



UNIVERSIDAD DE SEVILLA

Facultad de Química

Departamento de Química Inorgánica

CONSEJO SUPERIOR DE INVESTIGACIONES CIENTÍFICAS

Instituto de Investigaciones Químicas

Departamento de Química Inorgánica

**Synthesis, Structure and Reactivity of Dialkyl Terphenyl  
Phosphine Complexes of Late Transition Metals**

**Mario Marín Gómez**

**Tesis Doctoral**

**Sevilla 2019**



**Synthesis, Structure and Reactivity of Dialkyl Terphenyl  
Phosphine Complexes of Late Transition Metals**

Por

**Mario Marín Gómez**

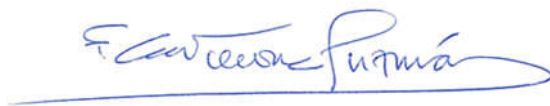
Trabajo presentado para aspirar  
al Título de Doctor en Química

Sevilla, 2019



Mario Marín Gómez

Directores de Tesis:



Ernesto Carmona Guzmán

Catedrático

Química Inorgánica

Universidad de Sevilla



M. Carmen Nicasio Jaramillo

Catedrática

Química Inorgánica

Universidad de Sevilla



*A la memoria de mi abuela Ana*

*A mis santos padres*



## **AGRADECIMIENTOS**

Se agradecen las siguientes contribuciones a esta tesis:

- Estudios sobre la optimización de las síntesis de las fosfinas por Carlos Navarro-Gilabert y Riccardo Peloso.
- Estudios de difracción de rayos X por el Dr. Eleuterio Álvarez (CSIC), la Dra. Celia Maya (Universidad de Sevilla) y Francisco Molina (Universidad de Huelva).
- Apoyo en los cálculos DFT por el Dr. Juan José Moreno y el Dr. Joaquín López-Serrano.





Cualquiera que haya estado a mi alrededor durante los últimos cuatro años y medio sabrá que el doctorado no ha sido un período fácil. Ni tiene que serlo. No lo repetiría, pero tampoco lo cambiaría. Me ha hecho la persona que soy ahora, en muchos aspectos, en lo bueno y lo no tan bueno. Incluso si decido no continuar en la investigación académica, las facetas de mi carácter que el doctorado ha mejorado, directa e indirectamente, se quedan conmigo para las siguientes etapas de mi camino. También he tenido la oportunidad de aprender en abundancia de todas y cada una de las personas con las que me he cruzado, tanto científicamente como personalmente. Y, por supuesto, también me llevo todas las relaciones que he formado como consecuencia del doctorado.

Esta Tesis es la culminación de mi etapa como doctorando, y no existe gracias únicamente a mí, ni mucho menos. Por tanto, me gustaría agradecer a todas las personas que han contribuido, científica y/o moralmente, a este trabajo.

En primer lugar, quiero agradecer a mis dos directores, Ernesto y M. Carmen, todo el esfuerzo que han dedicado tanto a la ciencia que se recoge en esta Tesis como al propio proceso de escritura. Creo que no hace falta decir que, sin ellos, indudablemente, todo mi trabajo no tendría ni raíces ni frutos.

En segundo lugar, pero no por ello menos importante, me gustaría extender mi agradecimiento al otro par de personas sin las que, evidentemente, tampoco habría llegado hasta aquí: mis padres, Adela y Sebastián. Ellos me educaron en el valor del esfuerzo y la dedicación, me han aguantado en las malas y me han acompañado en las buenas. Por todo lo que habéis hecho y seguís haciendo por mí, gracias.

Durante estos cuatro años y medio, he compartido laboratorios con una serie de personas (y personajes) que han hecho la vida en ellos más amena y que, en más de una ocasión, me han aportado una perspectiva distinta ante los diversos problemas que han surgido. Raquel y Carlos han sido probablemente los que me han aguantado en mayor proporción durante mi etapa en la Facultad de

Química, que no es poco. También compartí momentos con dos personas a las que les tengo mucho cariño, Paloma y Georgiana, y con dos personajazos con peculiares sentidos del humor, Miky y Antonio. No me puedo olvidar de otros dos amigos químicos, Alba y Vitor, aunque con ellos no haya compartido departamento durante el doctorado.

Luego me incorporé a los laboratorios del cicCartuja (en los que ya había estado intermitentemente sintetizando fosfina), donde me encontré con dos individuos a los que ya conocía: Carlos, al que me presentaron durante mis primeros pinitos en la investigación (allá por el 2011), y el gran JuanJo, compañero de grado, de máster y de doctorado. Poco a poco, se unieron los nuevos fichajes: Marina, domadora del molibdeno; Nere, secretaria extraoficial del 202; Juanín, competidor por el primer puesto de rompe-vidrio del laboratorio, y Macarena, que empieza ahora que yo termino. Más tarde conocí a Lola, una personita que se ha vuelto bastante importante en los últimos meses (¡y los que quedan!). Por último, pero no por ello menos importantes, las apodadas M&M's, María y Sonia. No me puedo olvidar de los que han pasado por el 1-2 y ya no están, José y JuanJe, y de los que, aunque no trabajan en él, son parte de esta gran familia, Tomás y Pablo. Aunque no estén (normalmente) en el laboratorio, también quiero dar las gracias a Joaquín, Riccardo y Jesús por enriquecer mi doctorado con sus conocimientos y experiencia. Esta tesis tampoco sería posible sin el trabajo de los cristalógrafos: Celia, Eleuterio y Paco; ni sin el del personal de RMN del CITIUS (Manolo, Belén, Miguel Ángel y Encarna) y el de los diversos servicios del IIQ: Fran, José Manuel, Guadalupe, Gloria y José Tomás.

Más allá del mundo de la química, existen en mi vida una serie de personas a las que valoro muchísimo y que también han estado acompañándome a lo largo de este camino. Tengo una familia extraordinaria y cualquiera que me conozca un poco sabrá cuánto aprecio el tiempo que paso con ellos: las paellas y barbacoas en el campo, las rutas de senderismo y de recogida de castañas, los viajes, las

comidas y cenas de navidad, los cumpleaños... Entre todos los miembros de mi familia que forman parte de mi vida y a los cuales agradezco todo el cariño y apoyo, me gustaría destacar a mi hermano Adrián, mi tía Ele y mi primo Alejandro.

Y en lo que a la amistad respecta, tampoco tengo nada que envidiarle a nadie. Mis queridas patinadoras, Cris, Leo y Bea, que son un tesoro; JuanMari, el neurólogo más joven y rubio de La Paz; Carlos, un campeón en muchos aspectos; Xexuh, al que conozco desde que éramos dos mocosos; Rocío y Ana, a las que veo menos de lo que me gustaría, y Pablo y Sara (y la pequeña Matilde).

Durante estos últimos años, el deporte me sirvió en muchas ocasiones como válvula de escape, por lo que me gustaría mencionar brevemente a mi equipo de hockey línea, los Sevilla Dragons, y a mis compañeros y monitores de natación de Hytasa.

Finally, I would also like to thank the friends I have made abroad. Luke, whom I met while I was an Erasmus student in Sheffield and with whom I am so very glad of still being in touch. Josh, Kedar and the people I met in Oxford and made my stay there much more enjoyable. Simon Aldridge, for having me in his group for those three months, and Jamie, for investing some of his time teaching and helping me in the lab.



# TABLE OF CONTENTS

Abbreviations	1
List of Compounds	5
Prefacio	11
Resumen	21

## **CHAPTER I. SYNTHESIS AND STUDY OF DIALKYL TERPHENYL PHOSPHINES AND MEASUREMENT OF THE TOLMAN ELECTRONIC PARAMETER**

### **I.1. INTRODUCTION** **27**

I.1.1. Tertiary phosphine ligands.	27
I.1.2. Metal carbonyl complexes.	30
I.1.3. Determination of the electronic properties of ligands.	32
I.1.4. Aims.	35

### **I.2. RESULTS AND DISCUSSION** **37**

I.2.1. Synthesis and properties of new dialkyl terphenyl phosphines.	37
I.2.2. Solid state structure of the $\text{PR}_2\text{Ar}''$ phosphines.	43
I.2.3. Synthesis and characterisation of $\text{Ni}(\text{CO})_3(\text{PR}_2\text{Ar}'')$ complexes of the dialkyl terphenyl phosphines ( $\text{R} = \text{Me, Et}$ ) and measurement of the Tolman electronic parameter.	48
I.2.4. Synthesis and characterisation of $\text{Ni}(\text{CO})_2(\text{PR}_2\text{Ar}'')$ complexes of the dialkyl terphenyl phosphines ( $\text{R} = \textit{i}\text{Pr, Cyp, Cy}$ ).	56
I.2.5. Interconversion between $\text{Ni}(\text{CO})_n(\text{PR}_2\text{Ar}'')$ species: experimental and DFT studies.	65
I.2.6. Reactivity of $\text{Ni}(\text{CO})_n(\text{PR}_2\text{Ar}'')$ complexes towards oxidative addition.	70

I.2.7. Synthesis and characterisation of iridium(I) and rhodium(I) carbonyl complexes of the dialkyl terphenyl phosphines.	74
--	----

---

<b>I.3. SUMMARY OF THE RESULTS</b>	<b>85</b>
------------------------------------	-----------

---

<b>I.4. EXPERIMENTAL SECTION</b>	<b>87</b>
----------------------------------	-----------

I.4.1. General considerations.	87
I.4.2. Synthesis of phosphine ligands.	88
I.4.3. Nickel carbonyl complexes.	98
I.4.4. Oxidative addition products.	110
I.4.5. Iridium carbonyl complexes.	113
I.4.6. Rhodium carbonyl complexes.	119
I.4.7. Computational details.	124

---

<b>I.5. BIBLIOGRAPHY</b>	<b>125</b>
--------------------------	------------

## **CHAPTER II. SYNTHESIS AND STUDY OF NICKEL, PALLADIUM AND PLATINUM COMPLEXES OF DIALKYL TERPHENYL PHOSPHINES**

---

<b>II.1. INTRODUCTION</b>	<b>135</b>
---------------------------	------------

II.1.1. Pd(II) and Pt(II) complexes with low coordination number.	138
II.1.2. $\eta^3$ -Allyl transition metal complexes. Generalities.	140
II.1.3. Zerovalent phosphine complexes of the group-10 metals.	145
II.1.4. Aims.	148

---

<b>II.2. RESULTS AND DISCUSSION</b>	<b>149</b>
-------------------------------------	------------

II.2.1. Dichloride Pd(II) and Pt(II) complexes of dialkyl terphenyl phosphines.	150
---	-----

II.2.2. Allylpalladium(II) and allylnickel(II) complexes of dialkyl terphenyl phosphines.	175
II.2.3. Zerovalent low-coordinate complexes of nickel, palladium and platinum stabilised by dialkyl terphenyl phosphines.	212
<b>II.3. SUMMARY OF THE RESULTS</b>	<b>229</b>
<b>II.4. EXPERIMENTAL SECTION</b>	<b>231</b>
II.4.1. General considerations.	231
II.4.2. Platinum dichloride adducts.	232
II.4.3. Palladium dichloride adducts.	235
II.4.4. Reactivity of the palladium dichloride adducts towards Lewis bases.	238
II.4.5. Neutral $\eta^3$ -allylpalladium complexes.	242
II.4.6. Cationic $\eta^3$ -allylpalladium complexes.	253
II.4.7. Neutral $\eta^3$ -allylnickel complexes.	259
II.4.8. Cationic $\eta^3$ -allylnickel complexes.	263
II.4.9. Nickel(0), palladium(0) and platinum(0) complexes.	268
<b>II.5. BIBLIOGRAPHY</b>	<b>273</b>
Conclusiones	287





## ABBREVIATIONS

R, R', R''	alkyl group
Me	methyl, $-\text{CH}_3$
Et	ethyl, $-\text{CH}_2\text{CH}_3$
<sup>i</sup> Pr	isopropyl, $-\text{CH}(\text{CH}_3)_2$
<sup>n</sup> Bu	<i>n</i> -butyl, $-\text{CH}_2\text{CH}_2\text{CH}_2\text{CH}_3$
<sup>t</sup> Bu	<i>tert</i> -butyl, $-\text{C}(\text{CH}_3)_3$
Cyp	cyclopentyl, $-\text{C}_5\text{H}_9$
Cy	cyclohexyl, $-\text{C}_6\text{H}_{11}$
Ac	acetyl, $-\text{C}(\text{O})\text{CH}_3$
Tf	triflate, $-\text{OS}(\text{O})_2\text{CF}_3$
Ar	aryl group
Ph	phenyl, $-\text{C}_6\text{H}_5$
Xyl	xylyl (2,6-dimethylphenyl), $-\text{C}_6\text{H}_3-2,6-(\text{CH}_3)_2$
Xyl'	3,5-dimethylphenyl, $-\text{C}_6\text{H}_3-3,5-(\text{CH}_3)_2$
Mes	mesityl, (2,4,6-trimethylphenyl), $-\text{C}_6\text{H}_2-2,4,6-(\text{CH}_3)_3$
Dipp	2,6-diisopropylphenyl, $-\text{C}_6\text{H}_3-2,6-^i\text{Pr}_2$
Tripp	2,4,6-triisopropylphenyl, $-\text{C}_6\text{H}_2-2,4,6-^i\text{Pr}_3$
Dtbp	3,5-di- <i>tert</i> -butylphenyl, $-\text{C}_6\text{H}_3-3,5-^t\text{Bu}_2$
Ar <sup>F</sup>	3,5-bis(trifluoromethyl)phenyl, $-\text{C}_6\text{H}_3-3,5-(\text{CF}_3)_2$
Ar'	biaryl group
Ar <sup>Tripp</sup>	2-(2,4,6-triisopropylphenyl)phenyl, $-\text{C}_6\text{H}_4-2\text{-Tripp}$
Ar''	<i>m</i> -terphenyl group
Ar <sup>Ph2</sup>	2,6-diphenylphenyl, $-\text{C}_6\text{H}_3-2,6-\text{Ph}_2$
Ar <sup>Xyl2</sup>	2,6-bis(2,6-dimethylphenyl)phenyl, $-\text{C}_6\text{H}_3-2,6-\text{Xyl}_2$

## Abbreviations

Ar <sup>Xyl'</sup> <sub>2</sub>	2,6-bis(3,5-dimethylphenyl)phenyl, -C <sub>6</sub> H <sub>3</sub> -2,6-Xyl' <sub>2</sub>
Ar <sup>Mes</sup> <sub>2</sub>	2,6-bis(2,4,6-trimethylphenyl)phenyl, -C <sub>6</sub> H <sub>3</sub> -2,6-Mes <sub>2</sub>
Ar <sup>Dipp</sup> <sub>2</sub>	2,6-bis(2,6-diisopropylphenyl)phenyl, -C <sub>6</sub> H <sub>3</sub> -2,6-Dipp <sub>2</sub>
Ar <sup>Tripp</sup> <sub>2</sub>	2,6-bis(2,4,6-triisopropylphenyl)phenyl, -C <sub>6</sub> H <sub>3</sub> -2,6-Tripp <sub>2</sub>
Ar <sup>Dtbp</sup> <sub>2</sub>	2,6-bis(3,5-di-tert-butylphenyl)phenyl, -C <sub>6</sub> H <sub>3</sub> -2,6-Dtbp <sub>2</sub>
acac	acetylacetonate, CH <sub>3</sub> C(O)CHC(O)CH <sub>3</sub>
L, L'	2-electron donor ligand
PR <sub>3</sub>	tertiary phosphine
NHC	N-heterocyclic carbene
CAAC	cyclic alkyl amino carbene
cod	1,5-cyclooctadiene
coe	cyclooctene
dvds	1,3-divinyltetramethyldisiloxane
κ	ligand hapticity
η	number of carbon atoms directly bound to a metal centre
μ	bridging ligand
<i>o</i>	<i>ortho</i>
<i>m</i>	<i>meta</i>
<i>p</i>	<i>para</i>
THF	tetrahydrofuran, C <sub>4</sub> H <sub>8</sub> O
TEP	Tolman Electronic Parameter
<i>v</i>	vibrational wavenumber (cm <sup>-1</sup> )
DFT	density functional theory
TS	transition state
ORTEP	Oak Ridge Thermal Ellipsoid Plot
IR	infrared
ESMS	electrospray mass spectrometry

## Abbreviations

r.t.	room temperature
ca.	<i>circa</i>
ref.	reference

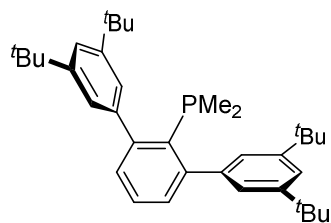
### **NMR abbreviations**

NMR	nuclear magnetic resonance
$\delta$	chemical shift
ppm	parts per million
COSY	$^1\text{H}$ - $^1\text{H}$ Correlation Spectroscopy
NOESY	Nuclear Overhauser Effect Spectroscopy
DOSY	Diffusion Ordered Spectroscopy
DEPTQ	Distortionless Enhancement by Polarization Transfer with retention of Quaternary carbons
HSQC	Heteronuclear Single Quantum Coherence
HMQC	Heteronuclear Multiple Quantum Coherence
s	singlet
d	doublet
t	triplet
q	quartet
sept	septet
m	multiplet
br	broad
$^nJ_{\text{AB}}$	coupling constant between nuclei A and B separated by n bonds
$J_{\text{app}}$	apparent coupling constant
Tol- $d_8$	toluene- $d_8$ , $\text{C}_6\text{D}_5\text{CD}_3$

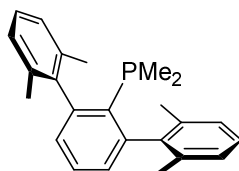


# LIST OF COMPOUNDS

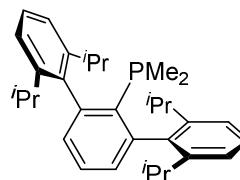
## CHAPTER I (LIGANDS)



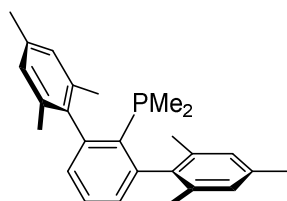
$\text{PMe}_2\text{Ar}^{\text{Dtbp}2}$ , **L1**



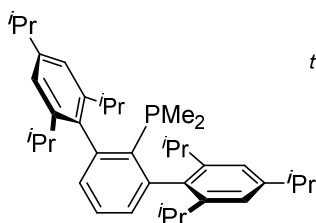
$\text{PMe}_2\text{Ar}^{\text{Xyl}2}$ , **L2**



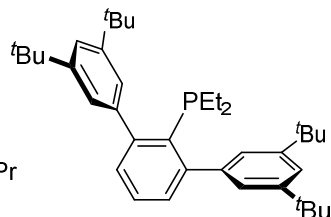
$\text{PMe}_2\text{Ar}^{\text{Dipp}2}$ , **L3**



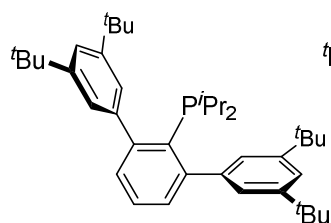
$\text{PMe}_2\text{Ar}^{\text{Mes}2}$ , **L4**



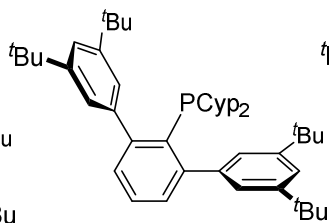
$\text{PMe}_2\text{Ar}^{\text{Tripp}2}$ , **L5**



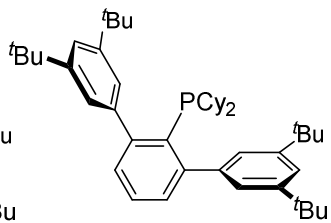
$\text{PEt}_2\text{Ar}^{\text{Dtbp}2}$ , **L6**



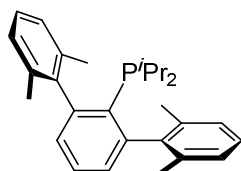
$\text{P}^i\text{Pr}_2\text{Ar}^{\text{Dtbp}2}$ , **L7**



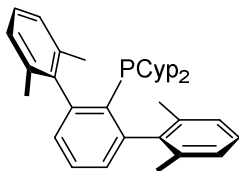
$\text{PCyp}_2\text{Ar}^{\text{Dtbp}2}$ , **L8**



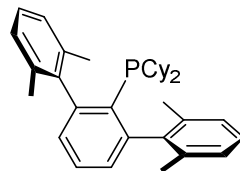
$\text{PCy}_2\text{Ar}^{\text{Dtbp}2}$ , **L9**



$\text{P}^i\text{Pr}_2\text{Ar}^{\text{Xyl}2}$ , **L10**



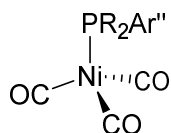
$\text{PCyp}_2\text{Ar}^{\text{Xyl}2}$ , **L11**



$\text{PCy}_2\text{Ar}^{\text{Xyl}2}$ , **L12**

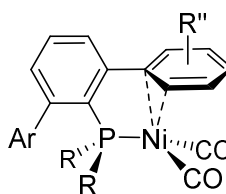
List of Compounds

CHAPTER I (COMPLEXES)



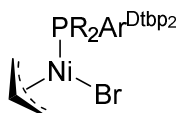
**1·PR<sub>2</sub>Ar''**

PR<sub>2</sub>Ar'' = L1-L6, XPhos

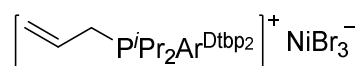


**2·PR<sub>2</sub>Ar''**

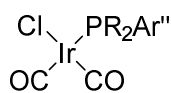
PR<sub>2</sub>Ar'' = L7-L12



R = Me, **3·L1**  
R = Et, **3·L6**

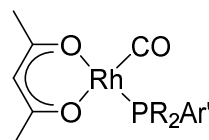


**4·L7**



**5·PR<sub>2</sub>Ar''**

PR<sub>2</sub>Ar'' = L1, L6-L12

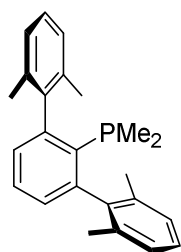


**6·PR<sub>2</sub>Ar''**

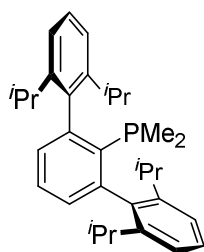
PR<sub>2</sub>Ar'' = L1-L12, XPhos

List of Compounds

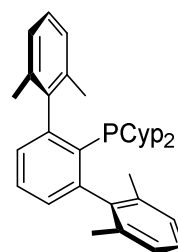
CHAPTER II (LIGANDS)



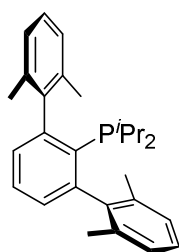
$\text{PMe}_2\text{Ar}^{\text{Xyl}_2}$ , L1



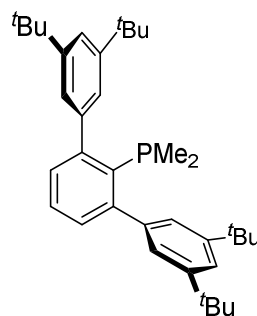
$\text{PMe}_2\text{Ar}^{\text{Dipp}_2}$ , L2



$\text{PCyp}_2\text{Ar}^{\text{Xyl}_2}$ , L3

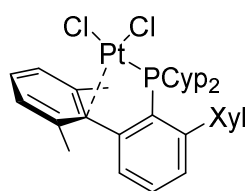


$\text{P}^i\text{Pr}_2\text{Ar}^{\text{Xyl}_2}$ , L4

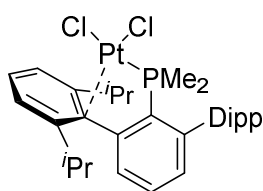


$\text{PMe}_2\text{Ar}^{\text{D}^t\text{Bu}_2}$ , L5

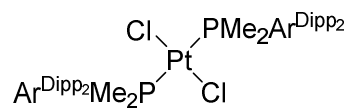
CHAPTER II (COMPLEXES)



1-L3



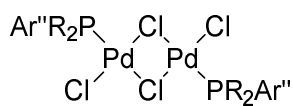
1-L2



2-L2

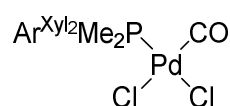
List of Compounds

CHAPTER II (COMPLEXES, cont.)

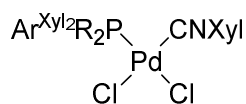


**3·PR<sub>2</sub>Ar''**

PR<sub>2</sub>Ar'' = L1-L3

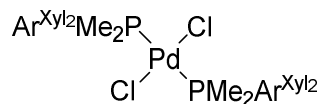


**4·L1**

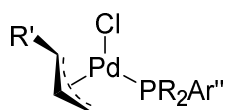


R = Me, **5·L1**

R = Cyp, **5·L3**



**6·L1**

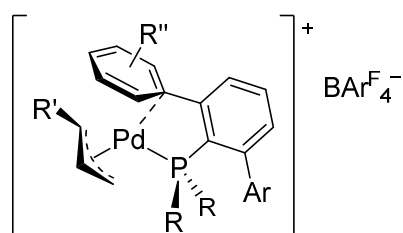


R' = H, **7·PR<sub>2</sub>Ar''**

R' = Me, **8·PR<sub>2</sub>Ar''**

R' = Ph, **9·PR<sub>2</sub>Ar''**

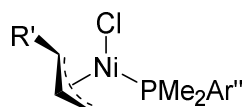
PR<sub>2</sub>Ar'' = L1-L3



R' = H, **10·PR<sub>2</sub>Ar''**

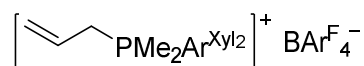
R' = Ph, **11·PR<sub>2</sub>Ar''**

PR<sub>2</sub>Ar'' = L2, L4



R' = H, **12·L1, 12·L2**

R' = Me, **13·L1**

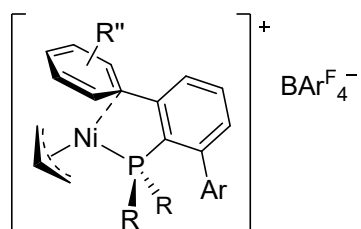


**14·L1**

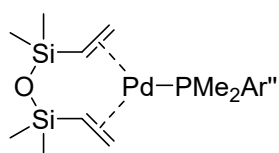


List of Compounds

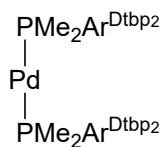
CHAPTER II (COMPLEXES, cont.)



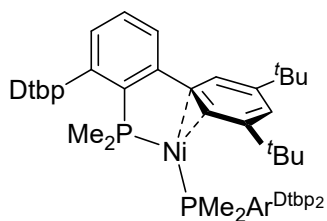
**15·PR<sub>2</sub>Ar''**  
PR<sub>2</sub>Ar'' = L2-L4



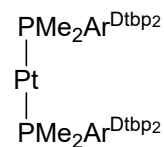
**16·L1**  
**16·L2**



**17·L5**



**18·L5**



**19·L5**



## PREFACIO

El avance de la especie humana ha ido, y sigue yendo, de la mano con el avance de la ciencia. Desde el descubrimiento del fuego y la invención de la rueda hasta los más modernos desarrollos en la lucha contra el cáncer y en la producción de fármacos, la curiosidad y el ingenio del ser humano han hecho frente a los problemas que han surgido a lo largo de la Historia, y han puesto a nuestra sociedad en el lugar en el que hoy nos encontramos. A pesar del inexplicable escepticismo que aún algunas personas muestran ante diversos hechos y fenómenos que actualmente están respaldados por la casi totalidad de la comunidad científica, como el cambio climático y la efectividad de las vacunas, la contribución que la investigación científica ha tenido y tiene en el desarrollo de la humanidad es incuestionable.

Puesto que toda la materia conocida se encuentra formada por los 118 elementos de la tabla periódica, dando lugar a moléculas y compuestos de todos los tipos y tamaños, la investigación química en particular juega un papel fundamental en dicho desarrollo. Muchos de los avances científicos en campos tan diversos como la biología, la medicina, la agrología, la ciencia de materiales, etc., pasan en algún punto de su proceso, en mayor o menor medida, por la Química.

Un área para nada pequeña de esta ciencia es la Química Organometálica, que se fundamenta sobre el estudio del enlace entre los elementos metálicos y el carbono. La principal razón de que algo que *a priori* parece tan concreto como un tipo de enlace constituya la base de toda un área de la química es la riqueza en propiedades y reactividad que los metales, especialmente los que se encuentran en la serie de transición, poseen. Como se discutirá más adelante, los compuestos organometálicos han tenido un gran impacto en la Catálisis Homogénea. Esta, a

## Prefacio

su vez, resulta esencial tanto para ciertos procesos industriales como para la investigación en otras áreas de la ciencia. La importancia de la simbiosis entre la Química Organometálica y la Catálisis Homogénea se ha visto reflejada en tres de los premios Nobel de Química que se han concedido en las últimas dos décadas, otorgados a científicos que han contribuido de forma indiscutible a ambos campos::

- En 2001 a William S. Knowles y Ryoji Noyori "*for their work on chirally catalysed hydrogenation reactions*" y a K. Barry Sharpless "*for his work on chirally catalysed oxidation reactions*".
- En 2005 a Yves Chauvin, Robert H. Grubbs y Richard R. Schrock "*for the development of the metathesis method in organic synthesis*".
- En 2010 a Richard F. Heck, Ei-ichi Negishi y Akira Suzuki "*for palladium-catalyzed cross couplings in organic synthesis*".

El trabajo que se ha desarrollado durante esta Tesis Doctoral se enmarca dentro de la línea de investigación de Química Organometálica y Catálisis Homogénea y se ha llevado a cabo tanto en la Facultad de Química de la Universidad de Sevilla como en el Instituto de Investigaciones Químicas (centro mixto Universidad de Sevilla – CSIC). En concreto, los estudios que aquí se describen se centran en la descripción de una nueva familia de ligandos fosfina voluminosos, estables al aire, que poseen un sustituyente de tipo terfenilo, y su aplicación en la síntesis de una gran variedad de complejos de metales de la parte derecha de la series de transición, níquel y paladio, aunque también se incluyen otros de platino, iridio y rodio. Por una parte, se han determinado las características electrónicas y estéricas de los ligandos fosfina y sus diferentes modos de coordinación: el modo clásico a través del átomo de fósforo,  $\kappa^1\text{-P}$ , y la coordinación bidentada,  $\kappa^1\text{-P}, \eta^x\text{-C}_{\text{areno}}$ , que incluye la interacción adicional  $\text{M}\cdots\text{C}_{\text{areno}}$  con uno de los anillos laterales del grupo terfenilo. Por otra, se pone de manifiesto la capacidad que tienen estos ligandos voluminosos para estabilizar

## Prefacio

compuestos en bajo número de coordinación con diferentes metales. Algunos de los compuestos descritos podrían resultar de interés en procesos catalíticos diversos, como los de acoplamiento cruzado. Los compuestos preparados se han caracterizado mediante espectroscopía de RMN multinuclear, mono y bidimensional, y espectrofotometría IR, y una buena parte de ellos han sido caracterizados estructuralmente mediante difracción de rayos X. Las determinaciones cristalográficas se llevaron a cabo de manera independiente a este trabajo por la Dra. Celia Maya (Universidad de Sevilla), el Dr. Eleuterio Álvarez (Consejo Superior de Investigaciones Científicas) y Francisco Molina (CIQSO-Universidad de Huelva).

Esta tesis consta de dos capítulos, estructurados de la forma habitual: introducción, resultados y discusión, parte experimental, conclusiones y bibliografía. La numeración tanto de las referencias bibliográficas como de los esquemas, figuras y tablas es independiente en cada capítulo, así como la numeración de los compuestos.

Como parte del programa de Formación del Personal Investigador (FPI), he realizado una estancia de tres meses de duración (de junio a agosto de 2018, ambos inclusive) en la Universidad de Oxford, bajo la supervisión del Prof. Simon Aldridge. Allí, combiné la experiencia adquirida en el tratamiento de complejos de los metales de transición con los conocimientos que el grupo aceptor posee sobre la química de los elementos del grupo principal, dando lugar a novedosos compuestos que contienen enlaces entre unos y otros, y que podrían presentar una reactividad inédita.

Dicha estancia constituye uno de los prerrequisitos para optar a la Mención de Doctor Internacional (RD99/2011, normativa regulada por acuerdo 7.2/CG 17-6-11). Con objeto de obtener dicha mención, parte de la tesis debe ser redactada en un idioma extranjero. Por esta razón, los Capítulos I y II se han escrito en inglés, mientras que el Prefacio, el Resumen y las Conclusiones se han

## Prefacio

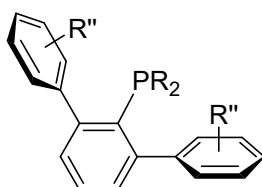
redactado en español. Se incluye también una relación de compuestos (*List of Compounds*) obtenidos y caracterizados a lo largo de esta tesis.

Una parte de los resultados obtenidos se ha publicado, bajo el título “*Synthesis, Structure and Nickel Carbonyl Complexes of Dialkylterphenyl Phosphines*”, en la revista *Chemistry – A European Journal* (año 2019, vol. 25, núm. 1, págs. 260-272). Asimismo, contribuí en otra publicación científica, no relacionada directamente con esta tesis, titulada “*Ni-Catalyzed Amination Reactions: An Overview*”, de la revista *The Chemical Record* (año 2016, vol. 16, núm. 4, págs. 1819-1832).

## RESUMEN

Esta Tesis Doctoral se estructura en dos capítulos. El primero de ellos está dedicado a la síntesis y al estudio de las propiedades electrónicas de una familia de fosfinas terciarias voluminosas que contiene un anillo de terfenilo en su estructura.

Este primer capítulo se divide en cuatro secciones. En las dos primeras, se describen la preparación y las propiedades estructurales de un total de doce dialquil terfenil fosfinas, cuya estructura general se muestra en la figura.



Estas fosfinas muestran una marcada estabilidad frente a la oxidación por exposición al aire, tanto en estado sólido como en disolución, resaltando las diferentes propiedades que los sustituyentes alquilo en el átomo de fósforo les confieren. Se han identificado tres posibles conformaciones para las fosfinas, que se interconvierten fácilmente mediante la rotación alrededor del enlace P-C<sub>ipso</sub>.

Las dos últimas secciones del primer capítulo de esta Memoria se dedican al estudio de las propiedades electrónicas de las terfenil fosfinas mediante medidas de las frecuencias de vibración de los enlaces C–O en los compuestos del tipo Ni(CO)<sub>3</sub>(PR<sub>2</sub>Ar'') y IrCl(CO)<sub>2</sub>(PR<sub>2</sub>Ar''). Se han preparado los tricarbonylos de níquel con los miembros menos voluminosos de las terfenil fosfinas y se ha determinado, mediante espectroscopía de IR, la capacidad donadora de los correspondientes ligandos fosfina, comparándola con otros ligandos de interés descritos en la bibliografía. Para fosfinas con sustituyentes más voluminosos (grupos cíclicos o ramificados) en el átomo de fósforo, no se han podido obtener

## Resumen

los correspondientes derivados de tricarbonilo. En estos casos, se observa la formación de productos de composición  $\text{Ni}(\text{CO})_2(\text{PR}_2\text{Ar}'')$ , en los que una molécula de CO se ha sustituido por la interacción débil  $\text{Ni}\cdots\text{C}_{\text{areno}}$  con uno de los anillos laterales del sustituyente terfenilo. Las estructuras cristalinas de estos compuestos constituyen los primeros ejemplos de compuestos de fórmula  $\text{Ni}(\text{CO})_2(\text{PR}_3)$  caracterizados estructuralmente. Dada la imposibilidad de medir las propiedades electrónicas de las fosfinas más voluminosas en los complejos de níquel, se exploran alternativas basadas en compuestos de iridio,  $\text{IrCl}(\text{CO})_2(\text{PR}_2\text{Ar}'')$ , y de rodio,  $\text{Rh}(\text{acac})(\text{CO})(\text{PR}_2\text{Ar}'')$ ; no obstante, no se encuentra una buena correlación entre los valores de la frecuencia de vibración del ligando carbonilo obtenidos para estos sistemas y los hallados en el caso de los complejos de níquel.

En el segundo capítulo, se emplea una selección de cinco de las terfenil fosfinas descritas en el capítulo anterior ( $\text{PMe}_2\text{Ar}^{\text{Xyl}_2}$ ,  $\text{PMe}_2\text{Ar}^{\text{Dipp}_2}$ ,  $\text{PCyp}_2\text{Ar}^{\text{Xyl}_2}$ ,  $\text{P}^i\text{Pr}_2\text{Ar}^{\text{Xyl}_2}$  y  $\text{PMe}_2\text{Ar}^{\text{Dtbp}_2}$ ) para preparar una variedad de compuestos de níquel, paladio y platino en diferentes estados de oxidación. En la primera sección, se aborda la síntesis y caracterización estructural de dicloruros de platino(II) y paladio(II) con estas fosfinas. Como complemento a los trabajos con platino desarrollados con anterioridad en nuestro grupo de investigación, se han preparado dos nuevos dicloruros de platino(II),  $\text{PtCl}_2(\text{PCyp}_2\text{Ar}^{\text{Xyl}_2})$  y *trans*- $\text{PtCl}_2(\text{PMe}_2\text{Ar}^{\text{Dipp}_2})_2$ . En el primero de ellos, se observa la coordinación bidentada de la fosfina  $\text{PCyp}_2\text{Ar}^{\text{Xyl}_2}$ , que se une al centro metálico tanto por el átomo de fósforo como a través del carbono *ipso* de uno de los anillo laterales de la fosfina. Los compuestos análogos de paladio, de fórmula empírica  $\text{PdCl}_2(\text{PR}_2\text{Ar}'')$ , a diferencia de los de platino, presentan una estructura dinuclear con ligandos cloruro puentes en el estado sólido. Sin embargo, en disolución se observan mezclas de las especies mononucleares y dinucleares cuya composición depende la naturaleza del ligando fosfina y de la polaridad del disolvente. Los estudios de



## Resumen

reactividad de los dicloruros de paladio(II) frente a diversas bases de Lewis (CO, CNXyl, PR<sub>2</sub>Ar'') completan esta sección.

A continuación, se discute la preparación de una serie de complejos de paladio(II) y níquel(II) con ligandos  $\eta^3$ -alilo de composición MCl( $\eta^3$ -C<sub>3</sub>H<sub>4</sub>R') (PR<sub>2</sub>Ar'') (M = Pd, Ni). Los compuestos se han caracterizado por técnicas de RMN y de difracción de rayos X de monocristal. Los derivados de paladio constituyen la familia más extensa, habiéndose sintetizado combinaciones con casi todas las fosfinas empleadas y diferentes grupos alilo (C<sub>3</sub>H<sub>5</sub>, alilo; C<sub>3</sub>H<sub>4</sub>Me, crotilo; C<sub>3</sub>H<sub>4</sub>Ph, cinamilo). A la temperatura ambiente, estos complejos presentan un comportamiento dinámico en disolución que afecta al ligando alilo y que se pone de manifiesto en sus espectros de RMN de <sup>1</sup>H. Este comportamiento fluxional es compatible con un mecanismo que implica un cambio de hapticidad del ligando alilo del tipo  $\eta^3$ - $\eta^1$ - $\eta^3$ . La facilidad con la que se da este proceso fluxional depende tanto de la naturaleza de la fosfina como del sustituyente R' en el fragmento alilo. El tratamiento de estos derivados con NaBAR<sub>4</sub><sup>F</sup> ha permitido el aislamiento de compuestos catiónicos, de fórmula [Pd( $\eta^3$ -C<sub>3</sub>H<sub>4</sub>R') (PR<sub>2</sub>Ar'')]BAR<sub>4</sub><sup>F</sup>, en los que el ligando cloruro se sustituye por la interacción entre el átomo de paladio y uno de los anillos laterales del grupo terfenilo, tal como demuestran las estructuras de difracción de rayos X. Mediante este procedimiento se ha podido incorporar la fosfina voluminosa P'Pr<sub>2</sub>Ar<sup>Xyl</sup> a este tipo de aductos. A diferencia de los derivados neutros, los compuestos catiónicos no muestran evidencia del proceso dinámico mencionado anteriormente.

Respecto al níquel, sólo se han podido sintetizar los complejos análogos de composición NiCl( $\eta^3$ -C<sub>3</sub>H<sub>5</sub>) (PMe<sub>2</sub>Ar'') con las fosfinas dimetiladas PMe<sub>2</sub>Ar<sup>Xyl</sup> y PMe<sub>2</sub>Ar<sup>Dipp</sup>, y únicamente se ha podido aislar un derivado de crotilo con la primera de ellas. Los estudios de RMN parecen indicar que el proceso dinámico que experimentan estos complejos es el intercambio *sin-sin anti-anti*, mediante una rotación del plano alílico alrededor del eje que conecta al níquel con el centro de

## Resumen

masas del fragmento alilo. Para finalizar esta sección, se describen los correspondientes aductos catiónicos de níquel,  $[\text{Ni}(\eta^3\text{-C}_3\text{H}_5)(\text{PR}_2\text{Ar}'')] \text{BAr}^{\text{F}_4}$ , que incorporan tanto la fosfina dimetilada  $\text{PMe}_2\text{Ar}^{\text{Dipp}_2}$  como las voluminosas  $\text{PCyp}_2\text{Ar}^{\text{Xyl}_2}$  y  $\text{P}^i\text{Pr}_2\text{Ar}^{\text{Xyl}_2}$ . Como en el caso de los derivados catiónicos de paladio, la cuarta posición de coordinación de estos complejos está ocupada por una interacción débil con uno de los anillos laterales de la fosfina, tal como se confirmó por difracción de rayos X.

En la última sección del segundo capítulo, se detalla la síntesis de compuestos de níquel, paladio y platino en los que el metal se encuentra en el estado de oxidación 0. En primer lugar, se presentan dos compuestos de paladio(0), de composición  $\text{Pd}(\text{dvds})(\text{PMe}_2\text{Ar}'')$  para  $\text{Ar}'' = \text{Ar}^{\text{Xyl}_2}$  y  $\text{Ar}^{\text{Dipp}_2}$  y  $\text{dvds} = 1,3\text{-diviniltetrametildisiloxano}$ , que se obtienen mediante la reducción de los dicloruros de paladio(II), descritos en la primera sección, con zinc en polvo en presencia de la diolefina  $\text{dvds}$ . Estos presentan una geometría trigonal plana, con dos de las posiciones de coordinación ocupadas por los dobles enlaces del ligando  $\text{dvds}$  y la tercera por la fosfina actuando como ligando monodentado. A partir de la reducción del alilo de paladio  $\text{PdCl}(\eta^3\text{-C}_3\text{H}_5)(\text{PMe}_2\text{Ar}^{\text{Dtbp}_2})$  en presencia de un segundo equivalente de fosfina en medio fuertemente básico ( $\text{KO}^t\text{Bu}/i\text{PrOH}$ ), se ha podido aislar el compuesto homoléptico dicoordinado  $\text{Pd}(\text{PMe}_2\text{Ar}^{\text{Dtbp}_2})_2$ . La estructura de rayos X del este compuesto revela que la mitad de los sustituyentes  $^t\text{Bu}$  del terfenilo se sitúan alrededor del centro de paladio, otorgándole, presumiblemente, una relativa estabilidad. El complejo análogo de níquel,  $\text{Ni}(\text{PMe}_2\text{Ar}^{\text{Dtbp}_2})_2$ , se ha podido obtener a través de la hidrogenación de  $\text{Ni}(\text{cod})_2$  en presencia de la fosfina. Aunque con la misma fórmula molecular que el derivado de paladio, la estructura en estado sólido de este compuesto muestra una geometría trigonal del átomo de níquel, con la tercera posición de coordinación ocupada por una interacción  $\eta^2$  con uno de los anillos de  $\text{Dtbp}$ . Durante el seguimiento de la reacción mediante RMN, se pudo detectar la formación de un intermedio cuya estructura se ha determinado por difracción de rayos X,

## Resumen

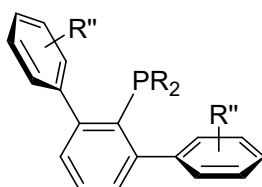
confirmando que se trata de la especie  $\text{Ni}(\text{coe})(\text{PMe}_2\text{Ar}^{\text{Dtbp}_2})$  (coe = cicloocteno), la cual contiene una molécula de cicloocteno que proviene de la hidrogenación parcial del ciclooctadieno. En este compuesto, el ligando fosfina también exhibe un modo de coordinación bidentado. Para completar la tríada, se ha llevado a cabo la síntesis del complejo  $\text{Pt}(\text{PMe}_2\text{Ar}^{\text{Dtbp}_2})_2$ , el cual se genera mediante el tratamiento del precursor  $\text{K}_2\text{PtCl}_4$  con KOH en etanol en presencia de dos equivalentes del ligando fosfina. Como cabe esperar, este compuesto posee una estructura molecular en el estado sólido prácticamente idéntica a la del análogo de paladio.



## ABSTRACT

This PhD thesis consists of two chapters. The first one focuses on the synthesis and study of the electronic properties of a family of bulky tertiary phosphines which contain a terphenyl group in their structure.

This first chapter is divided into four sections. In the first two sections, the preparation and the structural features of twelve different dialkyl terphenyl phosphines (of which the general structure is depicted in the figure below) are described.



These phosphines exhibit a marked stability towards oxidation by air, both in the solid state and in solution, highlighting the different properties conferred by the alkyl substituents on the phosphorus atom. Three possible conformations for these phosphines have been identified, facily interconverting through the rotation around the P-C<sub>ipso</sub> bond.

The two last sections of the first chapter of this thesis are dedicated to the study of the electronic properties of the terphenyl phosphines. This is achieved via the measurement of the C–O vibration frequencies in compounds of the type Ni(CO)<sub>3</sub>(PR<sub>2</sub>Ar'') and IrCl(CO)<sub>2</sub>(PR<sub>2</sub>Ar''). Nickel tricarbonyls of the less bulky terphenyl phosphines were prepared and the donor capacity of the ligands was determined by IR spectroscopy and compared to those of other ligands of interest described in the literature. The corresponding tricarbonyl derivatives of the phosphines with bulkier (branched or cyclic) alkyl groups on the phosphorus atom could not be obtained. Instead, complexes Ni(CO)<sub>2</sub>(PR<sub>2</sub>Ar'') were formed where a

## Abstract

second carbonyl ligand has been replaced by a weak Ni...C<sub>arene</sub> interaction with one the side rings of the terphenyl substituent. The crystal structures of these compounds are the first examples of compounds of formula Ni(CO)<sub>2</sub>(PR<sub>3</sub>) structurally characterised. Given the unfeasibility of measuring the electronic properties of the bulkier phosphines in the nickel complexes, alternatives based on iridium, IrCl(CO)<sub>2</sub>(PR<sub>2</sub>Ar''), and rhodium complexes, Rh(acac)(CO)(PR<sub>2</sub>Ar''), were explored. However, no correlation was found between the C–O vibration frequencies obtained for these systems and those acquired for the nickel complexes.

In the second chapter, a selection of five out of the twelve terphenyl phosphines described in the previous chapter (PMe<sub>2</sub>Ar<sup>Xyl<sub>2</sub></sup>, PMe<sub>2</sub>Ar<sup>Dipp<sub>2</sub></sup>, PCyp<sub>2</sub>Ar<sup>Xyl<sub>2</sub></sup>, P<sup>i</sup>Pr<sub>2</sub>Ar<sup>Xyl<sub>2</sub></sup> y PMe<sub>2</sub>Ar<sup>Dtbp<sub>2</sub></sup>) are employed to prepare various nickel, palladium and platinum complexes in different oxidation states. In the first section, the synthesis and structural characterisation of platinum(II) and palladium(II) dichloride compounds with these phosphines are addressed. Complementing the work on platinum previously developed in our research group, two new platinum(II) dichlorides, PtCl<sub>2</sub>(PCyp<sub>2</sub>Ar<sup>Xyl<sub>2</sub></sup>) and *trans*-PtCl<sub>2</sub>(PMe<sub>2</sub>Ar<sup>Dipp<sub>2</sub></sup>)<sub>2</sub>, have been prepared. In the former, a bidentate coordination of the phosphine PCyp<sub>2</sub>Ar<sup>Xyl<sub>2</sub></sup> is observed, binding to the metal centre both by the phosphorus atom and through the *ipso* carbon of one of the side rings of the phosphine. The palladium analogues, PdCl<sub>2</sub>(PR<sub>2</sub>Ar''), unlike those based on platinum, exhibit a dinuclear structure with bridging chloride ligands in the solid state. Nevertheless, a mixture of both the mononuclear and dinuclear species is observed, with the ratio between the two depending on the nature of the phosphine ligand and the polarity of the solvent. The study of the reactivity of the palladium(II) dichlorides towards different Lewis bases (CO, CNXyl, PR<sub>2</sub>Ar'') complete this section.

Next, the preparation of a series of palladium(II) and nickel(II) complexes bearing η<sup>3</sup>-allyl ligands of composition MCl(η<sup>3</sup>-C<sub>3</sub>H<sub>4</sub>R')(PR<sub>2</sub>Ar'') (M = Pd, Ni) is

## Abstract

discussed. These compounds have been characterised by NMR and single crystal X-ray diffraction techniques. The palladium derivatives represent the broader family, combining the majority of phosphines employed and different allyl groups ( $C_3H_5$ , allyl;  $C_3H_4Me$ , crotyl;  $C_3H_4Ph$ , cinnamyl). At room temperature, these complexes display a dynamic behaviour in solution involving the allyl ligand, as inferred from their  $^1H$  NMR spectra. This fluxional behaviour is compatible with a mechanism comprising a change in the hapticity of the allyl ligand of the type  $\eta^3$ - $\eta^1$ - $\eta^3$ . The rate of this fluxional process depends on both the nature of the phosphine ligand and the R' substituent on the allyl moiety. Treatment of these derivatives with  $NaBAR^F_4$  allowed for the isolation of cationic complexes of formula  $[Pd(\eta^3-C_3H_4R')(PR_2Ar'')]BAR^F_4$ , where the chloride ligand is replaced by an interaction between the palladium atom and one of the side rings of the terphenyl group, as confirmed by X-ray diffraction studies. Following this procedure, the bulky  $P'Pr_2Ar^{Xyl_2}$  phosphine could be incorporated into this type of adducts. Unlike the neutral derivatives, the cationic complexes do not seem to exhibit the dynamic behaviour mentioned above.

Concerning the nickel analogues, only those of composition  $NiCl(\eta^3-C_3H_5)(PMe_2Ar'')$  with dimethyl-substituted phosphines  $PMe_2Ar^{Xyl_2}$  and  $PMe_2Ar^{Dipp_2}$ , and the crotyl derivative bearing the former, could be isolated. NMR studies apparently indicate that the dynamic process undergone by these complexes is the *syn-syn anti-anti* exchange, via rotation of the allylic plane around the axis connecting the nickel atom with the mass centre of the allyl moiety. Finally, the corresponding nickel cationic adducts,  $[Ni(\eta^3-C_3H_5)(PR_2Ar'')]BAR^F_4$ , bearing dimethyl-substituted  $PMe_2Ar^{Dipp_2}$  as well as bulky  $PCyp_2Ar^{Xyl_2}$  and  $P'Pr_2Ar^{Xyl_2}$ , are described. As in the case of the cationic palladium derivatives, the fourth coordination position in these complexes is occupied by a weak interaction with one of the side rings of the phosphine, as confirmed by X-ray diffraction studies.

## Abstract

In the last section of the second chapter, the syntheses of nickel, palladium and platinum compounds where the metal is in oxidation state zero are detailed. Firstly, two palladium(0) complexes, of composition  $\text{Pd}(\text{dvds})(\text{PMe}_2\text{Ar}'')$  (for  $\text{Ar}'' = \text{Ar}^{\text{Xyl}_2}$  and  $\text{Ar}^{\text{Dipp}_2}$  and  $\text{dvds} = 1,3\text{-divinyltetramethyldisiloxane}$ ), are presented, obtained by reduction of the palladium(II) dichlorides described in the first section by zinc powder in the presence of the diolefin  $\text{dvds}$ . These complexes display a trigonal geometry, with two coordination positions occupied by the double bonds of the  $\text{dvds}$  ligand and the third position by the phosphine acting as a monodentate ligand. From the reduction of the palladium allyl  $\text{PdCl}(\eta^3\text{-C}_3\text{H}_5)(\text{PMe}_2\text{Ar}^{\text{Dtbp}_2})$  in the presence of a second equivalent of phosphine in a strongly basic medium ( $\text{KO}^t\text{Bu}/i\text{PrOH}$ ), the homoleptic bisphosphine compound  $\text{Pd}(\text{PMe}_2\text{Ar}^{\text{Dtbp}_2})_2$  could be isolated. The X-ray structure of this complex reveals that half the  $^t\text{Bu}$  substituents on the terphenyl group are positioned around the palladium centre, presumably conferring the complex a relative stability. The nickel analogue,  $\text{Ni}(\text{PMe}_2\text{Ar}^{\text{Dtbp}_2})_2$ , was obtained by the hydrogenation of  $\text{Ni}(\text{cod})_2$  in the presence of the phosphine. Although with the same molecular formula than the palladium derivative, the solid state structure of this compound displays a trigonal geometry of the nickel atom, with the third coordination position occupied by a weak  $\eta^2$  interaction with on the  $\text{Dtbp}$  rings. During the reaction monitoring by NMR, the formation of an intermediate was detected and its identity was determined by X-ray diffraction to be  $\text{Ni}(\text{coe})(\text{PMe}_2\text{Ar}^{\text{Dtbp}_2})$  ( $\text{coe} = \text{cyclooctene}$ ), where the cyclooctene ligand originates from the partial hydrogenation of cyclooctadiene. In this compound, the phosphine ligand also exhibits a bidentate mode of coordination. To complete the triad, complex  $\text{Pt}(\text{PMe}_2\text{Ar}^{\text{Dtbp}_2})_2$  was synthesised by the treatment of the precursor  $\text{K}_2\text{PtCl}_4$  with  $\text{KOH}$  in ethanol in the presence of two equivalents of the phosphine ligand. As expected, this compound displays a solid state structure almost identical to the palladium analogue.



## **CHAPTER I.**

---

Synthesis and study of dialkyl terphenyl  
phosphines and measurement of the  
Tolman Electronic Parameter



## I.1. INTRODUCTION

### I.1.1. Tertiary phosphine ligands.

Tertiary phosphines and related P(III)-containing compounds ( $PX_3$ ,  $X = R$ , OR,  $NR_2$ , etc.) have become indispensable ligands in organometallic chemistry and homogeneous catalysis.<sup>1-3</sup> For instance, most transition metal complexes studied during the second half of the past century include an alkyl or aryl phosphine (e.g.  $PMe_3$ ,  $P^iPr_3$ ,  $PCy_3$ ,  $PPh_3$ , etc.). This fact is also reflected on the prominence of some metal-phosphine complexes, as the ones shown on Figure 1, with applications as varied as olefin hydrogenation (**I**),<sup>4</sup> olefin metathesis (**II**)<sup>5</sup> or cross-coupling (**III**),<sup>6</sup> among others. Their widespread use stems from their remarkable versatility, as their properties can be finely tuned by changing the nature and structure of the substituents on the phosphorus atom. Despite all of this, scant progress had been made on the synthesis of new monodentate phosphines until fairly recently.<sup>7</sup>

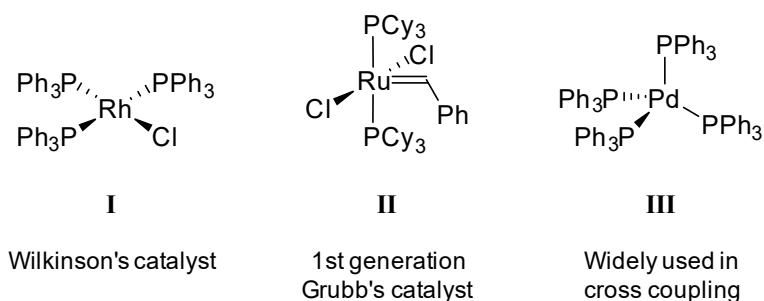


Figure 1. Notable examples of transition metal-phosphine complexes.



the first transition metal complex with a quintuple metal-metal bond (**VI**) discovered by Power and coworkers,<sup>19a</sup> and a terphenyl isocyanide ligand developed by Figueroa *et al.*<sup>20b</sup> (**VII**). Besides, many other researchers including ourselves<sup>19g-i</sup> have favourably exploited this strategy.<sup>19-21</sup>

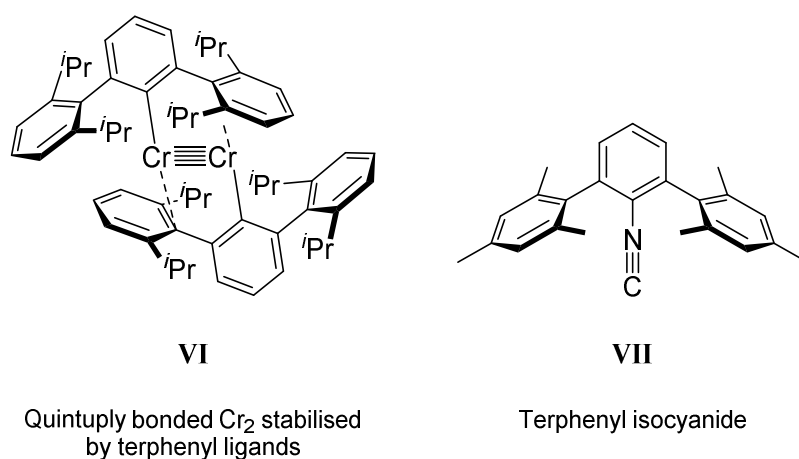


Figure 3. Representative examples of a terphenyl group as an aryl ligand (**VI**) and as part of a Lewis base (**VII**).

Considering the above and our own expertise in the use of terphenyl groups,<sup>19g-l</sup> we decided to develop a new family of terphenyl phosphines and explore their characteristics as ligands coordinated to different transition metals. Our previous reports focused on Rh, Ir, Pt and Au complexes of ligands  $\text{PMe}_2\text{Ar}''$  ( $\text{Ar}'' = \text{Ar}^{\text{Xyl}_2}, \text{Ar}^{\text{Mes}_2}, \text{Ar}^{\text{Dipp}_2}$  and  $\text{Ar}^{\text{Tripp}_2}$ ) and demonstrated their capacity to stabilise coordinatively unsaturated structures and to adopt different coordination modes. The latter situation arises when classical P-bonding becomes complemented with a relatively weak  $\text{M}\cdots\text{C}_{\text{arene}}$  interaction with a flanking ring of the terphenyl moiety (Figure 4).<sup>22</sup>

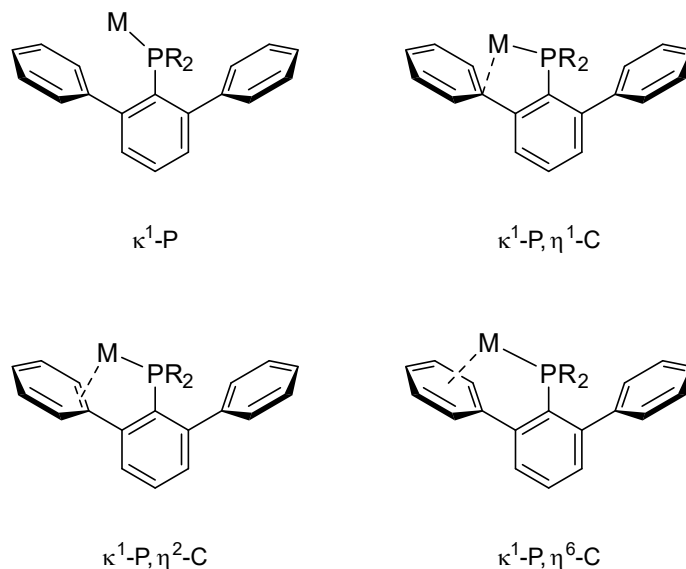


Figure 4. Different coordination modes found for terphenyl phosphines (substituents on the aryl rings omitted for clarity).

### I.1.2. Metal carbonyl complexes.

Carbon monoxide has been known since ancient Greece, although its composition was not unveiled until 1800.<sup>23</sup> Its notoriety in Chemistry emanates from its aptitude to bind to transition metal atoms, which was first disclosed in 1868, when Schützenberger prepared the complex  $\text{PtCl}_2(\text{CO})_2$ .<sup>24</sup> However, the most conspicuous example of a carbonyl complex of a transition metal atom is doubtless  $\text{Ni}(\text{CO})_4$  (**VIII** in Figure 5), first unexpectedly synthesised in 1890 by Mond via the reaction of finely divided metallic nickel with carbon monoxide.<sup>24a</sup> Its surprisingly high volatility (b.p. 43 °C) provided a practical way to purify nickel ores, known as the Mond process.<sup>24b</sup> This discovery sparked the preparation of many other binary metal carbonyls, both mononuclear, such as  $\text{Fe}(\text{CO})_5$  (**IX**) and  $\text{Mo}(\text{CO})_6$  (**X**), and polynuclear, e.g.  $\text{Co}_2(\text{CO})_8$  (**XI**).

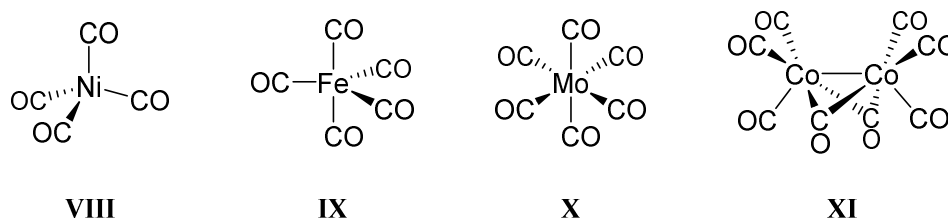


Figure 5. First examples of homoleptic metal carbonyl complexes.

Unlike in classical Werner-type complexes, where the ligand acts exclusively as  $\sigma$  donor, the bonding in metal carbonyls is comprised of a  $\sigma$  component and an even more important  $\pi$  backdonation (Figure 6):

- The former arises from the donation of the carbonyl ligand HOMO to an empty  $d(\sigma)$  orbital of the metal (**A**).
- As for the latter, the electron density is provided by a filled  $d(\pi)$  orbital of the metal atom and is transferred to the  $\pi^*$  orbitals of CO, thus debilitating the C–O bond (**B**).

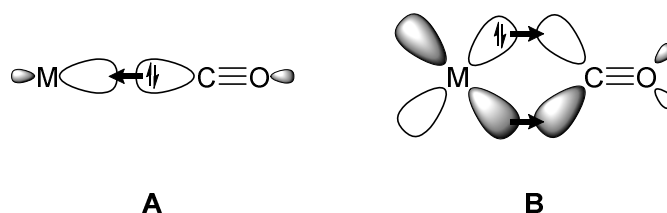
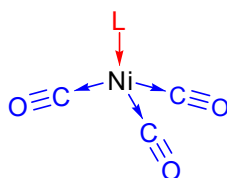


Figure 6. Schematic representation of the bonding in metal carbonyl complexes.

The influence of the  $M \Rightarrow CO$   $\pi$  backdonation on the C–O bond is evinced in the infrared vibrational spectra (IR and Raman) of the complexes, where the stretching vibration of said bond for terminal carbonyl ligands appears at a lower wavenumber (*ca.* 2120-1850  $\text{cm}^{-1}$ ) than that in free CO (2143  $\text{cm}^{-1}$ ) and somewhat closer to that observed for C=O groups in organic molecules (1820-1670  $\text{cm}^{-1}$ ).

### I.1.3. Determination of the electronic properties of ligands.

In account of the abovementioned effect of the  $M \Rightarrow CO$   $\pi$  backdonation on the C–O bond, the stretching frequencies of the carbonyl ligands in a given complex are greatly influenced by the electron density on the metal atom. In his pioneering work, Tolman generated a series of  $Ni(CO)_3(L)$  complexes of a wide range of tertiary phosphines and other three-coordinate P-donor species by reaction of  $Ni(CO)_4$  and L in  $CH_2Cl_2$  at room temperature. Tolman's method relies on the notion that the electron density provided by the ligand L to the metal centre can be passed on to the  $\pi^*$  orbitals of the coordinated CO ligands. Accordingly, the symmetric ( $A_1$ ) C–O stretching vibration,  $\nu_{CO}$ , reflects the donicity of ligand L (Figure 7), so that the lower the stretching frequency of CO, the stronger the  $\sigma$ -donor properties of the ligand L. Thus, Tolman measured and tabulated the corresponding  $\nu_{CO}$  of seventy monodentate phosphorus ligands and proposed a substituent additivity rule for accurately predicting the parameter later known as Tolman Electronic Parameter (TEP).<sup>25</sup>



Example of highly electron-donating L:  $P^tBu_3$  ( $\nu_{CO} = 2056\text{ cm}^{-1}$ )  
 Example of poorly electron-donating L:  $PCl_3$  ( $\nu_{CO} = 2097\text{ cm}^{-1}$ )

( $\rightarrow$ : L-to-Ni  $\sigma$  bonding,  $\rightarrow$ : Ni-to-CO  $\pi$  backbonding)

Figure 7. Schematic representation of the influence of the electron-donor capacity of ligand L in the C–O stretching frequencies of complexes  $Ni(CO)_3(L)$ .

Given the major influence of electronic effects on catalytic performance,<sup>11a,3b,26</sup> it is crucial to determine the overall electron-donor capacity of the ligands accompanying the metal centre throughout the catalytic cycle. In



this context, Tolman's work had a long-standing impact in organometallic chemistry and catalysis, as it constitutes the cornerstone of ligand parameterisation.

Considering the above, it is surprising that scant structural data can be found on  $\text{Ni}(\text{CO})_3(\text{L})$  complexes of commonly used, commercially available phosphines, such as  $\text{PPh}_3$ ,  $\text{PCy}_3$ ,  $\text{PMe}_3$  and others, with the notable exception of  $\text{Ni}(\text{CO})_3(\text{P}^t\text{Bu}_3)$ .<sup>27a</sup> On the other hand, some ferrocenyl phosphine<sup>27b</sup> and fluoroalkyl phosphine<sup>27c</sup>  $\text{Ni}(\text{CO})_3(\text{L})$  complexes (see **XII** and **XIII**, respectively, in Figure 8), among others, have been structurally characterised, as well as an admixture of composition  $(\text{CO})_n\text{Ni}(\text{P-P})\text{Ni}(\text{CO})_n$  ( $\text{P-P} = 1,4\text{-bis}(2\text{-diisopropylphosphino})\text{phenyl}(\text{benzene}))$ , where 80% of the nickel centres are bound to three carbonyl ligands and the remaining 20% bear two carbonyl ligands (**XIV** in Figure 8).<sup>27d</sup>

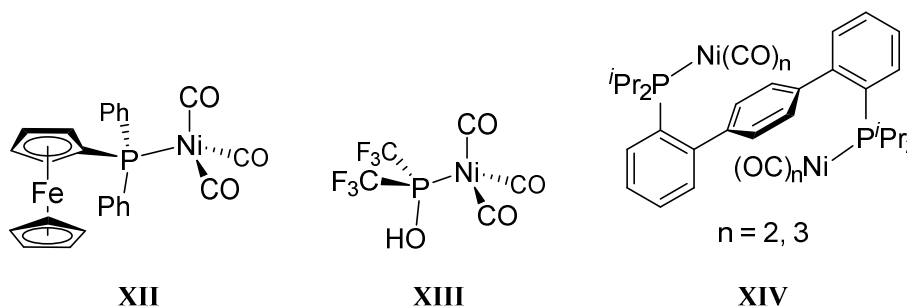


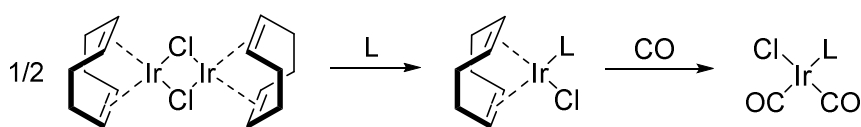
Figure 8. Examples of crystallographically characterised  $\text{Ni}(\text{CO})_n(\text{L})$  complexes with a ferrocenyl phosphine (**XII**), a fluoroalkyl phosphine (**XIII**) and a p-terphenyl bidentate phosphine (**XIV**).

The strategy developed by Tolman encounters, however, some disadvantages, not least the extreme toxicity and volatility of the  $\text{Ni}(\text{CO})_4$  starting material, as well as the apparent lack of reactivity towards certain bulky ligands, such as Buchwald's biaryl phosphines,<sup>28</sup> and the formation of three-coordinate  $\text{Ni}(\text{CO})_2(\text{L})$  complexes of sterically demanding NHC ligands.<sup>29</sup> To overcome these

## Chapter I

problems, several alternative approaches have been developed.

In the method developed by Crabtree,<sup>30a</sup> and later refined by Nolan,<sup>30b</sup>  $[\text{Ir}(\mu\text{-Cl})(\text{cod})]_2$  (cod = 1,5-cyclooctadiene) was reacted with a ligand L to form  $\text{IrCl}(\text{cod})(\text{L})$ , and later treated with excess carbon monoxide to yield complexes of formula  $\text{IrCl}(\text{CO})_2(\text{L})$  (Scheme 1). The infrared frequencies arising from the carbonyl ligands of these complexes, along with those already reported in the literature,<sup>31</sup> were then compared with those for analogous  $\text{Ni}(\text{CO})_3(\text{L})$  complexes. A linear regression was obtained that can be used to predict the TEP using the  $\text{Ir}(\text{I})$  derivatives. This method avoids the handling of dangerous  $\text{Ni}(\text{CO})_4$ . Moreover, due to the reduced steric bulkiness of a square-planar metal centre, it allows for the measurement of the TEP of bulky phosphine<sup>28</sup> and NHC ligands.<sup>30b</sup> Similar approaches include the use of square-planar  $\text{Rh}(\text{I})$  carbonyl complexes.<sup>32</sup>



Scheme 1. Schematic synthesis of complexes  $\text{IrCl}(\text{CO})_2(\text{L})$ .

Recently, other parameters have been proposed for the description of the electronic properties of ligands. One such parameter, developed by Huynh *et al.*,<sup>33</sup> involves the measurement of the  $^{13}\text{C}$  NMR spectrum of a metallic complex containing the NHC 1,3-diisopropylbenzimidazolin-2-ylidene ( $i\text{Pr}_2\text{-bimy}$ ) reporter ligand. Since backdonation from a Lewis-acidic  $\text{Pd}(\text{II})$  centre is insignificant, the chemical shift of the carbenic  $^{13}\text{C}$  in a *trans*- $\text{PdBr}_2(i\text{Pr}_2\text{-bimy})(\text{L})$  complex (**XV** in Figure 9) will reflect primarily the  $\sigma$ -donor capacity of ligand L. This approach can be applied to a much broader scope of ligands, and purportedly removes the  $\pi$ -backdonation component in the M–L bonding. Furthermore, similar systems can be used for the determination of the electronic parameter of bulkier and of

bidentate ligands, as shown in the structures of  $[\text{Au}(\text{}^i\text{Pr}_2\text{-bimy})(\text{L})]\text{BF}_4$  (**XVI**) and  $[\text{PdBr}(\text{}^i\text{Pr}_2\text{-bimy})(\text{L}_2)]\text{PF}_6$  (**XVII**), respectively.

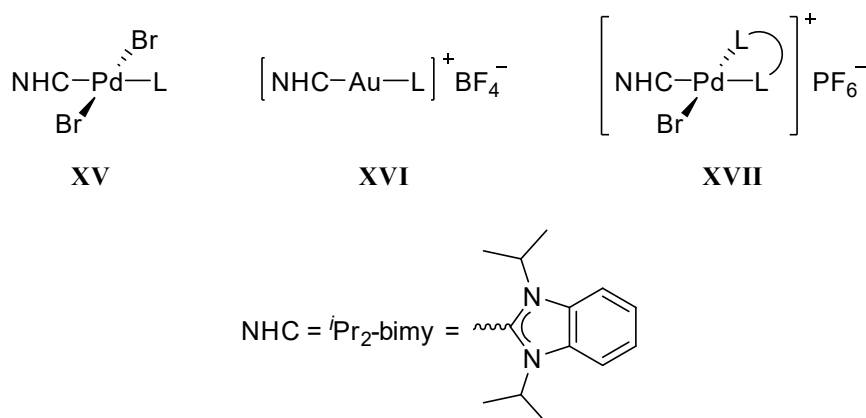


Figure 9. Systems developed by Huynh et al. for the determination of the electronic properties of ligands.

#### I.1.4. Aims.

Considering all of the above, the research presented in this chapter pursues the following objectives:

- The synthesis of new dialkyl terphenyl phosphines,  $\text{PR}_2\text{Ar}''$ , where the terphenyl moiety contains two 3,5-di-tert-butylphenyl substituents at the 2,6 positions of the central aryl ring (in short  $\text{Ar}^{\text{Dtbp}_2}$ ), with various alkyl substituents, namely  $R = \text{Me}, \text{Et}, \text{}^i\text{Pr}, \text{Cyp}$  and  $\text{Cy}$ .
- The synthesis of new derivatives of the already described  $\text{PR}_2\text{Ar}^{\text{Xyl}_2}$  ( $R = \text{Me}, \text{Et}, \text{C}_3\text{H}_5$  and  $\text{C}_4\text{H}_7$ ) with bulkier secondary alkyl groups ( $R = \text{}^i\text{Pr}, \text{Cyp}$  and  $\text{Cy}$ ).
- The assessment of the electronic properties of the new phosphines, as well as of the already reported  $\text{PMe}_2\text{Ar}''$  ( $\text{Ar}'' = \text{Ar}^{\text{Xyl}_2}, \text{Ar}^{\text{Mes}_2}, \text{Ar}^{\text{Dipp}_2}$  and  $\text{Ar}^{\text{Tripp}_2}$ ), by the measurement of the C–O stretching frequencies in  $\text{Ni}(\text{CO})_3(\text{PR}_2\text{Ar}'')$  and  $\text{IrCl}(\text{CO})_2(\text{PR}_2\text{Ar}'')$  complexes.



## I.2. RESULTS AND DISCUSSION

### I.2.1. Synthesis and properties of new dialkyl terphenyl phosphines.

The first section of this chapter focuses on the synthesis of the new dialkyl terphenyl phosphines recently developed in our research group. Characteristic NMR spectroscopic properties and their reactivity towards air are also discussed. In turn, their reactivity towards a source of Ni(CO)<sub>4</sub> and their electronic properties are studied in the next sections, along with those of previously described terphenyl phosphines. Thus, the structures of all the phosphines used in this study are shown in Figure 10.

The syntheses of ligands **L2-L5** were performed according to procedures previously described in the literature, by Protasiewicz (for **L4**<sup>16a</sup>) and by our group (for **L2**<sup>22a</sup>, **L3**<sup>22e</sup> and **L5**<sup>22d</sup>), and thus will not be discussed further. Phosphines **L1** and **L6**, bearing linear methyl and ethyl groups on the phosphorus atom, respectively, were prepared from the corresponding dihalophosphine (PX<sub>2</sub>Ar'', X = Cl, Br) following the method described by our group<sup>22d</sup> for similar phosphines (Scheme 2A). However, application of the same approach to branched or cyclic alkyl groups led to either no reaction or intractable mixtures of unidentified products. Emulating the synthesis of biaryl phosphines,<sup>34</sup> an overstoichiometric amount of copper chloride was added prior to the treatment with the corresponding alkylmagnesium bromide (in a PX<sub>2</sub>Ar'':CuI:RMgBr ratio of *ca.* 1:1.5:4), leading to the isolation of the sought phosphines in moderate yields (Scheme 2B).

Chapter I

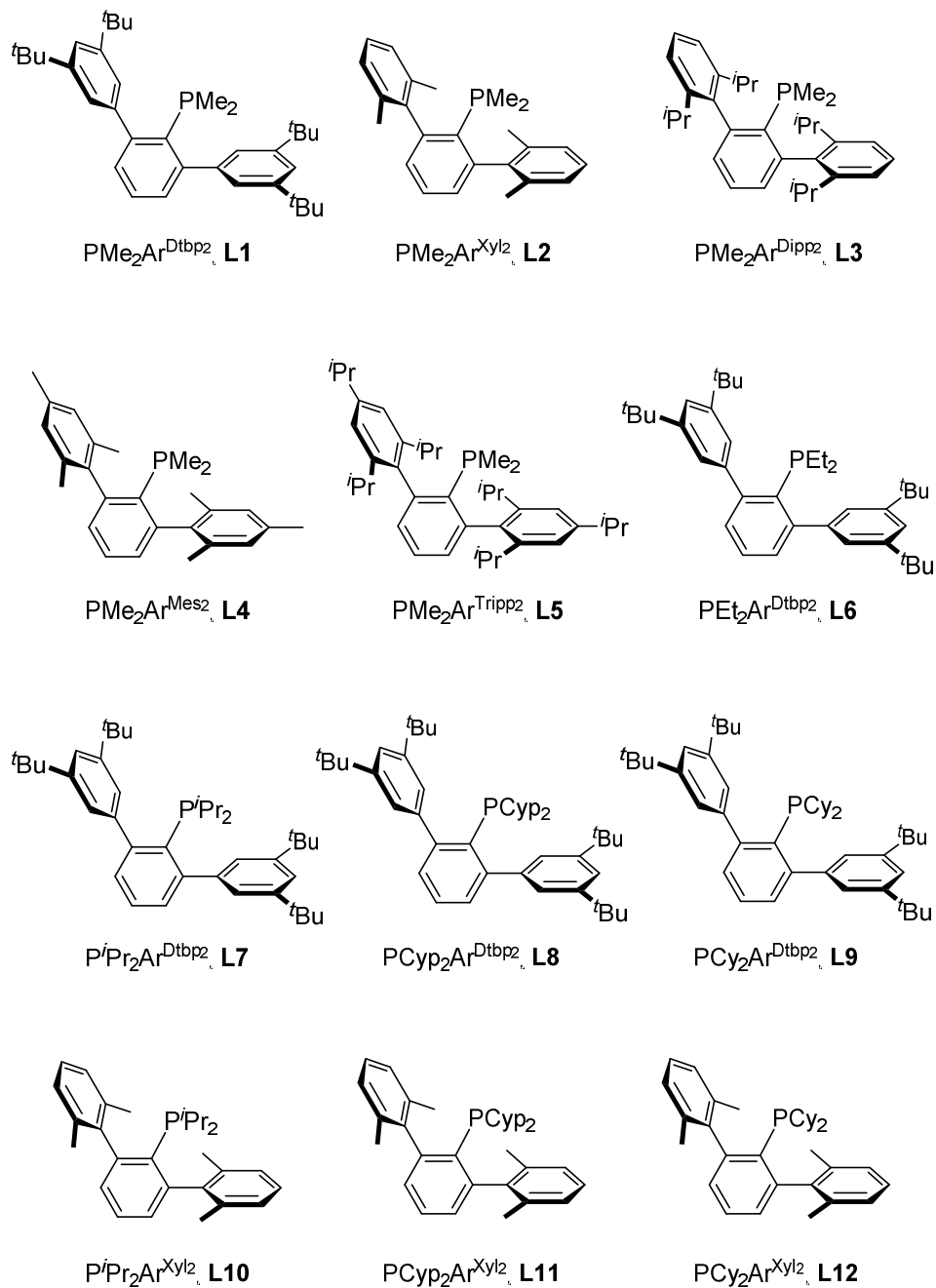
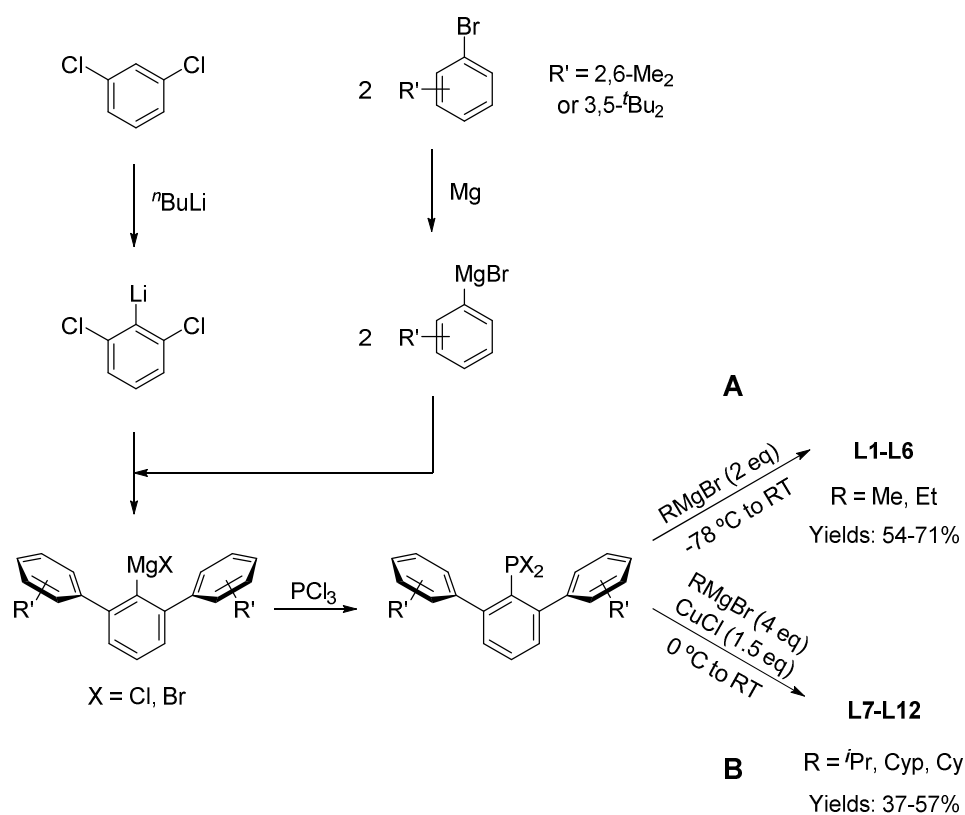


Figure 10. Structures of the dialkyl terphenyl phosphines used in this chapter.



Scheme 2. Syntheses of phosphines **L1-L6** (A) and **L7-L12** (B).

All phosphines were obtained as pure white solids, soluble in common organic solvents, and quite air-stable, particularly in the solid state (*vide infra*). If necessary, they could be crystallised from EtOH/Et<sub>2</sub>O or MeOH/Et<sub>2</sub>O mixtures at  $-30^\circ\text{C}$ .  $^1\text{H}$  and  $^{13}\text{C}\{^1\text{H}\}$  NMR spectra are generally simple and suggest a high degree of apparent symmetry, originated by the rotation around the P–C<sub>ipso</sub> bond. In the example shown in Figure 11, corresponding to the  $^1\text{H}$  NMR spectrum of **L1** in C<sub>6</sub>D<sub>6</sub> (as aromatic signals are better differentiated in this solvent rather than CDCl<sub>3</sub>), this can be noticed in the existence of only one signal for the <sup>t</sup>Bu groups and one set of signals for the side aryl rings of the terphenyl fragment. Coupling with the  $^{31}\text{P}$  nucleus can be observed in the  $^1\text{H}$  and  $^{13}\text{C}$  resonances due to the P–Me groups, as well as in those arising from the aromatic carbons in close vicinity (Figure 12).

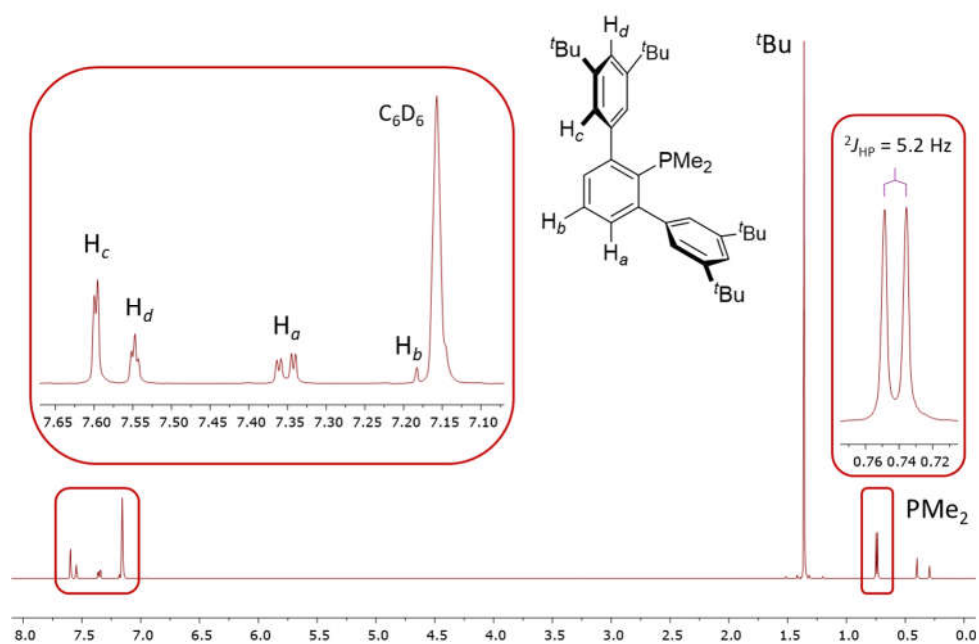


Figure 11.  $^1\text{H}$  NMR spectrum of **L1** in  $\text{C}_6\text{D}_6$  at  $25^\circ\text{C}$ .

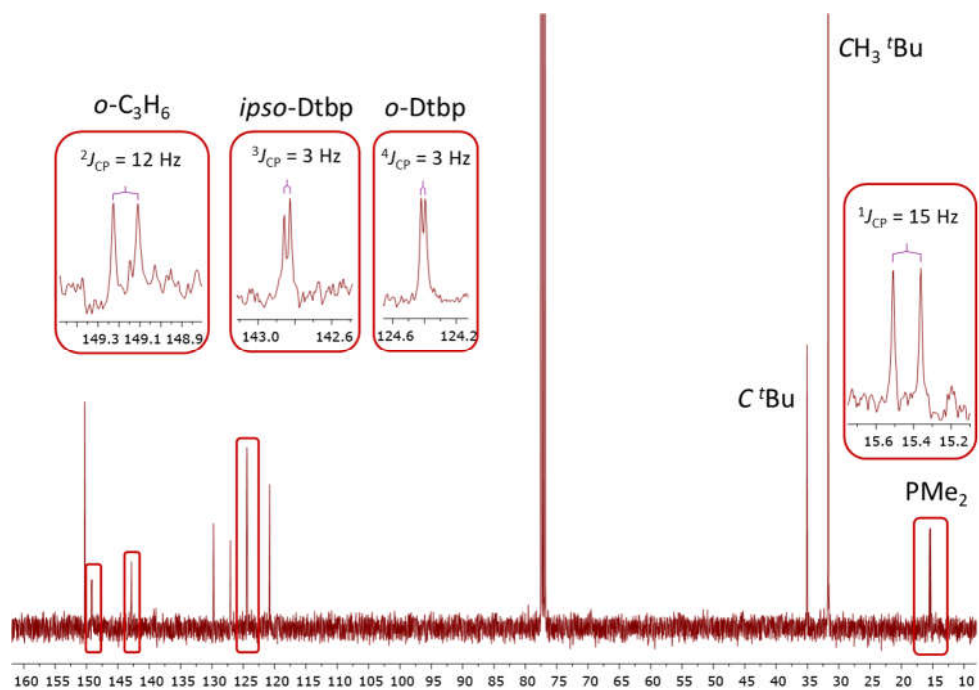


Figure 12.  $^{13}\text{C}\{^1\text{H}\}$  NMR spectrum of **L1** in  $\text{CDCl}_3$  at  $25^\circ\text{C}$ .



$^{31}\text{P}\{^1\text{H}\}$  NMR chemical shifts vary considerably depending mainly on the nature of the alkyl substituents on the phosphorus atom,<sup>9,35</sup> and span a range of over 50 ppm (Table 1). As will be discussed in following sections, the  $^{31}\text{P}\{^1\text{H}\}$  NMR chemical shifts can be indicative of the coordination mode adopted by the phosphine.

	Phosphine	$\delta$ (ppm)
<b>L1</b>	$\text{PMe}_2\text{Ar}^{\text{Dtbp}_2}$	-36.6
<b>L2</b>	$\text{PMe}_2\text{Ar}^{\text{Xyl}_2}$	-40.4
<b>L3</b>	$\text{PMe}_2\text{Ar}^{\text{Dipp}_2}$	-41.3
<b>L4</b>	$\text{PMe}_2\text{Ar}^{\text{Mes}_2}$	-36.9
<b>L5</b>	$\text{PMe}_2\text{Ar}^{\text{Tripp}_2}$	-40.7
<b>L6</b>	$\text{PEt}_2\text{Ar}^{\text{Dtbp}_2}$	-12.8
<b>L7</b>	$\text{P}^i\text{Pr}_2\text{Ar}^{\text{Dtbp}_2}$	12.6
<b>L8</b>	$\text{PCyp}_2\text{Ar}^{\text{Dtbp}_2}$	0.9
<b>L9</b>	$\text{PCy}_2\text{Ar}^{\text{Dtbp}_2}$	1.6
<b>L10</b>	$\text{P}^i\text{Pr}_2\text{Ar}^{\text{Xyl}_2}$	16.2
<b>L11</b>	$\text{PCyp}_2\text{Ar}^{\text{Xyl}_2}$	4.6
<b>L12</b>	$\text{PCy}_2\text{Ar}^{\text{Xyl}_2}$	10.1

Table 1.  $^{31}\text{P}\{^1\text{H}\}$  NMR chemical shifts of phosphines **L1-L12**.

Among the by-products generated in the synthesis of bulky  $\text{PR}_2\text{Ar}''$  ( $\text{R} = {}^i\text{Pr}, \text{Cyp}, \text{Cy}$ ), it is worth mentioning the formation of secondary phosphines  $\text{PH}(\text{R})\text{Ar}''$ . For instance,  $\text{PH}({}^i\text{Pr})\text{Ar}^{\text{Xyl}_2}$  was isolated from the preparation of **L10** and characterised by  $^{31}\text{P}\{^1\text{H}\}$  and  $^1\text{H}$  NMR. This phosphine features a distinctive  $\text{PH}$  signal at 3.15 ppm that presents a coupling constant to the phosphorus nucleus of  $^1J_{\text{HP}} = 221.9$  Hz.

In order to assess their stability towards oxidation in a more precise manner, a study was carried out where phosphines **L1**, **L8** and **L11** were exposed

## Chapter I

to air, both as ground solids and in a toluene solution. The relative quantity of  $P(O)R_2Ar''$  present was determined by means of  $^{31}P\{^1H\}$  NMR in non-deuterated toluene. Even in the case of dimethyl-substituted **L1**, no  $P(O)R_2Ar''$  is detected after up to 20 days exposure in the solid state, and less than 5% oxidation is observed until after 30 days. As expected, oxidation is faster in solution, although only 6% of the most air-stable **L8** ( $PCyp_2Ar^{Dtbp_2}$ ) is converted into the oxide after more than 15 days (Figure 13). This is in line with the findings by Buchwald's group on the oxidation of dicyclohexyl biaryl phosphines in air.<sup>36</sup>

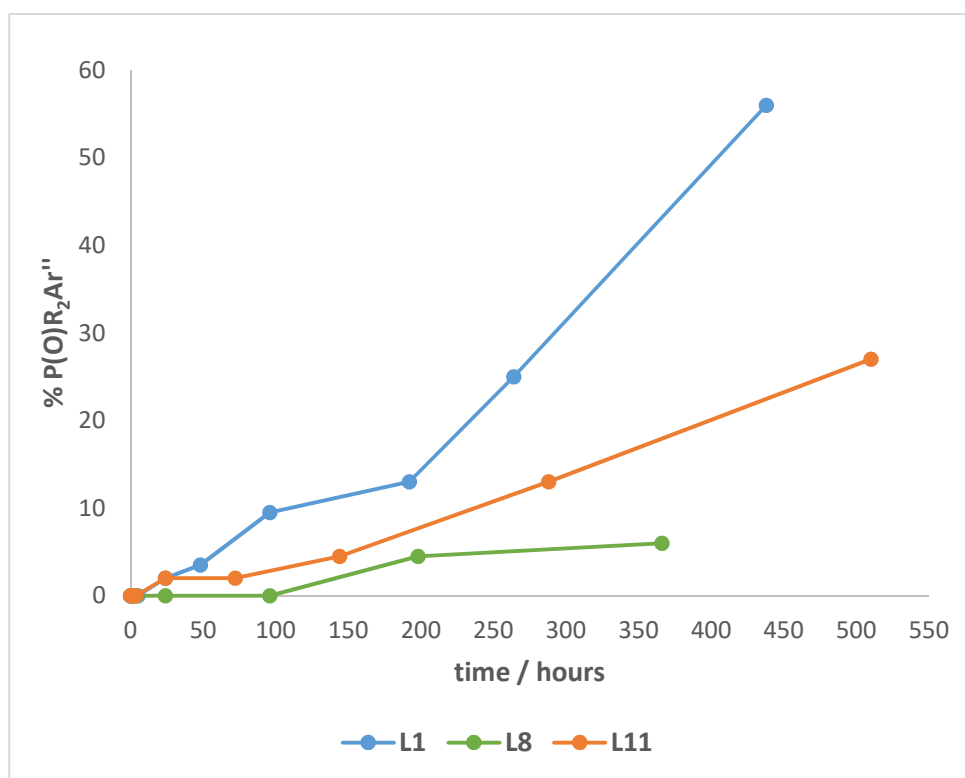


Figure 13. Oxidation of ligands **L1**, **L8** and **L11** over time in toluene solution.

### I.2.2. Solid state structure of the $PR_2Ar''$ phosphines.

Single crystals suitable for X-ray studies were grown for a few selected phosphines. By way of examples, only the structures of **L1**, **L2**<sup>37</sup> and **L7**<sup>37</sup> will be discussed here and mentions of the others,<sup>38</sup> as well as those previously reported,<sup>17a,22d</sup> will be made when appropriate.

Consideration of all the crystal structures existent for dialkyl terphenyl phosphines permits three different possible conformations to be distinguished, labelled as **A**, **B** and **C** in Figure 14, which formally interconvert by rotation of the  $P-C_{ipso}$  bond. The conformation adopted by a particular phosphine in the solid state is determined by, on the one hand, steric repulsions between the alkyl substituents on the phosphorus atom and on the flanking aryl rings and, on the other hand, electron-electron repulsion between the lone pair and the  $\pi$  systems of the side rings.

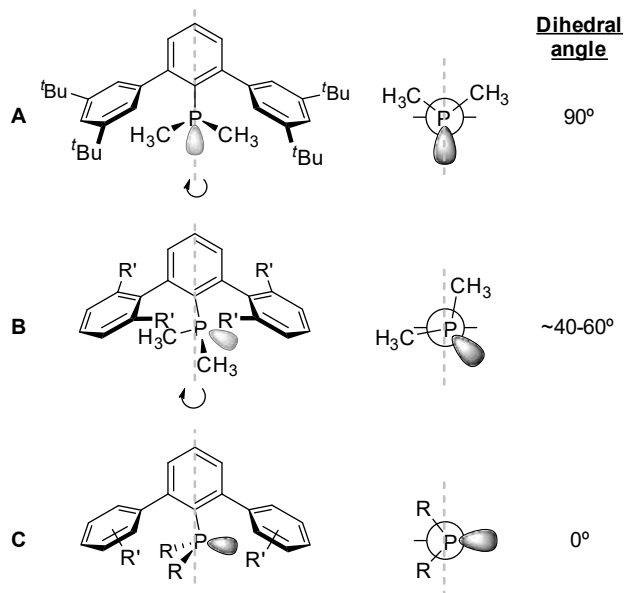


Figure 14. Different conformations adopted by dialkyl terphenyl phosphines in the solid state.

In conformation **A**, the alkyl substituents on the phosphorus atom are symmetrically distributed with respect to a plane perpendicular to the central aryl ring, while the lone pair, which is contained in the mentioned plane, is pointing towards a void region of space. Structure **A** is the preferred geometry for the least sterically demanding  $\text{PR}_2\text{Ar}'$  phosphines, namely  $\text{PMe}_2\text{Ar}^{\text{Dtbp}_2}$  (**L1**) and  $\text{PMe}_2\text{Ar}^{\text{Ph}_2}$ ,<sup>38</sup> as well as for  $\text{PH}_2\text{Ar}^{\text{Mes}_2}$  and  $\text{PMe}_2\text{Ar}^{\text{Xyl}'_2}$  ( $\text{Xyl}' = 3,5\text{-C}_6\text{H}_3\text{Me}_2$ ), reported by Wehmschulte and coworkers.<sup>17a</sup> Figure 15 shows two views of the molecular structure of **L1**, emphasizing the regular distribution of the  $\text{PMe}_2$  fragment. It

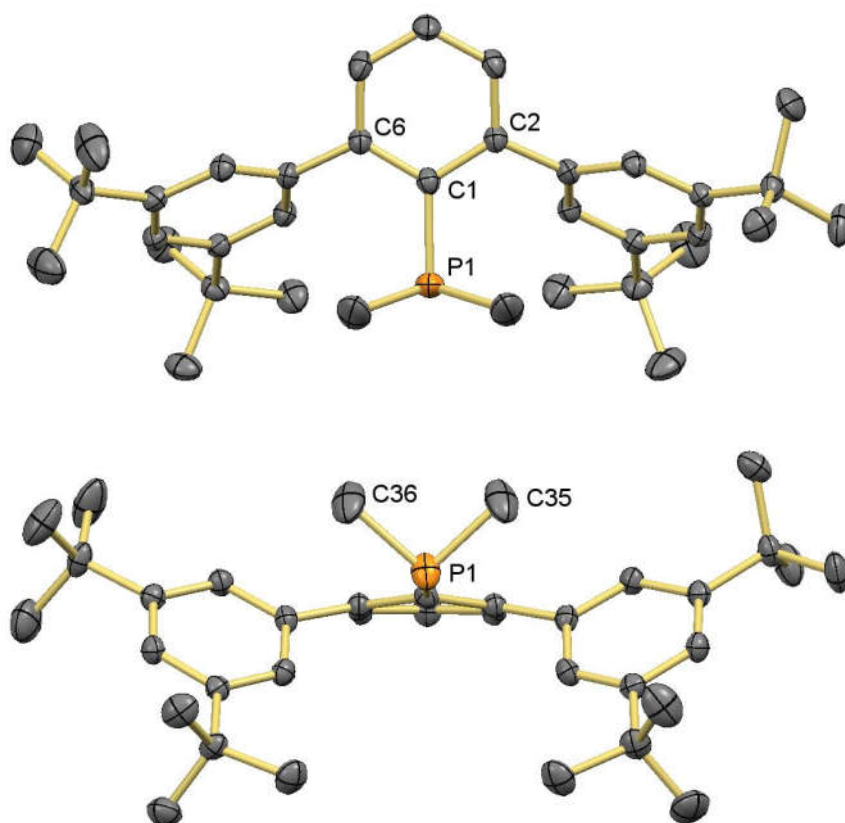


Figure 15. Two ORTEP views of phosphine **L1**. Hydrogen atoms are omitted for clarity and thermal ellipsoids are set at 50% level probability. Selected bond distances (Å) and angles (°): P1-C1 1.864(3), P1-C35 1.848(3), P1-C36 1.851(3), C35-P1-C36 95.2(2), C1-P1-C35 101.4(1), C1-P1-C36 101.9(1), P1-C1-C2 121.3(2), P1-C1-C6 121.4(2).

should be noted that, due to the absence of substituents in the *ortho* positions of the lateral rings, these are rotated around the  $C_{ortho}-C_{ipso'}$  bond from the almost perpendicular arrangement in relation to the central aryl ring present in the X-ray structures of other phosphines. As a result, an angle of  $48^\circ$  is measured between the planes containing the side rings and the plane of the central ring, considerably smaller than the average of *ca.*  $85^\circ$  observed in  $PMe_2Ar^{Xyl_2}$ . Another significant feature is the deviation of the *ipso* carbons of the flanking aryl rings from the plane of the central ring by *ca.*  $0.32-0.33 \text{ \AA}$ , causing two methyl groups of the <sup>t</sup>Bu substituents in opposite rings to approach to a distance of about  $4.77 \text{ \AA}$ , only *ca.* 20% longer than twice the van der Waals radius of a methyl group ( $2.0 \text{ \AA}$ ).<sup>39</sup> However, this distortion cannot be attributed to London dispersion forces, as  $PMe_2Ar^{Ph_2}$ , lacking substituents on the side rings, exhibits a similar deformation.

$PMe_2Ar^{Xyl_2}$  (**L2**) displays a solid-state structure of type **B** (Figure 16), where one of the methyl groups on the phosphorus atom is nearly coplanar with the central aryl ring, displaying a  $C(Me)-P-C_{ipso}-C_{ortho}$  torsion angle of  $19.2^\circ$ . Additionally, due to steric repulsion between said methyl group and the neighbouring side aryl ring, the pertinent  $P-C_{ipso}-C_{ortho}$  angle increases to  $127.6(2)^\circ$ , at the expense of the other ( $114.2(2)^\circ$ ). A conformation of type **B** is also found in the molecular structures of  $PMe_2Ar^{Dipp_2}$  (**L3**)<sup>38</sup> and of previously reported<sup>17a,22d</sup>  $PMe_2Ar^{Mes_2}$ ,  $P(C\equiv CH)_2Ar^{Mes_2}$  and  $P(CH_2CH=CH_2)_2Ar^{Dipp_2}$ . Presumably, the enlarged steric impediments brought in by the substituents in the *ortho* positions of the side aryl rings, combined with the opening of one of the  $P-C_{ipso}-C_{ortho}$  angle, would make conformation **B** somewhat more favourable than **A** for these phosphines.

Finally, due to steric hindrance among the bulky R groups and the flanking aryl rings, molecules of  $P^iPr_2Ar^{Dtbbp_2}$  (**L7**) and other isopropyl-, cyclopentyl- and cyclohexyl-substituted terphenyl phosphines (namely **L8**, **L10**, **L11** and **L12**)<sup>38</sup> place their two R groups in opposite regions of space relative to the plane of the terphenyl central aryl ring, in the conformation labelled **C**. Similarly to

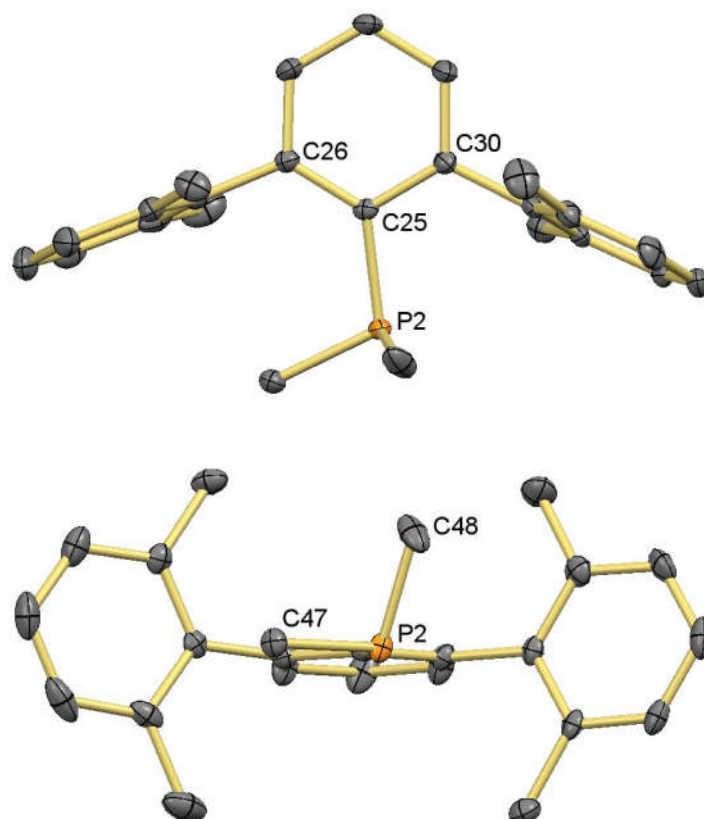


Figure 16. Two ORTEP views of phosphine **L2**. Hydrogen atoms are omitted for clarity and thermal ellipsoids are set at 50% level probability. Selected bond distances (Å) and angles (°): P2-C25 1.847(2), P2-C47 1.833(3), P2-C48 1.832(3), C47-P2-C48 97.7(1), C25-P2-C47 109.7(1), C25-P2-C48 102.6(1), P2-C25-C26 127.6(2), P2-C25-C30 114.2(2).

conformation **B**, this results in two different P- $C_{ipso}$ - $C_{ortho}$  angles, the wider at 127.2(2)° and the smaller at 114.8(1)° in the case of **L7** (Figure 17). Interestingly, along with the phosphines mentioned, all the sterically demanding dialkyl biaryl phosphines analysed by the group of Buchwald,<sup>36</sup> or by others,<sup>40</sup> feature also a structure of type **C**. Furthermore, the preference of these phosphines for conformation **C** could be the reason behind their relatively low reactivity towards molecular oxygen, as already noted by Buchwald *et al.* for dicyclohexyl biaryl phosphines.<sup>36</sup>

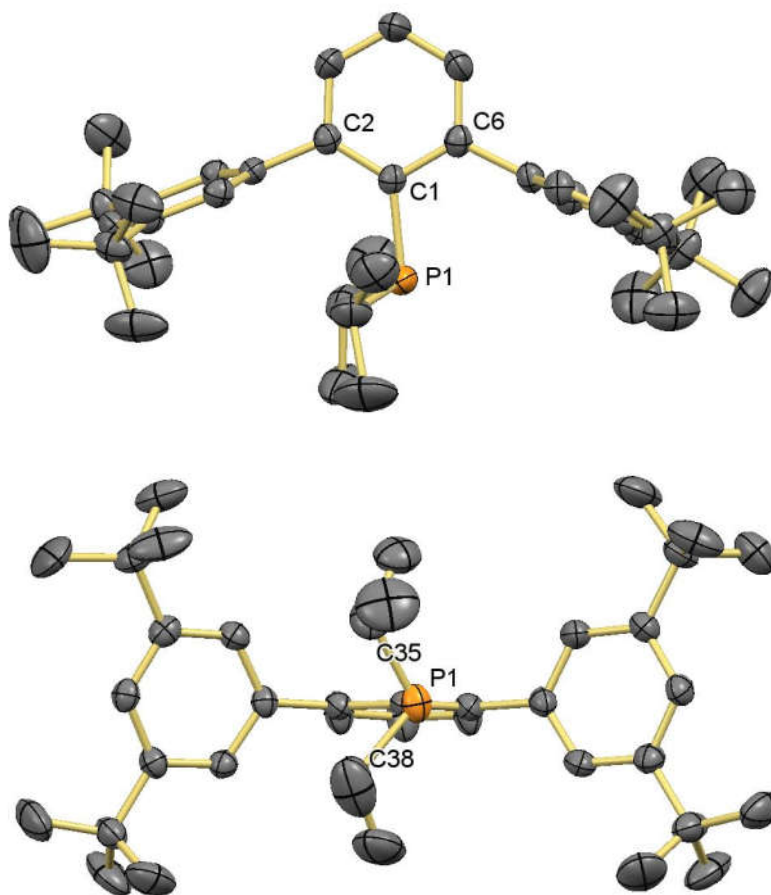


Figure 17. Two ORTEP views of phosphine **L7**. Hydrogen atoms are omitted for clarity and thermal ellipsoids are set at 50% level probability. Selected bond distances (Å) and angles (°): P1-C1 1.872(2), P1-C35 1.860(3), P1-C36 1.863(3), C35-P1-C38 105.1(1), C1-P1-C35 104.3(1), C1-P1-C38 101.3(1), P1-C1-C6 127.2(2), P1-C1-C2 114.8(2).

In order to gain insight into the solution behaviour of terphenyl phosphines, variable temperature NMR experiments and complementary computational studies were carried out<sup>38,41</sup> on  $\text{PMe}_2\text{Ar}^{\text{Dtbp}_2}$  (**L1**, structure **A**) and  $\text{P}^i\text{Pr}_2\text{Ar}^{\text{Dtbp}_2}$  (**L7**, structure **C**). Computational calculations revealed that rotation around the P-C<sub>ipso</sub> bond is a very facile process (*ca.* 3-3.5 kcal·mol<sup>-1</sup>) in the case of **L1**, whereas ring exchange in **L7** needs surmounting an energy barrier of *ca.* 14 kcal·mol<sup>-1</sup>. This is in accordance with solution NMR data down to -80 °C, where

## Chapter I

both flanking rings in **L1** remain equivalent. In contrast, the  $^1\text{H}$  NMR spectrum of **L7** at that temperature reveals inequivalence of the two rings. An energy barrier of  $\Delta G^\ddagger \approx 11.7 \text{ kcal}\cdot\text{mol}^{-1}$  can be estimated using the value of the rate constant determined at the coalescence temperature of  $-50 \text{ }^\circ\text{C}$ .

In view of all the aforementioned, some conclusions can be drawn regarding the coordination capabilities of the different terphenyl phosphines. Since all conformations **A**, **B** and **C** are readily accessible for dimethyl-substituted phosphines, both classical  $\kappa^1\text{-P}$  and bidentate  $\kappa^1\text{-P}, \eta^n\text{-C}_{\text{arene}}$  coordination modes can be foreseen, contingent on metal needs. Contrary to this situation, structure **C** is substantially favoured for bulky phosphines, where the electron density of the phosphorus lone pair faces the nearby aryl ring, thus facilitating the formation of complementary  $\text{M}\cdots\text{C}_{\text{arene}}$  bonds, i.e.  $\kappa^1\text{-P}, \eta^n\text{-C}_{\text{arene}}$  coordination. As discussed later, these considerations are in excellent agreement with the reactivity found for terphenyl phosphines towards  $\text{Ni}(\text{CO})_4$ .

### **1.2.3. Synthesis and characterisation of $\text{Ni}(\text{CO})_3(\text{PR}_2\text{Ar}'')$ complexes of the dialkyl terphenyl phosphines (R = Me, Et) and measurement of the Tolman electronic parameter.**

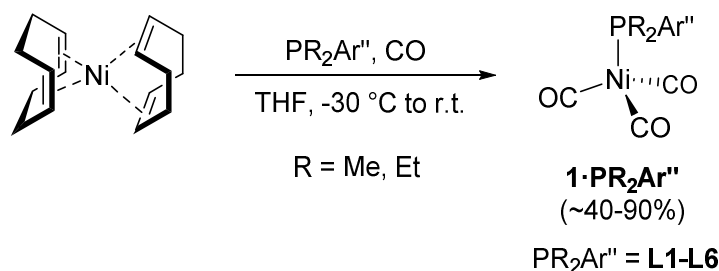
Once the whole series of phosphines represented in Figure 10 were prepared, it was considered of interest to ascertain their electronic properties when bound to a metal centre. Following Tolman's approach,<sup>25</sup> we studied their coordination chemistry towards  $\text{Ni}(\text{CO})_4$  in a 1:1 ratio and analysed the IR spectra of the resulting compounds.

For this purpose,  $\text{Ni}(\text{CO})_4$  was generated by the treatment of  $\text{Ni}(\text{cod})_2$  with 1 atm of CO in THF as solvent. Similar results were obtained whether this process was carried out prior to reaction with  $\text{PR}_2\text{Ar}''$  or in the presence of the phosphine.



For convenience in handling, the latter approach was then optimised and employed for all cases.

Thus, methyl- and ethyl-substituted phosphines **L1-L6** produced the expected  $\text{Ni}(\text{CO})_3(\text{PR}_2\text{Ar}'')$  complexes (**1-L1** through **1-L6**) by substitution of a carbonyl ligand from  $\text{Ni}(\text{CO})_4$  in differing reaction times that spanned the range from 3 hours (for  $\text{PEt}_2\text{Ar}^{\text{Dtbp}_2}$ ) to 3-4 days (for  $\text{PMe}_2\text{Ar}^{\text{Dipp}_2}$ ), presumably due to steric reasons (Scheme 3). It was later found that removing the CO atmosphere following the complete conversion of  $\text{Ni}(\text{cod})_2$  into  $\text{Ni}(\text{CO})_4$  (which was accompanied by the loss of the yellow colour caused by the former) accelerated the reaction, but this method was not further optimised.



Scheme 3. Synthesis of complexes  $\text{Ni}(\text{CO})_3(\text{PR}_2\text{Ar}'')$ , **1-L1** through **1-L6**.

Out of the six  $\text{Ni}(\text{CO})_3(\text{PR}_2\text{Ar}'')$  complexes generated, only **1-L1-1-L3** and **1-L6** were isolated as white solids by removing the volatiles from the reaction mixtures and washing with cold MeOH. It is worth mentioning that, in the reaction with **L6** to produce **1-L6**, it was necessary to maintain the temperature of the vessel at  $-30\text{ }^\circ\text{C}$  while operating under vacuum. This was done in order to minimise the generation of the yellow-coloured by-product later identified as the dicarbonyl adduct (*vide infra*). In this case, analytically pure samples could be obtained by crystallisation from pentane at  $-30\text{ }^\circ\text{C}$  in a considerably lower yield. Complexes **1-L4** and **1-L5** were analysed by IR spectroscopy immediately after

## Chapter I

generation as it was not considered of interest to isolate and further characterise them.

In the  $^1\text{H}$  and  $^{13}\text{C}\{^1\text{H}\}$  NMR spectra of all isolated complexes, the substituents on the side aryl rings give rise to only one set of signals (see Figure 18 for the  $^1\text{H}$  NMR spectrum of **1·L2**), due to a symmetrical environment around the terphenyl moiety and a facile rotation of the P- $C_{ipso}$  bond. Moreover, only one resonance for the carbonyl ligands is observed around 197-198 ppm in the  $^{13}\text{C}\{^1\text{H}\}$  NMR. These chemical shifts are in line with those reported for other  $\text{Ni}(\text{CO})_3(\text{L})$  complexes in the literature.<sup>29b,42</sup> Lastly, the  $^{31}\text{P}\{^1\text{H}\}$  NMR shifts for these complexes fall around 30-41 ppm to higher frequency compared to the free phosphines (Table 2). This is consistent with the difference in  $^{31}\text{P}$  NMR chemical shift of  $\Delta\delta \approx 30\text{-}40$  ppm found for a  $\kappa^1\text{-P}$  coordination mode of this kind of ligands in other complexes throughout this thesis as well as in the literature.<sup>16,22</sup>

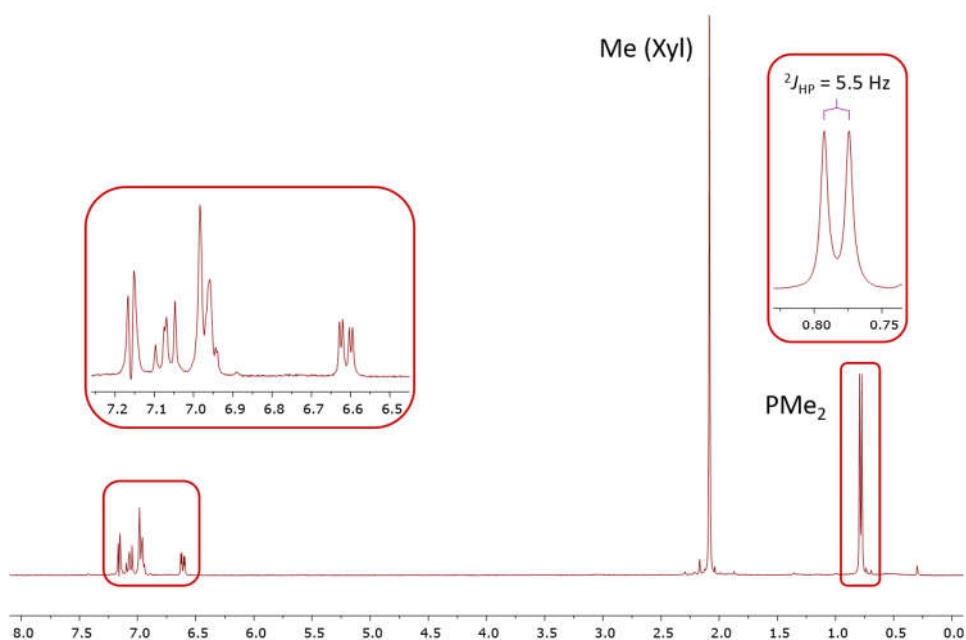


Figure 18.  $^1\text{H}$  NMR spectrum of complex **1·L2** in  $\text{C}_6\text{D}_6$  at 25 °C.

Ligand	Complex	$\delta$ (ppm)	$\Delta\delta$ (ppm)
<b>L1</b>	Ni(CO) <sub>3</sub> (PMe <sub>2</sub> Ar <sup>Dtbp<sub>2</sub></sup> )	4.7	41.3
<b>L2</b>	Ni(CO) <sub>3</sub> (PMe <sub>2</sub> Ar <sup>Xyl<sub>2</sub></sup> )	-7.7	32.7
<b>L3</b>	Ni(CO) <sub>3</sub> (PMe <sub>2</sub> Ar <sup>Dipp<sub>2</sub></sup> )	-4.3	37.0
<b>L4</b>	Ni(CO) <sub>3</sub> (PMe <sub>2</sub> Ar <sup>Mes<sub>2</sub></sup> )	-7 <sup>a</sup>	30
<b>L5</b>	Ni(CO) <sub>3</sub> (PMe <sub>2</sub> Ar <sup>Tripp<sub>2</sub></sup> )	-5 <sup>a</sup>	36
<b>L6</b>	Ni(CO) <sub>3</sub> (PEt <sub>2</sub> Ar <sup>Dtbp<sub>2</sub></sup> )	22.9	35.8

Table 2. <sup>31</sup>P{<sup>1</sup>H} NMR chemical shifts ( $\delta$ ) of complexes **1**·**PR<sub>2</sub>Ar''** and difference with the corresponding free phosphines ( $\Delta\delta$ ). <sup>a</sup>Recorded in non-deuterated THF.

The structure of some of these complexes were confirmed by single crystal X-ray diffraction studies (Figures 19-21). All of them present the expected slightly distorted tetrahedral geometry around the nickel centre and, in all cases, the coordinated phosphine adopts a conformation of type **A**. As free, non-coordinated molecules, only **L1** presents this conformation, while **L2** and **L3** prefer

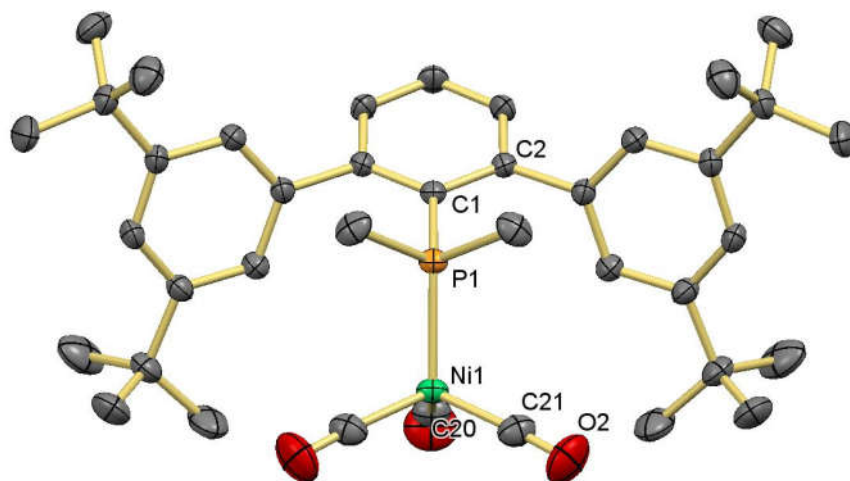


Figure 19. ORTEP view of complex **1**·**L1**. Hydrogen atoms are omitted for clarity and thermal ellipsoids are set at 50% level probability. Selected bond distances (Å) and angles (°): Ni1-P1 2.2401(7), Ni1-C21 1.797(3), Ni1-C20 1.782(3), C21-O2 1.135(4), P1-Ni1-C21 107.51(8), C20-Ni1-C21 112.46(9), Ni1-P1-C1-C2 -91.24(19).

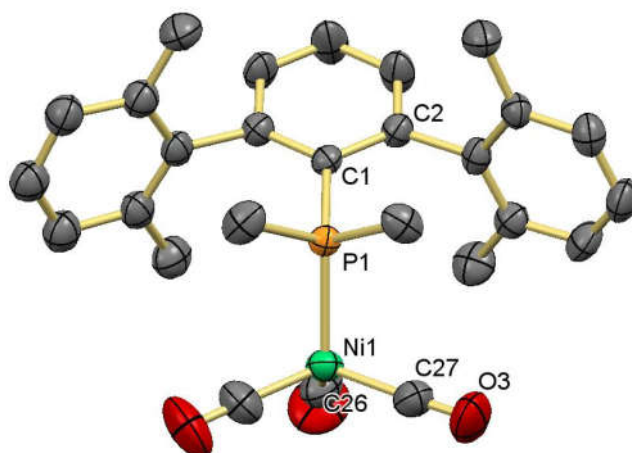


Figure 20. ORTEP view of complex **1·L2**. Hydrogen atoms and minor disorder are omitted for clarity and thermal ellipsoids are set at 50% level probability. Selected bond distances (Å) and angles (°): Ni1-P1 2.248(1), Ni1-C27 1.782(7), Ni1-C26 1.783(7), C27-O3 1.144(9), P1-Ni1-C27 101.5(2), C27-Ni1-C26 110.6(3), Ni1-P1-C1-C2 -87.5(4).

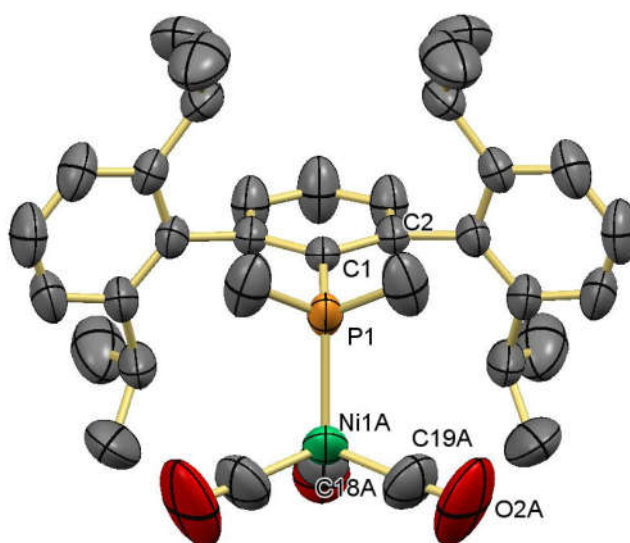


Figure 21. ORTEP view of complex **1·L3**. Hydrogen atoms and minor disorder are omitted for clarity and thermal ellipsoids are set at 50% level probability. Selected bond distances (Å) and angles (°): Ni1A-P1 2.294(2), Ni1-C19A 1.771(6), Ni1-C18A 1.785(8), C19A-O2A 1.15(1), P1-Ni1A-C19A 104.6(3), C19A-Ni1A-C18A 113.3(3), Ni1-P1-C1-C2 85.3(3).

a structure of type **B**. Given the trivial differences in energy between conformations **A** and **B** in the free phosphines, it is not surprising that, in order to minimise strain between the Ni(CO)<sub>3</sub> fragment and the phosphine ligand, conformation **A** becomes favoured in the Ni(CO)<sub>3</sub>(PR<sub>2</sub>Ar'') complexes.

For comparative purposes, the reactions of Ni(CO)<sub>4</sub> with two dialkyl biaryl phosphines, namely PCy<sub>2</sub>Ar<sup>Tripp</sup> (XPhos) and P<sup>t</sup>Bu<sub>2</sub>Ar<sup>Tripp</sup> (<sup>t</sup>BuXPhos), were also examined under the same conditions. Although, in accordance with previous studies, the latter originated no isolable products,<sup>28</sup> Ni(CO)<sub>3</sub>(XPhos) was actually isolated and completely characterised. The <sup>31</sup>P{<sup>1</sup>H} NMR spectrum of this complex displays a very broad resonance (width at half height  $\Delta\delta_{1/2} \approx 2$  ppm) at *ca.* 57.5 ppm. The isopropyl groups on the side aryl ring give rise to two sets of signals in a 2:1 ratio in the <sup>1</sup>H NMR spectrum, with two different signals for the diastereotopic CH<sub>3</sub> groups of the *ortho* substituents (Figure 22).

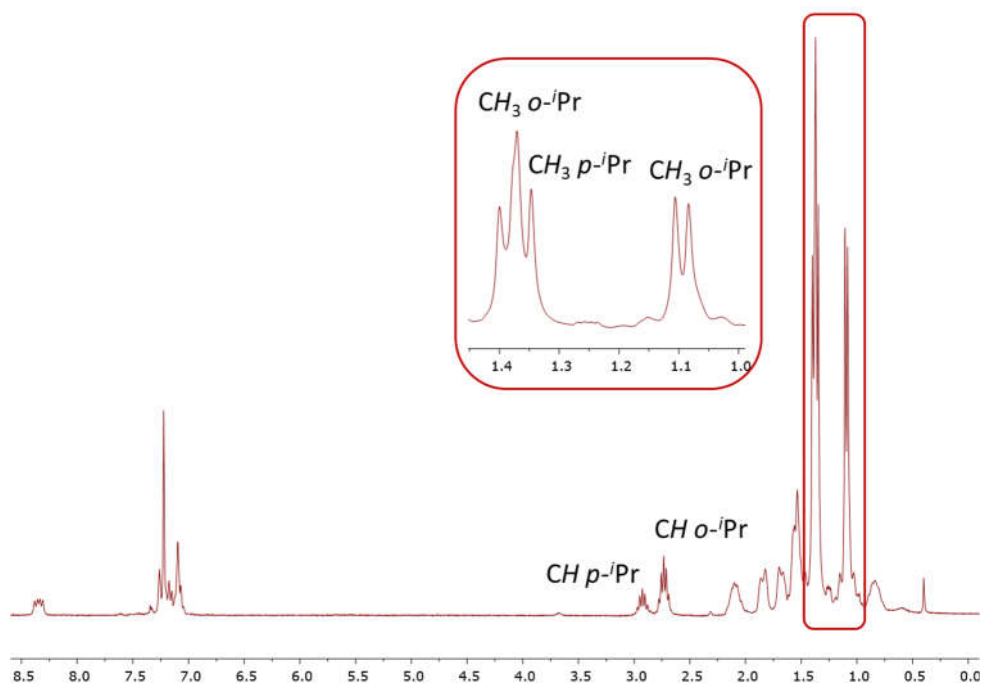


Figure 22. <sup>1</sup>H NMR spectrum of Ni(CO)<sub>3</sub>(XPhos) in C<sub>6</sub>D<sub>6</sub> at 25 °C.

## Chapter I

As was mentioned in the introduction to this chapter, crystallographic data pertaining  $\text{Ni}(\text{CO})_3(\text{PR}_3)$  complexes of commonly used phosphines are scarce. For this reason, it was considered of interest to isolate and structurally characterise  $\text{Ni}(\text{CO})_3(\text{PPh}_3)$  by single crystal X-ray diffraction (Figure 23).

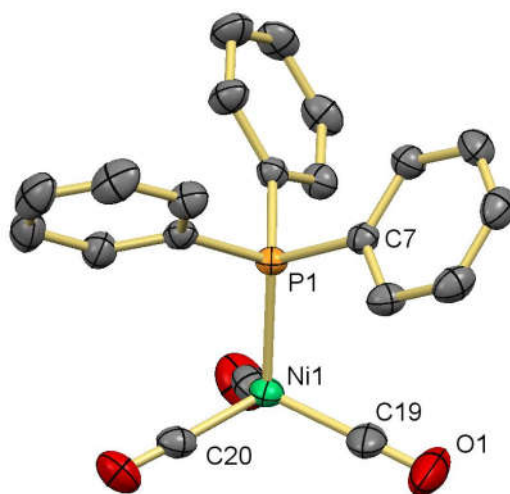


Figure 23. ORTEP view of complex  $\text{Ni}(\text{CO})_3(\text{PPh}_3)$ . Hydrogen atoms are omitted for clarity and thermal ellipsoids are set at 50% level probability. Selected bond distances ( $\text{\AA}$ ) and angles ( $^\circ$ ): Ni1-P1 2.2235(5), Ni1-C19 1.794(3), C19-O1 1.133(3), P1-C7 1.831(1), P1-Ni1-C19 106.05(7), C7-P1-Ni1 115.72(5), C19-Ni1-C20 113.62(9).

Table 3 collects Ni–P and Ni–CO bond distances for the crystallographically characterised **1·L1·L3** and  $\text{Ni}(\text{CO})_3(\text{PPh}_3)$  complexes, as well as for  $\text{Ni}(\text{CO})_3(\text{L})$  adducts of  $\text{P}^t\text{Bu}_3$ ,<sup>27a</sup> the N-heterocyclic carbene (NHC)  $\text{IPr}^{29b}$  and the cyclic alkyl amino carbene (CAAC)  $\text{CAAC}^{\text{Methyl}}$ .<sup>42b</sup> The Ni–P distances in **1·L1** and **1·L2** are very similar and comparable to that in  $\text{Ni}(\text{CO})_3(\text{PPh}_3)$ , while the more sterically demanding **L3** forms the longest bond in this series, closer to that found in  $\text{Ni}(\text{CO})_3(\text{P}^t\text{Bu}_3)$ . Ni–CO bond distances cluster around 1.78  $\text{\AA}$  for the three **1·PR<sub>2</sub>Ar''** complexes, falling shorter than in  $\text{Ni}(\text{CO})_4$  (*ca.* 1.82  $\text{\AA}$ ), but comparable to those in  $\text{Ni}(\text{CO})_3(\text{L})$  containing  $\text{PPh}_3$ ,  $\text{NHC}^{29b}$  or CAAC ligands.<sup>42b</sup> Probably, Ni–CO bond

distances in these complexes are mainly influenced by steric reasons rather than by the electron density at the Ni(0) centre.

Ligand	Complex	Ni–P (Å)	Ni–CO (average, Å)
<b>L1</b>	Ni(CO) <sub>3</sub> (PMe <sub>2</sub> Ar <sup>Dtbp<sub>2</sub></sup> )	2.240	1.792
<b>L2</b>	Ni(CO) <sub>3</sub> (PMe <sub>2</sub> Ar <sup>Xyl<sub>2</sub></sup> )	2.248	1.780
<b>L3</b>	Ni(CO) <sub>3</sub> (PMe <sub>2</sub> Ar <sup>Dipp<sub>2</sub></sup> )	2.294	1.776
PPh <sub>3</sub>	Ni(CO) <sub>3</sub> (PPh <sub>3</sub> )	2.224	1.800
P <sup>t</sup> Bu <sub>3</sub>	Ni(CO) <sub>3</sub> (P <sup>t</sup> Bu <sub>3</sub> ) <sup>a</sup>	2.289	1.721
IPr	Ni(CO) <sub>3</sub> (IPr) <sup>b</sup>	-	1.792
CAAC <sup>Methyl</sup>	Ni(CO) <sub>3</sub> (CAAC <sup>Methyl</sup> ) <sup>c</sup>	-	1.800

Table 3. Ni–P and Ni–CO distances for Ni(CO)<sub>3</sub>(L) complexes of tertiary phosphines and nucleophilic carbene ligands. <sup>a</sup>From ref. 27a. <sup>b</sup>From ref. 29b. <sup>c</sup>From ref. 42b.

The carbonyl region of the IR spectra of all Ni(CO)<sub>3</sub>(L) complexes studied exhibit a narrow signal around 2061–2064 cm<sup>-1</sup>, corresponding to the symmetric A<sub>1</sub> stretching vibration, and a broad band around 1985–1988 cm<sup>-1</sup> for the degenerate asymmetric E vibrations (Figure 24). IR wavenumbers for the C–O stretching vibrations in the new Ni(CO)<sub>3</sub>(L) complexes are gathered in Table 4, along with those obtained for other related ligands, collected from the literature for the sake of comparison. C–O stretching frequencies for complex Ni(CO)<sub>3</sub>(PCy<sub>2</sub>Ar<sup>Dtbp<sub>2</sub></sup>) (*vide infra*) and Ni(CO)<sub>3</sub>(PCyp<sub>3</sub>), obtained for the sake of completeness, are also included in Table 4.

All dimethyl-substituted terphenyl phosphines (**L1–L5**) in Table 4 feature TEPs, given by the symmetric (A<sub>1</sub>) C–O stretching frequencies, encompassed in the narrow range 2062–2064 cm<sup>-1</sup>, below the values for the parent phenyl-substituted PMe<sub>2</sub>Ph (2065.3 cm<sup>-1</sup>) and even PMe<sub>3</sub> (2064.1 cm<sup>-1</sup>). Similarly, the TEP of 2061 cm<sup>-1</sup> registered for PEt<sub>2</sub>Ar<sup>Dtbp<sub>2</sub></sup> (**L6**) lies lower than that corresponding to its analogue PEt<sub>2</sub>Ph (2063.7 cm<sup>-1</sup>). Lastly, although no record exists on the

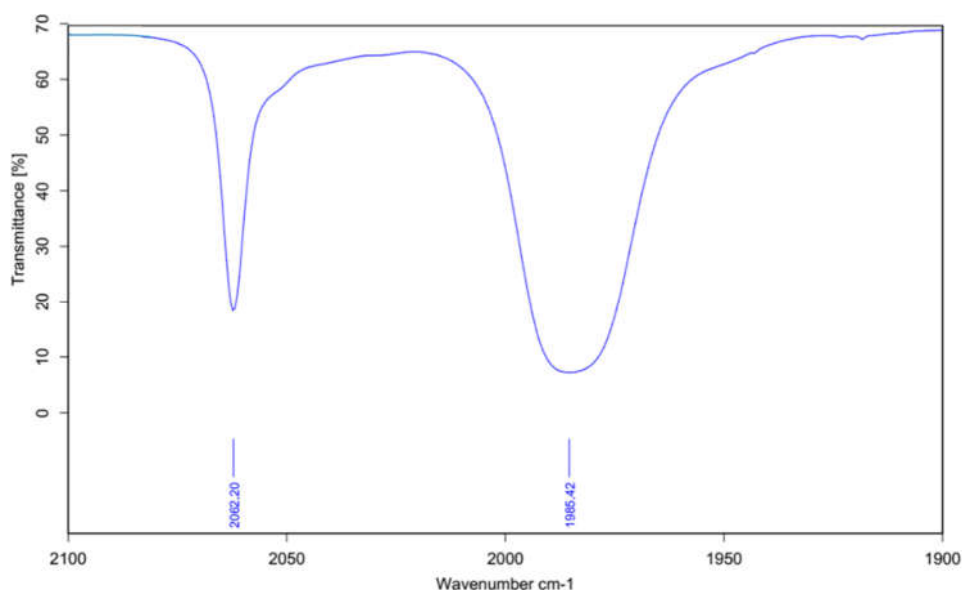


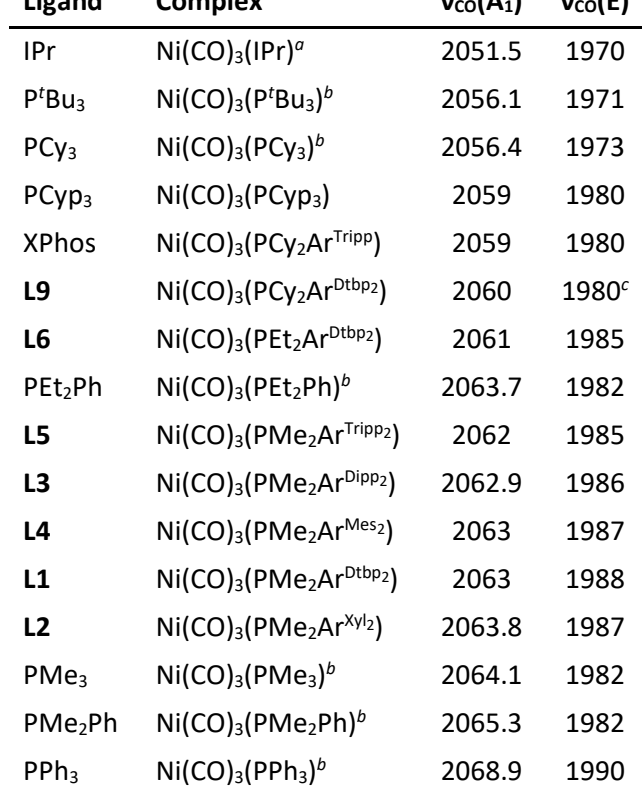
Figure 24. Carbonyl region of the IR spectrum of complex **1-L5**.

experimental TEP value corresponding to  $\text{PCy}_2\text{Ph}$ , a calculated TEP of  $2060.6\text{ cm}^{-1}$  can be obtained using Tolman's substituent contributions,<sup>25</sup> falling marginally higher than that measured for  $\text{PCy}_2\text{Ar}^{\text{Dtbp}_2}$  ( $2060\text{ cm}^{-1}$ ) and the biaryl phosphine  $\text{PCy}_2\text{Ar}^{\text{Tripp}}$  ( $2059\text{ cm}^{-1}$ ). Taking all these data into account, it can be concluded that terphenyl groups confer a slightly higher electron-donor capacity to phosphine ligands than a phenyl substituent.

#### 1.2.4. Synthesis and characterisation of $\text{Ni}(\text{CO})_2(\text{PR}_2\text{Ar}'')$ complexes of the dialkyl terphenyl phosphines ( $\text{R} = \textit{i}\text{Pr}, \text{Cyp}, \text{Cy}$ ).

Terphenyl phosphines bearing branched or cyclic alkyl groups on the phosphorus atom (i.e. **L7-L12**) did not react with  $\text{Ni}(\text{CO})_4$  under the conditions used above, even when irradiated with ultraviolet light. For these phosphines, it was necessary to remove the carbon monoxide atmosphere and, in most cases,



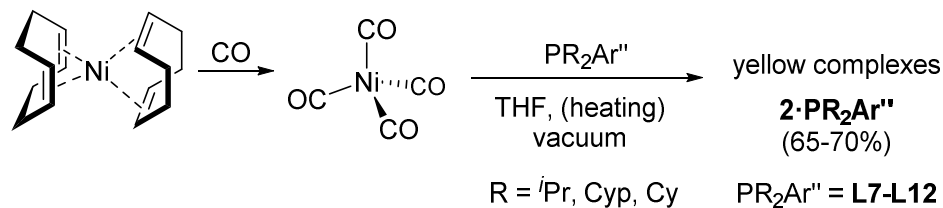


Ligand	Complex	$\nu_{\text{CO}}(\text{A}_1)$	$\nu_{\text{CO}}(\text{E})$
IPr	$\text{Ni}(\text{CO})_3(\text{IPr})^a$	2051.5	1970
$\text{P}^t\text{Bu}_3$	$\text{Ni}(\text{CO})_3(\text{P}^t\text{Bu}_3)^b$	2056.1	1971
$\text{PCy}_3$	$\text{Ni}(\text{CO})_3(\text{PCy}_3)^b$	2056.4	1973
$\text{PCyp}_3$	$\text{Ni}(\text{CO})_3(\text{PCyp}_3)$	2059	1980
XPhos	$\text{Ni}(\text{CO})_3(\text{PCy}_2\text{Ar}^{\text{Tripp}})$	2059	1980
<b>L9</b>	$\text{Ni}(\text{CO})_3(\text{PCy}_2\text{Ar}^{\text{Dtbp}_2})$	2060	1980 <sup>c</sup>
<b>L6</b>	$\text{Ni}(\text{CO})_3(\text{PEt}_2\text{Ar}^{\text{Dtbp}_2})$	2061	1985
$\text{PEt}_2\text{Ph}$	$\text{Ni}(\text{CO})_3(\text{PEt}_2\text{Ph})^b$	2063.7	1982
<b>L5</b>	$\text{Ni}(\text{CO})_3(\text{PMe}_2\text{Ar}^{\text{Tripp}_2})$	2062	1985
<b>L3</b>	$\text{Ni}(\text{CO})_3(\text{PMe}_2\text{Ar}^{\text{Dipp}_2})$	2062.9	1986
<b>L4</b>	$\text{Ni}(\text{CO})_3(\text{PMe}_2\text{Ar}^{\text{Mes}_2})$	2063	1987
<b>L1</b>	$\text{Ni}(\text{CO})_3(\text{PMe}_2\text{Ar}^{\text{Dtbp}_2})$	2063	1988
<b>L2</b>	$\text{Ni}(\text{CO})_3(\text{PMe}_2\text{Ar}^{\text{Xyl}_2})$	2063.8	1987
$\text{PMe}_3$	$\text{Ni}(\text{CO})_3(\text{PMe}_3)^b$	2064.1	1982
$\text{PMe}_2\text{Ph}$	$\text{Ni}(\text{CO})_3(\text{PMe}_2\text{Ph})^b$	2065.3	1982
$\text{PPh}_3$	$\text{Ni}(\text{CO})_3(\text{PPh}_3)^b$	2068.9	1990

Table 4. IR wavenumbers ( $\text{cm}^{-1}$ ) for the C–O stretching vibrations in some  $\text{Ni}(\text{CO})_3(\text{L})$  complexes in  $\text{CH}_2\text{Cl}_2$  solution, ordered from lowest to highest  $\nu_{\text{CO}}(\text{A}_1)$ . <sup>a</sup>From ref. 29b. <sup>b</sup>From ref. 25. <sup>c</sup>Partially obscured band.

increase the reaction temperature to 50–80 °C to achieve a reaction, giving rise to bright yellow complexes **2·L7** through **2·L12** (Scheme 4).

As was the case with the phosphines discussed in the previous section, **L7–L12** present different degrees of reactivity towards  $\text{Ni}(\text{CO})_4$ , with two notable examples. The reaction with **L7** needs a vast emptied headspace or, alternatively, a repetitive vacuum at several moments during the reaction for complete conversion to be achieved. On the other hand, **2·L10** seems to decompose rapidly at the temperature needed for reaction to proceed, resulting in a mixture of the final product, metallic nickel and free phosphine. It was found that a short time (30 min) at 100 °C yielded better results than a longer time at a lower



*Scheme 4. Synthesis of complexes **2-PR<sub>2</sub>Ar''**.*

temperature. It is also worth mentioning that minor quantities of  $\text{Ni}(\text{CO})_3(\text{PCy}_2\text{Ar}^{\text{Dtpb}_2})$  could be observed in the IR spectrum recorded for **2-L9**. However, attempts to isolate and further characterise this tricarbonyl complex were unsatisfactory.

Similarly to the  $\text{Ni}(\text{CO})_3(\text{PR}_2\text{Ar}'')$  compounds, only complexes **2-L7** and **2-L11** were isolated and characterised, spectroscopically and crystallographically, while all others were generated in solution and analysed solely by IR spectroscopy. IR spectra recorded for the newly generated complexes display an entirely different carbonyl region than those for the complexes discussed in the previous section: wavenumbers are considerably smaller (*ca.* 1995 and 1923  $\text{cm}^{-1}$ ) and the two bands appear narrow (Figure 25). These values are collected in Table 6 and discussed below.

The  $^{31}\text{P}\{^1\text{H}\}$  NMR shifts of these complexes deviate by 44-50 ppm downfield from the free phosphines (Table 5), which points to a different mode of coordination of the ligands in these derivatives.<sup>22</sup> In the  $^1\text{H}$  NMR spectrum of **2-L11**, the methyl substituents on the flanking aryl rings give rise to two distinct signals at room temperature (Figure 26). On the other hand, all signals due to the terphenyl moiety in the room temperature  $^1\text{H}$  NMR spectrum of complex **2-L7** appear as broad resonances that resolve into sharp peaks on cooling at  $-30\text{ }^\circ\text{C}$ . No significant change can be discerned for those corresponding to the isopropyl

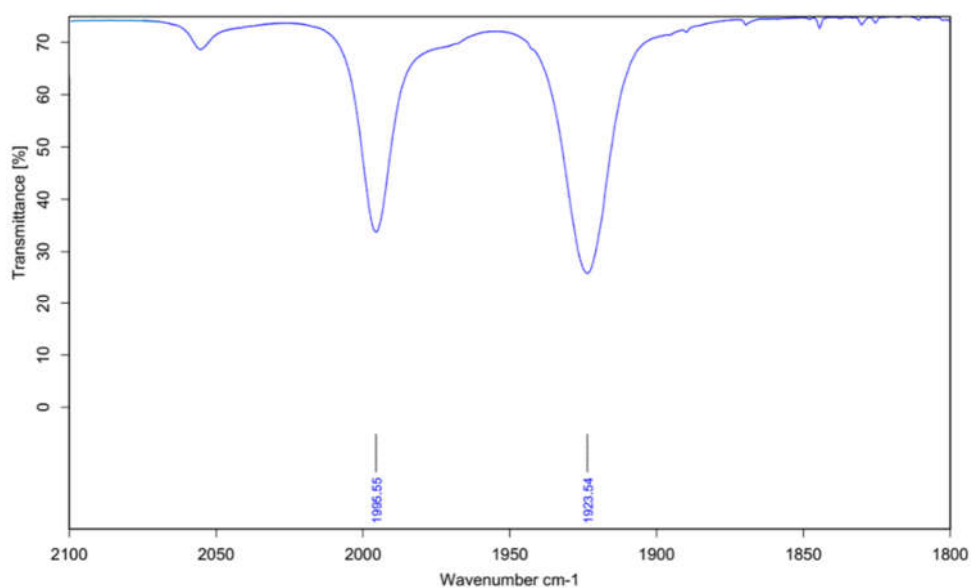


Figure 25. Carbonyl region of the IR spectrum of complex **2-L11**.

groups on the phosphorus atom (Figure 27). The value of the rate constant for exchange determined by  $^1\text{H}$  NMR at the coalescence temperature of around 15 °C is  $\Delta G^\ddagger \approx 15 \text{ kcal}\cdot\text{mol}^{-1}$ . The carbonyl ligands appear at around 198-199 ppm in the  $^{13}\text{C}\{^1\text{H}\}$  NMR as doublets with coupling constants  $^2J_{\text{CP}} = 10\text{-}11 \text{ Hz}$ .

Complex	$\delta$ (ppm)	$\Delta\delta$ (ppm)
<b>2-L7</b>	60.7	48.1
<b>2-L8</b>	50.3	49.4
<b>2-L9</b>	49 <sup>a</sup>	47
<b>2-L10</b>	62 <sup>a</sup>	46
<b>2-L11</b>	53.5	48.9
<b>2-L12</b>	54 <sup>a</sup>	44

Table 5.  $^{31}\text{P}\{^1\text{H}\}$  NMR chemical shifts ( $\delta$ ) of complexes **2-PR<sub>2</sub>Ar''** and difference with the corresponding free phosphines ( $\Delta\delta$ ). <sup>a</sup>Recorded in non-deuterated THF.

Chapter I

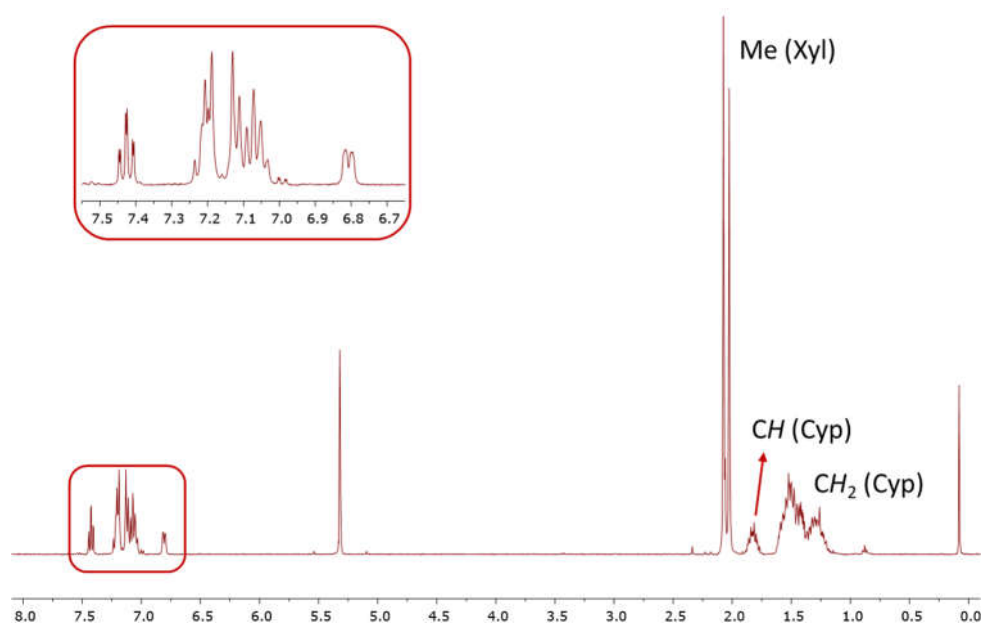


Figure 26.  $^1\text{H}$  NMR spectrum of complex **2-L11** in  $\text{CD}_2\text{Cl}_2$  at  $25\text{ }^\circ\text{C}$ .

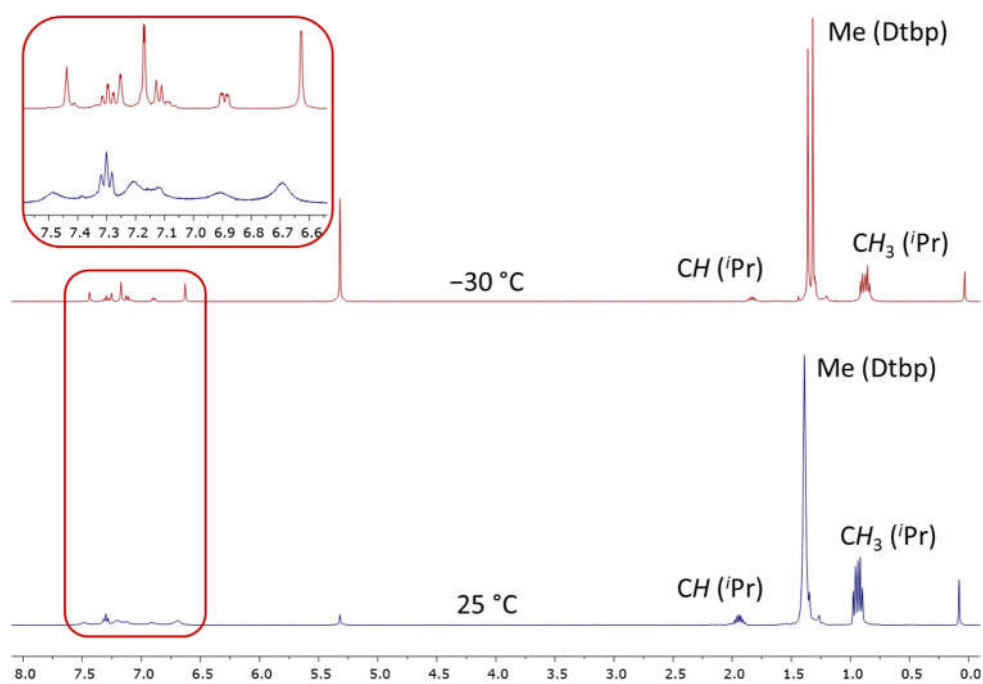


Figure 27.  $^1\text{H}$  NMR spectra of complex **2-L7** in  $\text{CD}_2\text{Cl}_2$  at  $-30\text{ }^\circ\text{C}$  (top) and  $25\text{ }^\circ\text{C}$  (bottom).

To gain insight into the structure of these complexes, single crystals of both isolated  $\text{Ni}(\text{CO})_2(\text{PR}_2\text{Ar}'')$  complexes, **2·L7** and **2·L11**, were grown and analysed by X-ray diffraction. These studies unveiled the substitution of a second carbonyl ligand from the initial  $\text{Ni}(\text{CO})_4$  by a relatively weak  $\text{Ni}-\eta^2\text{-C}_{ipso,Cortho}$  interaction with one of the side aryl rings (Figures 28 and 29). Thus, both structures display four-coordinated nickel centres, with a very uncommon oblique triangular pyramidal geometry. The weak  $\text{Ni}-\eta^2\text{-C}_{ipso,Cortho}$  interaction is characterised by fairly long  $\text{Ni}\cdots\text{C}_{arene}$  distances, namely 2.449(2) (to  $\text{C}_{ipso}$ ) and 2.332(2) Å (to  $\text{C}_{ortho}$ ) in **2·L7**, and 2.438(3) (to  $\text{C}_{ipso}$ ) and 2.414(3) Å (to  $\text{C}_{ortho}$ ) in **2·L11**, all of them standing well above the 1.97 Å value of the sum of the covalent radii of  $\text{C}_{sp^2}$  (0.73 Å) and Ni (1.24 Å).<sup>43</sup> These distances are also significantly longer than in known Ni(0)-olefin complexes, such as  $\text{Ni}(\text{cod})_2$  (Ni-C bond distances in the range 2.11-2.13 Å)<sup>44a</sup> and  $\text{Ni}(\text{C}_2\text{H}_4)(\text{PPh}_3)_2$  (close to 2.0 Å).<sup>44b</sup> To the best of our knowledge, these are the first examples of complexes with the formula  $\text{Ni}(\text{CO})_2(\text{PR}_3)$ , thus preventing further comparison of the crystallographic data. Moreover, unlike **2·L7** and **2·L11**, reported  $\text{Ni}(\text{CO})_2(\text{L})$  complexes of carbene ligands<sup>29,45</sup> do not feature a secondary interaction with said ligands, resulting in a triangular planar geometry of the nickel centre.

Once the structures of these complexes had been elucidated, the dynamic behaviour of **2·L7** in solution was studied in more depth by variable temperature  $^1\text{H}$  NMR and DFT calculations. Two different processes can be envisioned to take place. First, an interchange between the two degenerate conformations where the nickel centre is coordinated in a  $\eta^2$  fashion to the *ipso* and one of the *ortho* carbons of the Dtbp ring engaged in bonding, through a  $\eta^1\text{-C}_{ipso}$  transition state (Figure 30), which is expected to be fast (1.7 kcal·mol<sup>-1</sup> energy barrier according to DFT calculations). This process generates an effective plane of symmetry containing the central ring of the terphenyl moiety and the Ni-P bond, thus rendering the two isopropyl groups equivalent, as well as the two *tert*-butyl substituents of each Dtbp ring. Conversely, temporary cleavage of the  $\text{Ni}-\eta^2\text{-C}_{arene}$

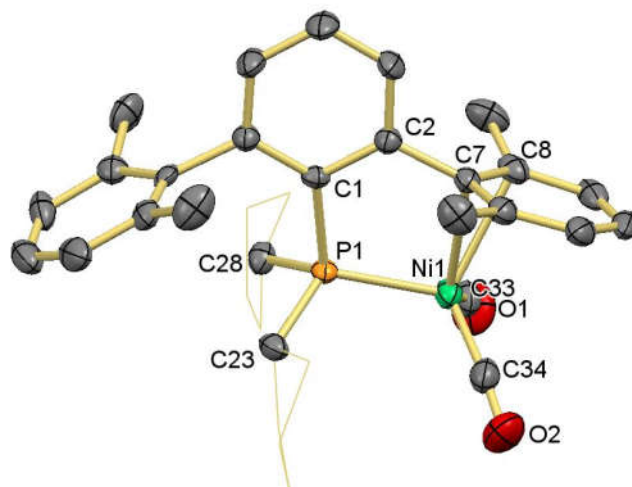


Figure 28. ORTEP view of complex **2-L17**. Hydrogen atoms and minor disorder are omitted, some atoms from the cyclopentyl substituents are drawn in wireframe for clarity and thermal ellipsoids are set at 50% level probability. Selected bond distances (Å) and angles (°): Ni1-P1 2.2037(8), Ni1-C33 1.767(4); Ni1-C34 1.770(4), Ni1-C7 2.438(3), Ni1-C8 2.414(3), P1-C1 1.850(2), P1-C23 1.845(3), P1-C28 1.845(3), C23-P1-C28 104.2(1), C23-P1-C1 107.7(1), C28-P1-C1 104.3(1), Ni1-P1-C1-C2 -1.5(2).

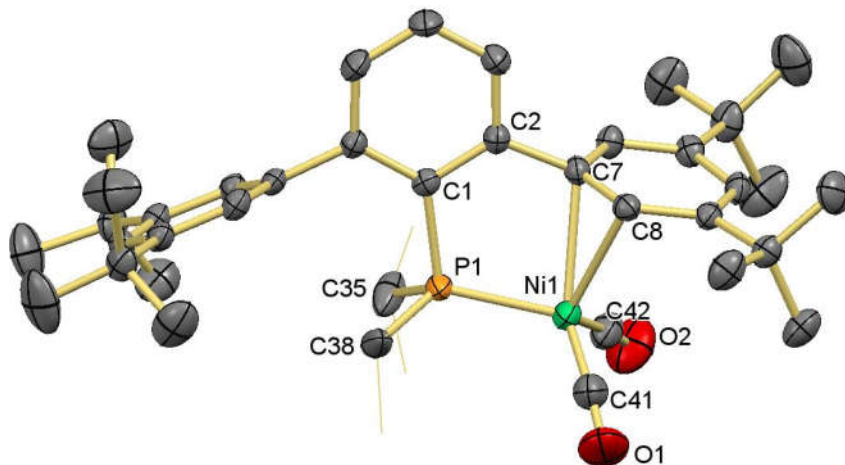


Figure 29. ORTEP view of complex **2-L11**. Hydrogen atoms and minor disorder are omitted, some atoms from the isopropyl substituents are drawn in wireframe for clarity and thermal ellipsoids are set at 50% level probability. Selected bond distances (Å) and angles (°): Ni1-P1 2.2056(6), Ni1-C41 1.763(3), Ni1-C42 1.776(3), Ni1-C7 2.449(2), Ni1-C8 2.332(2), P1-C1 1.849(2), P1-C35 1.863(3), P1-C38 1.848(3), C35-P1-C38 106.1(2), C35-P1-C1 104.0(1), C38-P1-C1 104.5(1), Ni1-P1-C1-C2 11.08(18).

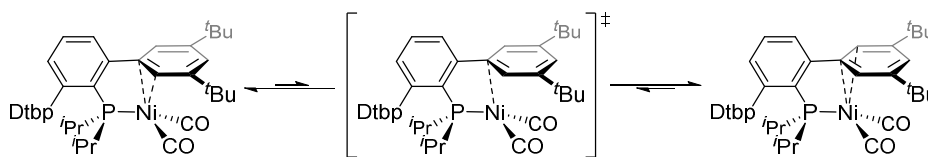


Figure 30. Exchange between the two degenerate Ni- $\eta^2$ -Carene structures of complex **2·L7**.

interaction to generate a truly three-coordinate intermediate, followed by rotation around the P- $C_{ipso}$  bond, results in the swap of the two Dtbp rings. An exhaustive DFT study revealed the complexity of the latter process, where the transition states for the rotation of the isopropyl groups previous to decoordination of the Ni(CO)<sub>2</sub> moiety are even higher in the potential energy surface than those corresponding to the cleavage of the Ni- $\eta^2$ -Carene interaction (Figure 31). This could explain the difference between the room temperature NMR spectra of **2·L7** and **2·L11**. The highest transition state is calculated to be 10.5 kcal·mol<sup>-1</sup> above the conformation observed in the X-ray structure, which supports a low energy process, as already inferred from the variable temperature NMR data. It is thus clear that complexes Ni(CO)<sub>2</sub>(PR<sub>2</sub>Ar'') can be considered a source of unsaturated, three-coordinate, sixteen valence electron species.

The symmetric and antisymmetric C–O stretching frequencies found for complexes Ni(CO)<sub>2</sub>(PR<sub>2</sub>Ar'') are displayed in Table 6. The structural peculiarity of these complexes limits comparison of the IR data with four-coordinate Ni(CO)<sub>2</sub>(PR<sub>3</sub>)<sub>2</sub> complexes and also with the few known examples of truly three-coordinate Ni(CO)<sub>2</sub>(L) derivatives of carbene ligands.<sup>29,45</sup> Entries for ligands **L6** and XPhos have been included in Table 6, since dicarbonyl complexes of these phosphines could be generated in low conversion from the corresponding tricarbonyl species (*vide infra*).

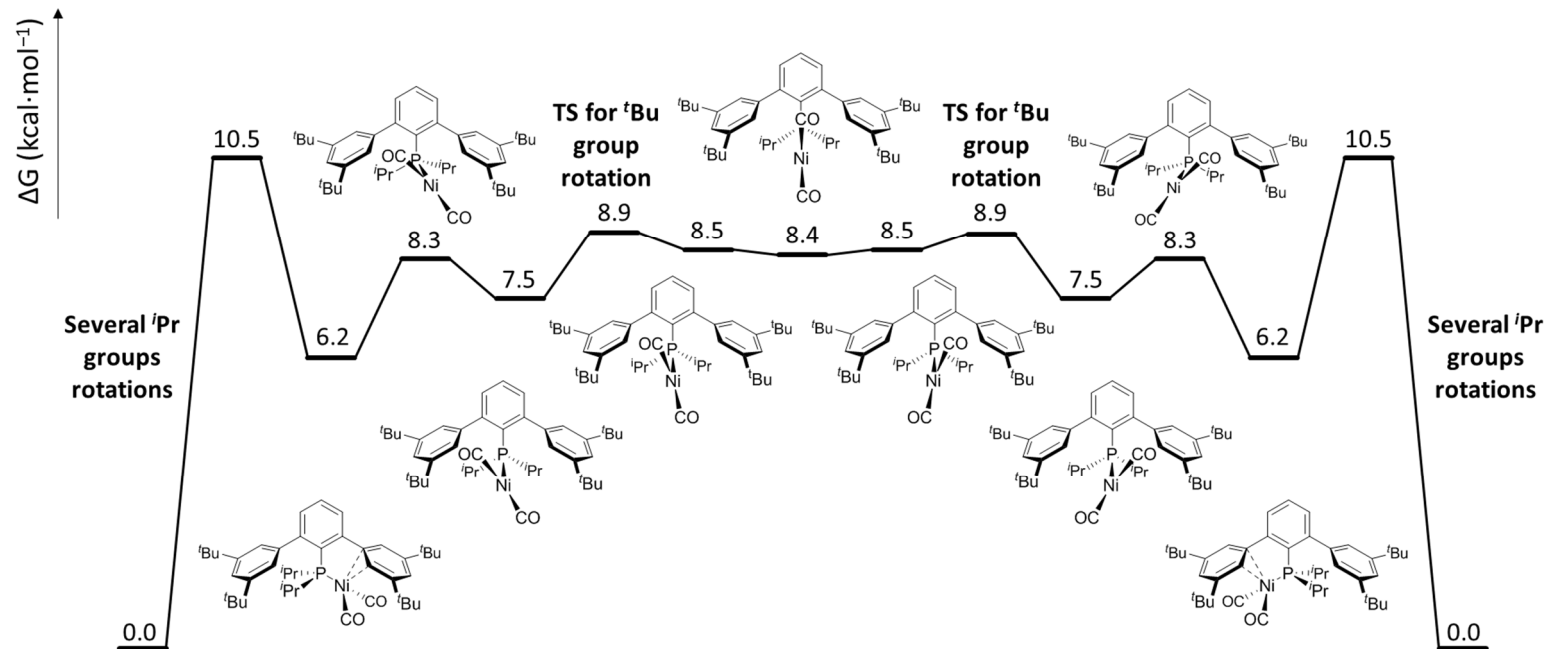


Figure 31. Free energy profile for the cleavage of the Ni- $\eta^2$ -Carene interaction, rotation of the Ni(CO)<sub>2</sub> fragment and subsequent recoordination to recover the initial conformation in complex 2-L7.



Ligand	Complex	$\nu_{\text{sym}}$	$\nu_{\text{asym}}$
<b>L6</b>	$\text{Ni}(\text{CO})_2(\text{PEt}_2\text{Ar}^{\text{Dtbp}_2})$	1996 <sup>c</sup>	1923
<b>L7</b>	$\text{Ni}(\text{CO})_2(\text{P}^i\text{Pr}_2\text{Ar}^{\text{Dtbp}_2})$	1995	1923
<b>L8</b>	$\text{Ni}(\text{CO})_2(\text{PCyp}_2\text{Ar}^{\text{Dtbp}_2})$	1995	1923
<b>L9</b>	$\text{Ni}(\text{CO})_2(\text{PCy}_2\text{Ar}^{\text{Dtbp}_2})$	1993	1921
<b>L10</b>	$\text{Ni}(\text{CO})_2(\text{P}^i\text{Pr}_2\text{Ar}^{\text{Xyl}_2})$	1996	1924
<b>L11</b>	$\text{Ni}(\text{CO})_2(\text{PCyp}_2\text{Ar}^{\text{Xyl}_2})$	1996	1924
<b>L12</b>	$\text{Ni}(\text{CO})_2(\text{PCy}_2\text{Ar}^{\text{Xyl}_2})$	1993	1923
XPhos	$\text{Ni}(\text{CO})_2(\text{PCy}_2\text{Ar}^{\text{Tripp}})$	1995 <sup>c</sup>	1918
IAd	$\text{Ni}(\text{CO})_2(\text{IAd})^a$	2007	1926
I <sup>t</sup> Bu	$\text{Ni}(\text{CO})_2(\text{I}^t\text{Bu})^a$	2010	1929
C(PPh <sub>3</sub> ) <sub>2</sub>	$\text{Ni}(\text{CO})_2(\text{C}(\text{PPh}_3)_2)^b$	1976	1895

Table 6. IR wavenumbers ( $\text{cm}^{-1}$ ) for the C–O stretching vibrations in  $\text{Ni}(\text{CO})_2(\text{L})$  complexes in  $\text{CH}_2\text{Cl}_2$  solution (unless otherwise stated). <sup>a</sup>In hexane solution, see ref. 29b. <sup>b</sup>In Nujol, see ref. 45. <sup>c</sup>Partially obscured band.

### 1.2.5. Interconversion between $\text{Ni}(\text{CO})_n(\text{PR}_2\text{Ar}'')$ species: experimental and DFT studies.

A study was carried out concerning the conversion of the tricarbonyl complexes into the corresponding dicarbonyl species and *vice versa*. First, complexes **1·L2** and **1·L3** of the dimethyl-substituted terphenyl phosphines  $\text{PMe}_2\text{Ar}^{\text{Xyl}_2}$  and  $\text{PMe}_2\text{Ar}^{\text{Dipp}_2}$ , respectively, were heated under vacuum. This resulted in the development of a yellow colour and some decomposition into free phosphine and metallic nickel, but no sign of the  $\text{Ni}(\text{CO})_2(\text{PMe}_2\text{Ar}'')$  complexes could be observed by spectroscopic techniques. Application of the same approach to  $\text{Ni}(\text{CO})_3(\text{PEt}_2\text{Ar}^{\text{Dtbp}_2})$ , **1·L6**, and  $\text{Ni}(\text{CO})_3(\text{XPhos})$  produced the corresponding  $\text{Ni}(\text{CO})_2(\text{L})$  species in low conversions, even when the vacuum was iterative. The  $\text{Ni}(\text{CO})_3(\text{L})/\text{Ni}(\text{CO})_2(\text{L})$  admixtures were analysed by IR spectroscopy and the values recorded for  $\nu_{\text{CO}}$  are included in Table 6.

## Chapter I

On the other hand, a solution of  $\text{Ni}(\text{CO})_2(\text{PCyp}_2\text{Ar}^{\text{Xyl}_2})$ , **2-L11**, was placed under an atmosphere of CO (1 bar) at room temperature, leading to the quick disappearance of the yellow colour. Analysis by  $^{31}\text{P}\{^1\text{H}\}$  NMR revealed the presence of free phosphine as the only P-containing species. Ostensibly, **2-L11** evolves under these conditions to  $\text{Ni}(\text{CO})_4$  and uncoordinated phosphine, as already reported by Nolan *et al.* for their  $\text{Ni}(\text{CO})_2(\text{NHC})$  species.<sup>29b</sup> When this process was repeated at low temperature ( $-30\text{ }^\circ\text{C}$ ), an intermediate, stable up to  $-15\text{ }^\circ\text{C}$ , could be observed by NMR with a  $^{31}\text{P}\{^1\text{H}\}$  chemical shift of 47.3 ppm, *ca.* 6.5 ppm to lower frequency compared to the original compound. The  $^1\text{H}$  NMR spectrum of this intermediate at  $-15\text{ }^\circ\text{C}$ , presumably  $\text{Ni}(\text{CO})_3(\text{PCyp}_2\text{Ar}^{\text{Xyl}_2})$ , features an asymmetric chemical environment around the terphenyl moiety, as evinced by the two distinct signals for the methyl groups on the side aryl rings (Figure 32). As discussed below, DFT studies reveal the preference of the phosphine ligand to

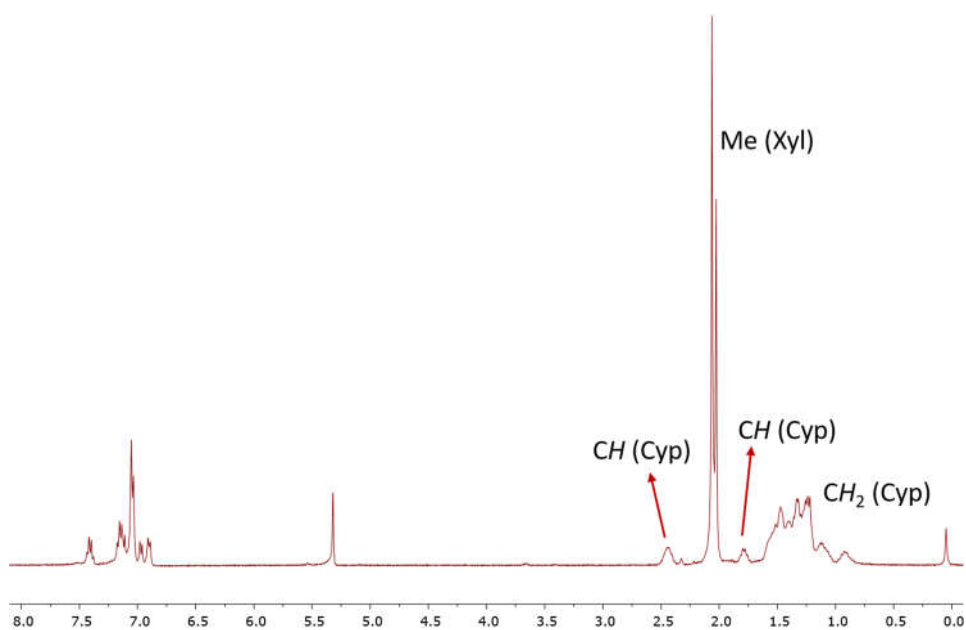


Figure 32.  $^1\text{H}$  NMR spectrum recorded from the reaction of **2-L11** with CO at low temperature, in  $\text{CD}_2\text{Cl}_2$  at  $-15\text{ }^\circ\text{C}$ .

retain a conformation of type **C** when coordinated to the  $\text{Ni}(\text{CO})_3$  fragment, which would explain this observation. As expected, the intermediate quickly decomposes to free phosphine and  $\text{Ni}(\text{CO})_4$  at higher temperatures and evolves to the original dicarbonyl species in the absence of a CO atmosphere, preventing its characterisation by IR spectroscopy.

In order to attain a better understanding on the different reactivities of the phosphines towards  $\text{Ni}(\text{CO})_4$ , a computational study was carried out. For convenience, of the twelve phosphines represented in Figure 10, only those with isolated  $\text{Ni}(\text{CO})_n(\text{PR}_2\text{Ar}'')$  complexes were selected for this study.

First, an optimisation of the geometries of complexes  $\text{Ni}(\text{CO})_3(\text{PR}_2\text{Ar}'')$  was carried out. Two possible conformations were found. They are interchangeable by rotation around the  $\text{P}-\text{C}_{\text{ipso}}$  bond, and correspond to the **A** and **C** structures of the uncoordinated phosphines (Figure 33). As expected considering the X-ray structures (see Figures 19-21), complexes bearing dimethyl- and diethyl-substituted phosphines favour conformation **A'**. On the other hand,

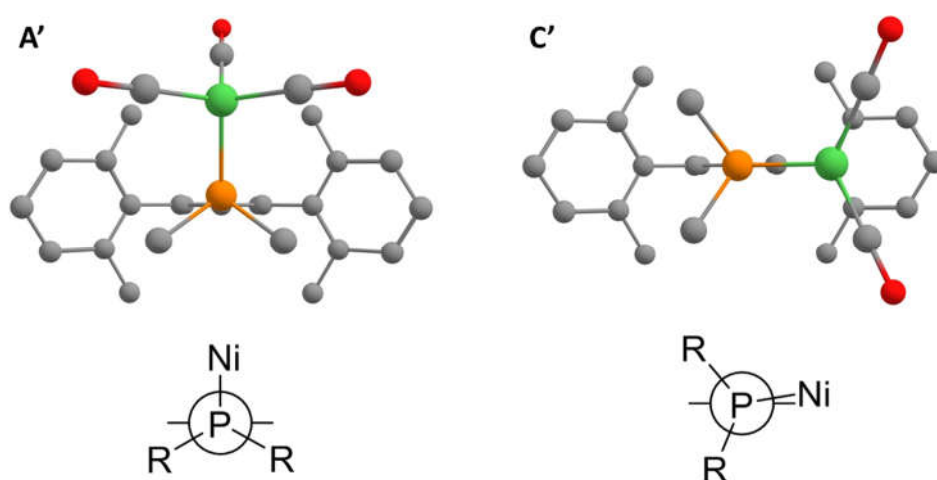


Figure 33. Calculated conformations for  $\text{Ni}(\text{CO})_3(\text{PR}_2\text{Ar}'')$  complexes. Top: calculated geometry of the  $\text{Ni}(\text{CO})_3(\text{PMe}_2\text{Ar}^{\text{Xyl}/2})$  complex in conformations **A'** (left) and **C'** (right). Bottom: View along  $\text{P}-\text{C}_{\text{ipso}}$  bond.

$\text{Ni}(\text{CO})_3(\text{PCyp}_2\text{Ar}^{\text{Xyl}_2})$  and  $\text{Ni}(\text{CO})_3(\text{P}^i\text{Pr}_2\text{Ar}^{\text{Dtbp}_2})$  prefer a conformation where the metal centre sits very close to one of the side rings of the terphenyl moiety, labelled **C'**.

As stated above, due to steric hindrance between the alkyl groups on the phosphorus atom and the side rings of the terphenyl moiety, bulky  $\text{PR}_2\text{Ar}''$  phosphines (i.e. those with  $\text{R} = ^i\text{Pr}$ , Cyp or Cy) adopt a structure of type **C** in the solid state (see Figure 17). Analogously, according to DFT calculations, in the tricarbonyl adducts this would also cause a destabilisation of conformation **A'** in favour of the alternative **C'** for  $\text{PCyp}_2\text{Ar}^{\text{Xyl}_2}$  (Figure 34) and for  $\text{P}^i\text{Pr}_2\text{Ar}^{\text{Dtbp}_2}$ . The differences in free energy between the two conformations for all six complexes studied are collected in the first column of Table 7.

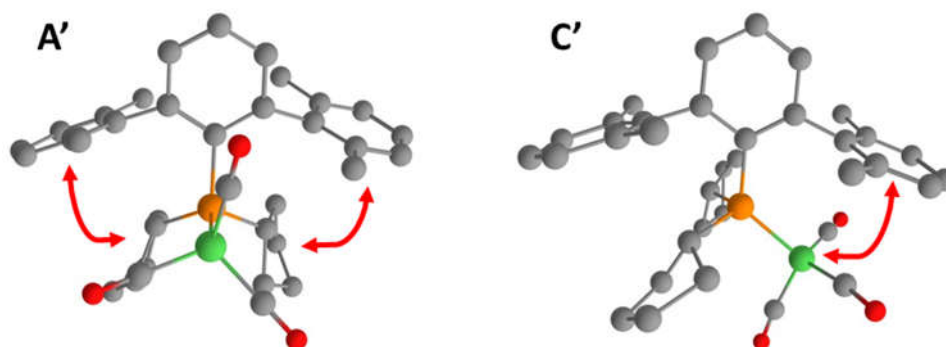


Figure 34. Molecular geometries of  $\text{Ni}(\text{CO})_3(\text{PCyp}_2\text{Ar}^{\text{Xyl}_2})$  in conformations **A'** (left) and **C'** (right), with red arrows representing steric hindrance between the terphenyl moiety and other fragments of the complex.

The geometries of the complexes  $\text{Ni}(\text{CO})_2(\text{PR}_2\text{Ar}'')$  were optimised and the energies compared to those for the  $\text{Ni}(\text{CO})_3(\text{PR}_2\text{Ar}'')$  complexes in the favoured conformation, **A'** or **C'**, for each case. These data are collected in the fourth data column of Table 7 below. Although all these energies are positive, it must be noted that reactions are carried out under vacuum, thus shifting the equilibrium towards

the loss of CO. As expected,  $\text{Ni}(\text{CO})_2(\text{PR}_2\text{Ar}'')$  complexes of methyl- and ethyl-substituted phosphines are higher in energy than those for the bulkier isopropyl- and cyclopentyl-substituted ones. This difference is less marked in the case of  $\text{PMe}_2\text{Ar}^{\text{Xyl}_2}$ , but analysis of the obtained data did not shed any light upon the reason behind this peculiarity.

The configuration of the transition states could be obtained by performing a relaxed potential energy surface (PES) scan of the loss of a carbonyl ligand from the two conformations. It was found that the transition states reached by starting from conformation **C'** had a lower energy (*ca.* 4-8 kcal/mol) than from conformation **A'**, as they include a favourable interaction between the nickel centre and the aryl side ring (Figure 35).

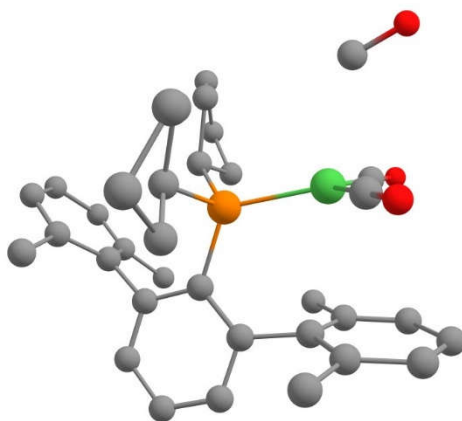


Figure 35. Molecular geometry of the transition state for CO loss from complex  $\text{Ni}(\text{CO})_3(\text{PCyp}_2\text{Ar}^{\text{Xyl}_2})$ .

In all cases, the free energy required to reach the transition state from conformation **C'** falls in the narrow range 11.2-13.0 kcal·mol<sup>-1</sup> (Table 7, second data column), as this process is barely affected by steric bulkiness. Since conformation **C'** is the energy well in the systems containing the bulkier phosphines, the overall free energy barrier for conversion from  $\text{Ni}(\text{CO})_3(\text{PR}_2\text{Ar}'')$

to  $\text{Ni}(\text{CO})_2(\text{PR}_2\text{Ar}'')$  remains around  $12.8 \text{ kcal}\cdot\text{mol}^{-1}$ . However, tricarbonyl complexes of the methyl- and ethyl-substituted phosphines must attain the cited conformation from the favoured **A'**, which means that an additional, though small, energy barrier, corresponding to the change in conformation, must be overcome (Table 7, third data column). This difference is exemplified in the free energy profiles for the global reactions depicted in Figures 36 and 37 (representing the cases for  $\text{PMe}_2\text{Ar}^{\text{Dtbp}_2}$  and  $\text{PCyp}_2\text{Ar}^{\text{Xyl}_2}$ , respectively) and could be the cause of the different reactivities. Again,  $\text{PMe}_2\text{Ar}^{\text{Xyl}_2}$  arises as an outlier, but no reason could be found behind this anomaly.

Phosphine	$\Delta G (\text{A}' \rightarrow \text{C}')$	$\Delta G^\ddagger (\text{from C}')$	$\Delta G^\ddagger (\text{overall})$	$\Delta G (\text{reaction})$
$\text{PMe}_2\text{Ar}^{\text{Dtbp}_2}$	3.8	12.9	16.6	10.1
$\text{PMe}_2\text{Ar}^{\text{Xyl}_2}$	2.0	11.9	13.9	7.1
$\text{PMe}_2\text{Ar}^{\text{Dipp}_2}$	6.4	11.2	17.6	11.6
$\text{PEt}_2\text{Ar}^{\text{Dtbp}_2}$	7.3	12.4	19.7	11.3
$\text{P}^i\text{Pr}_2\text{Ar}^{\text{Dtbp}_2}$	-1.8	12.5	12.5	3.0
$\text{PCyp}_2\text{Ar}^{\text{Xyl}_2}$	-8.7	13.0	13.0	4.4

Table 7. Changes in calculated free energies involved in the loss of a carbonyl ligand from  $\text{Ni}(\text{CO})_3(\text{PR}_2\text{Ar}'')$  complexes.

### 1.2.6. Reactivity of $\text{Ni}(\text{CO})_n(\text{PR}_2\text{Ar}'')$ complexes towards oxidative addition.

To complete the study of the nickel carbonyl complexes bearing dialkyl terphenyl phosphines, their capacity to undergo oxidative addition reactions was explored. No changes were observed upon addition of 4-bromotoluene at room temperature to tricarbonyl complexes **1·L1** and **1·L3** and to dicarbonyl **2·L7**. Heating at around  $70 \text{ }^\circ\text{C}$  resulted in decomposition to metallic nickel. Furthermore, complex **2·L11** did not oxidatively add iodomethane.

Despite these failures, complexes **1·L1** and **1·L6** reacted smoothly at room temperature with 3-bromo-1-propene by displacement of the carbonyl ligands

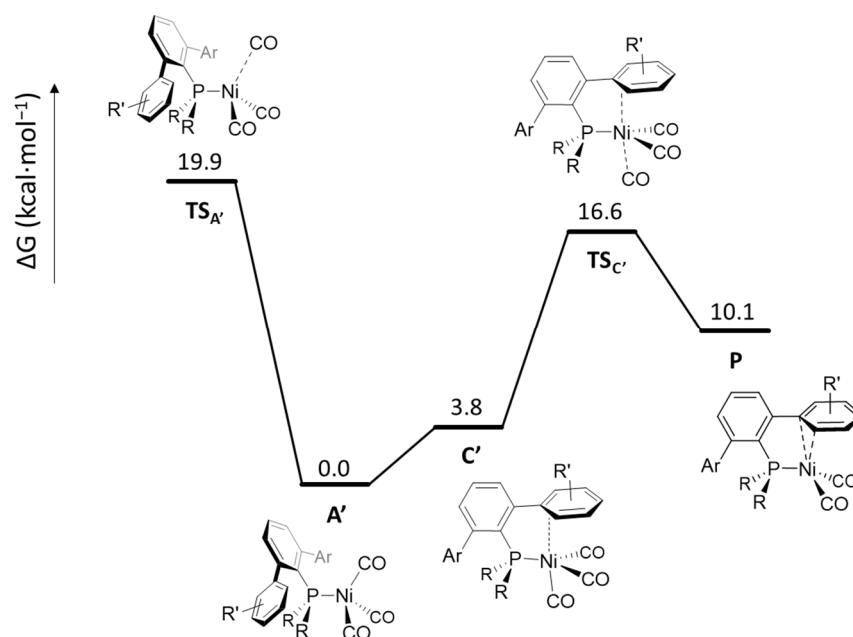


Figure 36. Free energy profile for the loss of a carbonyl ligand in complex  $\text{Ni}(\text{CO})_3(\text{PMe}_2\text{Ar}^{\text{Dtbp}_2})$ .

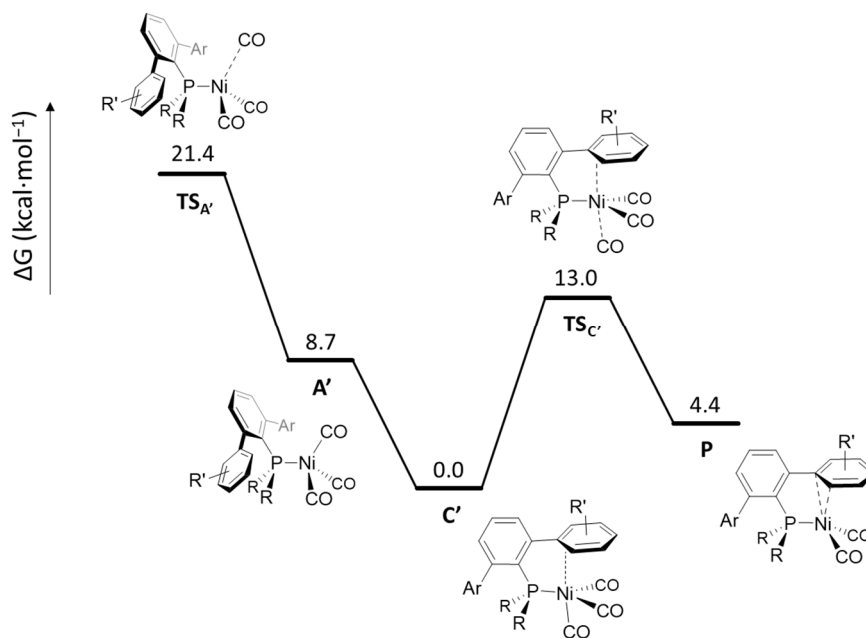
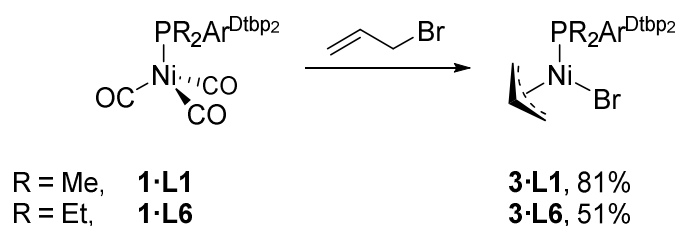


Figure 37. Free energy profile for the loss of a carbonyl ligand in complex  $\text{Ni}(\text{CO})_3(\text{PCyp}_2\text{Ar}^{\text{Xyl}_2})$ .

## Chapter I

and subsequent formation of the allylnickel(II) compounds  $\text{NiBr}(\eta^3\text{-C}_3\text{H}_5)(\text{PR}_2\text{Ar}^{\text{Dtbp}_2})$  ( $\text{R} = \text{Me}$ , **3·L1**;  $\text{R} = \text{Et}$ , **3·L6**) as the only organometallic products (Scheme 5). Both complexes were isolated as orange solids, soluble in THF, pentane and  $\text{C}_6\text{H}_6$ , and characterised by NMR and elemental analysis.  $^{31}\text{P}\{^1\text{H}\}$  NMR singlets appear at  $-2.5$  (**3·L1**) and  $23.2$  ppm (**3·L6**), thus shifted *ca.* 35 ppm downfield relative to the free phosphine ligands, in accordance with a  $\kappa^1$  coordination mode of the  $\text{PR}_2\text{Ar}''$  in these complexes. The spectroscopic features of these derivatives will be discussed in Chapter II, along with those obtained for other allylnickel(II) complexes.

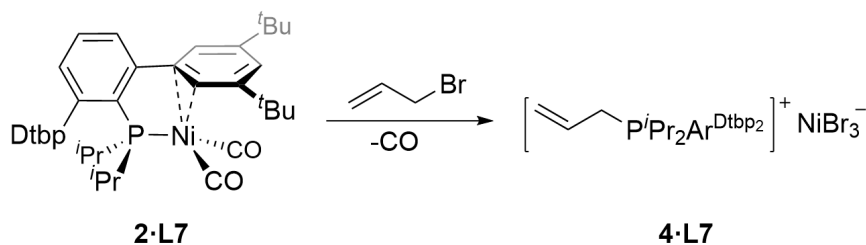


*Scheme 5. Reactivity of complexes **1·L1** and **1·L6** towards oxidative addition of allyl bromide.*

In contrast, reaction of dicarbonyl complex **2·L7** with allyl bromide yielded a green solid, insoluble in benzene, but soluble in acetone and acetonitrile. These characteristics are in agreement with a salt-like formulation, comprised of an allyl phosphonium cation,  $[(\text{C}_3\text{H}_5)\text{P}^i\text{Pr}_2\text{Ar}^{\text{Dtbp}_2}]^+$ , and a tribromonickelate anion,  $[\text{NiBr}_3]^-$  (**4·L7**, Scheme 6).

This proposal finds support in elemental analysis, as well as in NMR and ESMS spectra recorded for the phosphonium cation. Thus, in the  $^1\text{H}$  NMR spectrum (Figure 38), the allyl moiety gives rise to two signals in the olefin region and one in the aliphatic region, in a 1:2:2 ratio. The latter resonance appears as a doublet of doublets due to coupling with the phosphorus atom and with the





*Scheme 6. Reactivity of complex 2·L7 towards allyl bromide.*

neighbouring olefinic proton. The  $^{31}\text{P}\{^1\text{H}\}$  NMR spectrum displays a singlet at 42.2 ppm. Although the tribromonickelate anion could not be observed by means of ESMS, its definitive structural characterisation was not considered necessary, since there exists precedent in the literature for this anion.<sup>46</sup>

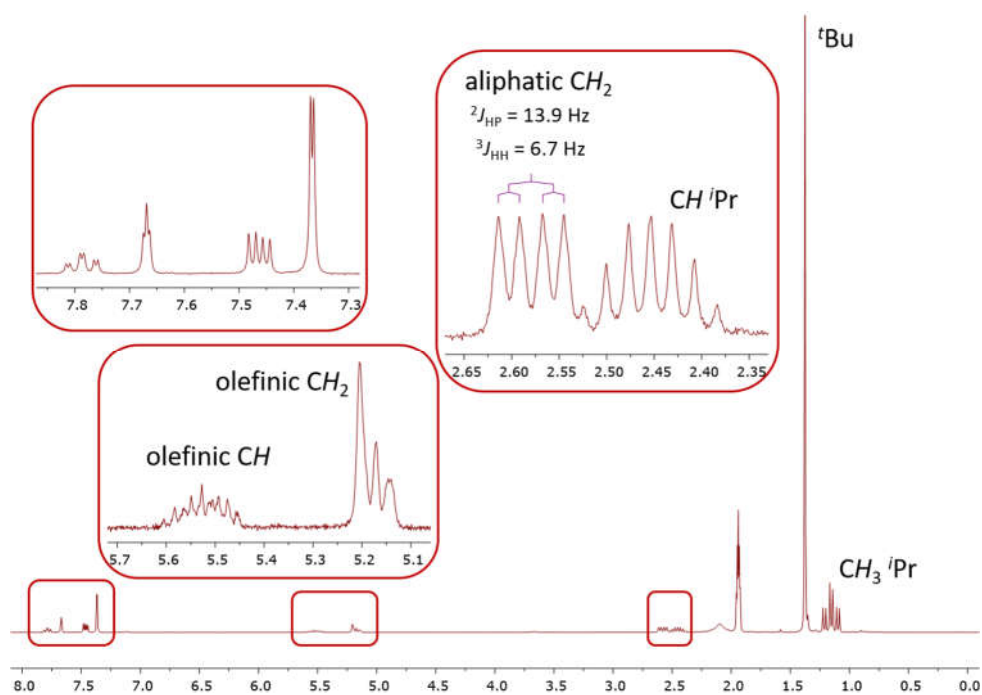
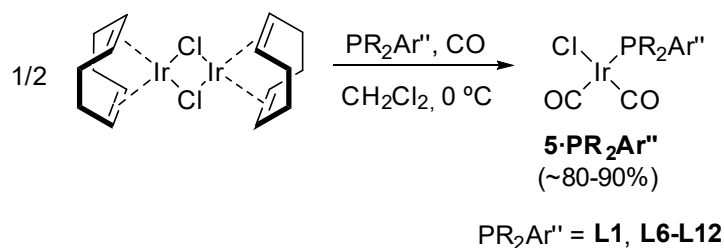


*Figure 38.  $^1\text{H}$  NMR spectrum of 4·L7 in  $\text{CD}_3\text{CN}$  at 25 °C.*

### 1.2.7. Synthesis and characterisation of iridium(I) and rhodium(I) carbonyl complexes of the dialkyl terphenyl phosphines.

Given that appropriate evaluation of the electronic properties of the bulkier phosphine ligands could not be completed through the study of their  $\text{Ni}(\text{CO})_3(\text{PR}_2\text{Ar}'')$  complexes, an alternative approach was considered, consisting on the synthesis of Ir(I) and Rh(I) carbonyl adducts of the dialkyl terphenyl phosphines. In a previous work carried out in our research group, a series of  $\text{IrCl}(\text{CO})_2(\text{PR}_2\text{Ar}'')$  complexes ( $\text{PR}_2\text{Ar}'' = \text{L2-L5}$ ) were synthesised and characterised.<sup>22d,47</sup> Thus, it was deemed of interest to complete this family with the remaining phosphines of this study, i.e. **L1** and **L6-L12** (Scheme 7).



Scheme 7. Synthesis of complexes  $\text{IrCl}(\text{CO})_2(\text{PR}_2\text{Ar}'')$ , **5-L1** and **5-L6** through **5-L12**.

Complexes bearing the phosphines **L1**, **L7**, **L10** and **L11** were isolated and spectroscopically characterised and all others were analysed by IR spectroscopy immediately after generation.  $^{31}\text{P}\{^1\text{H}\}$  NMR chemical shifts found for these complexes span a broad range, mainly depending on the nature of the R substituents, *ca.* 15-33 ppm toward higher frequency relative to the free phosphine ligands (Table 8).  $^1\text{H}$  NMR spectra feature a symmetrical environment around the terphenyl moiety, implying that no significant interaction exists between the metal centre and the side aryl rings, as shown in the  $^1\text{H}$  NMR

spectrum of **5·L1** (Figure 39). Finally, in the  $^{13}\text{C}\{^1\text{H}\}$  NMR spectra, two different signals can be observed arising from the carbonyl ligands, one at around 175-180 ppm ( $^2J_{\text{CP}} \approx 115\text{-}125$  Hz), corresponding to the CO ligand *trans* to the phosphine, and the other at around 165-170 ppm ( $^2J_{\text{CP}} \approx 11\text{-}13$  Hz), from the CO ligand in the *cis* position (Figure 40).

Ligand	Complex	$\delta$ (ppm)	$\Delta\delta$ (ppm)
<b>L1</b>	$\text{IrCl}(\text{CO})_2(\text{PMe}_2\text{Ar}^{\text{Dtbp}_2})$	-3.5	33.1
<b>L7</b>	$\text{IrCl}(\text{CO})_2(\text{P}^i\text{Pr}_2\text{Ar}^{\text{Dtbp}_2})$	40.6	28.0
<b>L10</b>	$\text{IrCl}(\text{CO})_2(\text{P}^i\text{Pr}_2\text{Ar}^{\text{Xyl}_2})$	38.7	22.5
<b>L11</b>	$\text{IrCl}(\text{CO})_2(\text{PCyp}_2\text{Ar}^{\text{Xyl}_2})$	20.0	15.4

Table 8.  $^{31}\text{P}\{^1\text{H}\}$  NMR chemical shifts ( $\delta$ ) of complexes **5·PR<sub>2</sub>Ar''** and difference with the corresponding free phosphines ( $\Delta\delta$ ).

The structure of **5·L1** was confirmed by X-ray diffraction studies (Figure 41). Just as **5·L2** and **5·L3** retain a phosphine configuration akin to **B** in the solid state,<sup>22d</sup> **L1** maintains conformation **A** in complex **5·L1**. Ostensibly, due to the lower steric requirements of a square-planar  $\text{IrCl}(\text{CO})_2$  fragment, relative to the tetrahedral  $\text{Ni}(\text{CO})_3$ , conformation **B** remains favoured for **L2** and **L3** when coordinated to iridium. It is worth mentioning that, while in **5·L2** and **5·L3**, the  $\text{IrCl}(\text{CO})_2$  moiety is placed parallel to the neighbouring side ring, in **5·L1** one of the carbonyl ligands is positioned nearly parallel to the  $\text{P}-\text{C}_{\text{ipso}}$  bond ( $\text{C}_{\text{ipso}}\text{-P-Ir-CO}$  torsion =  $-6.2(1)^\circ$ ). As a result, the  $\text{Ir}(\text{CO})_2\text{Cl}$  plane is nearly perpendicular to the central aryl ring, with a small distortion that could be ascribed to crystal packing effects.

On the other hand, in the solid state structure of **5·L7** (Figure 42), the phosphine ligand displays a conformation akin to **B**, with one of the isopropyl groups almost eclipsed with the central aryl ring ( $\text{C}^i\text{Pr}-\text{P}-\text{C}_{\text{ipso}}-\text{C}_{\text{ortho}}$  torsion angle =  $3.0(5)^\circ$ ), instead of the expected conformation **C** adopted by the free,

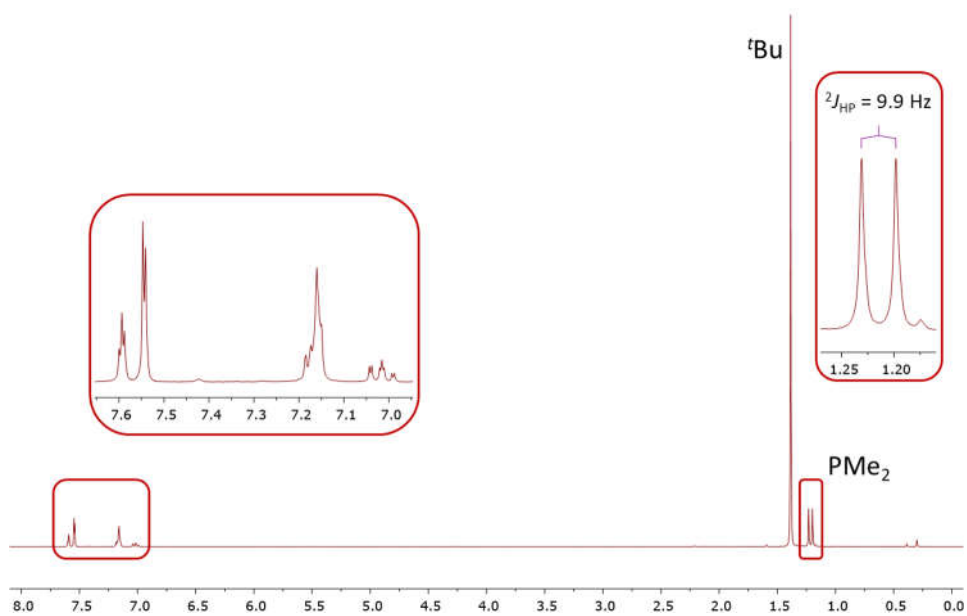


Figure 39.  $^1\text{H}$  NMR spectra of complex **5-L1** in  $\text{C}_6\text{D}_6$  at  $25^\circ\text{C}$ .

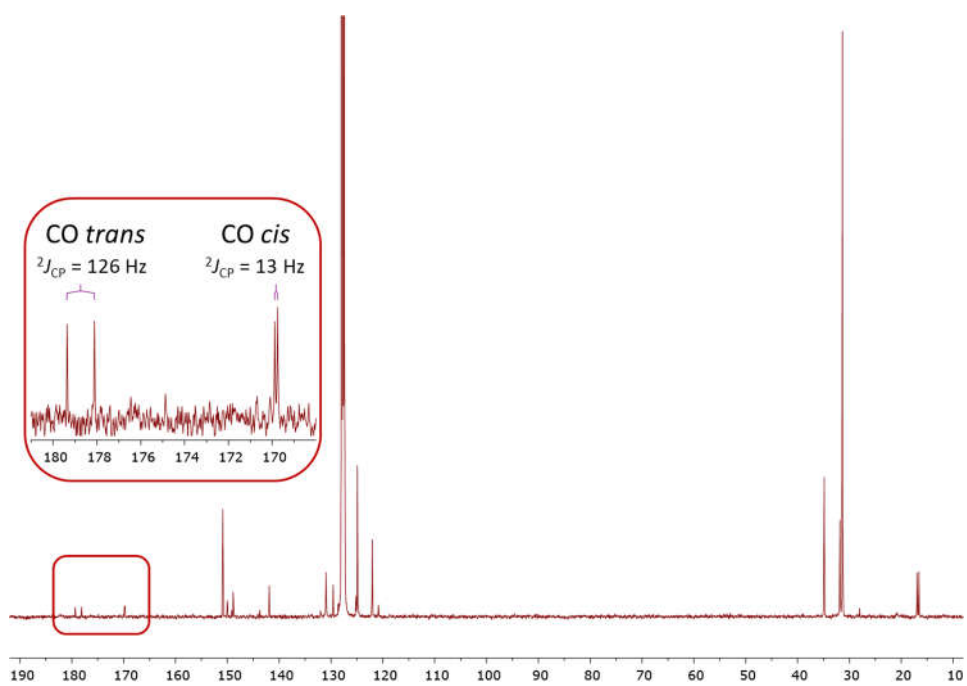


Figure 40.  $^{13}\text{C}\{^1\text{H}\}$  NMR spectra of complex **5-L1** in  $\text{C}_6\text{D}_6$  at  $25^\circ\text{C}$ .

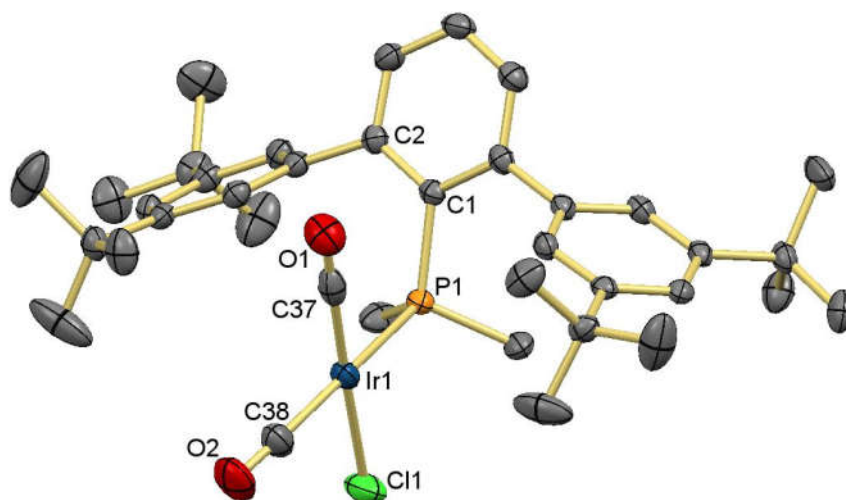


Figure 41. ORTEP view of complex **5-L1**. Hydrogen atoms and minor disorder are omitted for clarity and thermal ellipsoids are set at 50% level probability. Selected bond distances (Å) and angles (°): Ir1-P1 2.3599(6), Ir1-Cl1 2.3552(7), Ir1-C38 1.910(3), Ir1-C37 1.854(3), C37-O1 1.081(3), C38-O2 1.119(3), C37-Ir1-C38 92.85(12), C38-Ir1-Cl1 87.43(9), Cl1-Ir1-P1 87.48(2), P1-Ir1-C37 92.40(8), Ir1-P1-C1-C2 -87.50(17).

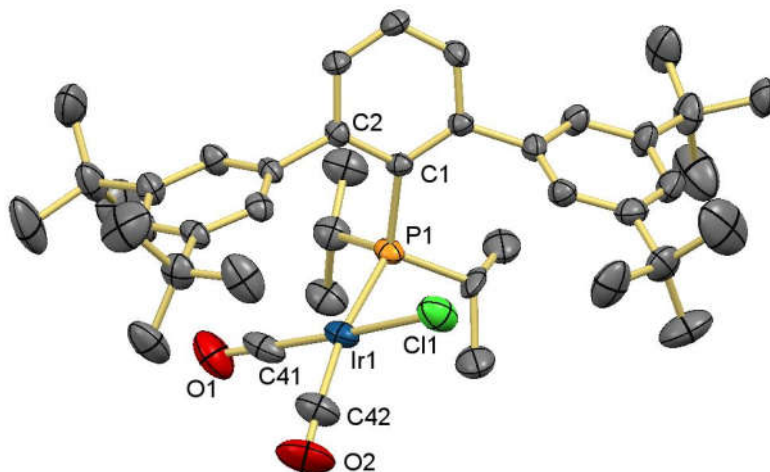


Figure 42. ORTEP view of complex **5-L7**. Hydrogen atoms and minor disorder are omitted for clarity and thermal ellipsoids are set at 50% level probability. Selected bond distances (Å) and angles (°): Ir1-P1 2.387(1), Ir1-Cl1 2.349(2), Ir1-C42 1.884(5), Ir1-C41 1.824(7), C41-O1 1.145(9), C42-O2 1.135(7), C41-Ir1-C42 90.5(3), C42-Ir1-Cl1 88.8(2), Cl1-Ir1-P1 87.33(5), P1-Ir1-C41 93.9(2), Ir-P1-C1-C2 -60.6(4).

## Chapter I

uncoordinated phosphine molecule. Presumably, such conformation would still be disfavoured due to steric hindrance between the metal centre and the nearby side aryl ring. This is manifested in the deviation from planarity of the iridium centre, as the carbonyl ligand *trans* to the phosphine ligand bends away from the neighbouring ring, leading to a P-Ir-CO angle of 170.1(2)°.

The C–O stretching frequencies recorded for complexes **5-PR<sub>2</sub>Ar''** are collected in Table 9. As already mentioned in the introduction to this chapter, the TEP of the ligands can be determined from these values by using a correlation developed by Crabtree<sup>30a</sup> and later refined by Nolan *et al.*:<sup>30b</sup>

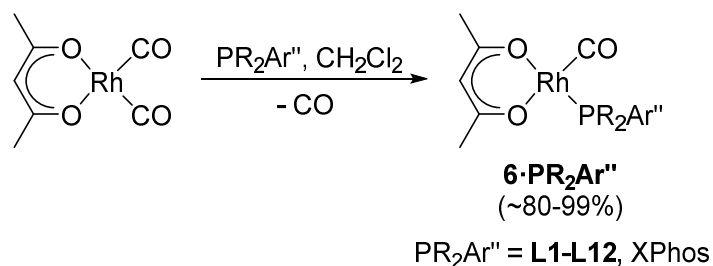
$$\text{TEP}(\text{Ir}) = 0.847 \cdot \nu_{\text{CO}}(\text{average}) + 336 \text{ cm}^{-1}$$

Where  $\nu_{\text{CO}}(\text{average})$  is the arithmetic average of the two carbonyl stretching frequencies. It is clear, however, that TEP values obtained from the IrCl(CO)<sub>2</sub>(L) complexes of terphenyl phosphines **L1-L6** and **L9** as well as biaryl phosphine XPhos differ from those observed for Ni(CO)<sub>3</sub>(L) by as much as 12 cm<sup>-1</sup> (for **L1**). Furthermore, variation among the values for similar phosphines is rather large (see, for example, the five dimethyl-substituted PMe<sub>2</sub>Ar'' phosphines, or dicyclohexyl-substituted **L9**, **L12** and XPhos<sup>28</sup>). Thus, interpretation of the IR data for the bulkier terphenyl phosphines should be made with caution.

For the sake of completeness, complexes Rh(acac)(CO)(PR<sub>2</sub>Ar'') bearing dialkyl terphenyl phosphines and biaryl phosphine XPhos were also synthesised and characterised (Scheme 8). A few representative examples, namely **6-L1**, **6-L6**,

**6-L9** and **6-L11**, were isolated and spectroscopically characterised, whereas others were analysed solely by means of IR spectroscopy directly from the reaction mixture.

As in the case of the iridium complexes, the <sup>1</sup>H NMR spectra of these compounds are relatively simple, with only one set of signals for the side aryl rings

Scheme 8. Synthesis of complexes Rh(acac)(CO)(PR<sub>2</sub>Ar''), **6·L1** through **6·L12**.

Ligand	Complex	$\nu_{\text{sym}}$	$\nu_{\text{asym}}$	TEP (Ir) <sup>a</sup>	TEP (Ni)
<b>L1</b>	IrCl(CO) <sub>2</sub> (PMe <sub>2</sub> Ar <sup>Dtbp</sup> <sub>2</sub> )	2063	1984	2051.1	2063
<b>L2</b>	IrCl(CO) <sub>2</sub> (PMe <sub>2</sub> Ar <sup>Xyl</sup> <sub>2</sub> ) <sup>b</sup>	2068	1987	2054.5	2063.8
<b>L3</b>	IrCl(CO) <sub>2</sub> (PMe <sub>2</sub> Ar <sup>Dipp</sup> <sub>2</sub> ) <sup>b</sup>	2067	1987	2054.1	2062.9
<b>L4</b>	IrCl(CO) <sub>2</sub> (PMe <sub>2</sub> Ar <sup>Mes</sup> <sub>2</sub> ) <sup>b</sup>	2066	1986	2053.2	2063
<b>L5</b>	IrCl(CO) <sub>2</sub> (PMe <sub>2</sub> Ar <sup>Tripp</sup> <sub>2</sub> ) <sup>b</sup>	2065	1986	2052.8	2062
<b>L6</b>	IrCl(CO) <sub>2</sub> (PEt <sub>2</sub> Ar <sup>Dtbp</sup> <sub>2</sub> )	2061	1983	2049.8	2061
<b>L7</b>	IrCl(CO) <sub>2</sub> (P <sup>i</sup> Pr <sub>2</sub> Ar <sup>Dtbp</sup> <sub>2</sub> )	2060	1980	2048.2	-
<b>L8</b>	IrCl(CO) <sub>2</sub> (PCyp <sub>2</sub> Ar <sup>Dtbp</sup> <sub>2</sub> )	2058	1978	2046.5	-
<b>L9</b>	IrCl(CO) <sub>2</sub> (PCy <sub>2</sub> Ar <sup>Dtbp</sup> <sub>2</sub> )	2056	1980	2046.5	2060
<b>L10</b>	IrCl(CO) <sub>2</sub> (P <sup>i</sup> Pr <sub>2</sub> Ar <sup>Xyl</sup> <sub>2</sub> )	2064	1982	2050.7	-
<b>L11</b>	IrCl(CO) <sub>2</sub> (PCyp <sub>2</sub> Ar <sup>Xyl</sup> <sub>2</sub> )	2063	1979	2049.0	-
<b>L12</b>	IrCl(CO) <sub>2</sub> (PCy <sub>2</sub> Ar <sup>Xyl</sup> <sub>2</sub> )	2062	1980	2049.0	-
XPhos	IrCl(CO) <sub>2</sub> (PCy <sub>2</sub> Ar <sup>Tripp</sup> ) <sup>c</sup>	2070	1985	2053.3	2059
PMe <sub>2</sub> Ph	IrCl(CO) <sub>2</sub> (PMe <sub>2</sub> Ph) <sup>d</sup>	2084	1999	2066.4	2065.3 <sup>e</sup>

Table 9. IR wavenumbers (cm<sup>-1</sup>) for the C–O stretching vibrations in some IrCl(CO)<sub>2</sub>(L) complexes in CH<sub>2</sub>Cl<sub>2</sub> solution. <sup>a</sup>Calculated using the correlation found in ref. 28. <sup>b</sup>From ref. 47. <sup>c</sup>From ref. 28. <sup>d</sup>From ref. 30a. <sup>e</sup>From ref. 25.

of the phosphine (Figure 43). It should be noted that, in the spectrum shown for **6·L1**, the Dtbp rings show some fluxionality, but this was not investigated further. Also, the methyl groups give rise to somewhat broadened signals, though with discernable coupling to both the <sup>103</sup>Rh and the <sup>31</sup>P nuclei, giving rise to a doublet of doublets (<sup>2</sup>J<sub>HP</sub> = 9.1 Hz, <sup>3</sup>J<sub>HRh</sub> = 1.9 Hz). The carbonyl ligand resonance, which

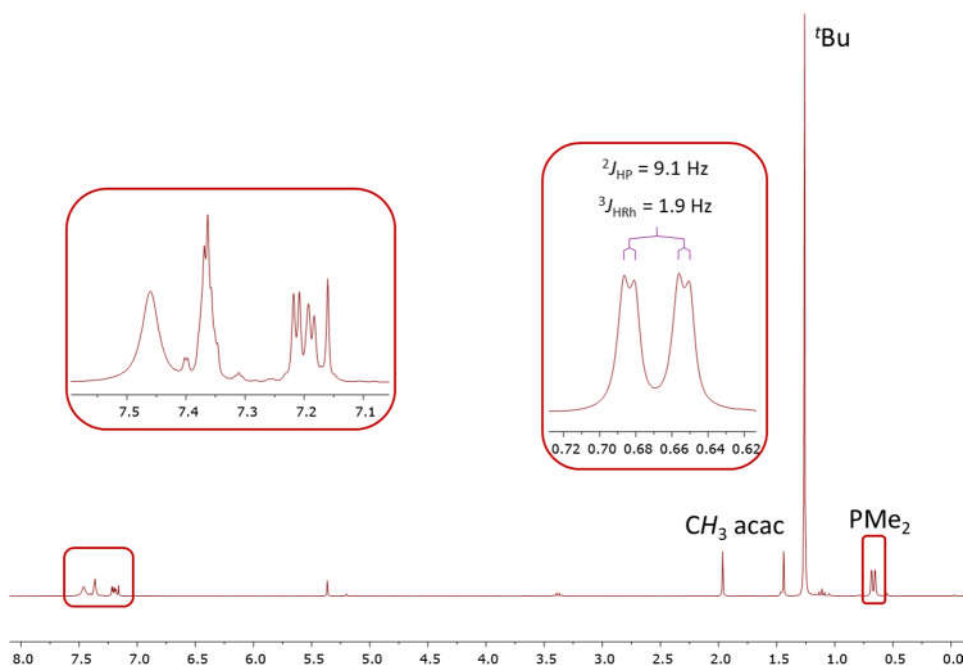


Figure 43.  $^1\text{H}$  NMR spectrum of complex **6-L1** in  $\text{C}_6\text{D}_6$  at 25 °C.

appears at a chemical shift around 190-192 ppm in the  $^{13}\text{C}\{^1\text{H}\}$  NMR spectrum, also shows the coupling with the two magnetically active nuclei ( $^1J_{\text{CRh}} \approx 77$  Hz,  $^2J_{\text{CP}} \approx 24$  Hz). The  $^{31}\text{P}\{^1\text{H}\}$  NMR spectra of **6-PR<sub>2</sub>Ar''** exhibit doublets ( $^1J_{\text{PRh}}$  between 166-184 Hz) at *ca.* 54-68 ppm to higher frequency with respect to the uncoordinated phosphines (Table 10), quite uncommon for a  $\kappa^1$  mode of coordination.

Ligand	Complex	$\delta$ (ppm)	$\Delta\delta$ (ppm)
<b>L1</b>	$\text{Rh}(\text{acac})(\text{CO})(\text{PMe}_2\text{Ar}^{\text{Dtbp}_2})$	28.4	65.0
<b>L6</b>	$\text{Rh}(\text{acac})(\text{CO})(\text{PEt}_2\text{Ar}^{\text{Dtbp}_2})$	52.4	65.2
<b>L9</b>	$\text{Rh}(\text{acac})(\text{CO})(\text{PCy}_2\text{Ar}^{\text{Dtbp}_2})$	69.4	67.8
<b>L11</b>	$\text{Rh}(\text{acac})(\text{CO})(\text{PCyp}_2\text{Ar}^{\text{Xyl}_2})$	58.3	53.7

Table 10.  $^{31}\text{P}\{^1\text{H}\}$  NMR chemical shifts ( $\delta$ ) of complexes **6-PR<sub>2</sub>Ar''** and difference with the corresponding free phosphines ( $\Delta\delta$ ).



In the solid state structure, **6·L1** shows a disposition similar to its iridium analogue **5·L1**, with the phosphine adopting a conformation of type **A** and the Rh(acac)(CO) fragment contained in the symmetry plane perpendicular to the central aryl ring of the terphenyl moiety (Figure 44).

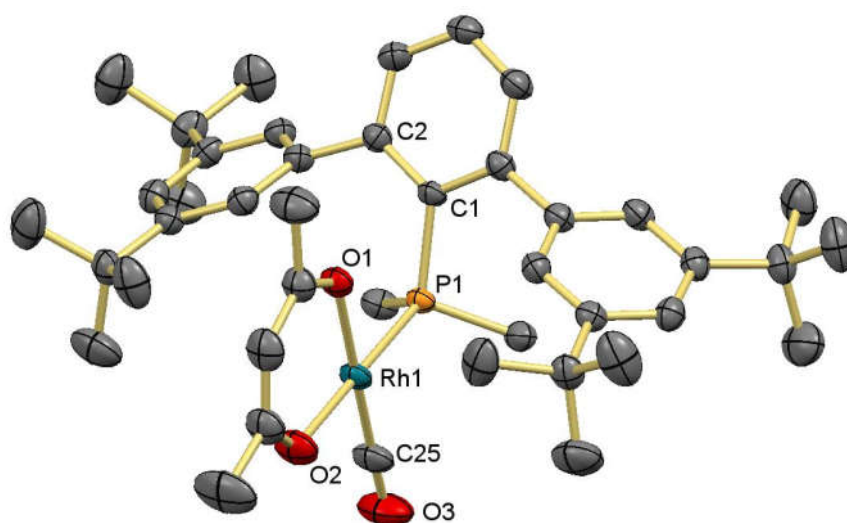


Figure 44. ORTEP view of complex **6·L1**. Hydrogen atoms and minor disorder are omitted for clarity and thermal ellipsoids are set at 50% level probability. Selected bond distances (Å) and angles (°): Rh1-P1 2.2374(11), Rh1-O1 2.051(3), Rh1-O2 2.068(3), Rh1-C25 1.797(5), C25-O3 1.162(7), P1-Rh1-O1 92.22(9), O1-Rh1-O2 88.65(14), O2-Rh1-C25 91.90(19), C25-Rh1-P1 87.23(16), Rh1-P1-C1-C2 -94.0(3).

C–O stretching frequencies recorded for these complexes are collected in Table 11, spanning the range 1954–1963  $\text{cm}^{-1}$ . As in the case of the iridium complexes discussed above, IR data do not correlate well with the TEPs observed in the  $\text{Ni}(\text{CO})_3(\text{L})$  complexes nor, in some cases, with the trends based on predicted electron-donating capacities (for instance, a higher  $\nu_{\text{CO}}$  for **6·XPhos** than for adducts of the dimethyl-substituted  $\text{PMe}_2\text{Ar}''$  phosphines **6·L1** through **6·L5**).

Ligand	Complex	$\nu_{\text{CO}}$	TEP (Ni)
L1	Rh(acac)(CO)(PMe <sub>2</sub> Ar <sup>Dtbp<sub>2</sub></sup> )	1961	2063
L2	Rh(acac)(CO)(PMe <sub>2</sub> Ar <sup>Xyl<sub>2</sub></sup> )	1960	2063.8
L3	Rh(acac)(CO)(PMe <sub>2</sub> Ar <sup>Dipp<sub>2</sub></sup> )	1962	2062.9
L4	Rh(acac)(CO)(PMe <sub>2</sub> Ar <sup>Mes<sub>2</sub></sup> )	1960	2063
L5	Rh(acac)(CO)(PMe <sub>2</sub> Ar <sup>Tripp<sub>2</sub></sup> )	1960	2062
L6	Rh(acac)(CO)(PEt <sub>2</sub> Ar <sup>Dtbp<sub>2</sub></sup> )	1959	2061
L7	Rh(acac)(CO)(P <sup>i</sup> Pr <sub>2</sub> Ar <sup>Dtbp<sub>2</sub></sup> )	1958	-
L8	Rh(acac)(CO)(PCyp <sub>2</sub> Ar <sup>Dtbp<sub>2</sub></sup> )	1957	-
L9	Rh(acac)(CO)(PCy <sub>2</sub> Ar <sup>Dtbp<sub>2</sub></sup> )	1957	2060
L10	Rh(acac)(CO)(P <sup>i</sup> Pr <sub>2</sub> Ar <sup>Xyl<sub>2</sub></sup> )	1958	-
L11	Rh(acac)(CO)(PCyp <sub>2</sub> Ar <sup>Xyl<sub>2</sub></sup> )	1956	-
L12	Rh(acac)(CO)(PCy <sub>2</sub> Ar <sup>Xyl<sub>2</sub></sup> )	1954	-
XPhos	Rh(acac)(CO)(PCy <sub>2</sub> Ar <sup>Tripp</sup> )	1963	2059
PMe <sub>2</sub> Ph	Rh(acac)(CO)(PMe <sub>2</sub> Ph) <sup>a</sup>	1971	2065.3

Table 11. IR wavenumbers ( $\text{cm}^{-1}$ ) for the C–O stretching vibrations in some Rh(acac)(CO)(L) complexes in CH<sub>2</sub>Cl<sub>2</sub> solution. <sup>a</sup>From ref. 48.

On the other hand, as shown in Figure 45, there is a moderately good correlation ( $R^2 = 0.9223$ ) between the  $\nu_{\text{CO}}$  values in IrCl(CO)<sub>2</sub>(L) and Rh(acac)(CO)(L) complexes of the phosphines considered in this section. Two possible reasons for this correlation that appears not to be extendable to the Ni(CO)<sub>3</sub>(L) complexes, could be: (a) some effect other than electronics (e.g. sterics) affecting the TEPs of the nickel complexes or (b) the same effect (e.g. a weak M $\cdots$ C<sub>arene</sub> interaction) influencing the square-planar IrCl(CO)<sub>2</sub>(L) and Rh(acac)(CO)(L) complexes.

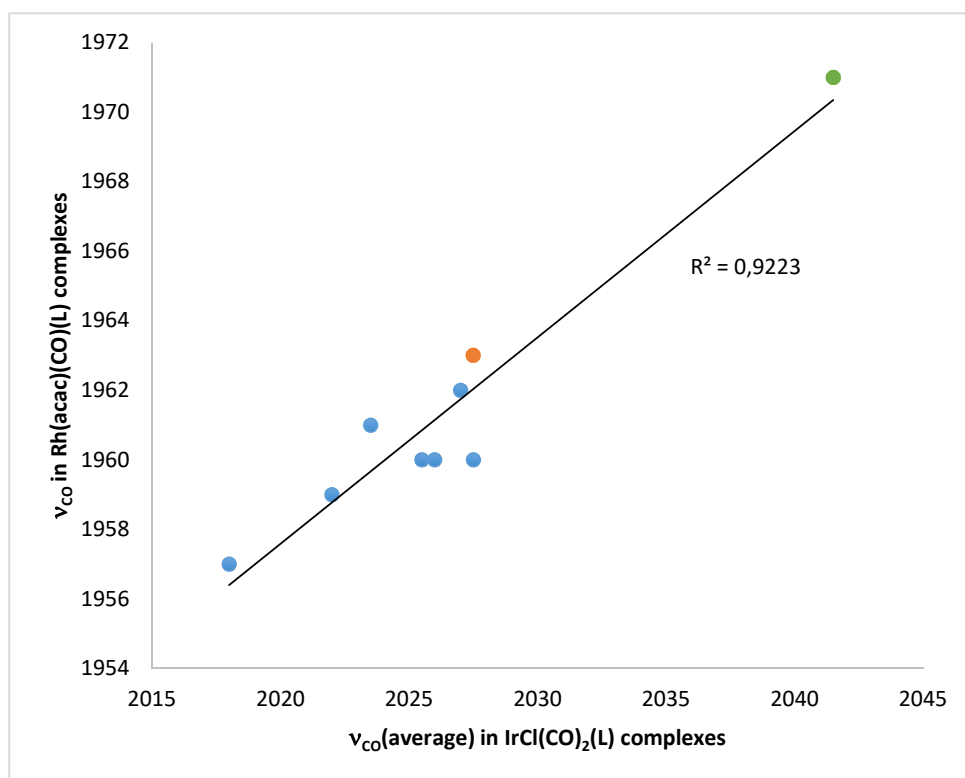


Figure 45. Correlation between  $\text{IrCl}(\text{CO})_2(\text{L})$   $\nu_{\text{CO}}(\text{average})$  and  $\text{Rh}(\text{acac})(\text{CO})(\text{L})$   $\nu_{\text{CO}}$  values. Orange point: XPhos, green point:  $\text{PMe}_2\text{Ph}$ .



### I.3. SUMMARY OF THE RESULTS

A series of dialkyl terphenyl phosphines,  $\text{PR}_2\text{Ar}''$ , have been synthesised, characterised and their stabilities towards oxidation by air probed. In the solid state, both new and previously reported  $\text{PR}_2\text{Ar}''$  molecules adopt one of three conformations, depending on the disposition of the alkyl groups.

$\text{Ni}(\text{CO})_3(\text{PR}_2\text{Ar}'')$  complexes of the less bulky phosphines (with R = Me or Et) were synthesised and characterised. By measuring their IR spectra, it can be inferred that  $\text{PR}_2\text{Ar}''$  phosphines lead to slightly lower TEP values than their  $\text{PR}_2\text{Ph}$  analogues, indicating a higher donor capacity of the former.

For the bulkier members of the family (R = *i*Pr, Cyp or Cy), heating under vacuum resulted in compounds of formula  $\text{Ni}(\text{CO})_2(\text{PR}_2\text{Ar}'')$ , where a second carbonyl ligand has been replaced by a weak  $\eta^2$  interaction with one of the side aryl rings of the phosphine.

DFT calculations suggest that the presence of bulky alkyl groups on the phosphorus atom causes destabilisation of  $\text{Ni}(\text{CO})_3(\text{PR}_2\text{Ar}'')$  molecules, thus facilitating the loss of a carbonyl ligand.

TEP values obtained from the IR spectra of  $\text{IrCl}(\text{CO})_2(\text{PR}_2\text{Ar}'')$  complexes do not correlate well with those found in the  $\text{Ni}(\text{CO})_3(\text{PR}_2\text{Ar}'')$  system.



## I.4. EXPERIMENTAL SECTION

### I.4.1. General considerations.

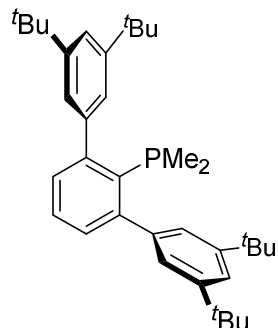
All preparations and manipulations were carried out under an atmosphere of dry oxygen-free nitrogen by means of standard Schlenk techniques or glovebox techniques. Solvents were rigorously dried and degassed before use. Ar''MgBr were prepared by following the synthesis reported by Power<sup>49</sup> for the related Ar<sup>Xyl</sup><sub>2</sub> compounds without adding I<sub>2</sub> in the last step of the preparation. Ligands **L2-L5**<sup>16a,22a,22d,22e</sup> and **L11**,<sup>38</sup> and complexes Ni(cod)<sub>2</sub><sup>50</sup> and [Ir(μ-Cl)(cod)]<sub>2</sub><sup>51</sup> were synthesised by following previously reported procedures. PCl<sub>3</sub> was distilled prior to use and kept under a nitrogen atmosphere. Other chemicals were purchased from commercial sources and used as received. Solution NMR spectra were recorded on Bruker Avance DPX-300, DRX-400 and DRX-500, and 400 Ascend/R spectrometers. The <sup>1</sup>H and <sup>13</sup>C resonances of the solvent were used as the internal standard and the chemical shifts are reported relative to TMS while <sup>31</sup>P was referenced to external H<sub>3</sub>PO<sub>4</sub>. Infrared spectra were recorded on a Bruker Vector 22 spectrometer and at the Infrared Spectroscopy Service of the Instituto de Ciencia de Materiales de Sevilla (ICMS). Microanalyses were performed by the Microanalytical Service of the Instituto de Investigaciones Químicas (IIQ). X-ray diffraction data were collected on Bruker KAPPA APEX II diffractometer (CITIUS) and Bruker Nonius X8 APEX-II Diffractometer (IIQ) and processed by Dr. Eleuterio Álvarez and Dr. Celia Maya. Mass spectra were performed by the Mass Spectrometry Service of the Instituto de Investigaciones Químicas (IIQ).

## **I.4.2. Synthesis of phosphine ligands.**

### **I.4.2.1. General procedure for the synthesis of $\text{PMe}_2\text{Ar}^{\text{Dtbp}_2}$ (L1) and $\text{PEt}_2\text{Ar}^{\text{Dtbp}_2}$ (L6).**

A freshly prepared solution of  $\text{Ar}^{\text{Dtbp}_2}\text{MgBr}$  (3.6 mmol) in THF (*ca.* 20 mL) was added dropwise to a solution of an equimolar amount of  $\text{PCl}_3$  in THF (0.30 mL, 3.6 mmol) at  $-80\text{ }^\circ\text{C}$ . The reaction mixture was allowed to reach slowly the room temperature and stirred overnight. All volatiles were removed by evaporation under reduced pressure and the solid residue was extracted three times with pentane ( $3 \times 10\text{ mL}$ ). The combined organic fractions were dried under vacuum giving a mixture of the three dihalophosphines  $\text{PCl}_2\text{Ar}^{\text{Dtbp}_2}$ ,  $\text{PBr}_2\text{Ar}^{\text{Dtbp}_2}$ , and  $\text{PCl}(\text{Br})\text{Ar}^{\text{Dtbp}_2}$ , as a pale yellow solid, which was redissolved in THF (*ca.* 20 mL). A commercial solution of  $\text{RMgBr}$  (7.8 mmol) was added dropwise at  $-80\text{ }^\circ\text{C}$ , the mixture was allowed to reach slowly the room temperature, and stirred overnight. The volatiles were removed under reduced pressure and the solid residue was extracted with pentane ( $3 \times 10\text{ mL}$ ). The combined organic fractions were taken to dryness affording a pale yellow solid which was washed with MeOH at  $0\text{ }^\circ\text{C}$ .



**I.4.2.1.1.  $\text{PMe}_2\text{Ar}^{\text{Dtbp}_2}$  (L1).**

$^1\text{H}$  NMR ( $\text{CDCl}_3$ , 400.1 Hz, 298 K):  $\delta$  7.44 (s, 2 H, *p*-Dtbp), 7.38 (t, 1 H,  $^3J_{\text{HH}} = 7.5$  Hz, *p*- $\text{C}_6\text{H}_3$ ), 7.33 (s, 4 H, *o*-Dtbp), 7.29 (d, 2 H,  $^3J_{\text{HH}} = 7.5$  Hz, *m*- $\text{C}_6\text{H}_3$ ), 1.40 (s, 36 H,  $\text{CH}_3$   $^t\text{Bu}$ ), 0.69 (d, 6 H,  $^2J_{\text{HP}} = 5.0$  Hz, *P*- $\text{CH}_3$ ).

$^{13}\text{C}\{^1\text{H}\}$  NMR ( $\text{CDCl}_3$ , 100.6 Hz, 298 K):  $\delta$  150.3 (s, *m*-Dtbp), 149.2 (d,  $^2J_{\text{CP}} = 12$  Hz, *o*- $\text{C}_6\text{H}_3$ ), 142.9 (d,  $^3J_{\text{CP}} = 3$  Hz, *ipso*-Dtbp), 129.8 (s, *m*- $\text{C}_6\text{H}_3$ ), 127.2 (s, *p*- $\text{C}_6\text{H}_3$ ), 124.5 (d,  $^4J_{\text{CP}} = 3$  Hz, *o*-Dtbp), 120.9 (s, *p*-Dtbp), 35.1 (s, C  $^t\text{Bu}$ ), 31.8 (s,  $\text{CH}_3$   $^t\text{Bu}$ ), 15.5 (d,  $^1J_{\text{CP}} = 15$  Hz, *P*- $\text{CH}_3$ ).

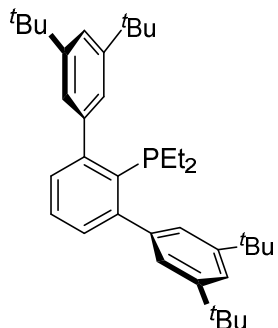
$^{31}\text{P}\{^1\text{H}\}$  NMR ( $\text{CDCl}_3$ , 162.0 MHz, 298 K):  $\delta$  -36.6 (s).

Elemental analysis (%), calculated (found) for  $\text{C}_{36}\text{H}_{51}\text{P}$ : C, 84.00 (83.89); H, 9.99 (10.01).

Yield: 1.31 g, 71%.

Chapter I

**I.4.2.1.2.  $\text{PEt}_2\text{Ar}^{\text{Dtbp}_2}$  (L6).**



$^1\text{H}$  NMR ( $\text{CDCl}_3$ , 400.1 Hz, 298 K):  $\delta$  7.42 (s, 2 H, *p*-Dtbp), 7.37 (t, 1 H,  $^3J_{\text{HH}} = 7.5$  Hz, *p*- $\text{C}_6\text{H}_3$ ), 7.25 (d, 2 H,  $^3J_{\text{HH}} = 6.6$  Hz, *m*- $\text{C}_6\text{H}_3$ ), 7.19 (s, 4 H, *o*-Dtbp), 1.38 (s, 36 H,  $\text{CH}_3$   $^t\text{Bu}$ ), 1.30-1.14 (m, 2 H,  $\text{CH}_2$  Et), 0.82 (dt,  $^2J_{\text{HP}} = 15.3$  Hz,  $^3J_{\text{HH}} = 7.2$  Hz, 6 H,  $\text{CH}_3$  Et).

$^{13}\text{C}\{^1\text{H}\}$  NMR ( $\text{CDCl}_3$ , 100.6 Hz, 298 K):  $\delta$  151.4 (d,  $^2J_{\text{CP}} = 15$  Hz, *o*- $\text{C}_6\text{H}_3$ ), 149.5 (s, *m*-Dtbp), 142.8 (d,  $^3J_{\text{CP}} = 5$  Hz, *ipso*-Dtbp), 133.1 (d,  $^1J_{\text{CP}} = 31$  Hz, *ipso*- $\text{C}_6\text{H}_3$ ), 130.0 (d,  $^2J_{\text{CP}} = 3$  Hz, *m*- $\text{C}_6\text{H}_3$ ), 127.5 (s, *p*- $\text{C}_6\text{H}_3$ ), 124.4 (d,  $^4J_{\text{CP}} = 2$  Hz, *o*-Dtbp), 120.7 (s, *p*-Dtbp), 35.0 (s, C  $^t\text{Bu}$ ), 31.7 (s,  $\text{CH}_3$   $^t\text{Bu}$ ), 20.38 (d,  $^1J_{\text{CP}} = 13$  Hz,  $\text{CH}_2$  Et), 11.1 (d,  $^1J_{\text{CP}} = 18$  Hz,  $\text{CH}_3$  Et).

$^{31}\text{P}\{^1\text{H}\}$  NMR ( $\text{CDCl}_3$ , 162.0 MHz, 298 K):  $\delta$  -12.8 (s).

Elemental analysis (%), calculated (found) for  $\text{C}_{36}\text{H}_{51}\text{P}$ : C, 84.04 (83.81); H, 10.21 (10.37).

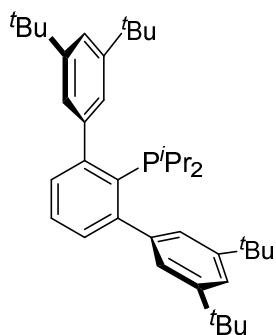
Yield: 1.27 g, 65%.

**I.4.2.2. General procedure for the synthesis of bulky dialkyl terphenyl phosphines,  $\text{PR}_2\text{Ar}''$  (R = *i*Pr, Cyp, Cy; L7-L12).**

A freshly prepared solution of alkyl magnesium bromide in THF (4 eq, diluted to *ca.* 0.5 M) was added dropwise at  $-20\text{ }^\circ\text{C}$  to a stirred solution of  $\text{PX}_2\text{Ar}''$  (1 eq, *ca.* 2 g) in THF (20 mL) in the presence of CuCl (1.5 eq). After addition was completed, the dark reaction mixture was allowed to slowly reach room temperature while stirring overnight. The insoluble material was removed by filtration. Volatiles were removed from the resulting solution under reduced pressure and the residue was extracted with pentane ( $4 \times 25\text{ mL}$ ). The combined organic fractions were again taken to dryness under reduced pressure yielding a pale yellow oil, which was treated with HCl (1 eq, 1 M in  $\text{Et}_2\text{O}$ ). A colourless solid separated out immediately, which was collected by filtration, washed with pentane ( $3 \times 10\text{ mL}$ ), and treated with excess aqueous ammonia (25%). The aqueous phase was then extracted with  $\text{CH}_2\text{Cl}_2$  ( $1 \times 20 + 2 \times 10\text{ mL}$ ) in a separating funnel. The combined organic phases were dried over  $\text{MgSO}_4$  and the solvent was removed in a rotary evaporator. The resulting pale yellow solid (sticky in some cases) was washed with methanol MeOH ( $2 \times 5\text{ mL}$ ) at  $0\text{ }^\circ\text{C}$  and, if necessary, recrystallised from  $\text{Et}_2\text{O}/\text{EtOH}$  (*ca.* 1:2) at  $-32\text{ }^\circ\text{C}$ .

Chapter I

**1.4.2.2.1. P<sup>i</sup>Pr<sub>2</sub>Ar<sup>Dtbp<sub>2</sub></sup> (L7).**



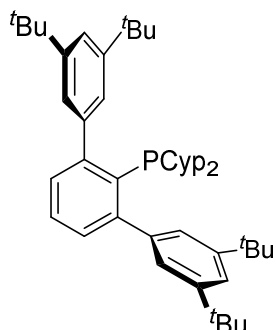
<sup>1</sup>H NMR (CDCl<sub>3</sub>, 400.1 Hz, 298 K): δ 7.34 (t, 2 H, <sup>4</sup>J<sub>HH</sub> = 1.7 Hz, *p*-Dtbp), 7.32 (t, 1 H, <sup>3</sup>J<sub>HH</sub> = 7.5 Hz, *p*-C<sub>6</sub>H<sub>3</sub>), 7.19 (dd, 2 H, <sup>4</sup>J<sub>HP</sub> = 1.6 Hz, <sup>3</sup>J<sub>HH</sub> = 7.5 Hz, *m*-C<sub>6</sub>H<sub>3</sub>), 7.09 (d, 4 H, <sup>4</sup>J<sub>HH</sub> = 1.7 Hz, *o*-Dtbp), 1.59 (dsept, 2 H, <sup>3</sup>J<sub>HH</sub> ≈ <sup>2</sup>J<sub>HP</sub> ≈ 6.9 Hz, CH<sup>*i*</sup>Pr), 1.33 (s, 36 H, CH<sub>3</sub><sup>*t*</sup>Bu), 0.84 (dd, 6 H, <sup>3</sup>J<sub>HH</sub> = 6.9 Hz, <sup>3</sup>J<sub>HP</sub> = 13.0 Hz, CH<sub>3</sub><sup>*i*</sup>Pr), 0.74 (dd, 6 H, <sup>3</sup>J<sub>HH</sub> = 6.9 Hz, <sup>3</sup>J<sub>HP</sub> = 16.0 Hz, CH<sub>3</sub><sup>*i*</sup>Pr).

<sup>13</sup>C{<sup>1</sup>H} NMR (CDCl<sub>3</sub>, 100.6 Hz, 298 K): δ 151.2 (d, <sup>2</sup>J<sub>CP</sub> = 14 Hz, *o*-C<sub>6</sub>H<sub>3</sub>), 149.3 (s, *m*-Dtbp), 143.4 (d, <sup>3</sup>J<sub>CP</sub> = 5 Hz, *ipso*-Dtbp), 130.1 (s, *m*-C<sub>6</sub>H<sub>3</sub>), 127.5 (s, *p*-C<sub>6</sub>H<sub>3</sub>), 124.7 (s, *o*-Dtbp), 120.2 (s, *p*-Dtbp), 35.1 (s, C<sup>*t*</sup>Bu), 31.8 (s, CH<sub>3</sub><sup>*t*</sup>Bu), 25.5 (d, <sup>2</sup>J<sub>CP</sub> = 17 Hz, CH<sup>*i*</sup>Pr), 22.8 (d, <sup>2</sup>J<sub>CP</sub> = 15 Hz, CH<sub>3</sub><sup>*i*</sup>Pr), 22.4 (d, <sup>2</sup>J<sub>CP</sub> = 29 Hz, CH<sub>3</sub><sup>*i*</sup>Pr).

<sup>31</sup>P{<sup>1</sup>H} NMR (CDCl<sub>3</sub>, 162.0 MHz, 298 K): δ 12.6 (s).

Elemental analysis (%), calculated (found) for C<sub>40</sub>H<sub>59</sub>P: C, 84.16 (84.24); H, 10.42 (10.12).

Yield: 1.00 g, 49%.

**I.4.2.2.2. PCyp<sub>2</sub>Ar<sup>Dtbp<sub>2</sub></sup> (L8).**

<sup>1</sup>H NMR (CDCl<sub>3</sub>, 400.1 Hz, 298 K): δ 7.35 (s, 2 H, *p*-Dtbp), 7.31 (t, 1 H, <sup>3</sup>J<sub>HH</sub> = 7.5 Hz, *p*-C<sub>6</sub>H<sub>3</sub>), 7.17 (d, 2 H, <sup>3</sup>J<sub>HH</sub> = 7.5 Hz, *m*-C<sub>6</sub>H<sub>3</sub>), 7.11 (d, 4 H, <sup>4</sup>J<sub>HH</sub> = 1.7 Hz, *o*-Dtbp), 1.80-1.56 (m, 4 H, CH and CH<sub>2</sub> Cyp), 1.54-0.91 (m, 14 H, CH<sub>2</sub> Cyp), 1.33 (s, 36 H, CH<sub>3</sub> <sup>t</sup>Bu).

<sup>13</sup>C{<sup>1</sup>H} NMR (CDCl<sub>3</sub>, 100.6 Hz, 298 K): δ 151.4 (br s, *o*-C<sub>6</sub>H<sub>3</sub>), 149.2 (s, *m*-Dtbp), 143.4 (s, *ipso*-Dtbp), 135.3 (d, <sup>1</sup>J<sub>CP</sub> = 30 Hz, *ipso*-C<sub>6</sub>H<sub>3</sub>), 130.0 (s, *m*-C<sub>6</sub>H<sub>3</sub>), 127.3 (s, *p*-C<sub>6</sub>H<sub>3</sub>), 124.7 (s, *o*-Dtbp), 120.3 (s, *p*-Dtbp), 36.6 (d, <sup>1</sup>J<sub>CP</sub> = 14 Hz, CH Cyp), 35.0 (s, C <sup>t</sup>Bu), 32.6 (d, J<sub>CP</sub> = 30 Hz, CH<sub>2</sub> Cyp), 32.2 (d, J<sub>CP</sub> = 16 Hz, CH<sub>2</sub> Cyp), 31.7 (s, CH<sub>3</sub> <sup>t</sup>Bu), 27.1 (d, J<sub>CP</sub> = 9 Hz, CH<sub>2</sub> Cyp), 25.8 (d, J<sub>CP</sub> = 7 Hz, CH<sub>2</sub> Cyp).

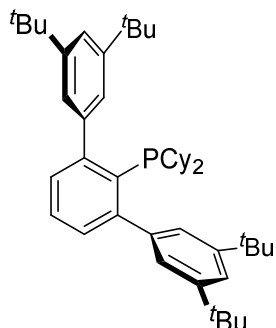
<sup>31</sup>P{<sup>1</sup>H} NMR (CDCl<sub>3</sub>, 162.0 MHz, 298 K): δ 0.9 (s).

Elemental analysis (%), calculated (found) for C<sub>44</sub>H<sub>63</sub>P: C, 84.83 (85.19); H, 10.19 (9.81).

Yield: 0.83 g, 37%.

Chapter I

**I.4.2.2.3. PCy<sub>2</sub>Ar<sup>Dtbp</sup><sub>2</sub> (L9).**



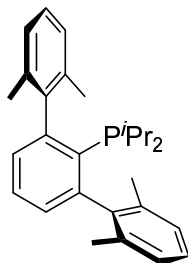
<sup>1</sup>H NMR (CDCl<sub>3</sub>, 400 Hz, 298 K): δ 7.42 (t, 2 H, <sup>4</sup>J<sub>HH</sub> = 1.7 Hz, *p*-Dtbp), 7.36 (t, 1 H, <sup>3</sup>J<sub>HH</sub> = 7.5 Hz, *p*-C<sub>6</sub>H<sub>3</sub>), 7.23 (dd, 2 H, <sup>3</sup>J<sub>HH</sub> = 7.5 Hz, <sup>4</sup>J<sub>HP</sub> = 1.7 Hz, *m*-C<sub>6</sub>H<sub>3</sub>), 7.13 (d, 4 H, <sup>4</sup>J<sub>HH</sub> = 1.7 Hz, *o*-Dtbp), 1.66-1.42 (m, 12 H, CH and CH<sub>2</sub> Cy), 1.40 (s, 36 H, CH<sub>3</sub> <sup>t</sup>Bu), 1.19-0.83 (m, 10 H, CH<sub>2</sub> Cy).

<sup>13</sup>C{<sup>1</sup>H} NMR (CDCl<sub>3</sub>, 101 Hz, 298 K): δ 151.2 (d, <sup>2</sup>J<sub>CP</sub> = 15 Hz, *o*-C<sub>6</sub>H<sub>3</sub>), 149.2 (s, *m*-Dtbp), 143.6 (d, <sup>3</sup>J<sub>CP</sub> = 5 Hz, *ipso*-Dtbp), 133.1 (d, <sup>1</sup>J<sub>CP</sub> = 30 Hz, *ipso*-C<sub>6</sub>H<sub>3</sub>), 130.1 (d, <sup>3</sup>J<sub>CP</sub> = 2 Hz, *m*-C<sub>6</sub>H<sub>3</sub>), 127.2 (s, *p*-C<sub>6</sub>H<sub>3</sub>), 124.4 (s, *o*-Dtbp), 120.2 (s, *p*-Dtbp), 34.9 (s, C <sup>t</sup>Bu), 34.5 (d, <sup>1</sup>J<sub>CP</sub> = 17 Hz, CH Cy), 32.8 (d, <sup>1</sup>J<sub>CP</sub> = 27 Hz, CH<sub>2</sub> Cy), 31.6 (s, CH<sub>3</sub> <sup>t</sup>Bu), 31.3 (d, <sup>1</sup>J<sub>CP</sub> = 12 Hz, CH<sub>2</sub> Cy), 26.9 (d, <sup>1</sup>J<sub>CP</sub> = 9 Hz, CH<sub>2</sub> Cy), 26.6 (d, <sup>1</sup>J<sub>CP</sub> = 14 Hz, CH<sub>2</sub> Cy), 26.3 (s, CH<sub>2</sub> Cy).

<sup>31</sup>P{<sup>1</sup>H} NMR (CDCl<sub>3</sub>, 162 MHz, 298 K): δ 1.6 (s).

Elemental analysis (%), calculated (found) for C<sub>46</sub>H<sub>67</sub>P: C, 84.87 (84.95); H, 10.37 (10.04).

Yield: 1.20 g, 51%.

**1.4.2.2.4. P<sup>i</sup>Pr<sub>2</sub>Ar<sup>Xyl</sup><sub>2</sub> (L10).**

<sup>1</sup>H NMR (CDCl<sub>3</sub>, 400 Hz, 298 K): δ 7.36 (t, 1 H, <sup>3</sup>J<sub>HH</sub> = 7.4 Hz, *p*-C<sub>6</sub>H<sub>3</sub>), 7.15 (t, 2 H, <sup>3</sup>J<sub>HH</sub> = 7.4 Hz, *p*-Xyl), 7.06 (d, 4 H, <sup>3</sup>J<sub>HH</sub> = 7.4 Hz, *m*-Xyl), 6.99 (d, 2 H, <sup>3</sup>J<sub>HH</sub> = 7.4 Hz, *m*-C<sub>6</sub>H<sub>3</sub>), 2.04 (s, 12 H, CH<sub>3</sub> Xyl), 1.83 (dsept, 2 H, <sup>3</sup>J<sub>HH</sub> ≈ <sup>2</sup>J<sub>HP</sub> ≈ 7.0 Hz, CH <sup>i</sup>Pr), 0.84 (dd, 6 H, <sup>3</sup>J<sub>HH</sub> = 7.0 Hz, <sup>3</sup>J<sub>HP</sub> = 18.7 Hz, CH<sub>3</sub> <sup>i</sup>Pr), 0.51 (dd, 6 H, <sup>3</sup>J<sub>HH</sub> = 7.0 Hz, <sup>3</sup>J<sub>HP</sub> = 11.4 Hz, CH<sub>3</sub> <sup>i</sup>Pr).

<sup>13</sup>C{<sup>1</sup>H} NMR (CDCl<sub>3</sub>, 126 MHz, 298 K): δ 148.9 (d, <sup>2</sup>J<sub>CP</sub> = 17 Hz, *o*-C<sub>6</sub>H<sub>3</sub>), 143.7 (d, <sup>3</sup>J<sub>CP</sub> = 5 Hz, *ipso*-Xyl), 137.5 (d, <sup>1</sup>J<sub>CP</sub> = 35 Hz, *ipso*-C<sub>6</sub>H<sub>3</sub>), 136.2 (d, <sup>3</sup>J<sub>CP</sub> = 1 Hz, *o*-Xyl), 130.0 (d, <sup>3</sup>J<sub>CP</sub> = 3 Hz, *m*-C<sub>6</sub>H<sub>3</sub>), 128.7 (s, *p*-C<sub>6</sub>H<sub>3</sub>), 127.4 (s, *m*-Xyl), 127.1 (s, *p*-Xyl), 25.3 (d, <sup>2</sup>J<sub>CP</sub> = 31 Hz, CH <sup>i</sup>Pr), 22.7 (d, <sup>1</sup>J<sub>CP</sub> = 17 Hz, CH<sub>3</sub> <sup>i</sup>Pr), 21.7 (d, <sup>5</sup>J<sub>CP</sub> = 1 Hz, CH<sub>3</sub> Xyl), 22.1 (d, <sup>1</sup>J<sub>CP</sub> = 12 Hz, CH<sub>3</sub> <sup>i</sup>Pr).

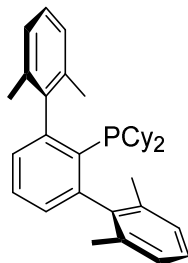
<sup>31</sup>P{<sup>1</sup>H} NMR (CDCl<sub>3</sub>, 162 MHz, 298 K): δ 16.2 (s).

Elemental analysis (%), calculated (found) for C<sub>28</sub>H<sub>35</sub>P: C, 83.54 (83.60); H, 8.76 (8.57).

Yield: 1.18 g, 57%.

Chapter I

**1.4.2.2.5. PCy<sub>2</sub>Ar<sup>Xyl</sup><sub>2</sub> (L12).**



<sup>1</sup>H NMR (CDCl<sub>3</sub>, 500 Hz, 298 K): δ 7.35 (t, 1 H, <sup>3</sup>J<sub>HH</sub> = 7.5 Hz, *p*-C<sub>6</sub>H<sub>3</sub>), 7.14 (t, 2 H, <sup>3</sup>J<sub>HH</sub> = 7.5 Hz, *p*-Xyl), 7.07 (d, 4 H, <sup>3</sup>J<sub>HH</sub> = 7.5 Hz, *m*-Xyl), 7.00 (dd, 2 H, <sup>3</sup>J<sub>HH</sub> = 7.5 Hz, <sup>4</sup>J<sub>HP</sub> = 1.5 Hz, *m*-C<sub>6</sub>H<sub>3</sub>), 2.05 (s, 12 H, CH<sub>3</sub> Xyl), 1.61-1.36 (m, 10 H, CH and CH<sub>2</sub> Cy), 1.15-0.72 (m, 12 H, CH<sub>2</sub> Cy).

<sup>13</sup>C{<sup>1</sup>H} NMR (CDCl<sub>3</sub>, 101 Hz, 298 K): δ 149.0 (d, <sup>2</sup>J<sub>CP</sub> = 17 Hz, *o*-C<sub>6</sub>H<sub>3</sub>), 143.9 (d, <sup>3</sup>J<sub>CP</sub> = 5 Hz, *ipso*-Xyl), 136.5 (d, <sup>1</sup>J<sub>CP</sub> = 37 Hz, *ipso*-C<sub>6</sub>H<sub>3</sub>), 136.1 (d, <sup>4</sup>J<sub>CP</sub> = 1 Hz, *o*-Xyl), 130.0 (d, <sup>3</sup>J<sub>CP</sub> = 3 Hz, *m*-C<sub>6</sub>H<sub>3</sub>), 128.9 (s, *p*-C<sub>6</sub>H<sub>3</sub>), 128.0 (s, *m*-Xyl), 126.9 (s, *p*-Xyl), 35.0 (d, <sup>1</sup>J<sub>CP</sub> = 28 Hz, PCH), 33.1 (d, J<sub>CP</sub> = 18 Hz, CH<sub>2</sub>), 30.8 (d, J<sub>CP</sub> = 12 Hz, CH<sub>2</sub>), 27.8 (s, CH<sub>2</sub>), 27.8 (d, J<sub>CP</sub> = 23 Hz, CH<sub>2</sub>), 21.7 (d, <sup>5</sup>J<sub>CP</sub> = 1 Hz, CH<sub>3</sub>).

<sup>31</sup>P{<sup>1</sup>H} NMR (CDCl<sub>3</sub>, 202 MHz, 298 K): δ 10.1 (s).

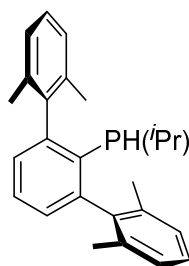
Elemental analysis (%), calculated (found) for C<sub>34</sub>H<sub>43</sub>P: C, 84.60 (84.54); H, 8.98 (8.98).

Yield: 1.40 g, 56%.



**I.4.2.2.6. PH(*i*Pr)Ar<sup>Xyl</sup><sub>2</sub>.**

This compound is formed as a by-product in the preparation of **L6**. It was isolated as a colourless solid. Selected spectroscopic data are detailed below.

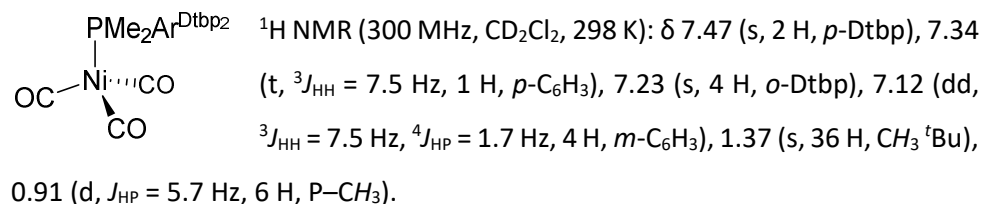


<sup>1</sup>H NMR (CDCl<sub>3</sub>, 400 Hz, 298 K): δ 7.29 (t, <sup>3</sup>J<sub>HH</sub> = 7.5 Hz, 1 H, *p*-C<sub>6</sub>H<sub>3</sub>), 7.09 (t, <sup>3</sup>J<sub>HH</sub> = 7.4 Hz, 2 H, *p*-Xyl), 7.04-6.95 (m, 6 H, *m*-Xyl, *m*-C<sub>6</sub>H<sub>3</sub>), 3.15 (dd, <sup>1</sup>J<sub>HP</sub> = 221.9 Hz, <sup>3</sup>J<sub>HH</sub> = 8.8 Hz, 1 H, PH), 2.03 (s, 6 H, CH<sub>3</sub> Xyl), 1.97 (s, 6 H, CH<sub>3</sub> Xyl), 1.20 (br, 1 H, CH *i*Pr), 0.76 (dd, 3 H, <sup>3</sup>J<sub>HP</sub> = 6.8 Hz, <sup>3</sup>J<sub>HH</sub> = 6.7 Hz, CH<sub>3</sub> *i*Pr), 0.53 (dd, <sup>3</sup>J<sub>HP</sub> = 20.8 Hz, <sup>3</sup>J<sub>HH</sub> = 7.2 Hz, 3 H, CH<sub>3</sub> *i*Pr).

<sup>31</sup>P{<sup>1</sup>H} NMR (CDCl<sub>3</sub>, 116 MHz, 298 K): δ -37.7 (s).

**I.4.3. Nickel carbonyl complexes.****I.4.3.1. General procedure for the synthesis of Ni(CO)<sub>3</sub>(PMe<sub>2</sub>Ar'') (1·PMe<sub>2</sub>Ar''; PMe<sub>2</sub>Ar'' = L1-L3).**

THF (2-5 mL) was added to an ampoule charged with PMe<sub>2</sub>Ar'' and Ni(cod)<sub>2</sub> (1.0-1.1 eq), cooled to -15 °C. The vessel was then charged with CO (1 bar) and the cool bath removed. Reaction with PMe<sub>2</sub>Ar<sup>Xyl</sup><sub>2</sub> and PMe<sub>2</sub>Ar<sup>Dtbp</sup><sub>2</sub> was complete within 1 day at room temperature, while for PMe<sub>2</sub>Ar<sup>Dipp</sup><sub>2</sub> 3-4 days were needed. After removal of volatiles under vacuum, the solid residues were washed with cold (-30 °C) methanol. Samples suitable for X-ray diffraction were obtained by crystallisation from pentane.

**I.4.3.1.1. Ni(CO)<sub>3</sub>(PMe<sub>2</sub>Ar<sup>Dtbp</sup><sub>2</sub>) (1·L1).**

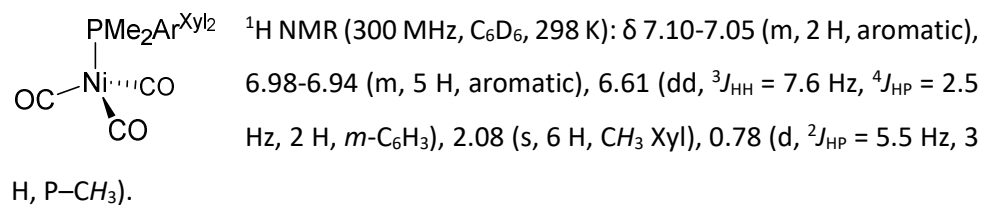
<sup>13</sup>C{<sup>1</sup>H} NMR (100 MHz, CD<sub>2</sub>Cl<sub>2</sub>, 298 K): δ 197.2 (s, CO), 151.0 (s, *o*-Dtbp), 147.9 (d, <sup>2</sup>J<sub>CP</sub> = 8 Hz, *o*-C<sub>6</sub>H<sub>3</sub>), 143.1 (d, <sup>3</sup>J<sub>CP</sub> = 3 Hz, *ipso*-Dtbp), 136.3 (d, <sup>1</sup>J<sub>CP</sub> = 21 Hz, *ipso*-C<sub>6</sub>H<sub>3</sub>), 131.8 (d, <sup>3</sup>J<sub>CP</sub> = 5 Hz, *m*-C<sub>6</sub>H<sub>3</sub>), 127.7 (s, *p*-C<sub>6</sub>H<sub>3</sub>), 124.6 (s, *m*-Dtbp), 122.4 (s, *p*-Dtbp), 35.3 (s, C<sup>t</sup>Bu), 31.7 (s, CH<sub>3</sub><sup>t</sup>Bu), 22.6 (d, <sup>1</sup>J<sub>CP</sub> = 24 Hz, P-CH<sub>3</sub>).

<sup>31</sup>P{<sup>1</sup>H} NMR (121 MHz, CD<sub>2</sub>Cl<sub>2</sub>, 298 K): δ 4.7 (s).

IR (CH<sub>2</sub>Cl<sub>2</sub>): 2063 cm<sup>-1</sup> (ν<sub>CO</sub>, A<sub>1</sub>), 1988 cm<sup>-1</sup> (ν<sub>CO</sub>, E).

Elemental analysis (%), calculated (found) for C<sub>39</sub>H<sub>51</sub>NiO<sub>3</sub>P: C, 71.24 (71.24); H, 7.82 (7.66).

Yield: 0.030 g, 47%.

**I.4.3.1.2. Ni(CO)<sub>3</sub>(PMe<sub>2</sub>Ar<sup>Xyl2</sup>) (1·L2).**

<sup>13</sup>C{<sup>1</sup>H} NMR (100 MHz, C<sub>6</sub>D<sub>6</sub>, 298 K): δ 196.7 (s, CO), 144.8 (d, <sup>2</sup>J<sub>CP</sub> = 7 Hz, *o*-C<sub>6</sub>H<sub>3</sub>), 142.5 (s, *ipso*-Xyl), 136.6 (s, *o*-Xyl), 130.9 (d, <sup>3</sup>J<sub>CP</sub> = 5 Hz, *m*-C<sub>6</sub>H<sub>3</sub>), 129.6 (s, *p*-C<sub>6</sub>H<sub>3</sub>), 128.3 (s, *p*-Xyl), 127.9 (s, *m*-Xyl), 22.1 (s, CH<sub>3</sub> Xyl), 21.3 (d, <sup>1</sup>J<sub>CP</sub> = 24 Hz, P-CH<sub>3</sub>).

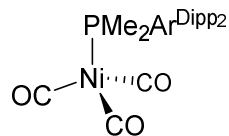
<sup>31</sup>P{<sup>1</sup>H} NMR (162 MHz, C<sub>6</sub>D<sub>6</sub>, 298 K): δ -7.7 (s).

IR (CH<sub>2</sub>Cl<sub>2</sub>): 2063.8 cm<sup>-1</sup> (ν<sub>CO</sub>, A<sub>1</sub>), 1987 cm<sup>-1</sup> (ν<sub>CO</sub>, E).

Elemental analysis (%), calculated (found) for C<sub>27</sub>H<sub>27</sub>NiO<sub>3</sub>P: C, 66.29 (65.93); H, 5.56 (5.91).

Yield: 0.234 g, 64%.

**I.4.3.1.3. Ni(CO)<sub>3</sub>(PMe<sub>2</sub>Ar<sup>Dipp2</sup>) (1·L3).**



<sup>1</sup>H NMR (300 MHz, C<sub>6</sub>D<sub>6</sub>, 298 K): δ 7.29-7.23 (m, 2 H, aromatic), 7.15-7.13 (m, 4 H, aromatic), 7.01-6.97 (m, 2 H, aromatic), 6.91-6.85 (m, 1 H, aromatic), 2.83 (sept, <sup>3</sup>J<sub>HH</sub> = 6.7 Hz, 4 H, CH <sup>i</sup>Pr), 1.38 (d, <sup>3</sup>J<sub>HH</sub> = 6.8 Hz, 12 H, CH<sub>3</sub> <sup>i</sup>Pr), 1.02 (d, <sup>3</sup>J<sub>HH</sub> = 6.7 Hz, 12 H, CH<sub>3</sub> <sup>i</sup>Pr), 0.88 (d, <sup>2</sup>J<sub>HP</sub> = 5.7 Hz, 6 H, P-CH<sub>3</sub>).

<sup>13</sup>C{<sup>1</sup>H} NMR (100 MHz, C<sub>6</sub>D<sub>6</sub>, 298 K): δ 197.1 (s, CO), 147.0 (s, *o*-Dipp), 142.5 (d, <sup>2</sup>J<sub>CP</sub> = 10 Hz, *o*-C<sub>6</sub>H<sub>3</sub>), 140.6 (s, *ipso*-Dipp), 134.7 (d, <sup>1</sup>J<sub>CP</sub> = 16 Hz, *ipso*-C<sub>6</sub>H<sub>3</sub>), 133.5 (d, <sup>3</sup>J<sub>CP</sub> = 6 Hz, *m*-C<sub>6</sub>H<sub>3</sub>), 129.3 (s, *p*-Dipp), 126.4 (s, *p*-C<sub>6</sub>H<sub>3</sub>), 123.1 (s, *m*-Dipp), 31.4 (s, CH <sup>i</sup>Pr), 25.9 (s, CH<sub>3</sub> <sup>i</sup>Pr), 22.7 (s, CH<sub>3</sub> <sup>i</sup>Pr), 22.5 (d, J<sub>CP</sub> = 23 Hz, P-CH<sub>3</sub>).

<sup>31</sup>P{<sup>1</sup>H} NMR (121 MHz, C<sub>6</sub>D<sub>6</sub>, 298 K): δ -4.3 (s).

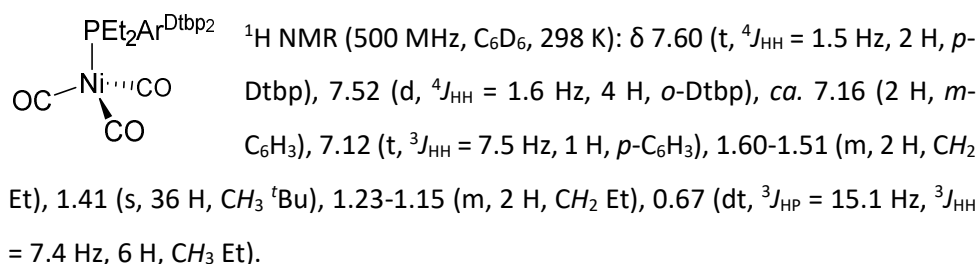
IR (CH<sub>2</sub>Cl<sub>2</sub>): 2062.9 cm<sup>-1</sup> (ν<sub>CO</sub>, A<sub>1</sub>), 1986 cm<sup>-1</sup> (ν<sub>CO</sub>, E).

Elemental analysis (%), calculated (found) for C<sub>35</sub>H<sub>43</sub>NiO<sub>3</sub>P: C, 69.90 (69.57); H, 7.21 (7.54).

Yield: 0.093 g, 39%.

**1.4.3.2. Synthesis and characterisation of Ni(CO)<sub>3</sub>(PEt<sub>2</sub>Ar<sup>Dtbp<sub>2</sub></sup>) (1·L6).**

THF (2 mL) was added to an ampoule charged with Ni(cod)<sub>2</sub> (0.041 g, 0.149 mmol, 10 % excess) and PEt<sub>2</sub>Ar<sup>Dtbp<sub>2</sub></sup> (0.073 g, 0.135 mmol), cooled to –30 °C. The vessel was then charged with CO (1 bar) and the cool bath was removed. The reaction mixture was stirred at room temperature for 3 h, after which all volatiles were removed under vacuum at –30 °C. The resulting off-white residue was extracted with pentane at room temperature and filtered. Subsequent removal of volatiles under vacuum, first at –30 °C and then at room temperature, rendered the sought product as a yellowish white solid. Yield: 0.083 g, 90%. This solid contains a small amount of Ni(CO)<sub>2</sub>(PEt<sub>2</sub>Ar<sup>Dtbp<sub>2</sub></sup>) (<5% by NMR), but is suitable for spectroscopic characterisation. Analytically pure samples can be obtained by crystallisation from pentane at –30 °C.



<sup>13</sup>C{<sup>1</sup>H} NMR (100 MHz, C<sub>6</sub>D<sub>6</sub>, 298 K): δ 197.7 (s, CO), 150.9 (s, *m*-Dtbp), 148.9 (d, <sup>2</sup>J<sub>CP</sub> = 7 Hz, *o*-C<sub>6</sub>H<sub>3</sub>), 143.8 (d, <sup>3</sup>J<sub>CP</sub> = 2 Hz, *ipso*-Dtbp), 132.3 (d, <sup>3</sup>J<sub>CP</sub> = 5 Hz, *m*-C<sub>6</sub>H<sub>3</sub>), 132.0 (d, <sup>1</sup>J<sub>CP</sub> = 18 Hz, *ipso*-C<sub>6</sub>H<sub>3</sub>), *ca.* 128.8 (*p*-C<sub>6</sub>H<sub>3</sub>), 124.5 (s, *o*-Dtbp), 122.4 (s, *p*-Dtbp), 35.1 (s, C <sup>t</sup>Bu), 31.6 (s, CH<sub>3</sub> <sup>t</sup>Bu), 21.1 (d, <sup>1</sup>J<sub>CP</sub> = 20 Hz, CH<sub>2</sub> Et), 8.5 (s, CH<sub>3</sub> Et).

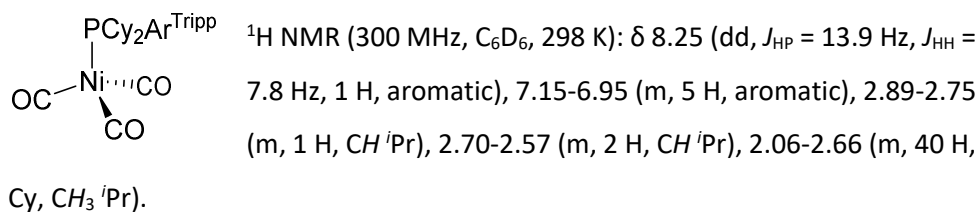
<sup>31</sup>P{<sup>1</sup>H} NMR (121 MHz, C<sub>6</sub>D<sub>6</sub>, 298 K): δ 22.9 (s).

IR (CH<sub>2</sub>Cl<sub>2</sub>): 2061 cm<sup>-1</sup> (ν<sub>CO</sub>, A<sub>1</sub>), 1985 cm<sup>-1</sup> (ν<sub>CO</sub>, E).

Elemental analysis (%), calculated (found) for C<sub>41</sub>H<sub>55</sub>NiO<sub>3</sub>P: C, 71.83 (71.82); H, 8.09 (8.05).

**I.4.3.3. Synthesis and characterisation of Ni(CO)<sub>3</sub>(PCy<sub>2</sub>Ar<sup>Tripp</sup>) (1·XPhos).**

THF (2 mL) was added to an ampoule charged with Ni(cod)<sub>2</sub> (0.033 g, 0.120 mmol, 20 % excess) and XPhos (0.048 g, 0.100 mmol), cooled to -35 °C. The vessel was then charged with CO (1 bar) and the cool bath removed. After the yellow colour due to Ni(cod)<sub>2</sub> faded from the solution, the mixture was frozen using a liquid N<sub>2</sub> bath and all gases were removed under vacuum. The reaction mixture was stirred at room temperature for 3 h, after which all volatiles were removed under vacuum at -20 °C. The resulting off-white residue was extracted with pentane at room temperature and filtered. Removal of volatiles under vacuum, first at 0 °C and then at room temperature rendered the sought product as an off-white solid. Yield: 0.027 g, 44%.



<sup>13</sup>C{<sup>1</sup>H} NMR (100 MHz, C<sub>6</sub>D<sub>6</sub>, 298 K): δ 198.1 (s, CO), 149.1 (s, C aromatic), 146.8 (s, C aromatic), 142.9 (br s, C aromatic), 138.8 (br, CH aromatic), 137.6 (s, C aromatic), 134.1 (d, *J* = 4 Hz, CH aromatic), 133.2 (d, *J* = 17 Hz, C aromatic), *ca.* 128.0 (CH aromatic), 126.5 (d, *J* = 13 Hz, CH aromatic), 121.3 (s, CH aromatic), 35.8 (br, Cy), 34.9 (s, CH<sup>*i*</sup>Pr), 31.3-31.2 (m, Cy), 31.0 (s, CH<sup>*i*</sup>Pr), 27.5-27.2 (m, Cy), 26.5 (s, CH<sub>3</sub><sup>*i*</sup>Pr), 26.2 (s, Cy), 24.3 (s, CH<sub>3</sub><sup>*i*</sup>Pr), 22.5 (s, CH<sub>3</sub><sup>*i*</sup>Pr).

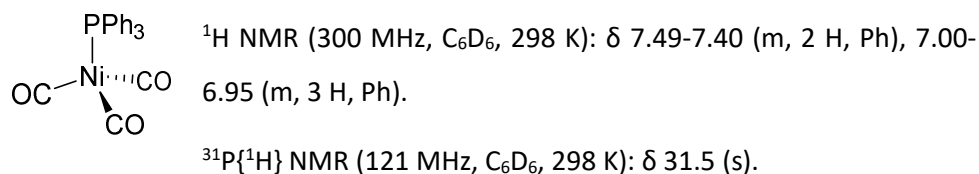
<sup>31</sup>P{<sup>1</sup>H} NMR (121 MHz, C<sub>6</sub>D<sub>6</sub>, 298 K): δ 57.5 (b).

IR (CH<sub>2</sub>Cl<sub>2</sub>): 2059 cm<sup>-1</sup> (ν<sub>CO</sub>, A<sub>1</sub>), 1980 cm<sup>-1</sup> (ν<sub>CO</sub>, E).

Elemental analysis (%), calculated (found) for C<sub>36</sub>H<sub>49</sub>NiO<sub>3</sub>P: C, 69.80 (69.57); H, 7.97 (8.29).

**I.4.3.4. Synthesis and characterisation of Ni(CO)<sub>3</sub>(PPh<sub>3</sub>).**

THF (3 mL) was added to an ampoule charged with Ni(cod)<sub>2</sub> (0.069 g, 0.250 mmol, 25% excess) and PPh<sub>3</sub> (0.053 g, 0.200 mmol), cooled to -30 °C. The vessel was then charged with CO (1 bar) and the cool bath removed. The mixture was stirred at room temperature for 6 hours, after which volatiles were removed under vacuum. The resulting solid was extracted with pentane, filtered and the solution concentrated and kept at -30 °C. Crystals suitable for X-ray diffraction were obtained by crystallisation from pentane at -30 °C.



IR (CH<sub>2</sub>Cl<sub>2</sub>): 2069 cm<sup>-1</sup> (ν<sub>CO</sub>, A<sub>1</sub>), 1995 cm<sup>-1</sup> (ν<sub>CO</sub>, E).

**I.4.3.5. Synthesis of Ni(CO)<sub>3</sub>(PMe<sub>2</sub>Ar<sup>Mes</sup>) (1·L4).**

THF (1 mL) was added to an ampoule charged with Ni(cod)<sub>2</sub> (0.016 g, 0.058 mmol, 15% excess) and PMe<sub>2</sub>Ar<sup>Mes</sup> (0.026 g, 0.050 mmol), cooled to -40 °C. The vessel was then charged with CO (1 bar) and the cool bath removed. When the yellow colour of Ni(cod)<sub>2</sub> faded, the mixture was frozen using a liquid N<sub>2</sub> bath and all gases were removed under vacuum. The mixture was stirred at room temperature for 2 hours, after which removal of volatiles under vacuum resulted in an off-white sticky solid. CH<sub>2</sub>Cl<sub>2</sub> (1 mL) was added and the resulting solution was analysed by means of IR spectroscopy.

IR (CH<sub>2</sub>Cl<sub>2</sub>): 2063 cm<sup>-1</sup> (ν<sub>CO</sub>, A<sub>1</sub>), 1987 cm<sup>-1</sup> (ν<sub>CO</sub>, E).

#### **I.4.3.6. Synthesis of Ni(CO)<sub>3</sub>(PMe<sub>2</sub>Ar<sup>Tripp2</sup>) (1·L5).**

THF (1 mL) was added to an ampoule charged with Ni(cod)<sub>2</sub> (0.016 g, 0.058 mmol, 15% excess) and PMe<sub>2</sub>Ar<sup>Tripp2</sup> (0.027 g, 0.051 mmol), cooled to -30 °C. The vessel was then charged with CO (1 bar) and the cool bath removed. When the yellow colour of Ni(cod)<sub>2</sub> faded, the mixture was frozen using a liquid N<sub>2</sub> bath and all gases were removed under vacuum. The reaction mixture was stirred at room temperature for 2 hours, after which removal of volatiles under vacuum resulted in a white solid. CH<sub>2</sub>Cl<sub>2</sub> (1 mL) was added and the resulting solution was analysed by means of IR spectroscopy.

IR (CH<sub>2</sub>Cl<sub>2</sub>): 2062 cm<sup>-1</sup> (ν<sub>CO</sub>, A<sub>1</sub>), 1985 cm<sup>-1</sup> (ν<sub>CO</sub>, E).

#### **I.4.3.7. Synthesis of Ni(CO)<sub>3</sub>(PCyp<sub>3</sub>).**

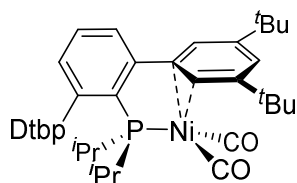
To an ampoule charged with Ni(cod)<sub>2</sub> (0.016 g, 0.057 mmol, 15% excess), cooled to -40 °C, a solution of PCyp<sub>3</sub> (1 mL, 0.05 M in THF, 0.05 mmol) was added. The vessel was then charged with CO (1 bar) and the cool bath removed. The reaction mixture was stirred at room temperature for 30 minutes, after which removal of volatiles under vacuum resulted in an off-white sticky solid. CH<sub>2</sub>Cl<sub>2</sub> (1 mL) was added and the resulting solution was analysed by means of IR spectroscopy.

IR (CH<sub>2</sub>Cl<sub>2</sub>): 2059 cm<sup>-1</sup> (ν<sub>CO</sub>, A<sub>1</sub>), 1980 cm<sup>-1</sup> (ν<sub>CO</sub>, E).



**I.4.3.8. Synthesis and characterisation of Ni(CO)<sub>2</sub>(κ<sup>1</sup>-P-η<sup>2</sup>-C,C-P<sup>i</sup>Pr<sub>2</sub>Ar<sup>Dtbp<sub>2</sub></sup>) (2·L7).**

THF (3 mL) was added to a 100 mL ampoule charged with Ni(cod)<sub>2</sub> (0.045 g, 0.163 mmol, 25% excess) and P<sup>i</sup>Pr<sub>2</sub>Ar<sup>Dtbp<sub>2</sub></sup> (0.073 g, 0.128 mmol), cooled to -30 °C. The vessel was then charged with CO (1 bar) and the cool bath removed. When the yellow colour of Ni(cod)<sub>2</sub> disappeared, the mixture was frozen using a liquid N<sub>2</sub> bath and all gases were removed under vacuum. The mixture was stirred at 50 °C for 2 hours, after which removal of volatiles under vacuum resulted in a yellow tacky residue. Crystallisation from a MeOH/Et<sub>2</sub>O mixture at -30 °C yielded the sought compound as a yellow crystalline solid. Yield: 0.057 g, 65%. Although the former method of crystallisation resulted in the best yield, traces of free phosphine were found by NMR. Analytically pure samples could be obtained by further recrystallisation from pentane at -30 °C.



<sup>1</sup>H NMR (400 MHz, CD<sub>2</sub>Cl<sub>2</sub>, 298 K): δ 7.49 (br, 1 H, aromatic), 7.30 (br, 2 H, aromatic), 7.20-7.11 (br, 3 H, aromatic), 6.90 (br, 1 H, aromatic), 6.69 (br, 2 H, aromatic), 1.94 (dsept, <sup>2</sup>J<sub>HP</sub> = 13.3 Hz, <sup>3</sup>J<sub>HH</sub> = 6.6 Hz, 2 H, CH <sup>i</sup>Pr), 1.39 (br s, 36 H, CH<sub>3</sub> <sup>t</sup>Bu), 0.98-0.90 (m, 12 H, CH<sub>3</sub> <sup>i</sup>Pr).

<sup>1</sup>H NMR (400 MHz, CD<sub>2</sub>Cl<sub>2</sub>, 243 K): δ 7.43 (t, <sup>4</sup>J<sub>HH</sub> = 1.5 Hz, 1 H, *p*-Dtbp), 7.30 (td, <sup>3</sup>J<sub>HH</sub> = 7.6 Hz, <sup>5</sup>J<sub>HP</sub> = 1.4 Hz, 1 H, *p*-C<sub>6</sub>H<sub>3</sub>), 7.26-7.24 (m, 1 H, *p*-Dtbp), 7.17 (d, <sup>4</sup>J<sub>HH</sub> = 1.7 Hz, 2 H, *o*-Dtbp), 7.12 (d, <sup>3</sup>J<sub>HH</sub> = 7.4 Hz, 1 H, *m*-C<sub>6</sub>H<sub>3</sub>), 6.89 (ddd, <sup>3</sup>J<sub>HH</sub> = 7.6 Hz, <sup>4</sup>J<sub>HP</sub> = 2.8 Hz, <sup>4</sup>J<sub>HH</sub> = 1.2 Hz, 1 H, *m*-C<sub>6</sub>H<sub>3</sub>), 6.63 (d, <sup>4</sup>J<sub>HH</sub> = 0.9 Hz, 2 H, *o*-Dtbp), 1.83 (dsept, <sup>2</sup>J<sub>HP</sub> = 13.5 Hz, <sup>3</sup>J<sub>HH</sub> = 6.6 Hz, 2 H, CH <sup>i</sup>Pr), 1.36 (s, 18 H, CH<sub>3</sub> <sup>t</sup>Bu), 1.32 (s, 18 H, CH<sub>3</sub> <sup>t</sup>Bu), 0.92-0.84 (m, 12 H, CH<sub>3</sub> <sup>i</sup>Pr).

<sup>13</sup>C{<sup>1</sup>H} NMR (100 MHz, CD<sub>2</sub>Cl<sub>2</sub>, 243 K): δ 198.9 (d, <sup>2</sup>J<sub>CP</sub> = 10 Hz, CO), 152.4 (d, <sup>1</sup>J<sub>CP</sub> = 31 Hz, *ipso*-C<sub>6</sub>H<sub>3</sub>), 151.6 (s, *m*-Dtbp), 149.7 (s, *m*-Dtbp), 146.9 (s, *ipso*-Dtbp), 141.2 (s, *ipso*-Dtbp), 134.0 (d, <sup>3</sup>J<sub>CP</sub> = 20 Hz, *o*-C<sub>6</sub>H<sub>3</sub>), 132.3 (d, <sup>3</sup>J<sub>CP</sub> = 6 Hz, *o*-C<sub>6</sub>H<sub>3</sub>), 130.8 (s, *m*-C<sub>6</sub>H<sub>3</sub>), 130.7 (d, *J*<sub>CP</sub> = 9 Hz, *m*-C<sub>6</sub>H<sub>3</sub>), 128.2 (s, *p*-C<sub>6</sub>H<sub>3</sub>), 123.4 (s, *o*-Dtbp), 121.4 (s,

Chapter I

*p*-Dtbp), 120.7 (s, *p*-Dtbp), 110.4 (s, *o*-Dtbp), 35.1 (s, C<sup>t</sup>Bu), 34.8 (s, C<sup>t</sup>Bu), 31.2 (s, CH<sub>3</sub><sup>t</sup>Bu), 31.0 (s, CH<sub>3</sub><sup>t</sup>Bu), 26.8 (d, <sup>1</sup>J<sub>CP</sub> = 18 Hz, CH<sup>i</sup>Pr), 20.37 (m, CH<sub>3</sub><sup>i</sup>Pr) ppm.

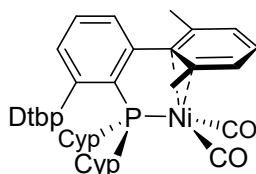
<sup>31</sup>P{<sup>1</sup>H} NMR (162 MHz, CD<sub>2</sub>Cl<sub>2</sub>, 298 K): δ 60.4 (s).

IR (CH<sub>2</sub>Cl<sub>2</sub>): 1995 cm<sup>-1</sup> (ν<sub>CO</sub>, symmetric), 1923 cm<sup>-1</sup> (ν<sub>CO</sub>, asymmetric).

Elemental analysis (%), calculated (found) for C<sub>42</sub>H<sub>61</sub>NiO<sub>2</sub>P: C, 73.36 (73.66); H, 8.94 (8.64).

### 1.4.3.9. Synthesis and characterisation of $\text{Ni}(\text{CO})_2(\kappa^1\text{-P-}\eta^2\text{-C,C-PCyp}_2\text{Ar}^{\text{Xyl}_2})$ (2·L11).

THF (10 mL) was added to an ampoule charged with  $\text{Ni}(\text{cod})_2$  (0.094 g, 0.342 mmol, 10% excess) and  $\text{PCyp}_2\text{Ar}^{\text{Xyl}_2}$  (0.141 g, 0.311 mmol), cooled to  $-15^\circ\text{C}$ . The vessel was then charged with CO (1 bar) and the cool bath removed. When the yellow colour of  $\text{Ni}(\text{cod})_2$  faded, the mixture was frozen using a liquid  $\text{N}_2$  bath and all gases were removed under vacuum. The mixture was stirred at  $80^\circ\text{C}$  for 2 hours, after which removal of volatiles under vacuum resulted in a yellow sticky solid. Washing with cold ( $0^\circ\text{C}$ ) methanol rendered the sought compound as a yellow solid. Yield: 0.123 g, 70%. Samples suitable for X-ray diffraction were obtained by crystallisation from a pentane/ $\text{Et}_2\text{O}$  mixture.



$^1\text{H NMR}$  (400 MHz,  $\text{CD}_2\text{Cl}_2$ , 298 K):  $\delta$  7.43 (td,  $^3J_{\text{HH}} = 7.6$ ,  $^5J_{\text{HP}} = 1.6$  Hz, 1 H, *p*- $\text{C}_6\text{H}_3$ ), 7.24-7.19 (m, 3 H, aromatic), 7.13-7.03 (m, 4 H, aromatic), 6.81 (bd,  $^4J_{\text{HH}} = 7.6$ , 1 H, *m*- $\text{C}_6\text{H}_3$ ), 2.07 (s, 6 H,  $\text{CH}_3$  Xyl), 2.03 (s, 6 H,  $\text{CH}_3$  Xyl), 1.89-1.77 (m, 2

H, CH Cyp), 1.61-1.20 (m, 16 H,  $\text{CH}_2$  Cyp).

$^{13}\text{C}\{^1\text{H}\}$  NMR (100 MHz,  $\text{C}_6\text{D}_6$ , 298 K):  $\delta$  198.4 (d,  $^2J_{\text{CP}} = 11$  Hz, CO), 150.1 (d,  $^1J_{\text{CP}} = 34$  Hz, *ipso*- $\text{C}_6\text{H}_3$ ), 145.8 (s, C aromatic), 141.4 (s, C aromatic), 136.9 (s, C aromatic), 137.5 (d,  $^3J_{\text{CP}} = 13$  Hz, *o*- $\text{C}_6\text{H}_3$ ), 131.9 (s, C aromatic), 131.1 (s, CH aromatic), 130.6 (d,  $J_{\text{CP}} = 8$  Hz, *m*- $\text{C}_6\text{H}_3$ ), 129.9 (s, CH aromatic), 129.6 (s, CH aromatic), 128.7 (s, C aromatic), 127.4 (s, CH aromatic), 125.4 (s, CH aromatic), 38.8 (d,  $^1J_{\text{CP}} = 19$  Hz, CH Cyp), 32.9 (d,  $^3J_{\text{CP}} = 10$  Hz,  $\text{CH}_2$  Cyp), 31.5 (d,  $^2J_{\text{CP}} = 12$  Hz,  $\text{CH}_2$  Cyp), 26.0 (d,  $^3J_{\text{CP}} = 10$  Hz,  $\text{CH}_2$  Cyp), 23.3 (s,  $\text{CH}_3$  Xyl), 21.6 (s,  $\text{CH}_3$  Xyl).

$^{31}\text{P}\{^1\text{H}\}$  NMR (162 MHz,  $\text{CD}_2\text{Cl}_2$ , 298 K):  $\delta$  53.8 (s).

IR ( $\text{CH}_2\text{Cl}_2$ ):  $1996\text{ cm}^{-1}$  ( $\nu_{\text{CO}}$ , symmetric),  $1924\text{ cm}^{-1}$  ( $\nu_{\text{CO}}$ , asymmetric).

Elemental analysis (%), calculated (found) for  $\text{C}_{34}\text{H}_{39}\text{NiO}_2\text{P}$ : C, 71.73 (71.46); H, 6.90 (7.08).

**I.4.3.10. Synthesis of Ni(CO)<sub>2</sub>(κ<sup>1</sup>-P-η<sup>2</sup>-C,C-PCyp<sub>2</sub>Ar<sup>Dtbp<sub>2</sub></sup>) (2·L8).**

THF (2 mL) was added to an ampoule charged with Ni(cod)<sub>2</sub> (0.038 g, 0.137 mmol, 7% excess) and PCyp<sub>2</sub>Ar<sup>Dtbp<sub>2</sub></sup> (0.080 g, 0.128 mmol), cooled to -10 °C. The vessel was then charged with CO (1 bar) and the cool bath removed. After the yellow colour of Ni(cod)<sub>2</sub> faded, the mixture was frozen using a liquid N<sub>2</sub> bath and all gases were removed under vacuum. The reaction mixture was stirred at room temperature for 16 hours, after which removal of volatiles under vacuum resulted in a yellow sticky solid. Several attempts were made to isolate the sought compound pure by NMR, but none of them were successful.

IR (CH<sub>2</sub>Cl<sub>2</sub>): 1995 cm<sup>-1</sup> (ν<sub>CO</sub>, symmetric), 1923 cm<sup>-1</sup> (ν<sub>CO</sub>, asymmetric).

**I.4.3.11. Synthesis of Ni(CO)<sub>2</sub>(κ<sup>1</sup>-P-η<sup>2</sup>-C,C-PCy<sub>2</sub>Ar<sup>Dtbp<sub>2</sub></sup>) (2·L9).**

THF (1 mL) was added to an ampoule charged with Ni(cod)<sub>2</sub> (0.016 g, 0.057 mmol, 15% excess) and PCy<sub>2</sub>Ar<sup>Dtbp<sub>2</sub></sup> (0.033 g, 0.050 mmol), cooled to -30 °C. The vessel was then charged with CO (1 bar) and the cool bath removed. After the yellow colour of Ni(cod)<sub>2</sub> faded, the mixture was frozen using a liquid N<sub>2</sub> bath and all gases were removed under vacuum. The reaction mixture was stirred at room temperature for 16 hours, after which removal of volatiles under vacuum resulted in a yellow sticky solid. CH<sub>2</sub>Cl<sub>2</sub> (1 mL) was added and the resulting solution was analysed by means of IR spectroscopy.

IR (CH<sub>2</sub>Cl<sub>2</sub>): 1993 cm<sup>-1</sup> (ν<sub>CO</sub>, symmetric), 1921 cm<sup>-1</sup> (ν<sub>CO</sub>, asymmetric).

A low intensity band could be discerned belonging to the species Ni(CO)<sub>3</sub>(PCy<sub>2</sub>Ar<sup>Dtbp<sub>2</sub></sup>). IR (CH<sub>2</sub>Cl<sub>2</sub>): 2060 cm<sup>-1</sup> (ν<sub>CO</sub>, A<sub>1</sub>).

**I.4.3.12. Synthesis of Ni(CO)<sub>2</sub>(κ<sup>1</sup>-P-η<sup>2</sup>-C,C-P<sup>i</sup>Pr<sub>2</sub>Ar<sup>Xyl<sub>2</sub></sup>) (2·L10).**

A solution of Ni(cod)<sub>2</sub> (0.0060 g, 0.022 mmol, 10% excess) and P<sup>i</sup>Pr<sub>2</sub>Ar<sup>Xyl<sub>2</sub></sup> (0.0081 g, 0.020 mmol) in THF (0.6 mL) was charged with CO (1 bar). After the yellow colour of the Ni(cod)<sub>2</sub> faded from the solution, the mixture was frozen using a liquid N<sub>2</sub> bath and all gases were removed under vacuum. The reaction mixture was stirred at 100 °C for 30 min, resulting in a yellow solution and some black metallic residue. The solution was then filtered, the solvent removed under vacuum and the resulting solid dissolved in CH<sub>2</sub>Cl<sub>2</sub> to be analysed by means of IR spectroscopy.

IR (CH<sub>2</sub>Cl<sub>2</sub>): 1996 cm<sup>-1</sup> (ν<sub>CO</sub>, symmetric), 1924 cm<sup>-1</sup> (ν<sub>CO</sub>, asymmetric).

**I.4.3.13. Synthesis of Ni(CO)<sub>2</sub>(κ<sup>1</sup>-P-η<sup>2</sup>-C,C-PCy<sub>2</sub>Ar<sup>Xyl<sub>2</sub></sup>) (2·L12).**

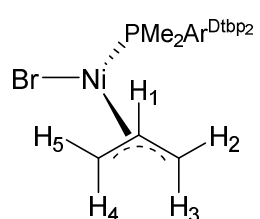
THF (1 mL) was added to an ampoule charged with Ni(cod)<sub>2</sub> (0.016 g, 0.058 mmol, 15% excess) and PCy<sub>2</sub>Ar<sup>Xyl<sub>2</sub></sup> (0.024 g, 0.050 mmol), cooled to -30 °C. The vessel was then charged with CO (1 bar) and the cool bath removed. After the yellow colour of the Ni(cod)<sub>2</sub> faded from the solution, the mixture was frozen using a liquid N<sub>2</sub> bath and all gases were removed under vacuum. Reaction progress was monitored using <sup>31</sup>P NMR and, after each aliquot was analysed and then returned to the reaction vessel, the liquid N<sub>2</sub>-vacuum procedure was repeated. Thus, the mixture was stirred for 16 hours at room temperature and analysed. Then heated up to 50 °C for 2 hours and analysed again. A final analysis after further 16 hours at 50 °C showed enough conversion to the sought product. Volatiles were removed under vacuum, CH<sub>2</sub>Cl<sub>2</sub> (1 mL) was added and the solution was examined by IR spectroscopy.

IR (CH<sub>2</sub>Cl<sub>2</sub>): 1993 cm<sup>-1</sup> (ν<sub>CO</sub>, symmetric), 1923 cm<sup>-1</sup> (ν<sub>CO</sub>, asymmetric).

#### I.4.4. Oxidative addition products.

##### I.4.4.1. Synthesis and characterisation of NiBr(C<sub>3</sub>H<sub>5</sub>)(PMe<sub>2</sub>Ar<sup>Dtbp<sub>2</sub></sup>) (3·L1).

THF (1 mL) was added to an ampoule charged with Ni(cod)<sub>2</sub> (0.016 g, 0.057 mmol, 15% excess) and PMe<sub>2</sub>Ar<sup>Dtbp<sub>2</sub></sup> (0.026 g, 0.050 mmol), cooled to -30 °C. The vessel was then charged with CO (1 bar) and the cool bath removed. After the yellow colour of the Ni(cod)<sub>2</sub> faded from the solution, the mixture was frozen using a liquid N<sub>2</sub> bath and all gases were removed under vacuum. The mixture was stirred at room temperature for 90 min, after which all volatiles were removed under vacuum. The resulting white solid was dissolved in THF (1 mL) and allyl bromide (17 μL, 0.196 mmol, 4 eq) were added. After 30 min, the mixture was taken to dryness, extracted in pentane and filtered. Removal of volatiles under vacuum yielded the sought product as an orange powder. Yield: 0.028 g, 81%.



<sup>1</sup>H NMR (500 MHz, C<sub>6</sub>D<sub>6</sub>, 298 K): δ 7.57-7.54 (m, 6 H, *o*-Dtbp, *p*-Dtbp), 7.16 (dd, <sup>3</sup>J<sub>HH</sub> = 7.5 Hz, <sup>4</sup>J<sub>HP</sub> = 2.6 Hz, 2 H, *m*-C<sub>6</sub>H<sub>3</sub>), 7.07-7.02 (m, 1 H, *p*-C<sub>6</sub>H<sub>3</sub>), 4.26-4.17 (m, 1 H, H<sub>1</sub>), 3.81-3.79 (m, 1 H, H<sub>5</sub>), 2.55 (dd, <sup>3</sup>J<sub>HH</sub> = 14.2 Hz, <sup>3</sup>J<sub>HP</sub> = 5.4 Hz, 1 H, H<sub>4</sub>), 2.10-2.07 (m, 1 H, H<sub>2</sub>), 1.36 (s, 18 H, CH<sub>3</sub> <sup>t</sup>Bu), 1.35 (s, 18 H, CH<sub>3</sub> <sup>t</sup>Bu), 1.30 (d, <sup>2</sup>J<sub>HP</sub> = 7.7 Hz, 3 H, CH<sub>3</sub> Me), 1.22 (d, <sup>2</sup>J<sub>HP</sub> = 7.7 Hz, 3 H, CH<sub>3</sub> Me), 1.02 (dd, <sup>3</sup>J<sub>HH</sub> = 12.7 Hz, <sup>3</sup>J<sub>HP</sub> = 2.9 Hz, 1 H, H<sub>3</sub>).

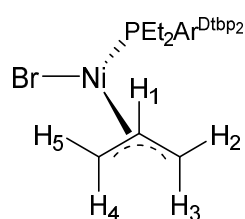
<sup>13</sup>C{<sup>1</sup>H} NMR (100 MHz, C<sub>6</sub>D<sub>6</sub>, 298 K): δ 150.6 (s, *m*-Dtbp), 149.2 (d, <sup>2</sup>J<sub>CP</sub> = 10 Hz, *o*-C<sub>6</sub>H<sub>3</sub>), 143.1 (d, <sup>3</sup>J<sub>CP</sub> = 5 Hz, *ipso*-Dtbp), 131.3 (d, <sup>3</sup>J<sub>CP</sub> = 6 Hz, *m*-C<sub>6</sub>H<sub>3</sub>), *ca.* 131.1 (*ipso*-C<sub>6</sub>H<sub>3</sub>), 129.0 (s, *p*-C<sub>6</sub>H<sub>3</sub>), 126.0 (s, *o*-Dtbp), 125.5 (s, *o*-Dtbp), 121.7 (s, *p*-Dtbp), 108.7 (s, C<sub>meso</sub>), 69.2 (d, <sup>2</sup>J<sub>CP</sub> = 23 Hz, C<sub>trans-P</sub>), 49.9 (d, <sup>2</sup>J<sub>CP</sub> = 6 Hz, C<sub>cis-P</sub>), 35.1 (s, C <sup>t</sup>Bu), 31.7 (s, CH<sub>3</sub> <sup>t</sup>Bu), 18.3 (d, <sup>1</sup>J<sub>CP</sub> = 27 Hz, CH<sub>3</sub> Me), 17.3 (d, <sup>1</sup>J<sub>CP</sub> = 28 Hz, CH<sub>3</sub> Me).

<sup>31</sup>P{<sup>1</sup>H} NMR (121 MHz, C<sub>6</sub>D<sub>6</sub>, 298 K): δ -2.5 (s).

Elemental analysis (%), calculated (found) for C<sub>39</sub>H<sub>56</sub>BrNiP: C, 67.45 (67.40); H, 8.13 (8.08).

#### I.4.4.2. Synthesis and characterisation of NiBr(C<sub>3</sub>H<sub>5</sub>)(PEt<sub>2</sub>Ar<sup>Dtbp2</sup>) (3·L6).

A solution of Ni(CO)<sub>3</sub>(PEt<sub>2</sub>Ar<sup>Dtbp2</sup>) (**1·L6**) (0.078 g, 0.113 mmol) in THF (2 mL) was treated with allyl bromide (40 μL, 0.462 mmol, 4 eq). After 1 h stirring at room temperature, the mixture was taken to dryness, dissolved in pentane and filtered. Removal of volatiles under vacuum rendered the sought product as an orange solid. Yield: 0.042 g, 51%.



<sup>1</sup>H NMR (400 MHz, C<sub>6</sub>D<sub>6</sub>, 298 K): δ 7.65-7.59 (br m, 4 H, *o*-Dtbp), 7.54 (t, <sup>4</sup>J<sub>HH</sub> = 1.8 Hz, 2 H, *p*-Dtbp), 7.08 (dd, <sup>3</sup>J<sub>HH</sub> = 7.6 Hz, <sup>4</sup>J<sub>HP</sub> = 2.5 Hz, 2 H, *m*-C<sub>6</sub>H<sub>3</sub>), 6.97-6.93 (m, 1 H, *p*-C<sub>6</sub>H<sub>3</sub>), 4.23-4.13 (m, 1 H, H<sub>1</sub>), 3.91-3.88 (m, 1 H, H<sub>5</sub>), 2.57 (dd, <sup>3</sup>J<sub>HH</sub> = 14.3 Hz, <sup>3</sup>J<sub>HP</sub> = 5.1 Hz, 1 H, H<sub>4</sub>), 2.09-2.00 (m, 2 H, H<sub>2</sub>, CH<sub>2</sub> Et), 1.67-1.57 (m, 1 H, CH<sub>2</sub> Et), 1.54-1.44 (m, 1 H, CH<sub>2</sub> Et), 1.38 (s, 36 H, CH<sub>3</sub> <sup>t</sup>Bu), 1.36-1.27 (m, 1 H, CH<sub>2</sub> Et), 1.05 (dt, <sup>3</sup>J<sub>HP</sub> = 17.6 Hz, <sup>3</sup>J<sub>HH</sub> = 7.6 Hz, 3 H, CH<sub>3</sub> Et), 0.89 (d, <sup>3</sup>J<sub>HH</sub> = 12.7 Hz, 1 H, H<sub>3</sub>), 0.84 (dt, <sup>3</sup>J<sub>HP</sub> = 15.5 Hz, <sup>3</sup>J<sub>HH</sub> = 7.6 Hz, 3 H, CH<sub>3</sub> Et).

<sup>13</sup>C{<sup>1</sup>H} NMR (100 MHz, C<sub>6</sub>D<sub>6</sub>, 298 K): δ 150.2 (d, *J* = 5 Hz, *m*-Dtbp), 148.8 (d, *J* = 9 Hz, *o*-C<sub>6</sub>H<sub>3</sub>), 143.2 (d, *J* = 4 Hz, *ipso*-Dtbp), 131.5 (d, *J* = 6 Hz, *m*-C<sub>6</sub>H<sub>3</sub>), 129.6 (d, *J* = 33 Hz, *ipso*-C<sub>6</sub>H<sub>3</sub>), *ca.* 128 (*p*-C<sub>6</sub>H<sub>3</sub>), 125.9 (s, *o*-Dtbp), 125.7 (s, *o*-Dtbp), 121.6 (s, *p*-Dtbp), 108.9 (s, C<sub>meso</sub>), 69.6 (d, <sup>2</sup>J<sub>CP</sub> = 21 Hz, C<sub>trans-p</sub>), 47.8 (d, <sup>2</sup>J<sub>CP</sub> = 6 Hz, C<sub>cis-p</sub>), 35.1 (s, C<sup>t</sup>Bu), 31.7 (s, CH<sub>3</sub> <sup>t</sup>Bu), 20.60 (d, <sup>1</sup>J<sub>CP</sub> = 24 Hz, CH<sub>2</sub> Et), 19.44 (d, <sup>1</sup>J<sub>CP</sub> = 24 Hz, CH<sub>2</sub> Et), 10.6 (s, CH<sub>3</sub> Et), 9.5 (s, CH<sub>3</sub> Et).

<sup>31</sup>P{<sup>1</sup>H} NMR (121 MHz, C<sub>6</sub>D<sub>6</sub>, 298 K): δ 23.2 (s).

Elemental analysis (%), calculated (found) for C<sub>41</sub>H<sub>60</sub>BrNiP: C, 68.16 (68.21); H, 8.37 (8.52).

**1.4.4.3. Synthesis and characterisation of  $[(\text{CH}_2=\text{CHCH}_2)\text{P}^i\text{Pr}_2\text{Ar}^{\text{Dtbp}_2}][\text{NiBr}_3]$  (4-L7).**

A solution of  $\text{Ni}(\text{CO})_2(\text{P}^i\text{Pr}_2\text{Ar}^{\text{Dtbp}_2})$  (**2-L7**) (0.056 g, 0.0812 mmol) in THF (2 mL) was treated with allyl bromide (28  $\mu\text{L}$ , 0.324 mmol, 4 eq). After 6 h stirring at room temperature, the reaction mixture was taken to dryness and washed with pentane, yielding the product as a bluish green solid. Yield: 0.048 g, 79%.

$[(\text{CH}_2=\text{CHCH}_2)\text{P}^i\text{Pr}_2\text{Ar}^{\text{Dtbp}_2}]^+ \text{NiBr}_3^-$   $^1\text{H}$  NMR (300 MHz,  $\text{CD}_3\text{CN}$ , 298 K):  $\delta$  7.79 (td,  $^3J_{\text{HH}} = 7.8$  Hz,  $^5J_{\text{HP}} = 2.2$  Hz, 1 H, *p*- $\text{C}_6\text{H}_3$ ), 7.67 (d,  $^4J_{\text{HH}} = 1.7$  Hz, 2 H, *p*-Dtbp), 7.46 (dd,  $^3J_{\text{HH}} = 7.7$  Hz,  $^4J_{\text{HP}} = 3.9$  Hz, 2 H, *m*- $\text{C}_6\text{H}_3$ ), 7.37 (d,  $^4J_{\text{HH}} = 1.7$  Hz, 4 H, *o*-Dtbp), 5.61-5.46 (m, 1 H,  $\text{CH}=\text{CH}_2$ ), 5.21-5.14 (m, 2 H,  $\text{CH}=\text{CH}_2$ ), 2.58 (dd,  $^2J_{\text{HP}} = 13.9$  Hz,  $^3J_{\text{HH}} = 6.7$  Hz, 2 H, *P*- $\text{CH}_2$ ), 2.45 (dsept,  $^2J_{\text{HP}} = 13.6$  Hz,  $^3J_{\text{HH}} = 7.1$  Hz, 2 H,  $\text{CH}^i\text{Pr}$ ), 1.38 (s, 36 H,  $\text{CH}_3^t\text{Bu}$ ), 1.18 (td,  $^3J_{\text{HP}} = 17.3$  Hz,  $^3J_{\text{HH}} = 7.2$  Hz, 6 H,  $\text{CH}_3^i\text{Pr}$ ), 1.13 (dd,  $^3J_{\text{HP}} = 17.1$ ,  $^3J_{\text{HH}} = 7.1$  Hz, 6 H,  $\text{CH}_3^i\text{Pr}$ ).

$^{13}\text{C}\{^1\text{H}\}$  NMR (100 MHz, acetone- $d_6$ , 298 K):  $\delta$  151.1 (s, *m*-Dtbp), 150.2 (d,  $^2J_{\text{CP}} = 8$  Hz, *o*- $\text{C}_6\text{H}_3$ ), 140.2 (d,  $^3J_{\text{CP}} = 2$  Hz, *ipso*-Dtbp), 134.3 (d,  $^3J_{\text{CP}} = 10$  Hz, *m*- $\text{C}_6\text{H}_3$ ), 133.2 (s, *p*- $\text{C}_6\text{H}_3$ ), 127.3 (d,  $^2J_{\text{CP}} = 8$  Hz,  $\text{CH}=\text{CH}_2$ ), 124.4 (s, *o*-Dtbp), 124.0 (d,  $^3J_{\text{CP}} = 14$  Hz,  $\text{CH}=\text{CH}_2$ ), 123.6 (s, *p*-Dtbp) ppm, 114.0 (d,  $^1J_{\text{CP}} = 70$  Hz, *ipso*- $\text{C}_6\text{H}_3$ ), 34.7 (s,  $\text{C}^t\text{Bu}$ ), 31.0 (s,  $\text{CH}_3^t\text{Bu}$ ), 27.2 (d,  $^1J_{\text{CP}} = 41$  Hz,  $\text{CH}^i\text{Pr}$ ), 25.3 (d,  $^1J_{\text{CP}} = 44$  Hz, *P*- $\text{CH}_2$ ), 18.8 (d,  $^2J_{\text{CP}} = 78$  Hz,  $\text{CH}_3^i\text{Pr}$ ).

$^{31}\text{P}\{^1\text{H}\}$  NMR (121 MHz,  $\text{CD}_3\text{CN}$ , 298 K):  $\delta$  42.2 (s).

Elemental analysis (%), calculated (found) for  $\text{C}_{43}\text{H}_{63}\text{Br}_3\text{NiP}$ : C, 56.73 (56.41); H, 7.09 (7.39).

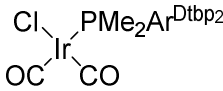
MS/ESI  $m/z$  (%): 611.7 ( $(\text{CH}_2=\text{CHCH}_2)\text{P}^i\text{Pr}_2\text{Ar}^{\text{Dtbp}_2}$ , 100).



#### I.4.5. Iridium carbonyl complexes.

##### I.4.5.1. Synthesis and characterisation of IrCl(CO)<sub>2</sub>(PMe<sub>2</sub>Ar<sup>Dtbp2</sup>) (5·L1).

CH<sub>2</sub>Cl<sub>2</sub> (3 mL) was added to a Schlenk tube charged with [Ir(μ-Cl)(cod)]<sub>2</sub> (0.0337, 0.050 mmol) and PMe<sub>2</sub>Ar<sup>Dtbp2</sup> (0.0570 g, 0.105 mmol, 5% excess). After stirring for 30 min, the vessel was cooled to 0 °C and charged with CO (0.9 bar). After the cool bath was removed, the solution was left to evolve from the initial red into yellow (*ca.* 1 h). The volatiles were evaporated under vacuum and the resulting residue was washed with pentane at –30 °C, rendering an intensely coloured yellow solid. Yield: 0.0677 g, 85%. Samples suitable for X-ray diffraction were obtained by slow evaporation from a pentane solution at room temperature.


<sup>1</sup>H NMR (300 MHz, C<sub>6</sub>D<sub>6</sub>, 298 K): δ 7.59 (t, <sup>4</sup>J<sub>HH</sub> = 1.8 Hz, 2 H, *p*-Dtbp), 7.54 (d, <sup>4</sup>J<sub>HH</sub> = 1.8 Hz, 4 H, *o*-Dtbp), *ca.* 7.16 (*m*-C<sub>6</sub>H<sub>3</sub>), 7.04–6.99 (m, 1 H, *p*-C<sub>6</sub>H<sub>3</sub>), 1.39 (s, 36 H, CH<sub>3</sub> <sup>t</sup>Bu), 1.21 (d, <sup>2</sup>J<sub>HP</sub> = 9.8 Hz, 6 H, CH<sub>3</sub> Me).

<sup>13</sup>C{<sup>1</sup>H} NMR (100 MHz, C<sub>6</sub>D<sub>6</sub>, 298 K): δ 179.1 (d, <sup>2</sup>J<sub>CP</sub> = 126 Hz, CO *trans* P), 170.2 (d, <sup>2</sup>J<sub>CP</sub> = 13 Hz, CO *cis* P), 151.2 (s, *m*-Dtbp), 149.2 (d, <sup>2</sup>J<sub>CP</sub> = 9 Hz, *o*-C<sub>6</sub>H<sub>3</sub>), 142.3 (d, <sup>3</sup>J<sub>CP</sub> = 4 Hz, *ipso*-Dtbp), 131.4 (d, <sup>3</sup>J<sub>CP</sub> = 8 Hz, *m*-C<sub>6</sub>H<sub>3</sub>), 130.0 (d, <sup>4</sup>J<sub>CP</sub> = 2 Hz, *p*-C<sub>6</sub>H<sub>3</sub>), *ca.* 129 (*ipso*-C<sub>6</sub>H<sub>3</sub>), 125.3 (s, *o*-Dtbp), 122.4 (s, *p*-Dtbp), 35.2 (s, C(CH<sub>3</sub>)<sub>3</sub> <sup>t</sup>Bu), 31.7 (s, CH<sub>3</sub> <sup>t</sup>Bu), 17.1 (d, <sup>2</sup>J<sub>CP</sub> = 38 Hz, CH<sub>3</sub> Me).

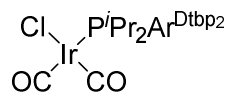
<sup>31</sup>P{<sup>1</sup>H} NMR (121 MHz, C<sub>6</sub>D<sub>6</sub>, 298 K): δ –3.5 (s).

IR (CH<sub>2</sub>Cl<sub>2</sub>): 2063 cm<sup>–1</sup> (ν<sub>CO</sub>, symmetric), 1984 cm<sup>–1</sup> (ν<sub>CO</sub>, asymmetric).

Elemental analysis (%), calculated (found) for C<sub>38</sub>H<sub>51</sub>ClIrO<sub>2</sub>P: C, 57.16 (56.81); H, 6.44 (6.84).

**I.4.5.2. General procedure for the synthesis of  $\text{IrCl}(\text{CO})_2(\text{PR}_2\text{Ar}'')$  ( $\text{R} = \textit{i}\text{Pr}, \text{Cyp}; \text{Ar}'' = \text{Ar}^{\text{Xyl}_2}, \text{Ar}^{\text{Dtbp}_2}$ ).**

$\text{CH}_2\text{Cl}_2$  (3-6 mL) was added to a Schlenk tube charged with equimolar amounts of  $\text{PR}_2\text{Ar}''$  (**L7**, **L10** or **L11**) and  $[\text{Ir}(\mu\text{-Cl})(\text{cod})]_2$ . The vessel was then cooled to 0 °C and charged with CO (0.9 bar). After the cool bath was removed, the solution was left to evolve from the initial red into yellow (*ca.* 1 h), after which volatiles were evaporated under vacuum. The resulting residue was extracted in pentane and filtered. Removal of the solvent under reduced pressure rendered the sought compounds as intense yellow solids in good yields.

**I.4.5.2.1. IrCl(CO)<sub>2</sub>(P<sup>i</sup>Pr<sub>2</sub>Ar<sup>Dtbp2</sup>) (5·L7).**

<sup>1</sup>H NMR (500 MHz, C<sub>6</sub>D<sub>6</sub>, 298 K): δ 7.62 (s, 4 H, *o*-Dtbp), 7.59 (s, 2 H, *p*-Dtbp), 7.09 (dd, <sup>3</sup>J<sub>HH</sub> = 7.5 Hz, <sup>4</sup>J<sub>HP</sub> = 2.7 Hz, 2 H, *m*-C<sub>6</sub>H<sub>3</sub>), 6.91 (br t, <sup>3</sup>J<sub>HH</sub> = 7.1 Hz, 1 H, *p*-C<sub>6</sub>H<sub>3</sub>), 2.91 (dsept, 2 H, <sup>1</sup>J<sub>HP</sub> = 12.7 Hz, <sup>3</sup>J<sub>HH</sub> = 7.2 Hz, CH <sup>i</sup>Pr), 1.46-1.40 (m, 42 H, CH<sub>3</sub> <sup>i</sup>Pr, CH<sub>3</sub> <sup>t</sup>Bu), 1.01 (dd, <sup>3</sup>J<sub>HP</sub> = 14.6 Hz, <sup>3</sup>J<sub>HH</sub> = 7.1 Hz, 6 H, CH<sub>3</sub> <sup>i</sup>Pr).

<sup>13</sup>C{<sup>1</sup>H} NMR (100 MHz, C<sub>6</sub>D<sub>6</sub>, 298 K): δ 178.4 (d, <sup>2</sup>J<sub>CP</sub> = 118 Hz, CO *trans* P), 169.5 (d, <sup>2</sup>J<sub>CP</sub> = 11 Hz, CO *cis* P), 150.3 (s, *o*-Dtbp), 149.9 (d, <sup>2</sup>J<sub>CP</sub> = 8 Hz, *o*-C<sub>6</sub>H<sub>3</sub>), 142.8 (d, <sup>3</sup>J<sub>CP</sub> = 4 Hz, *ipso*-Dtbp), 133.3 (d, <sup>3</sup>J<sub>CP</sub> = 7 Hz, *m*-C<sub>6</sub>H<sub>3</sub>), 129.1 (d, <sup>4</sup>J<sub>CP</sub> = 2 Hz, *p*-C<sub>6</sub>H<sub>3</sub>), 125.8 (s, *m*-Dtbp), 122.6 (s, *p*-Dtbp), 35.2 (s, C(CH<sub>3</sub>)<sub>3</sub> <sup>t</sup>Bu), 31.6 (s, CH<sub>3</sub> <sup>t</sup>Bu), 30.5 (d, <sup>1</sup>J<sub>CP</sub> = 11 Hz, CH <sup>i</sup>Pr), 28.4 (s, CH<sub>3</sub> <sup>i</sup>Pr), 22.5 (d, <sup>2</sup>J<sub>CP</sub> = 3 Hz, CH<sub>3</sub> <sup>i</sup>Pr).

<sup>13</sup>C{<sup>1</sup>H} NMR (126 MHz, CD<sub>2</sub>Cl<sub>2</sub>, 298 K): δ 178.1 (d, <sup>2</sup>J<sub>CP</sub> = 116 Hz, CO *trans* P), 168.8 (d, <sup>2</sup>J<sub>CP</sub> = 12 Hz, CO *cis* P), 150.2 (s, *m*-Dtbp), 149.9 (d, <sup>2</sup>J<sub>CP</sub> = 8 Hz, *o*-C<sub>6</sub>H<sub>3</sub>), 142.5 (d, <sup>3</sup>J<sub>CP</sub> = 4 Hz, *ipso*-Dtbp), 133.3 (d, <sup>3</sup>J<sub>CP</sub> = 7 Hz, *m*-C<sub>6</sub>H<sub>3</sub>), 129.0 (d, <sup>4</sup>J<sub>CP</sub> = 2 Hz, *p*-C<sub>6</sub>H<sub>3</sub>), 128.1 (d, <sup>1</sup>J<sub>CP</sub> = 38 Hz, *ipso*-C<sub>6</sub>H<sub>3</sub>), 125.6 (s, *o*-Dtbp), 122.7 (s, *p*-Dtbp), 35.3 (s, C(CH<sub>3</sub>)<sub>3</sub> <sup>t</sup>Bu), 31.6 (s, CH<sub>3</sub> <sup>t</sup>Bu), 30.6 (d, <sup>1</sup>J<sub>CP</sub> = 28 Hz, CH <sup>i</sup>Pr), 28.4 (s, CH<sub>3</sub> <sup>i</sup>Pr), 22.5 (d, <sup>2</sup>J<sub>CP</sub> = 3 Hz, CH<sub>3</sub> <sup>i</sup>Pr).

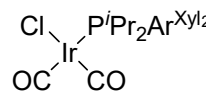
<sup>31</sup>P{<sup>1</sup>H} NMR (202 MHz, C<sub>6</sub>D<sub>6</sub>, 298 K): δ 40.7 (s).

IR (CH<sub>2</sub>Cl<sub>2</sub>): 2060 cm<sup>-1</sup> (ν<sub>CO</sub>, symmetric), 1980 cm<sup>-1</sup> (ν<sub>CO</sub>, asymmetric).

Elemental analysis (%), calculated (found) for C<sub>42</sub>H<sub>59</sub>ClIrO<sub>2</sub>P: C, 59.03 (59.01); H, 6.96 (7.31).

Yield: 0.1156 g, 80%.

**I.4.5.2.2. IrCl(CO)<sub>2</sub>(P<sup>i</sup>Pr<sub>2</sub>Ar<sup>Xyl<sub>2</sub></sup>) (5·L10).**


<sup>1</sup>H NMR (400 MHz, CDCl<sub>3</sub>, 298 K): δ 7.48 (td, <sup>3</sup>J<sub>HH</sub> = 7.6 Hz, <sup>5</sup>J<sub>HP</sub> = 1.9 Hz, 2 H, *p*-C<sub>6</sub>H<sub>3</sub>), 7.22-7.18 (m, 2 H, *p*-Xyl), 7.13-7.11 (m, 4 H, *m*-Xyl), 7.04 (dd, <sup>3</sup>J<sub>HH</sub> = 7.6 Hz, <sup>4</sup>J<sub>HP</sub> = 2.9 Hz, 2 H, *m*-C<sub>6</sub>H<sub>3</sub>), 2.59-2.46 (m, 2 H, CH <sup>i</sup>Pr), 2.19 (s, 12 H, CH<sub>3</sub> Xyl), 1.45 (dd, <sup>3</sup>J<sub>HP</sub> = 18.8 Hz, <sup>3</sup>J<sub>HH</sub> = 7.3 Hz, 6 H, CH<sub>3</sub> <sup>i</sup>Pr), 0.88 (dd, <sup>3</sup>J<sub>HP</sub> = 12.6 Hz, <sup>3</sup>J<sub>HH</sub> = 7.1 Hz, 6 H, CH<sub>3</sub> <sup>i</sup>Pr).

<sup>13</sup>C{<sup>1</sup>H} NMR (100 MHz, CDCl<sub>3</sub>, 298 K): δ 175.8 (d, <sup>2</sup>J<sub>CP</sub> = 118 Hz, CO *trans* P), 167.5 (d, <sup>2</sup>J<sub>CP</sub> = 11 Hz, CO *cis* P), 147.5 (d, <sup>2</sup>J<sub>CP</sub> = 8 Hz, *o*-C<sub>6</sub>H<sub>3</sub>), 143.1 (d, <sup>3</sup>J<sub>CP</sub> = 3 Hz, *ipso*-Xyl), 137.2 (s, *o*-Xyl), 132.9 (d, <sup>3</sup>J<sub>CP</sub> = 7 Hz, *m*-C<sub>6</sub>H<sub>3</sub>), 131.03 (d, <sup>1</sup>J<sub>CP</sub> = 33 Hz, *ipso*-C<sub>6</sub>H<sub>3</sub>), 130.5 (s, *p*-C<sub>6</sub>H<sub>3</sub>), 128.3 (s, *m*-Xyl), 128.0 (s, *p*-Xyl), 29.8 (d, <sup>1</sup>J<sub>CP</sub> = 25 Hz, CH <sup>i</sup>Pr), 24.0 (br s, CH<sub>3</sub> <sup>i</sup>Pr), 22.7 (s, Xyl), 21.2 (d, <sup>2</sup>J<sub>CP</sub> = 5 Hz, CH<sub>3</sub> <sup>i</sup>Pr).

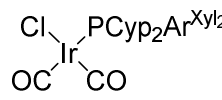
<sup>31</sup>P{<sup>1</sup>H} NMR (121 MHz, CDCl<sub>3</sub>, 298 K): δ 38.7 (s).

IR (CH<sub>2</sub>Cl<sub>2</sub>): 2064 cm<sup>-1</sup> (ν<sub>CO</sub>, symmetric), 1982 cm<sup>-1</sup> (ν<sub>CO</sub>, asymmetric).

Elemental analysis (%), calculated (found) for C<sub>30</sub>H<sub>35</sub>ClIrO<sub>2</sub>P: C, 52.51 (52.30); H, 5.14 (5.27).

Yield: 0.1740, 87%.

**I.4.5.2.3. IrCl(CO)<sub>2</sub>(PCyp<sub>2</sub>Ar<sup>Xyl<sub>2</sub></sup>) (5·L11).**


<sup>1</sup>H NMR (400 MHz, CD<sub>2</sub>Cl<sub>2</sub>, 298 K): δ 7.50 (td, <sup>3</sup>J<sub>HH</sub> = 7.6 Hz, <sup>5</sup>J<sub>HP</sub> = 1.9 Hz, 1 H, *p*-C<sub>6</sub>H<sub>3</sub>), 7.23-7.19 (m, 2 H, *p*-Xyl), 7.14-7.12 (m, 4 H, *m*-Xyl), 7.03 (dd, <sup>3</sup>J<sub>HH</sub> = 7.6 Hz, <sup>4</sup>J<sub>HP</sub> = 2.9 Hz, 2 H, *m*-C<sub>6</sub>H<sub>3</sub>), 2.45-2.34 (br m, 2 H, CH Cyp), 2.16 (s, 12 H, CH<sub>3</sub> Xyl), 2.00 (br, 2 H, CH<sub>2</sub> Cyp), 1.83 (br m, 2 H, CH<sub>2</sub> Cyp), 1.58 (br, 6 H, CH<sub>2</sub> Cyp), 1.39 (br, 2 H, CH<sub>2</sub> Cyp), 1.21 (br, 4 H, CH<sub>2</sub> Cyp).

<sup>13</sup>C{<sup>1</sup>H} NMR (100 MHz, C<sub>6</sub>D<sub>6</sub>, 298 K): δ 176.2 (d, <sup>2</sup>J<sub>CP</sub> = 119 Hz, CO *trans* P), 168.3 (d, <sup>2</sup>J<sub>CP</sub> = 12 Hz, CO *cis* P), 147.6 (d, <sup>2</sup>J<sub>CP</sub> = 8 Hz, *o*-C<sub>6</sub>H<sub>3</sub>), 143.3 (d, <sup>3</sup>J<sub>CP</sub> = 3 Hz, *ipso*-Xyl), 137.4 (s, *o*-Xyl), 132.8 (d, <sup>3</sup>J<sub>CP</sub> = 7 Hz, *m*-C<sub>6</sub>H<sub>3</sub>), 132.7 (d, <sup>1</sup>J<sub>CP</sub> = 35 Hz, *ipso*-C<sub>6</sub>H<sub>3</sub>), 130.8 (d, <sup>4</sup>J<sub>CP</sub> = 2 Hz, *p*-C<sub>6</sub>H<sub>3</sub>), 128.6 (s, *m*-Xyl), 128.2 (s, *p*-Xyl), 40.4 (d, <sup>1</sup>J<sub>CP</sub> = 29 Hz, CH Cyp), 33.2 (br, CH<sub>2</sub> Cyp), 31.6 (s, CH<sub>2</sub> Cyp), 26.9 (d, <sup>2</sup>J<sub>CP</sub> = 10 Hz, CH<sub>2</sub> Cyp), 25.5 (d, <sup>2</sup>J<sub>CP</sub> = 12 Hz, CH<sub>2</sub> Cyp), 22.6 (s, Xyl).

<sup>31</sup>P{<sup>1</sup>H} NMR (121 MHz, CD<sub>2</sub>Cl<sub>2</sub>, 298 K): δ 20.0 (s).

IR (CH<sub>2</sub>Cl<sub>2</sub>): 2063 cm<sup>-1</sup> (ν<sub>CO</sub>, symmetric), 1979 cm<sup>-1</sup> (ν<sub>CO</sub>, asymmetric).

Elemental analysis (%), calculated (found) for C<sub>34</sub>H<sub>39</sub>ClIrO<sub>2</sub>P: C, 55.31 (55.25); H, 5.32 (5.34).

Yield: 0.1845 g, 84%.

**I.4.5.3. General procedure for the synthesis of non-isolated  $\text{IrCl}(\text{CO})_2(\text{PR}_2\text{Ar}'')$  (**5-PR<sub>2</sub>Ar''**).**

$\text{CH}_2\text{Cl}_2$  (1-2 mL) was added to an ampoule charged with  $[\text{Ir}(\mu\text{-Cl})(\text{cod})]_2$  (0.010-0.025 mmol) and  $\text{PR}_2\text{Ar}''$  (0.022-0.055 mmol, 10% excess). The vessel was then charged with CO (1 bar) at 0 °C and the cool bath was then removed. The reaction mixture was stirred out at room temperature for 1 hour and analysed by means of IR spectroscopy.

**$\text{IrCl}(\text{CO})_2(\text{PEt}_2\text{Ar}^{\text{Dtbp}_2})$  (**5-L6**).**

IR ( $\text{CH}_2\text{Cl}_2$ ): 2065  $\text{cm}^{-1}$  ( $\nu_{\text{CO}}$ , symmetric), 1984  $\text{cm}^{-1}$  ( $\nu_{\text{CO}}$ , asymmetric).

**$\text{IrCl}(\text{CO})_2(\text{PCyp}_2\text{Ar}^{\text{Dtbp}_2})$  (**5-L8**).**

IR ( $\text{CH}_2\text{Cl}_2$ ): 2058  $\text{cm}^{-1}$  ( $\nu_{\text{CO}}$ , symmetric), 1978  $\text{cm}^{-1}$  ( $\nu_{\text{CO}}$ , asymmetric).

**$\text{IrCl}(\text{CO})_2(\text{PCy}_2\text{Ar}^{\text{Dtbp}_2})$  (**5-L9**).**

IR ( $\text{CH}_2\text{Cl}_2$ ): 2056  $\text{cm}^{-1}$  ( $\nu_{\text{CO}}$ , symmetric), 1980  $\text{cm}^{-1}$  ( $\nu_{\text{CO}}$ , asymmetric).

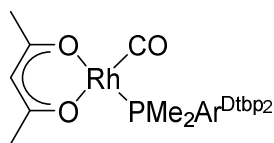
**$\text{IrCl}(\text{CO})_2(\text{PCy}_2\text{Ar}^{\text{Xyl}_2})$  (**5-L12**).**

IR ( $\text{CH}_2\text{Cl}_2$ ): 2062  $\text{cm}^{-1}$  ( $\nu_{\text{CO}}$ , symmetric), 1980  $\text{cm}^{-1}$  ( $\nu_{\text{CO}}$ , asymmetric).

#### I.4.6. Rhodium carbonyl complexes.

##### I.4.6.1. Synthesis and characterisation of Rh(acac)(CO)(PMe<sub>2</sub>Ar<sup>Dtbp2</sup>) (6·L1).

THF (2 mL) was added to a Schlenk tube charged with Rh(acac)(CO)<sub>2</sub> (0.0129 g, 0.050 mmol) and PMe<sub>2</sub>Ar<sup>Dtbp2</sup> (0.0271 g, 0.053 mmol). The mixture was stirred for 90 minutes and then taken to dryness. The resulting residue was washed with pentane, extracted in CH<sub>2</sub>Cl<sub>2</sub> and filtered to a weighed vial. Removal of volatiles, first under a N<sub>2</sub> flow and then under vacuum, rendered the sought product as a yellow solid. Yield: 0.0297 g, 80%. The samples thus obtained are suitable for most purposes, but contain 5% of phosphine according to <sup>1</sup>H NMR; analytically pure samples can be obtained by recrystallisation from a hexane/CH<sub>2</sub>Cl<sub>2</sub> mixture at -30 °C. Samples suitable for X-ray diffraction studies can be obtained by slow evaporation from a pentane solution.



<sup>1</sup>H NMR (300 MHz, CDCl<sub>3</sub>, 298 K): δ 7.56 (br, 4 H, *o*-Dtbp), 7.50-7.45 (m, 3 H, *p*-C<sub>6</sub>H<sub>3</sub>, *p*-Dtbp), 7.30 (dd, <sup>3</sup>J<sub>HH</sub> = 7.4 Hz, <sup>4</sup>J<sub>HP</sub> = 3.0 Hz, 2 H, *m*-C<sub>6</sub>H<sub>3</sub>), 5.47 (s, 1 H, CH acac), 2.06 (s, 3 H, CH<sub>3</sub> acac), 1.54 (s, 3 H, CH<sub>3</sub> acac), 1.36 (s, 36 H, CH<sub>3</sub> <sup>t</sup>Bu), 0.77 (dd, <sup>2</sup>J<sub>HP</sub> = 9.1 Hz, <sup>3</sup>J<sub>HRh</sub> = 1.9 Hz, 6 H, P-CH<sub>3</sub>).

<sup>13</sup>C{<sup>1</sup>H} NMR (100 MHz, CDCl<sub>3</sub>, 298 K): δ 189.7 (dd, <sup>1</sup>J<sub>CRh</sub> = 78 Hz, <sup>2</sup>J<sub>CP</sub> = 27 Hz, CO), 187.8 (s, CO acac), 184.8 (s, CO acac), 151.0 (s, *m*-Dtbp), 147.9 (d, <sup>2</sup>J<sub>CP</sub> = 7 Hz, *o*-C<sub>6</sub>H<sub>3</sub>), 142.5 (d, <sup>3</sup>J<sub>CP</sub> = 3 Hz, *ipso*-Dtbp), 130.7 (d, <sup>1</sup>J<sub>CP</sub> = 41 Hz, *ipso*-C<sub>6</sub>H<sub>3</sub>), 130.5 (d, <sup>3</sup>J<sub>CP</sub> = 7 Hz, *m*-C<sub>6</sub>H<sub>3</sub>), 128.6 (d, <sup>4</sup>J<sub>CP</sub> = 2 Hz, *p*-C<sub>6</sub>H<sub>3</sub>), 124.7 (s, *m*-Dtbp), 121.7 (s, *p*-Dtbp), 100.5 (d, <sup>4</sup>J<sub>CP</sub> = 2 Hz, CH acac), 35.1 (s, C <sup>t</sup>Bu), 31.7 (s, CH<sub>3</sub> <sup>t</sup>Bu), 27.8 (d, <sup>4</sup>J<sub>CP</sub> = 5 Hz, CH<sub>3</sub> acac), 27.3 (s, CH<sub>3</sub> acac), 20.4 (dd, <sup>1</sup>J<sub>CP</sub> = 38 Hz, <sup>3</sup>J<sub>CRh</sub> = 2 Hz, P-CH<sub>3</sub>).

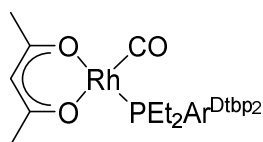
<sup>31</sup>P{<sup>1</sup>H} NMR (121 MHz, CD<sub>2</sub>Cl<sub>2</sub>, 298 K): δ 28.4 (d, <sup>1</sup>J<sub>PRh</sub> = 167 Hz).

IR (CH<sub>2</sub>Cl<sub>2</sub>): 1961 cm<sup>-1</sup> (ν<sub>CO</sub>).

Elemental analysis (%), calculated (found) for C<sub>42</sub>H<sub>58</sub>O<sub>3</sub>PRh: C, 67.73 (67.99); H, 7.85 (7.47).

**I.4.6.2. Synthesis and characterisation of Rh(acac)(CO)(PEt<sub>2</sub>Ar<sup>Dtbp2</sup>) (6·L6).**

THF (2 mL) was added to a Schlenk tube charged with Rh(acac)(CO)<sub>2</sub> (0.0130 g, 0.050 mmol) and PEt<sub>2</sub>Ar<sup>Dtbp2</sup> (0.0271 g, 0.050 mmol). The mixture was stirred for 2 h and then taken to dryness. The resulting residue was extracted in CH<sub>2</sub>Cl<sub>2</sub> and filtered to a weighed vial. Removal of volatiles, first under a N<sub>2</sub> flow and then under vacuum, rendered the sought product as a yellow solid. Yield: 0.0384 g, 99%. Analytically pure samples can be obtained by recrystallisation from pentane at -30 °C.



<sup>1</sup>H NMR (400 MHz, CDCl<sub>3</sub>, 298 K): δ 7.59 (br s, 4 H, *o*-Dtbp), 7.46-7.42 (m, 3 H, *m*-Dtbp, *p*-C<sub>6</sub>H<sub>3</sub>), 7.26 (br dd, <sup>3</sup>J<sub>HH</sub> = 7.4 Hz, <sup>4</sup>J<sub>HP</sub> = 2.3 Hz, 1 H, *m*-C<sub>6</sub>H<sub>3</sub>), 5.46 (s, 1 H, CH acac), 2.07 (s, 3 H, CH<sub>3</sub> acac), 1.52 (s, 3 H, CH<sub>3</sub> acac), 1.37 (s, 36 H, CH<sub>3</sub> <sup>t</sup>Bu), 1.17-1.06 (m, 4 H, CH<sub>2</sub> Et), 0.65 (dt, <sup>3</sup>J<sub>HP</sub> = 15.5 Hz, <sup>3</sup>J<sub>HH</sub> = 7.4 Hz, 6 H, CH<sub>3</sub> Et).

<sup>13</sup>C{<sup>1</sup>H} NMR (100 MHz, CDCl<sub>3</sub>, 298 K): δ 190.5 (dd, <sup>1</sup>J<sub>CRh</sub> = 78 Hz, <sup>2</sup>J<sub>CP</sub> = 25 Hz, CO), 187.8 (s, CO acac), 184.7 (s, CO acac), 150.6 (s, *m*-Dtbp), 148.4 (d, <sup>2</sup>J<sub>CP</sub> = 6 Hz, *o*-C<sub>6</sub>H<sub>3</sub>), 143.0 (d, <sup>3</sup>J<sub>CP</sub> = 1 Hz, *ipso*-Dtbp), 131.1 (d, <sup>3</sup>J<sub>CP</sub> = 7 Hz, *m*-C<sub>6</sub>H<sub>3</sub>), 128.2 (s, *p*-C<sub>6</sub>H<sub>3</sub>), 127.4 (d, <sup>1</sup>J<sub>CP</sub> = 36 Hz, *ipso*-C<sub>6</sub>H<sub>3</sub>), 124.6 (s, *m*-Dtbp), 121.6 (s, *p*-Dtbp), 100.6 (s, CH acac), 35.1 (s, C <sup>t</sup>Bu), 31.7 (s, CH<sub>3</sub> <sup>t</sup>Bu), 27.8 (d, <sup>4</sup>J<sub>CP</sub> = 6 Hz, CH<sub>3</sub> acac), 27.2 (s, CH<sub>3</sub> acac), 19.7 (d, <sup>1</sup>J<sub>CP</sub> = 33 Hz, CH<sub>2</sub> Et), 9.0 (d, <sup>2</sup>J<sub>CP</sub> = 2 Hz, CH<sub>3</sub> Et).

<sup>31</sup>P{<sup>1</sup>H} NMR (162 MHz, CD<sub>2</sub>Cl<sub>2</sub>, 298 K): δ 52.4 (d, <sup>1</sup>J<sub>PRh</sub> = 168 Hz).

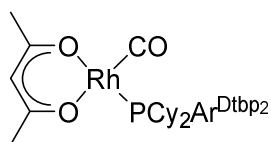
IR (CH<sub>2</sub>Cl<sub>2</sub>): 1959 cm<sup>-1</sup> (ν<sub>CO</sub>).

Elemental analysis (%), calculated (found) for C<sub>44</sub>H<sub>62</sub>O<sub>3</sub>PRh: C, 68.38 (68.18); H, 8.09 (8.16).



**I.4.6.3. Synthesis and characterisation of Rh(acac)(CO)(PCy<sub>2</sub>Ar<sup>Dtbp<sub>2</sub></sup>) (6-L9).**

THF (2 mL) was added to a Schlenk tube charged with Rh(acac)(CO)<sub>2</sub> (0.0129 g, 0.050 mmol) and PCy<sub>2</sub>Ar<sup>Dtbp<sub>2</sub></sup> (0.0328 g, 0.050 mmol). The mixture was stirred for 90 minutes and then taken to dryness. The resulting residue was extracted in pentane and filtered to a weighed vial. Removal of volatiles, first under a N<sub>2</sub> flow and then under vacuum, rendered the sought product as an orange solid. Yield: 0.0428 g, 97%. The samples thus obtained are suitable for most purposes, but contain *ca.* 9% of unknown impurities according to <sup>31</sup>P NMR; analytically pure samples can be obtained by crystallisation from pentane at -30 °C.



<sup>1</sup>H NMR (400 MHz, CDCl<sub>3</sub>, 298 K): δ 7.66 (d, <sup>4</sup>J<sub>HH</sub> = 1.8 Hz, 4 H, *o*-Dtbp), 7.44 (t, <sup>4</sup>J<sub>HH</sub> = 1.8 Hz, 2 H, *p*-Dtbp), 7.33-7.37 (m, 1 H, *p*-C<sub>6</sub>H<sub>3</sub>), 7.19 (dd, <sup>3</sup>J<sub>HH</sub> = 7.6 Hz, <sup>4</sup>J<sub>HP</sub> = 2.6 Hz, 2 H, *m*-C<sub>6</sub>H<sub>3</sub>), 5.39 (s, 1 H, CH acac), 2.08-2.02 (m, 6 H, CH<sub>3</sub> acac), 1.93-1.83 (br m, 3 H, Cy), 1.66-1.57 (br, 6 H, Cy), 1.38 (s, 36 H, CH<sub>3</sub> <sup>t</sup>Bu), 1.17-1.07 (br m, 4 H, Cy), 1.03-0.93 (br m, 3 H, Cy), 0.83-0.72 (br m, 2 H, Cy), 0.68-0.57 (br m, 2 H, Cy).

<sup>13</sup>C{<sup>1</sup>H} NMR (100 MHz, CDCl<sub>3</sub>, 298 K): δ 191.7 (dd, <sup>1</sup>J<sub>CRh</sub> = 76 Hz, <sup>2</sup>J<sub>CP</sub> = 22 Hz, CO), 187.6 (s, CO acac), 184.2 (s, CO acac), 150.2 (s, *m*-Dtbp), 149.1 (d, <sup>2</sup>J<sub>CP</sub> = 6 Hz, *o*-C<sub>6</sub>H<sub>3</sub>), 144.1 (d, <sup>3</sup>J<sub>CP</sub> = 2 Hz, *ipso*-Dtbp), 133.3 (d, <sup>3</sup>J<sub>CP</sub> = 7 Hz, *m*-C<sub>6</sub>H<sub>3</sub>), 127.6 (d, <sup>4</sup>J<sub>CP</sub> = 2 Hz, *p*-C<sub>6</sub>H<sub>3</sub>), 127.3 (d, <sup>1</sup>J<sub>CP</sub> = 27 Hz, *ipso*-C<sub>6</sub>H<sub>3</sub>), 125.0 (s, *m*-Dtbp), 122.0 (s, *p*-Dtbp), 100.8 (d, <sup>4</sup>J<sub>CP</sub> = 2 Hz, CH acac), 39.4 (d, <sup>1</sup>J<sub>CP</sub> = 25 Hz, CH Cy), 35.1 (s, C <sup>t</sup>Bu), 31.9-31.6 (m, CH<sub>2</sub> Cy, CH<sub>3</sub> <sup>t</sup>Bu), 30.9-30.8 (m, CH<sub>2</sub> Cy, CH<sub>3</sub> acac), 28.1 (d, J<sub>CP</sub> = 13 Hz, CH<sub>2</sub> Cy), 27.9-27.8 (m, CH<sub>2</sub> Cy, CH<sub>3</sub> acac), 26.0 (s, CH<sub>2</sub> Cy).

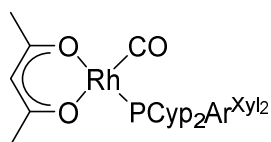
<sup>31</sup>P{<sup>1</sup>H} NMR (162 MHz, CD<sub>2</sub>Cl<sub>2</sub>, 298 K): δ 69.4 (d, <sup>1</sup>J<sub>PRh</sub> = 171 Hz).

IR (CH<sub>2</sub>Cl<sub>2</sub>): 1957 cm<sup>-1</sup> (ν<sub>CO</sub>).

Elemental analysis (%), calculated (found) for C<sub>57</sub>H<sub>74</sub>O<sub>3</sub>PRh: C, 70.89 (70.97); H, 8.47 (8.47).

**I.4.6.4. Synthesis and characterisation of Rh(acac)(CO)(PCyp<sub>2</sub>Ar<sup>Xyl<sub>2</sub></sup>) (6-L11).**

THF (2 mL) was added to a Schlenk tube charged with Rh(acac)(CO)<sub>2</sub> (0.0128 g, 0.050 mmol) and PCyp<sub>2</sub>Ar<sup>Xyl<sub>2</sub></sup> (0.0229 g, 0.050 mmol). The mixture was stirred for 5 days and then taken to dryness. The resulting residue was extracted in pentane and filtered to a weighed vial. Removal of volatiles, first under a N<sub>2</sub> flow and then under vacuum, rendered the sought product as a yellow solid. Yield: 0.0310 g, 91%. Analytically pure samples can be obtained by recrystallisation from pentane at -80 °C.



<sup>1</sup>H NMR (400 MHz, CDCl<sub>3</sub>, 298 K): δ 7.47 (td, <sup>4</sup>J<sub>HH</sub> = 7.5 Hz, <sup>5</sup>J<sub>HP</sub> = 1.7 Hz, 1 H, *p*-C<sub>6</sub>H<sub>3</sub>), 7.11 (t, <sup>3</sup>J<sub>HH</sub> = 7.5 Hz, 2 H, *p*-Xyl), 7.07 (dd, <sup>3</sup>J<sub>HH</sub> = 7.5 Hz, <sup>4</sup>J<sub>HP</sub> = 2.4 Hz, 2 H, *m*-C<sub>6</sub>H<sub>3</sub>), 7.01 (d, <sup>3</sup>J<sub>HH</sub> = 7.6 Hz, 4 H, *m*-Xyl), 5.31 (s, 1 H, CH acac), 2.10 (s, 12 H, CH<sub>3</sub> Xyl), 1.99-1.86 (m, 6 H, Cyp, CH<sub>3</sub> acac), 1.81-1.70 (m, 5 H, Cyp, CH<sub>3</sub> acac), 1.62-1.43 (m, 6 H, Cyp), 1.39-1.18 (m, 7 H, Cyp).

<sup>13</sup>C{<sup>1</sup>H} NMR (100 MHz, CDCl<sub>3</sub>, 298 K): δ 190.8 (dd, <sup>1</sup>J<sub>CRh</sub> = 77 Hz, <sup>2</sup>J<sub>CP</sub> = 22.2 Hz, CO), 186.7 (s, CO acac), 182.7 (s, CO acac), 147.6 (br s, *o*-C<sub>6</sub>H<sub>3</sub>), 143.2 (d, <sup>3</sup>J<sub>CP</sub> = 4 Hz, *ipso*-Xyl), 136.4 (s, *o*-Xyl), 135.5 (d, <sup>1</sup>J<sub>CP</sub> = 27 Hz, *ipso*-C<sub>6</sub>H<sub>3</sub>), 131.7 (d, <sup>3</sup>J<sub>CP</sub> = 7 Hz, *m*-C<sub>6</sub>H<sub>3</sub>), 129.8 (s, *p*-C<sub>6</sub>H<sub>3</sub>), 127.4 (*m*-Xyl), 127.1 (*p*-Xyl), 100.8 (CH acac), 41.7 (d, <sup>1</sup>J<sub>CP</sub> = 29 Hz, CH Cyp), 32.5 (d, *J*<sub>CP</sub> = 8 Hz, CH<sub>2</sub> Cyp), 31.2 (d, *J*<sub>CP</sub> = 3 Hz, CH<sub>2</sub> Cyp), 28.0 (d, <sup>4</sup>J<sub>CP</sub> = 6 Hz, CH<sub>3</sub> acac), 26.4-25.6 (m, CH<sub>2</sub> Cyp, CH<sub>3</sub> acac), 22.3 (s, CH<sub>3</sub> Xyl).

<sup>31</sup>P{<sup>1</sup>H} NMR (162 MHz, CD<sub>2</sub>Cl<sub>2</sub>, 298 K): δ 58.3 (d, <sup>1</sup>J<sub>PRh</sub> = 184 Hz).

IR (CH<sub>2</sub>Cl<sub>2</sub>): 1956 cm<sup>-1</sup> (ν<sub>CO</sub>).

Elemental analysis (%), calculated (found) for C<sub>38</sub>H<sub>46</sub>O<sub>3</sub>PRh: C, 66.66 (66.47); H, 6.77 (7.03).

**I.4.6.5. General procedure for the synthesis of non-isolated Rh(acac)(CO)(PR<sub>2</sub>Ar'') (6·PR<sub>2</sub>Ar'').**

CH<sub>2</sub>Cl<sub>2</sub> (0.5-1 mL) was added to a vial containing Rh(acac)(CO)<sub>2</sub> (0.0026 g, 0.010 mmol) and PR<sub>2</sub>Ar'' (0.011 mmol, 10% excess). After CO stopped evolving from the solution (a few minutes), the reaction mixture was analysed by IR spectroscopy. Most complexes thus generated are accompanied by varying quantities of starting Rh(acac)(CO)<sub>2</sub> ( $\nu_{\text{CO}}$ : 2084 cm<sup>-1</sup>, 2012 cm<sup>-1</sup>).

**Rh(acac)(CO)(PMe<sub>2</sub>Ar<sup>Xyl</sup>)<sub>2</sub> (6·L2).**

IR (CH<sub>2</sub>Cl<sub>2</sub>): 1960 cm<sup>-1</sup> ( $\nu_{\text{CO}}$ ).

**Rh(acac)(CO)(PMe<sub>2</sub>Ar<sup>Dipp</sup>)<sub>2</sub> (6·L3).**

IR (CH<sub>2</sub>Cl<sub>2</sub>): 1962 cm<sup>-1</sup> ( $\nu_{\text{CO}}$ ).

**Rh(acac)(CO)(PMe<sub>2</sub>Ar<sup>Mes</sup>)<sub>2</sub> (6·L4).**

IR (CH<sub>2</sub>Cl<sub>2</sub>): 1960 cm<sup>-1</sup> ( $\nu_{\text{CO}}$ ).

**Rh(acac)(CO)(PMe<sub>2</sub>Ar<sup>Tripp</sup>)<sub>2</sub> (6·L5).**

IR (CH<sub>2</sub>Cl<sub>2</sub>): 1960 cm<sup>-1</sup> ( $\nu_{\text{CO}}$ ).

**Rh(acac)(CO)(P<sup>i</sup>Pr<sub>2</sub>Ar<sup>Dtbp</sup>)<sub>2</sub> (6·L7).**

IR (CH<sub>2</sub>Cl<sub>2</sub>): 1958 cm<sup>-1</sup> ( $\nu_{\text{CO}}$ ).

**Rh(acac)(CO)(PCyp<sub>2</sub>Ar<sup>Dtbp</sup>)<sub>2</sub> (6·L8).**

IR (CH<sub>2</sub>Cl<sub>2</sub>): 1957 cm<sup>-1</sup> ( $\nu_{\text{CO}}$ ).

**Rh(acac)(CO)(P<sup>i</sup>Pr<sub>2</sub>Ar<sup>Xyl</sup>)<sub>2</sub> (6·L10).**

IR (CH<sub>2</sub>Cl<sub>2</sub>): 1958 cm<sup>-1</sup> ( $\nu_{\text{CO}}$ ).

**Rh(acac)(CO)(PCy<sub>2</sub>Ar<sup>Xyl</sup>)<sub>2</sub> (6·L12).**

A reaction time of 2 h was needed in this case.

IR (CH<sub>2</sub>Cl<sub>2</sub>): 1954 cm<sup>-1</sup> ( $\nu_{\text{CO}}$ ).

#### **I.4.7. Computational details.**

Calculations were performed at the DFT level with the Gaussian09 program.<sup>52</sup> The Head-Gordon hybrid functional  $\omega$ B97X-D,<sup>53</sup> which includes empirical dispersion, was used throughout the computational study. Geometry optimizations were carried out without geometry constraints, using the 6-31G(d,p) basis set<sup>54</sup> to represent the C, H, P and O atoms and the Stuttgart/Dresden Effective Core Potential and its associated basis set (SDD)<sup>55</sup> to model the Ni atoms. The stationary points of the Potential Energy Surface and their nature as minima or saddle points (TS) were characterised by vibrational analysis, which also produced enthalpy (H), entropy (S) and Gibbs energy (G) data. The minima connected by a given transition state were determined by Intrinsic Reaction Coordinate (IRC) calculations or by perturbing the transition states along the TS coordinate and optimizing to the nearest minimum.

## I.5. BIBLIOGRAPHY

1. a) *Transition Metal Complexes of Phosphorus, Arsenic and Antimony Ligands*; McAuliffe, C. A., Ed.; Macmillan Education UK: London, 1973; b) *Phosphine, Arsine and Stibine Complexes of the Transition Elements*; McAuliffe, C. A., Levason, W., Eds.; Elsevier: Amsterdam, 1979; c) Malatesta, L.; Cenini, S. *Zerovalent Compounds of Metals*; Academic Press: London, 1974; d) *Homogeneous Catalysis with Metal Phosphine Complexes*; Pignolet, L. H., Ed.; Springer US: Boston, MA, 1983.
2. a) Bochmann, M. *Organometallics and Catalysis. An Introduction*; Oxford University Press: Oxford, 2015; b) Crabtree, R. H. *The Organometallic Chemistry of the Transition Metals*, 4th Ed.; John Wiley & Sons, Inc.: Hoboken, NJ, USA, 2005; c) Hartwig, J. F. *Organotransition Metal Chemistry: From Bonding to Catalysis*; University Science Books: Sausalito, 2010.
3. a) Valentine Jr., D. H.; Hillhouse, J. H. *Synthesis* **2003**, 2437–2460; b) Crabtree, R. H. *J. Organomet. Chem.* **2005**, 690, 5451–5457; c) Fleckenstein, C. A.; Plenio, H. *Chem. Soc. Rev.* **2010**, 39, 694–711.
4. a) Osborn, J. A.; Jardine, F. H.; Young, J. F.; Wilkinson, G. J. *Chem. Soc. A* **1966**, 1711–1732; b) Birch, A. J.; Williamson, D. H. Homogeneous Hydrogenation Catalysts in Organic Synthesis. In *Organic Reactions*; John Wiley & Sons, Inc.: Hoboken, NJ, USA, 2011; pp 1–186.
5. a) Schwab, P.; France, M. B.; Ziller, J. W.; Grubbs, R. H. *Angew. Chem. Int. Ed. Engl.* **1995**, 34, 2039–2041; b) Schwab, P.; Grubbs, R. H.; Ziller, J. W. *J. Am. Chem. Soc.* **1996**, 118, 100–110.
6. van Leeuwen, P. W. N. M. *Homogeneous Catalysis*; Springer Netherlands: Dordrecht, 2004.
7. Kendall, A. J.; Tyler, D. R. *Dalton Trans.* **2015**, 44, 12473–12483.

## Chapter I

8. a) Wu, K.; Doyle, A. G. *Nat. Chem.* **2017**, *9*, 779–784; b) Niemeyer, Z. L.; Milo, A.; Hickey, D. P.; Sigman, M. S. *Nat. Chem.* **2016**, *8*, 610–617; c) Christian, A. H.; Niemeyer, Z. L.; Sigman, M. S.; Toste, F. D. *ACS Catal.* **2017**, *7*, 3973–3978.
9. Keller, J.; Schlierf, C.; Nolte, C.; Mayer, P.; Straub, B. F. *Synthesis* **2006**, 354–365.
10. a) Petušková, J.; Patil, M.; Holle, S.; Lehmann, C. W.; Thiel, W.; Alcarazo, M. *J. Am. Chem. Soc.* **2011**, *133*, 20758–20760; b) Petušková, J.; Bruns, H.; Alcarazo, M. *Angew. Chem. Int. Ed.* **2011**, *50*, 3799–3802; c) Alcarazo, M. *Acc. Chem. Res.* **2016**, *49*, 1797–1805.
11. a) Chen, L.; Ren, P.; Carrow, B. P. *J. Am. Chem. Soc.* **2016**, *138*, 6392–6395; b) Buß, F.; Mehlmann, P.; Mück-Lichtenfeld, C.; Bergander, K.; Dielmann, F. *J. Am. Chem. Soc.* **2016**, *138*, 1840–1843; c) McAtee, J. R.; Yap, G. P. A.; Watson, D. A. *J. Am. Chem. Soc.* **2014**, *136*, 10166–10172; d) Proutiere, F.; Lyngvi, E.; Aufiero, M.; Sanhueza, I. A.; Schoenebeck, F. *Organometallics* **2014**, *33*, 6879–6884.
12. a) Kondoh, A.; Yorimitsu, H.; Oshima, K. *J. Am. Chem. Soc.* **2007**, *129*, 6996–6997; b) Lugo, C. A.; Moore, C. E.; Rheingold, A. L.; Lavallo, V. *Inorg. Chem.* **2015**, *54*, 2094–2096; c) Doherty, S.; Knight, J. G.; Ward, N. A. B.; Bittner, D. M.; Wills, C.; McFarlane, W.; Clegg, W.; Harrington, R. W. *Organometallics* **2013**, *32*, 1773–1788; d) Horak, K. T.; VanderVelde, D. G.; Agapie, T. *Organometallics* **2015**, *34*, 4753–4765.
13. a) Tolman, C. A.; Seidel, W. C.; Gosser, L. W. *Organometallics* **1983**, *2*, 1391–1396; b) Hu, R.-B.; Zhang, H.; Zhang, X.-Y.; Yang, S.-D. *Chem. Commun.* **2014**, *50*, 2193–2195; c) Zhang, H.; Hu, R.-B.; Zhang, X.-Y.; Li, S.-X.; Yang, S.-D. *Chem. Commun.* **2014**, *50*, 4686–4689.

14. Qiu, X.; Wang, M.; Zhao, Y.; Shi, Z. *Angew. Chem. Int. Ed.* **2017**, *56*, 7233–7237.
15. a) Surry, D. S.; Buchwald, S. L. *Angew. Chem. Int. Ed.* **2008**, *47*, 6338–6361; b) Martin, R.; Buchwald, S. L. *Acc. Chem. Res.* **2008**, *41*, 1461–1473; c) Surry, D. S.; Buchwald, S. L. *Chem. Sci.* **2011**, *2*, 27–50.
16. a) Smith, R. C.; Woloszynek, R. A.; Chen, W.; Ren, T.; Protasiewicz, J. D. *Tetrahedron Lett.* **2004**, *45*, 8327–8330; b) Partyka, D. V.; Washington, M. P.; Updegraff, J. B.; Chen, X.; Incarvito, C. D.; Rheingold, A. L.; Protasiewicz, J. D. *J. Organomet. Chem.* **2009**, *694*, 1441–1446.
17. a) Buster, B.; Diaz, A. A.; Graham, T.; Khan, R.; Khan, M. A.; Powell, D. R.; Wehmschulte, R. J. *Inorganica Chim. Acta* **2009**, *362*, 3465–3474; b) Diaz, A. A.; Young, J. D.; Khan, M. A.; Wehmschulte, R. J. *Inorg. Chem.* **2006**, *45*, 5568–5575.
18. a) Sasaki, S.; Chowdhury, R.; Yoshifuji, M. *Tetrahedron Lett.* **2004**, *45*, 9193–9196; b) Sasaki, S.; Izawa, M.; Yoshifuji, M. *Phosphorus Sulfur Silicon Relat. Elem.* **2014**, *189*, 1207–1215; c) Fujihara, T.; Semba, K.; Terao, J.; Tsuji, Y. *Angew. Chem. Int. Ed.* **2010**, *49*, 1472–1476.
19. a) Nguyen, T.; Sutton, A. D.; Brynda, M.; Fettinger, J. C.; Long, G. J.; Power, P. P. *Science* **2005**, *310*, 844–847; b) Wright, R. J.; Steiner, J.; Beaini, S.; Power, P. P. *Inorganica Chim. Acta* **2006**, *359*, 1939–1946; c) Wolf, R.; Brynda, M.; Ni, C.; Long, G. J.; Power, P. P. *J. Am. Chem. Soc.* **2007**, *129*, 6076–6077; d) Ni, C.; Ellis, B. D.; Fettinger, J. C.; Long, G. J.; Power, P. P. *Chem. Commun.* **2008**, 1014–1016; e) Ni, C.; Power, P. P. In *Metal-Metal Bonding*; Parkin, G., Ed.; Springer Berlin Heidelberg: Berlin, Heidelberg, 2010; pp 59–111; f) Bukhryakov, K. V.; Schrock, R. R.; Hoveyda, A. H.; Müller, P.; Becker, J. *Org. Lett.* **2017**, *19*, 2607–2609; g) Carrasco, M.; Faust, M.; Peloso, R.; Rodríguez, A.; López-Serrano, J.; Álvarez, E.; Maya, C.;

## Chapter I

- Power, P. P.; Carmona, E. *Chem. Commun.* **2012**, *48*, 3954–3956;
- h) Carrasco, M.; Mendoza, I.; Faust, M.; López-Serrano, J.; Peloso, R.; Rodríguez, A.; Álvarez, E.; Maya, C.; Power, P. P.; Carmona, E. *J. Am. Chem. Soc.* **2014**, *136*, 9173–9180; i) Carrasco, M.; Mendoza, I.; Álvarez, E.; Grrirane, A.; Maya, C.; Peloso, R.; Rodríguez, A.; Falceto, A.; Álvarez, S.; Carmona, E. *Chem. Eur. J.* **2015**, *21*, 410–421.
20. a) Gerber, L. C. H.; Schrock, R. R.; Müller, P.; Takase, M. K. *J. Am. Chem. Soc.* **2011**, *133*, 18142–18144; b) Fox, B. J.; Sun, Q. Y.; DiPasquale, A. G.; Fox, A. R.; Rheingold, A. L.; Figueroa, J. S. *Inorg. Chem.* **2008**, *47*, 9010–9020; c) Barnett, B. R.; Neville, M. L.; Moore, C. E.; Rheingold, A. L.; Figueroa, J. S. *Angew. Chem. Int. Ed.* **2017**, *56*, 7195–7199; d) Klare, H. F. T.; Oestreich, M.; Ito, J.; Nishiyama, H.; Ohki, Y.; Tatsumi, K. *J. Am. Chem. Soc.* **2011**, *133*, 3312–3315; e) Jones, C.; Waugh, M. *J. Organomet. Chem.* **2007**, *692*, 5086–5090; f) Hinz, A.; Schulz, A.; Villinger, A. *Inorg. Chem.* **2016**, *55*, 3692–3699; g) Nutz, M.; Borthakur, B.; Dewhurst, R. D.; Deißberger, A.; Dellermann, T.; Schäfer, M.; Krummenacher, I.; Phukan, A. K.; Braunschweig, H. *Angew. Chem. Int. Ed.* **2017**, *56*, 7975–7979; h) Braunschweig, H.; Dewhurst, R. D.; Hupp, F.; Nutz, M.; Radacki, K.; Tate, C. W.; Vargas, A.; Ye, Q. *Nature* **2015**, *522*, 327–330; i) Ghana, P.; Arz, M. I.; Das, U.; Schnakenburg, G.; Filippou, A. C. *Angew. Chem. Int. Ed.* **2015**, *54*, 9980–9985; j) Graham, C. M. E.; Pritchard, T. E.; Boyle, P. D.; Valjus, J.; Tuononen, H. M.; Ragogna, P. J. *Angew. Chem. Int. Ed.* **2017**, *56*, 6236–6240.
21. a) Carrasco, M.; Peloso, R.; Rodríguez, A.; Álvarez, E.; Maya, C.; Carmona, E. *Chem. Eur. J.* **2010**, *16*, 9754–9757; b) Carrasco, M.; Peloso, R.; Resa, I.; Rodríguez, A.; Sánchez, L.; Álvarez, E.; Maya, C.; Andreu, R.; Calvente, J. J.; Galindo, A.; et al. *Inorg. Chem.* **2011**, *50*, 6361–6371.
22. a) Campos, J.; Ortega-Moreno, L.; Conejero, S.; Peloso, R.; López-Serrano, J.; Maya, C.; Carmona, E. *Chem. Eur. J.* **2015**, *21*, 8883–8896; b) Espada, M.



- F.; Campos, J.; López-Serrano, J.; Poveda, M. L.; Carmona, E. *Angew. Chem. Int. Ed.* **2015**, *54*, 15379–15384; c) Moreno, J. J.; Espada, M. F.; Krüger, E.; López-Serrano, J.; Campos, J.; Carmona, E. *Eur. J. Inorg. Chem.* **2018**, 2309–2321; d) Ortega-Moreno, L.; Fernández-Espada, M.; Moreno, J. J.; Navarro-Gilbert, C.; Campos, J.; Conejero, S.; López-Serrano, J.; Maya, C.; Peloso, R.; Carmona, E. *Polyhedron* **2016**, *116*, 170–181; e) Ortega-Moreno, L.; Peloso, R.; Maya, C.; Suárez, A.; Carmona, E. *Chem. Commun.* **2015**, *51*, 17008–17011.
23. Nicholson, W. *A Journal of Natural Philosophy, Chemistry and the Arts: Volume 5*; Ulan Press, 1801.
24. a) Bhatt, V. Metal Carbonyls. In *Essentials of Coordination Chemistry*; Elsevier, 2016; pp 191–236; b) *Nature* **1898**, *59*, 63–64.
25. Tolman, C. A. *J. Am. Chem. Soc.* **1970**, *92*, 2953–2956.
26. a) Alcarazo, M. *Chem. Eur. J.* **2014**, *20*, 7868–7877; b) Gu, L.; Wolf, L. M.; Zieliński, A.; Thiel, W.; Alcarazo, M. *J. Am. Chem. Soc.* **2017**, *139*, 4948–4953.
27. a) Pickardt, J.; Rösch, L.; Schumann, H. *Z. Anorg. Allg. Chem.* **1976**, *426*, 66–76; b) Schaarschmidt, D.; Kühnert, J.; Tripke, S.; Alt, H. G.; Görl, C.; Ruffer, T.; Ecorchard, P.; Walfort, B.; Lang, H. *J. Organomet. Chem.* **2010**, *695*, 1541–1549; c) Zakharov, A. V.; Vishnevskiy, Y. V.; Allefeld, N.; Bader, J.; Kurscheid, B.; Steinhauer, S.; Hoge, B.; Neumann, B.; Stammler, H.-G.; Berger, R. J. F.; Mitzel, N. W. *Eur. J. Inorg. Chem.* **2013**, 3392–3404; d) Velian, A.; Lin, S.; Miller, A. J. M.; Day, M. W.; Agapie, T. *J. Am. Chem. Soc.* **2010**, *132*, 6296–6297.
28. Diebolt, O.; Fortman, G. C.; Clavier, H.; Slawin, A. M. Z.; Escudero-Adán, E. C.; Benet-Buchholz, J.; Nolan, S. P. *Organometallics* **2011**, *30*, 1668–1676.
29. a) Dorta, R.; Stevens, E. D.; Hoff, C. D.; Nolan, S. P. *J. Am. Chem. Soc.* **2003**,

## Chapter I

- 125, 10490–10491; b) Dorta, R.; Stevens, E. D.; Scott, N. M.; Costabile, C.; Cavallo, L.; Hoff, C. D.; Nolan, S. P. *J. Am. Chem. Soc.* **2005**, *127*, 2485–2495.
30. a) Chianese, A. R.; Li, X.; Janzen, M. C.; Faller, J. W.; Crabtree, R. H. *Organometallics* **2003**, *22*, 1663–1667; b) Kelly III, R. A.; Clavier, H.; Giudice, S.; Scott, N. M.; Stevens, E. D.; Bordner, J.; Samardjiev, I.; Hoff, C. D.; Cavallo, L.; Nolan, S. P. *Organometallics* **2008**, *27*, 202–210.
31. Chen, W.; Esteruelas, M. A.; Martín, M.; Oliván, M.; Oro, L. A. *J. Organomet. Chem.* **1997**, *534*, 95–103.
32. Wolf, S.; Plenio, H. *J. Organomet. Chem.* **2009**, *694*, 1487–1492.
33. a) Huynh, H. V.; Han, Y.; Ho, J. H. H.; Tan, G. K. *Organometallics* **2006**, *25*, 3267–3274; b) Huynh, H. V.; Han, Y.; Jothibasur, R.; Yang, J. A. *Organometallics* **2009**, *28*, 5395–5404; c) Guo, S.; Sivaram, H.; Yuan, D.; Huynh, H. V. *Organometallics* **2013**, *32*, 3685–3696; d) Teng, Q.; Huynh, H. V. *Dalton Trans.* **2017**, *46*, 614–627.
34. a) Kaye, S.; Fox, J. M.; Hicks, F. A.; Buchwald, S. L. *Adv. Synth. Catal.* **2001**, *343*, 789–794; b) Hoshiya, N.; Buchwald, S. L. *Adv. Synth. Catal.* **2012**, *354*, 2031–2037.
35. *Phosphorus-31 NMR Spectroscopy*; Kühl, O., Ed.; Springer Berlin Heidelberg: Berlin, Heidelberg, 2009.
36. Barder, T. E.; Buchwald, S. L. *J. Am. Chem. Soc.* **2007**, *129*, 5096–5101.
37. Single crystals were grown and analysed by X-ray diffraction independently to this thesis.
38. Marín, M.; Moreno, J. J.; Navarro-Gilabert, C.; Álvarez, E.; Maya, C.; Peloso, R.; Nicasio, M. C.; Carmona, E. *Chem. Eur. J.* **2019**, *25*, 260–272.
39. Pauling, L. *The Nature of the Chemical Bond*; Cornell University Press: Ithaca, New York (United States), 1960.

40. a) Bonnafoux, L.; Leroux, F. R.; Colobert, F. *Beilstein J. Org. Chem.* **2011**, *7*, 1278–1287; b) Pratap, R.; Parrish, D.; Gunda, P.; Venkataraman, D.; Lakshman, M. K. *J. Am. Chem. Soc.* **2009**, *131*, 12240–12249.
41. Both made by Dr. J. J. Moreno as part of a collaborative effort to explain the behaviour of these phosphines.
42. a) Paul, U. S. D.; Radius, U. *Organometallics* **2017**, *36*, 1398–1407; b) Paul, U. S. D.; Sieck, C.; Haehnel, M.; Hammond, K.; Marder, T. B.; Radius, U. *Chem. Eur. J.* **2016**, *22*, 11005–11014.
43. Cordero, B.; Gómez, V.; Platero-Prats, A. E.; Revés, M.; Echeverría, J.; Cremades, E.; Barragán, F.; Alvarez, S. *Dalton Trans.* **2008**, 2832–2838.
44. a) Bogdanović, B.; Kröner, M.; Wilke, G. *Justus Liebigs Ann. Chem.* **1966**, *699*, 1–23; b) Cook, C. D.; Koo, C. H.; Nyburg, S. C.; Shiomi, M. T. *Chem. Commun. (London)* **1967**, 426b–427.
45. Petz, W.; Weller, F.; Uddin, J.; Frenking, G. *Organometallics* **1999**, *18*, 619–626.
46. Stucky, G.; D'Agostino, S.; McPherson, G. *J. Am. Chem. Soc.* **1966**, *88*, 4828–4831.
47. Moreno Díaz, J. J. Preparación, Estructura y Reactividad de Diversos Complejos de Iridio con Ligandos Fosfina Voluminosos. Master's Degree Dissertation, Universidad de Sevilla, 2013.
48. Serron, S.; Huang, J.; Nolan, S. P. *Organometallics* **1998**, *17*, 534–539.
49. a) Schiemenz, B.; Power, P. P. *Organometallics* **1996**, *15*, 958–964; b) Simons, R. S.; Haubrich, S. T.; Mork, B. V.; Niemeyer, M.; Power, P. P. *Main Group Chem.* **1998**, *2*, 275–283.
50. Wielandt, J. W.; Ruckerbauer, D., *Inorg. Synth.* **2010**, *35*, 120–125.

## Chapter I

51. Herde, J. L.; Lambert, J. C.; Senoff, C. V.; Cushing, M. A., *Inorg. Synth.*, **2007**, *15*, 18–20.
52. Gaussian 09, Revision B.01. Firsch, M. J.; Trucks, G. W.; Shlegel, H. B.; Scuseria, G. E.; Robb, M. A.; Cheeseman, J. R.; Scalmani, G.; Barone, V.; Mennucci, B.; Petersson, G. A.; Nakatsuji, H.; Caricato, M.; Li, X.; Hratchian, H.P.; Izmaylov, A. F.; Bloino, J.; Zheng, G.; Sonnenberg, J. L.; Hada, M.; Ehara, M.; Toyota, K.; Fukuda, R.; Hasegawa, J.; Ishida, M.; Nakajima, T.; Honda, Y.; Kitao, O.; Nakai, H.; Vreven, T.; Montgomery Jr., J. A.; Peralta, J. E.; Ogliaro, F.; Bearpark, M.; Heyd, J. J.; Brothers, E.; Kudin, K. N.; Staroverov, V. N.; Keith, T.; Kobayashi, R.; Normand, J.; Raghavachari, K.; Rendell, A.; Burant, J. C.; Iyengar, S. S.; Tomasi, J.; Cossi, M.; Rega, N.; Millam, J. M.; Klene, M.; Knox, J. E.; Cross, J. B.; Bakken, V.; Adamo, C.; Jaramillo, J.; CGomperts, R.; Stratmann, R. E.; Yazyev, O.; Austin, A. J.; Cammi, R.; Pomelli, C.; Ochterski, J. W.; Martin, R. L.; Morokuma, K.; Zakrzewski, V. G.; Voth, G. A.; Salvador, P.; Dannenberg, J. J.; Dapprich, S.; Daniels, A. D.; Farkas, O.; Foresman, J. B.; Ortiz, J. V.; Cioslowski, J.; Fox, D.J. Gaussian, Inc., Wallingford CT, **2010**.
53. Chai, J.-D.; Head-Gordon, M. *Phys. Chem. Chem. Phys.* **2008**, *10*, 6615.
54. a) Hehre, W. J.; Ditchfield, R.; Pople, J. A. *J. Chem. Phys.* **1972**, *56*, 2257–2261; b) Hariharan, P. C.; Pople, J. A. *Theor. Chim. Acta* **1973**, *28*, 213–222; c) Francl, M. M.; Pietro, W. J.; Hehre, W. J.; Binkley, J. S.; Gordon, M. S.; DeFrees, D. J.; Pople, J. A. *J. Chem. Phys.* **1982**, *77*, 3654–3665.
55. Andrae, D.; Häussermann, U.; Dolg, M.; Stoll, H.; Preuss, H. *Theor. Chim. Acta* **1990**, *77*, 123–141.

## **CHAPTER II.**

---

Synthesis and study of nickel, palladium  
and platinum complexes of dialkyl  
terphenyl phosphines



## II.1. INTRODUCTION

Nickel, palladium and platinum, the group-10 metals, have been instrumental in the development of Organometallic Chemistry.<sup>1</sup> As a prominent example, platinum(II) complex  $K[PtCl_3(\eta^2-C_2H_4)] \cdot H_2O$  (**I** in Figure 1), named Zeise's salt, discovered as early as 1831,<sup>2</sup> was the first organometallic compound bearing an organic ligand bonded to the metal centre. However, it was not until the 1950s that Zeise's salt was characterised as a  $\pi$ -alkene complex.<sup>3</sup> Since then, the chemistry of  $\pi$ -complexes (alkenes and alkynes) has expanded considerably. As stated in the Introduction to Chapter I,  $Ni(CO)_4$  (**II**) is a representative example of another important family of organometallic compound, metal carbonyls. The platinum methyl complex of empirical formula  $Pt(Me)_3I$  (**III**), synthesised in 1907 by Pope and Peachy,<sup>4a</sup> is among the earliest examples of transition metal alkyls. Its tetrameric structure was not disclosed until more than 50 years later.<sup>4b</sup> The finding in 1958 by Reppe and co-workers of the cyclic oligomerisation of

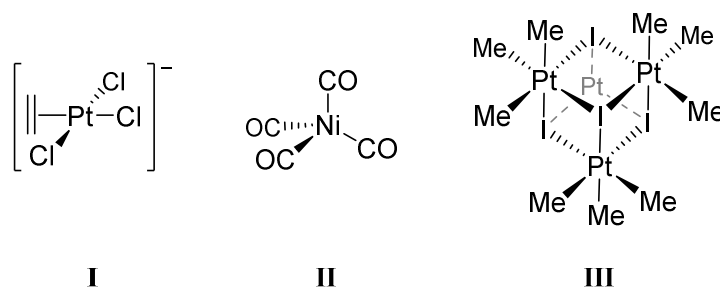


Figure 1. Examples of early organometallic complexes of the group-10 metals.

## Chapter II

acetylenes catalysed by Ni(II) complexes<sup>5</sup> caused a surge of interest that led to the discovery in 1960 of  $\pi$ -allyl complexes, of which those based on Pd(II) are the most numerous.

In addition to this, contributions of the group-10 triad to the field of homogeneous catalysis have been particularly significant. Among the three metals, palladium is by far the most versatile and widely used transition metal in modern organic synthesis.<sup>6</sup> Its applications span from the synthesis of polymers to pharmaceuticals. Palladium-mediated processes include oxidations,<sup>7</sup> hydrogenations,<sup>8</sup> carbonylations,<sup>9</sup> cycloisomerisations<sup>10</sup> and C–C and C–heteroatom bond forming reactions.<sup>11,12</sup> The use of palladium in organic chemistry was stimulated by the discovery, in the late 1950s, that ethylene was oxidised to acetaldehyde by air in the presence of a Pd(II) catalyst, the key reaction of the industrial Wacker process for the synthesis of acetaldehyde (Figure 2).<sup>13</sup>

This finding inspired the work of T. Mizoroki<sup>14</sup> and R. Heck,<sup>15</sup> which independently demonstrated the coupling reaction between an aryl halide and an alkene using Pd(II) catalysis (Figure 3). This reaction, known as the Heck-Mizoroki reaction, laid the foundations of one of the most powerful tools for the creation of C–C bonds: the palladium-catalysed cross-coupling reactions.<sup>11,16</sup> The extraordinary impact of palladium catalysis in contemporary organic chemistry was recognised in 2010 with the Nobel Prize in Chemistry, awarded to R. Heck, E. Negishi and A. Suzuki for their pioneering work on the formation of carbon-carbon single bonds through palladium-catalysed cross-coupling reactions.<sup>17</sup>

Since the organometallic chemistry of nickel, palladium and platinum are well developed, the following sections of the Introduction will review only some aspects that are in line with the results described in this chapter.



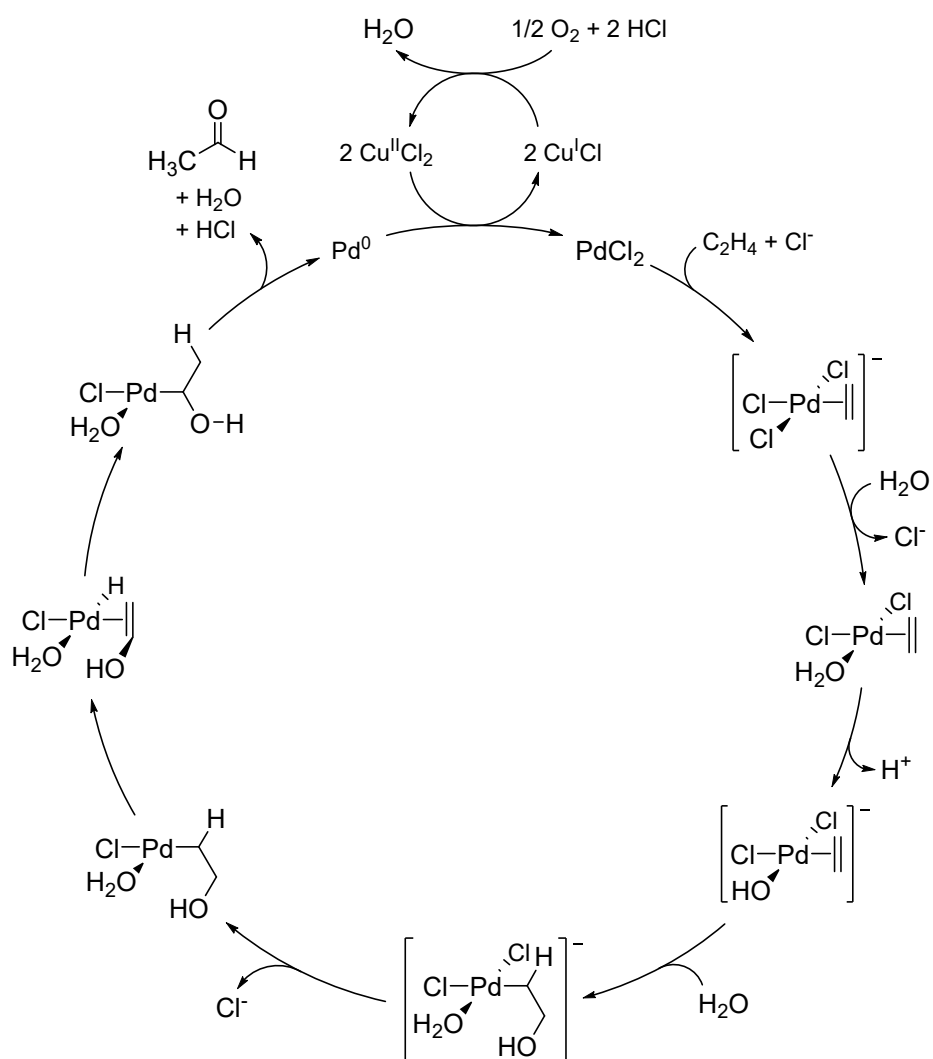
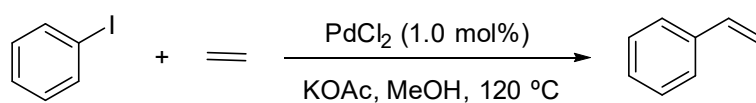
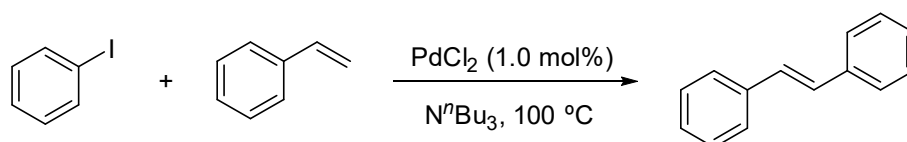


Figure 2. Proposed mechanism for the palladium-catalysed oxidation of ethylene to acetaldehyde in the Wacker process.

## Chapter II



Mizoroki 1971



Heck 1972

Figure 3. Cross-coupling reactions first reported by Mizoroki (top) and Heck (bottom).

### II.1.1. Pd(II) and Pt(II) complexes with low coordination number.

The most common oxidation state for group-10 elements is M(II). Whereas Ni(II) complexes can be found in a variety of coordination geometries (square-planar or tetrahedral for a coordination number of 4, trigonal bipyramidal or square pyramidal for a coordination number of 5 and octahedral for a coordination number of 6), Pd(II) and Pt(II) usually form four-coordinated complexes with square-planar geometry.<sup>1a</sup> Three-coordinate Pd(II) and Pt(II) complexes have been proposed as intermediates in stoichiometric and catalytic transformations. For example, in palladium-catalysed cross-coupling reactions, three-coordinate organopalladium(II) complexes are claimed to be the species that form the C–C or C–heteroatom bond in the product during the reductive eliminations from palladium complexes with monodentate ligands.<sup>18–20</sup>

There are few examples of unsaturated three-coordinate Pd(II)<sup>21</sup> and Pt(II)<sup>22</sup> complexes that have been isolated and they usually exhibit a T-shaped geometry (**VIII** and **IX** in Figure 10, respectively). From a kinetic viewpoint, other species can also be considered three-coordinate. We refer to those complexes that feature a weak interaction with a solvent molecule or with a bond that is located at the fourth coordination site of the metal centre.<sup>23</sup> This weak ligand,

which can be easily displaced in solution, provides an additional stabilisation of the complex. This is the situation often encountered for palladium(II) complexes bearing Buchwald's phosphines. The bulkiness of the biaryl phosphine ligands blocks the coordination of solvent/ligand to the palladium centre while the biaryl group provides stabilisation through secondary interactions between the  $\pi$ -system of the lower ring (see, for example, **IV** in Figure 9).<sup>24</sup>

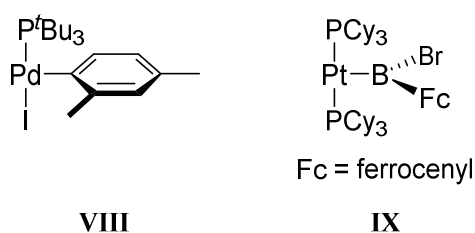


Figure 10. Three-coordinate T-shaped Pd(II) and Pt(II) complexes.

This hemilabile interaction has also been observed in transition metal complexes bearing dialkyl terphenyl phosphines.<sup>25,26</sup> More particularly, several examples of low-coordinate platinum complexes stabilised by these phosphines have been prepared recently in our group, including Pt(II) compounds of formula  $\text{PtCl}_2(\text{PMe}_2\text{Ar}'')$ .<sup>26</sup> These were synthesised by addition of the corresponding terphenyl phosphine ( $\text{PMe}_2\text{Ar}^{\text{Dipp}_2}$  or  $\text{PMe}_2\text{Ar}^{\text{Tripp}_2}$ ) to commercial  $\text{PtCl}_2$ , as illustrated in Figure 11.

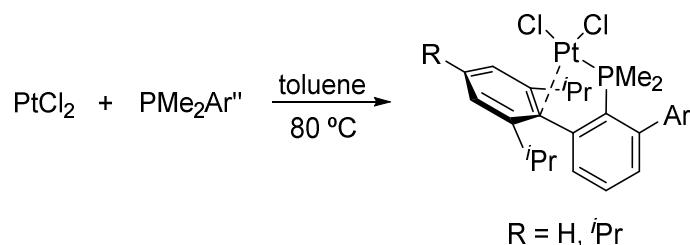


Figure 11. Synthesis of complexes  $\text{PtCl}_2(\text{PMe}_2\text{Ar}'')$ .

With the object of expanding this line of work, we set out to prepare new  $\text{PtCl}_2(\text{PR}_2\text{Ar}'')$  complexes of terphenyl phosphines bearing bulkier alkyl groups, as well as to extend this methodology to the synthesis of the  $\text{PdCl}_2(\text{PR}_2\text{Ar}'')$  analogues.

### II.1.2. $\eta^3$ -Allyl transition metal complexes. Generalities.

The allyl ligand ( $\text{CH}_2\text{CHCH}_2$ ) is a ubiquitous organic ligand in organometallic chemistry, forming moderately stable complexes with almost all the transition metal series.<sup>27,28</sup> The allyl ligand binds to a metal centre with  $\eta^3$  hapticity, that is, through all three carbon atoms, serving as a 3-electron donor (Figure 4-A), or as a  $\eta^1$  ligand, formally acting as a 1-electron donor (Figure 4-B). Moreover, the  $\eta^3$ -allyl ligand can also bridge two metal centres in a symmetric  $\eta^3$  mode (Figure 4-C),<sup>29</sup> or in a more unusual  $\eta^1, \eta^2$  or  $\eta^1, \eta^3$  fashion (Figure 4-D).<sup>30</sup>

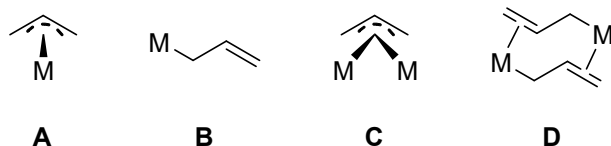


Figure 4. Different coordination modes of the allyl ligand. **A:**  $\eta^3$ , **B:**  $\eta^1$ , **C** and **D:** bridging.

The allyl ligand is most frequently found, both in homoleptic and mixed-ligand complexes, in a  $\eta^3$  coordination mode. In this binding mode, the orbital interactions comprise donation of the  $\pi$ -electrons from the HOMO of the allyl moiety to the metal centre and  $\pi$  back-donation of the metal  $d$ -electrons to the LUMO of the allyl group. Due to this interaction, the plane that contains the three carbon atoms of the allyl group is tilted in such a way that the central carbon becomes more distant to the metal centre than the terminal carbons. As a consequence, the two hydrogen atoms in *anti* position with respect to the central

H atom are placed much closer to the metal centre than the other three (Figure 5-**A**).<sup>31a</sup> In contrast, when the terminal carbons of the allyl moiety bear substituents, these do not lie in the same plane defined by the three allyl carbon atoms. The substituents in *syn* position move away from the metal centre whereas those in *anti* position move closer (Figure 5-**B**).<sup>31b</sup>

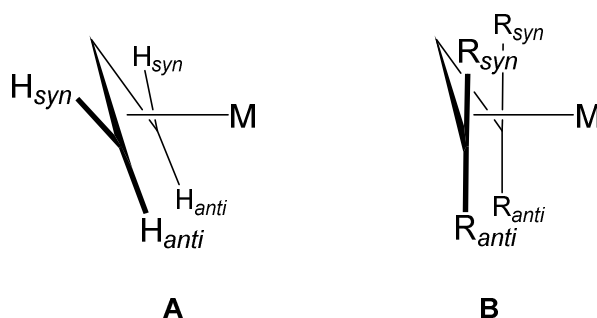


Figure 5. Spatial disposition of an unsubstituted (**A**) and a tetrasubstituted (**B**)  $\eta^3$ -allyl ligand.

The chloride-bridged dimer  $[\text{Pd}(\eta^3\text{-C}_3\text{H}_5)(\mu\text{-Cl})_2]_2$ , the first compound that was correctly described as a  $\eta^3$ -allyl metal complex, was prepared by Smidt and Hafner in 1959 from the reaction of palladium chloride with allyl alcohol (Figure 6-**A**).<sup>32a</sup> On the other hand,  $\text{Ni}(\eta^3\text{-C}_3\text{H}_5)_2$  was the first homoleptic allyl metal complex to be isolated. This compound was obtained by Wilke from the addition of a solution of allylmagnesium chloride in ether to anhydrous nickel bromide at  $-10\text{ }^\circ\text{C}$  (Figure 6-**B**).<sup>32b</sup>

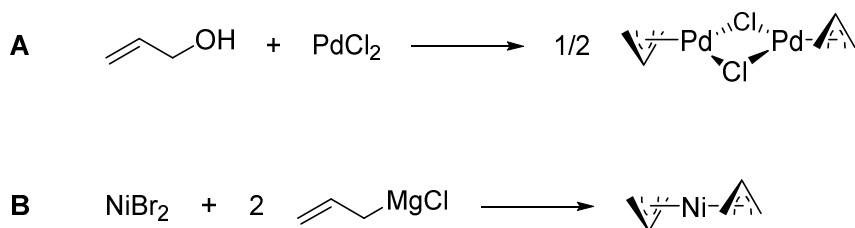


Figure 6. Syntheses of two transition metal  $\eta^3$ -allyl complexes.

## Chapter II

When the  $\eta^3$ -allyl ligand is not involved in any fluxional process in solution, it displays a characteristic pattern of signals in the  $^1\text{H}$  NMR spectrum. Since *anti* protons, as mentioned above, are closer to the metal centre, they experience a larger shielding than the *syn* protons. Consequently, the former appear at higher frequencies (between 1-3 ppm) than the latter (between 2-5 ppm). The resonance of the central proton usually appears between 4-6.5 ppm and exhibits strong couplings with the *syn* and *anti* protons (coupling constant values of about 7 and 11 Hz, respectively). However, dynamic behaviour is frequently observed in solution for many  $\eta^3$ -allyl complexes. Although these fluxional processes will be discussed in more detail later on, they will be briefly commented here. One of these dynamic processes is the rapid  $\eta^3$ - $\eta^1$ - $\eta^3$  isomerisation, which at the  $\eta^1$  stage allows the free rotation around the single C-C and M-C bonds, thus exchanging the position of the *syn* and *anti* protons of the allyl terminus directly bound to the metal (Figure 7-A). A second fluxional process involving the formal rotation along the metal-allyl axis has also been observed (Figure 7-B).

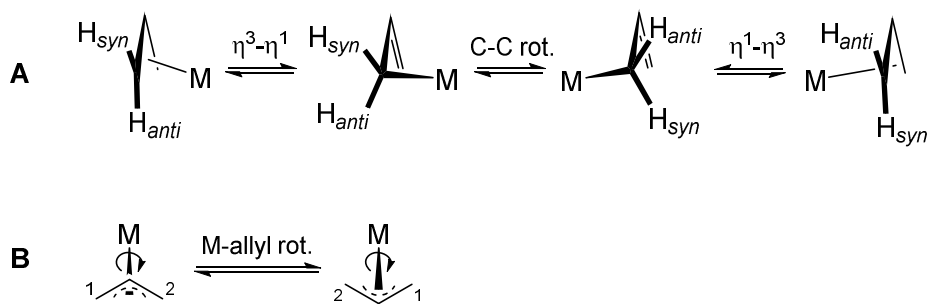


Figure 7. Two isomerisation processes commonly undergone by allyl complexes.

$\eta^3$ -Allyl nickel and palladium complexes participate in various catalytic transformations. For example,  $\text{Ni}(\eta^3\text{-C}_3\text{H}_5)_2$  catalyses a variety of cyclooligomerisations of butadiene, a process that was extensively studied by Wilke, Jolly and co-workers.<sup>33</sup> The cyclotrimerisation of butadiene to

cyclododecatriene was the first organometallic reaction subjected to a detailed mechanistic study, which revealed the occurrence of nickel  $\eta^3$ -allyl species as intermediates in the catalytic cycle.<sup>34</sup>

Palladium  $\eta^3$ -allyl complexes also play a part in diverse catalytic processes, such as diene telomerisation,<sup>35</sup> intramolecular alkene and alkyne insertions<sup>36</sup> and, even more importantly, allylic substitution reactions.<sup>37</sup> The latter transformations can be carried out enantioselectively and have been employed for the synthesis of natural products.<sup>38</sup> The generally accepted catalytic cycle for these transformations is depicted in Figure 8.

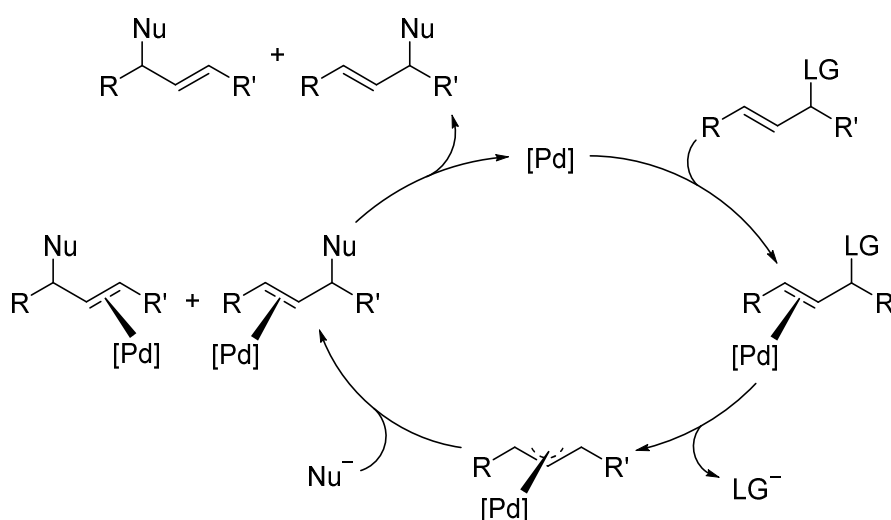


Figure 8. General cycle of a palladium-catalysed allylic substitution.

In recent years,  $\eta^3$ -allylpalladium complexes, accommodating both N-heterocyclic carbenes (NHC)<sup>39</sup> and phosphine ligands,<sup>40</sup> including Buchwald's phosphines,<sup>40b</sup> have been shown to be highly efficient precatalysts in C–C and C–heteroatom cross-coupling reactions.<sup>11,41</sup> These precatalysts are easily activated to the monoligated Pd<sup>0</sup>L active species in the presence of a base (e.g. NaO<sup>t</sup>Bu or even weaker bases such as K<sub>3</sub>PO<sub>4</sub>). By replacing the halide ligand by a weakly

## Chapter II

coordinating anion (i.e. triflate), complexes of the bulkier members of the dialkyl biaryl phosphine family could be obtained (**IV** in Figure 9).<sup>24b</sup> Concerning the allyl moiety in these complexes, introduction of a phenyl substituent on the terminal position of the allyl group (**V**) leads to somewhat more active precatalysts.<sup>24b</sup> Colacot and co-workers have demonstrated that the use of substituted allyl and/or bulky ligands suppresses the formation of  $\mu$ -allyl-bridged palladium(I) dimers (**VI**), which is deleterious for the catalytic activity.<sup>24b</sup> In this regard, Hazari and co-workers have found that the incorporation of a  $\eta^3$ -indenyl group (**VII**) into the compound structure inhibits the formation of inactive Pd(I) dimers, considerably improving the catalytic performance of these palladium precatalysts.<sup>42</sup>

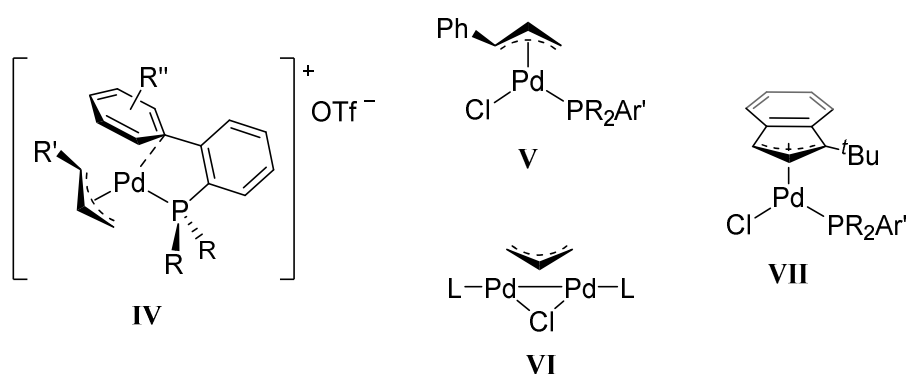


Figure 9. Some examples of  $\eta^3$ -allyl palladium complexes relevant in cross-coupling reactions.

Considering the increasing interest in first-row transition metal catalysis,<sup>43,44</sup> analogous  $\eta^3$ -allyl nickel complexes with NHC ligands have been used as precatalysts in bond-forming reactions, although to a lesser extent.<sup>45</sup> Interestingly, allyl nickel compounds supported by phosphine ligands have scarcely been applied in cross-coupling chemistry. Hartwig and co-workers have described the use of complex  $\text{NiCl}(\eta^3\text{-C}_3\text{H}_4\text{Ph})(\text{dppf})$  ( $\text{dppf} = 1,1'$ -



bis(diphenylphosphino)ferrocene) as a highly reactive precatalyst for Suzuki-Miyaura coupling of heteroaryl chlorides and heteroaryl boronic acids.<sup>46</sup> To the best of our knowledge, no reports on the synthesis and catalytic applications of  $\text{NiX}(\eta^3\text{-allyl})(\text{PR}_2\text{Ar}')$  complexes stabilised by Buchwald's phosphine ligands have been issued to date.

In view of the above, we thought of interest to prepare  $\eta^3$ -allyl derivatives of Ni(II) and Pd(II) stabilised by the terphenyl phosphines, which could be used to compare the performance of our phosphines and that of Buchwald's ligands in cross-coupling. In this chapter, a description of the synthesis and the details on the spectroscopic and structural properties of  $\text{MX}(\eta^3\text{-allyl})(\text{PR}_2\text{Ar}')$  complexes ( $\text{M} = \text{Ni}, \text{Pd}$ ) will be provided. However, the study of their catalytic activities in C–C and C–N bond forming reactions will not be presented, as it is the subject of another PhD Thesis that it is currently underway in our group.

### II.1.3. Zerovalent phosphine complexes of the group-10 metals.

Tetracarbonylnickel,  $\text{Ni}(\text{CO})_4$ , was the first coordination compound prepared in which the metal was in a low oxidation state. However, by the time Mond synthesised this adduct, the nature of the M–CO bond had not yet been established<sup>47</sup> and the compound was considered anomalous owing to its chemical and physical properties.

It was in the 1940s and 1950s when the interest in coordination compounds of zerovalent metals experienced a significant rise, particularly those based on  $d^{10}$  metals, i.e. Ni(0), Pd(0) and Pt(0). Between 1942 and 1943, the complexes  $\text{K}_4[\text{Ni}(\text{CN})_4]$ <sup>48a</sup> and  $\text{K}_4[\text{Pd}(\text{CN})_4]$ <sup>48b</sup> were obtained and, for the first time, the oxidation state zero was demonstrated for a metal in a complex anion and with a ligand different to CO.<sup>49</sup> The stability of these zerovalent compounds was rationalised in terms of metal-to-ligand  $\pi$  back-donation. When a poor  $\sigma$ -donor ligand possesses vacant low-energy orbitals of a suitable symmetry, these can

## Chapter II

interact with non-bonding metal *d* orbitals, thus forming  $\pi$ -bonds and contributing to the stabilisation of the *d* electrons of the metal.<sup>50</sup>

Malatesta and co-workers were pioneers in the preparation of Pd(0) and Pt(0) complexes with tertiary phosphine ligands by reducing Pd(II) or Pt(II) phosphine derivatives with different reductants like hydrazine, ethanolic potassium hydroxide or excess phosphine (Figure 12-A).<sup>51</sup> Tetra-coordinated Ni(0) phosphine complexes were prepared by Wilke later, in the early 1960s, by reduction of Ni(II) salts with trialkyl aluminium compounds in the presence of phosphine ligand (Figure 12-B).<sup>52</sup>

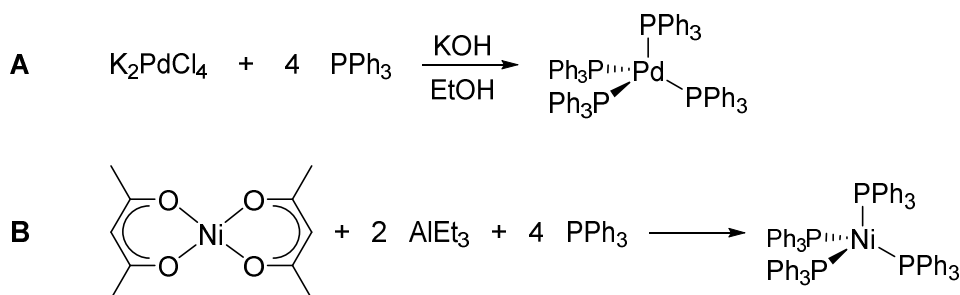
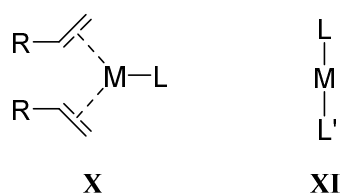


Figure 12. Syntheses of Pd(PPh<sub>3</sub>)<sub>4</sub> (A) and Ni(PPh<sub>3</sub>)<sub>4</sub> (B).

The homoleptic tertiary phosphine complexes of the  $d^{10}$ -metal triad display a variable stoichiometry, with coordination number of four and three observed for the large majority of compounds.<sup>53</sup> Remarkably, two-coordinated, 14-electron  $\text{M}^0(\text{PR}_3)_2$  species have also been described for the heavier members of the group-10 metals, palladium<sup>54</sup> and platinum.<sup>54c,55</sup> Regarding the nickel analogues, very few examples of di-coordinated compounds have been reported, containing  $\pi$ -acidic phosphite ligands.<sup>56</sup>

Monoligated  $\text{M}^0\text{L}$  species (L = bulky tertiary phosphine or NHC ligand) have been proposed as the active catalysts for many C–C and C–heteroatom bond-

forming reactions catalysed by group-10 metal complexes.<sup>57</sup> In recent years, a significant amount of interest has been placed in the development of precatalysts that can easily undergo ligand dissociation to generate the monoligated catalytically active species. These include complexes of general formula  $\text{Pd}(\text{olefin})_2(\text{L})$ <sup>58</sup> (**X** in Figure 13) as well as bisphosphine,<sup>59</sup> bis(NHC)<sup>60</sup> and mixed NHC/phosphine<sup>60h,61</sup>  $\text{PdL}_2$  complexes (**XI**). Many of these systems have been demonstrated to efficiently catalyse a variety of organic transformations and to serve as models for mechanistic investigations into the elementary steps of a catalytic cycle.



M = Ni, Pd or Pt

L, L' = NHC, phosphine ligands

*Figure 13. Coordinatively unsaturated zerovalent complexes of the group-10 metals.*

It is worth highlighting that examples of complexes similar to those depicted in Figure 13 but bearing Buchwald's phosphines are scarce and limited to palladium as metal centre.<sup>24a,59a</sup> Moreover, to the best of our knowledge, [1,4-bis{2-(diisopropylphosphino)phenyl}benzene]nickel(0) (Figure 14) is the only example of a  $\text{Ni}^0(\text{PR}_3)_2$  species containing a bidentate phosphine ligand that has been characterised.<sup>62</sup> However, analogous systems bearing monodentate phosphines remain unexplored.

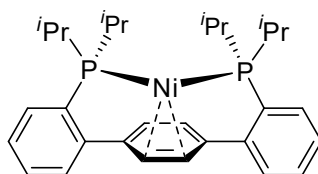


Figure 14. Only example of  $\text{Ni}^0(\text{PR}_3)_2$  complex reported in the literature.

Recently, in our group, a research line comprising the study of  $\text{Pt}(0)$  complexes stabilised by the terphenyl phosphine ligands has been initiated.<sup>63</sup> Complexes of composition  $\text{Pt}(\text{olefin})_{1-2}(\text{PMe}_2\text{Ar}'')$  ( $n = 1, 2$ ) have been synthesised which have turned out to be a source of monoligated, 12-electron  $\text{Pt}(\text{PMe}_2\text{Ar}'')$  fragments in solution. As a continuation of this work, we have focused here on the preparation of mixed-ligand  $\text{M}(\text{olefin})_{1-2}(\text{PR}_2\text{Ar}'')$  and homoleptic bisphosphine  $\text{M}(\text{PR}_2\text{Ar}'')$ <sub>2</sub> complexes of nickel, palladium and platinum. The results of this study will be described at the end of this chapter.

#### II.1.4. Aims.

The research presented in this chapter pursues the following objectives:

- *The assessment of the capabilities of the dialkyl terphenyl phosphines to stabilise metal complexes with low coordination number.*
- *The synthesis and characterisation of a family of  $\eta^3$ -allyl complexes based on palladium(II) and nickel(II) containing dialkyl terphenyl phosphines.*
- *The synthesis and characterisation of heteroleptic olefin-phosphine and homoleptic bisphosphine complexes of the group-10 metals in oxidation state zero stabilised by dialkyl terphenyl phosphines.*

## II.2. RESULTS AND DISCUSSION

This chapter addresses the synthesis, characterisation and reactivity of some nickel, palladium and platinum complexes, in different oxidation states, bearing dialkyl terphenyl phosphines. Of the twelve phosphines studied in Chapter I, five were selected for the studies that are described in the following sections. For convenience, the numbering scheme for these phosphines has been modified, as represented in Figure 15.

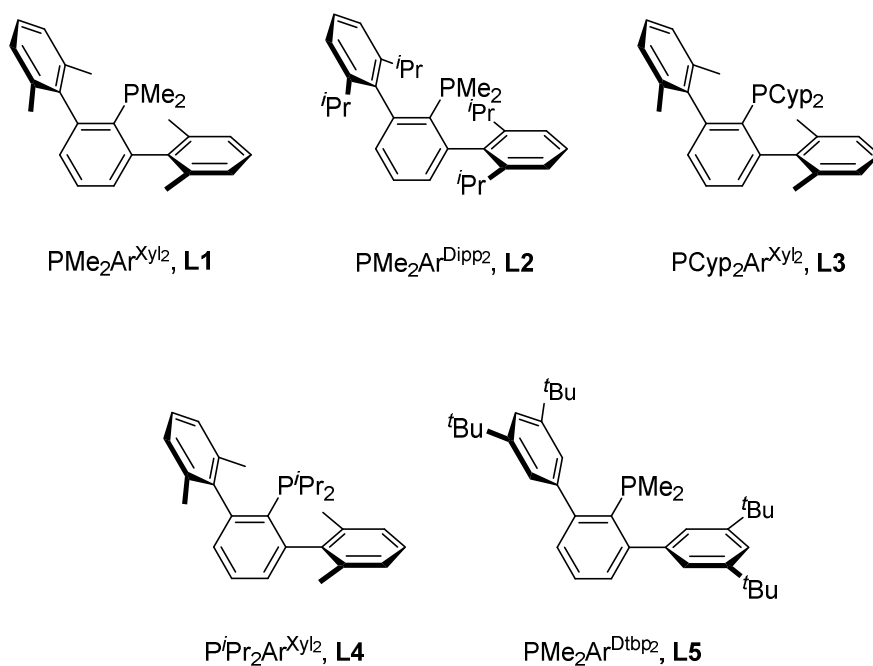


Figure 15. Dialkyl terphenyl phosphines used in this chapter.

### II.2.1. Dichloride Pd(II) and Pt(II) complexes of dialkyl terphenyl phosphines.

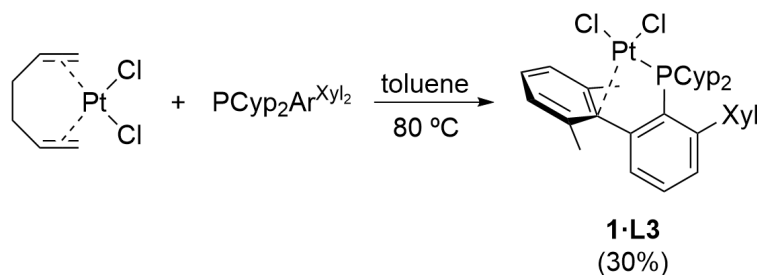
In a previous work carried out in our research group, some low-coordinate, formally 14-electron  $\text{PtCl}_2(\text{PMe}_2\text{Ar}'')$  complexes ( $\text{Ar}'' = \text{Ar}^{\text{Dipp}_2}$  or  $\text{Ar}^{\text{Tripp}_2}$ ) were synthesised by heating a mixture of  $\text{PtCl}_2$  and the corresponding phosphine in toluene.<sup>26a,63</sup> These compounds feature a weak  $\text{Pt}\cdots\text{C}_{\text{arene}}$  interaction with the *ipso* carbon of a flanking aryl ring of the terphenyl moiety. This interaction was easily displaced by Lewis bases such as CO or  $\text{PR}_3$ .<sup>64</sup>

Thus, it was considered of interest to extend this family of unsaturated Pt(II) complexes as well as to synthesise analogous Pd(II) dichloride monophosphine adducts. The reactivity of the resulting complexes towards various Lewis bases was probed.

#### II.2.1.1. Synthesis and characterisation of $\text{PtCl}_2(\text{PR}_2\text{Ar}'')$ ( $n = 1, 2$ ) complexes.

When  $\text{PtCl}_2$  and  $\text{PCyp}_2\text{Ar}^{\text{Xyl}_2}$  (**L3**), in a 1:1 molar ratio, were heated in toluene at 80 °C, a mixture of products was obtained in low yields, results that contrast sharply with those found previously for the phosphines  $\text{PMe}_2\text{Ar}^{\text{Dipp}_2}$  (**L2**) and  $\text{PMe}_2\text{Ar}^{\text{Tripp}_2}$ .<sup>26a,63</sup> Accordingly, other synthetic approaches involving different Pt(II) precursors were explored. No reaction was observed between phosphine **L3** and  $\text{PtCl}_2(\text{SMe}_2)_2$  in  $\text{CH}_2\text{Cl}_2$  at room temperature, and heating the reaction mixture in toluene at 100 °C resulted in a complex mixture of products. On the other hand, as shown in Scheme 1, reaction with  $\text{PtCl}_2(\text{hxd})$  ( $\text{hxd} = 1,5\text{-hexadiene}$ ) in toluene at 80 °C rendered the sought product,  $\text{PtCl}_2(\text{PCyp}_2\text{Ar}^{\text{Xyl}_2})$  (**1·L3**), as an air-stable orange solid, albeit in low yield (30%).

Complex **1·L3** was characterised by microanalysis and NMR spectroscopy. Its  $^{31}\text{P}\{^1\text{H}\}$  NMR spectrum contains a resonance centred at 39.6 ppm ( $^1J_{\text{Pt}} = 3308$  Hz), i.e. shifted to higher frequencies by 35 ppm with respect to the free phosphine. This shift is significantly lower than that of 49 ppm found for



Scheme 1. Synthesis of complex  $\text{PtCl}_2(\text{PCyp}_2\text{Ar}^{\text{Xyl}_2})$  (**1-L3**).

$\text{Ni}(\text{CO})_2(\text{PCyp}_2\text{Ar}^{\text{Xyl}_2})$ , for which a bidentate binding mode of the phosphine was observed. However, the  $^1\text{H}$  NMR spectrum of complex **1-L3** (Figure 16) shows an unsymmetrical environment around the terphenyl moiety, with two different sets of signals for the two xylyl groups. This is in agreement with the NMR features obtained for analogous complex  $\text{PtCl}_2(\text{PMe}_2\text{Ar}^{\text{Dipp}_2})$  (**1-L2**), where the phosphine is acting as a bidentate  $\kappa^1\text{-P}, \eta^1\text{-C}_{\text{ipso}}$  ligand.<sup>26a,63</sup> On that basis, a similar coordination mode for the phosphine  $\text{PCyp}_2\text{Ar}^{\text{Xyl}_2}$  is proposed in **1-L3**.

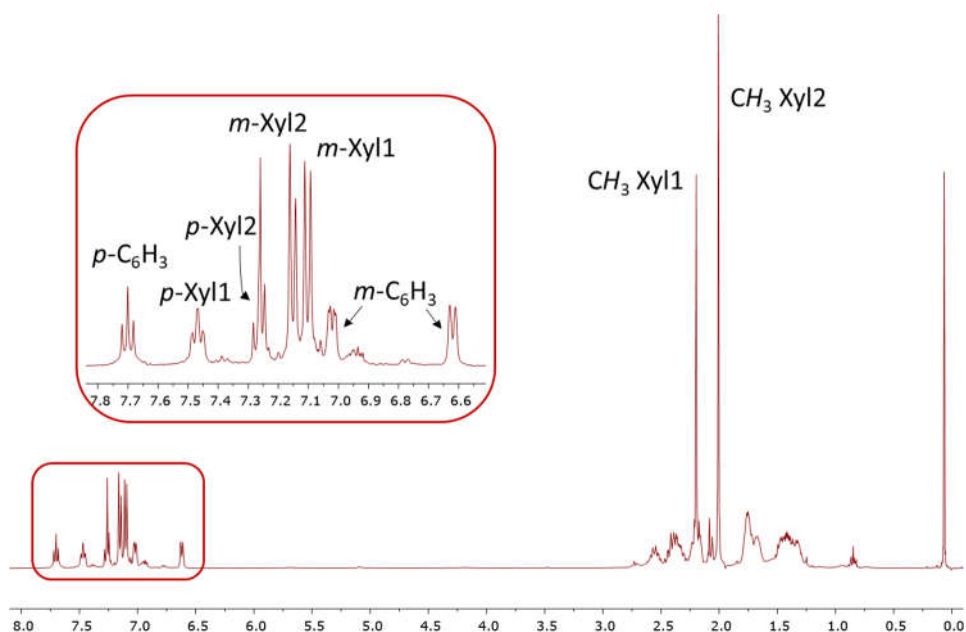


Figure 16.  $^1\text{H}$  NMR spectrum of complex **1-L3** in  $\text{CDCl}_3$  at  $25\text{ }^\circ\text{C}$ .

In order to confirm the molecular structure of **1·L3**, single crystals were grown by slow evaporation from a hexane/CH<sub>2</sub>Cl<sub>2</sub> mixture and analysed by X-ray diffraction. As illustrated in Figure 17, the platinum centre features a distorted square-planar geometry, with the abovementioned  $\eta^1\text{-C}_{ipso}$  interaction with one of the xylyl rings occupying the fourth coordination position. To facilitate this interaction, the terphenyl fragment undergoes two evident distortions. First, the central aryl ring bends towards the metal, resulting in a narrowing of the corresponding P-C<sub>ipso</sub>-C<sub>ortho</sub> angle (113.0(2)°) at the expense of the other (127.0(2)°). Also, as depicted in Figure 18, the interacting arene bends away from the metal by  $\alpha = 22.1^\circ$ . Further discussion of the structural features of **1·L3** will be presented in Section II.2.1.4, along with other related complexes.

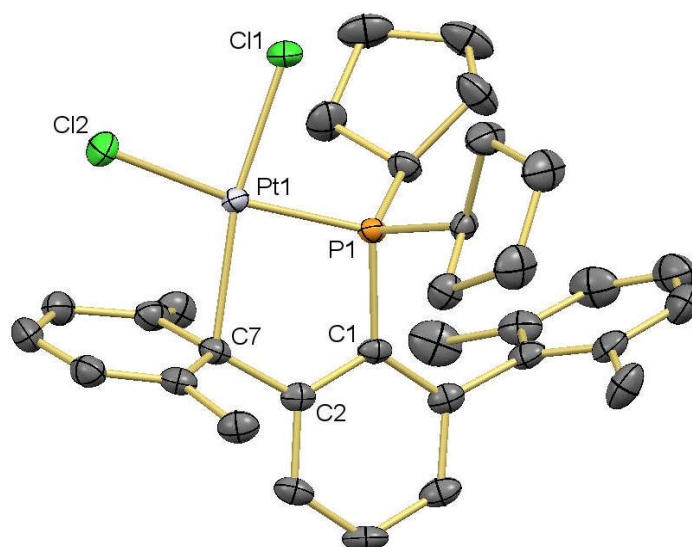


Figure 17. ORTEP view of complex **1·L3**. Hydrogen atoms are omitted for clarity and thermal ellipsoids are set at 50% level probability. Selected bond distances (Å) and angles (°): Pt1-P1 2.2298(9), Pt1-Cl1 2.303(1), Pt1-Cl2 2.3711(8), Pt1-C7 2.269(3), P1-Pt1-Cl1 86.78(3), Cl1-Pt1-Cl2 84.73(3), Cl2-Pt1-C7 104.94(8), C7-Pt1-P1 83.15(8), P1-C1-C2 113.0(2), Pt1-P1-C1-C2 -8.5(2).



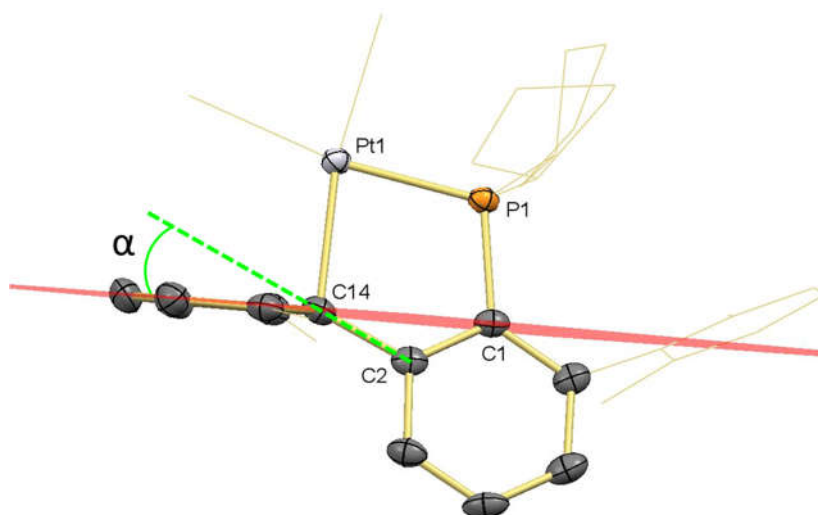
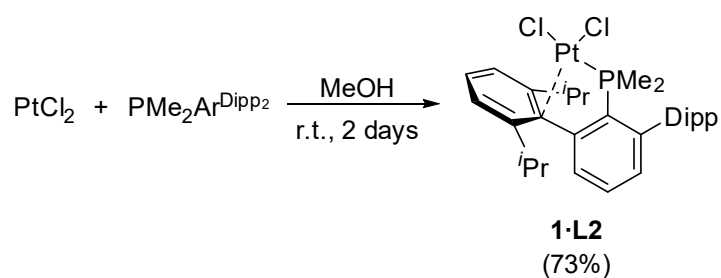


Figure 18. Simplified ORTEP showing the bending of the interacting side aryl ring away from the metal atom by an angle  $\alpha$ .

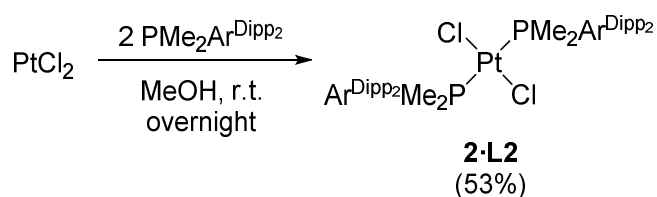
We further investigated an alternative synthetic route to the already reported complex  $\text{PtCl}_2(\text{PMe}_2\text{Ar}^{\text{Dipp}_2})$  (**1·L2**)<sup>63</sup> which eliminated the need for prolonged heating. After some experimentation, it was found that stirring the reaction mixture in MeOH at room temperature for 2 days rendered the desired product **1·L2** in 78% yield, slightly lower than the reported 89% (Scheme 2).



Scheme 2. New synthesis of complex  $\text{PtCl}_2(\text{PMe}_2\text{Ar}^{\text{Dipp}_2})$  (**1·L2**).

## Chapter II

During the reaction in MeOH, small amounts of an insoluble by-product were formed, which turned out to be the bisphosphine complex *trans*-PtCl<sub>2</sub>(PMe<sub>2</sub>Ar<sup>Dipp<sub>2</sub></sup>)<sub>2</sub> (**2·L2**). Thus, the reaction conditions were optimised for the synthesis of the bisphosphine complex by using a 1:2 ratio of Pt:PMe<sub>2</sub>Ar<sup>Dipp<sub>2</sub></sup> (Scheme 3). Under these conditions, **2·L2** was obtained as a white solid by washing with MeOH until the orange colouration of unwanted **1·L2** disappeared.



Scheme 3. Synthesis of complex PtCl<sub>2</sub>(PMe<sub>2</sub>Ar<sup>Dipp<sub>2</sub></sup>)<sub>2</sub> (**2·L2**).

The analytical and spectroscopic data obtained for **2·L2** are in agreement with the proposed formulation. Thus, the methyl groups on the phosphorus atom, as well as some of the CH groups and quaternary carbons of the central aryl ring, appear as triplets in the <sup>1</sup>H and <sup>13</sup>C{<sup>1</sup>H} NMR spectra of **2·L2** (Figure 19) due to virtual coupling with the mutually *trans* <sup>31</sup>P nuclei.<sup>65</sup> The <sup>31</sup>P{<sup>1</sup>H} NMR spectrum displays a singlet at -5.8 ppm (<sup>1</sup>J<sub>CP</sub> = 2448 Hz), shifted by 35.5 ppm downfield relative to the free PMe<sub>2</sub>Ar<sup>Dipp<sub>2</sub></sup>. These spectroscopic features resemble those found for the complex *trans*-PtCl<sub>2</sub>(PMe<sub>2</sub>Ar<sup>Xyl<sub>2</sub></sup>)<sub>2</sub> previously prepared in our group.<sup>26a</sup>

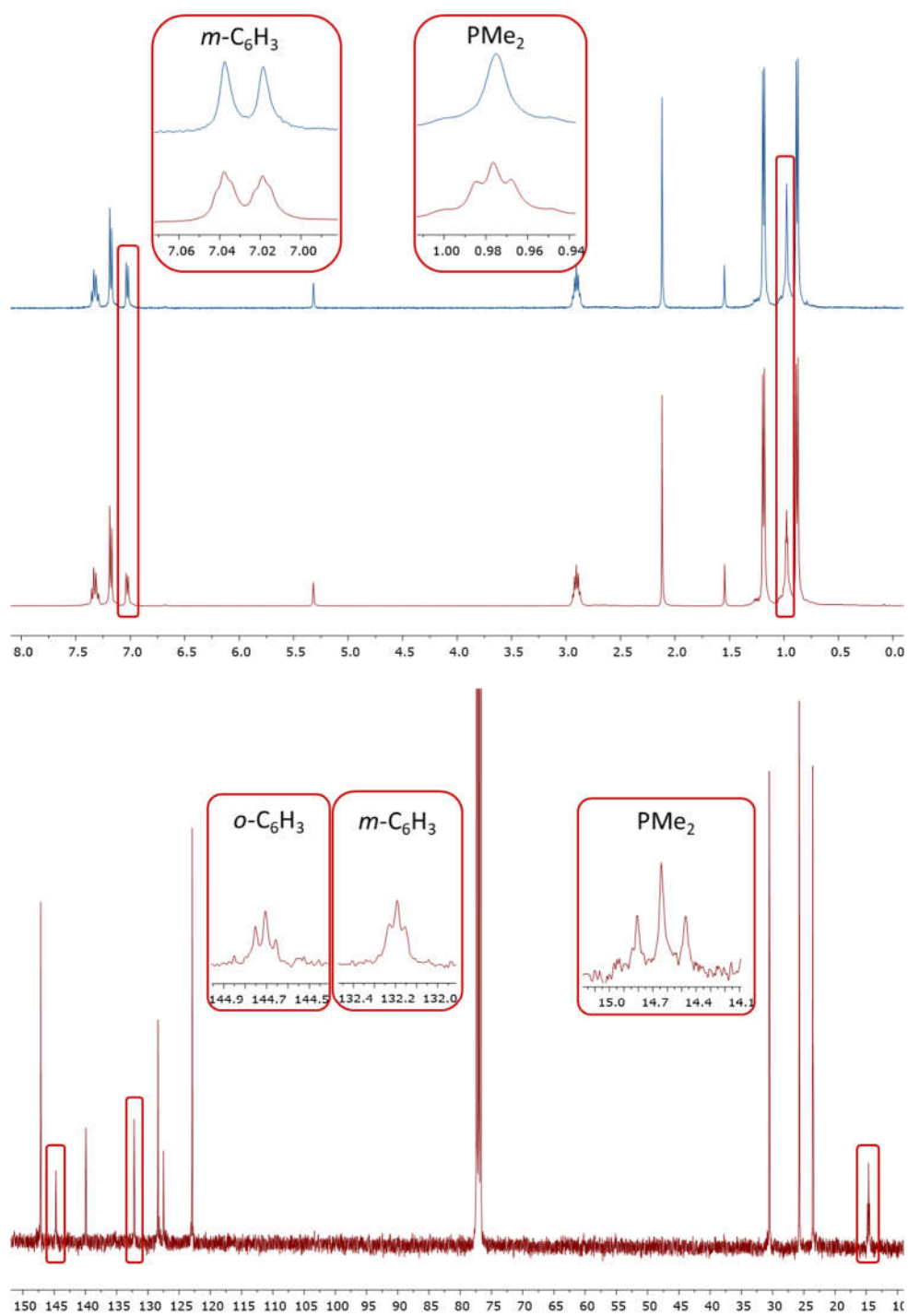


Figure 19. <sup>1</sup>H{<sup>31</sup>P} (top), <sup>1</sup>H (middle) and <sup>13</sup>C{<sup>1</sup>H} (bottom) NMR spectra of complex 2-L2 in CD<sub>2</sub>Cl<sub>2</sub> at 25 °C.

## Chapter II

As anticipated, the molecular structure proposed for complex **2·L2** was confirmed by single crystal X-ray diffraction studies. As depicted in Figure 20, this complex exhibits the expected square-planar environment around the metal centre, with two coordination sites occupied by chloride ligands and the other two by the  $\text{PMe}_2\text{Ar}^{\text{DipP}_2}$  ligands, in a mutually *trans* disposition. The phosphine ligands retain in this complex a conformation of type **B** (see Chapter I), with a  $\text{Pt-P-C}_{\text{ipso}}\text{-C}_{\text{ortho}}$  dihedral angle of  $50.1(4)^\circ$ . Other structural features of complex **2·L2** will be discussed in Section II.2.1.4.

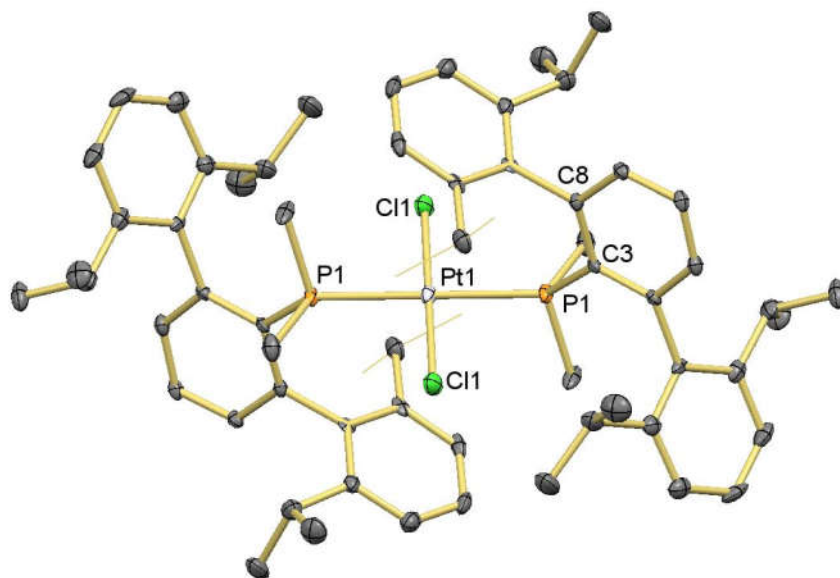
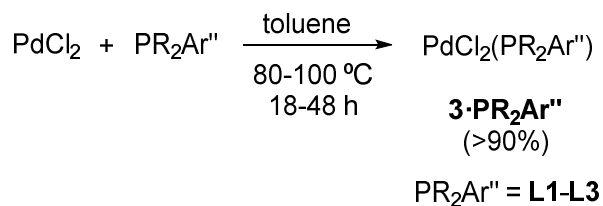


Figure 20. ORTEP view of complex **2·L2**. Hydrogen atoms are omitted for clarity, some atoms from the isopropyl substituents are drawn in wireframe and thermal ellipsoids are set at 50% level probability. Selected bond distances (Å) and angles (°):  $\text{Pt1-P1}$  2.3189(11),  $\text{Pt1-Cl1}$  2.2984(12),  $\text{Cl1-Pt1-P1}$   $87.30(4)$ ,  $\text{Pt1-P1-C3-C8}$   $-50.1(4)$ .

### II.2.1.2. Synthesis and characterisation of $[\text{PdCl}(\mu\text{-Cl})(\text{PR}_2\text{Ar}'')]_2$ complexes.

Next, we turned our attention to the preparation of monophosphine Pd(II) analogues. Thus, commercial  $\text{PdCl}_2$  was heated in toluene at high temperature (80-100 °C) with an equimolar amount of phosphines **L1**, **L2** and **L3** for a prolonged

period of time, affording orange compounds (Scheme 4). Reaction with phosphine  $P^iPr_2Ar^{Xyl_2}$  (**L4**) gave rise to a mixture of several products, which partially evolved over time to an unidentified red solid, insoluble in common organic solvents.



*Scheme 4. Synthesis of complexes 3·L1 through 3·L3.*

The orange solids obtained from the reactions with **L1-L3** were found by elemental analysis to agree with a  $PdCl_2(PR_2Ar'')$  formulation. However, in the  $^1H$  and  $^{13}C\{^1H\}$  NMR spectra in  $C_6D_6$  of **3·L1** and **3·L2** the two flanking aryl rings of the terphenyl moiety are equivalent, giving rise to only one set of signals (see Figure 21 for the  $^1H$  NMR spectrum of **3·L2**). This indicates both a symmetrical conformation of the phosphine and a rapid rotation around the  $P-C_{ipso}$  bond. However, their  $^{31}P\{^1H\}$  NMR spectra consists of a singlet centred at 6.3 (**3·L1**) and 6.5 ppm (**3·L2**), around 48-50 ppm at a higher frequency relative to the free phosphines, suggesting possibly a bidentate coordination of the phosphine ligands in these complexes.

To unambiguously establish the molecular structure of these two palladium(II) complexes, single crystals of **3·L2**, obtained from a petroleum ether/ $CH_2Cl_2$  mixture, were studied by X-ray diffraction. As shown in Figure 22, complex **3·L2** is a dinuclear species formed by two  $[PdCl_2PMe_2Ar^{Dipp_2}]$  units linked by two bridging chloride ligands. The Pd(II) centres exhibit a distorted square-planar geometry with no interaction between the two metal ions, as evinced in the Pd-Pd distance of 3.4196(4) Å, much higher than double the covalent radius

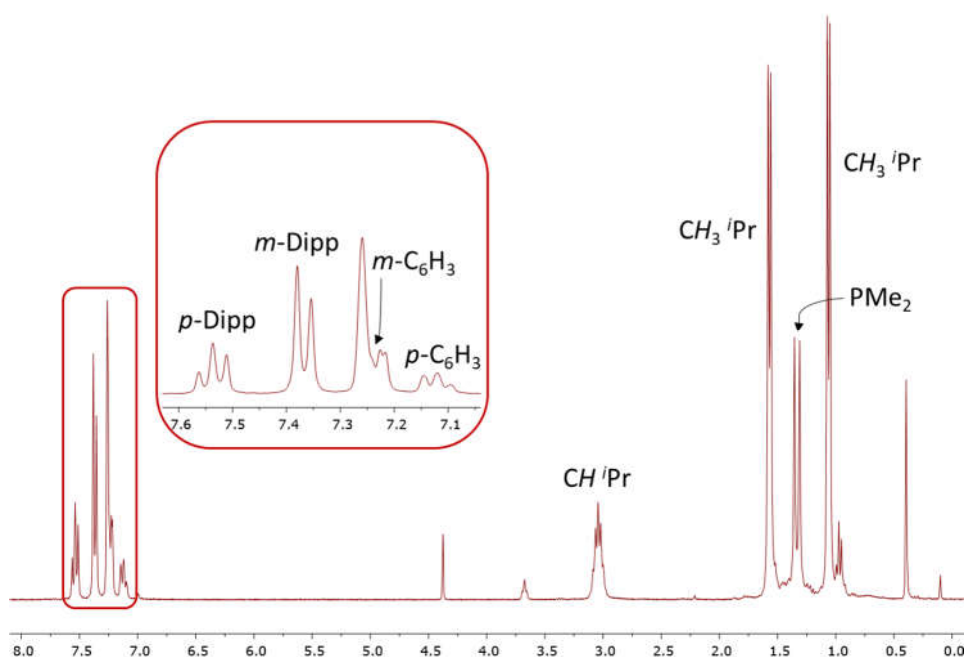


Figure 21.  $^1\text{H}$  NMR spectrum of complex **3·L2** in  $\text{C}_6\text{D}_6$  at 25 °C.

of a Pd atom (1.39 Å).<sup>66</sup> Interestingly, the  $[\text{Pd}(\mu\text{-Cl})_2\text{-Pd}]$  moiety does not display a planar arrangement, with an angle between the two  $[\text{Pd}(\mu\text{-Cl})_2]$  planes of 151° and the P atoms bent by *ca.* 10° from the  $[\text{PdCl}_3]$  planes. These distortions are not observed in the structures for other phosphine analogues. For instance, both  $[\text{PdCl}(\mu\text{-Cl})(\text{PPh}_3)]_2$ <sup>67</sup> and  $[\text{PdCl}(\mu\text{-Cl})(\text{SPhos})]_2$ <sup>61</sup> (SPhos = 2-Dicyclohexylphosphino-2',6'-dimethoxybiphenyl) exhibit an entirely planar  $[\text{P}(\text{Cl})\text{Pd}(\mu\text{-Cl})_2\text{Pd}(\text{Cl})\text{P}]$  fragment.

The behaviour of adduct **3·L3** in solution was found to be significantly different. Although the  $^{31}\text{P}\{^1\text{H}\}$  NMR chemical shift of the phosphine ligand in **3·L3** recorded in  $\text{C}_6\text{D}_6$  agrees with a monodentate coordination mode (36.1 ppm, with a change of 31.5 ppm downfield with respect to the uncoordinated phosphine), the  $^1\text{H}$  NMR spectrum does not provide any useful information, as all resonances due to the complex appear broad at room temperature. When the compound is dissolved in  $\text{CDCl}_3$ , its  $^{31}\text{P}$  resonance moves to a chemical shift of 68.9 ppm (i.e.

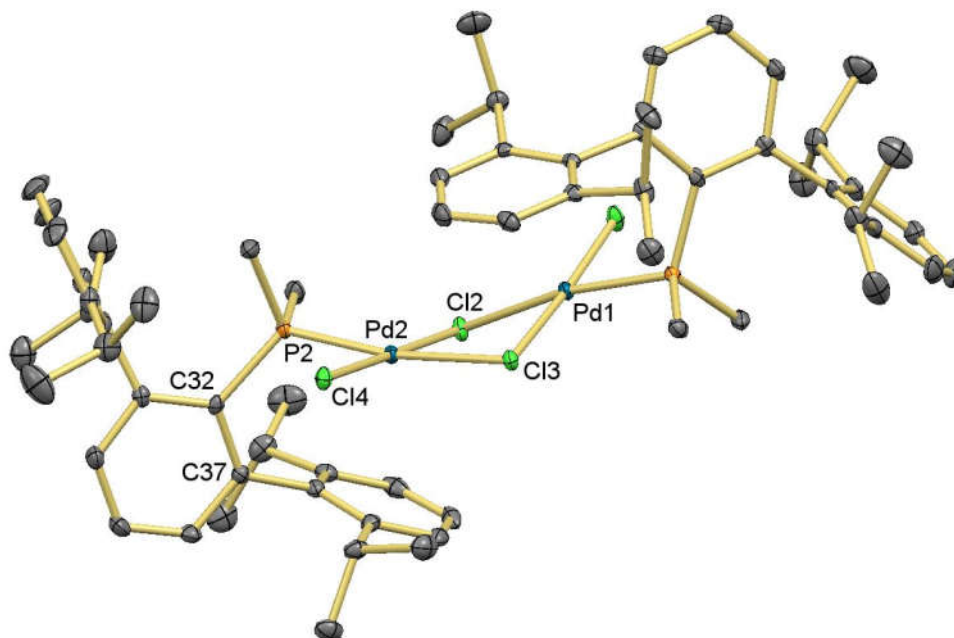


Figure 22. ORTEP view of complex **3·L2**. Hydrogen atoms are omitted for clarity and thermal ellipsoids are set at 50% level probability. Selected bond distances (Å) and angles (°): Pd2-P2 2.219(1), Pd2-Cl2 2.3302(7), Pd2-Cl3 2.439(1), Pd2-Cl4 2.3093(7), Cl2-Pd2-Cl3 84.68(3), Cl3-Pd2-Cl4 94.78(3), Cl4-Pd2-P2 86.01(3), P2-Pd2-Cl2 94.43(3), Pd2-P2-C32-C37 -47.9(3).

64.3 ppm at higher frequency relative to the free phosphine). Furthermore, both the  $^1\text{H}$  (Figure 23) and  $^{13}\text{C}\{^1\text{H}\}$  NMR spectra of **3·L3** recorded in this solvent at room temperature resemble those corresponding to the monophosphine platinum derivative **1·L3**, indicating that a monomeric complex could be present in this solvent with the phosphine acting as a P,C-bidentate ligand. Although this coordination mode of a phosphine ligand in a  $\text{PdCl}_2(\text{L})$  complex is not commonly encountered, there exist instances in the literature where such complexes have been structurally characterised, as in the case of  $\text{PdCl}_2(\text{Sym-Phos})$  (Sym-Phos = dicyclohexyl-[3-(2,4,6-trimethoxyphenyl)-4-methoxynaphth-2-yl]phosphine).<sup>68</sup>

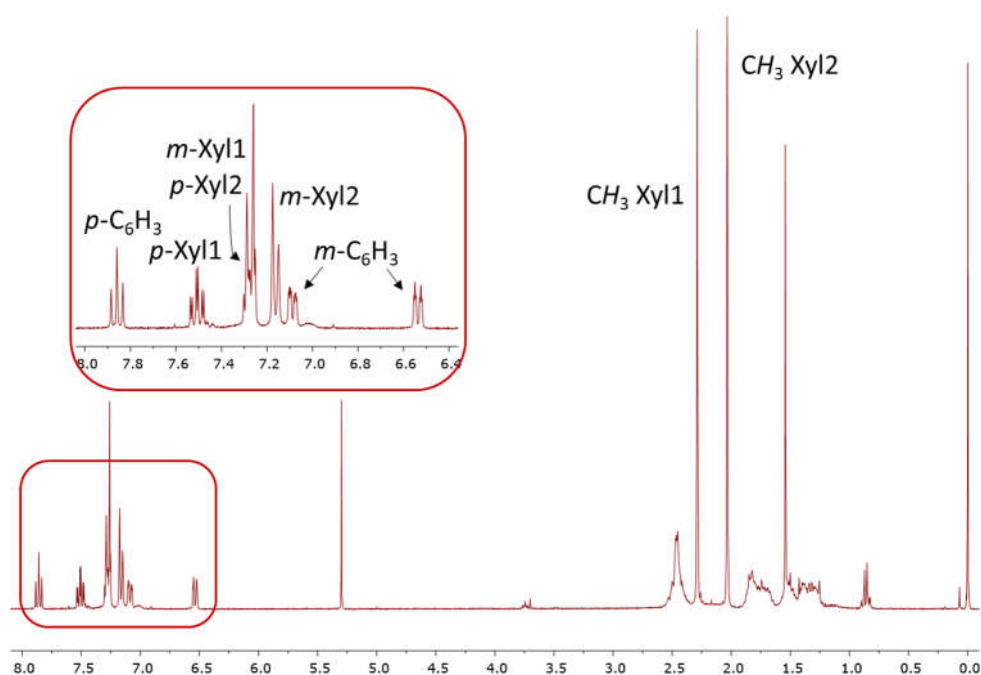


Figure 23.  $^1\text{H}$  NMR spectrum of **3·L3** in  $\text{CDCl}_3$  at 25 °C.

Surprisingly, analysis of the solid state structure of **3·L3** by X-ray crystallography revealed that it consists of a dinuclear Pd(II) species with a molecular structure analogous to that observed for **3·L2** (Figure 24) but with subtle differences. For example, the  $\text{P}(\text{Cl})\text{Pd}(\mu\text{-Cl})_2\text{Pd}(\text{Cl})\text{P}$  unit is planar in the structure of **3·L3**. It is worth mentioning that, although the free phosphine **L3** exhibits a structure of type **C**, it adopts a conformation **B** in complex **3·L2** (Pd-P- $C_{\text{ipso}}\text{-}C_{\text{ortho}}$  dihedral angle of  $40.4(3)^\circ$ ). This is presumably due to the steric strain arising from the introduction of the planar  $[\text{PdCl}_3]$  fragment, as is the case of the structure found for  $\text{IrCl}(\text{CO})_2(\text{P}^i\text{Pr}_2\text{Ar}^{\text{Dtbp}_2})$  discussed in the previous chapter. It is worth mentioning that the already mentioned  $[\text{PdCl}(\mu\text{-Cl})(\text{SPhos})]_2$ , although structurally characterised as a dinuclear species,<sup>61</sup> presents a  $^{31}\text{P}\{^1\text{H}\}$  NMR chemical shift in  $\text{CD}_2\text{Cl}_2$  solution of 53.3 ppm ( $\Delta\delta = 61.9$  ppm), possibly indicative of its existence as a mononuclear complex with a bidentate P,C-coordination of SPhos.



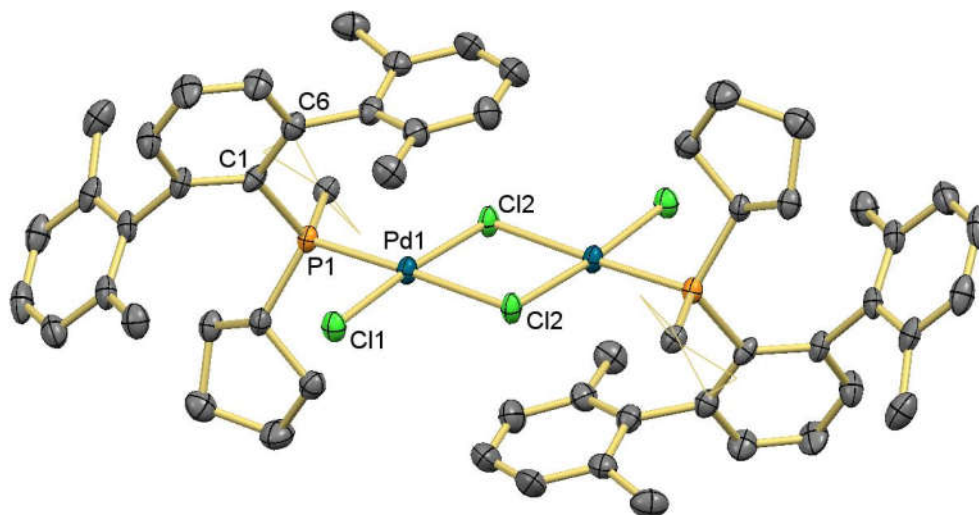


Figure 24. ORTEP view of complex **3·L3**. Hydrogen atoms are omitted for clarity, some atoms from the cyclopentyl substituents are drawn in wireframe and thermal ellipsoids are set at 50% level probability. Selected bond distances (Å) and angles (°): Pd1-P1 2.2408(10), Pd1-Cl1 2.2878(10), Pd1-Cl2(cis-P1) 2.3423(10), Pd1-Cl2(trans-P1) 2.4285(9), P1-Pd1-Cl1 86.11(4), Cl1-Pd1-Cl2(trans-P) 91.28(3), Cl2-Pd1-Cl2 84.90(3), P1-Pd1-Cl2 97.68(3), Pd1-P1-C1-C6 40.4(3).

Motivated by these findings, the NMR spectra of **3·L1** and **3·L2** were recorded in CDCl<sub>3</sub>. In direct opposition to **3·L3**, the NMR features of **3·L1** experience no significant change with respect to those recorded in C<sub>6</sub>D<sub>6</sub>. On the other hand, **3·L2** appears to exist in CDCl<sub>3</sub> as a mixture of the dinuclear and mononuclear species in *ca.* 80:20 ratio (Figure 25).

Similarly, a combination of both forms of **3·L3** can be obtained by dissolving it in a toluene/CH<sub>2</sub>Cl<sub>2</sub> mixture. Predictably, the ratio between the two compounds depends on the relative quantity of the solvents used, as shown in Figure 26, with the quantity of mononuclear species increasing as CH<sub>2</sub>Cl<sub>2</sub> is added. Furthermore, in very concentrated CDCl<sub>3</sub> samples of **3·L3**, a small amount of dinuclear species can be observed.

Chapter II

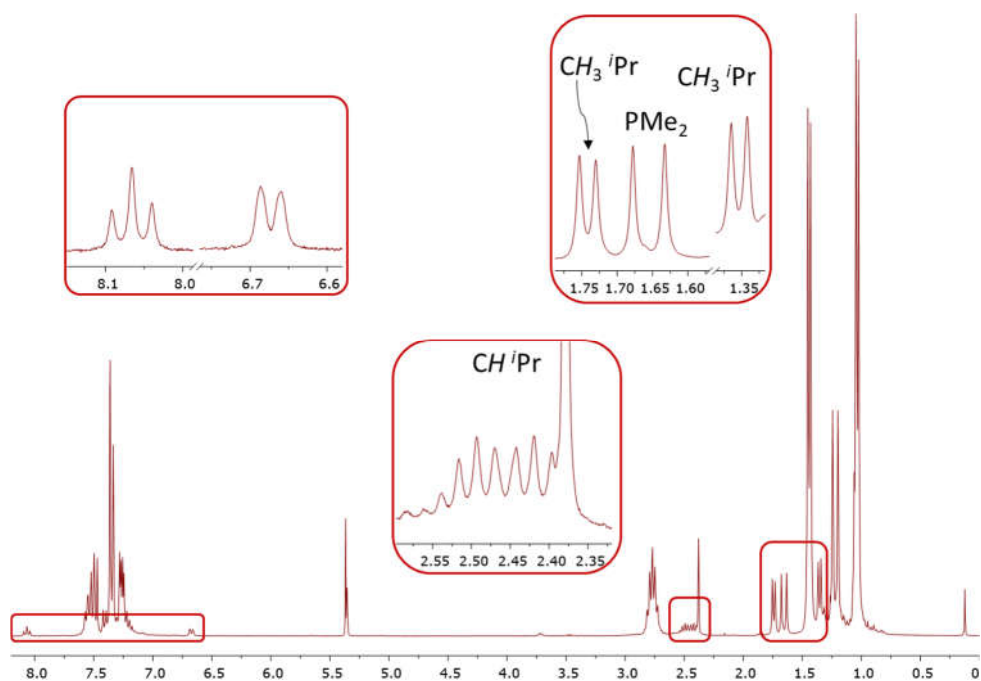


Figure 25.  $^1\text{H}$  NMR spectrum of complex **3·L2** in  $\text{CDCl}_3$ , emphasizing the signals due to the mononuclear species.

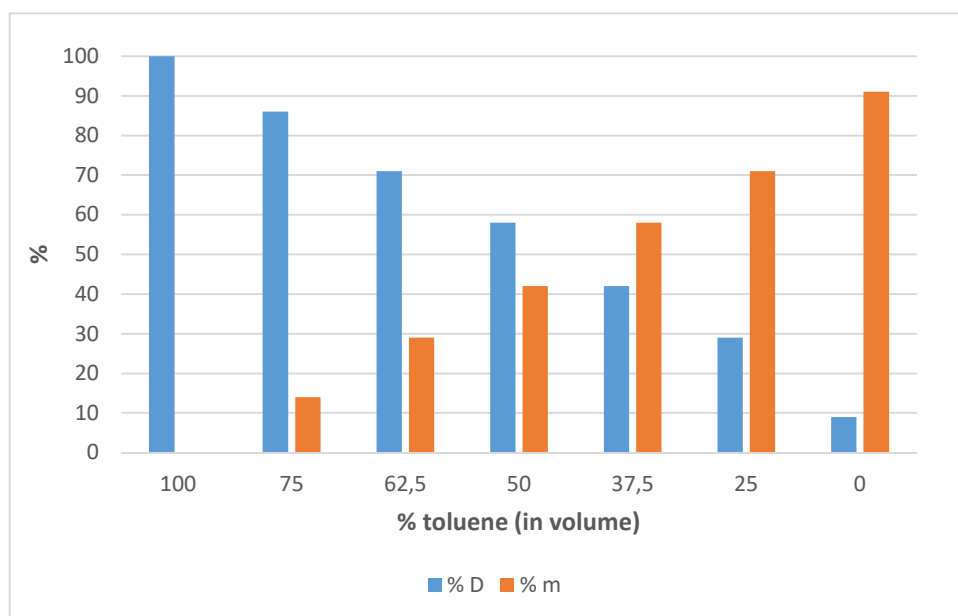


Figure 26. Variation of the relative quantities of the dinuclear (D) and mononuclear (m) forms of **3·L3** in toluene/ $\text{CH}_2\text{Cl}_2$  solution.

In order to examine this behaviour in more depth, a Diffusion Ordered Spectroscopy (DOSY) study was carried out. The DOSY spectra of **3·L3** were recorded in toluene-*d*<sub>8</sub> and in CDCl<sub>3</sub>. For comparative purposes, the DOSY spectra of **3·L1**, **1·L3** and the adduct PdCl<sub>2</sub>(CNXyl)(PCyp<sub>2</sub>Ar<sup>Xyl<sub>2</sub></sup>) (**5·L3**, *vide infra*) were also recorded in CDCl<sub>3</sub>. The diffusion coefficients obtained by relaxation analysis of the NMR data, along with the hydrodynamic radii calculated from said coefficients, are gathered in Table 1. The hydrodynamic radius of **3·L3** visibly increases from CDCl<sub>3</sub> (3.3 Å) to toluene-*d*<sub>8</sub> solution (5.5 Å), by a proportion of 1.7. The value for **3·L1**, which, as stated above, exists in solution as a dimer, is slightly lower at 5.2 Å, probably due to the reduced steric bulk of the PMe<sub>2</sub> moiety compared to PCyp<sub>2</sub>. On the other hand, a radius of 4.3 Å is obtained for the mononuclear platinum analogue **1·L3**, somewhat higher than expected, but still closer to the value obtained for **3·L3** in CDCl<sub>3</sub> than to that in toluene-*d*<sub>8</sub>. In contrast, the *r*<sub>H</sub> obtained for the adduct **5·L3** bears more similarity to that of the dimer than that of the monomer (with a ratio of 1.6), probably due to the introduced steric bulk of the xyllyl isocyanide moiety.

	Complex	Solvent	D (10 <sup>-10</sup> m <sup>2</sup> s <sup>-1</sup> )	<i>r</i> <sub>H</sub> (Å)	ratio
<b>3·L3</b>	PdCl <sub>2</sub> (PCyp <sub>2</sub> Ar <sup>Xyl<sub>2</sub></sup> )	CDCl <sub>3</sub>	11.7	3.3	
<b>3·L3</b>	[PdCl(μ-Cl)(PCyp <sub>2</sub> Ar <sup>Xyl<sub>2</sub></sup> )] <sub>2</sub>	Tol- <i>d</i> <sub>8</sub>	6.7	5.5	1.7
<b>3·L1</b>	[PdCl(μ-Cl)(PMe <sub>2</sub> Ar <sup>Xyl<sub>2</sub></sup> )] <sub>2</sub>	CDCl <sub>3</sub>	7.4	5.2	1.6
<b>1·L3</b>	PtCl <sub>2</sub> (PCyp <sub>2</sub> Ar <sup>Xyl<sub>2</sub></sup> )	CDCl <sub>3</sub>	8.9	4.3	1.3
<b>5·L3</b>	PdCl <sub>2</sub> (CNXyl)(PCyp <sub>2</sub> Ar <sup>Xyl<sub>2</sub></sup> )	CDCl <sub>3</sub>	7.2	5.3	1.6

Table 1. Diffusion coefficients (*D*) and hydrodynamic radii (*r*<sub>H</sub>) gathered from the DOSY studies of **3·L3**, **3·L1**, **1·L3** and **5·L3**. The last data column compares the corresponding values of *r*<sub>H</sub> relative to that obtained for **3·L3** in CDCl<sub>3</sub>.

This study seems to support the assumption that complexes **3·PR<sub>2</sub>Ar''** exist in solution as a mixture of mononuclear PdCl<sub>2</sub>(PR<sub>2</sub>Ar'') and dinuclear [PdCl(μ-

## Chapter II

$\text{Cl}(\text{PR}_2\text{Ar}'')$  species in dynamic equilibrium (Figure 27), where the ratio between the two depends on the nature of the phosphine ligand, the polarity of the solvent and the concentration. Although, as mentioned above, there is precedent in the literature for  $\text{PdCl}_2(\text{L})$  complexes presenting either of the two molecular structures,<sup>61,67,68</sup> to the best of our knowledge, no studies have been reported concerning the dependence of the nuclearity of these complexes on the nature of the solvent.

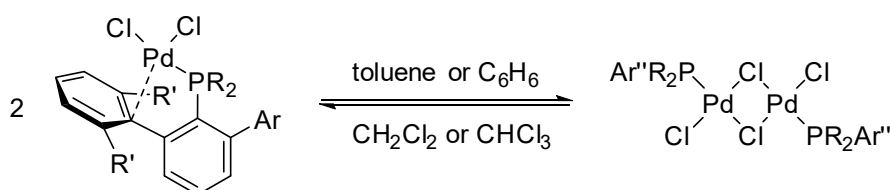


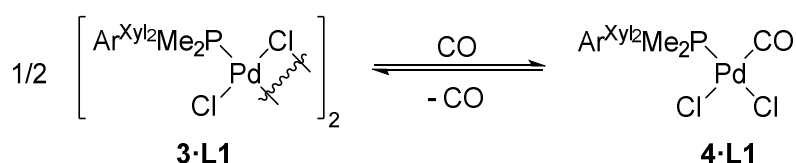
Figure 27. Equilibrium between the mononuclear and dinuclear forms of complexes **3·PR<sub>2</sub>Ar''**.

### II.2.1.3. Reactivity of $[\text{PdCl}(\mu\text{-Cl})(\text{PR}_2\text{Ar}'')]_2$ complexes towards Lewis bases.

For the sake of completeness, we considered of interest the study of the reactivity of the  $[\text{PdCl}(\mu\text{-Cl})(\text{PR}_2\text{Ar}'')]_2$  complexes towards some Lewis bases, namely CO and CNXyl. Although similar studies with different isocyanides have been reported,<sup>69a</sup> few of the corresponding adducts have been characterised both spectroscopically and structurally.<sup>69b</sup> Furthermore, no examples of analogous studies with CO were found in the literature.

When a solution of complex **3·L1** in  $\text{CH}_2\text{Cl}_2$  was placed under a carbon monoxide atmosphere (1 bar), a change in colour of the solution from orange to pale yellow was observed. The IR spectrum of the resulting solution displays an absorption band at  $2131 \text{ cm}^{-1}$ , somewhat close to the value of the C–O stretching frequency measured for the platinum complex  $\text{PtCl}_2(\text{CO})(\text{PMe}_2\text{Ar}^{\text{Dipp}_2})$  ( $2114 \text{ cm}^{-1}$  in Nujol).<sup>64</sup> However, when the CO atmosphere was removed, the newly formed

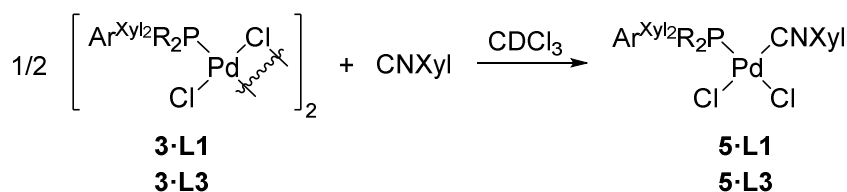
complex, **4·L1**, reverted back to **3·L1** (Scheme 5). It is worth mentioning that the reversibility of this process is in clear contrast with what is observed for  $\text{PtCl}_2(\text{CO})(\text{PMe}_2\text{Ar}^{\text{Dipp}_2})$ .<sup>64</sup> In order to spectroscopically characterise **4·L1**, the reaction was carried out in  $\text{CDCl}_3$  in an NMR tube.



Scheme 5. Reversible reaction of **3·L1** with CO to form **4·L1**.

The  $^1\text{H}$  and DEPTQ  $^{13}\text{C}\{^1\text{H}\}$  NMR spectra of **4·L1** (Figure 28) displays a symmetrical environment around the phosphine ligand, as expected for a  $\kappa^1$  mode of coordination. Moreover, the  $^{13}\text{C}$  resonance corresponding to the CO ligand appears as a doublet centred at 167.8 ppm with a coupling constant to the  $^{31}\text{P}$  nucleus of 4 Hz, indicative of a *cis* arrangement with respect to the phosphine ligand.<sup>70</sup> Finally, the  $^{31}\text{P}$  signal for **4·L1** (7.3 ppm) remains practically unchanged relative to the starting material (7.8 ppm in  $\text{CDCl}_3$ ).

Similarly, complexes **3·L1** and **3·L3** reacted in  $\text{CDCl}_3$  with the isocyanide  $\text{CNXyl}$  in stoichiometric ratio, leading to complexes **5·L1** and **5·L3**, respectively (Scheme 6).



Scheme 6. Reaction of complexes **3·L1** and **3·L3** with  $\text{CNXyl}$  to form **5·L1** and **5·L3**, respectively.

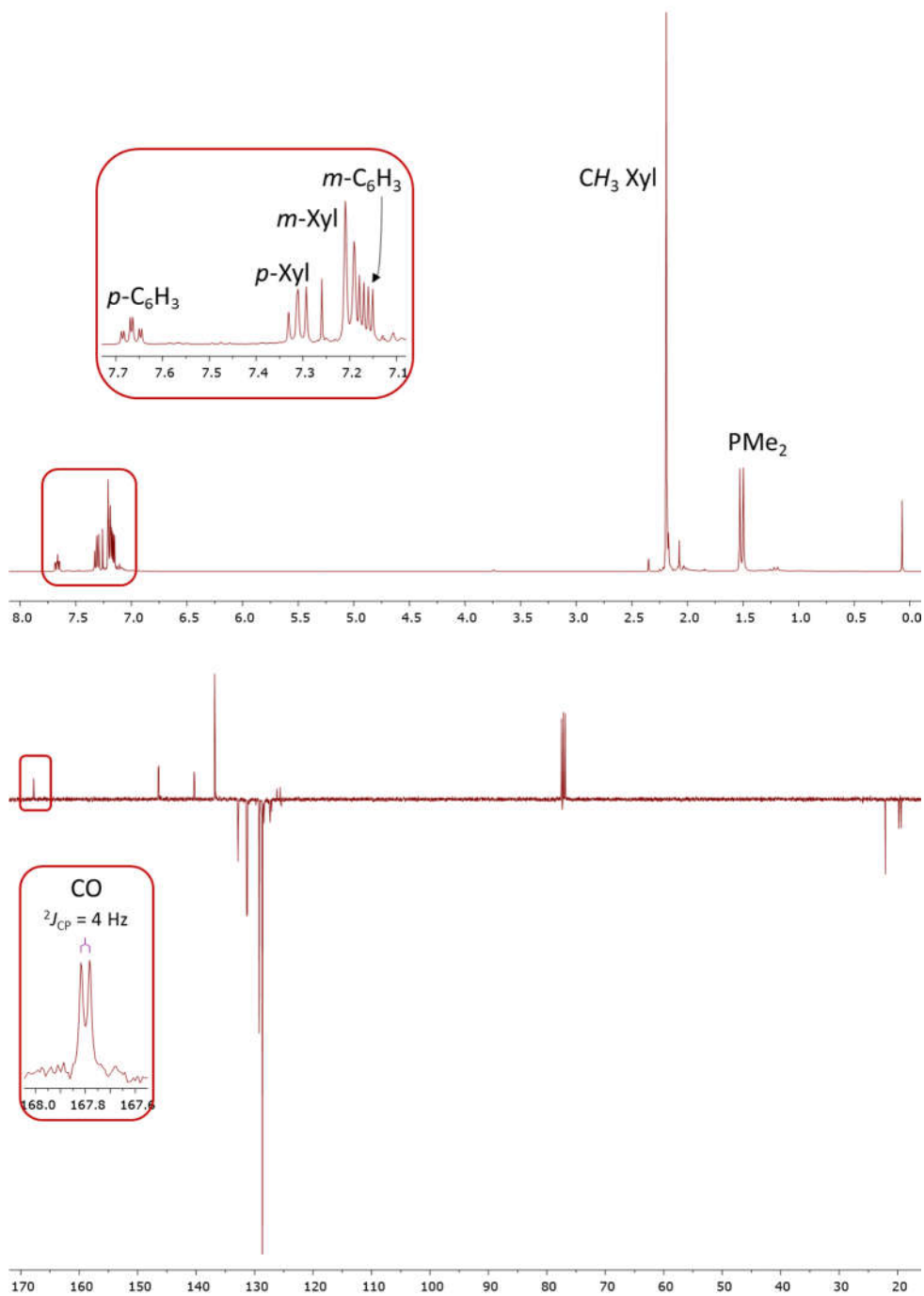


Figure 28. <sup>1</sup>H (top) and DEPTQ <sup>13</sup>C{<sup>1</sup>H} (bottom) NMR spectra of complex 4-L1 in CDCl<sub>3</sub> at 25 °C.

The NMR features of complex **5·L1** (see Figure 29 for the  $^1\text{H}$  NMR spectrum) resemble those observed for the carbon monoxide adduct **4·L1**, with a symmetrical environment around the terphenyl moiety due to facile rotation around the P–C<sub>arene</sub> bond. Interestingly, the carbon atom in the isocyanide ligand directly bonded to the metal does not appear in the  $^{13}\text{C}\{^1\text{H}\}$  NMR spectrum, as is the case of similar Pd(II) isonitrile adducts reported in the literature.<sup>69</sup>

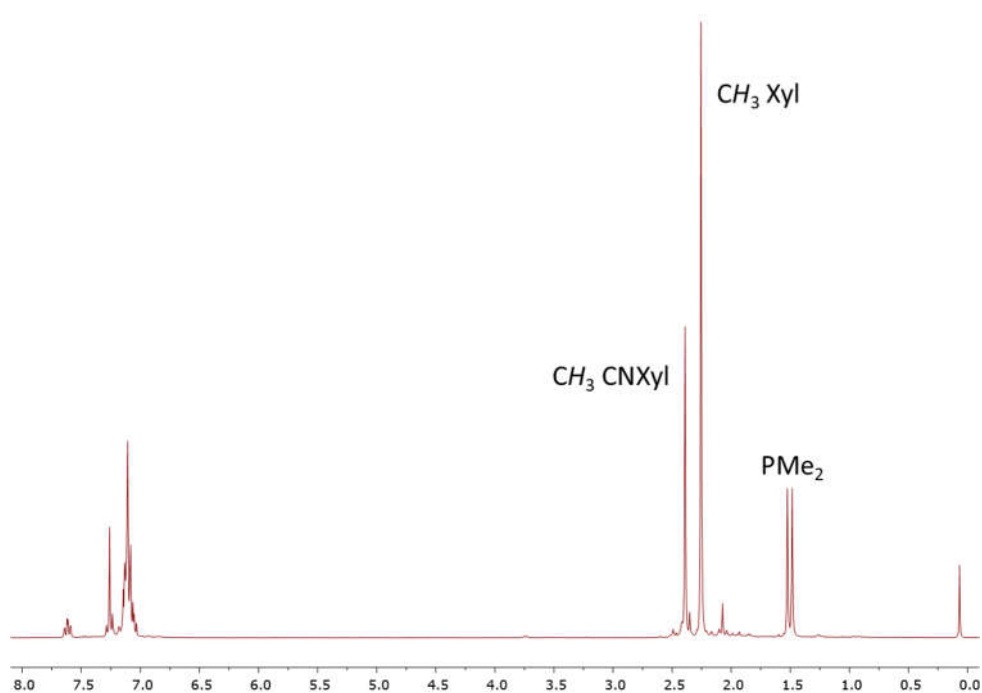


Figure 29.  $^1\text{H}$  NMR spectrum of complex **5·L1** in  $\text{CDCl}_3$  at 25 °C.

Complex **5·L3** exhibits a slightly different NMR behaviour, with some broad resonances both in the room temperature  $^1\text{H}$  (Figure 30-B) and  $^{13}\text{C}\{^1\text{H}\}$  NMR spectra, probably due to a slower rotation of the terphenyl moiety around the Pd–C<sub>ipso</sub> bond induced by the bulky cyclopentyl substituents. Cooling down the sample to –45 °C completely stops this fluxional process in the  $^1\text{H}$  NMR timescale, causing the four methyl substituents on the side aryl rings of the terphenyl group to

appear as four different signals (Figure 30-A). Conversely, heating up to 55 °C provides a simpler, though still somewhat broadened, spectrum, with only one resonance for the xylyl CH<sub>3</sub> substituents of the phosphine ligand (Figure 30-C).

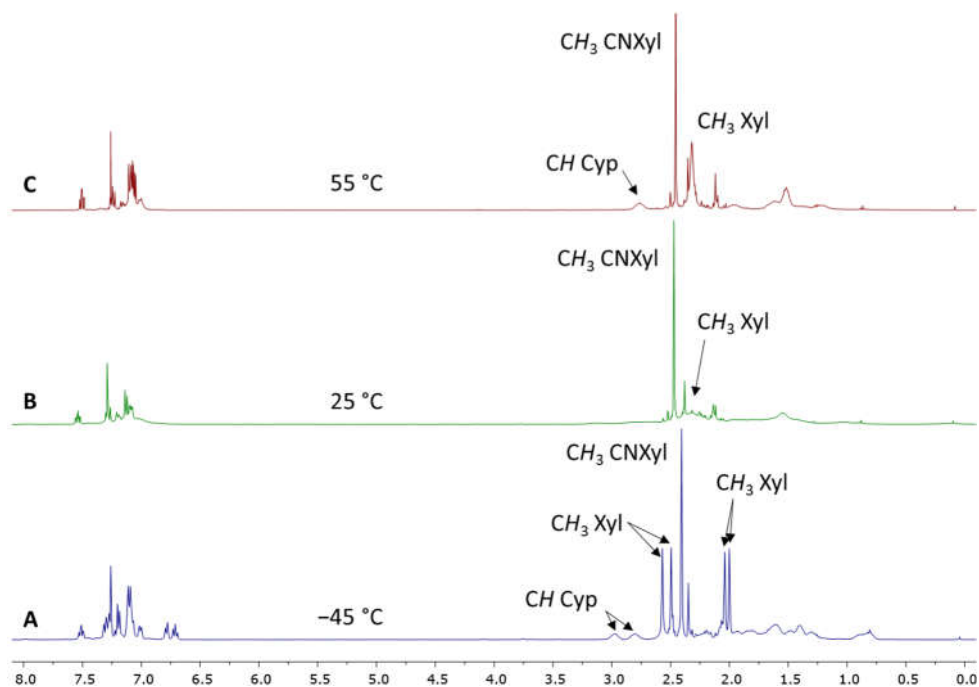


Figure 30. <sup>1</sup>H NMR spectra of complex **5·L3** in CDCl<sub>3</sub> at 55 °C (**C**), 25 °C (**B**) and -45 °C (**A**).

The structure of **5·L3** was unambiguously confirmed by X-ray diffraction studies and it is shown in Figure 31. This complex is structurally similar to the parent **3·L3**, with the palladium centre featuring a square-planar coordination environment. The isocyanide and the phosphine ligands are in mutually *cis* disposition, with the latter again adopting a conformation of type **B**. Other structural features will be discussed further below.



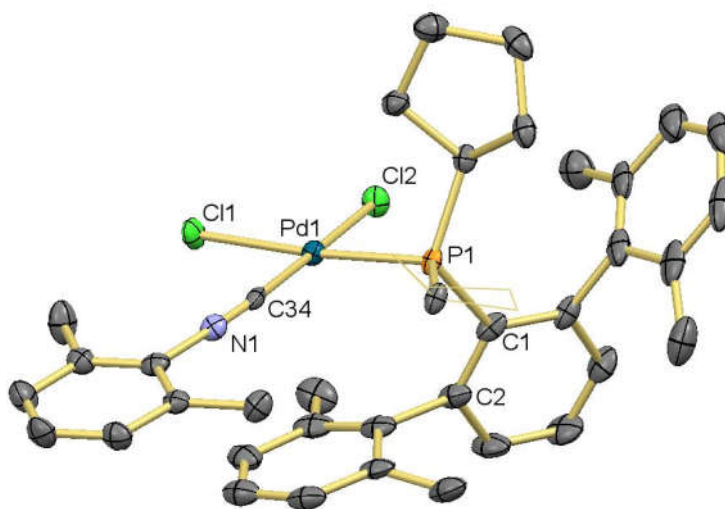
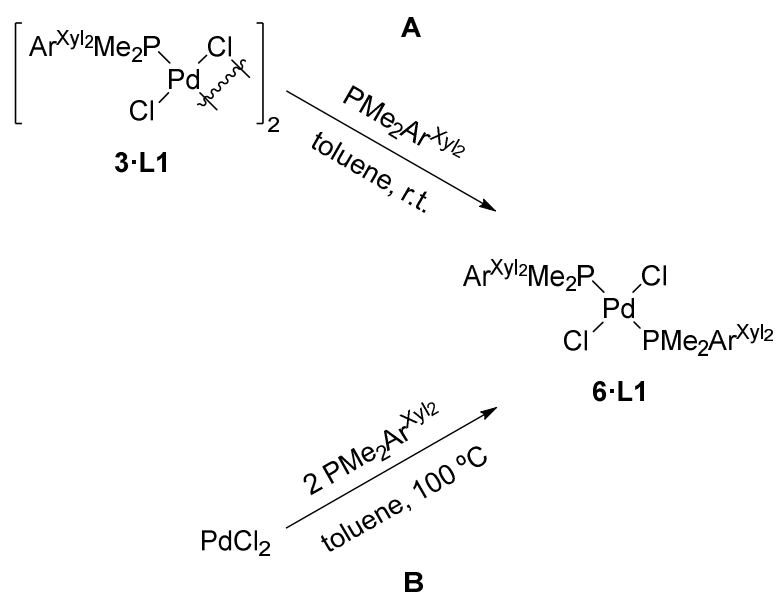


Figure 31. ORTEP view of complex **5·L3**. Hydrogen atoms are omitted for clarity, some atoms from the cyclopentyl substituents are drawn in wireframe and thermal ellipsoids are set at 50% level probability. Selected bond distances (Å) and angles (°): Pd1-P1 2.2735(10), Pd1-Cl1 2.3536(9), Pd1-Cl2 2.3137(10), Pd1-C34 1.939(4), C34-N1 1.142(5), P1-Pd1-Cl2 85.72(3), Cl2-Pd1-Cl1 90.27(4), Cl1-Pd1-C34 86.67(10), P1-Pd1-C34 97.45(10), Pd1-P1-C1-C2 -43.8(3).

To complement the study done on *trans*-PtCl<sub>2</sub>(PMe<sub>2</sub>Ar'')<sub>2</sub>,<sup>26a</sup> the reactions of complexes **3·PR<sub>2</sub>Ar''** towards a second equivalent of the corresponding dialkyl terphenyl phosphine were examined. Thus, an equimolar solution of **3·L1** and **L1** in toluene was stirred for 2 hours, resulting in the clean formation of the bisphosphine complex *trans*-PdCl<sub>2</sub>(PMe<sub>2</sub>Ar<sup>Xyl</sup>)<sub>2</sub>, **6·L1** (Scheme 7A). This new species was also identified as an intermediate when the synthesis of **3·L1** was monitored by <sup>31</sup>P{<sup>1</sup>H} NMR, indicating that, PdCl<sub>2</sub> first reacts with two equivalents of the phosphine to form **6·L1**, which evolved to the dinuclear species **3·L1** by reacting with the remaining PdCl<sub>2</sub>. Following this reasoning, **6·L1** was directly synthesised by heating a mixture of PdCl<sub>2</sub> with two equivalents of **L1** (Scheme 7B).



Scheme 7. Syntheses of complex *trans*-PdCl<sub>2</sub>(PMe<sub>2</sub>Ar<sup>Xyl</sup><sub>2</sub>) (**6-L1**) from **3-L1** (path **A**) and from PdCl<sub>2</sub> (path **B**).

The corresponding product obtained from applying either of these two synthetic strategies to phosphine **L2** was rather insoluble in common organic solvents and all attempts at purification were unsuccessful. Moreover, no reaction was observed between **3-L3** and a second equivalent of **L3** in CH<sub>2</sub>Cl<sub>2</sub>, even after two weeks.

The <sup>1</sup>H and DEPTQ <sup>13</sup>C{<sup>1</sup>H} NMR spectra (Figure 32) of **6-L1** exhibit the expected high symmetry already observed for the platinum(II) analogue **2-L2**. Also, some <sup>1</sup>H and <sup>13</sup>C aromatic resonances, as well as those corresponding to the PMe<sub>2</sub> groups, appear as virtual triplets, demonstrating the *trans* arrangement of the two phosphine ligands in **6-L1**. The <sup>31</sup>P{<sup>1</sup>H} NMR chemical shift of -10.8 ppm (Δδ = 29.6 ppm) observed is typical of a monodentate mode of coordination of the phosphine.

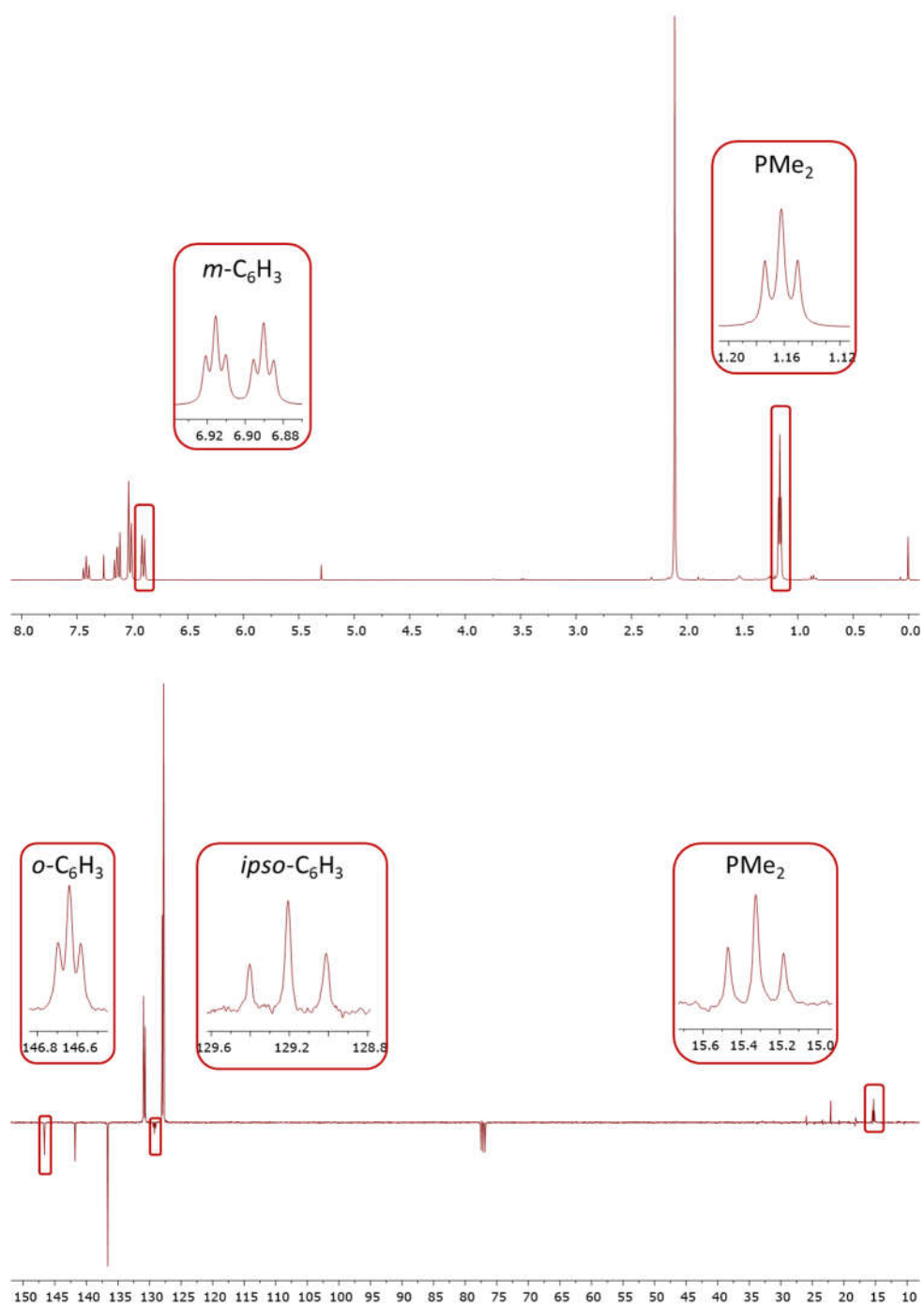


Figure 32. <sup>1</sup>H (top) and DEPTQ <sup>13</sup>C{<sup>1</sup>H} (bottom) NMR spectra of complex 6-L1 in CDCl<sub>3</sub> at 25 °C.

Figure 33 shows the solid-state molecular structure of **6·L1**. The Pd-P distance (2.3275(5) Å) is significantly longer than that found in **3·L2** (2.219(1) Å), almost certainly due to the stronger *trans* influence of the phosphine ligand in **6·L1** compared to the chloride ligand in complex **3·L2**. Furthermore, this value is considerably close to the Pt-P distance in **2·L2** (2.3189(11) Å), owing to the similar sizes of palladium and platinum.<sup>66</sup>

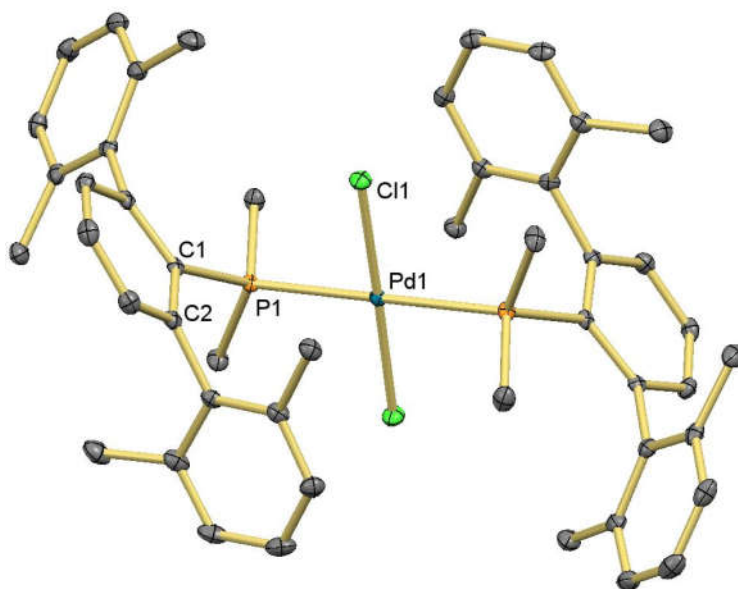


Figure 33. ORTEP view of complex **6·L1**. Hydrogen atoms are omitted for clarity and thermal ellipsoids are set at 50% level probability. Selected bond distances (Å) and angles (°): Pd1-P1 2.3275(5), Pd1-Cl1 2.3005(5), Cl1-Pd1-P1 82.38(2), Pd1-P1-C1-C2 -52.4(1).

#### II.2.1.4. Summary of spectroscopic and structural data pertaining $\text{MCl}_2(\text{PR}_2\text{Ar}'')$ and related complexes.

In view of the amount of spectroscopic and structural data presented for similar complexes in the previous sections, it seems appropriate to gather selected features of these compounds. Table 2 displays the  $^{31}\text{P}\{^1\text{H}\}$  NMR chemical shifts of all new complexes, along with the variation with respect to the uncoordinated

phosphines. As discussed in the previous chapter, these values often reflect the coordination mode of the phosphine ligand in the complex. Thus, a classical  $\kappa^1$ -P coordination of the phosphine usually causes the  $^{31}\text{P}\{^1\text{H}\}$  resonances to be shifted by 30-40 ppm to higher frequencies whereas additional binding of a flanking aryl ring leads to differences of 40-50 ppm in chemical shifts. However, based on the data collected in Table 2, no obvious trend can be inferred from these values concerning the coordination mode of the  $\text{PR}_2\text{Ar}''$  ligands in  $\text{MCl}_2(\text{PR}_2\text{Ar}'')$  complexes and their derivatives.

	Complex	$\delta(^{31}\text{P})$	$\Delta\delta$
<b>1•L2</b>	$\text{PtCl}_2(\text{PMe}_2\text{Ar}^{\text{Dipp}_2})$	10.9 <sup>a</sup>	52.2
<b>1•L3</b>	$\text{PtCl}_2(\text{PCyp}_2\text{Ar}^{\text{Xyl}_2})$	39.6	35.0
	$\text{PtCl}_2(\text{PMe}_2\text{Ar}^{\text{Xyl}_2})_2$	-17.3 <sup>b</sup>	23.1
<b>2•L2</b>	$\text{PtCl}_2(\text{PMe}_2\text{Ar}^{\text{Dipp}_2})_2$	-5.8	35.5
<b>3•L1</b>	$[\text{PdCl}(\mu\text{-Cl})(\text{PMe}_2\text{Ar}^{\text{Xyl}_2})]_2$	7.8	48.2
<b>3•L2</b>	$[\text{PdCl}(\mu\text{-Cl})(\text{PMe}_2\text{Ar}^{\text{Dipp}_2})]_2$	6.5	47.8
<b>3•L3 (D)</b>	$[\text{PdCl}(\mu\text{-Cl})(\text{PCyp}_2\text{Ar}^{\text{Xyl}_2})]_2$	36.1	31.5
<b>3•L3 (m)</b>	$\text{PdCl}_2(\text{PCyp}_2\text{Ar}^{\text{Xyl}_2})$	68.9	64.3
<b>4•L1</b>	$\text{PdCl}_2(\text{CO})(\text{PMe}_2\text{Ar}^{\text{Xyl}_2})$	7.3	47.7
<b>5•L1</b>	$\text{PdCl}_2(\text{CNXyl})(\text{PMe}_2\text{Ar}^{\text{Xyl}_2})$	4.1	44.5
<b>5•L3</b>	$\text{PdCl}_2(\text{CNXyl})(\text{PCyp}_2\text{Ar}^{\text{Xyl}_2})$	35.3	30.7
<b>6•L1</b>	$\text{PdCl}_2(\text{PMe}_2\text{Ar}^{\text{Xyl}_2})_2$	-10.8	29.6

Table 2.  $^{31}\text{P}\{^1\text{H}\}$  NMR chemical shifts of new complexes. <sup>a</sup>From ref. 63. <sup>b</sup>From ref. 26a.

Table 3 collects relevant structural data from the crystallographically characterised complexes. The increased *trans* influence of the phosphines with respect to the chloride ligands is reflected in the variation of *ca.* 0.10 Å in metal-P bond distances from monophosphine complexes **1•L2**,<sup>63</sup> **1•L3**, **3•L2** and **3•L3** to bisphosphine adducts **2•L2** and **6•L1**. This is further evinced in the different Pd-Cl

## Chapter II

bond distances in complexes **3·L2** and **3·L3** to those chloride ligands located in *trans* position to the phosphine ligands (*ca.* 2.44 Å) as compared to those in *cis* position (around 2.29-2.34 Å). These features are less marked in the structures of platinum complexes **1·L2** and **1·L3**, where the phosphine acts as a bidentate ligand, and isocyanide palladium(II) adduct **5·L3**, doubtless due to the increased *trans* influence of the  $\eta^1\text{-C}_{ipso}$  interaction and of the isocyanide ligand, respectively, compared to a chloride ligand.

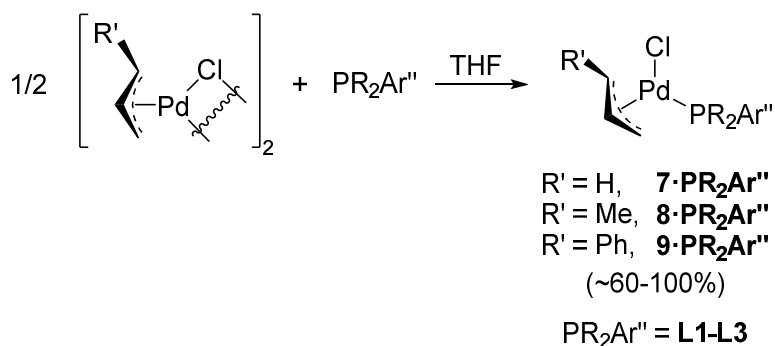
Complex	distances (Å)			$\theta$ (°)	Conf. <sup>a</sup>
	M-P	M-Cl <sub>cis</sub>	M-Cl <sub>trans</sub>		
<b>1·L2</b> PtCl <sub>2</sub> (PMe <sub>2</sub> Ar <sup>Dipp</sup> ) <sub>2</sub> <sup>b</sup>	2.22	2.35	2.40	-11.1	<b>C</b>
<b>1·L3</b> PtCl <sub>2</sub> (PCyp <sub>2</sub> Ar <sup>Xyl</sup> ) <sub>2</sub>	2.23	2.30	2.37	-8.5	<b>C</b>
<b>2·L2</b> PtCl <sub>2</sub> (PMe <sub>2</sub> Ar <sup>Dipp</sup> ) <sub>2</sub>	2.32	2.30	-	50.1	<b>B</b>
<b>3·L2</b> [PdCl(μ-Cl)(PMe <sub>2</sub> Ar <sup>Dipp</sup> ) <sub>2</sub> ] <sub>2</sub>	2.22	2.33 2.31	2.44	47.9	<b>B</b>
<b>3·L3</b> [PdCl(μ-Cl)(PCyp <sub>2</sub> Ar <sup>Xyl</sup> ) <sub>2</sub> ] <sub>2</sub>	2.24	2.34 2.29	2.43	40.4	<b>B</b>
<b>5·L3</b> PdCl <sub>2</sub> (CNXyl)(PCyp <sub>2</sub> Ar <sup>Xyl</sup> ) <sub>2</sub>	2.27	2.31	2.35	43.8	<b>B</b>
<b>6·L1</b> PdCl <sub>2</sub> (PMe <sub>2</sub> Ar <sup>Xyl</sup> ) <sub>2</sub>	2.33	2.30	-	52.4	<b>B</b>

Table 3. Selected bond distances and M-P-C<sub>ipso</sub>-C<sub>ortho</sub> dihedral angle ( $\theta$ ) in structurally characterised complexes. <sup>a</sup>Conformation of the phosphine ligand in the complex. <sup>b</sup>From ref. 26a.

## II.2.2. Allylpalladium(II) and allylnickel(II) complexes of dialkyl terphenyl phosphines.

### II.2.2.1. Synthesis and characterisation of $\text{PdCl}(\eta^3\text{-C}_3\text{H}_4\text{R}')(\text{PR}_2\text{Ar}'')$ ( $\text{R}' = \text{H, Me, Ph}$ ) complexes.

A series of  $\text{PdCl}(\eta^3\text{-C}_3\text{H}_4\text{R}')(\text{PR}_2\text{Ar}'')$  complexes were synthesised by reaction between the corresponding  $[\text{Pd}(\eta^3\text{-C}_3\text{H}_4\text{R}')(\mu\text{-Cl})]_2$  dimer ( $\text{R}' = \text{H, Me, Ph}$ ) and phosphines **L1**, **L2** and **L3** in THF at room temperature, according to Scheme 8. No pure products could be separated from the reactions with **L4**. The resulting complexes, **7-PR<sub>2</sub>Ar''** ( $\text{R}' = \text{H}$ ), **8-PR<sub>2</sub>Ar''** ( $\text{R}' = \text{Me}$ ) and **9-PR<sub>2</sub>Ar''** ( $\text{R}' = \text{Ph}$ ), are moderately air-stable in solution but can be stored in air for a long period of time. They are highly soluble in common organic solvents like  $\text{Et}_2\text{O}$ , benzene,  $\text{CH}_2\text{Cl}_2$  and  $\text{CHCl}_3$ .



Scheme 8. Synthesis of complexes  $\text{PdCl}(\eta^3\text{-C}_3\text{H}_4\text{R}')(\text{PR}_2\text{Ar}'')$ , for  $\text{R}' = \text{H}$  (**7-PR<sub>2</sub>Ar''**), Me (**8-PR<sub>2</sub>Ar''**), Ph (**9-PR<sub>2</sub>Ar''**).

The complexes were identified by analytical and spectroscopic methods. Due to the similarity between the NMR data for complexes  $\text{PdCl}(\eta^3\text{-C}_3\text{H}_5)(\text{PMe}_2\text{Ar}^{\text{Xyl}_2})$  (**7-L1**) and  $\text{PdCl}(\eta^3\text{-C}_3\text{H}_5)(\text{PMe}_2\text{Ar}^{\text{Dipp}_2})$  (**7-L2**), only those pertaining **7-L1** will be discussed; the conclusions drawn from them can be

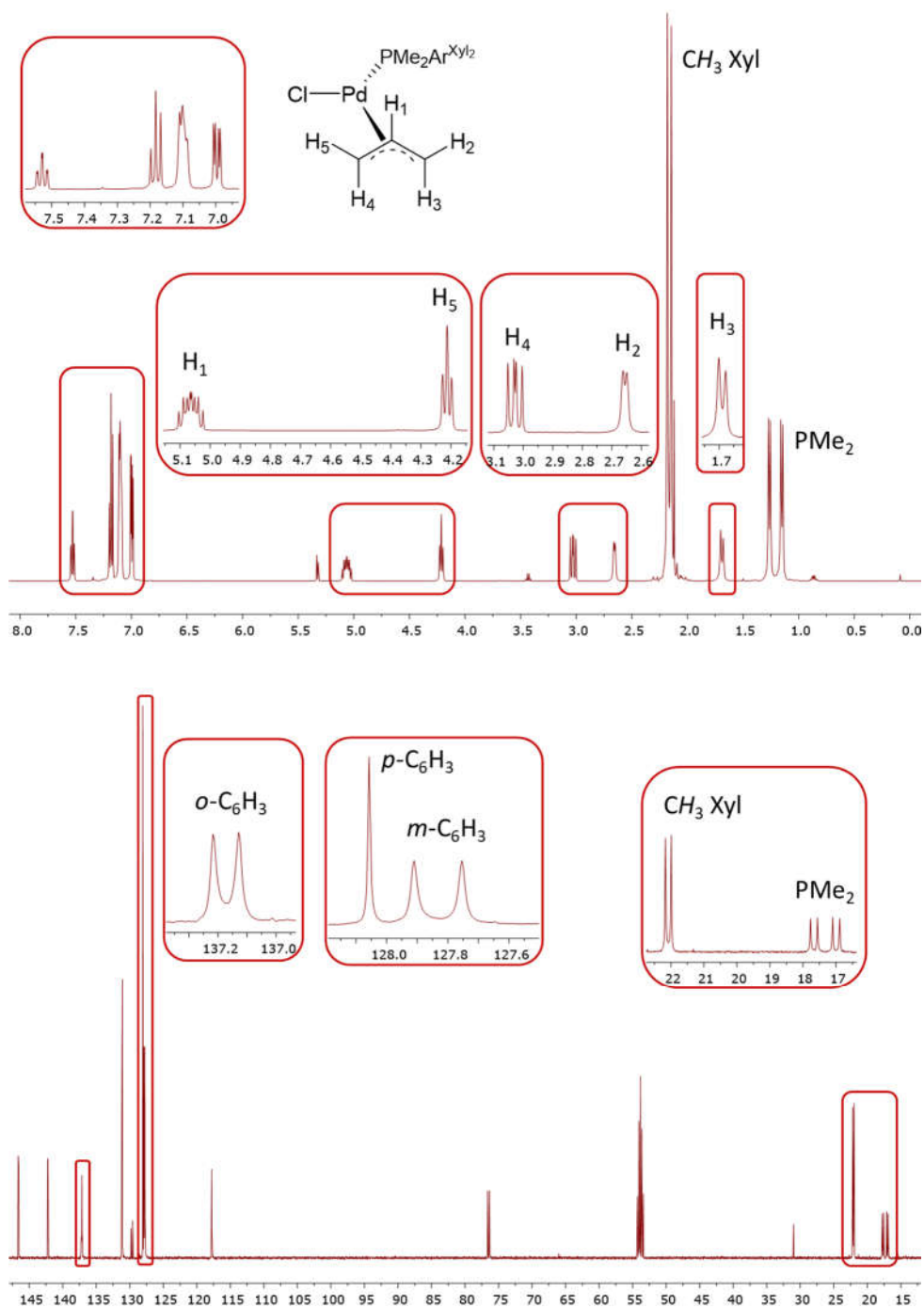


Figure 34.  $^1\text{H}$  (top) and  $^{13}\text{C}\{^1\text{H}\}$  (bottom) NMR spectra of complex **7-L1** in  $\text{CD}_2\text{Cl}_2$  at  $25^\circ\text{C}$ .



extended to **7·L2**. As shown in Figure 34, the  $^1\text{H}$  and  $^{13}\text{C}\{^1\text{H}\}$  NMR spectra of **7·L1** at room temperature display two different doublets for the methyl groups on the phosphorus atom ( $^2J_{\text{HP}} \approx 8.5$  Hz and  $^1J_{\text{CP}} \approx 27$  Hz) and only two singlets for the four methyl groups on the side xylyl rings. Furthermore, in the  $^{13}\text{C}\{^1\text{H}\}$  NMR spectrum only two resonances are observed for the CH groups in *meta* position of the flanking rings and two additional singlets are detected for the quaternary carbons in *ortho* position. On the other hand, the two *para* CH groups of the xylyl rings give rise to only one signal in both  $^1\text{H}$  and  $^{13}\text{C}\{^1\text{H}\}$  NMR spectra. In view of these spectroscopic features, it can be concluded that, at room temperature, a rapid rotation around the P- $C_{\text{ipso}}$  bond of the phosphine generates an effective  $C_2$  axis of symmetry on the NMR timescale, making the two xylyl rings equivalent (Figure 35). Their  $^{31}\text{P}\{^1\text{H}\}$  NMR data will be discussed at the end of this section, along with those of the other neutral palladium(II) allyl complexes.

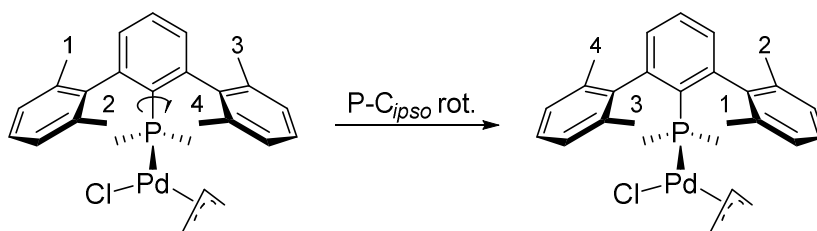


Figure 35. Rotation of the P- $C_{\text{ipso}}$  bond making the xylyl rings equivalent by an effective  $C_2$  axis.

The protons of the allyl moiety cause five different signals in the  $^1\text{H}$  NMR spectrum, with the resonance due to the central CH group exhibiting coupling with the other four, as depicted in the COSY spectrum of **7·L1** in Figure 36. Careful analysis of the NMR data, particularly the  $^1\text{H}$ - $^1\text{H}$  and  $^1\text{H}$ - $^{31}\text{P}$  coupling constants, allows for identification of each proton within the allyl ligand. Namely, protons  $\text{H}_2$  and  $\text{H}_5$ , being in *syn* position with respect to the central proton  $\text{H}_1$ , couple with the latter with  $^3J_{\text{HH}}$  coupling constants of 6.2 and 7.5 Hz, respectively. However,  $\text{H}_3$  and

## Chapter II

H<sub>4</sub>, in *anti* position, exhibit coupling constants to H<sub>1</sub> of 11.8 and 13.8 Hz.<sup>70</sup> Furthermore, the two protons from the CH<sub>2</sub> group in *trans* position relative to the phosphine ligand (i.e. H<sub>5</sub> and H<sub>4</sub>) present visible coupling to the phosphorus nucleus (<sup>3</sup>J<sub>HP</sub> = 7.5 and 10.2 Hz, respectively). Concerning the <sup>1</sup>H NMR chemical shifts, these are also in agreement with the expected situation for asymmetric PdCl(η<sup>3</sup>-C<sub>3</sub>H<sub>5</sub>)(L) complexes,<sup>70</sup> with both protons *trans* to the phosphine ligand (H<sub>5</sub> and H<sub>4</sub>) appearing at higher frequencies than those in *cis* position, due to the marked *trans* influence of the phosphines. Moreover, each *anti* proton (H<sub>3</sub> and H<sub>4</sub>) is observed at lower frequencies than the *syn* analogue (H<sub>2</sub> and H<sub>5</sub>), owing to their spatial proximity to the metal centre (see Figure 5 in the Introduction to this chapter).

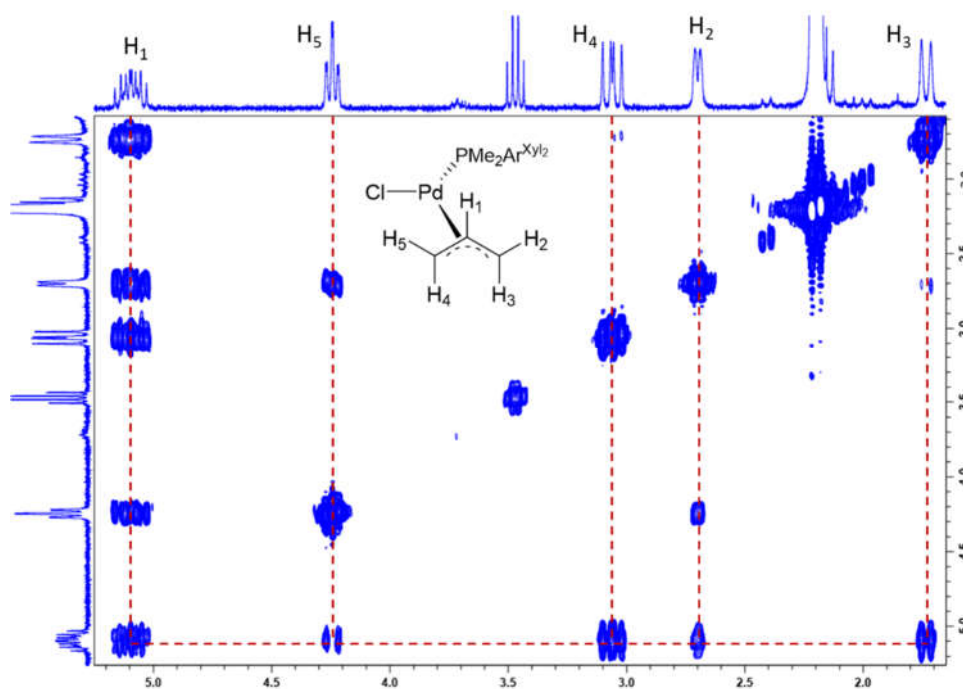


Figure 36. Allylic region of the COSY spectrum of complex **7-L1** in CDCl<sub>3</sub> at 25 °C, showing the coupling between the allylic protons.

The central proton, H<sub>1</sub>, of the allyl ligand originates a complex resonance due to the couplings to the other four allyl protons. As mentioned above, each of these exhibits a different  $^3J_{\text{HH}}$  value. However, the pattern for this signal obtained through a simulation differs from that observed in the  $^1\text{H}$  NMR spectrum (see Figure 37-A and B). In order to gain insight into this phenomenon, a Nuclear Overhauser Effect Spectroscopy (NOESY) experiment was carried out (Figure 38), revealing that hydrogen atoms H<sub>2</sub> and H<sub>3</sub>, both bound to the terminal C atom in *cis* position to the phosphine ligand, are interchanging. This exchange is slow enough not to cause coalescence of the resonances due to these two nuclei, but fast enough to affect their coupling constants with the central allyl proton, H<sub>1</sub>. As a result, the observed H<sub>1</sub> signal resembles more closely the simulation taking into account said exchange (Figure 37-C).<sup>71</sup>

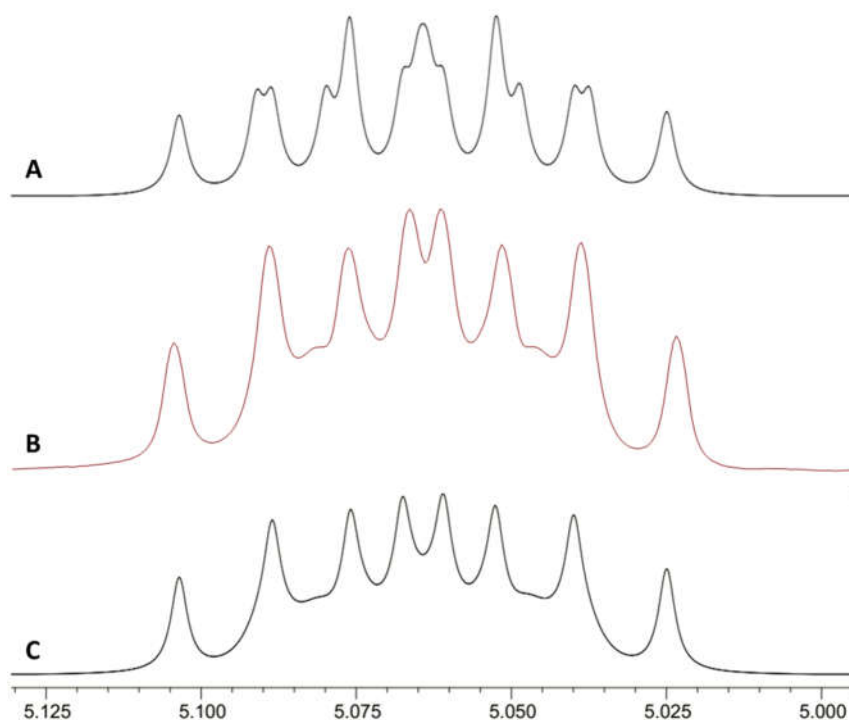


Figure 37.  $^1\text{H}$  NMR resonance of the allyl central CH of complex **7-L1**, observed (B) and simulated with (C) and without exchange (A).

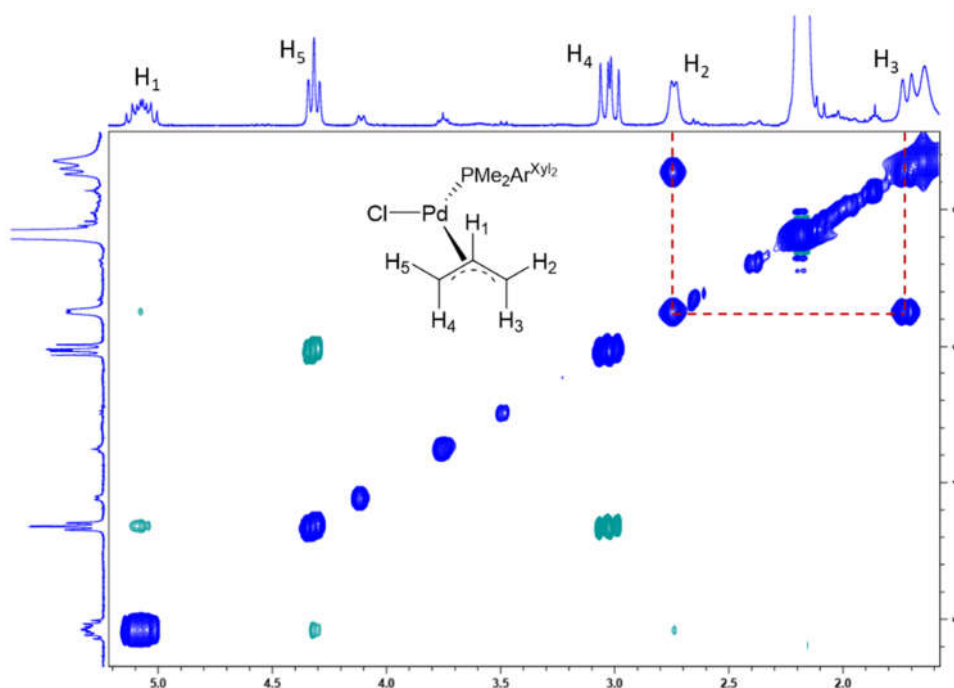


Figure 38. Allyl region of the NOESY spectrum of **7-L1** in  $\text{CDCl}_3$  at  $25\text{ }^\circ\text{C}$ , showing the exchange cross peak between  $\text{H}_2$  and  $\text{H}_3$ .

The process that accounts for the observed exchange between the germinal *syn* and *anti* hydrogens ( $\text{H}_2$  and  $\text{H}_3$ ) of the C atom in *cis* position to the phosphine ligand is termed the *syn-anti* exchange. It is commonly observed in allyl complexes at high temperature and can either affect one side of the allyl moiety or both of them. This exchange is associated with an allyl  $\eta^3$ - $\eta^1$ - $\eta^3$  isomerisation, as illustrated in Figure 39.<sup>72</sup> The coordination mode of the allyl moiety first changes from  $\eta^3$  to  $\eta^1$ , followed by a rotation around the C–C simple bond, which interchanges the protons  $\text{H}_2$  and  $\text{H}_3$ , and a subsequent regeneration of the  $\eta^3$  mode of coordination of the allyl. Since the bonding between the *trans* terminus of the allyl fragment and the palladium centre is expected to be weaker due to the *trans* influence of the phosphine ligand, this process seems to affect only the  $\text{CH}_2$  in *cis* position, although it is very slow at room temperature, as discussed above.

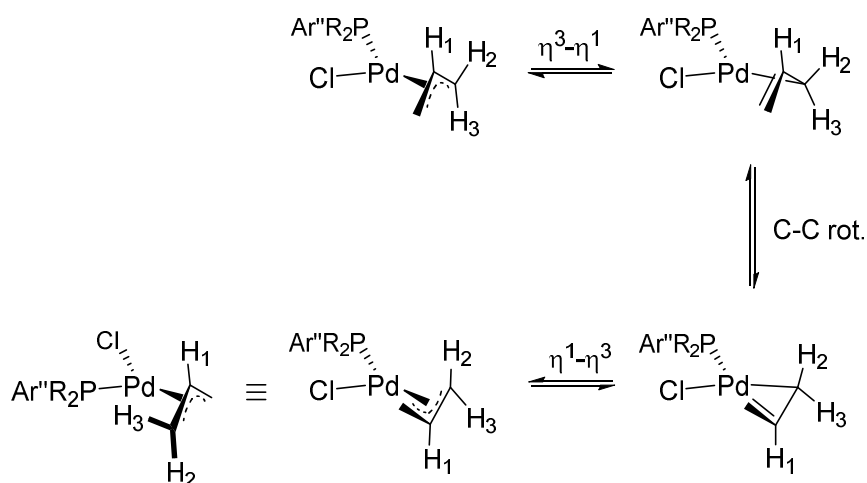


Figure 39. Proposed mechanism for the *syn-anti* exchange of  $H_2$  and  $H_3$  through a  $\eta^3$ - $\eta^1$ - $\eta^3$  isomerisation.

This situation is even more pronounced in the case of **7·L3**. The protons bound to the C atom in *cis* position to the phosphine ligand are not observed in the room temperature  $^1\text{H}$  NMR spectrum of this complex and they cause no cross peaks in any of the 2D NMR spectra at the same temperature (see Figure 40 for the  $^1\text{H}$ - $^{13}\text{C}$  HSQC spectrum). This apparent higher rate of exchange could be explained by the greater electron-donor capacity of  $\text{PCyp}_2\text{Ar}^{\text{Xyl}_2}$  compared to the dimethyl-substituted phosphines **L1** and **L2**, weakening even further the bonding between the palladium centre and the  $\text{CH}_2$  in *trans* position. Interestingly, only one signal is observed in the  $^1\text{H}$  and  $^{13}\text{C}\{^1\text{H}\}$  NMR spectra for the methyl groups on the xylyl rings of this complex. If both the *syn-anti* exchange and the rotation around the Pd–P bond are fast enough, an effective plane of symmetry perpendicular to the central aryl ring of the phosphine is created (Figure 41).

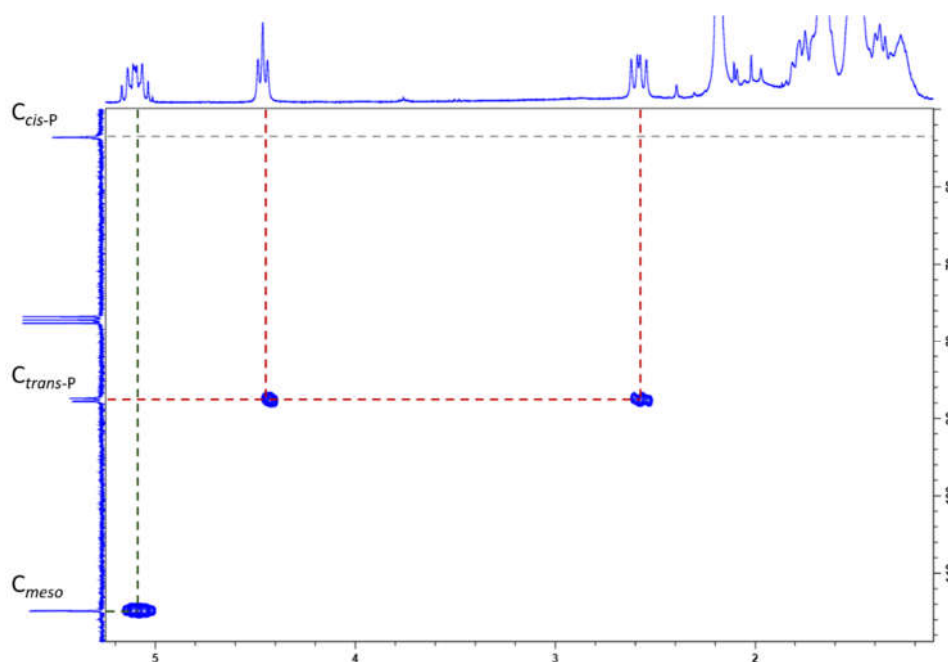


Figure 40. Allylic region of the  $^1\text{H}$ - $^{13}\text{C}$  HSQC spectrum of complex **7-L3** in  $\text{CDCl}_3$  at 25 °C.

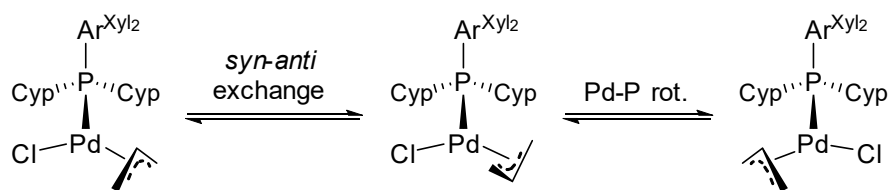


Figure 41. Proposed processes creating an effective plane of symmetry containing the  $\text{Pd-P}$  and  $\text{P-Ar}^{\text{Xyl}_2}$  bonds.

Complex **8-L1**, bearing a methyl-substituted allyl ligand (crotyl group), displays very similar NMR spectra to the parent analogue **7-L1** (see Figure 42 for the  $^1\text{H}$  NMR spectrum of **8-L1**). The allyl central proton is again affected by the *syn-anti* exchange between the two hydrogen atoms of the  $\text{CH}_2$  *cis* to the phosphine ligand. On the other hand, the  $^1\text{H}$  NMR resonances due to the *meta* positions and the methyl substituents on the xyllyl rings, as well as to the  $\text{PMe}_2$  moiety, appear somewhat broadened, indicating that this exchange might be slightly faster than

in **7·L1** at room temperature. Proton  $H_4$  couples to the vicinal methyl group as well as to the phosphorus atom and  $H_1$ , appearing as a doublet of doublet of quartets. In turn, the methyl group on the allyl ligand exhibits coupling to both the phosphorus atom and  $H_4$ . In view of these data, the proposed disposition of the crotyl group is presented in Figure 42, with the CHMe group located *trans* to the phosphine ligand.

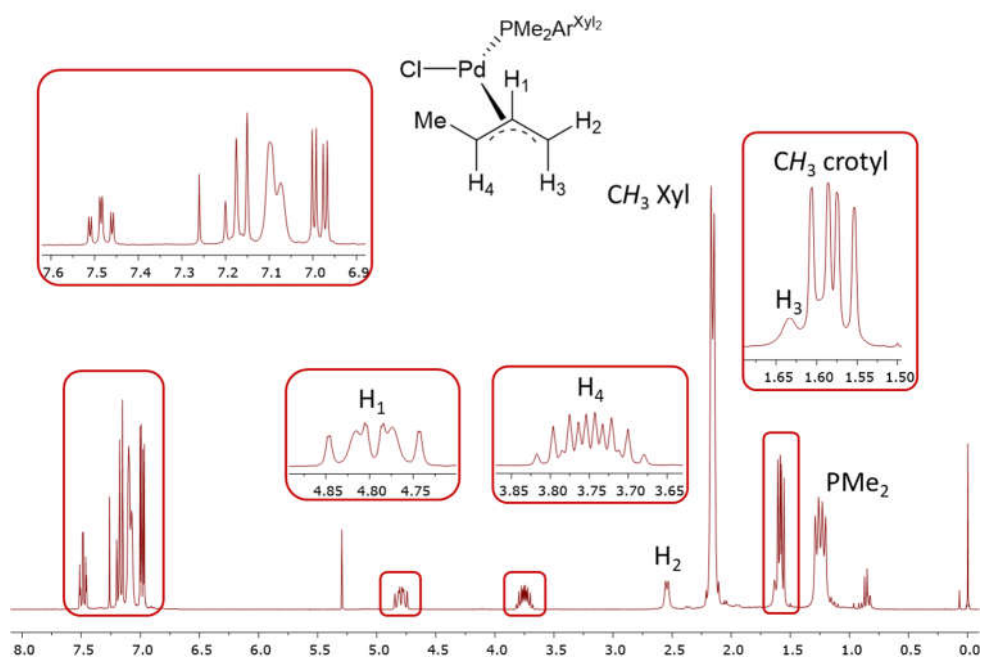


Figure 42.  $^1\text{H}$  NMR spectrum of **8·L1** in  $\text{CDCl}_3$  at  $25\text{ }^\circ\text{C}$ .

Following the series, complex **8·L2** bearing the somewhat bulkier  $\text{PMe}_2\text{Ar}^{\text{Dipp}_2}$  phosphine, appears to be slightly more fluxional than **8·L1**. This fluxional behaviour is responsible for the increased broadness of certain signals in the room temperature  $^1\text{H}$  NMR, such as the one corresponding to  $H_2$ , and the appearance of only one set of resonances for the  $^i\text{Pr}$  groups on the side aryl rings

## Chapter II

and for the  $\text{PMe}_2$  fragment (Figure 43). Lastly, **8-L3** behaves in solution very similarly to its analogue **7-L3**.

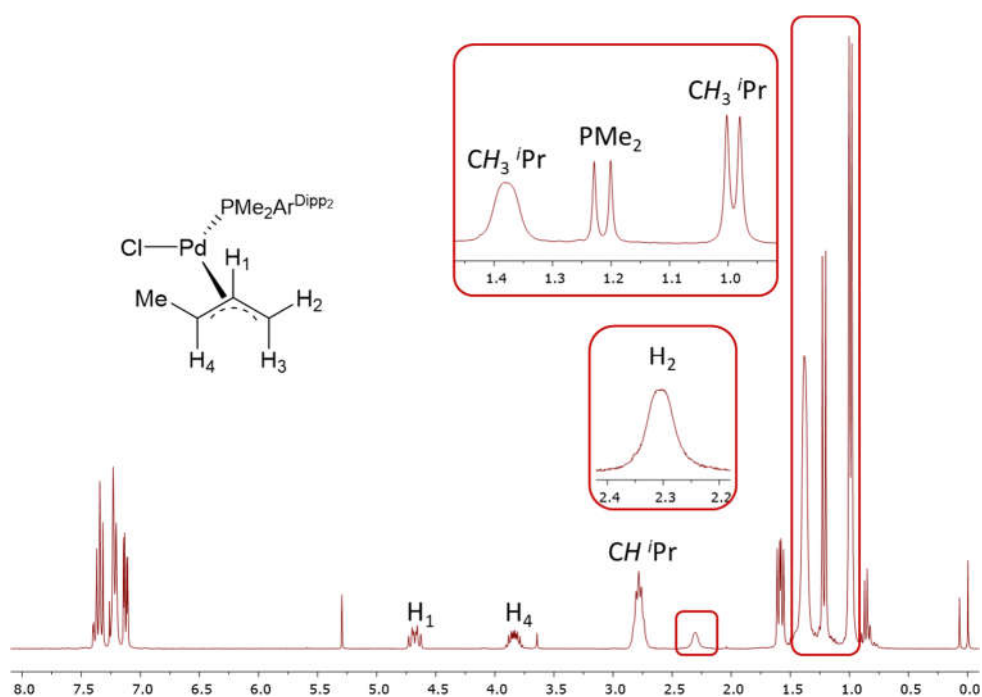


Figure 43.  $^1\text{H}$  NMR spectrum of **8-L2** in  $\text{CDCl}_3$  at 25 °C.

Concerning the cinnamyl derivatives, **9-L1** through **9-L3**, the *syn-anti* exchange becomes even faster. The room temperature  $^1\text{H}$  NMR spectrum of complex **9-L1** (Figure 44) exhibits broadened signals for  $\text{H}_2$  and  $\text{H}_3$ , while said signals disappear in the case of **9-L2**. Also, both the  $^1\text{H}$  and  $^{13}\text{C}\{^1\text{H}\}$  NMR of these two complexes display an apparently symmetric environment around the phosphine ligand. Another interesting feature of derivatives **9-L1** and **9-L2** is the presence of a minor isomer in solution. The major species present the same allyl moiety conformation as their crotyl analogues, as deduced from their  $^1\text{H}$  and  $^{13}\text{C}\{^1\text{H}\}$  NMR data (see Figure 44 for the  $^1\text{H}$  NMR spectrum of complex **9-L1**). In the minor species, however, the cinnamyl is coordinated in such a way that the



unsubstituted CH<sub>2</sub> terminus is placed in *trans* position to the phosphine ligand and the CHPh terminus in *cis* position. The *syn-anti* exchange is impeded in these cases due to the presence of the phenyl substituent on the allylic carbon *cis* to the phosphine ligand.<sup>72b</sup> As a result, there exists an asymmetric environment around the PMe<sub>2</sub>Ar'' ligands in the minor isomers, as evinced in the appearance in the <sup>1</sup>H NMR spectra of two sets of signals for the alkyl substituents on the side aryl rings as well as two different doublets for the PMe<sub>2</sub> groups.

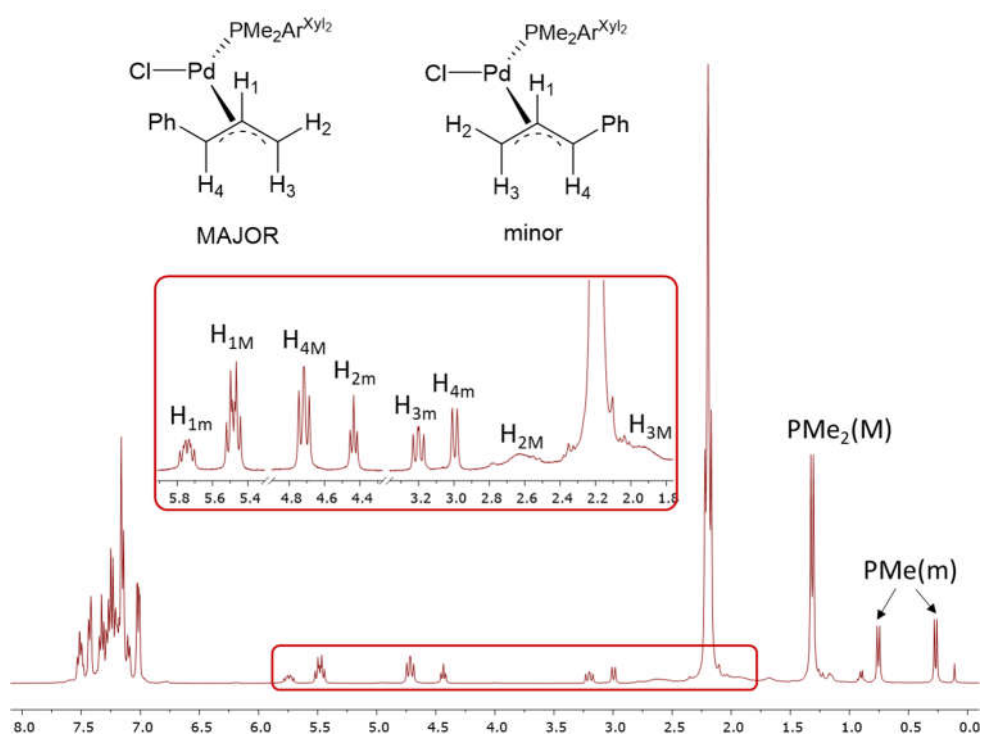


Figure 44. <sup>1</sup>H NMR spectrum of complex **9-L1** in CDCl<sub>3</sub> at 25 °C.

A variable temperature NMR study of complex **9-L1** was carried out, revealing that the H<sub>2</sub> and H<sub>3</sub> resonances resolved into the expected doublets upon lowering the temperature (Figure 45).

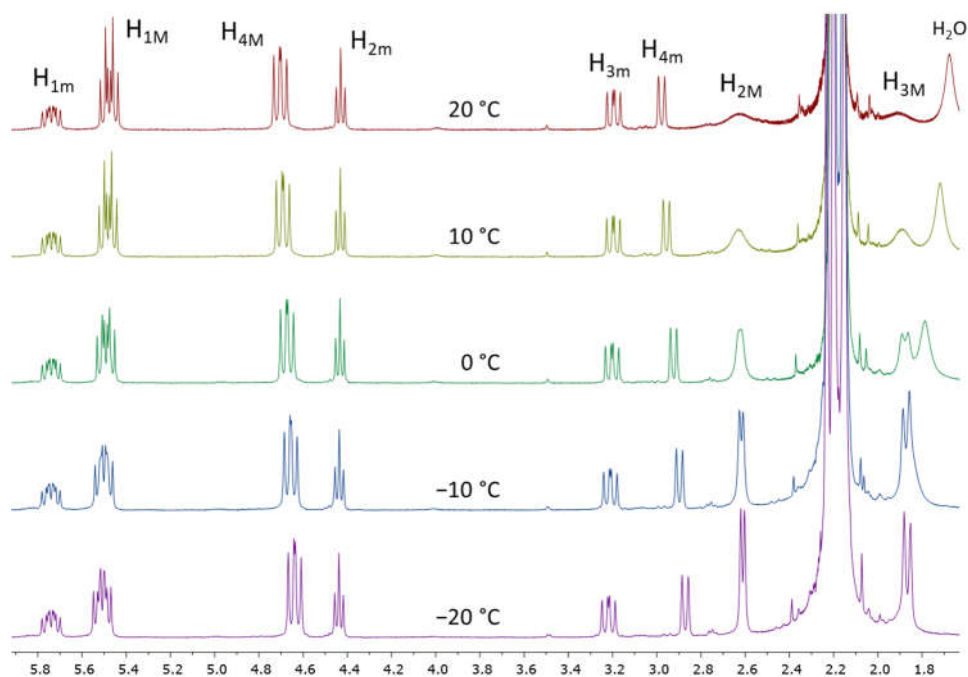


Figure 45. Allylic region of the  $^1\text{H}$  NMR spectra of complex **9·L1** in  $\text{CDCl}_3$  at different temperatures.

In order to discern if an exchange was ongoing between the two isomers of **9·L1**, a NOESY spectrum was recorded at 40 °C. Several weak same-phase cross peaks can be discerned connecting signals of the major isomer with those corresponding to the minor isomer, such as those caused by the  $\text{PMe}_2$  groups and the allylic protons  $\text{H}_1$  and  $\text{H}_4$  (Figure 46). This seems to indicate that a very slow exchange is ongoing between the two isomers. It is worth mentioning that no cross peaks are observed for the resonances of  $\text{H}_2$  and  $\text{H}_3$  due to their pronounced broadness in the case of the major isomer.

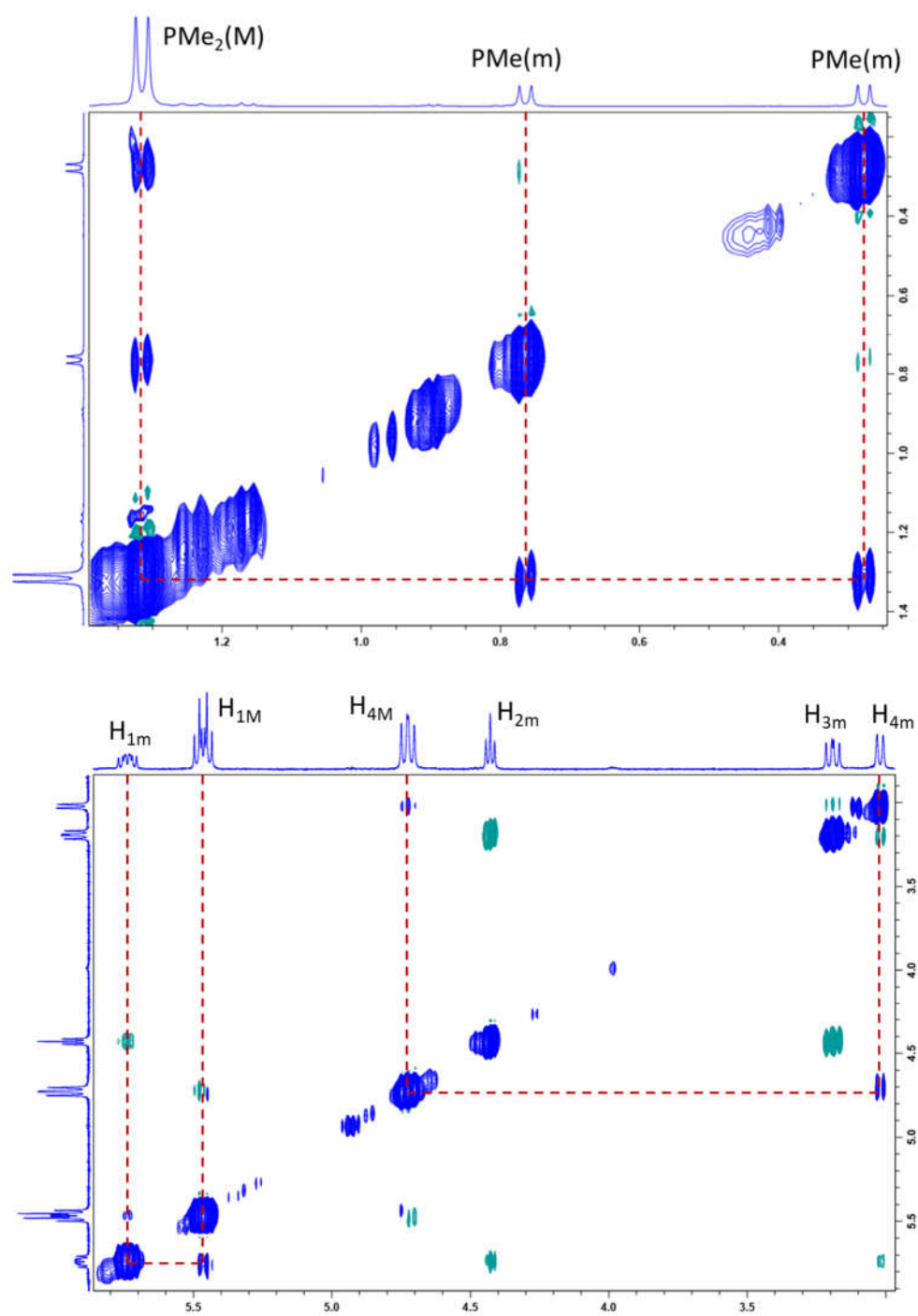


Figure 46. PMe<sub>2</sub> (top) and allylic (bottom) regions of the NOESY spectrum of 9-L1 in CDCl<sub>3</sub> at 40 °C.

## Chapter II

Finally, the faster rate of interchange for the cinnamyl derivatives is even more evident in the appearance of only one broad signal for both H<sub>2</sub> and H<sub>3</sub> protons in the <sup>1</sup>H NMR spectrum of **9·L3** (Figure 47). In contrast to **9·L1** and **9·L2**, only one species was detected in the NMR spectra of **9·L3**.

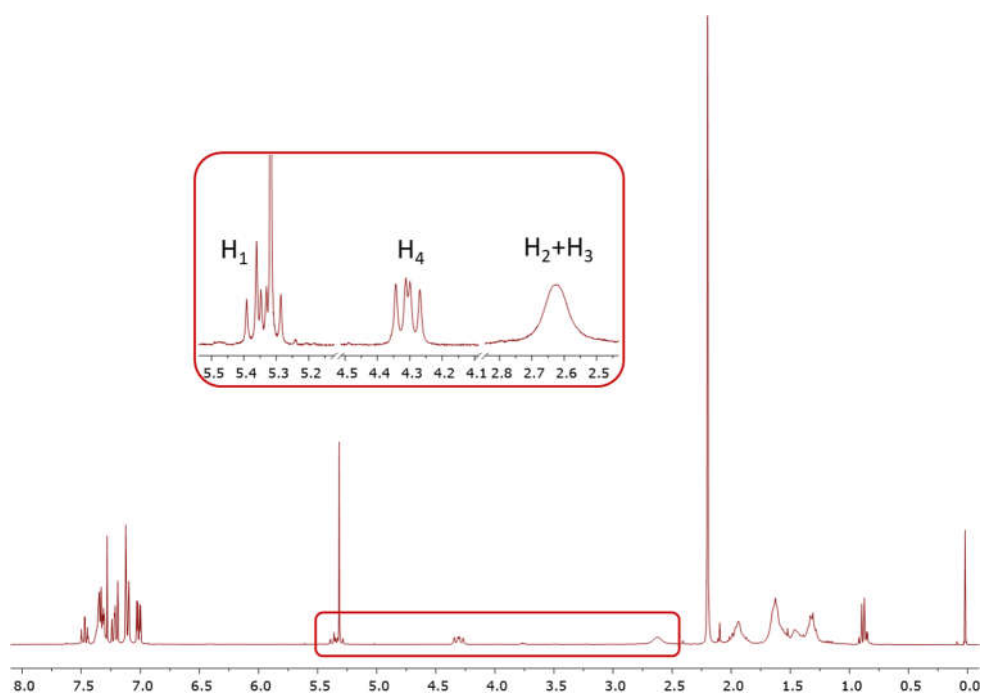


Figure 47. <sup>1</sup>H NMR spectrum of complex **9·L3** in CDCl<sub>3</sub> at 25 °C.

To further confirm the structures of the palladium(II) allyl derivatives inferred from the NMR data, the molecular structure of complex **9·L2** was studied by single crystal X-ray diffraction (Figure 48). The palladium atom exhibits the expected pseudo-square planar geometry, with the cinnamyl moiety occupying two coordination positions. Due to the preference of the phosphine ligand for a conformation of type **B**, one of the flanking rings of the terphenyl moiety is positioned just above the metal centre. However, the shortest Pd-C<sub>arene</sub> distance is 3.287(3) Å, far above the sum of their covalent radii (2.12 Å).<sup>66</sup> In fact, this Dipp

ring is slightly bent away from the metal by 8.3° (see Figure 18 for a representation of this measurement). A similar phenomenon is observed for half the molecules in the crystal structure of the biaryl phosphine adduct PdCl( $\eta^3$ -C<sub>3</sub>H<sub>5</sub>)(RuPhos) (RuPhos = 2-dicyclohexylphosphino-2',6'-diisopropoxybiphenyl), where the phosphine ligand adopts a conformation akin to type **C**, with the side aryl ring located above the palladium centre (shortest Pd-C<sub>arene</sub> distance of 3.307(2) Å).<sup>24b</sup> Concerning the cinnamyl moiety, although two isomers can be observed in the crystal structure, in a 66:34 ratio, the phenyl-substituted terminus of the allyl ligand is placed in *trans* position with respect to the phosphine in both cases. Thus, these two conformers are correlated by the  $\eta^3$ - $\eta^1$ - $\eta^3$  isomerisation discussed above (see Figure 39). The Pd-C<sub>allyl</sub> bond distances follow the expected trend based on the *trans* influence of the phosphine and the chloride ligands. Thus, the Pd-C<sub>*trans*-P</sub> bonds (*ca.* 2.27 Å) are significantly longer than the Pd-C<sub>*cis*-P</sub> bonds (2.10-2.16 Å).

Finally, a brief comment concerning the <sup>31</sup>P{<sup>1</sup>H} NMR chemical shifts of the above discussed complexes, collected in Table 4, will be made. All the resonances appear at around 30-35 ppm at higher frequency compared to the free phosphine ligands, quite typical of complexes where a  $\kappa^1$ -P mode of coordination of the phosphine is observed (as, for example, with the Ni(CO)<sub>3</sub>(PR<sub>2</sub>Ar'') complexes discussed in the previous chapter).

#### II.2.2.2. Synthesis and characterisation of some [Pd( $\eta^3$ -C<sub>3</sub>H<sub>4</sub>R')](PR<sub>2</sub>Ar'')BAr<sup>f</sup><sub>4</sub> (R' = H, Me, Ph) complexes.

Inspired by Colacot's report on the synthesis of cationic allylpalladium adducts of bulky ligands,<sup>24b</sup> we set out to study analogous systems using the dialkyl terphenyl phosphines.

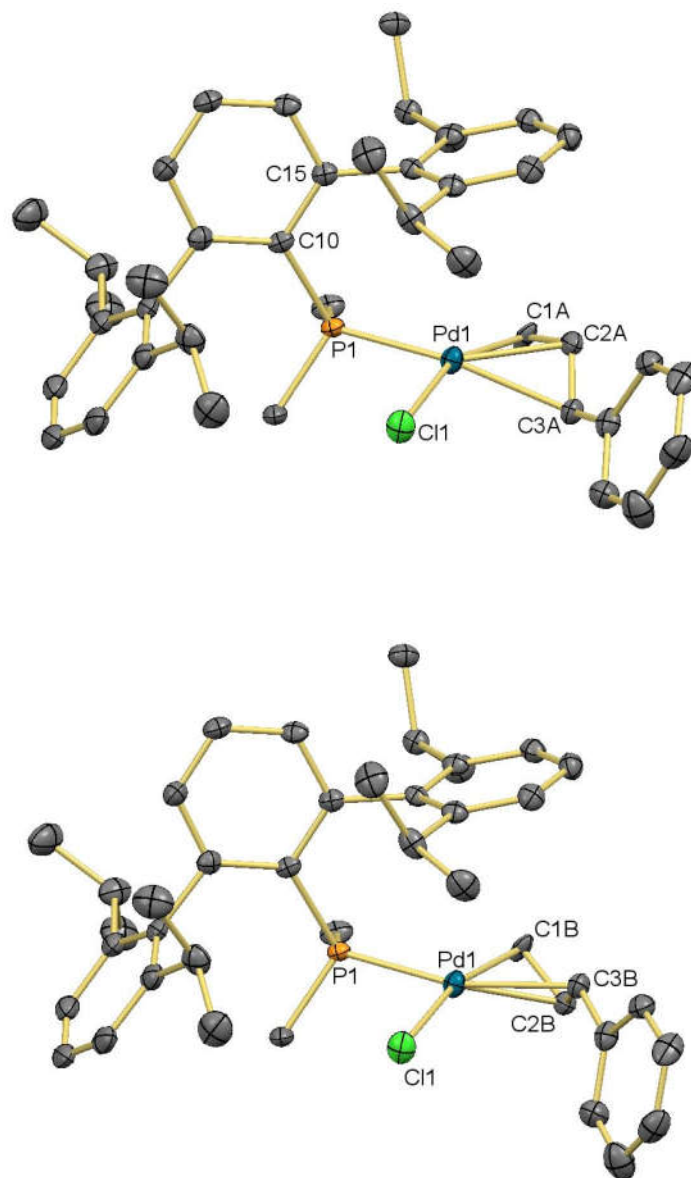


Figure 48. ORTEP views of the two conformers of complex **9·L2**. Hydrogen atoms are omitted for clarity and thermal ellipsoids are set at 50% level probability. Selected bond distances (Å) and angles (°): Pd1-P1 2.2943(9), Pd1-Cl1 2.369(1), Pd1-C1A 2.10(1), Pd1-C2A 2.155(5), Pd1-C3A 2.269(4), C1A-C2A 1.37(1), C2A-C3A 1.396(7), P1-Pd1-Cl1 93.54(3), Cl1-Pd1-C3A 94.4(1), C3A-Pd1-C1A 66.4(3), C1A-Pd1-P1 102.7(2), C3A-C2A-C1A 120.5(6), Pd1-P1-C10-C15 43.3(3).

	Complex	$\delta(^{31}\text{P})$	$\Delta\delta$
<b>7·L1</b>	$\text{PdCl}(\eta^3\text{-C}_3\text{H}_5)(\text{PMe}_2\text{Ar}^{\text{Xyl}_2})$	-10.4	30.0
<b>7·L2</b>	$\text{PdCl}(\eta^3\text{-C}_3\text{H}_5)(\text{PMe}_2\text{Ar}^{\text{Dipp}_2})$	-8.9	32.4
<b>7·L3</b>	$\text{PdCl}(\eta^3\text{-C}_3\text{H}_5)(\text{PCyp}_2\text{Ar}^{\text{Xyl}_2})$	33.2	28.6
<b>8·L1</b>	$\text{PdCl}(\eta^3\text{-C}_3\text{H}_4\text{Me})(\text{PMe}_2\text{Ar}^{\text{Xyl}_2})$	-9.7	30.7
<b>8·L2</b>	$\text{PdCl}(\eta^3\text{-C}_3\text{H}_4\text{Me})(\text{PMe}_2\text{Ar}^{\text{Dipp}_2})$	-8.5	32.8
<b>8·L3</b>	$\text{PdCl}(\eta^3\text{-C}_3\text{H}_4\text{Me})(\text{PCyp}_2\text{Ar}^{\text{Xyl}_2})$	36.2	31.6
<b>9·L1 Major</b>	$\text{PdCl}(\eta^3\text{-C}_3\text{H}_4\text{Ph})(\text{PMe}_2\text{Ar}^{\text{Xyl}_2})$	-7.3	33.1
<b>9·L1 minor</b>	$\text{PdCl}(\eta^3\text{-C}_3\text{H}_4\text{Ph})(\text{PMe}_2\text{Ar}^{\text{Xyl}_2})$	-10.9	29.5
<b>9·L2 Major</b>	$\text{PdCl}(\eta^3\text{-C}_3\text{H}_4\text{Ph})(\text{PMe}_2\text{Ar}^{\text{Dipp}_2})$	-5.6	35.7
<b>9·L2 minor</b>	$\text{PdCl}(\eta^3\text{-C}_3\text{H}_4\text{Ph})(\text{PMe}_2\text{Ar}^{\text{Dipp}_2})$	-9.0	32.3
<b>9·L3</b>	$\text{PdCl}(\eta^3\text{-C}_3\text{H}_4\text{Ph})(\text{PCyp}_2\text{Ar}^{\text{Xyl}_2})$	37.9	33.3

Table 4.  $^{31}\text{P}\{^1\text{H}\}$  NMR chemical shifts of the allylpalladium complexes.

Thus, complex **9·L2** was made to react with one equivalent of the sodium salt of a weakly coordinating anion, namely sodium tetrakis(3,5-bis(trifluoromethyl)phenyl)borate,  $\text{NaBAR}^{\text{F}_4}$ . This led to the formation of a new complex, **11·L2**, where the chloride ligand was replaced by the already mentioned weak  $\eta^1\text{-C}$  interaction with the *ipso* carbon of one of the side aryl rings (Scheme 9-A). Application of this approach to *in situ* generated, rather than previously isolated, **7·L2** produced the corresponding analogue, **10·L2**. Hence, this simpler direct synthetic route to this type of complexes was successfully used to synthesise the cationic adducts of the bulkier phosphine  $\text{P}^i\text{Pr}_2\text{Ar}^{\text{Xyl}_2}$ , **L4** (Scheme 9-B). It is worth iterating that attempts at preparing neutral allylpalladium(II) complexes of **L4** were unsuccessful. All four new complexes were isolated as air-stable yellow or pale yellow solids, insoluble in nonpolar solvents (e.g. pentane), but quite soluble THF,  $\text{CH}_2\text{Cl}_2$  or  $\text{CHCl}_3$ . Interestingly, obtaining single crystals of these complexes was easier than for the neutral derivatives discussed in the previous section, presumably due to their salt-like formulation.





NMR spectrum of **10·L4** ( $H_1$ ,  $H_2$ ,  $H_4$ ,  $H_3$  and  $H_5$ ) differs from that observed for the neutral derivatives discussed in the previous section (i.e.  $H_1$ ,  $H_5$ ,  $H_4$ ,  $H_2$ ,  $H_3$ ), possibly due to the difference in nature between the chloride ligand and the  $\eta^1$ - $C_{ipso}$  interaction. In addition, judging by the sharpness observed for the resonances due to  $H_2$  and  $H_3$  and the absence of exchange cross peaks in the NOESY spectrum, complex **10·L4**, and more broadly all the members of this series of compounds, do not seem to undergo the  $\eta^3$ - $\eta^1$ - $\eta^3$  isomerisation commented in the previous section. A stronger bonding between the formally tricoordinate palladium centre and the allyl moiety in these complexes could constitute the reason behind this difference in behaviour.

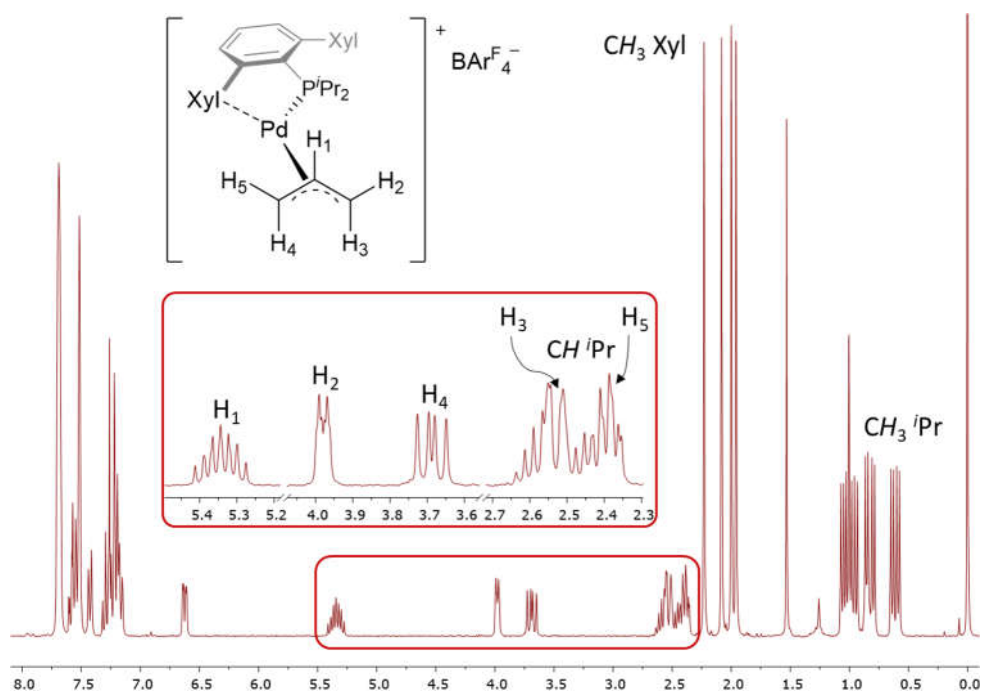


Figure 49.  $^1\text{H}$  NMR spectrum of complex **10·L4** in  $\text{CDCl}_3$  at 25 °C.

Similarly to the neutral analogue  $\text{PdCl}(\eta^3\text{-C}_3\text{H}_4\text{Ph})(\text{PMe}_2\text{Ar}^{\text{Dipp}_2})$  (**9·L2**), cationic complex  $[\text{Pd}(\eta^3\text{-C}_3\text{H}_4\text{Ph})(\text{PMe}_2\text{Ar}^{\text{Dipp}_2})]\text{BARF}_4$  (**11·L2**) appears in the NMR

## Chapter II

spectra as a mixture of isomers in different proportion, varying in the position of the unsubstituted and phenyl-substituted allyl termini relative to the phosphine ligand. The different dispositions of the cinnamyl group in the two isomers are clearly discerned in the  $^1\text{H}$ - $^{31}\text{P}$  HMQC experiment shown in Figure 50. The  $^{31}\text{P}\{^1\text{H}\}$  NMR signal of the major isomer exhibits a strong correlation with only one  $^1\text{H}$  NMR signal, corresponding to  $\text{H}_4$ , while that of the minor isomer couples with two different allyl protons,  $\text{H}_2$  and  $\text{H}_3$ .

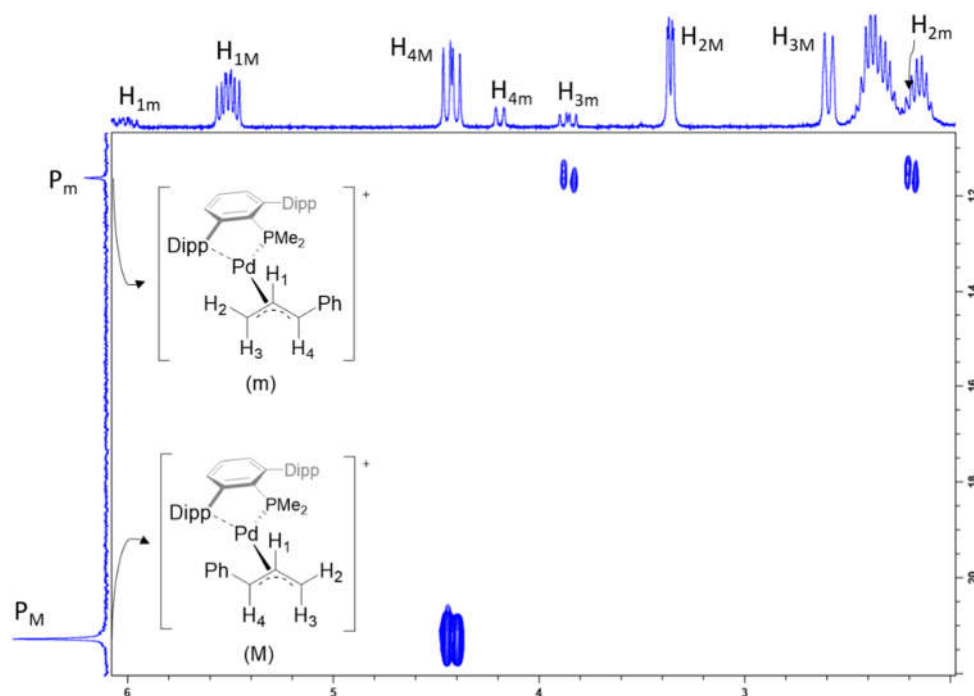


Figure 50.  $^1\text{H}$ - $^{31}\text{P}$  HMQC spectrum of **11·L2** in  $\text{CDCl}_3$  at  $25\text{ }^\circ\text{C}$ .

On the contrary, complex  $[\text{Pd}(\eta^3\text{-C}_3\text{H}_4\text{Ph})(\text{P}^i\text{Pr}_2\text{Ar}^{\text{Xyl}_2})]\text{BAr}^{\text{F}_4}$  (**11·L4**) resembles  $\text{PdCl}(\eta^3\text{-C}_3\text{H}_4\text{Ph})(\text{PCyp}_2\text{Ar}^{\text{Xyl}_2})$  (**9·L3**) in that only one species is detected by NMR spectroscopy. The impeded  $\text{P-C}_{ipso}$  rotation, the coupling between the  $^{31}\text{P}$  and  $^{13}\text{C}$  nuclei and the presence of a phenyl substituent on the allyl moiety considerably complicated the correct assignment of the  $^{13}\text{C}\{^1\text{H}\}$  NMR spectra of

both **11·L2** and **11·L4**. A  $^{13}\text{C}\{^1\text{H}, ^{31}\text{P}\}$  NMR of the latter was recorded, facilitating the identification of the different aromatic  $^{13}\text{C}$  nuclei and the measuring of their coupling constants to the  $^{31}\text{P}$  nucleus (Figure 51).

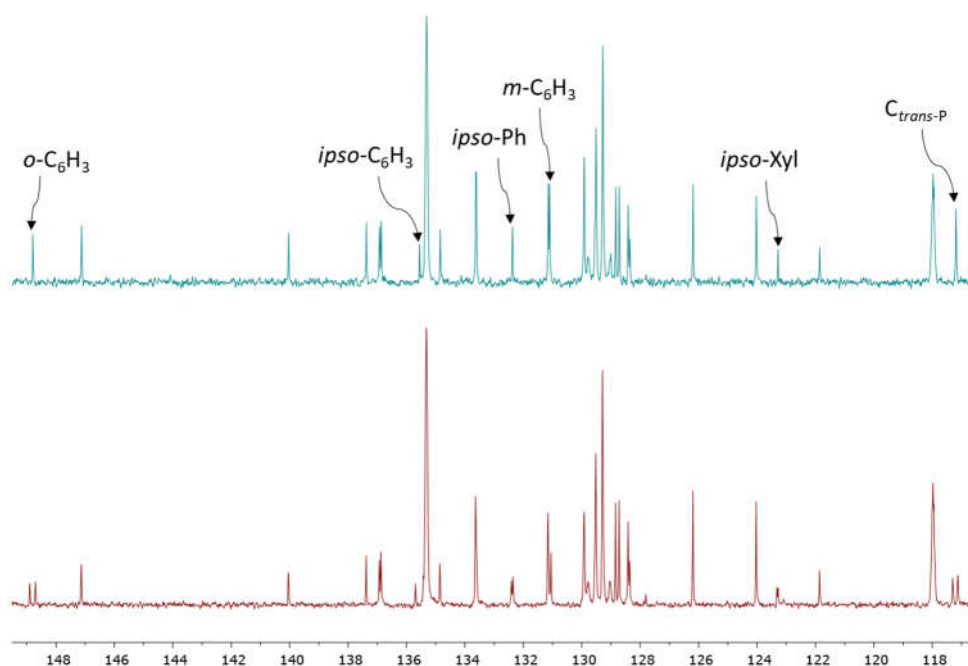


Figure 51.  $^{13}\text{C}\{^1\text{H}\}$  (bottom) and  $^{13}\text{C}\{^1\text{H}, ^{31}\text{P}\}$  (top) NMR spectra of **11·L4** in  $\text{CD}_2\text{Cl}_2$  at 25 °C.

The structures of complexes **10·L2**, **11·L2** and **11·L4** were confirmed by single crystal X-ray diffraction studies and the molecular structures of the cationic species are displayed in Figures 52-54 ( $\text{BAR}^{\text{F}_4^-}$  anions have been omitted for clarity). To facilitate comparison, selected structural data are contained in Table 6, and only distances and angles pertaining the major conformers will be discussed here. The Pd- $\text{C}_{\text{allyl}}$  bond distances in **10·L2** (2.25(1) Å to  $\text{C}_{\text{trans-P}}$  and 2.106(6) Å to  $\text{C}_{\text{cis-P}}$ ) are very similar to those observed in the neutral  $\eta^3$ -cinnamyl complex **9·L2** (2.269(4) and 2.10(1) Å, respectively) and only slightly different from those in  $[\text{Pd}(\eta^3\text{-C}_3\text{H}_5)(\text{RuPhos})]\text{OTf}$  (ca. 2.21 and 2.16 Å).<sup>24b</sup> In comparison, the Pd- $\text{C}_{\text{trans-P}}$

## Chapter II

bonds in cationic  $\eta^3$ -cinnamyl complexes **11·L2** and **11·L4** are considerably elongated (2.388(7) and 2.452(3) Å, respectively), presumably due to steric repulsion between the phenyl substituent and the interacting arene. Strikingly, these distances are actually longer than the Pd $\cdots$ C<sub>ipso</sub> distances to the latter (2.276(3) and 2.273(2) Å). These observations are in line with other similar complexes in the literature, such as [Pd( $\eta^3$ -C<sub>3</sub>H<sub>4</sub>Ph)(<sup>t</sup>BuXPhos)]OTf (<sup>t</sup>BuXPhos = 2-di-*tert*-butylphosphino-2',4',6'-triisopropylbiphenyl), and are thought to be the reason behind the higher rate of activation of palladium(II) complexes bearing substituted allyl ligands compared to their unsubstituted analogues.<sup>24b,40b,73</sup> Another interesting feature of these complexes is the bending of the interacting arene away from the metal centre (labelled  $\alpha$  in Figure 18) by 20–26°. At the same time, the central aryl ring bends towards the metal, resulting in P-C<sub>ipso</sub>-C<sub>ortho</sub> angle of *ca.* 113–114°. It is also worth mentioning that, as in the case of neutral complex **9·L2**, the cationic species in **10·L2** and **11·L4** appear as a mixture of two conformers, in ratios of 73:27 and 84:16, respectively.

Selected distances and angles	<b>10·L2</b>	<b>11·L2</b>	<b>11·L4</b>	<b>9·L2</b>
Pd-P	2.298	2.263	2.2887	2.2943
Pd-C <sub>trans-P</sub>	2.25	2.388	2.452	2.269
Pd-C <sub>meso</sub>	2.16	2.191	2.188	2.155
Pd-C <sub>cis-P</sub>	2.106	2.098	2.100	2.10
Pd $\cdots$ C <sub>ipso</sub>	2.314	2.276	2.272	-
C <sub>trans-P</sub> -C <sub>meso</sub>	1.29	1.356	1.370	1.396
C <sub>meso</sub> -C <sub>cis-P</sub>	1.40	1.40	1.417	1.37
C <sub>trans-P</sub> -C <sub>meso</sub> -C <sub>cis-P</sub>	126.2	122.6	121.3	120.5
Ar plane deviation ( $\alpha$ )	20.4	26.2	23.9	8.3

Table 6. Selected distances (Å) and angles (°) in the major isomers of the cationic allylpalladium complexes (data for neutral complex **9·L2** included for comparison).

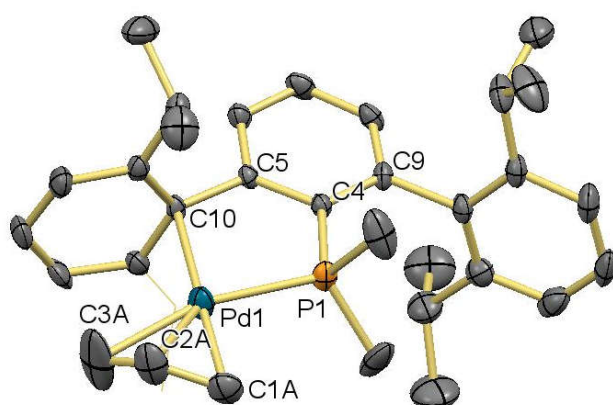


Figure 52. ORTEP view of the major conformer of cation in complex **10-L2**. Hydrogen atoms are omitted for clarity, the atoms of an isopropyl substituent are drawn in wireframe and thermal ellipsoids are set at 50% level probability. Selected bond distances (Å) and angles (°): Pd1-P1 2.298(1), Pd1-C1A 2.106(6), Pd1-C2A 2.16(1), Pd1-C3A 2.25(1), Pd1-C10 2.314(4), C1A-C2A 1.40(1), C2A-C3A 1.29(1), C1A-Pd1-P1 95.9(1), P1-Pd1-C10 83.58(9), C10-Pd1-C3A 113.5(3), C3A-Pd1-C1A 67.1(3), C1A-C2A-C3A 126.2(9), P1-C4-C5 113.9(3), C4-C5-C10 125.6(3), P1-C4-C9 127.0(3), Pd1-P1-C4-C5 9.0(3).

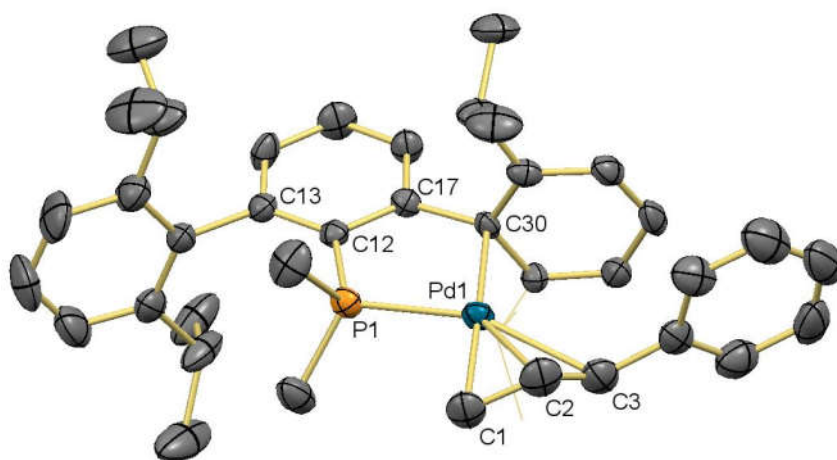


Figure 53. ORTEP view of the cation in complex **11-L2**. Hydrogen atoms are omitted for clarity, the atoms of an isopropyl substituent are drawn in wireframe and thermal ellipsoids are set at 50% level probability. Selected bond distances (Å) and angles (°): Pd1-P1 2.263(1), Pd1-C1 2.098(5), Pd1-C2 2.191(6), Pd1-C3 2.388(7), Pd1-C30 2.276(3), C1-C2 1.40(1), C2-C3 1.356(9), P1-Pd1-C1 94.5(2), C1-Pd1-C3 64.8(2), C3-Pd1-C30 116.3(2), C30-Pd1-P1 83.4(1), C1-C2-C3 122.6(6), P1-C12-C17 113.3(3), P1-C12-C13 127.3(3), Pd1-P1-C12-C17 -3.3(3).

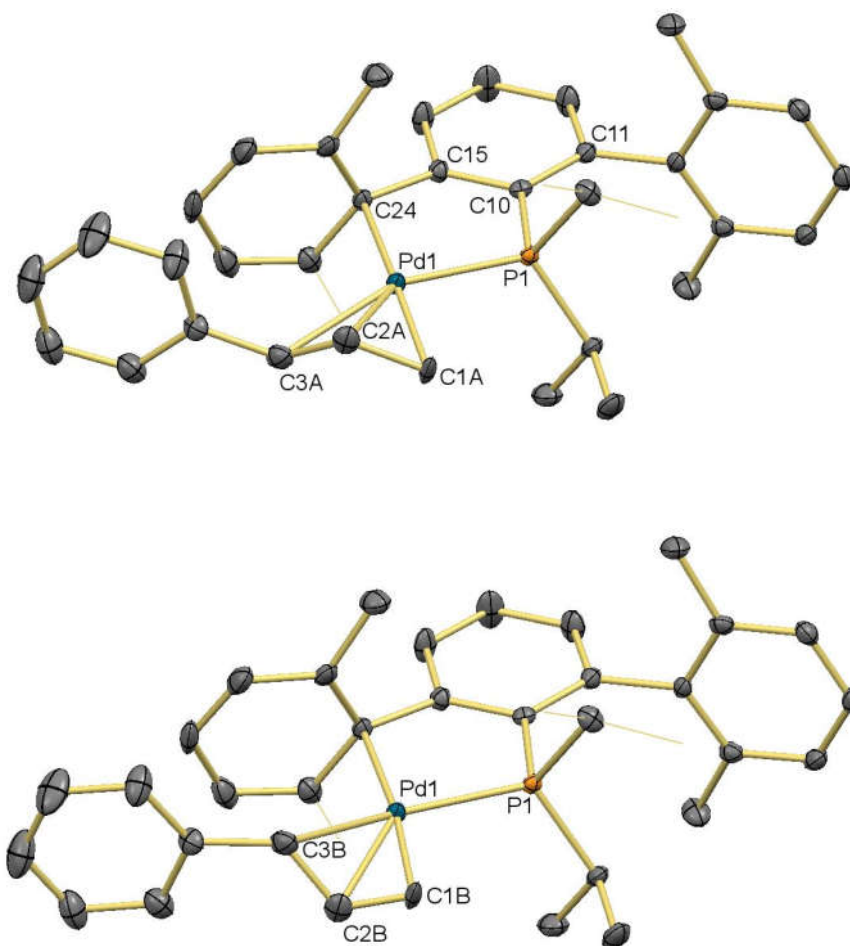
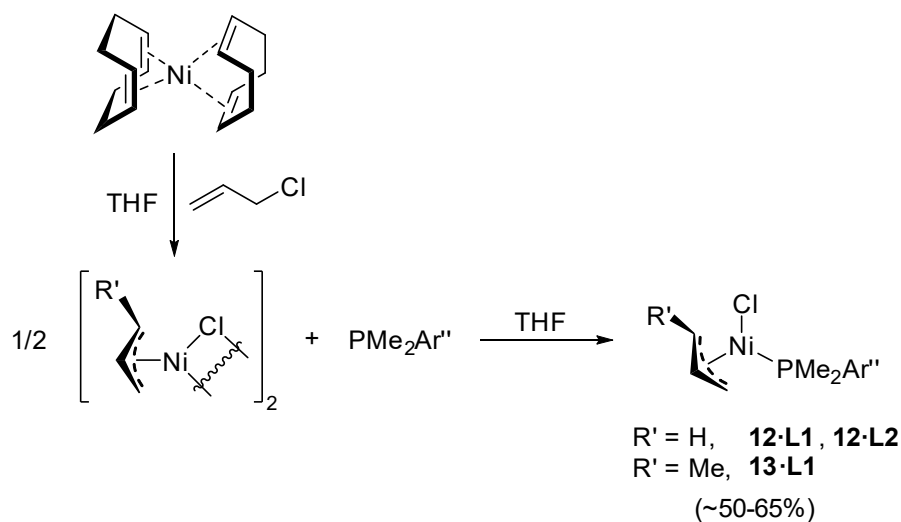


Figure 54. ORTEP views of the two conformers of the cation in complex **11-L4**. Hydrogen atoms are omitted for clarity, the atoms of an isopropyl and a methyl substituent are drawn in wireframe and thermal ellipsoids are set at 50% level probability. Selected bond distances (Å) and angles (°): Pd1-P1 2.2888(8), Pd1-C1A 2.109(7), Pd1-C2A 2.188(3), Pd1-C3A 2.452(3), Pd1-C24 2.273(2), C1A-C2A 1.448(7), C2A-C3A 1.366(5), P1-Pd1-C1A 94.6(2), C1A-Pd1-C3A 64.7(2), C3A-Pd1-C24 115.03(9), C24-Pd1-P1 84.92(6), C1A-C2A-C3A 121.7(4), P1-C10-C15 114.1(2), P1-C10-C11 127.3(2), Pd1-P1-C10-C15 0.5(2).

### II.2.2.3. Synthesis and characterisation of $\text{NiCl}(\eta^3\text{-C}_3\text{H}_4\text{R}')(\text{PMe}_2\text{Ar}'')$ ( $\text{R}' = \text{H, Me}$ ) complexes.

In contrast to palladium, we only succeeded in preparing neutral allylnickel(II) adducts with the dimethyl terphenyl phosphines  $\text{PMe}_2\text{Ar}^{\text{Xyl}_2}$  (**L1**) and  $\text{PMe}_2\text{Ar}^{\text{Dipp}_2}$  (**L2**). The synthesis of these Ni(II) complexes was accomplished by the addition of one equivalent of the phosphine (**L1** or **L2**) to a solution of allylnickel(II) chloride dimer, generated *in situ* via oxidative addition of allyl chloride to  $\text{Ni}(\text{cod})_2$  (Scheme 10). A similar reaction using crotyl chloride yielded the analogous complex **13·L1** with the smaller phosphine  $\text{PMe}_2\text{Ar}^{\text{Xyl}_2}$ , while the corresponding adduct of  $\text{PMe}_2\text{Ar}^{\text{Dipp}_2}$  could not be isolated in pure form. Finally, reactions with bulkier phosphines **L3** and **L4**, as well as with cinnamyl chloride, led to incomplete conversions and decomposition. The three isolated Ni(II)-allyl complexes were obtained as orange solids, partially soluble in pentane or benzene and quite soluble in  $\text{Et}_2\text{O}$ , THF and  $\text{CH}_2\text{Cl}_2$ . They are rather unstable, often decomposing if kept in solution for a while even under inert atmosphere and at low temperature.



Scheme 10. Synthesis of complexes  $\text{NiCl}(\eta^3\text{-C}_3\text{H}_4\text{R}')(\text{PR}_2\text{Ar}'')$ , for  $\text{R}' = \text{H}$  (**12·L1** and **12·L2**),  $\text{Me}$  (**13·L1**).

## Chapter II

These complexes were characterised by microanalysis, NMR spectroscopy and X-ray crystallography. Their NMR features do not substantially differ from those recorded for their palladium analogues. As an example, the  $^1\text{H}$  NMR spectrum of  $\text{NiCl}(\eta^3\text{-C}_3\text{H}_5)(\text{PMe}_2\text{Ar}^{\text{Xyl}_2})$  (**12·L1**) is presented in Figure 55. The most significant difference pertains the allyl moiety. Firstly, the signal due to the central allyl hydrogen  $\text{H}_1$  appears in the  $^1\text{H}$  NMR spectrum as a triplet of triplets, with the value of one coupling constant doubling the other. The resulting resonance resembles a pseudoseptet with a ratio of integrals of 1:2:3:4:3:2:1 (see Figure 56 for a simplified simulation of this phenomenon). Also, the *syn* allyl protons present a complex shape, with no discernable coupling constant values. As will be discussed later, this is probably due to a dynamic isomerisation process different from that discussed previously for the palladium analogues.

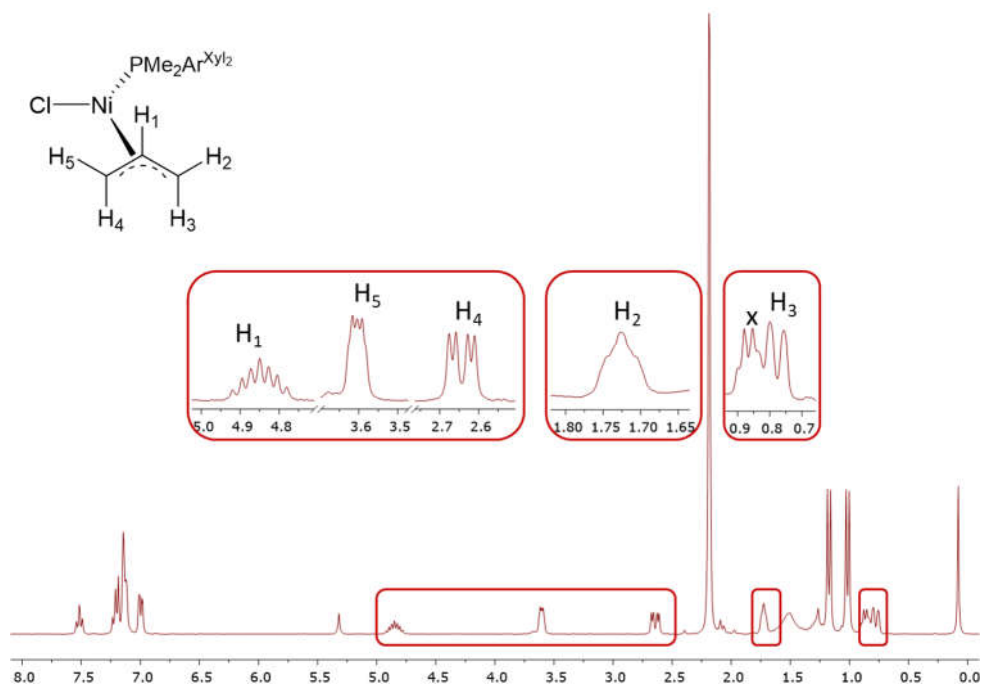


Figure 55.  $^1\text{H}$  NMR spectrum of **12·L1** in  $\text{CD}_2\text{Cl}_2$  at 25 °C.



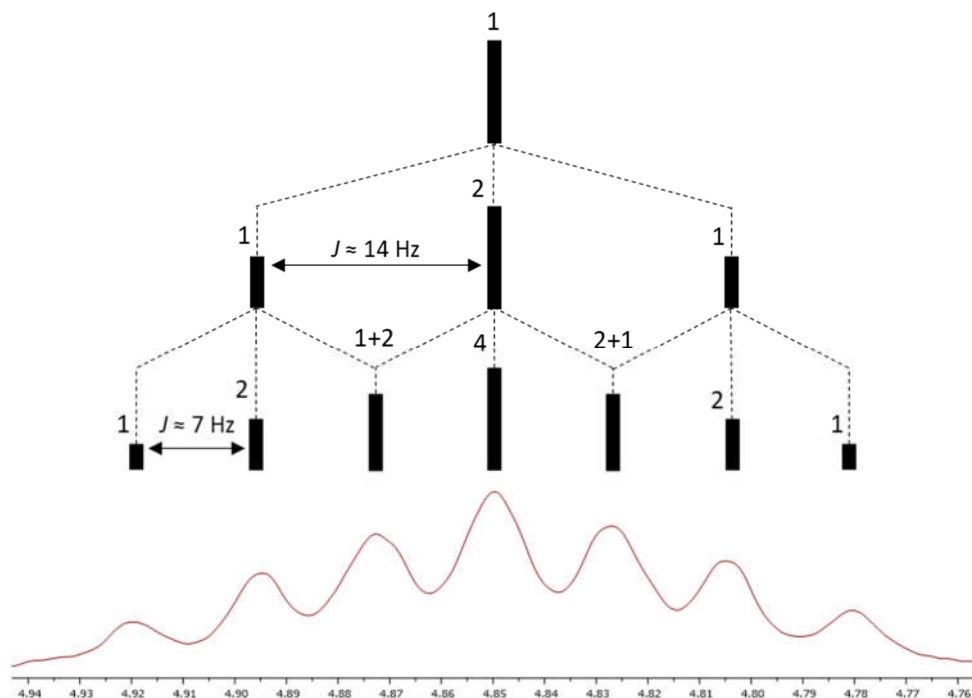


Figure 56. Schematic representation of the coupling pattern in proton  $H_1$  of complex **12-L1**.

At this point, it is worth commenting the spectroscopic features of complexes  $\text{NiBr}(\eta^3\text{-C}_3\text{H}_5)(\text{PR}_2\text{Ar}^{\text{Dtbp}_2})$  ( $\text{R} = \text{Me}, \text{Et}$ ), obtained, as described in Chapter I, by oxidative addition of allyl bromide to  $\text{Ni}(\text{CO})_3(\text{PR}_2\text{Ar}^{\text{Dtbp}_2})$ . As expected, their  $^1\text{H}$  and  $^{13}\text{C}\{^1\text{H}\}$  NMR spectra do not significantly differ from those corresponding to the latter. Also, in their  $^1\text{H}\{^{31}\text{P}\}$  NMR spectrum (see Figure 57 for the case of  $\text{NiBr}(\eta^3\text{-C}_3\text{H}_5)(\text{PMe}_2\text{Ar}^{\text{Dtbp}_2})$ ), the resonances due to the *syn* allyl protons ( $H_2$  and  $H_5$ ) resolve into simple, though somewhat broad, doublets, indicating that the dynamic process affects their coupling to the  $^{31}\text{P}$  nucleus.

Chapter II

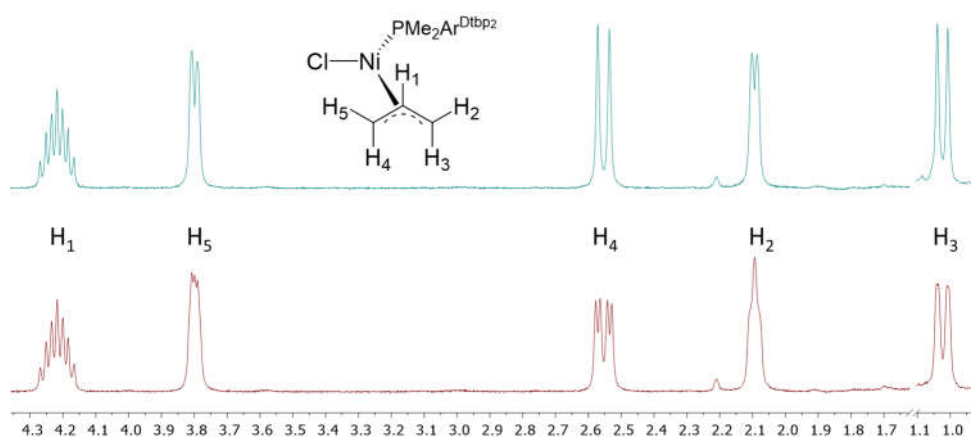


Figure 57.  $^1\text{H}$  (bottom) and  $^1\text{H}\{^{31}\text{P}\}$  (top) NMR spectra of complex  $\text{NiBr}(\eta^3\text{-C}_3\text{H}_5)(\text{PMe}_2\text{Ar}^{\text{Dtpb}_2})$  from Chapter I in  $\text{C}_6\text{D}_6$  at  $25^\circ\text{C}$ .

In order to understand this dynamic behaviour, the NOESY spectra of these two complexes were recorded (as shown in Figure 58 for that corresponding to  $\text{NiBr}(\eta^3\text{-C}_3\text{H}_5)(\text{PMe}_2\text{Ar}^{\text{Dtpb}_2})$ ). They both feature same-phase cross peaks

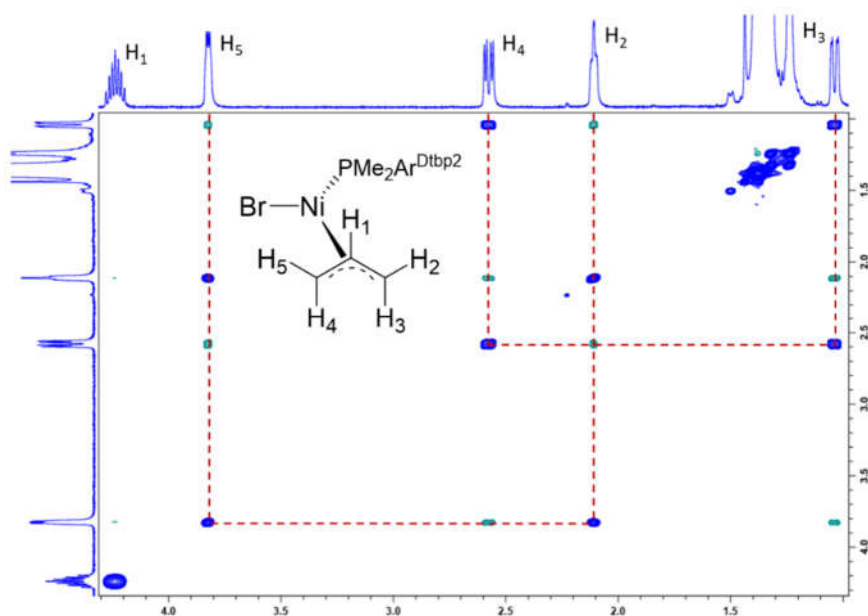


Figure 58. Allylic region in the NOESY spectrum of complex  $\text{NiBr}(\eta^3\text{-C}_3\text{H}_5)(\text{PMe}_2\text{Ar}^{\text{Dtpb}_2})$  in  $\text{C}_6\text{D}_6$  at  $25^\circ\text{C}$ .

connecting both allylic *syn* protons as well as the two *anti* protons, indicating a *syn-syn anti-anti* exchange. This type of fluxional process involves a rotation of the  $\eta^3$ -allyl moiety around the axis that links its mass centre with the nickel atom (Figure 59). This process is permitted in the allylnickel adducts due to the tetrahedral geometry of the intermediate, which is presumably characterised by a spin triplet state.<sup>74</sup>

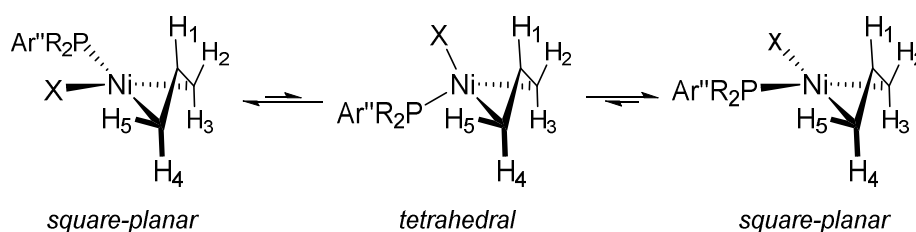


Figure 59. Proposed mechanism for the *syn-syn anti-anti* exchange in the  $\text{NiX}(\eta^3\text{-C}_3\text{H}_4\text{R}')(\text{PR}_2\text{Ar}'')$  complexes.

To finish the discussion about the NMR characteristics of the Ni(II)-allyl phosphine adducts, the  $^{31}\text{P}\{^1\text{H}\}$  NMR chemical shifts deserve some comments. Table 7 collects the  $^{31}\text{P}$  data, as well as  $\Delta\delta$  with respect to the free phosphines. As in the case of the neutral allylpalladium complexes discussed previously, the same trend is observed regarding the binding mode of the phosphine and  $\Delta\delta$  shift of the  $^{31}\text{P}$  resonance due to the phosphine ligand.

	Complex	$\delta(^{31}\text{P})$	$\Delta\delta$
<b>12-L1</b>	$\text{NiCl}(\eta^3\text{-C}_3\text{H}_5)(\text{PMe}_2\text{Ar}^{\text{Xyl}_2})$	-9.1	31.3
<b>12-L2</b>	$\text{NiCl}(\eta^3\text{-C}_3\text{H}_5)(\text{PMe}_2\text{Ar}^{\text{Dipp}_2})$	-7.8	33.5
<b>13-L1</b>	$\text{NiCl}(\eta^3\text{-C}_3\text{H}_4\text{Me})(\text{PMe}_2\text{Ar}^{\text{Xyl}_2})$	-7.1	33.3
	$\text{NiBr}(\eta^3\text{-C}_3\text{H}_5)(\text{PMe}_2\text{Ar}^{\text{Dtbp}_2})$	-2.5	34.1
	$\text{NiBr}(\eta^3\text{-C}_3\text{H}_5)(\text{PEt}_2\text{Ar}^{\text{Dtbp}_2})$	23.2	36.0

Table 7.  $^{31}\text{P}\{^1\text{H}\}$  NMR chemical shifts of the allylnickel complexes.

## Chapter II

All three complexes **12·L1**, **12·L2** and **13·L1** were also analysed by X-ray diffraction studies and their solid-state structures are depicted in Figures 60-62. They all feature a distorted square-planar geometry of the nickel centres, with the allyl ligands occupying two of the coordination positions and no interaction with the side aryl rings of the phosphines. Relevant structural data is gathered in Table 8. As expected, the Ni- $C_{trans-P}$  bonds are in all cases the longest of the Ni- $C_{allyl}$  distances, due to the stronger *trans* influence of the phosphines compared to the chloride ligand. The phosphine ligands adopt the expected conformation **B** in the three complexes.

Selected distances and angles	12·L1	12·L2	13·L1
Ni-P	2.1989	2.1869	2.1882
Ni- $C_{trans-P}$	2.053	2.080	2.098
Ni- $C_{meso}$	1.984	1.992	1.996
Ni- $C_{cis-P}$	1.997	1.947	1.975
$C_{trans-P}-C_{meso}$	1.377	1.370	1.381
$C_{meso}-C_{cis-P}$	1.409	1.407	1.381
$C_{trans-P}-C_{meso}-C_{cis-P}$	120.2	119.0	123.2

Table 8. Selected distances (Å) and angles (°) in the neutral allylnickel complexes.

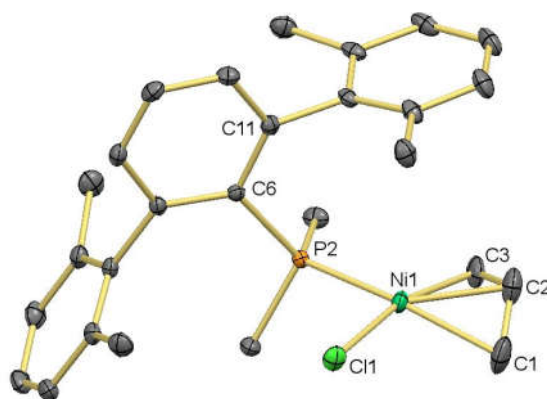


Figure 60. ORTEP views of complex **12·L1**. Hydrogen atoms are omitted for clarity and thermal ellipsoids are set at 50% level probability. Selected bond distances (Å) and angles (°): Ni1-P2 2.1989(5), Ni1-Cl1 2.2034(5), Ni1-C1 2.053(2), Ni1-C2 1.984(2), Ni1-C3 1.997(2), C1-C2 1.377(4), C2-C3 1.409(3), P2-Ni1-Cl1 96.17(2), Cl1-Ni1-C1 94.41(8), C1-Ni1-C3 73.2(1), C3-Ni1-P2 94.62(7), C1-C2-C3 120.2(2), Ni1-P2-C6-C11 57.8(1).

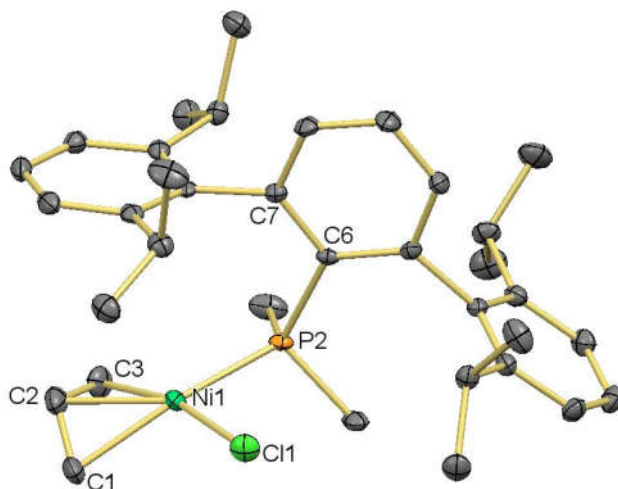


Figure 61. ORTEP view of the major conformer of complex **12-L2**. Hydrogen atoms are omitted for clarity and thermal ellipsoids are set at 50% level probability. Selected bond distances (Å) and angles (°): Ni1-P2 2.1869(5), Ni1-Cl1 2.1818(5), Ni1-C1 2.080(4), Ni1-C2 1.992(2), Ni1-C3 1.947(5), C1-C2 1.370(6), C2-C3 1.407(6), P2-Ni1-Cl1 92.99(2), Cl1-Ni1-C1 94.7(1), C1-Ni1-C3 72.8(2), C3-Ni1-P2 98.1(1), C1-C2-C3 119.0(3), Ni1-P2-C6-C7 -51.8(1).

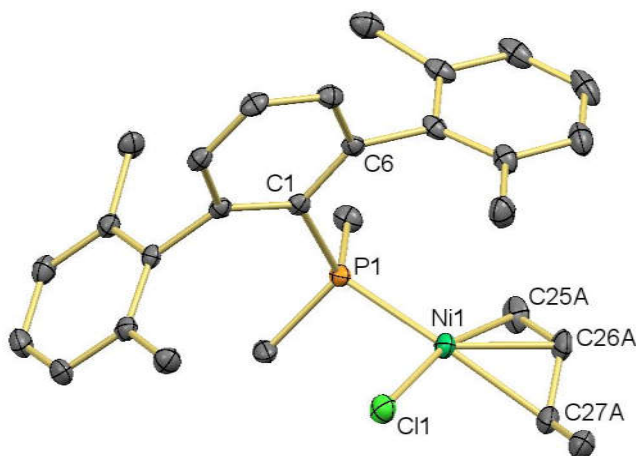


Figure 62. ORTEP view of the major conformer of complex **13-L1**. Hydrogen atoms are omitted for clarity and thermal ellipsoids are set at 50% level probability. Selected bond distances (Å) and angles (°): Ni1-P1 2.1882(6), Ni1-Cl1 2.2077(7), Ni1-C25A 1.975(4), Ni1-C26A 1.996(3), Ni1-C27A 2.098(3), C25A-C26A 1.381(5), C26A-C27A 1.381(4), P1-Ni1-C25A 95.8(1), C25A-Ni1-C27A 73.2(2), C27A-Ni1-Cl1 93.47(8), C25A-C26A-C27A 123.2(3), Ni1-P1-C1-C6 57.0(2).

**II.2.2.4. Synthesis and characterisation of  $[\text{Ni}(\eta^3\text{-C}_3\text{H}_5)(\text{PR}_2\text{Ar}'')] \text{BAr}^{\text{F}}_4$  complexes.**

In line with the allylpalladium(II) complexes, the chloride ligand in these Ni(II)-allyl compounds could be abstracted by treatment with  $\text{NaBAr}^{\text{F}}_4$ . However, performing the reactions of **12·L1** and **12·L2** with  $\text{NaBAr}^{\text{F}}_4$  in THF led to colourless compounds, which exhibit  $^{31}\text{P}$  resonances at 19.8 and 22.1 ppm, respectively, shifted by 29-30 ppm at higher frequency relative to the parent complexes. Moreover, the  $^1\text{H}$  and  $^{13}\text{C}\{^1\text{H}\}$  NMR spectra of these new species present resonances characteristic of the phosphine ligands but lack the signals due to the allyl moiety. Instead, new resonances are observed indicating the presence of an olefinic residue in these molecules; see for example Figure 63 for the  $^1\text{H}$  NMR spectrum of the product bearing  $\text{PMe}_2\text{Ar}^{\text{Xyl}2}$ , **14·L1**.

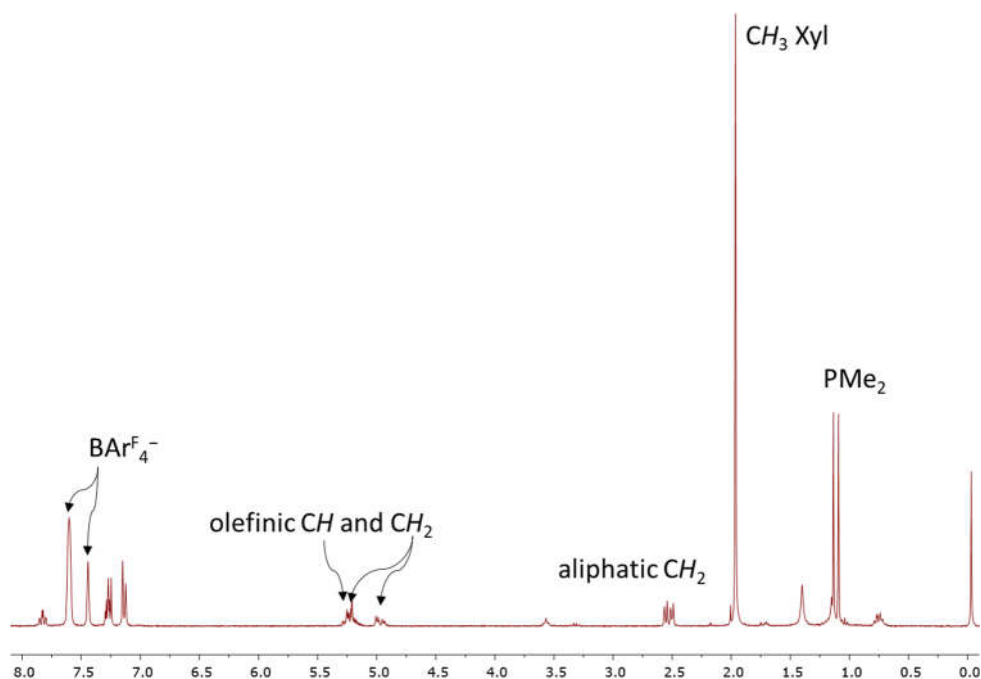
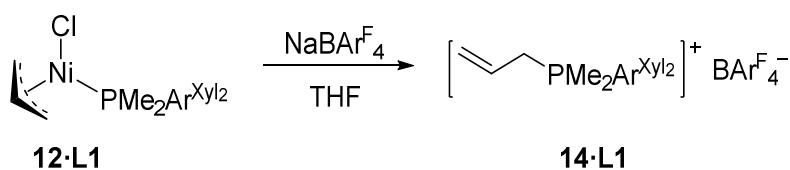


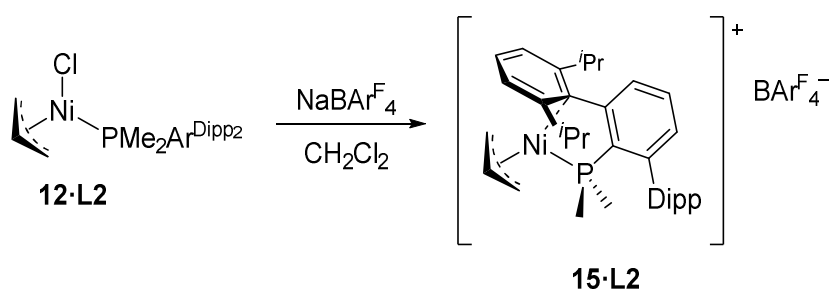
Figure 63.  $^1\text{H}$  NMR spectrum of **14·L1** in  $\text{CD}_2\text{Cl}_2$  at 25 °C.

Mass spectrometry revealed the presence of a non-nickel-containing cation, which agreed with the formulation  $[(\text{CH}_2=\text{CHCH}_2)\text{PMe}_2\text{Ar}^{\text{Xyl}_2}]^+$ , accompanied by a  $\text{BAR}^{\text{F}_4^-}$  anion. Presumably, after chloride abstraction, the resulting cationic allylnickel adducts would reductively eliminate the phosphonium cation, producing finely divided metallic nickel (Scheme 11).



Scheme 11. Formation of the phosphonium salt  $[(\text{CH}_2=\text{CHCH}_2)\text{PMe}_2\text{Ar}^{\text{Xyl}_2}]\text{BAR}^{\text{F}_4}$  (**14·L1**).

Nevertheless, it was found that conducting the reaction in  $\text{CH}_2\text{Cl}_2$ , in the case of complex  $\text{NiCl}(\eta^3\text{-C}_3\text{H}_5)(\text{PMe}_2\text{Ar}^{\text{Dipp}_2})$  (**12·L2**), afforded the desired cationic Ni(II) complex, **15·L2**, in good yield (Scheme 12). The corresponding cationic adduct of **L1** could not be isolated pure, as it often decomposed, even at low temperature.



Scheme 12. Synthesis of complex  $[\text{Ni}(\eta^3\text{-C}_3\text{H}_5)(\text{PMe}_2\text{Ar}^{\text{Dipp}_2})]\text{BAR}^{\text{F}_4}$  (**15·L2**).

The room temperature  $^1\text{H}$  and  $^{13}\text{C}\{^1\text{H}\}$  NMR spectra of **15·L2** show the expected asymmetric environment around the terphenyl moiety, brought about

## Chapter II

by the impeded rotation around the P–C<sub>ipso</sub> bond. Interestingly, the <sup>1</sup>H NMR signals due to allyl protons H<sub>2</sub> and H<sub>3</sub> are only observed upon lowering the temperature to –30 °C (Figure 64). In the room temperature NOESY spectrum, a broad, weak same-phase cross peak can be perceived connecting the signals for H<sub>4</sub> and H<sub>5</sub> with the region of the spectrum where the coalesced resonance for the other two protons is expected to appear. This observations seem to indicate that both *syn-anti* and *syn-syn anti-anti* exchanges are occurring at room temperature. However, this phenomenon was not investigated further.

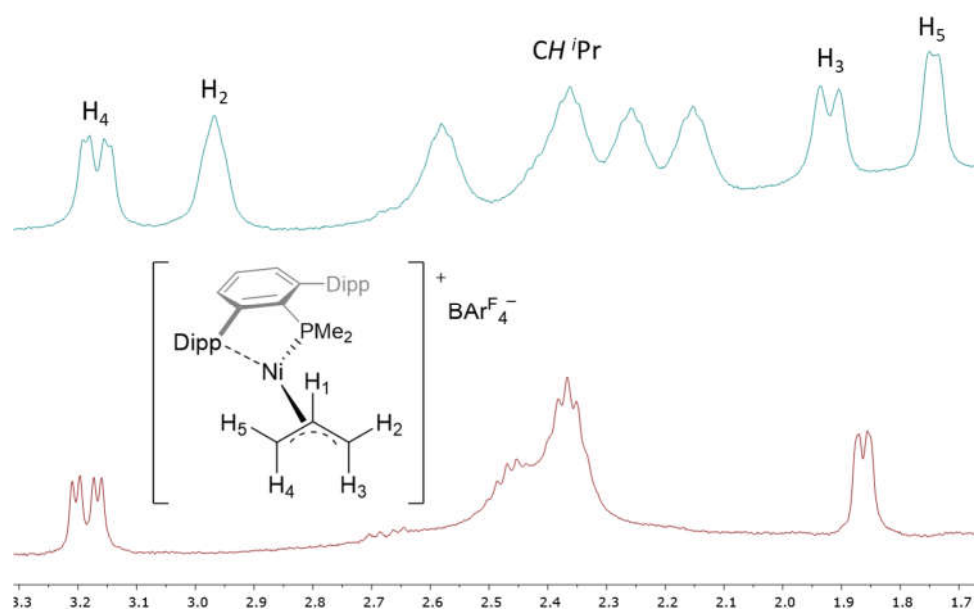


Figure 64. Selected region of the <sup>1</sup>H NMR spectra of complex **15·L2** in CD<sub>2</sub>Cl<sub>2</sub> at 25 °C (bottom) and –30 °C (top).

The structure of **15·L2** was confirmed by X-ray diffraction studies (Figure 65), revealing the expected similarity with the palladium analogue **10·L2**. The major variations arise from the difference in covalent radii, of 0.15 Å,<sup>66</sup> between nickel and palladium, thus affecting the bond distances and angles in which the metal atom is involved. In addition, the angle at which the interacting arene is



bent away from the metal centre is slightly ampler, at 22.4° (vs. 20.4° for **10·L2**). Once again, this complex exists in the crystal structure as a mixture of two conformers in a 74:26 ratio.

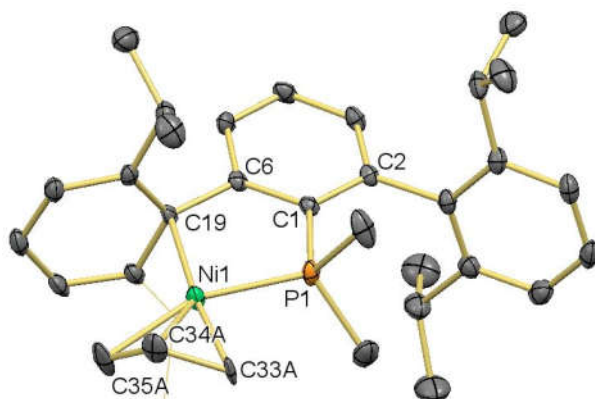
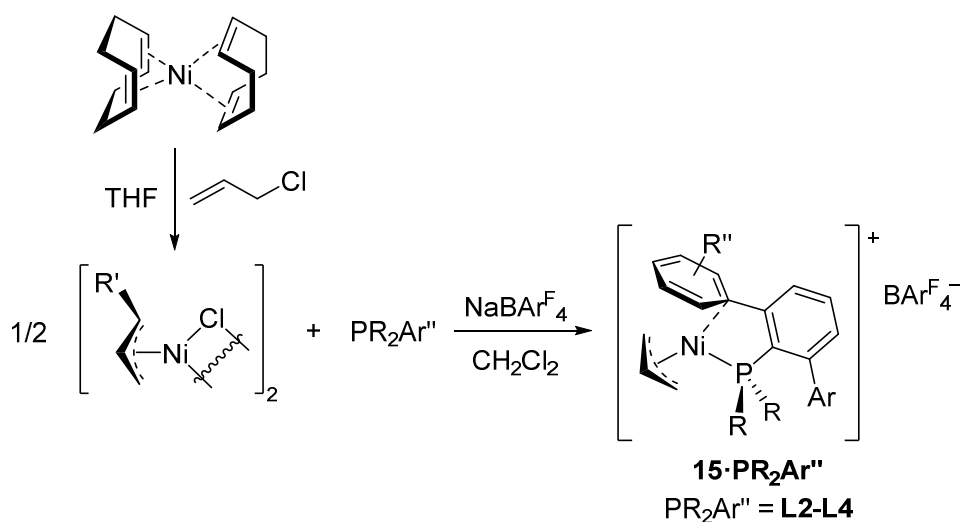


Figure 65. ORTEP view of the major conformer of cation in complex **15·L2**. Hydrogen atoms are omitted for clarity, the atoms of an isopropyl substituent are drawn in wireframe and thermal ellipsoids are set at 50% level probability. Selected bond distances (Å) and angles (°): Ni1-P1 2.1876(8), Ni1-C33A 2.006(8), Ni1-C34A 2.012(5), Ni1-C35A 2.113(5), Ni1-C19 2.146(3), P1-Ni1-C33A 88.1(2), C33A-Ni1-C35A 72.0(2), C33A-C34A 1.460(8), C34A-C35A 1.358(7), C35A-Ni1-C19 113.9(2), C19-Ni1-P1 86.23(7), P1-C1-C6 111.8(2), P1-C1-C2 128.5(2), P1-C1-C6-C19 -9.8(3).

As noted when discussing allylpalladium(II) systems, it was possible to isolate cationic Pd(II) derivatives with the bulkier terphenyl phosphine **L4**. Thus, a direct route towards cationic allylnickel(II) complexes with the sterically hindered phosphines **L3** and **L4**, starting from Ni(cod)<sub>2</sub>, was devised (Scheme 13). This procedure allowed for the preparation of complexes [Ni(η<sup>3</sup>-C<sub>3</sub>H<sub>5</sub>)(PCyp<sub>2</sub>Ar<sup>Xyl<sub>2</sub></sup>)]BAR<sub>4</sub><sup>F</sup> (**15·L3**) and [Ni(η<sup>3</sup>-C<sub>3</sub>H<sub>5</sub>)(P<sup>i</sup>Pr<sub>2</sub>Ar<sup>Xyl<sub>2</sub></sup>)]BAR<sub>4</sub><sup>F</sup> **15·L4**. However, they could not be isolated in pure form, since they were always accompanied by small amounts of another product, apparently the neutral analogues, which could not be separated even by crystallisation. Furthermore, substituted allyls (crotyl or cinnamyl groups) could not be incorporated into these complexes, as the resulting

## Chapter II

products partially decomposed and thus pure samples could not be obtained. It must be noted that all three  $[\text{Ni}(\eta^3\text{-C}_3\text{H}_5)(\text{PR}_2\text{Ar}'')] \text{BAr}^{\text{F}_4}$  complexes can be stored in the solid state, and even handled in solution for a short a period of time, in air.



*Scheme 13. Synthesis of complexes  $[\text{Ni}(\eta^3\text{-C}_3\text{H}_5)(\text{PR}_2\text{Ar}'')] \text{BAr}^{\text{F}_4}$  (**15·PR<sub>2</sub>Ar''**).*

In sharp contrast to the palladium analogues, complexes **15·L3** and **15·L4** display a fluxional behaviour in solution. Thus, in the room temperature  $^1\text{H}$  NMR spectra of both complexes, the terphenyl moiety appears symmetric and all allyl hydrogen resonances, except that for  $\text{H}_1$ , are undetected (see Figure 66 for the case of **15·L4**). This fluxional process slowed down at  $-40^\circ\text{C}$  giving rise to  $^1\text{H}$  NMR spectra consistent with the absence of symmetry in these molecules.

Single crystals of complex  $[\text{Ni}(\eta^3\text{-C}_3\text{H}_5)(\text{P}^i\text{Pr}_2\text{Ar}^{\text{Xyl}_2})] \text{BAr}^{\text{F}_4}$  (**15·L4**) were grown from a hexane/ $\text{CH}_2\text{Cl}_2$  mixture and analysed by X-ray crystallography, thus confirming the structure of this complex (Figure 67). No significant differences can be observed in comparison with  $[\text{Ni}(\eta^3\text{-C}_3\text{H}_5)(\text{PMe}_2\text{Ar}^{\text{Dipp}_2})] \text{BAr}^{\text{F}_4}$  (**15·L2**). It is possible that the chelating effect of the phosphine in a P,C-bidentate mode of coordination confers a higher stability to these complexes relative to the neutral adducts discussed above.

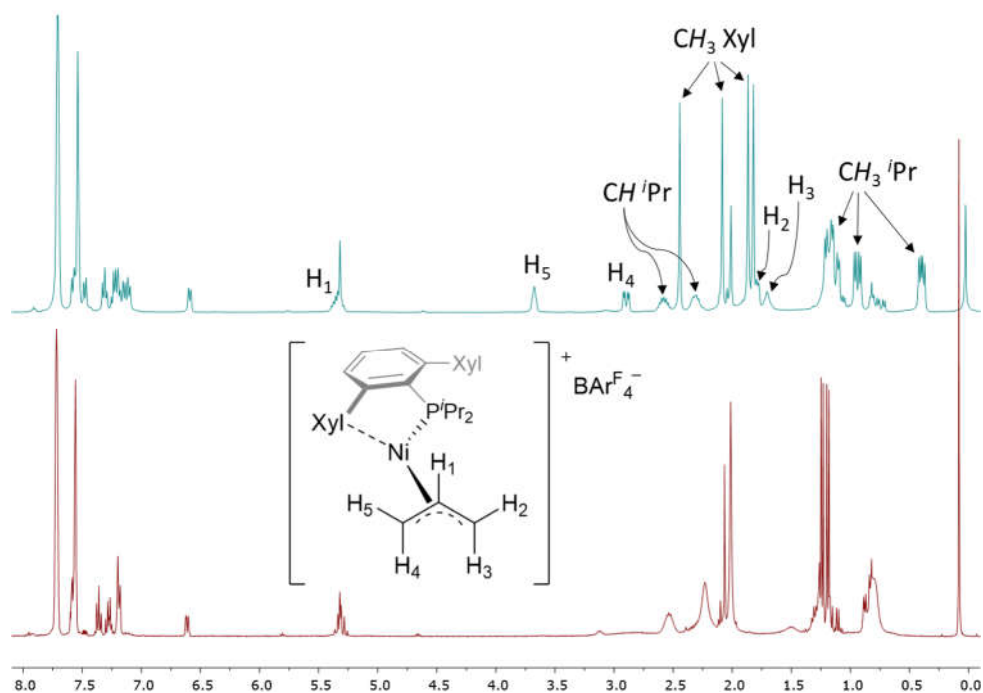


Figure 66.  $^1\text{H}$  NMR spectra of complex **15·L4** in  $\text{CD}_2\text{Cl}_2$  at 25 °C (bottom) and -40 °C (top).

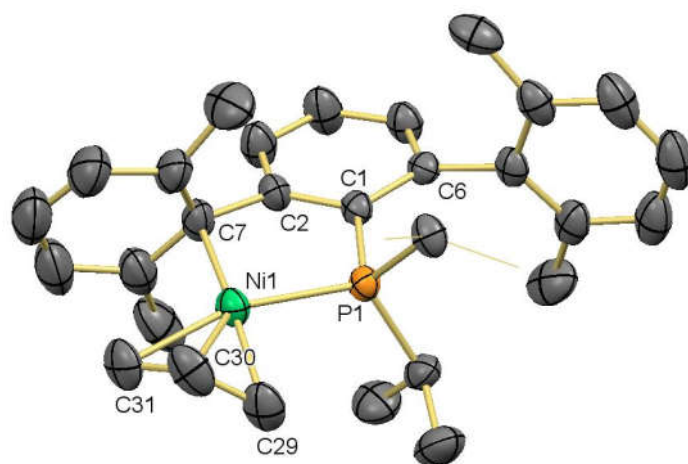


Figure 67. ORTEP view of the cation in complex **15·L4**. Hydrogen atoms are omitted for clarity, some atoms of an isopropyl substituent are drawn in wireframe and thermal ellipsoids are set at 50% level probability. Selected bond distances (Å) and angles (°): Ni1-P1 2.2065(9), Ni1-C29 2.012(4), Ni1-C30 2.000(5), Ni1-C31 2.109(4), Ni1-C7 2.159(4), C29-C30 1.375(6), C30-C31 1.373(7), P1-Ni1-C29 92.2(1), C29-Ni1-C31 70.3(2), C31-Ni1-C7 108.9(1), C7-Ni1-P1 87.43(9), C29-C30-C31 119.4(4), P1-C1-C2 113.6(2), P1-C1-C6 127.6(2), Ni1-P1-C1-C2 -5.9(2).

### **II.2.3. Zerovalent low-coordinate complexes of nickel, palladium and platinum stabilised by dialkyl terphenyl phosphines.**

As outlined in the Introduction to this chapter, unsaturated zerovalent complexes of nickel, palladium and platinum play a major role in many catalytic and stoichiometric transformations mediated by these metals. While dicoordinate Pd(0) and Pt(0) complexes stabilised by bulky phosphines or N-heterocyclic carbene (NHC) ligands are well known,<sup>54,59–61</sup> examples of nickel analogues are scarce, they have mostly been detected as intermediates<sup>75</sup> or have been prepared but poorly characterised.<sup>76</sup> As mentioned in the Introduction, only one example of a Ni<sup>0</sup>(PR<sub>3</sub>)<sub>2</sub> species, containing a bidentate phosphine ligand, has been characterised.<sup>62</sup>

In this section, we discuss the preparation of mixed-ligand and homoleptic low-coordinate complexes of nickel, palladium and platinum in zero oxidation state bearing dialkyl terphenyl phosphine ligands.

#### **II.2.3.1. Synthesis and characterisation of palladium(0) complexes.**

Our group has previously reported the reduction of PtCl<sub>2</sub>(PMe<sub>2</sub>Ar'') complexes in the presence of an olefin to generate low-coordinate Pt(0)-phosphine complexes, which acted as competent catalysts in the hydrosilylation of alkynes.<sup>63</sup>

Paralleling this work, the dinuclear palladium(II) complexes described in Section II.2.1.2 were reacted with Zn powder in THF in the presence of several olefins, namely ethylene, 3,3-dimethyl-1-butene, styrene, 1,5-cyclooctadiene and diethyl maleate. However, these attempts led to either decomposition or to complex mixtures of products. Conversely, when the reduction was carried out in the presence of the diolefin 1,3-divinyltetramethyldisiloxane (dvds), the desired palladium(0) complexes, **16·L1** and **16·L2**, were obtained (Scheme 14). These two



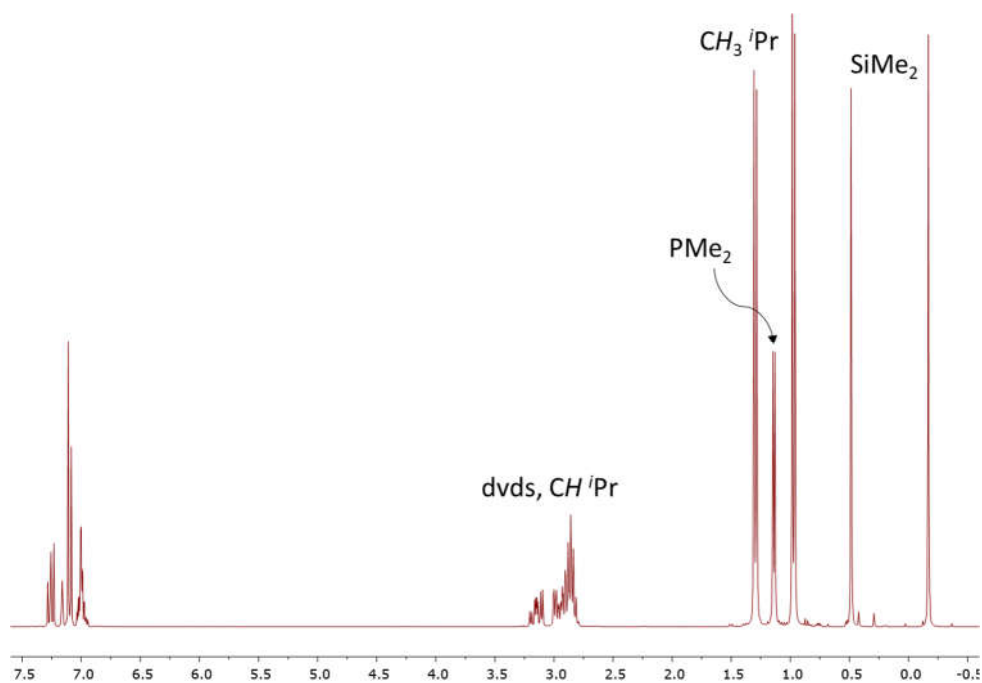


Figure 68.  $^1\text{H}$  NMR spectrum of complex **16·L2** in  $\text{C}_6\text{D}_6$  at 25 °C.

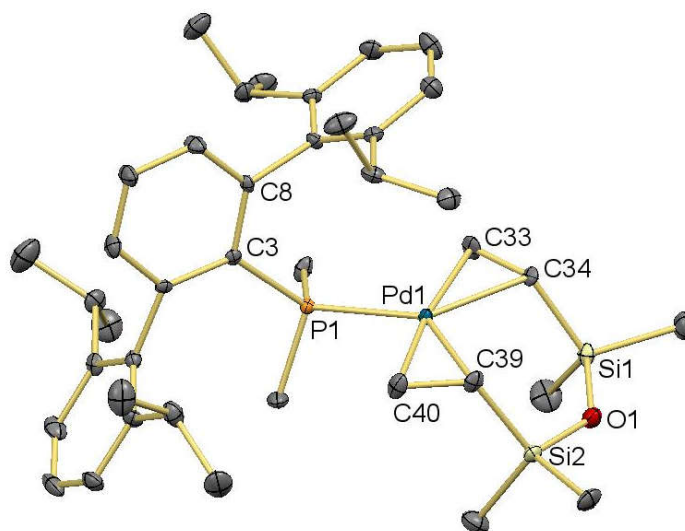
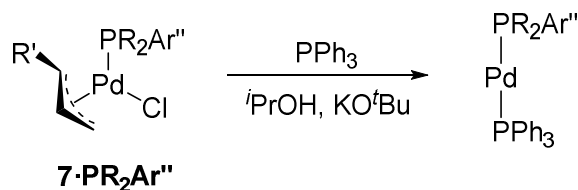


Figure 69. ORTEP view of complex **16·L2**. Hydrogen atoms are omitted for clarity and thermal ellipsoids are set at 50% level probability. Selected bond distances (Å) and angles (°): Pd1-P1 2.324(1), Pd1-C33 2.163(6), Pd1-C34 2.198(6), Pd1-C39 2.187(4), Pd1-C40 2.169(6), Pd1-P1-C3-C8 53.1(4).

Next, we turned our attention to the preparation of  $\text{Pd}^0(\text{PR}_3)_2$  complexes bearing dialkyl terphenyl phosphine ligands. Nolan and co-workers have devised a synthetic approach towards mixed  $\text{Pd}^0(\text{NHC})(\text{PR}_3)$  species consisting in the reaction of allylpalladium(II)-NHC complexes with the phosphine in the presence of a strong base,  $\text{KO}^t\text{Bu}$ , in  $i\text{PrOH}$  as the reaction medium.<sup>60h</sup> Following Nolan's method, the  $\text{PdCl}(\eta^3\text{-C}_3\text{H}_5)(\text{PR}_2\text{Ar}'')$  complexes, **7-PR<sub>2</sub>Ar''** for  $\text{PR}_2\text{Ar}'' = \text{PMe}_2\text{Ar}^{\text{Xyl}_2}$  (**L1**),  $\text{PMe}_2\text{Ar}^{\text{Dipp}_2}$  (**L2**) and  $\text{PCyp}_2\text{Ar}^{\text{Xyl}_2}$  (**L3**), described in Section II.2.2.1, were reacted with  $\text{PPh}_3$  under the same conditions (Scheme 15). Although the reaction involving **7-L1** was unsuccessful, in the cases of **7-L2** and **7-L3**, the resulting heteroleptic palladium(0) bisphosphine complexes  $\text{Pd}(\text{PPh}_3)(\text{PR}_2\text{Ar}'')$  could be detected by  $^{31}\text{P}\{^1\text{H}\}$  NMR as two mutually coupled doublets ( $^2J_{\text{PP}} \approx 190\text{-}200$  Hz). However, spontaneous decomposition in solution prevented the successful isolation of these compounds.

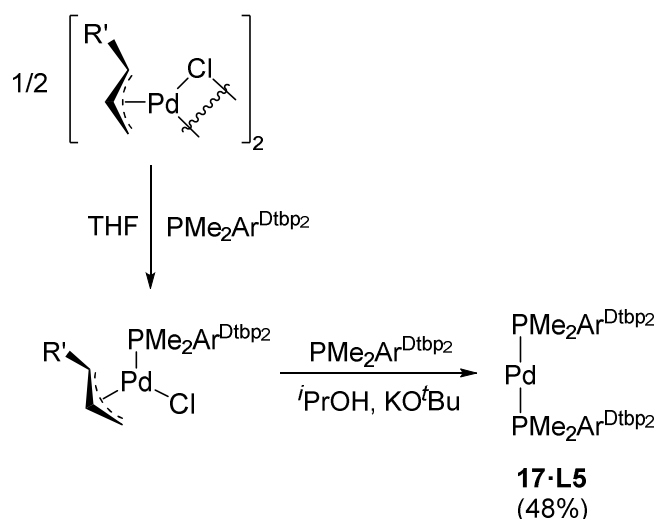


Scheme 15. Reduction of complexes **7-PR<sub>2</sub>Ar''** to form heteroleptic  $\text{Pd}(\text{PPh}_3)(\text{PR}_2\text{Ar}'')$ .

In light of these results, we focused our efforts on the synthesis of homoleptic  $\text{Pd}(\text{PR}_2\text{Ar}'')_2$  complexes. Thus, when the  $\eta^3$ -allyl complex **7-L2** was reacted with an additional equivalent of the phosphine **L2** under the conditions shown in Scheme 15, the resulting complex quickly decomposed in solution. Similar results were obtained when **7-L3** was used instead. We hypothesised that the phosphine  $\text{PMe}_2\text{Ar}^{\text{Dtbp}_2}$  (**L5**), which unlike the previous ones, bears *tert*-butyl groups on the farther *meta* positions of the side aryl rings, thus providing remote rather than proximal steric effects, would be a better candidate for attaining the

## Chapter II

target compound. Thus, the synthesis was carried out in two steps, involving the *in situ* generation of complex  $\text{PdCl}(\eta^3\text{-C}_3\text{H}_5)(\text{PMe}_2\text{Ar}^{\text{Dtbp}_2})$  by addition of **L5** to the palladium precursor  $[\text{Pd}(\mu\text{-Cl})(\eta^3\text{-C}_3\text{H}_5)]_2$ , followed by its reduction under the conditions cited above in the presence of an additional equivalent of the phosphine. In these conditions,  $\text{Pd}(\text{PMe}_2\text{Ar}^{\text{Dtbp}_2})_2$  (**19-L5**) was generated in moderate yield as a yellowish white solid (Scheme 16). Surprisingly, this complex exhibited a notably greater stability compared to its abovementioned non-isolated  $\text{Pd}(\text{PR}_2\text{Ar}'')_2$  analogues, hence allowing full characterisation.



Scheme 16. Two-step synthesis of complex  $\text{Pd}(\text{PMe}_2\text{Ar}^{\text{Dtbp}_2})_2$  (**17-L5**).

The most noteworthy signal observed in the  $^1\text{H}$  NMR spectrum of **17-L5** at room temperature (Figure 70-A) is a broadened virtual triplet at 0.94 ppm for the  $\text{PMe}_2$  groups. Interestingly, the hydrogens in *ortho* position of the Dtbp rings appear as a very broad signal centred at an unusual chemical shift of 8.16 ppm. Upon heating the NMR sample to 60 °C, this resonance resolved into the expected, although somewhat broadened, doublet due to a small coupling with the proton in *para* position with a value of  $^4J_{\text{HH}} \approx 1$  Hz (Figure 70-B). Contrary to the  $^1\text{H}$  NMR



spectrum, the room-temperature  $^{13}\text{C}\{^1\text{H}\}$  NMR spectrum of **17·L5** (Figure 71) exhibits a well-defined virtual triplet for the P-bound methyl groups (apparent  $^1J_{\text{CP}} = 19$  Hz), as well as two other virtual triplets for the resonances due to the quaternary carbons in *ortho* position ( $^2J_{\text{CP}} = 4$  Hz) and to the *ipso* carbon atom ( $^1J_{\text{CP}} = 7$  Hz). Lastly, complex **17·L5** features a singlet at  $-12.8$  ppm in the  $^{31}\text{P}\{^1\text{H}\}$  NMR spectrum, only  $23.8$  ppm at higher frequency compared to the free phosphine.

Definitive structural characterisation was attained by single crystal X-ray diffraction studies. The molecular structure of **17·L5** is outlined in Figure 72. As expected, the palladium centre displays an almost linear geometry (P-Pd-P angle of  $171.49(4)^\circ$ ) with both phosphine ligands coordinated in a  $\kappa^1\text{-P}$  mode of coordination. The phosphines adopt a pseudo-staggered conformation, with a  $\text{C}_{\text{ipso}}\text{-P-P-C}_{\text{ipso}}$  dihedral angle of  $92.3(1)^\circ$ , and retain a configuration of type **A**. The most striking feature of this molecular structure is the disposition of the  $^t\text{Bu}$  groups. The quaternary carbons of four of these groups share a plane with the Pd atom, closely surrounding the latter in a radius of *ca.*  $4.9$  Å (Figure 73). Moreover, two of the  $^t\text{Bu}$  substituents are located so that the closest distance between methyl groups is  $3.951(7)$  Å, marginally lower than twice the van der Waals radius of a  $\text{CH}_3$  moiety ( $2.0$  Å).<sup>47</sup> Presumably, these characteristics are behind the relatively high stability of this complex compared to the non-isolated  $\text{Pd}(\text{PR}_2\text{Ar}'')_2$  analogues. In contrast, in similar complexes found in the literature bearing dicyclohexyl biaryl phosphines, one of the ligands adopts a **C** conformation, with the side aryl ring in close proximity to the metal atom and the bulky cyclohexyl groups contributing to the steric congestion around the palladium centre.<sup>24a,59a</sup>

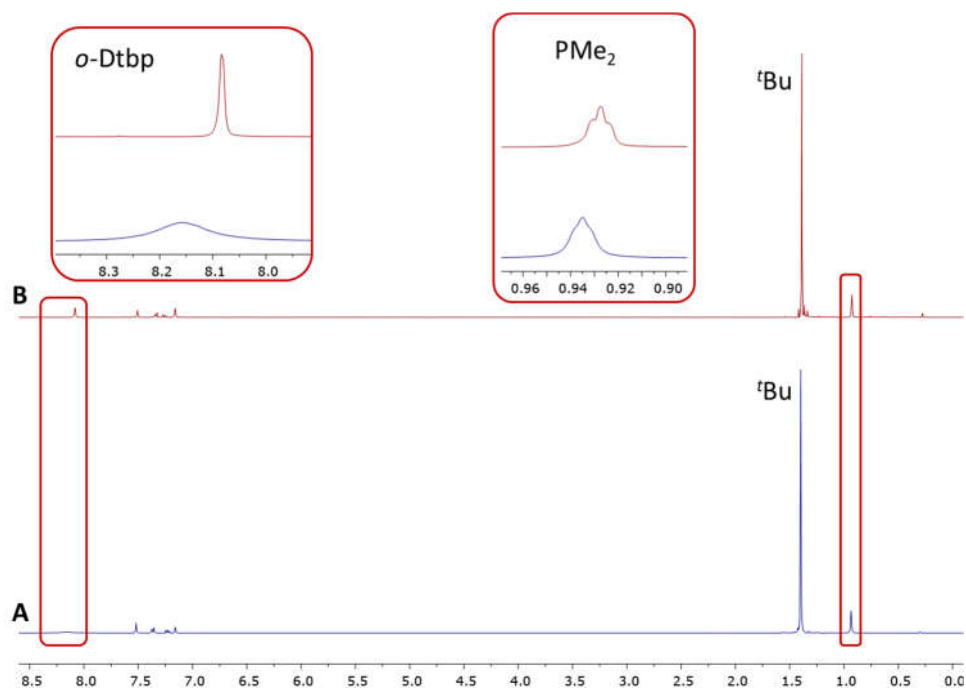


Figure 70.  $^1\text{H}$  NMR spectrum of complex **17-L5** in  $\text{C}_6\text{D}_6$  at 25 °C (A) and 60 °C (B).

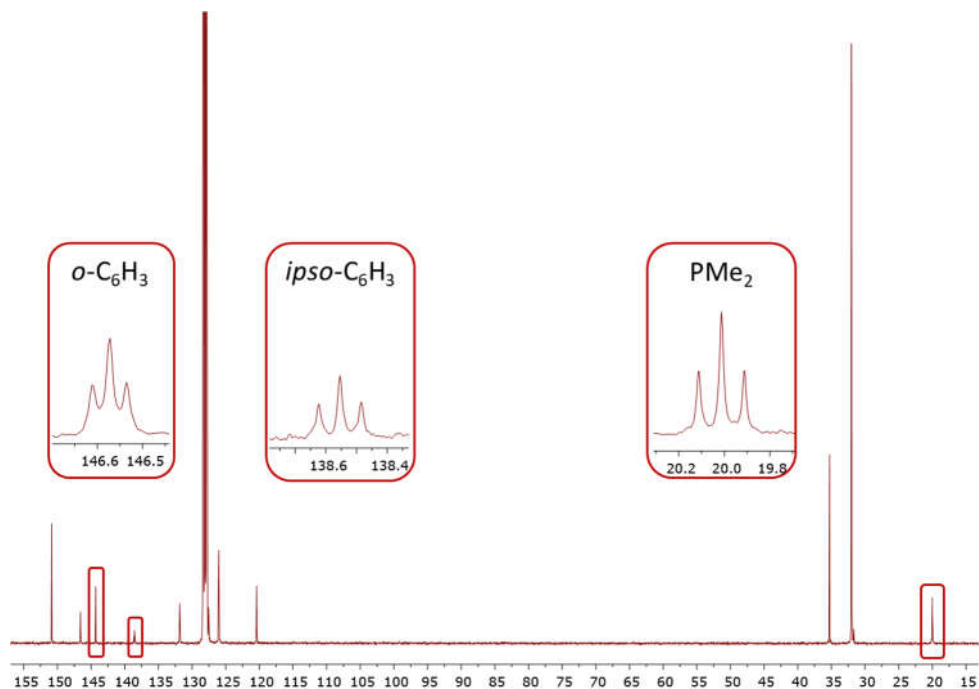


Figure 71.  $^{13}\text{C}\{^1\text{H}\}$  NMR spectrum of **17-L5** in  $\text{C}_6\text{D}_6$  at 25 °C.

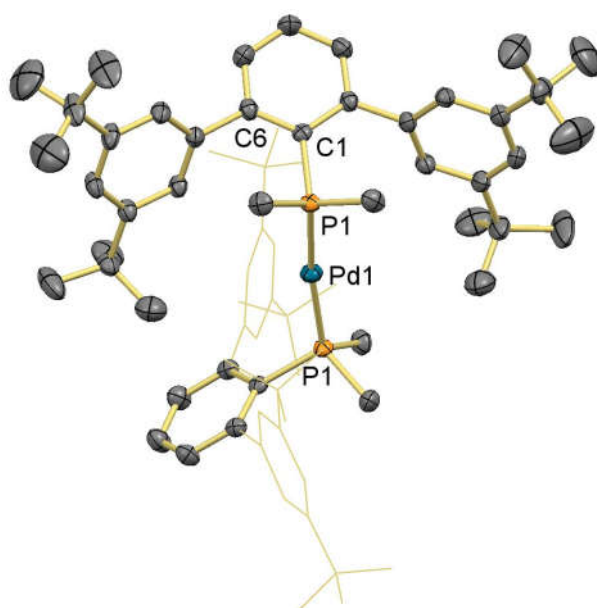


Figure 72. ORTEP view of complex **17·L5**. Hydrogen atoms are omitted for clarity, the side Dtbp rings of one of the terphenyl moieties are drawn in wireframe and thermal ellipsoids are set at 50% level probability. Selected bond distances (Å) and angles (°): Pd1-P1 2.2701(7), P1-Pd1-P1 171.49(4), Pd1-P1-C1-C6 89.5(2).

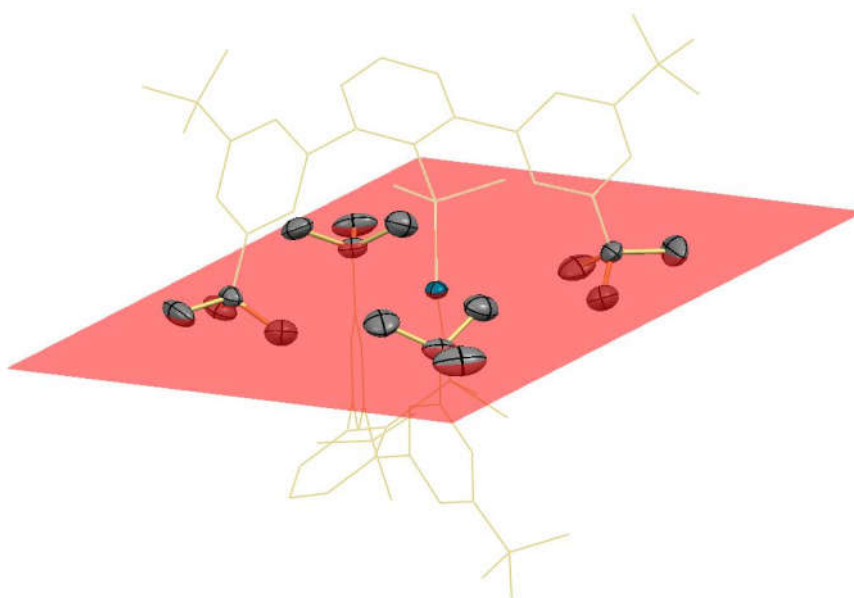
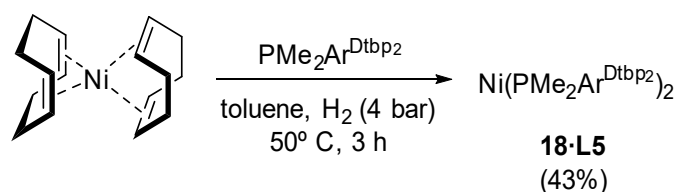


Figure 73. ORTEP view of complex **17·L5**, emphasizing the disposition of the <sup>t</sup>Bu groups around the palladium atom.

It is interesting to point out that only two examples of  $\text{Pd}^0(\text{PR}_2\text{Ar}')_2$  derivatives of dialkyl biaryl phosphines have been described to date. These two compounds have been isolated using the less sterically hindered 2-(dicyclohexylphosphino)biphenyl (dcpBiph or CyJohnPhos)<sup>59a</sup> and 2-(2',6'-dimethoxybiphenyl)dicyclohexylphosphine (SPhos) biaryl phosphines.<sup>24a</sup> More recently, an analogous complex containing the related naphthylaryl-substituted dicyclohexyl(2-(2-methoxynaphthalen-1-yl)phenyl)phosphine was synthesised.<sup>78</sup> Although this complex performed competently in the alkynyl Heck reaction towards substituted allenes, its use was limited by its poor stability upon storage, even at low temperature.<sup>78</sup>

### II.2.3.2. Synthesis and characterisation of $\text{Ni}(\text{PMe}_2\text{Ar}^{\text{Dtbp}_2})_2$ .

Encouraged by this result, we targeted the synthesis of the analogous Ni(0) complex. Recently, Ogoshi and co-workers have reported the synthesis of  $\text{Ni}(\eta^6\text{-arene})(\text{NHC})$  complexes by hydrogenation of  $\text{Ni}(\text{cod})_2$  in the presence of the NHC ligand in the arene (toluene or benzene) as the reaction medium.<sup>79</sup> Inspired by the work of Ogoshi,  $\text{Ni}(\text{cod})_2$  and the phosphine **L5** were dissolved in toluene under  $\text{H}_2$  pressure (Scheme 17). After careful monitoring of the reaction conditions, best results were achieved for a temperature of 50 °C, a pressure of 4 bar and a reaction time of 3 h. After work-up of the reaction, complex **18·L5** was isolated as a very dark brown solid. This compound was obtained pure by crystallisation from a saturated pentane solution at -30 °C. Elemental analysis supports the proposed composition of **18·L5** as  $\text{Ni}(\text{PMe}_2\text{Ar}^{\text{Dtbp}_2})_2$ . This complex is extremely air-sensitive, undergoing decomposition to an unidentified yellowish product almost instantly even in the solid state.



Scheme 17. Synthesis of complex  $\text{Ni}(\text{PMe}_2\text{Ar}^{\text{Dtbp}_2})_2$  (**18-L5**).

As illustrated in Figure 74, the  $^1\text{H}$  NMR spectrum of this complex exhibits a substantial broadening of most signals, especially those corresponding to the Dtbp rings, indicating a dynamic process is ongoing involving said groups. Although variable temperature NMR studies were carried out to gain insight into this fluxional behaviour, no conclusions could be drawn from them. Also,  $^1\text{H}$  and  $^{13}\text{C}\{^1\text{H}\}$  spectra recorded for the Ni(0) complex substantially differ from those recorded for the palladium analogue,  $\text{Pd}(\text{PMe}_2\text{Ar}^{\text{Dtbp}_2})_2$  (**17-L5**), discussed in the previous section, which only present broadening of the resonance due to the

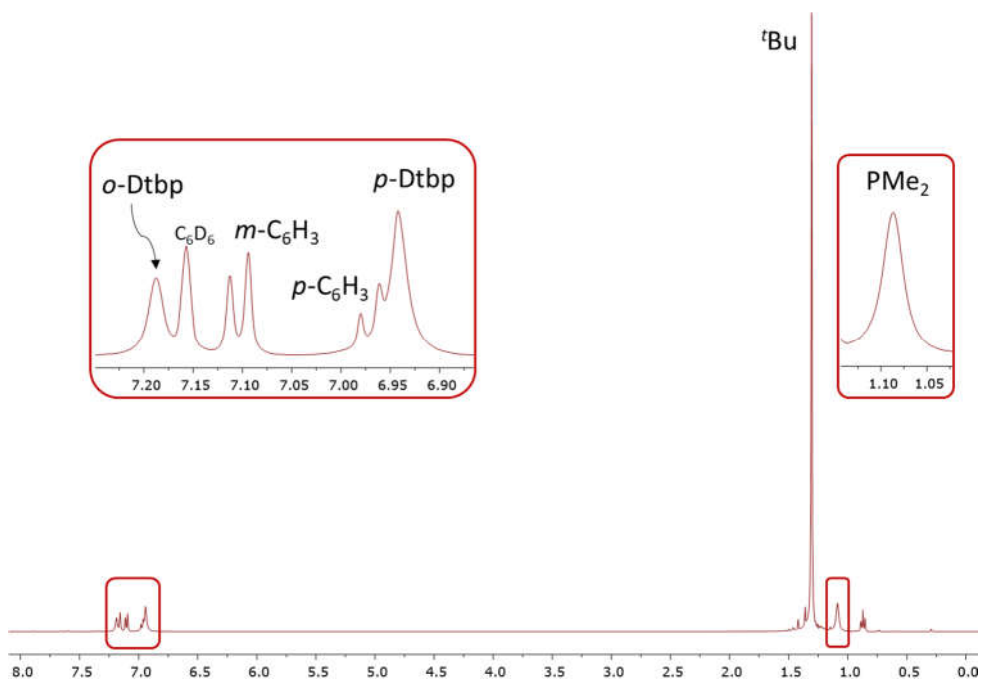


Figure 74.  $^1\text{H}$  NMR of complex **18-L5** in  $\text{C}_6\text{D}_6$  at  $25^\circ\text{C}$ .

hydrogen atoms in *ortho* position of the side aryl rings. Complex **18·L5** gives rise to a singlet in  $^{31}\text{P}\{^1\text{H}\}$  NMR at  $-4.3$  ppm ( $\Delta\delta = 32.3$  ppm), which suggests a monodentate coordination of the phosphine in solution at room temperature.

The structure of **18·L5** was analysed by single crystal X-ray diffraction and the molecular structure in the solid state is displayed in Figure 75. Surprisingly, unlike the linear palladium analogue, the nickel centre lies in a distorted trigonal coordination environment, with the third coordination site occupied by a  $\eta^2$ - $C_{ipso},C_{ortho}$  interaction with one of the Dtbp rings. This interaction features significantly shorter  $\text{Ni}\cdots C_{arene}$  distances ( $2.142(5)$  Å to  $C_{ipso}$  and  $2.294(6)$  Å to  $C_{ortho}$ ) than in the case of  $\text{Ni}(\text{CO})_2(\text{P}^i\text{Pr}_2\text{Ar}^{\text{Dtbp}_2})$  from Chapter I ( $2.449(2)$  Å to  $C_{ipso}$  and  $2.332(2)$  Å to  $C_{ortho}$ ). Interestingly, the  $\text{Ni}\cdots C_{ipso}$  distance presents the greater shortening, of around  $0.30$  Å. Still, both measurements lie well above the sum of

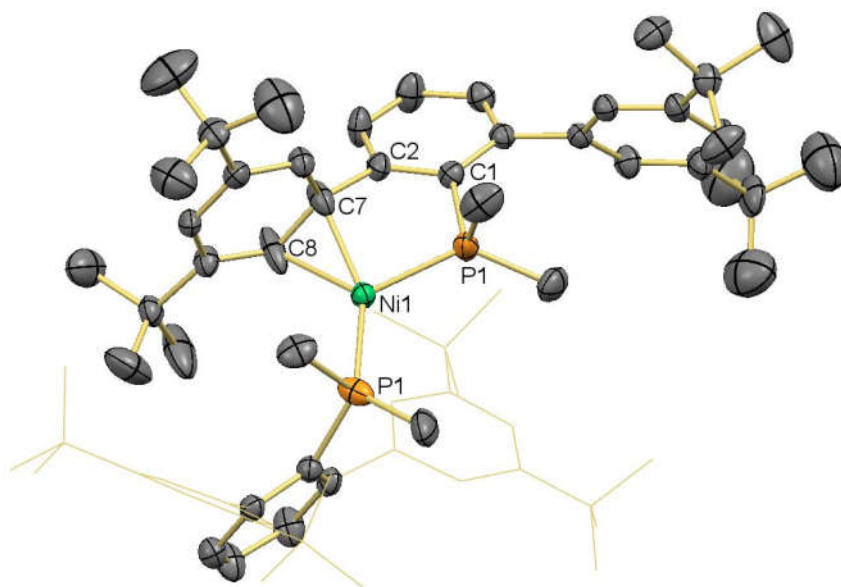


Figure 75. ORTEP view of complex **18·L5**. Hydrogen atoms are omitted for clarity, the side Dtbp rings of one of the terphenyl moieties are drawn in wireframe and thermal ellipsoids are set at 50% level probability. Selected bond distances (Å) and angles (°):  $\text{Ni1-P1}(\text{bidentate})$   $2.137(2)$ ,  $\text{Ni1-P1}(\text{monodentate})$   $2.220(2)$ ,  $\text{Ni1-C7}$   $2.142(5)$ ,  $\text{Ni1-C8}$   $2.294(6)$ ,  $\text{C7-C8}$   $1.412(8)$ ,  $\text{P1-Ni1-P1}$   $115.37(7)$ ,  $\text{P1-C1-C2}(\text{bidentate})$   $112.5(3)$ ,  $\text{Ni1-P1-C1-C2}(\text{bidentate})$   $8.4(3)$ ,  $\text{Ni1-P1-C1-C2}(\text{monodentate})$   $43.5(4)$ .

the covalent radii of the two atoms (1.97 Å),<sup>66</sup> and are also considerably longer than the Ni-C bond distances found in Ni(C<sub>2</sub>H<sub>4</sub>)(PPh<sub>3</sub>)<sub>2</sub> (*ca.* 2.01 Å)<sup>80</sup> and in [1,4-bis{2-(diisopropylphosphino)phenyl}benzene]nickel(0) (around 2.00 Å),<sup>62</sup> indicating that this interaction is weak and may be the cause of the dynamic behaviour of this species in solution. Concerning the conformation of the phosphines, the one presenting a bidentate mode of coordination adopts the expected type **C**, while the other exhibits a configuration of type **B**. To the best of our knowledge, this constitutes the first example of a structurally characterised Ni(PR<sub>3</sub>)<sub>2</sub> complex bearing monodentate phosphine ligands.

During the optimisation process of the reaction conditions, another species was detected appearing at a <sup>31</sup>P{<sup>1</sup>H} chemical shift of -8.0 ppm. This new species was generated before bisphosphine complex **18·L5** started to develop and was consumed at the same time that the concentration of the latter increased, suggesting that it may be a reaction intermediate. We succeeded in isolating this complex by cooling at -20 °C a pentane solution where this new species was the major component. The crystals obtained were suitable for X-ray diffraction studies, which revealed this intermediate to be a partially hydrogenated Ni(0)-olefin-phosphine complex, Ni(coe)(PMe<sub>2</sub>Ar<sup>Dtbp<sub>2</sub></sup>) (coe = cyclooctene, Figure 76). As in the structure of **18·L5**, the nickel centre in this complex adopts a trigonal geometry, with a bidentate mode of coordination of the phosphine and the third coordination position occupied by the olefin ligand. The Ni-C<sub>arene</sub> bond distances are shortened with respect to **18·L5**, with 2.017(3) Å to C<sub>ipso</sub> and 2.121(3) Å to C<sub>ortho</sub>, presumably due to a lower steric congestion around the metal centre. Strikingly, the interacting C<sub>ortho</sub> is bent out of the arene plane and towards the nickel atom by 0.161 Å. This feature is unobserved in other complexes with P,C-bidentate mode of coordination discussed throughout this thesis. On the other hand, as in all other structures, the plane of the arene is bent away from the metal centre by 24.5°. The Ni-C<sub>olefin</sub> bond distances (2.021(3) and 2.000(3) Å) are in good agreement with those observed in Ni(C<sub>2</sub>H<sub>4</sub>)(PPh<sub>3</sub>)<sub>2</sub>.<sup>80</sup>

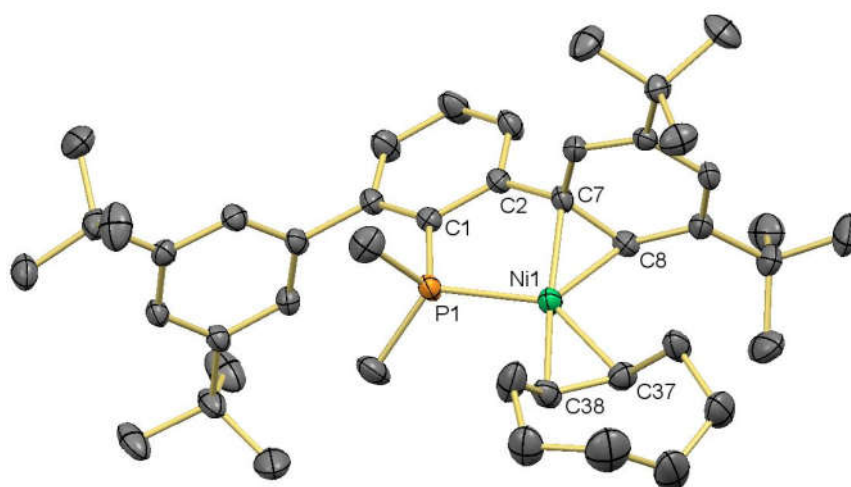
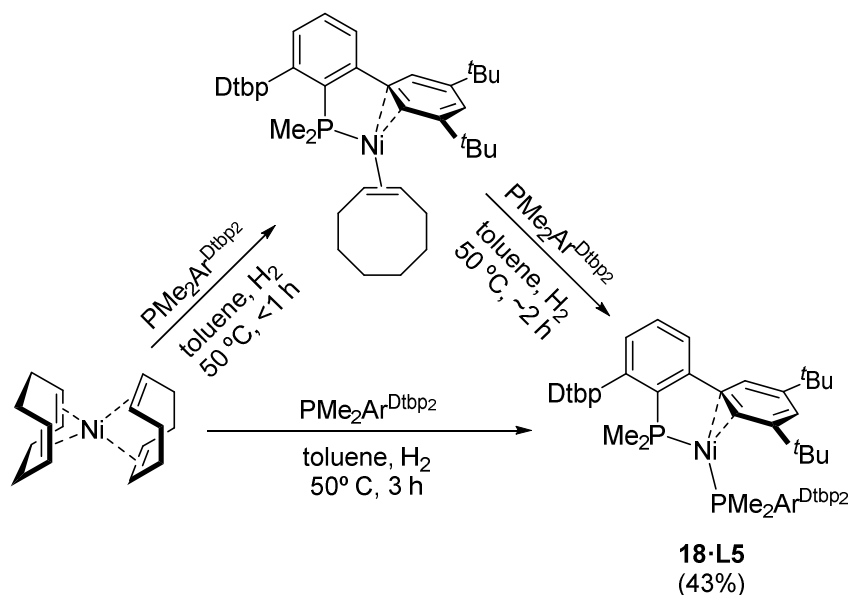


Figure 76. ORTEP view of  $\text{Ni}(\text{cod})(\text{PMe}_2\text{Ar}^{\text{Dtbp}2})$ . Hydrogen atoms are omitted for clarity, the side Dtbp rings of one of the terphenyl moieties are drawn in wireframe and thermal ellipsoids are set at 50% level probability. Selected bond distances (Å) and angles (°): Ni1-P1 2.1634(8), Ni1-C7 2.017(3), Ni1-C8 2.121(3), Ni1-C37 2.021(3), Ni1-C38 2.000(3), C7-C8 1.429(4), C37-C38 1.399(4), P1-C1-C2 109.9(2), Ni1-P1-C1-C2 -19.1(2).

Scheme 18 summarises the hydrogenation of  $\text{Ni}(\text{cod})_2$  in the presence of  $\text{PMe}_2\text{Ar}^{\text{Dtbp}2}$ .

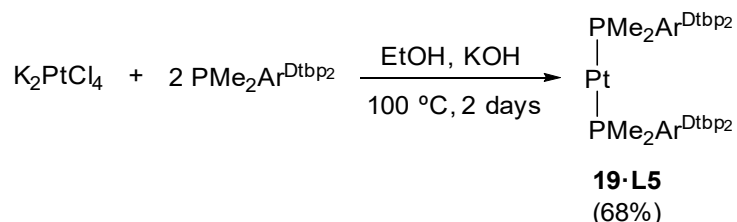


Scheme 18. Stepwise hydrogenation of  $\text{Ni}(\text{cod})_2$  in the presence of  $\text{PMe}_2\text{Ar}^{\text{Dtbp}2}$  (**L5**).



### II.2.3.3. Towards a platinum(0) bisphosphine complex.

Since both nickel and palladium  $M^0(\text{PMe}_2\text{Ar}^{\text{Dtbpp}_2})_2$  complexes had been successfully synthesised and characterised, it was considered of interest to obtain the platinum analogue. Several synthetic strategies were explored with this aim in mind, using as precursors different Pt-PMe<sub>2</sub>Ar<sup>Dipp<sub>2</sub></sup> complexes previously prepared in our group, such as the already mentioned PtCl<sub>2</sub>(PMe<sub>2</sub>Ar<sup>Dipp<sub>2</sub></sup>), PtMe<sub>2</sub>(PMe<sub>2</sub>Ar<sup>Dipp<sub>2</sub></sup>) or PtH(SiEt<sub>3</sub>)(PMe<sub>2</sub>Ar<sup>Dipp<sub>2</sub></sup>).<sup>63,64</sup> When none of these approaches yielded satisfactory results, a similar method to that described for the synthesis of Pt(P<sup>t</sup>Bu<sub>3</sub>)<sub>2</sub><sup>55b</sup> was undertaken. Thus, the platinum(II) precursor K<sub>2</sub>PtCl<sub>4</sub> was heated in EtOH in the presence of KOH and two equivalents of PMe<sub>2</sub>Ar<sup>Dtbpp<sub>2</sub></sup> (Scheme 19). This led to the precipitation of the desired Pt(PMe<sub>2</sub>Ar<sup>Dtbpp<sub>2</sub></sup>)<sub>2</sub> (**19·L5**), accompanied by a significant amount of free phosphine **L5** and metallic platinum. Washing of the solid with additional EtOH and subsequent extraction with pentane resulted in a mixture of **19·L5** and **L5**. Finally, washing with pentane at 0 °C rendered the sought product as a pale yellow solid in moderate yield (68%).



Scheme 19. Synthesis of complex Pt(PMe<sub>2</sub>Ar<sup>Dtbpp<sub>2</sub></sup>)<sub>2</sub> (**19·L5**).

As in the case of the palladium analogue **17·L5**, both the <sup>1</sup>H and <sup>13</sup>C{<sup>1</sup>H} NMR (Figure 77) spectra of **19·L5** exhibit virtual triplets for the nuclei in the vicinity of the phosphorus atom. In the <sup>1</sup>H NMR spectrum of this complex, the most striking feature is the pronounced broadness of the resonance due to the *ortho* protons in the Dtbp rings, almost indistinguishable from the baseline. Upon

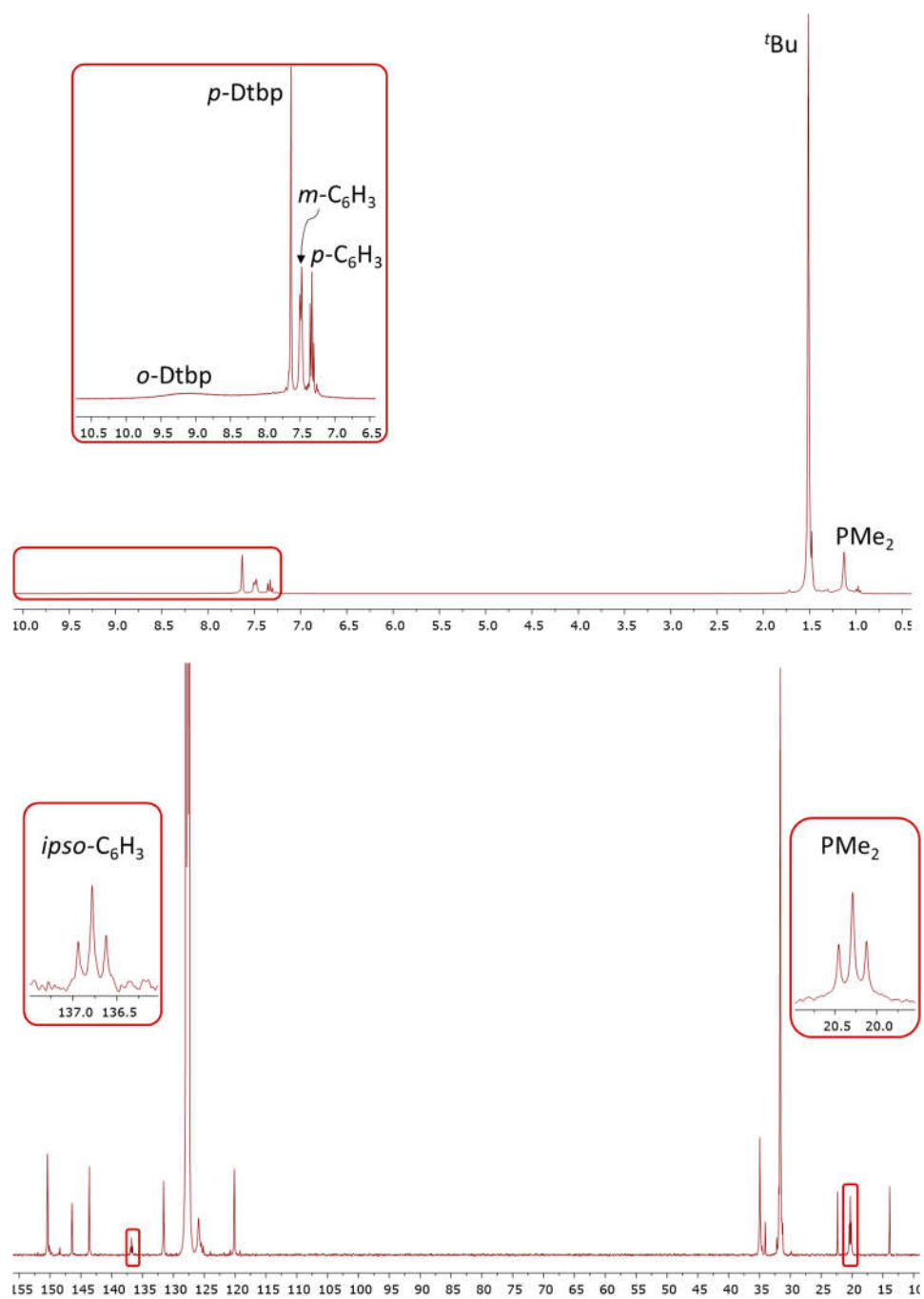


Figure 77.  $^1H$  (top) and  $^{13}C\{^1H\}$  (bottom) NMR spectra of complex **19-L5** in  $C_6D_6$  at 25 °C.

heating to 65 °C, this signal remains very broad, although it becomes more easily perceived. The major difference with the former lies in the  $^{13}\text{P}\{^1\text{H}\}$  NMR chemical shift, as **19·L5** appears as a singlet at 14.2 ppm (*versus* -12.8 ppm for **17·L5**), with a coupling to the  $^{195}\text{Pt}$  nucleus of  $^1J_{\text{Pt}} = 3794$  Hz.

This complex presents a molecular structure in the solid state almost identical to that of the palladium derivative **17·L5**, with minor differences in bond distances and angles (Figure 78). For example, the Pt-P bond distance stands at 2.2378(5) Å, only *ca.* 0.03 Å shorter than the Pd-P distance in **17·L5**, consistent with what is observed for similar complexes in the literature, such as  $\text{M}(\text{P}^t\text{Bu}_2\text{Ph})_2$  (M = Pd, Pt).<sup>54c</sup> In addition, the platinum atom displays a pseudo-linear geometry, with a P-Pt-P angle of 172.26(3)°, and the phosphines adopt a conformation of type **A** (Pt-P-*C*<sub>ipso</sub>-*C*<sub>ortho</sub> dihedral angle of -88.16(16)°).

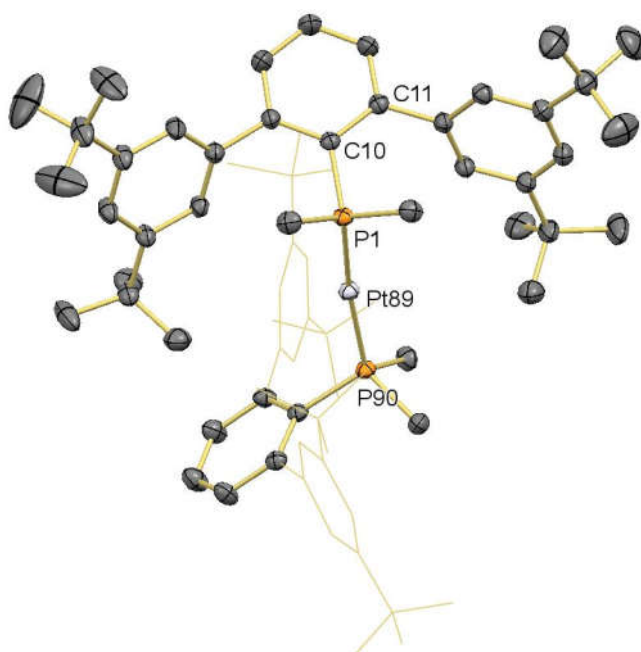


Figure 78. ORTEP view of complex **19·L5**. Hydrogen atoms are omitted for clarity, the side Dtbp rings of one of the terphenyl moieties are drawn in wireframe and thermal ellipsoids are set at 50% level probability. Selected bond distances (Å) and angles (°): Pt89-P1 2.2378(5), P1-Pt89-P90 172.26(3), Pt89-P1-C10-C11 -88.16(16).



### II.3. SUMMARY OF THE RESULTS

The studied dialkyl terphenyl phosphines ( $\text{PR}_2\text{Ar}''$ ) are, in most cases, capable of stabilising complexes of nickel, palladium and platinum in oxidation states 0 and +II, exhibiting competence in the generation of low-coordinate compounds.

Compounds of empirical formula  $\text{PdCl}_2(\text{PR}_2\text{Ar}'')$  exist in solution as mononuclear or chloride-bridged dinuclear species, according to NMR studies. The preference for one form or the other depends on several factors, such as the polarity of the solvent, concentration and nature of the phosphine ligand. These complexes react with Lewis bases to generate the corresponding  $\text{PdCl}_2(\text{L})(\text{PR}_2\text{Ar}'')$  adducts.

A large family of neutral and cationic  $\eta^3$ -allyl palladium(II) complexes, accommodating a wide variety of terphenyl phosphines in combination with different allyl ligands have been prepared. In the case of nickel, the stability of the  $\eta^3$ -allyl derivatives is conditioned by the size of the phosphine and allyl ligands. The dynamic behaviour of  $\eta^3$ -allyl complexes of nickel and palladium bearing dialkyl terphenyl phosphines has been investigated. The allyl moiety in palladium derivatives undergoes a *syn-anti* exchange, presumably via a  $\eta^3$ - $\eta^1$ - $\eta^3$  isomerisation mechanism. The natures of both the phosphine and the allyl ligands have an effect in the rate of this exchange. On the other hand, a *syn-syn anti-anti* exchange seems to be the cause of the fluxional behaviour of the nickel analogues.

## Chapter II

Complexes where the metal is in oxidation state 0 containing dialkyl terphenyl phosphines can be synthesised following different strategies. Coordinatively unsaturated compounds are stabilised by steric impediment or by interaction with the side aryl rings.

## II.4. EXPERIMENTAL SECTION

### II.4.1. General considerations.

All preparations and manipulations were carried out under an atmosphere of dry oxygen-free nitrogen or argon by means of conventional Schlenk or glovebox. Solvents were rigorously dried and degassed before use. Ligands **L1**<sup>23h</sup> and **L2**<sup>63</sup> and complexes Ni(cod)<sub>2</sub>,<sup>82</sup> [Pd(μ-Cl)(η<sup>3</sup>-C<sub>3</sub>H<sub>4</sub>R)]<sub>2</sub><sup>73</sup> and PtCl<sub>2</sub>(hxd)<sup>83</sup> were synthesized by following previously reported procedures. Other chemicals were purchased from commercial sources and used as received. NMR spectra were recorded on Bruker Avance DPX-300, Avance DRX-400, Avance DRX-500, 400 Ascend/R, AV 300 MHz and AVIII 300 MHz spectrometers. The <sup>1</sup>H and <sup>13</sup>C resonances of the solvent were used as the internal standard and the chemical shifts are reported relative to TMS while <sup>31</sup>P was referenced to external H<sub>3</sub>PO<sub>4</sub>. Infrared spectra were recorded on a Bruker Vector 22 spectrometer. Microanalyses were performed by the Microanalytical Service of the Instituto de Investigaciones Químicas (IIQ) and by the Chemical Analysis Service of the Centro de Investigación en Química Sostenible (CIQSO) at the Universidad de Huelva. X-ray diffraction data were collected on Bruker-AXSX8Kappa diffractometer (IIQ), Bruker Nonius X8 APEX-II Diffractometer (CITIUS) and Bruker-D8 QUEST ECO (CIQSO) and processed by Dr. Eleuterio Álvarez, Dr. Celia Maya and Mr. Francisco Molina. Mass spectra were performed by the Mass Spectrometry Service of the Instituto de Investigaciones Químicas (IIQ).

## II.4.2. Platinum dichloride adducts.

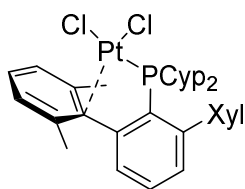
### II.4.2.1. New procedure for the synthesis of $\text{PtCl}_2(\text{PMe}_2\text{Ar}^{\text{Dipp}_2})$ (1·L2).

$\text{PtCl}_2$  (0.0588 g, 0.221 mmol, 10% excess) was stirred in commercial MeOH (5 mL) for 30 minutes, after which  $\text{PMe}_2\text{Ar}^{\text{Dipp}_2}$  (0.0916 g, 0.200 mmol) was added. The resulting mixture was stirred at room temperature for 2 days, filtered through a mixture of Celite and silica and the solvent removed under vacuum. The resulting orange powder was washed with pentane to yield the sought product as an orange solid. Yield: 0.1053 g, 73%. NMR data agree with those reported in the literature.<sup>63</sup>



#### II.4.2.2. Synthesis and characterization of PtCl<sub>2</sub>(PCyp<sub>2</sub>Ar<sup>Xyl</sup>)<sub>2</sub> (1·L3).

To an ampoule charged with PtCl<sub>2</sub>(hxd) (0.1044 g, 0.300 mmol) and PCyp<sub>2</sub>Ar<sup>Xyl</sup> (0.1432 g, 0.315 mmol, 5% excess), toluene (10 mL) was added. The reaction mixture was stirred at 80 °C for 1 day, after which the solution was filtered and petroleum ether added. Crystallisation from a toluene/petroleum ether mixture at -20 °C rendered the sought product as orange crystals. Yield: 0.0648 g, 30%. Crystals suitable for X-ray diffraction studies were obtained by slow evaporation from a hexane/CH<sub>2</sub>Cl<sub>2</sub> mixture at room temperature.



<sup>1</sup>H NMR (400 MHz, CDCl<sub>3</sub>, 298 K): δ 7.70 (t, <sup>3</sup>J<sub>HH</sub> = 7.6 Hz, 1 H, *p*-Xyl1), 7.47 (td, <sup>3</sup>J<sub>HH</sub> = 7.6 Hz, <sup>5</sup>J<sub>HP</sub> = 2.1 Hz, 1 H, *p*-C<sub>6</sub>H<sub>3</sub>), 7.26 (t, <sup>3</sup>J<sub>HH</sub> = 7.5 Hz, *p*-Xyl2), 7.15 (d, <sup>3</sup>J<sub>HH</sub> = 7.5 Hz, *m*-Xyl2), 7.10 (d, <sup>3</sup>J<sub>HH</sub> = 7.6 Hz, *m*-Xyl1), 7.02 (dd, <sup>3</sup>J<sub>HH</sub> = 7.4 Hz, <sup>4</sup>J<sub>HP</sub> = 2.8 Hz, *m*-C<sub>6</sub>H<sub>3</sub>), 6.62 (b d, <sup>3</sup>J<sub>HH</sub> = 7.5 Hz, *m*-C<sub>6</sub>H<sub>3</sub>), 2.63-2.50 (m, 2 H, Cyp), 2.46-2.31 (m, 4 H, Cyp), 2.20 (s, 6 H, CH<sub>3</sub> Xyl1), 2.01 (s, 6 H, CH<sub>3</sub> Xyl2), 1.79-1.73 (m, 6 H, Cyp), 1.51-1.30 (m, 6 H, Cyp).

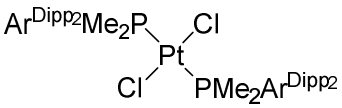
<sup>13</sup>C{<sup>1</sup>H} NMR (100 MHz, CDCl<sub>3</sub>, 298 K): δ 149.5 (d, <sup>2</sup>J<sub>CP</sub> = 19 Hz, *o*-C<sub>6</sub>H<sub>3</sub>), 145.1 (s, *o*-C<sub>6</sub>H<sub>3</sub>), 139.5 (s, *o*-Xyl1), 138.8 (s, *ipso*-Xyl2), 137.1 (s, *p*-Xyl1), 136.8 (s, *o*-Xyl2), 136.7 (d, <sup>1</sup>J<sub>CP</sub> = 47 Hz, *ipso*-C<sub>6</sub>H<sub>3</sub>), 132.7 (d, <sup>4</sup>J<sub>CP</sub> = 2 Hz, *p*-C<sub>6</sub>H<sub>3</sub>), 132.4 (d, <sup>3</sup>J<sub>CP</sub> = 7 Hz, *m*-C<sub>6</sub>H<sub>3</sub>), 131.1 (s, *m*-Xyl1), 130.5 (d, <sup>3</sup>J<sub>CP</sub> = 13 Hz, *m*-C<sub>6</sub>H<sub>3</sub>), 128.7 (s, *p*-Xyl2), 127.8 (s, *m*-Xyl2), 39.1 (d, <sup>1</sup>J<sub>CP</sub> = 37 Hz, CH Cyp), 33.6 (d, J<sub>CP</sub> = 4 Hz, CH<sub>2</sub> Cyp), 30.4 (s, CH<sub>2</sub> Cyp), 25.9 (d, J<sub>CP</sub> = 11 Hz, CH<sub>2</sub> Cyp), 25.0 (d, J<sub>CP</sub> = 14 Hz, CH<sub>2</sub> Cyp), 24.2 (s, CH<sub>3</sub> Xyl), 21.1 (s, CH<sub>3</sub> Xyl).

<sup>31</sup>P{<sup>1</sup>H} NMR (121 MHz, CDCl<sub>3</sub>, 298 K): δ 39.6 (<sup>1</sup>J<sub>PtP</sub> = 3308 Hz).

Elemental analysis (%), calculated (found) for C<sub>32</sub>H<sub>39</sub>Cl<sub>2</sub>Pt: C, 53.34 (53.33); H, 5.46 (5.70).

**II.4.2.3. Synthesis and characterization of PtCl<sub>2</sub>(PMe<sub>2</sub>Ar<sup>Dipp2</sup>)<sub>2</sub> (2·L2).**

To an ampoule charged with PtCl<sub>2</sub> (0.0267 g, 0.100 mmol) and PMe<sub>2</sub>Ar<sup>Dipp2</sup> (0.0965 g, 0.210 mmol, 5% excess), commercial MeOH (3 mL) was added. The resulting suspension was stirred overnight at room temperature. The solution was filtered off and the solid washed with MeOH until the resulting solution was colourless. Evaporation of remaining volatiles under vacuum rendered the product as an off-white solid. Yield: 0.0624 mg, 53%.


<sup>1</sup>H NMR (400 MHz, CD<sub>2</sub>Cl<sub>2</sub>, 298 K): δ 7.35-7.29 (m, 6 H, *p*-Dipp, *p*-C<sub>6</sub>H<sub>3</sub>), 7.18 (d, <sup>3</sup>J<sub>HH</sub> = 7.7 Hz, 8 H, *m*-Dipp), 7.03 (b d, <sup>3</sup>J<sub>HH</sub> = 7.5 Hz, 4 H, *m*-C<sub>3</sub>H<sub>6</sub>), 2.90 (sept, <sup>3</sup>J<sub>HH</sub> = 6.7 Hz, 8 H, CH <sup>*i*</sup>Pr), 1.19 (d, <sup>3</sup>J<sub>HH</sub> = 6.7 Hz, 24 H, CH<sub>3</sub> <sup>*i*</sup>Pr), 0.97 (virtual t, *J*<sub>app</sub> = 3.2 Hz, 12 H, P-CH<sub>3</sub>), 0.88 (d, <sup>3</sup>J<sub>HH</sub> = 6.7 Hz, 24 H, CH<sub>3</sub> <sup>*i*</sup>Pr).

<sup>13</sup>C{<sup>1</sup>H} NMR (100 MHz, CDCl<sub>3</sub>, 298 K): δ 147.3 (s, *o*-Dipp), 144.8 (virtual t, *J*<sub>app</sub> = 5 Hz, *o*-C<sub>6</sub>H<sub>3</sub>), 140.1 (s, *ipso*-Dipp), 132.3 (virtual t, *J*<sub>app</sub> = 4 Hz, *m*-C<sub>6</sub>H<sub>3</sub>), 128.5 (s, *p*-Dipp), 127.6 (s, *p*-C<sub>6</sub>H<sub>3</sub>), 123.0 (s, *m*-Dipp), 30.6 (s, CH <sup>*i*</sup>Pr), 25.9 (s, CH<sub>3</sub> <sup>*i*</sup>Pr), 23.7 (s, CH<sub>3</sub> <sup>*i*</sup>Pr), 14.8 (virtual t, *J*<sub>app</sub> = 17 Hz, P-CH<sub>3</sub>).

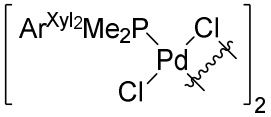
<sup>31</sup>P{<sup>1</sup>H} NMR (162 MHz, CD<sub>2</sub>Cl<sub>2</sub>, 298 K): δ -5.8 (<sup>1</sup>J<sub>Pt</sub> = 2448 Hz).

Elemental analysis (%), calculated (found) for C<sub>64</sub>H<sub>86</sub>Cl<sub>2</sub>P<sub>2</sub>Pt: C, 64.96 (64.72); H, 7.33 (7.63).

### II.4.3. Palladium dichloride adducts.

#### II.4.3.1. Synthesis and characterisation of $[\text{PdCl}(\mu\text{-Cl})(\text{PMe}_2\text{Ar}^{\text{Xyl}_2})]_2$ (**3·L1**).

To an ampoule charged with  $\text{PMe}_2\text{Ar}^{\text{Xyl}_2}$  (0.1039 g, 0.300 mmol) and  $\text{PdCl}_2$  (0.0532 g, 0.300 mmol), toluene (5 mL) was added, and the resulting mixture was heated at 100 °C for 2 days. The solvent was removed at reduced pressure and the resulting solid extracted in  $\text{CH}_2\text{Cl}_2$  and dried under vacuum, yielding the sought product as an orange solid. Yield: 0.1542 g, 98%.


 $^1\text{H NMR}$  (300 MHz,  $\text{C}_6\text{D}_6$ , 298 K):  $\delta$  7.30 (t,  $^3J_{\text{HH}} = 7.6$  Hz, 2 H, *p*-Xyl), 7.12 (d,  $^3J_{\text{HH}} = 7.6$  Hz, 4 H, *m*-Xyl), 6.99 (td,  $^3J_{\text{HH}} = 7.6$  Hz,  $^5J_{\text{HP}} = 2.1$  Hz, 1 H, *p*- $\text{C}_6\text{H}_3$ ), 6.61 (dd,  $^3J_{\text{HH}} = 7.6$  Hz,  $^4J_{\text{HP}} = 3.4$  Hz, 2 H, *m*- $\text{C}_6\text{H}_3$ ), 2.19 (s, 12 H,  $\text{CH}_3$  Xyl), 1.13 (d,  $^2J_{\text{HP}} = 13.2$  Hz, 6 H, P- $\text{CH}_3$ ).

$^1\text{H NMR}$  (400 MHz,  $\text{CDCl}_3$ , 298 K):  $\delta$  7.57 (td,  $^3J_{\text{HH}} = 7.6$  Hz,  $^5J_{\text{HP}} = 2.1$  Hz, 1 H, *p*- $\text{C}_6\text{H}_3$ ), 7.34 (t,  $^3J_{\text{HH}} = 7.6$  Hz, 2 H, *p*-Xyl), 7.19 (d,  $^3J_{\text{HH}} = 7.6$  Hz, 4 H, *m*-Xyl), 7.08 (dd,  $^3J_{\text{HH}} = 7.6$  Hz,  $^4J_{\text{HP}} = 3.4$  Hz, 2 H, *m*- $\text{C}_6\text{H}_3$ ), 2.17 (s, 12 H,  $\text{CH}_3$  Xyl), 1.21 (d,  $^2J_{\text{HP}} = 13.3$  Hz, 6 H, P- $\text{CH}_3$ ).

$^{13}\text{C}\{^1\text{H}\}$  NMR (101 MHz,  $\text{CDCl}_3$ , 298 K):  $\delta$  146.2 (d,  $^2J_{\text{CP}} = 10$  Hz, *o*- $\text{C}_6\text{H}_3$ ), 140.3 (s, *ipso*-Xyl), 136.7 (s, *o*-Xyl), 131.9 (s, *p*- $\text{C}_6\text{H}_3$ ), 131.0 (d,  $^3J_{\text{CP}} = 9$  Hz, *m*- $\text{C}_6\text{H}_3$ ), 129.2 (s, *p*-Xyl), 128.4 (s, *m*-Xyl), 127.5 (d,  $^1J_{\text{CP}} = 24$  Hz, *ipso*- $\text{C}_6\text{H}_3$ ), 22.2 (s,  $\text{CH}_3$  Xyl), 17.2 (d,  $^1J_{\text{CP}} = 37$  Hz, P- $\text{CH}_3$ ).

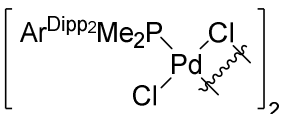
$^{31}\text{P}\{^1\text{H}\}$  NMR (121 MHz,  $\text{C}_6\text{D}_6$ , 298 K):  $\delta$  6.3 (s).

$^{31}\text{P}\{^1\text{H}\}$  NMR (162 MHz,  $\text{CDCl}_3$ , 298 K):  $\delta$  7.8 (s).

Elemental analysis (%), calculated (found) for  $\text{C}_{48}\text{H}_{54}\text{Cl}_4\text{P}_2\text{Pd}_2$ : C, 55.04 (55.12); H, 5.20 (5.37).

### II.4.3.2. Synthesis and characterisation of $[\text{PdCl}(\mu\text{-Cl})(\text{PMe}_2\text{Ar}^{\text{Dipp}_2})]_2$ (**3-L2**).

To an ampoule charged with  $\text{PMe}_2\text{Ar}^{\text{Dipp}_2}$  (0.3037 g, 0.662 mmol) and  $\text{PdCl}_2$  (0.1173 g, 0.662 mmol), toluene (5 mL) was added, and the resulting mixture was heated at 80 °C for 18 h. Removal of the solvent at reduced pressure yielded the sought product as an orange solid. Yield: 0.4096 g, 97%. Single crystals suitable for X-ray diffraction studies were obtained by crystallisation from a petroleum ether/ $\text{CH}_2\text{Cl}_2$  mixture at -20 °C.


 $^1\text{H}$  NMR (300 MHz,  $\text{C}_6\text{D}_6$ , 298 K):  $\delta$  7.54 (t,  $^3J_{\text{HH}} = 7.7$  Hz, 2 H, *p*-Dipp), 7.37 (d,  $^3J_{\text{HH}} = 7.7$  Hz, 4 H, *m*-Dipp), *ca.* 7.24 (*m*- $\text{C}_6\text{H}_3$ ), 7.12 (t,  $^3J_{\text{HH}} = 7.5$  Hz, 1 H, *p*- $\text{C}_6\text{H}_3$ ), 3.04 (sept,  $^3J_{\text{HH}} = 6.7$  Hz, 4 H, CH <sup>*i*</sup>Pr), 1.57 (d,  $^3J_{\text{HH}} = 6.6$  Hz, 12 H,  $\text{CH}_3$  <sup>*i*</sup>Pr), 1.33 (d,  $^2J_{\text{HP}} = 13.2$  Hz, 6 H, P- $\text{CH}_3$ ), 1.06 (d,  $^3J_{\text{HH}} = 6.6$  Hz, 12 H,  $\text{CH}_3$  <sup>*i*</sup>Pr).

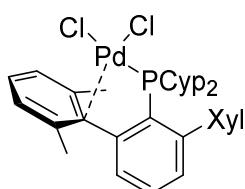
$^{13}\text{C}\{^1\text{H}\}$  NMR (100 MHz,  $\text{C}_6\text{D}_6$ , 298 K):  $\delta$  147.5 (s, *o*-Dipp), 144.9 (d,  $^2J_{\text{CP}} = 9$  Hz, *o*- $\text{C}_6\text{H}_3$ ), 138.6 (s, *ipso*-Dipp), 133.2 (d,  $^3J_{\text{CP}} = 10$  Hz, *m*- $\text{C}_6\text{H}_3$ ), 130.5 (s, *p*-Dipp), 128.5 (d,  $^1J_{\text{CP}} = 12$  Hz, *ipso*- $\text{C}_6\text{H}_3$ ), *ca.* 128.3 (*p*- $\text{C}_6\text{H}_3$ ), 123.8 (s, *m*-Dipp), 31.4 (s, CH <sup>*i*</sup>Pr), 26.5 (s,  $\text{CH}_3$  <sup>*i*</sup>Pr), 23.2 (s,  $\text{CH}_3$  <sup>*i*</sup>Pr), 18.4 (d,  $^1J_{\text{CP}} = 37$  Hz, P- $\text{CH}_3$ ).

$^{31}\text{P}\{^1\text{H}\}$  NMR (121 MHz,  $\text{C}_6\text{D}_6$ , 298 K):  $\delta$  6.5 (s).

Elemental analysis (%), calculated (found) for  $\text{C}_{64}\text{H}_{86}\text{Cl}_4\text{P}_2\text{Pd}_2$ : C, 60.43 (60.43); H, 6.82 (7.01).

### II.4.3.3. Synthesis and characterisation of $[\text{PdCl}(\mu\text{-Cl})(\text{PCyp}_2\text{Ar}^{\text{Xyl}_2})]_2$ (**3-L3**).

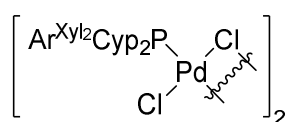
This complex was obtained following a similar procedure to that used for **3-L1**.



$^1\text{H}$  NMR (300 MHz,  $\text{CDCl}_3$ , 298 K):  $\delta$  7.86 (t,  $^3J_{\text{HH}} = 7.7$  Hz, 1 H, *p*-Xyl1), 7.51 (td,  $^3J_{\text{HH}} = 7.6$  Hz,  $^5J_{\text{HP}} = 2.3$  Hz, 1 H, *p*- $\text{C}_6\text{H}_3$ ), *ca.* 7.29 (*p*-Xyl2), *ca.* 7.28 (*m*-Xyl1), 7.16 (d,  $^3J_{\text{HH}} = 7.6$  Hz, 2 H, *m*-Xyl2), 7.09 (ddd,  $^3J_{\text{HH}} = 7.5$  Hz,  $^4J_{\text{HP}} = 2.5$  Hz,  $^4J_{\text{HH}} = 1.3$  Hz, 1 H, *m*- $\text{C}_6\text{H}_3$ ), 6.54 (ddd,  $^3J_{\text{HH}} = 7.5$  Hz,  $^4J_{\text{HP}} = 1.8$  Hz,  $^4J_{\text{HH}} = 1.3$  Hz, 1 H, *m*- $\text{C}_6\text{H}_3$ ), 2.57-2.35 (m, 6 H, Cyp), 2.29 (s, 6 H,  $\text{CH}_3$  Xyl1), 2.03 (s, 6 H,  $\text{CH}_3$  Xyl2), 1.89-1.64 (m, 6 H, Cyp), 1.50-1.24 (m, 6 H, Cyp).

$^{13}\text{C}\{^1\text{H}\}$  NMR (100 MHz,  $\text{CDCl}_3$ , 298 K):  $\delta$  148.1 (d,  $^2J_{\text{CP}} = 18$  Hz, *o*- $\text{C}_6\text{H}_3$ ), 145.0 (s, *o*- $\text{C}_6\text{H}_3$ ), 143.9 (s, *o*-Xyl1), 138.8 (s, *ipso*-Xyl2), 137.4 (d,  $^1J_{\text{CP}} = 35$  Hz, *ipso*- $\text{C}_6\text{H}_3$ ), 137.3 (s, *p*-Xyl1), 136.8 (s, *o*-Xyl2), 132.6 (d,  $^3J_{\text{CP}} = 9$  Hz, *p*- $\text{C}_6\text{H}_3$ ), 132.1 (d,  $J_{\text{CP}} = 6$  Hz, *m*- $\text{C}_6\text{H}_3$ ), 131.7 (s, *m*-Xyl1), 130.8 (d,  $^3J_{\text{CP}} = 15$  Hz, *m*- $\text{C}_6\text{H}_3$ ), 128.9 (s, *p*-Xyl2), 127.9 (s, *m*-Xyl2), 114.2 (d,  $^3J_{\text{CP}} = 3$  Hz, *ipso*-Xyl1), 41.3 (d,  $^1J_{\text{CP}} = 30$  Hz, CH Cyp), 33.6 (d,  $J_{\text{CP}} = 5$  Hz,  $\text{CH}_2$  Cyp), 31.5 (s,  $\text{CH}_2$  Cyp), 26.1 (d,  $J_{\text{CP}} = 11$  Hz,  $\text{CH}_2$  Cyp), 25.3 (d,  $J_{\text{CP}} = 14$  Hz,  $\text{CH}_2$  Cyp), 23.6 (s,  $\text{CH}_3$  Xyl), 21.2 (s,  $\text{CH}_3$  Xyl).

$^{31}\text{P}\{^1\text{H}\}$  NMR (121 MHz,  $\text{CDCl}_3$ , 298 K):  $\delta$  68.9 (s).



$^{31}\text{P}\{^1\text{H}\}$  NMR (121 MHz,  $\text{C}_6\text{D}_6$ , 298 K):  $\delta$  36.1 (s).

Elemental analysis (%), calculated (found) for  $\text{C}_{64}\text{H}_{78}\text{Cl}_4\text{P}_2\text{Pd}_2$ : C, 60.82 (60.56); H, 6.22 (6.36).

#### II.4.4. Reactivity of the palladium dichloride adducts towards Lewis bases.

##### II.4.4.1. Reaction of $[\text{PdCl}(\mu\text{-Cl})(\text{PMe}_2\text{Ar}^{\text{Xyl}_2})]_2$ (**3·L1**) with CO.

$[\text{PdCl}(\mu\text{-Cl})(\text{PMe}_2\text{Ar}^{\text{Xyl}_2})]_2$  (**3·L1**) (0.0524 g, 0.050 mmol) and  $\text{CDCl}_3$  (0.6 mL) were placed in an ampoule, the vessel was charged with CO (1.5 bar) and the reaction mixture left to stir overnight at room temperature and filtered to an NMR tube. Due to the reversibility of the process, compound **3·L1** could not be isolated. Hence, the characterisation of this CO adduct was carried out under a CO atmosphere (1.5 bar).

$$\begin{array}{c} \text{Ar}^{\text{Xyl}_2}\text{Me}_2\text{P} \quad \text{CO} \\ \quad \quad \quad \diagdown \quad / \\ \quad \quad \quad \text{Pd} \\ \quad \quad \quad / \quad \diagdown \\ \text{Cl} \quad \quad \quad \text{Cl} \end{array}$$
 $^1\text{H NMR}$  (400 MHz,  $\text{CDCl}_3$ , 298 K):  $\delta$  7.67 (td,  $^3J_{\text{HH}} = 7.6$  Hz,  $^5J_{\text{HP}} = 2.2$  Hz, 1 H, *p*- $\text{C}_6\text{H}_3$ ), 7.31 (t,  $^3J_{\text{HH}} = 7.6$  Hz, 2 H, *p*-Xyl), 7.20 (d,  $^3J_{\text{HH}} = 7.6$  Hz, 4 H, *m*-Xyl), 7.17 (dd,  $^3J_{\text{HH}} = 7.6$  Hz,  $^4J_{\text{HP}} = 3.8$  Hz, 2 H, *m*- $\text{C}_6\text{H}_3$ ), 2.19 (s, 12 H,  $\text{CH}_3$  Xyl), 1.51 (d,  $^2J_{\text{HP}} = 12.4$  Hz, 6 H,  $\text{P-CH}_3$ ).

$^{13}\text{C}\{^1\text{H}\}$  NMR (126 MHz,  $\text{CDCl}_3$ , 298 K):  $\delta$  167.8 (d,  $^2J_{\text{CP}} = 4$  Hz, CO), 146.4 (d,  $^2J_{\text{CP}} = 10$  Hz, *o*- $\text{C}_6\text{H}_3$ ), 140.3 (d,  $^3J_{\text{CP}} = 5$  Hz, *ipso*-Xyl), 136.8 (s, *o*-Xyl), 132.8 (d,  $^4J_{\text{CP}} = 3$  Hz, *p*- $\text{C}_6\text{H}_3$ ), 131.3 (d,  $^3J_{\text{CP}} = 9$  Hz, *m*- $\text{C}_6\text{H}_3$ ), 129.2 (s, *p*-Xyl), 128.7 (s, *m*-Xyl), 125.9 (d,  $^1J_{\text{CP}} = 58$  Hz, *ipso*- $\text{C}_6\text{H}_3$ ), 22.1 (s,  $\text{CH}_3$  Xyl), 19.6 (d,  $^1J_{\text{CP}} = 37$  Hz,  $\text{P-CH}_3$ ).

$^{31}\text{P}\{^1\text{H}\}$  NMR (162 MHz,  $\text{CDCl}_3$ , 298 K):  $\delta$  7.3 (s).

IR ( $\text{CH}_2\text{Cl}_2$ ): 2131  $\text{cm}^{-1}$  ( $\nu_{\text{CO}}$ ).

#### II.4.4.2. Reaction of [PdCl( $\mu$ -Cl)(PMe<sub>2</sub>Ar<sup>Xyl</sup>)<sub>2</sub>] (3·L1) with CNXyl.

To an NMR tube containing [PdCl( $\mu$ -Cl)(PMe<sub>2</sub>Ar<sup>Xyl</sup>)<sub>2</sub>] (3·L1) (0.0110 g, 0.011 mmol) and CNXyl (0.0028 g, 0.021 mmol), CDCl<sub>3</sub> (0.6 mL) was added. Reaction was instantaneous at room temperature. This complex was not isolated and only characterised by NMR.

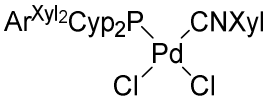
$$\begin{array}{c} \text{Ar}^{\text{Xyl}_2}\text{Me}_2\text{P} \\ \quad \quad \quad \diagdown \\ \quad \quad \quad \text{Pd} \\ \quad \quad \quad \diagup \\ \text{Cl} \quad \quad \text{Cl} \end{array} \text{CNXyl}$$
<sup>1</sup>H NMR (300 MHz, CDCl<sub>3</sub>, 298 K):  $\delta$  7.62 (td, <sup>3</sup>J<sub>HH</sub> = 7.6 Hz, <sup>5</sup>J<sub>HP</sub> = 2.2 Hz, 1 H, *p*-C<sub>6</sub>H<sub>3</sub>), 7.29-7.03 (m, 11 H, aromatic), 2.39 (s, 6 H, CH<sub>3</sub> CNXyl), 2.26 (s, 12 H, CH<sub>3</sub> Xyl), 1.50 (d, <sup>2</sup>J<sub>HP</sub> = 12.1 Hz, 6 H, P-CH<sub>3</sub>).

<sup>13</sup>C{<sup>1</sup>H} NMR (126 MHz, CDCl<sub>3</sub>, 298 K):  $\delta$  146.4 (d, <sup>2</sup>J<sub>CP</sub> = 10 Hz, *o*-C<sub>6</sub>H<sub>3</sub>), 140.8 (d?, <sup>3</sup>J<sub>CP</sub> = 5 Hz, *ipso*-Xyl), 137.1 (s, *o*-Xyl), 136.4 (s, *o*-XylINC), 132.1 (d, <sup>4</sup>J<sub>CP</sub> = 3 Hz, *p*-C<sub>6</sub>H<sub>3</sub>), 131.2 (d, <sup>3</sup>J<sub>CP</sub> = 9 Hz, *m*-C<sub>6</sub>H<sub>3</sub>), 130.2 (s, *p*-XylINC), 128.7 (s, *p*-Xyl), 128.4 (s, *m*-XylINC), 128.3 (s, *m*-Xyl), 127.3 (d, <sup>1</sup>J<sub>CP</sub> = 18 Hz, *ipso*-C<sub>6</sub>H<sub>3</sub>), 125.7 (s, *ipso*-XylINC) 22.3 (s, CH<sub>3</sub> Xyl), 19.8 (d, <sup>1</sup>J<sub>CP</sub> = 36 Hz, P-CH<sub>3</sub>), 19.7 (s, CH<sub>3</sub> CNXyl).

<sup>31</sup>P{<sup>1</sup>H} NMR (121 MHz, CDCl<sub>3</sub>, 298 K):  $\delta$  4.1 (s).

#### II.4.4.3. Reaction of [PdCl(μ-Cl)(PCyp<sub>2</sub>Ar<sup>Xyl<sub>2</sub></sup>)]<sub>2</sub> (**3·L3**) with CNXyl.

To an NMR tube containing [PdCl(μ-Cl)(PCyp<sub>2</sub>Ar<sup>Xyl<sub>2</sub></sup>)]<sub>2</sub> (**3·L3**) (0.0110 g, 0.011 mmol) and CNXyl (0.0028 g, 0.021 mmol), CDCl<sub>3</sub> (0.6 mL) was added. Reaction was instantaneous at room temperature. After analysis by NMR, samples suitable for single crystal X-ray diffraction studies were obtained by crystallisation from a pentane/CH<sub>2</sub>Cl<sub>2</sub> mixture at -5°C.


<sup>1</sup>H NMR (300 MHz, CDCl<sub>3</sub>, 298 K): δ 7.51 (td, <sup>3</sup>J<sub>HH</sub> = 7.6 Hz, <sup>5</sup>J<sub>HP</sub> = 2.3 Hz, 1 H, *p*-C<sub>6</sub>H<sub>3</sub>), 7.28-6.91 (m, 11 H, aromatic), 3.12-0.77 (very broad, Cyp, CH<sub>3</sub> Xyl), 2.44 (s, 6 H, CH<sub>3</sub> CNXyl), 0.13 (b, 1 H, Cyp).

<sup>1</sup>H NMR (400 MHz, CDCl<sub>3</sub>, 228 K): δ 7.51 (b td, <sup>3</sup>J<sub>HH</sub> = 7.7 Hz, <sup>5</sup>J<sub>HP</sub> = 2.2 Hz, 1 H, *p*-C<sub>6</sub>H<sub>3</sub>), *ca.* 7.32-7.25 (m, aromatic), 7.22-7.17 (m, 2 H, aromatic), 7.12-7.07 (m, 4 H, aromatic), 7.01 (b d, <sup>3</sup>J<sub>HH</sub> = 7.7 Hz, 1 H, *m*-C<sub>6</sub>H<sub>3</sub>), 6.79 (d, <sup>3</sup>J<sub>HH</sub> = 7.5 Hz, 1 H, *m*-Xyl), 6.71 (t, <sup>3</sup>J<sub>HH</sub> = 7.5 Hz, 1 H, *p*-Xyl), 2.98 (b, 1 H, Cyp), 2.80 (b, 1 H, Cyp), 2.57 (s, 3 H, CH<sub>3</sub> Xyl), 2.49 (s, 3 H, CH<sub>3</sub> Xyl), 2.41 (s, 6 H, CH<sub>3</sub> CNXyl), 2.04 (s, 3 H, CH<sub>3</sub> Xyl), 2.00 (s, 3 H, CH<sub>3</sub> Xyl), 1.96-1.24 (b, 13 H, Cyp), 0.93-0.77 (b, 2 H, Cyp), -0.20 (b, 1 H, Cyp).

<sup>1</sup>H NMR (400 MHz, CDCl<sub>3</sub>, 328 K): δ 7.51 (td, <sup>3</sup>J<sub>HH</sub> = 7.6 Hz, <sup>5</sup>J<sub>HP</sub> = 2.3 Hz, 1 H, *p*-C<sub>6</sub>H<sub>3</sub>), 7.26-7.22 (b m, 2 H, *p*-Xyl), 7.18-7.14 (b m, 1 H, *p*-XylINC), 7.10 (d, <sup>3</sup>J<sub>HH</sub> = 7.8 Hz, 4 H, *m*-Xyl), 7.06 (dd, <sup>3</sup>J<sub>HH</sub> = 7.6 Hz, <sup>4</sup>J<sub>HP</sub> = 3.3 Hz, 2 H, *m*-C<sub>6</sub>H<sub>3</sub>), 7.03-6.97 (b m, 2 H, *m*-XylINC), 2.76 (b, 2 H, Cyp), 2.46 (s, 6 H, CH<sub>3</sub> CNXyl), 2.32 (b s, 12 H, CH<sub>3</sub> Xyl), 2.02-1.97 (b m, 16 H, Cyp).

<sup>13</sup>C{<sup>1</sup>H} NMR (100 MHz, CDCl<sub>3</sub>, 293 K): δ 142.6 (b s, *o*-C<sub>6</sub>H<sub>3</sub>), 136.5 (s, *o*-Xyl), 132.7 (b s, *m*-C<sub>6</sub>H<sub>3</sub>), 130.8 (s, *p*-C<sub>6</sub>H<sub>3</sub>), 128.5 (s, Xyl), 128.3 (s, Xyl), 127.5 (very broad, aromatic), 126.1 (s, *ipso*-Xyl), 43.1-21.2 (several broad signals, Cyp, CH<sub>3</sub> CNXyl), 19.7 (s, CH<sub>3</sub> Xyl).

<sup>31</sup>P{<sup>1</sup>H} NMR (121 MHz, CDCl<sub>3</sub>, 298 K): δ 35.3 (s).

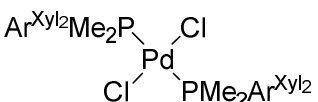


**II.4.4.4. Synthesis and characterisation of PdCl<sub>2</sub>(PMe<sub>2</sub>Ar<sup>Xyl</sup>)<sub>2</sub> (6-L1).**

This compound could be obtained following two different methods.

Method A: To an ampoule charged with [PdCl(μ-Cl)(PMe<sub>2</sub>Ar<sup>Xyl</sup>)<sub>2</sub>] (3-L1) (0.0262 g, 0.025 mmol) and PMe<sub>2</sub>Ar<sup>Xyl</sup> (0.0173 g, 0.050 mmol), toluene (1 mL) was added. After 2 hours stirring at room temperature, the solvent was removed under vacuum, and the resulting solid extracted in CH<sub>2</sub>Cl<sub>2</sub> and filtered. Removal of volatiles under reduced pressure yielded the sought product as a yellow powder.

Method B: A mixture of PdCl<sub>2</sub> (0.0560 g, 0.315 mmol) and PMe<sub>2</sub>Ar<sup>Xyl</sup> (0.2292 g, 0.662 mmol, 5% excess) in toluene (5 mL), placed in an ampoule, was heated at 100 °C for 15 hours. The solvent was removed under vacuum and the resulting solid washed with Et<sub>2</sub>O, extracted in CHCl<sub>3</sub> and filtered. Removal of volatiles under reduced pressure yielded the sought product as a yellow solid.


<sup>1</sup>H NMR (400 MHz, CDCl<sub>3</sub>, 298 K): δ 7.42 (td, <sup>3</sup>J<sub>HH</sub> = 7.6 Hz, 1 H, *p*-C<sub>6</sub>H<sub>3</sub>), 7.14 (dd, <sup>3</sup>J<sub>HH</sub> = 8.3 Hz, <sup>3</sup>J<sub>HH</sub> = 6.6 Hz, 2 H, *p*-Xyl), 7.02 (d, <sup>3</sup>J<sub>HH</sub> = 7.0 Hz, 4 H, *m*-Xyl), 6.90 (dt, <sup>3</sup>J<sub>HH</sub> = 7.5 Hz, J<sub>HP</sub>(app) = 1.6 Hz, 2 H, *m*-C<sub>6</sub>H<sub>3</sub>), 2.11 (s, 12 H, CH<sub>3</sub> Xyl), 1.16 (t, J<sub>HP</sub>(app) = 3.5 Hz, 6 H, P-CH<sub>3</sub>).

<sup>13</sup>C{<sup>1</sup>H} NMR (101 MHz, CDCl<sub>3</sub>, 298 K): δ 146.6 (t, J<sub>CP</sub>(app) = 6 Hz, *o*-C<sub>6</sub>H<sub>3</sub>), 141.8 (s, *ipso*-Xyl), 136.6 (s, *o*-Xyl), 130.9 (t, J<sub>CP</sub>(app) = 4 Hz, *m*-C<sub>6</sub>H<sub>3</sub>), 130.7 (s, *p*-C<sub>6</sub>H<sub>3</sub>), 129.2 (d, J<sub>CP</sub>(app) = 20 Hz, *ipso*-C<sub>6</sub>H<sub>3</sub>), 128.0 (s, *p*-Xyl), 127.8 (s, *m*-Xyl), 22.1 (s, CH<sub>3</sub> Xyl), 15.3 (t, J<sub>CP</sub>(app) = 15 Hz, P-CH<sub>3</sub>).

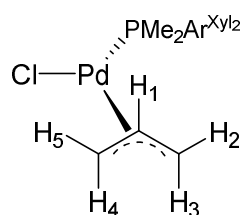
<sup>31</sup>P{<sup>1</sup>H} NMR (121 MHz, CDCl<sub>3</sub>, 298 K): δ -10.8 (s).

Elemental analysis (%), calculated (found) for C<sub>48</sub>H<sub>54</sub>Cl<sub>2</sub>P<sub>2</sub>Pd: C, 66.25 (66.09); H, 6.25 (6.41).

### II.4.5. General synthesis of complexes $\text{PdCl}(\eta^3\text{-C}_3\text{H}_4\text{R}')(\text{PR}_2\text{Ar}'')$ , $\text{R}' = \text{H}$ (**7**· $\text{PR}_2\text{Ar}''$ ), **Me** (**8**· $\text{PR}_2\text{Ar}''$ ), **Ph** (**9**· $\text{PR}_2\text{Ar}''$ ).

THF (5-15 mL) was added to a deoxygenated vessel charged with  $[\text{Pd}(\eta^3\text{-C}_3\text{H}_4\text{R})]_2(\mu\text{-Cl})_2$  (0.5 eq) and  $\text{PR}_2\text{Ar}''$  (1 eq) until complete dissolution. The mixture was stirred at room temperature for 4 h and then dried under vacuum. The remaining residue was extracted with  $\text{CH}_2\text{Cl}_2$  or a petroleum ether/ $\text{CH}_2\text{Cl}_2$  mixture and filtered. Evaporation of the solvent under reduced pressure or crystallisation (where specified) from a  $\text{CH}_2\text{Cl}_2$ /petroleum ether mixture rendered the sought products as yellow/pale yellow powder or pallid yellow crystals, respectively.

#### II.4.5.1. $\text{PdCl}(\eta^3\text{-C}_3\text{H}_5)(\text{PMe}_2\text{Ar}^{\text{Xyl}_2})$ (**7**·**L1**).



$^1\text{H}$  NMR (300 MHz,  $\text{CD}_2\text{Cl}_2$ , 298 K):  $\delta$  7.53 (td,  $^3J_{\text{HH}} = 7.6$  Hz,  $^5J_{\text{HP}} = 1.6$  Hz, 1 H, *p*- $\text{C}_6\text{H}_3$ ), 7.21-7.09 (m, 6 H, aromatic), 7.00 (dd,  $^3J_{\text{HH}} = 7.6$  Hz,  $^4J_{\text{HP}} = 2.8$  Hz, 2 H, *m*- $\text{C}_6\text{H}_3$ ), 5.06 (m, 1 H,  $\text{H}_1$ ), 4.21 (td,  $^3J_{\text{HH}} = ^3J_{\text{HP}} = 7.5$  Hz,  $^4J_{\text{HH}} = 1.6$  Hz, 1 H,  $\text{H}_5$ ), 3.03 (dd,  $^3J_{\text{HH}} = 13.8$  Hz,  $^3J_{\text{HP}} = 10.2$  Hz, 1 H,  $\text{H}_4$ ), 2.66 (bd,  $J_{\text{HH}} = 6.2$  Hz, 1 H,  $\text{H}_2$ ), 2.18 (s, 6 H,  $\text{CH}_3$  Xyl), 2.15 (s, 6 H,  $\text{CH}_3$  Xyl), 1.70 (bd,  $J_{\text{HH}} = 11.8$  Hz, 1 H,  $\text{H}_3$ ), 1.26 (d,  $^2J_{\text{HP}} = 8.4$  Hz, 3 H, *P*- $\text{CH}_3$ ), 1.16 (d,  $^2J_{\text{HP}} = 8.5$  Hz, 3 H, *P*- $\text{CH}_3$ ).

$^{13}\text{C}\{^1\text{H}\}$  NMR (75 MHz,  $\text{CD}_2\text{Cl}_2$ , 298 K):  $\delta$  146.6 (d,  $^2J_{\text{CP}} = 10$  Hz, *o*- $\text{C}_6\text{H}_3$ ), 142.2 (d,  $^3J_{\text{CP}} = 5$  Hz, *ipso*-Xyl), 137.2 (s, *o*-Xyl), 137.1 (s, *o*-Xyl), 131.2 (d,  $^4J_{\text{CP}} = 2$  Hz, *p*- $\text{C}_6\text{H}_3$ ), 131.1 (d,  $^3J_{\text{CP}} = 7$  Hz, *m*- $\text{C}_6\text{H}_3$ ), 129.7 (d,  $^1J_{\text{CP}} = 31$  Hz, *ipso*- $\text{C}_6\text{H}_3$ ), 128.1 (s, *p*-Xyl), 127.9 (s, *m*-Xyl), 127.8 (s, *m*-Xyl), 117.8 (d,  $^2J_{\text{CP}} = 6$  Hz,  $\text{C}_{\text{meso}}$ ), 76.5 (d,  $^2J_{\text{CP}} = 34$  Hz,  $\text{C}_{\text{trans-P}}$ ), 54.0 (d,  $^2J_{\text{CP}} = 2$  Hz,  $\text{C}_{\text{cis-P}}$ ), 22.2 ( $\text{CH}_3$  Xyl), 22.0 ( $\text{CH}_3$  Xyl), 17.7 (d,  $^1J_{\text{CP}} = 26$  Hz, *P*- $\text{CH}_3$ ), 17.0 (d,  $^1J_{\text{CP}} = 27$  Hz, *P*- $\text{CH}_3$ ).

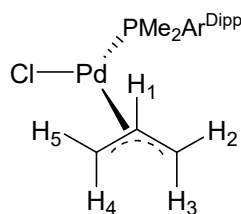
$^{31}\text{P}\{^1\text{H}\}$  NMR (121 MHz,  $\text{CD}_2\text{Cl}_2$ , 298 K):  $\delta$  -10.4 (s).

Elemental analysis (%), calculated (found) for  $\text{C}_{27}\text{H}_{32}\text{ClPPd}$ : C, 61.26 (60.68); H, 6.09 (5.98).

## Experimental Section

Yield: 0.0933 g, 68% (after recrystallisation).

*Alternative reaction work-up:* After reaction was complete, the mixture was filtered and the THF removed under reduced pressure (washing with petroleum ether was sometimes necessary to obtain a powder). Yield: 0.19 g, 90%.

II.4.5.2. PdCl( $\eta^3$ -C<sub>3</sub>H<sub>5</sub>)(PMe<sub>2</sub>Ar<sup>Dipp</sup>)<sub>2</sub> (7·L2).

<sup>1</sup>H NMR (300 MHz, C<sub>6</sub>D<sub>6</sub>, 298 K):  $\delta$  7.21-6.99 (m, 9 H, aromatic), 4.62 (m, 1 H, H<sub>1</sub>), 4.21 (td, <sup>3</sup>J<sub>HH</sub> = <sup>3</sup>J<sub>HP</sub> = 7.5 Hz, <sup>4</sup>J<sub>HH</sub> = 1.1 Hz, 1 H, H<sub>5</sub>), 3.09-2.93 (m, 5 H, CH <sup>i</sup>Pr, H<sub>4</sub>), 2.32 (bd, <sup>3</sup>J<sub>HH</sub> = 6.2 Hz, 1 H, H<sub>2</sub>), 1.49-1.42 (m, 13 H, CH<sub>3</sub> <sup>i</sup>Pr, H<sub>3</sub>), 1.32-1.26 (m, 6 H, P-CH<sub>3</sub>), 0.97 (d, <sup>3</sup>J<sub>HH</sub> = 6.7 Hz, 12 H, CH<sub>3</sub> <sup>i</sup>Pr).

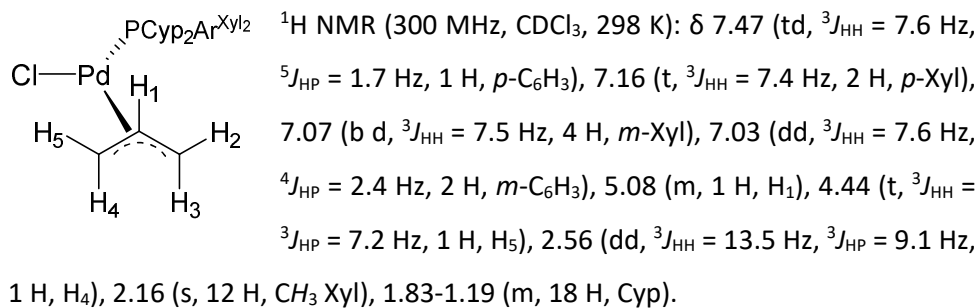
<sup>13</sup>C{<sup>1</sup>H} NMR (126 MHz, C<sub>6</sub>D<sub>6</sub>, 298 K):  $\delta$  147.5 (s, *o*-Dipp), 147.4 (s, *o*-Dipp), 144.8 (d, <sup>2</sup>J<sub>CP</sub> = 10 Hz, *o*-C<sub>6</sub>H<sub>3</sub>), 140.3 (d, <sup>3</sup>J<sub>CP</sub> = 4 Hz, *ipso*-Dipp), 133.4 (d, <sup>3</sup>J<sub>CP</sub> = 7 Hz, *m*-C<sub>6</sub>H<sub>3</sub>), 131.7 (d, <sup>1</sup>J<sub>CP</sub> = 29 Hz, *ipso*-C<sub>6</sub>H<sub>3</sub>), 129.1 (s, *p*-Dipp), 127.6 (d, <sup>4</sup>J<sub>CP</sub> = 2 Hz, *p*-C<sub>6</sub>H<sub>3</sub>), 123.4 (s, *m*-Dipp), 123.4 (s, *m*-Dipp), 117.7 (d, <sup>2</sup>J<sub>CP</sub> = 6 Hz, C<sub>meso</sub>), 75.1 (d, <sup>2</sup>J<sub>CP</sub> = 35 Hz, C<sub>trans-P</sub>), 53.3 (s, C<sub>cis-P</sub>), 31.4 (s, CH <sup>i</sup>Pr), 31.3 (s, CH <sup>i</sup>Pr), 26.2 (s, CH<sub>3</sub> <sup>i</sup>Pr), 23.5 (s, CH<sub>3</sub> <sup>i</sup>Pr), 18.2 (d, <sup>1</sup>J<sub>CP</sub> = 25 Hz, P-CH<sub>3</sub>), 18.0 (d, <sup>1</sup>J<sub>CP</sub> = 26 Hz, P-CH<sub>3</sub>).

<sup>31</sup>P{<sup>1</sup>H} NMR (121 MHz, C<sub>6</sub>D<sub>6</sub>, 298 K):  $\delta$  -8.9 (s).

Elemental analysis (%), calculated (found) for C<sub>35</sub>H<sub>48</sub>ClPPd: C, 65.52 (65.28); H, 7.54 (7.73).

Yield: 0.1088 g, 78%.

### II.4.5.3. PdCl( $\eta^3$ -C<sub>3</sub>H<sub>5</sub>)(PCyp<sub>2</sub>Ar<sup>Xyl</sup>)<sub>2</sub> (7·L3).

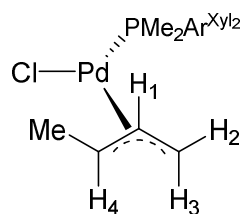


<sup>13</sup>C{<sup>1</sup>H} NMR (75 MHz, CDCl<sub>3</sub>, 298 K):  $\delta$  147.5 (d, <sup>2</sup>J<sub>CP</sub> = 9 Hz, *o*-C<sub>6</sub>H<sub>3</sub>), 142.5 (d, <sup>3</sup>J<sub>CP</sub> = 3 Hz, *ipso*-Xyl), 137.0 (s, *o*-Xyl), 134.4 (d, <sup>1</sup>J<sub>CP</sub> = 19 Hz, *ipso*-C<sub>6</sub>H<sub>3</sub>), 131.8 (d, <sup>3</sup>J<sub>CP</sub> = 6 Hz, *m*-C<sub>6</sub>H<sub>3</sub>), 130.0 (d, <sup>4</sup>J<sub>CP</sub> = 2 Hz, *p*-C<sub>6</sub>H<sub>3</sub>), 127.8 (s, *m*-Xyl), 127.2 (s, *p*-Xyl), 114.9 (d, <sup>2</sup>J<sub>CP</sub> = 5 Hz, C<sub>meso</sub>), 87.6 (d, <sup>2</sup>J<sub>CP</sub> = 29 Hz C<sub>trans-P</sub>), 53.6 (s, C<sub>cis-P</sub>), 40.8 (d, <sup>2</sup>J<sub>CP</sub> = 22 Hz, CH Cyp), 31.9 (d, J<sub>CP</sub> = 11 Hz, CH<sub>2</sub> Cyp), 31.1 (d, J<sub>CP</sub> = 5 Hz, CH<sub>2</sub> Cyp), 25.9-25.5 (m, CH<sub>2</sub> Cyp), 22.3 (s, CH<sub>3</sub> Xyl).

<sup>31</sup>P{<sup>1</sup>H} NMR (121 MHz, CD<sub>2</sub>Cl<sub>2</sub>, 298 K):  $\delta$  33.2 (s).

Elemental analysis (%), calculated (found) for C<sub>35</sub>H<sub>44</sub>ClPPd: C, 65.93 (66.00); H, 6.96 (7.04).

Yield: 0.0802 g, 63% (after recrystallisation).

II.4.5.4. PdCl( $\eta^3$ -C<sub>3</sub>H<sub>4</sub>Me)(PMe<sub>2</sub>Ar<sup>Xyl</sup>)<sub>2</sub> (8-L1).

<sup>1</sup>H NMR (300 MHz, CD<sub>2</sub>Cl<sub>2</sub>, 298 K):  $\delta$  7.51 (td, <sup>3</sup>J<sub>HH</sub> = 7.6 Hz, <sup>5</sup>J<sub>HP</sub> = 1.7 Hz, 1 H, *p*-C<sub>6</sub>H<sub>3</sub>), 7.18 (t, <sup>3</sup>J<sub>HH</sub> = 7.4 Hz, 2 H, *p*-Xyl), 7.09 (b d, <sup>3</sup>J<sub>HH</sub> = 7.6 Hz, 4 H, *m*-Xyl), 6.98 (dd, <sup>3</sup>J<sub>HH</sub> = 7.6 Hz, <sup>4</sup>J<sub>HP</sub> = 2.8 Hz, 2 H, *m*-C<sub>6</sub>H<sub>3</sub>), 4.79 (dt, <sup>3</sup>J<sub>HH</sub> = 12.9 Hz, <sup>3</sup>J<sub>HH</sub> = 9.4 Hz, H<sub>1</sub>), 3.75 (ddq, <sup>3</sup>J<sub>HH</sub> = 12.6 Hz, <sup>3</sup>J<sub>HP</sub> = 9.9 Hz, <sup>3</sup>J<sub>HH</sub> = 6.3 Hz, 1 H, H<sub>4</sub>), 2.54 (d, <sup>3</sup>J<sub>HH</sub> = 6.5 Hz, 1 H, H<sub>2</sub>), 2.17 (s, 6 H, CH<sub>3</sub> Xyl), 2.14 (s, 6 H, CH<sub>3</sub> Xyl), *ca.* 1.60 (H<sub>3</sub>), 1.58 (dd, <sup>4</sup>J<sub>HP</sub> = 9.5 Hz, <sup>3</sup>J<sub>HH</sub> = 6.3 Hz, 3 H, CH<sub>3</sub> crotyl), 1.29-1.20 (m, 6 H, P-CH<sub>3</sub>).

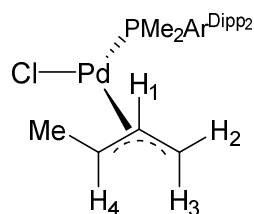
<sup>13</sup>C{<sup>1</sup>H} NMR (75 MHz, CD<sub>2</sub>Cl<sub>2</sub>, 298 K):  $\delta$  146.7 (d, <sup>2</sup>J<sub>CP</sub> = 10 Hz, *o*-C<sub>6</sub>H<sub>3</sub>), 142.4 (d, <sup>3</sup>J<sub>CP</sub> = 5 Hz, *ipso*-Xyl), 137.2 (s, *o*-Xyl), 131.2-131.1 (*p*-C<sub>6</sub>H<sub>3</sub>, *m*-C<sub>6</sub>H<sub>3</sub>), 130.3 (d, <sup>1</sup>J<sub>CP</sub> = 30 Hz, *ipso*-C<sub>6</sub>H<sub>3</sub>), 128.0 (s, *p*-Xyl), 127.9 (s, *m*-Xyl), 117.0 (d, <sup>3</sup>J<sub>CP</sub> = 5 Hz, C<sub>meso</sub>), 95.0 (d, <sup>2</sup>J<sub>CP</sub> = 30 Hz, C<sub>trans-P</sub>), 50.0 (d, <sup>2</sup>J<sub>CP</sub> = 1 Hz, C<sub>cis-P</sub>), 22.1 (s, CH<sub>3</sub> Xyl), 22.0 (s, CH<sub>3</sub> Xyl), 18.1-17.2 (m, P-CH<sub>3</sub>, CH<sub>3</sub> crotyl).

<sup>31</sup>P{<sup>1</sup>H} NMR (121 MHz, CD<sub>2</sub>Cl<sub>2</sub>, 298 K):  $\delta$  -9.7 (s).

Elemental analysis (%), calculated (found) for C<sub>28</sub>H<sub>34</sub>ClPPd: C, 61.89 (61.80); H, 6.31 (6.43).

Yield: 0.0879 g, 100%.

#### II.4.5.5. PdCl( $\eta^3$ -C<sub>3</sub>H<sub>4</sub>Me)(PMe<sub>2</sub>Ar<sup>Dipp</sup>)<sub>2</sub> (8-L2).



<sup>1</sup>H NMR (300 MHz, CDCl<sub>3</sub>, 298 K):  $\delta$  7.40-7.32 (m, 3 H, *p*-C<sub>6</sub>H<sub>3</sub>, *p*-Dipp), 7.22 (b d, <sup>3</sup>J<sub>HH</sub> = 7.6 Hz, 4 H, *m*-Dipp), 7.12 (dd, <sup>3</sup>J<sub>HH</sub> = 7.6 Hz, <sup>4</sup>J<sub>HP</sub> = 2.7 Hz, 2 H, *m*-C<sub>6</sub>H<sub>3</sub>), 4.68 (dt, <sup>3</sup>J<sub>HH</sub> = 12.6 Hz, <sup>3</sup>J<sub>HH</sub> = 9.1 Hz, 1 H, H<sub>1</sub>), 3.84 (ddq, <sup>3</sup>J<sub>HH</sub> = 12.6 Hz, <sup>3</sup>J<sub>HP</sub> = 9.9 Hz, <sup>3</sup>J<sub>HH</sub> = 6.2 Hz, 1 H, H<sub>4</sub>), 2.85-2.72 (b m, 4 H, CH<sup>*i*</sup>Pr), 2.30 (b, 1 H, H<sub>2</sub>), 1.58 (dd, <sup>4</sup>J<sub>HP</sub> = 9.6 Hz, <sup>3</sup>J<sub>HH</sub> = 6.3 Hz, 3 H, CH<sub>3</sub> crotyl), *ca.* 1.44 (H<sub>3</sub>), 1.38 (b, 12 H, CH<sub>3</sub><sup>*i*</sup>Pr), 1.21 (d, <sup>2</sup>J<sub>HP</sub> = 8.5 Hz, 6 H, P-CH<sub>3</sub>), 0.99 (d, <sup>3</sup>J<sub>HH</sub> = 6.7 Hz, 12 H, CH<sub>3</sub><sup>*i*</sup>Pr).

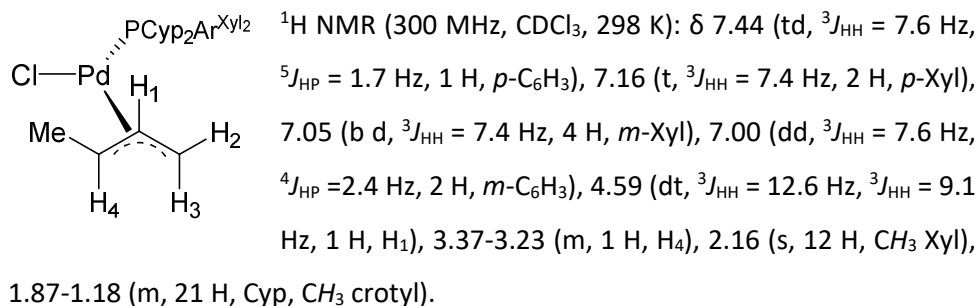
<sup>13</sup>C{<sup>1</sup>H} NMR (75 MHz, CDCl<sub>3</sub>, 298 K):  $\delta$  147.5 (s, *o*-Dipp), 144.4 (d, <sup>2</sup>J<sub>CP</sub> = 10 Hz, *o*-C<sub>6</sub>H<sub>3</sub>), 140.3 (d, <sup>3</sup>J<sub>CP</sub> = 4 Hz, *ipso*-Dipp), 133.6 (d, <sup>3</sup>J<sub>CP</sub> = 6 Hz, *m*-C<sub>6</sub>H<sub>3</sub>), 132.0 (d, <sup>1</sup>J<sub>CP</sub> = 29 Hz, *ipso*-C<sub>6</sub>H<sub>3</sub>), 129.0 (s, *p*-Dipp), 127.9 (d, <sup>4</sup>J<sub>CP</sub> = 2 Hz, *p*-C<sub>6</sub>H<sub>3</sub>), 123.4 (s, *m*-Dipp), 117.4 (d, <sup>2</sup>J<sub>CP</sub> = 5 Hz, C<sub>meso</sub>), 94.8 (d, <sup>2</sup>J<sub>CP</sub> = 30 Hz C<sub>trans-P</sub>), 49.9 (s, C<sub>cis-P</sub>), 31.4 (s, CH<sup>*i*</sup>Pr), 26.0 (s, CH<sub>3</sub><sup>*i*</sup>Pr), 23.4 (s, CH<sub>3</sub><sup>*i*</sup>Pr), 18.2 (m, P-CH<sub>3</sub>), 17.27 (d, <sup>3</sup>J<sub>CP</sub> = 4 Hz, CH<sub>3</sub> crotyl).

<sup>31</sup>P{<sup>1</sup>H} NMR (121 MHz, CDCl<sub>3</sub>, 298 K):  $\delta$  -8.5 (s).

Elemental analysis (%), calculated (found) for C<sub>36</sub>H<sub>50</sub>ClPPd: C, 65.95 (65.64); H, 7.69 (8.01).

Yield: 0.1627 g, 99%.

### II.4.5.6. PdCl( $\eta^3$ -C<sub>3</sub>H<sub>4</sub>Me)(PCyp<sub>2</sub>Ar<sup>Xyl</sup>)<sub>2</sub> (8-L3).



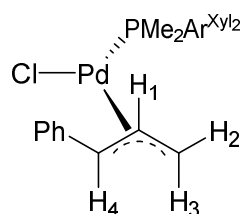
<sup>13</sup>C{<sup>1</sup>H} NMR (75 MHz, CDCl<sub>3</sub>, 298 K): δ 147.5 (s, *o*-C<sub>6</sub>H<sub>3</sub>), 142.9 (s, *ipso*-Xyl), 137.0 (s, *o*-Xyl), 134.8 (d, <sup>1</sup>J<sub>CP</sub> = 19 Hz, *ipso*-C<sub>6</sub>H<sub>3</sub>), 131.9 (d, <sup>3</sup>J<sub>CP</sub> = 6 Hz, *m*-C<sub>6</sub>H<sub>3</sub>), 129.9 (d, <sup>4</sup>J<sub>CP</sub> = 2 Hz, *p*-C<sub>6</sub>H<sub>3</sub>), 127.7 (s, *m*-Xyl), 127.2 (s, *p*-Xyl), 114.2 (d, <sup>2</sup>J<sub>CP</sub> = 4 Hz, C<sub>meso</sub>), 104.8 (d, <sup>2</sup>J<sub>CP</sub> = 25 Hz C<sub>trans-P</sub>), 48.2 (s, C<sub>cis-P</sub>), 41.2 (d, <sup>2</sup>J<sub>CP</sub> = 21 Hz, CH Cyp), 32.1 (d, J<sub>CP</sub> = 11 Hz, CH<sub>2</sub> Cyp), 31.3 (d, J<sub>CP</sub> = 5 Hz, CH<sub>2</sub> Cyp), 26.0 (d, J<sub>CP</sub> = 11 Hz, CH<sub>2</sub> Cyp), 25.6 (d, J<sub>CP</sub> = 12 Hz, CH<sub>2</sub> Cyp), 22.4 (s, CH<sub>3</sub>), 17.5 (d, <sup>3</sup>J<sub>CP</sub> = 4 Hz, CH<sub>3</sub> crotyl).

<sup>31</sup>P{<sup>1</sup>H} NMR (121 MHz, CDCl<sub>3</sub>, 298 K): δ 36.2 (s).

Elemental analysis (%), calculated (found) for C<sub>36</sub>H<sub>46</sub>ClPPd: C, 66.36 (66.36); H, 7.12 (6.96).

Yield: 0.0760 g, 78% (after recrystallisation).

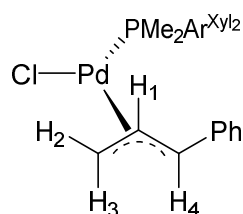


**II.4.5.7. PdCl( $\eta^3$ -C<sub>3</sub>H<sub>4</sub>Ph)(PMe<sub>2</sub>Ar<sup>Xyl2</sup>) (9·L1).****MAJOR ISOMER**

<sup>1</sup>H NMR (300 MHz, CD<sub>2</sub>Cl<sub>2</sub>, 298 K):  $\delta$  7.53 (td, <sup>3</sup>J<sub>HH</sub> = 7.6 Hz, <sup>5</sup>J<sub>HP</sub> = 1.7 Hz, 1 H, *p*-C<sub>6</sub>H<sub>3</sub>), 7.40-7.13 (m, 11 H, aromatic), 7.05 (dd, <sup>3</sup>J<sub>HH</sub> = 7.6 Hz, <sup>4</sup>J<sub>HP</sub> = 2.6 Hz, 2 H, *m*-C<sub>6</sub>H<sub>3</sub>), 5.46 (dt, <sup>3</sup>J<sub>HH</sub> = 13.0 Hz, <sup>3</sup>J<sub>HH</sub> = 9.2 Hz, 1 H, H<sub>1</sub>), 4.61 (dd, <sup>3</sup>J<sub>HH</sub> = 12.9 Hz, <sup>3</sup>J<sub>HP</sub> = 10.7 Hz, 1 H, H<sub>4</sub>), 2.60 (b, 1 H, H<sub>2</sub>), 2.16 (s, 12 H, CH<sub>3</sub> Xyl), 1.87 (b, 1 H, H<sub>3</sub>), 1.27 (d, <sup>2</sup>J<sub>HP</sub> = 8.9 Hz, 6 H, P-CH<sub>3</sub>).

<sup>13</sup>C{<sup>1</sup>H} NMR (100 MHz, CDCl<sub>3</sub>, 298 K) (selected signals)<sup>†</sup>:  $\delta$  146.4 (d, <sup>2</sup>J<sub>CP</sub> = 10 Hz, *o*-C<sub>6</sub>H<sub>3</sub>), 141.9 (d, <sup>3</sup>J<sub>CP</sub> = 5 Hz, *ipso*-Xyl), 111.4 (d, <sup>2</sup>J<sub>CP</sub> = 6 Hz, C<sub>meso</sub>), 96.9 (d, <sup>2</sup>J<sub>CP</sub> = 31 Hz, C<sub>trans-P</sub>), 50.1 (d, <sup>2</sup>J<sub>CP</sub> = 3 Hz, C<sub>cis-P</sub>), 22.1 (s, CH<sub>3</sub> Xyl), 17.8 (d, <sup>1</sup>J<sub>CP</sub> = 27 Hz, P-CH<sub>3</sub>).

<sup>31</sup>P{<sup>1</sup>H} NMR (121 MHz, CD<sub>2</sub>Cl<sub>2</sub>, 298 K):  $\delta$  -7.3 (s).

**MINOR ISOMER (selected signals) (16% by <sup>1</sup>H NMR)**

<sup>1</sup>H NMR (300 MHz, CD<sub>2</sub>Cl<sub>2</sub>, 298 K):  $\delta$  7.07 (b d, <sup>3</sup>J<sub>HH</sub> = 7.5 Hz, 2 H, aromatic), 5.74 (ddd, <sup>3</sup>J<sub>HH</sub> = 12.7 Hz, <sup>3</sup>J<sub>HH</sub> = 11.2 Hz, <sup>3</sup>J<sub>HH</sub> = 7.8 Hz, 1 H, H<sub>1</sub>), 4.31 (t, <sup>3</sup>J<sub>HH</sub> = <sup>3</sup>J<sub>HP</sub> = 7.8 Hz, 1 H, H<sub>2</sub>), 3.20 (ddd, <sup>3</sup>J<sub>HH</sub> = 13.7 Hz, <sup>3</sup>J<sub>HP</sub> = 10.5 Hz, <sup>4</sup>J<sub>HH</sub> = 0.8 Hz, 1 H, H<sub>3</sub>), 2.96 (b d, *J* = 11.3 Hz, H<sub>4</sub>), 2.18 (s, 6 H, CH<sub>3</sub> Xyl), 2.12 (s, 6 H, CH<sub>3</sub> Xyl), 0.65 (d, <sup>2</sup>J<sub>HP</sub> = 8.5 Hz, 3 H, P-CH<sub>3</sub>), 0.23 (d, <sup>2</sup>J<sub>HP</sub> = 8.9 Hz, 3 H, P-CH<sub>3</sub>).

<sup>13</sup>C{<sup>1</sup>H} NMR (75 MHz, CD<sub>2</sub>Cl<sub>2</sub>, 298 K) (selected signals):  $\delta$  114.8 (d, <sup>2</sup>J<sub>CP</sub> = 5 Hz, C<sub>meso</sub>), *ca.* 76.7 (C<sub>trans-P</sub>), 71.1 (d, <sup>2</sup>J<sub>CP</sub> = 5 Hz, C<sub>cis-P</sub>), 22.5 (s, CH<sub>3</sub> Xyl), 22.0 (s, CH<sub>3</sub> Xyl), 15.1 (d, <sup>1</sup>J<sub>CP</sub> = 27 Hz, P-CH<sub>3</sub>), 11.3 (d, <sup>1</sup>J<sub>CP</sub> = 25 Hz, P-CH<sub>3</sub>).

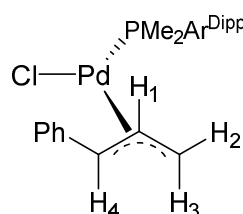
<sup>31</sup>P{<sup>1</sup>H} NMR (121 MHz, CD<sub>2</sub>Cl<sub>2</sub>, 298 K):  $\delta$  -10.9 (s).

Elemental analysis (%), calculated (found) for C<sub>33</sub>H<sub>36</sub>ClPPd: C, 65.46 (65.27); H, 5.99 (6.16).

Yield: 0.0822 g, 60% (after recrystallisation).

## Chapter II

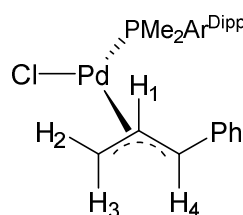
<sup>†</sup>Signals in the  $^{13}\text{C}\{^1\text{H}\}$  NMR spectrum are intermixed with those corresponding to the minor isomer, impeding a more thorough assignation. The rest of the aromatic signals are located between 137.4 and 127.0 ppm.

**II.4.5.8. PdCl( $\eta^3$ -C<sub>3</sub>H<sub>4</sub>Ph)(PMe<sub>2</sub>Ar<sup>Dipp</sup>)<sub>2</sub> (9-L2).****MAJOR ISOMER**

<sup>1</sup>H NMR (300 MHz, CDCl<sub>3</sub>, 298 K):  $\delta$  7.41-7.35 (m, 6 H, aromatic), 7.31-7.22 (m, 6 H, aromatic), 7.05 (dd, <sup>3</sup>J<sub>HH</sub> = 7.6 Hz, <sup>4</sup>J<sub>HP</sub> = 2.8 Hz, 2 H, *m*-C<sub>6</sub>H<sub>3</sub>), 5.30 (dt, <sup>3</sup>J<sub>HH</sub> = 13.2 Hz, <sup>3</sup>J<sub>HP</sub> = 9.2 Hz, 1 H, H<sub>1</sub>), 4.61 (dd, <sup>3</sup>J<sub>HH</sub> = 13.3 Hz, <sup>3</sup>J<sub>HP</sub> = 10.5 Hz, 1 H, H<sub>4</sub>), 2.76 (sept, <sup>3</sup>J<sub>HH</sub> = 6.7 Hz, 4 H, CH Dipp), 1.33 (b d, <sup>3</sup>J<sub>HH</sub> = 6.5 Hz, 12 H, CH<sub>3</sub> Dipp), 1.27 (d, <sup>2</sup>J<sub>HP</sub> = 9.0 Hz, 6 H, P-CH<sub>3</sub>), 0.98 (d, <sup>3</sup>J<sub>HH</sub> = 6.7 Hz, 12 H, CH<sub>3</sub> Dipp).

<sup>13</sup>C{<sup>1</sup>H} NMR (100 MHz, CDCl<sub>3</sub>, 298 K):  $\delta$  147.2 (s, *o*-Dipp), 144.1 (d, <sup>2</sup>J<sub>CP</sub> = 10 Hz, *o*-C<sub>6</sub>H<sub>3</sub>), 139.8 (d, <sup>3</sup>J<sub>CP</sub> = 4 Hz, *ipso*-Dipp), 136.6 (d, <sup>3</sup>J<sub>CP</sub> = 7 Hz, *ipso*-Ph), 133.3 (d, <sup>3</sup>J<sub>CP</sub> = 7 Hz, *m*-C<sub>6</sub>H<sub>3</sub>), 131.5 (d, <sup>1</sup>J<sub>CP</sub> = 31 Hz, *ipso*-C<sub>6</sub>H<sub>3</sub>), 128.8 (s, *p*-Dipp), 128.6 (d, <sup>5</sup>J<sub>CP</sub> = 2 Hz, *m*-Ph), 127.6-127.7 (m, *p*-Ph, *p*-C<sub>6</sub>H<sub>3</sub>), 127.6 (d, <sup>4</sup>J<sub>CP</sub> = 4 Hz, *o*-Ph), 123.2 (s, *m*-Dipp), 117.7 (d, <sup>2</sup>J<sub>CP</sub> = 6 Hz, C<sub>meso</sub>), 75.1 (d, <sup>2</sup>J<sub>CP</sub> = 35 Hz, C<sub>trans-P</sub>), 53.3 (s, C<sub>cis-P</sub>), 31.4 (s, CH <sup>*i*</sup>Pr), 31.3 (s, CH <sup>*i*</sup>Pr), 26.2 (s, CH<sub>3</sub> <sup>*i*</sup>Pr), 23.5 (s, CH<sub>3</sub> <sup>*i*</sup>Pr), 18.2 (d, <sup>1</sup>J<sub>CP</sub> = 25 Hz, P-CH<sub>3</sub>), 18.0 (d, <sup>1</sup>J<sub>CP</sub> = 26 Hz, P-CH<sub>3</sub>).

<sup>31</sup>P{<sup>1</sup>H} NMR (121 MHz, CD<sub>2</sub>Cl<sub>2</sub>, 298 K):  $\delta$  -5.6 (s).

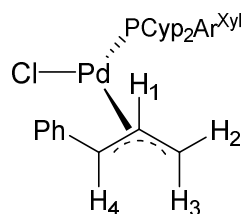
**MINOR ISOMER (selected signals) (12% by <sup>1</sup>H NMR)**

<sup>1</sup>H NMR (300 MHz, CD<sub>2</sub>Cl<sub>2</sub>, 298 K):  $\delta$  5.62 (m, 1 H, H<sub>1</sub>), 4.31 (t, <sup>3</sup>J<sub>HH</sub> = <sup>3</sup>J<sub>HP</sub> = 7.8 Hz, 1 H, H<sub>2</sub>), 3.23 (dd, <sup>3</sup>J<sub>HH</sub> = 13.2 Hz, <sup>3</sup>J<sub>HP</sub> = 11.3 Hz, 1 H, H<sub>3</sub>), 3.12 (b d, <sup>3</sup>J<sub>HH</sub> = 11.3 Hz, 1 H, H<sub>4</sub>), 0.64 (d, <sup>2</sup>J<sub>HP</sub> = 8.7 Hz, 3 H, P-CH<sub>3</sub>), 0.28 (d, <sup>2</sup>J<sub>HP</sub> = 9.0 Hz, 3 H, P-CH<sub>3</sub>).

<sup>31</sup>P{<sup>1</sup>H} NMR (121 MHz, CD<sub>2</sub>Cl<sub>2</sub>, 298 K):  $\delta$  -9.0 (s).

Elemental analysis (%), calculated (found) for C<sub>41</sub>H<sub>52</sub>ClPPd: C, 68.61 (68.75); H, 7.30 (7.59).

Yield: 0.150 g, 92%.

II.4.5.9. PdCl( $\eta^3$ -C<sub>3</sub>H<sub>4</sub>Ph)(PCyp<sub>2</sub>Ar<sup>Xyl</sup>)<sub>2</sub> (9-L3).

<sup>1</sup>H NMR (300 MHz, CDCl<sub>3</sub>, 298 K):  $\delta$  7.45 (td, <sup>3</sup>J<sub>HH</sub> = 7.6 Hz, <sup>5</sup>J<sub>HP</sub> = 1.7 Hz, 1 H, *p*-C<sub>6</sub>H<sub>3</sub>), 7.36-7.27 (m, 5 H, Ph), 7.20 (dd, <sup>3</sup>J<sub>HH</sub> = 8.3 Hz, <sup>3</sup>J<sub>HH</sub> = 6.6 Hz, 2 H, *p*-Xyl), 7.09 (b d, <sup>3</sup>J<sub>HH</sub> = 7.5 Hz, 4 H, *m*-Xyl), 6.99 (dd, <sup>3</sup>J<sub>HH</sub> = 7.6 Hz, <sup>4</sup>J<sub>HP</sub> = 2.5 Hz, 2 H, *m*-C<sub>6</sub>H<sub>3</sub>), 5.32 (dt, <sup>3</sup>J<sub>HH</sub> = 13.3 Hz, <sup>3</sup>J<sub>HH</sub> = 9.2 Hz, 1 H, H<sub>1</sub>), 4.29 (dd, <sup>3</sup>J<sub>HH</sub> = 13.3 Hz, <sup>3</sup>J<sub>HP</sub> = 9.1 Hz, 1 H, H<sub>4</sub>), 2.60 (b, 2 H, H<sub>2</sub>, H<sub>3</sub>), 2.18 (s, 12 H, CH<sub>3</sub> Xyl), 2.00-1.26 (m, 18 H, Cyp).

<sup>13</sup>C{<sup>1</sup>H} NMR (75 MHz, CDCl<sub>3</sub>, 298 K):  $\delta$  147.3 (b, *o*-C<sub>6</sub>H<sub>3</sub>), 142.5 (d, <sup>3</sup>J<sub>CP</sub> = 4 Hz, *ipso*-Xyl), 137.2 (s, *o*-Xyl), 136.6 (d, <sup>2</sup>J<sub>CP</sub> = 6 Hz, *ipso*-Ph), 134.8 (d, <sup>1</sup>J<sub>CP</sub> = 20 Hz, *ipso*-C<sub>6</sub>H<sub>3</sub>), 131.9 (d, <sup>3</sup>J<sub>CP</sub> = 6 Hz, *m*-C<sub>6</sub>H<sub>3</sub>), 130.0 (d, <sup>4</sup>J<sub>CP</sub> = 2 Hz, *p*-C<sub>6</sub>H<sub>3</sub>), 128.6 (d, <sup>5</sup>J<sub>CP</sub> = 2 Hz, *m*-Ph), 128.3 (d, <sup>4</sup>J<sub>CP</sub> = 3 Hz, *o*-Ph), 128.1 (d, <sup>5</sup>J<sub>CP</sub> = 2 Hz, *p*-Ph), 127.8 (s, *m*-Xyl), 127.4 (s, *p*-Xyl), 108.9 (d, <sup>2</sup>J<sub>CP</sub> = 5 Hz, C<sub>meso</sub>), 105.9 (b d, <sup>2</sup>J<sub>CP</sub> = 27 Hz C<sub>trans-P</sub>), 48.1 (s, C<sub>cis-P</sub>), 41.1 (d, <sup>2</sup>J<sub>CP</sub> = 21 Hz, CH Cyp), 32.0 (d, J<sub>CP</sub> = 7 Hz, CH<sub>2</sub> Cyp), 31.6 (d, J<sub>CP</sub> = 7 Hz, CH<sub>2</sub> Cyp), 26.2 (d, J<sub>CP</sub> = 11 Hz, CH<sub>2</sub> Cyp), 25.4 (d, J<sub>CP</sub> = 12 Hz, CH<sub>2</sub> Cyp), 22.5 (s, CH<sub>3</sub>).

<sup>31</sup>P{<sup>1</sup>H} NMR (121 MHz, CDCl<sub>3</sub>, 298 K):  $\delta$  37.9 (s).

Elemental analysis (%), calculated (found) for C<sub>41</sub>H<sub>48</sub>ClPPd: C, 69.00 (68.97); H, 6.78 (6.79).

Yield: 0.0913 g, 99%.

**II.4.6. General synthesis of cationic complexes [Pd( $\eta^3$ -C<sub>3</sub>H<sub>4</sub>R')](PR<sub>2</sub>Ar'')BAR<sup>F</sup><sub>4</sub>, R' = H (10-PR<sub>2</sub>Ar''), Ph (11-PR<sub>2</sub>Ar'').**

THF (5-15 mL) was added to a deoxygenated vessel charged with [Pd( $\eta^3$ -C<sub>3</sub>H<sub>4</sub>R)]<sub>2</sub>( $\mu$ -Cl)<sub>2</sub> (0.5 eq) and PR<sub>2</sub>Ar'' (1 eq) until complete dissolution. After stirring at room temperature for 1 h, NaBAR<sup>F</sup><sub>4</sub> (1 eq) was added and the reaction mixture stirred for a further 2 h. Solvent was then removed under vacuum and the remaining residue was extracted with CH<sub>2</sub>Cl<sub>2</sub> (for P<sup>i</sup>Pr<sub>2</sub>Ar<sup>Xyl</sup>) or a petroleum ether/CH<sub>2</sub>Cl<sub>2</sub> mixture (for PMe<sub>2</sub>Ar<sup>Dipp</sup>) and filtered. Evaporation of the solvent under reduced pressure or crystallisation (where specified) from a CH<sub>2</sub>Cl<sub>2</sub>/petroleum ether mixture rendered the sought products as yellow/pallid yellow powder or pallid yellow crystals, respectively.

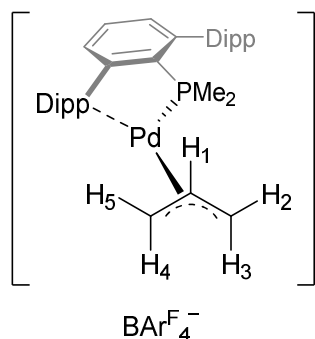
NMR resonances due to BAR<sup>F</sup><sub>4</sub><sup>-</sup>:

<sup>1</sup>H NMR (500 MHz, CD<sub>2</sub>Cl<sub>2</sub>):  $\delta$  7.74 (bm, 8 H, *o*-Ar<sup>F</sup>), 7.57 (bs, 4 H, *p*-Ar<sup>F</sup>).

<sup>13</sup>C{<sup>1</sup>H} NMR (126 MHz, CD<sub>2</sub>Cl<sub>2</sub>):  $\delta$  162.2 (q, <sup>1</sup>J<sub>CB</sub> = 50 Hz, *ipso*-Ar<sup>F</sup>), 135.3 (b s, *o*-Ar<sup>F</sup>), 129.4 (qq, <sup>2</sup>J<sub>CF</sub> = 34 Hz, <sup>4</sup>J<sub>CF</sub> = 3 Hz, *m*-Ar<sup>F</sup>), 125.1 (q, <sup>1</sup>J<sub>CF</sub> = 272 Hz, CF<sub>3</sub>), 117.9 (b m, *p*-Ar<sup>F</sup>).

<sup>1</sup>H NMR (500 MHz, CDCl<sub>3</sub>):  $\delta$  7.68 (bm, 8 H, *o*-Ar<sup>F</sup>), 7.51 (bs, 4 H, *p*-Ar<sup>F</sup>).

<sup>13</sup>C{<sup>1</sup>H} NMR (126 MHz, CDCl<sub>3</sub>):  $\delta$  161.9 (q, <sup>1</sup>J<sub>CB</sub> = 50 Hz, *ipso*-Ar<sup>F</sup>), 135.0 (b s, *o*-Ar<sup>F</sup>), 129.1 (qq, <sup>2</sup>J<sub>CF</sub> = 32 Hz, <sup>4</sup>J<sub>CF</sub> = 3 Hz, *m*-Ar<sup>F</sup>), 124.7 (q, <sup>1</sup>J<sub>CF</sub> = 273 Hz, CF<sub>3</sub>), 117.6 (b m, *p*-Ar<sup>F</sup>).

II.4.6.1.  $[\text{Pd}(\eta^3\text{-C}_3\text{H}_5)(\text{PMe}_2\text{Ar}^{\text{Dipp}})]\text{BAr}^{\text{F}_4}$  (10-L2).

$^1\text{H}$  NMR (300 MHz,  $\text{CDCl}_3$ , 298 K):  $\delta$  7.73 (dd,  $^3J_{\text{HH}} = 7.8$  Hz,  $^4J_{\text{HH}} = 1.0$  Hz, 1 H, *m*-Dipp), 7.62-7.56 (m, 2 H, *p*- $\text{C}_6\text{H}_3$ , Dipp), *ca.* 7.48 (1 H, Dipp), 7.39-7.28 (m, 4 H, *m*- $\text{C}_6\text{H}_3$ , Dipp), 6.79 (ddd,  $^3J_{\text{HH}} = 7.8$  Hz,  $^4J_{\text{HP}} = 3.1$  Hz,  $^4J_{\text{HH}} = 1.2$  Hz, *m*- $\text{C}_6\text{H}_3$ ), 5.46-5.32 (m, 1 H,  $\text{H}_1$ ), 3.64 (dd,  $^3J_{\text{HH}} = 14.2$  Hz,  $^3J_{\text{HP}} = 9.8$  Hz, 1 H,  $\text{H}_4$ ), 3.18 (d,  $^3J_{\text{HH}} = 6.5$  Hz, 1 H,  $\text{H}_2$ ), 2.48-2.21 (m, 6 H,  $\text{CH}^i\text{Pr}$ ,

$\text{H}_5$ ,  $\text{H}_3$ ), 1.44-1.25 (m, 18 H,  $\text{P-CH}_3$ ,  $\text{CH}_3^i\text{Pr}$ ), 1.09-0.98 (m, 12 H,  $\text{CH}_3^i\text{Pr}$ ).

$^{13}\text{C}\{^1\text{H}\}$  NMR (75 MHz,  $\text{CD}_2\text{Cl}_2$ , 298 K):  $\delta$  147.0 (s, *o*-Dipp), 146.5 (s, *o*-Dipp), 146.0 (s, *o*- $\text{C}_6\text{H}_3$ ), 145.5 (s, *o*-Dipp), 145.1 (d,  $^2J_{\text{CP}} = 29$  Hz, *o*- $\text{C}_6\text{H}_3$ ), *ca.* 135.0 (*ipso*-Dipp), 133.7 (d,  $^3J_{\text{CP}} = 5$  Hz, *m*- $\text{C}_6\text{H}_3$ ), 132.3 (d,  $^1J_{\text{CP}} = 46$  Hz, *ipso*- $\text{C}_6\text{H}_3$ ), 132.1 (d,  $^4J_{\text{CP}} = 2$  Hz, *p*- $\text{C}_6\text{H}_3$ ), 131.1 (d,  $^3J_{\text{CP}} = 14$  Hz, *m*- $\text{C}_6\text{H}_3$ ), 130.5 (s, *p*-Dipp), 127.8 (s, *m*-Dipp), 123.4 (s, *m*-Dipp), 122.8 (d,  $^2J_{\text{CP}} = 5$  Hz, *ipso*-Dipp), 121.2 (d,  $^3J_{\text{CP}} = 7$  Hz,  $\text{C}_{\text{meso}}$ ), 102.6 (d,  $^2J_{\text{CP}} = 29$  Hz,  $\text{C}_{\text{trans-P}}$ ), 53.7 (d,  $^2J_{\text{CP}} = 4$  Hz,  $\text{C}_{\text{cis-P}}$ ), 32.9 (s,  $\text{CH}^i\text{Pr}$ ), 31.5 (s,  $\text{CH}^i\text{Pr}$ ), 26.3 (s,  $\text{CH}_3^i\text{Pr}$ ), 25.4 (s,  $\text{CH}_3^i\text{Pr}$ ), 25.1 (s,  $\text{CH}_3^i\text{Pr}$ ), 24.1 (s,  $\text{CH}_3^i\text{Pr}$ ), 21.5 (s,  $\text{CH}_3^i\text{Pr}$ ), 21.5 (s,  $\text{CH}_3^i\text{Pr}$ ), 16.5 (d,  $^1J_{\text{CP}} = 30$  Hz,  $\text{P-CH}_3$ ), 15.5 (d,  $^1J_{\text{CP}} = 30$  Hz,  $\text{P-CH}_3$ ).

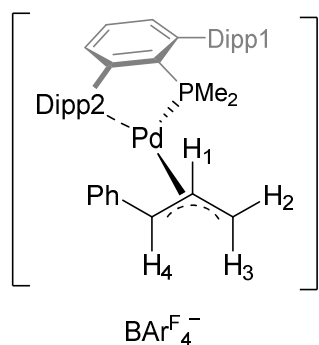
$^{31}\text{P}\{^1\text{H}\}$  NMR (121 MHz,  $\text{CDCl}_3$ , 298 K):  $\delta$  14.5 (s).

Elemental analysis (%), calculated (found) for  $\text{C}_{67}\text{H}_{70}\text{BF}_4\text{PPd}$ : C, 54.77 (54.49); H, 4.12 (4.27).

Yield: 0.1139 g, 78%.

### II.4.6.2. [Pd( $\eta^3$ -C<sub>3</sub>H<sub>4</sub>Ph)(PMe<sub>2</sub>Ar<sup>Dipp2</sup>)]BAR<sup>F</sup><sub>4</sub> (11·L2).

#### MAJOR ISOMER



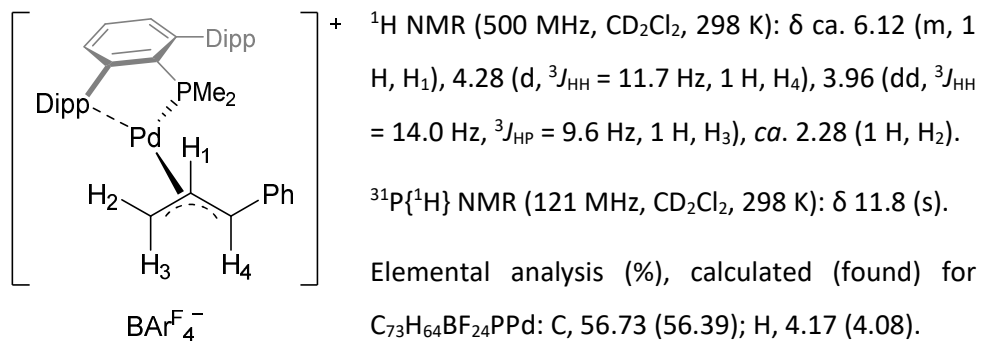
<sup>1</sup>H NMR (300 MHz, CD<sub>2</sub>Cl<sub>2</sub>, 298 K):  $\delta$  ca. 7.63-7.20 (m, 8 H, aromatic), 7.01 (d,  $J_{\text{HH}} = 7.6$  Hz, 1 H, *m*-Dipp2), 6.89 (d,  $J_{\text{HH}} = 7.4$  Hz, 2 H, aromatic), 6.83 (dd,  $^3J_{\text{HH}} = 7.5$  Hz,  $^4J_{\text{HP}} = 2.0$  Hz, 1 H, *m*-C<sub>6</sub>H<sub>3</sub>), 6.53 (d,  $J_{\text{HH}} = 7.6$  Hz, 1 H, *m*-Dipp2), 6.13 (t,  $J_{\text{HH}} = 7.6$  Hz, 1 H, *p*-Dipp2), 5.60 (ddd,  $^3J_{\text{HH}} = 14.0$  Hz,  $^3J_{\text{HH}} = 12.0$  Hz,  $^3J_{\text{HH}} = 6.9$  Hz, 1 H, H<sub>1</sub>), 4.48 (dd,  $^3J_{\text{HH}} = 14.0$  Hz,  $^3J_{\text{HP}} = 10.4$  Hz, 1 H, H<sub>4</sub>), 3.47 (dd,  $^3J_{\text{HH}} = 6.9$ ,  $^2J_{\text{HH}} = 2.0$  Hz, 1 H, H<sub>2</sub>), 2.69 (b d,  $^3J_{\text{HH}} = 11.1$  Hz, 1 H, H<sub>3</sub>), 2.52-2.10 (m, 4 H, CH <sup>*i*</sup>Pr), 1.56 (d,  $^2J_{\text{HP}} = 11.0$  Hz, 3 H, P-CH<sub>3</sub>), 1.50 (d,  $^2J_{\text{HP}} = 11.1$  Hz, 3 H, P-CH<sub>3</sub>), 1.34-1.29 (m, 9 H, 2 CH<sub>3</sub> <sup>*i*</sup>Pr1, CH<sub>3</sub> <sup>*i*</sup>Pr2), 1.17 (d,  $^3J_{\text{HH}} = 6.9$  Hz, 3 H, CH<sub>3</sub> <sup>*i*</sup>Pr2), 1.06-1.01 (m, 9 H, 2 CH<sub>3</sub> <sup>*i*</sup>Pr1, CH<sub>3</sub> <sup>*i*</sup>Pr2), 0.88 (d,  $^3J_{\text{HH}} = 6.9$  Hz, 3 H, CH<sub>3</sub> <sup>*i*</sup>Pr2).

<sup>13</sup>C{<sup>1</sup>H} NMR (75 MHz, CDCl<sub>3</sub>, 298 K):  $\delta$  147.0 (s, *o*-Dipp1), 145.9 (s, *o*-C<sub>6</sub>H<sub>3</sub>), 145.8 (d,  $^2J_{\text{CP}} = 28$  Hz, *o*-C<sub>6</sub>H<sub>3</sub>), 145.1 (s, *o*-Dipp2), 143.6 (s, *o*-Dipp2), ca. 135.0 (*ipso*-Dipp1), 133.7 (s, *m*-C<sub>6</sub>H<sub>3</sub>), 133.1 (d,  $^1J_{\text{CP}} = 46$  Hz, *ipso*-C<sub>6</sub>H<sub>3</sub>), 132.1 (d,  $^4J_{\text{CP}} = 2$  Hz, *p*-C<sub>6</sub>H<sub>3</sub>), 131.2-130.3 (m, CH aromatic, *ipso*-Ph), 129.7 (s, CH aromatic), 128.5 (s, *p*-Dipp2), 124.5 (s, *m*-Dipp2), 124.2 (s, *m*-Dipp2), 123.4 (*m*-Dipp1), 121.7 (s, *ipso*-Dipp2), 114.1 (d,  $^2J_{\text{CP}} = 24$  Hz, C<sub>*trans-p*</sub>), 108.7 (d,  $^3J_{\text{CP}} = 8$  Hz, C<sub>*meso*</sub>), 54.0 (d,  $^2J_{\text{CP}} = 4$  Hz, C<sub>*cis-p*</sub>), 32.6 (s, CH <sup>*i*</sup>Pr2), 32.3 (s, CH <sup>*i*</sup>Pr2), 31.5 (s, CH <sup>*i*</sup>Pr1), 31.4 (s, CH <sup>*i*</sup>Pr1), 26.4 (s, CH<sub>3</sub> <sup>*i*</sup>Pr1), 26.3 (s, CH<sub>3</sub> <sup>*i*</sup>Pr1), 25.8 (s, CH<sub>3</sub> <sup>*i*</sup>Pr2), 24.8 (s, CH<sub>3</sub> <sup>*i*</sup>Pr2), 24.1 (s, CH<sub>3</sub> <sup>*i*</sup>Pr2), 24.0 (s, CH<sub>3</sub> <sup>*i*</sup>Pr2), 21.5 (s, CH<sub>3</sub> <sup>*i*</sup>Pr1), 21.5 (s, CH<sub>3</sub> <sup>*i*</sup>Pr1), 16.8 (d,  $^1J_{\text{CP}} = 30$  Hz, P-CH<sub>3</sub>), 16.1 (d,  $^1J_{\text{CP}} = 30$  Hz, P-CH<sub>3</sub>).

<sup>31</sup>P{<sup>1</sup>H} NMR (121 MHz, CD<sub>2</sub>Cl<sub>2</sub>, 298 K):  $\delta$  21.4 (s).

Chapter II

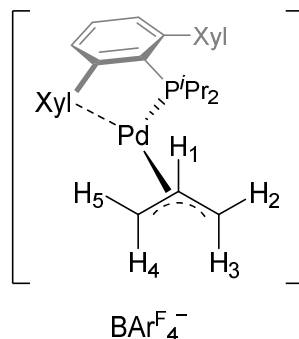
MINOR ISOMER (selected signals) (13% by  $^1\text{H}$  NMR)



Yield: 0.0758 g, 49% (after recrystallisation).



### II.4.6.3. $[\text{Pd}(\eta^3\text{-C}_3\text{H}_5)(\text{P}^i\text{Pr}_2\text{Ar}^{\text{Xyl}_2})]\text{BAr}^{\text{F}_4}$ (10·L4).



$^1\text{H}$  NMR (300 MHz,  $\text{CDCl}_3$ , 298 K):  $\delta$  7.60-7.54 (m, 2 H, aromatic), 7.43 (b d,  $^3J_{\text{HH}} = 7.6$  Hz, 1 H, aromatic), 7.32-7.15 (m, 5 H, aromatic), 6.63 (ddd,  $^3J_{\text{HH}} = 7.7$  Hz,  $^3J_{\text{HP}} = 2.7$  Hz,  $^4J_{\text{HH}} = 1.3$  Hz, 1 H, *m*- $\text{C}_6\text{H}_3$ ), 5.34 (dddd,  $^3J_{\text{HH}} = 14.3$  Hz,  $^3J_{\text{HH}} = 12.6$  Hz,  $^3J_{\text{HH}} = 7.9$  Hz,  $^3J_{\text{HH}} = 6.8$  Hz, 1 H,  $\text{H}_1$ ), 3.98 (dt,  $^3J_{\text{HH}} = 6.6$  Hz,  $^2J_{\text{HH}} = ^4J_{\text{HH}} = 2.2$  Hz, 1 H,  $\text{H}_2$ ), 3.69 (dd,  $^3J_{\text{HH}} = 14.1$  Hz,  $^3J_{\text{HP}} = 9.3$  Hz, 1 H,  $\text{H}_4$ ), 2.64-2.35 (m, 6 H,  $\text{CH}^i\text{Pr}$ ,  $\text{H}_3$ ,  $\text{H}_5$ ), 2.23 (s, 3 H,  $\text{CH}_3$  Xyl), 2.08 (s, 3 H,  $\text{CH}_3$  Xyl), 2.00 (s, 3 H,  $\text{CH}_3$  Xyl), 1.96 (s, 3 H,  $\text{CH}_3$  Xyl), 1.07-0.93 (m, 6 H,  $\text{CH}_3^i\text{Pr}$ ), 0.83 (dd,  $^3J_{\text{HP}} = 17.0$  Hz,  $^3J_{\text{HH}} = 6.8$  Hz, 3 H,  $\text{CH}_3^i\text{Pr}$ ), 0.61 (dd,  $^3J_{\text{HP}} = 15.0$  Hz,  $^3J_{\text{HH}} = 6.9$  Hz, 3 H,  $\text{CH}_3^i\text{Pr}$ ).

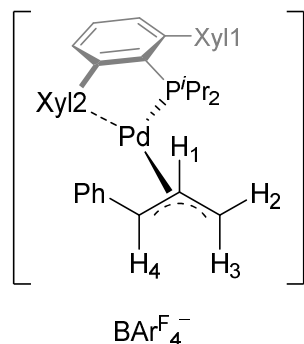
$^{13}\text{C}\{^1\text{H}\}$  NMR (100 MHz,  $\text{CDCl}_3$ , 298 K):  $\delta$  147.6 (d,  $^2J_{\text{CP}} = 25$  Hz, *o*- $\text{C}_6\text{H}_3$ ), 147.1 (s, *o*- $\text{C}_6\text{H}_3$ ), 139.5 (d,  $^3J_{\text{CP}} = 1$  Hz, *ipso*-Xyl), 138.7 (*o*-Xyl), 136.7 (*o*-Xyl), 136.3 (s, *o*-Xyl), 135.9 (s, *o*-Xyl), 134.4 (d,  $^1J_{\text{CP}} = 34$  Hz, *ipso*- $\text{C}_6\text{H}_3$ ), 133.4 (d,  $^4J_{\text{CP}} = 2$  Hz, *p*- $\text{C}_6\text{H}_3$ ), 133.2 (d,  $^3J_{\text{CP}} = 5$  Hz, *m*- $\text{C}_6\text{H}_3$ ), 132.2 (s, CH Xyl), 132.0 (CH Xyl), 130.8 (d,  $^3J_{\text{CP}} = 13$  Hz, *m*- $\text{C}_6\text{H}_3$ ), 130.3 (s, CH Xyl), 129.2 (s, CH Xyl), 129.0 (s, CH Xyl), 128.5 (s, CH Xyl), 123.9 (d,  $^3J_{\text{CP}} = 5$  Hz, *ipso*-Xyl), 119.2 (d,  $^3J_{\text{CP}} = 6$  Hz,  $\text{C}_{\text{meso}}$ ), 106.3 (d,  $^2J_{\text{CP}} = 27$  Hz,  $\text{C}_{\text{trans-P}}$ ), 54.4 (s,  $\text{C}_{\text{cis-P}}$ ), 27.4 (d,  $^1J_{\text{CP}} = 22$  Hz,  $\text{CH}^i\text{Pr}$ ), 26.7 (d,  $^1J_{\text{CP}} = 22$  Hz,  $\text{CH}^i\text{Pr}$ ), 25.7 (d,  $^2J_{\text{CP}} = 9$  Hz,  $\text{CH}_3^i\text{Pr}$ ), 24.2 (d,  $^2J_{\text{CP}} = 7$  Hz,  $\text{CH}_3^i\text{Pr}$ ), 22.5 (d,  $^2J_{\text{CP}} = 7$  Hz,  $\text{CH}_3^i\text{Pr}$ ), 21.2 (s,  $\text{CH}_3$  Xyl), 19.5 (s,  $\text{CH}_3$  Xyl), 19.1 (s,  $\text{CH}_3$  Xyl).

$^{31}\text{P}\{^1\text{H}\}$  NMR (121 MHz,  $\text{CDCl}_3$ , 298 K):  $\delta$  73.1 (s).

Elemental analysis (%), calculated (found) for  $\text{C}_{63}\text{H}_{52}\text{BF}_{24}\text{PPd}$ : C, 53.54 (53.36); H, 3.71 (3.97).

Yield: 0.2444 g, 86%.

#### II.4.6.4. [Pd( $\eta^3$ -C<sub>3</sub>H<sub>4</sub>Ph)(P<sup>i</sup>Pr<sub>2</sub>Ar<sup>Xyl2</sup>)]BAR<sup>F</sup><sub>4</sub> (11·L4).



+ <sup>1</sup>H NMR (300 MHz, CDCl<sub>3</sub>, 298 K):  $\delta$  ca. 7.60 (*p*-Ph, *p*-C<sub>6</sub>H<sub>3</sub>), 7.52 (t, <sup>3</sup>J<sub>HH</sub> = 7.6 Hz, 2 H, *m*-Ph), 7.31 (t, 1 H, <sup>3</sup>J<sub>HH</sub> = 7.6 Hz, *p*-Xyl1), 7.26-7.22 (m, 2 H, *m*-Xyl1, *m*-C<sub>6</sub>H<sub>3</sub>), 7.20 (d, 1 H, <sup>3</sup>J<sub>HH</sub> = 7.4 Hz, *m*-Xyl1), 7.00-6.98 (m, 2 H, *o*-Ph), 6.93 (d, <sup>3</sup>J<sub>HH</sub> = 7.5 Hz, 1 H, *m*-Xyl2), 6.68 (ddd, <sup>3</sup>J<sub>HH</sub> = 7.8 Hz, <sup>4</sup>J<sub>HP</sub> = 2.7 Hz, <sup>4</sup>J<sub>HH</sub> = 1.3 Hz, 1 H, *m*-C<sub>6</sub>H<sub>3</sub>), 6.35 (d, <sup>3</sup>J<sub>HH</sub> = 7.6 Hz, 1 H, *m*-Xyl2), 6.09 (t, <sup>3</sup>J<sub>HH</sub> = 7.6 Hz, 1 H, *p*-Xyl2), 5.49 (ddd, <sup>3</sup>J<sub>HH</sub> = 13.7 Hz, <sup>3</sup>J<sub>HH</sub> = 12.2 Hz, <sup>3</sup>J<sub>HH</sub> = 6.7 Hz, H<sub>1</sub>), 4.51 (dd, <sup>3</sup>J<sub>HH</sub> = 13.8 Hz, <sup>3</sup>J<sub>HP</sub> = 10.0 Hz, 1 H, H<sub>4</sub>), 4.27 (dd, <sup>3</sup>J<sub>HH</sub> = 6.7 Hz, <sup>2</sup>J<sub>HH</sub> = 2.1 Hz, H<sub>2</sub>), 2.81-2.71 (m, 2 H, H<sub>3</sub>, CH<sup>*i*</sup>Pr), 2.59 (dsept, <sup>2</sup>J<sub>HP</sub> = 12.7 Hz, <sup>3</sup>J<sub>HH</sub> = 7.1 Hz, 1 H, CH<sup>*i*</sup>Pr), 2.20 (s, 3 H, CH<sub>3</sub> Xyl2), 2.15 (s, 3 H, CH<sub>3</sub> Xyl1), 2.00 (s, 3 H, CH<sub>3</sub> Xyl1), 1.86 (s, 3 H, CH<sub>3</sub> Xyl2), 1.14 (dd, <sup>3</sup>J<sub>HP</sub> = 13.8 Hz, <sup>3</sup>J<sub>HH</sub> = 7.0 Hz, 3 H, CH<sub>3</sub><sup>*i*</sup>Pr), 1.10 (dd, <sup>3</sup>J<sub>HP</sub> = 14.5 Hz, <sup>3</sup>J<sub>HH</sub> = 6.9 Hz, 3 H, CH<sub>3</sub><sup>*i*</sup>Pr), 1.00 (dd, <sup>3</sup>J<sub>HP</sub> = 16.9 Hz, <sup>3</sup>J<sub>HH</sub> = 6.8 Hz, 3 H, CH<sub>3</sub><sup>*i*</sup>Pr), 0.75 (dd, <sup>3</sup>J<sub>HP</sub> = 14.9 Hz, <sup>3</sup>J<sub>HH</sub> = 6.9 Hz, 3 H, CH<sub>3</sub><sup>*i*</sup>Pr).

<sup>13</sup>C{<sup>1</sup>H} NMR (126 MHz, CD<sub>2</sub>Cl<sub>2</sub>, 298 K):  $\delta$  148.8 (d, <sup>2</sup>J<sub>CP</sub> = 24 Hz, *o*-C<sub>6</sub>H<sub>3</sub>-Xyl2), 147.1 (s, *o*-C<sub>6</sub>H<sub>3</sub>-Xyl1), 140.0 (d, <sup>3</sup>J<sub>CP</sub> = 1 Hz, *ipso*-Xyl1), 137.4 (s, *o*-Xyl1), 136.9 (s, *o*-Xyl2), 136.9 (s, *o*-Xyl1), 135.6 (d, <sup>1</sup>J<sub>CP</sub> = 34 Hz, *ipso*-C<sub>6</sub>H<sub>3</sub>), 134.9 (s, *o*-Xyl2), 133.6 (m, *p*-C<sub>6</sub>H<sub>3</sub>, *m*-C<sub>6</sub>H<sub>3</sub>), 132.4 (d, <sup>3</sup>J<sub>CP</sub> = 7 Hz, *ipso*-Ph), 131.2-131.1 (m, *m*-C<sub>6</sub>H<sub>3</sub>, *p*-Ph), 129.9 (d, <sup>4</sup>J<sub>CP</sub> = 2 Hz, *m*-Ph), 129.5 (s, *m*-Xyl2), 129.3 (m, *p*-Xyl1, *m*-Xyl2), 128.8 (s, *m*-Xyl1), 128.7 (s, *m*-Xyl1), 128.4 (s, *p*-Xyl2), 123.3 (d, <sup>3</sup>J<sub>CP</sub> = 5 Hz, *ipso*-Xyl2), 117.2 (d, <sup>3</sup>J<sub>CP</sub> = 22 Hz, C<sub>trans</sub>-P), 108.0 (d, <sup>2</sup>J<sub>CP</sub> = 7 Hz, C<sub>meso</sub>), 49.0 (d, <sup>2</sup>J<sub>CP</sub> = 3 Hz, C<sub>cis</sub>-P), 28.6 (d, <sup>1</sup>J<sub>CP</sub> = 21 Hz, CH<sup>*i*</sup>Pr), 28.1 (d, <sup>1</sup>J<sub>CP</sub> = 22 Hz, CH<sup>*i*</sup>Pr), 26.1 (d, <sup>2</sup>J<sub>CP</sub> = 9 Hz, CH<sub>3</sub><sup>*i*</sup>Pr), 24.4 (d, <sup>2</sup>J<sub>CP</sub> = 7 Hz, CH<sub>3</sub><sup>*i*</sup>Pr), 22.9 (s, CH<sub>3</sub> Xyl1), 22.4 (s, CH<sub>3</sub> Xyl1), 21.5 (s, CH<sub>3</sub> Xyl2), 21.4 (s, CH<sub>3</sub> Xyl2), 19.8 (d, <sup>2</sup>J<sub>CP</sub> = 2 Hz, CH<sub>3</sub><sup>*i*</sup>Pr), 19.6 (d, <sup>2</sup>J<sub>CP</sub> = 1.4 Hz, CH<sub>3</sub><sup>*i*</sup>Pr).

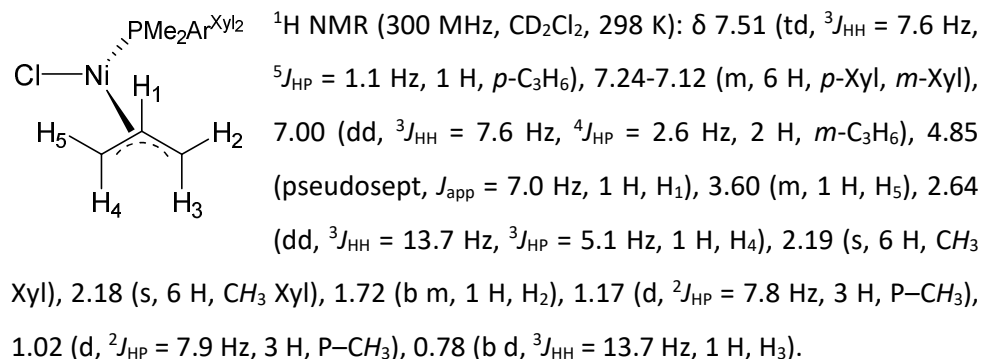
<sup>31</sup>P{<sup>1</sup>H} NMR (121 MHz, CD<sub>2</sub>Cl<sub>2</sub>, 298 K):  $\delta$  79.8 (s).

Elemental analysis (%), calculated (found) for C<sub>69</sub>H<sub>56</sub>BF<sub>24</sub>PPd: C, 55.64 (55.22); H, 3.79 (3.77).

Yield: 0.2868 g, 74%.

**II.4.7. General synthesis of complexes  $\text{NiCl}(\eta^3\text{-C}_3\text{H}_4\text{R}')(\text{PMe}_2\text{Ar}'')$ ,  $\text{R}' = \text{H}$  (**13**· $\text{PMe}_2\text{Ar}''$ ), Me (**14**· $\text{PMe}_2\text{Ar}''$ ).**

To a suspension of  $\text{Ni}(\text{cod})_2$  (1 eq) in THF (*ca.* 3 mL per 0.1 mmol), cooled to  $-60\text{ }^\circ\text{C}$ , allyl chloride (1-1.2 eq) was added. The mixture was warmed up to  $-20\text{ }^\circ\text{C}$  and stirred for 1 h at this temperature, after which  $\text{PMe}_2\text{Ar}''$  (1 eq) was added. The mixture was stirred at room temperature for 1 h and then the solvent was evaporated under vacuum. The resulting residue was extracted with  $\text{CH}_2\text{Cl}_2$  (for  $\text{PMe}_2\text{Ar}^{\text{Xyl}_2}$ ) or petroleum ether (for  $\text{PMe}_2\text{Ar}^{\text{Dipp}_2}$ ) and filtered. Crystallisation from  $\text{CH}_2\text{Cl}_2$ /petroleum ether mixtures or from petroleum ether, respectively, rendered the sought products as reddish orange crystals.

II.4.7.1.  $[\text{NiCl}(\eta^3\text{-C}_3\text{H}_5)(\text{PMe}_2\text{Ar}^{\text{Xyl}_2})]$  (13·L1).

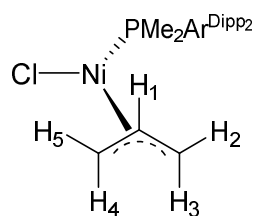
$^{13}\text{C}\{^1\text{H}\}$  NMR (75 MHz,  $\text{CD}_2\text{Cl}_2$ , 298 K):  $\delta$  146.5 (d,  $^2J_{\text{CP}} = 10$  Hz, *o*- $\text{C}_3\text{H}_6$ ), 142.4 (d,  $^3J_{\text{CP}} = 4$  Hz, *ipso*-Xyl), 137.3 (s, *o*-Xyl), 131.0 (d,  $^3J_{\text{CP}} = 7$  Hz, *m*- $\text{C}_3\text{H}_6$ ), 130.9 (d,  $^4J_{\text{CP}} = 2$  Hz, *p*- $\text{C}_3\text{H}_6$ ), 129.6 (d,  $^1J_{\text{CP}} = 29$  Hz, *ipso*- $\text{C}_6\text{H}_3$ ), 128.2 (s, *p*-Xyl), 128.0 (s, *m*-Xyl), 128.0 (s, *m*-Xyl), 111.0 (s,  $\text{C}_{\text{meso}}$ ), 71.5 (d,  $^2J_{\text{CP}} = 22$  Hz,  $\text{C}_{\text{trans-P}}$ ), 46.1 (d,  $^2J_{\text{CP}} = 6$  Hz,  $\text{C}_{\text{cis-P}}$ ), 22.2 (s,  $\text{CH}_3$  Xyl), 22.2 (s,  $\text{CH}_3$  Xyl), 16.3 (d,  $^1J_{\text{CP}} = 27$  Hz,  $\text{P-CH}_3$ ), 16.1 (d,  $^1J_{\text{CP}} = 28$  Hz,  $\text{P-CH}_3$ ).

$^{31}\text{P}\{^1\text{H}\}$  NMR (121 MHz,  $\text{CD}_2\text{Cl}_2$ , 298 K):  $\delta$  -9.1 (s).

Elemental analysis (%), calculated (found) for  $\text{C}_{27}\text{H}_{32}\text{ClNiP}$ : C, 67.33 (67.27); H, 6.70 (6.75).

Yield: 0.2188 g, 63%.

### II.4.7.2. $[\text{NiCl}(\eta^3\text{-C}_3\text{H}_5)(\text{PMe}_2\text{Ar}^{\text{Dipp}_2})]$ (13·L2).



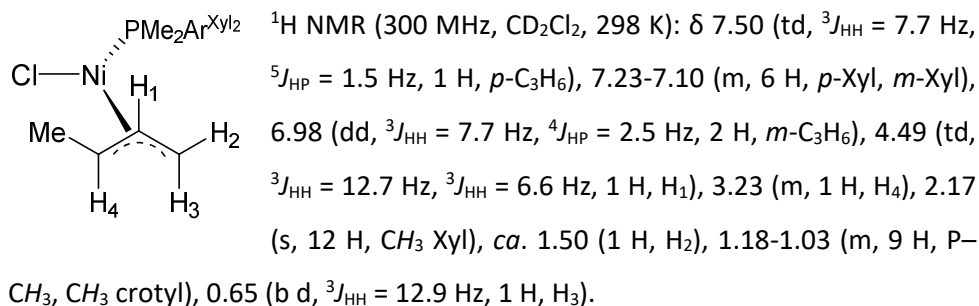
$^1\text{H}$  NMR (300 MHz,  $\text{C}_6\text{D}_6$ , 298 K):  $\delta$  7.31-7.01 (m, 9 H, aromatic), 4.55 (pseudosept,  $J_{\text{app}} = 6.8$  Hz, 1 H,  $\text{H}_1$ ), 3.82 (m, 1 H,  $\text{H}_5$ ), 3.04-2.84 (m, 4 H,  $\text{CH}^i\text{Pr}$ ), 2.76 (dd,  $^3J_{\text{HH}} = 13.6$  Hz,  $^3J_{\text{HP}} = 5.6$  Hz, 1 H,  $\text{H}_4$ ), 1.52-1.45 (m, 13 H,  $\text{H}_2$ ,  $\text{CH}_3^i\text{Pr}$ ), 1.29 (d,  $^2J_{\text{HP}} = 7.8$  Hz, 3 H,  $\text{P-CH}_3$ ), 1.07 (d,  $^2J_{\text{HP}} = 7.9$  Hz, 3 H,  $\text{P-CH}_3$ ), 0.97 (d,  $^3J_{\text{HP}} = 6.7$  Hz, 12 H,  $\text{CH}_3^i\text{Pr}$ ), 0.65 (b d,  $^3J_{\text{HH}} = 13.6$  Hz, 1 H,  $\text{H}_3$ ).

$^{13}\text{C}\{^1\text{H}\}$  NMR (75 MHz,  $\text{C}_6\text{D}_6$ , 298 K):  $\delta$  147.6 (s, *o*-Dipp), 144.6 (d,  $^2J_{\text{CP}} = 9$  Hz, *o*- $\text{C}_3\text{H}_6$ ), 140.3 (s, *ipso*-Dipp), 133.2 (d,  $^3J_{\text{CP}} = 5$  Hz, *m*- $\text{C}_3\text{H}_6$ ), 131.5 (d,  $^1J_{\text{CP}} = 29$  Hz, *ipso*- $\text{C}_6\text{H}_3$ ), 129.2 (s, *p*-Dipp), 127.3 (s, *p*- $\text{C}_3\text{H}_6$ ), 123.4 (s, *m*-Dipp), 123.3 (s, *m*-Dipp), 110.8 (s,  $\text{C}_{\text{meso}}$ ), 70.8 (d,  $^2J_{\text{CP}} = 22$  Hz,  $\text{C}_{\text{trans-p}}$ ), 46.2 (d,  $^2J_{\text{CP}} = 5$  Hz,  $\text{C}_{\text{cis-p}}$ ), 31.3 (s,  $\text{CH}^i\text{Pr}$ ), 31.3 (s,  $\text{CH}^i\text{Pr}$ ), 26.3 (s,  $\text{CH}_3^i\text{Pr}$ ), 23.5 (s,  $\text{CH}_3^i\text{Pr}$ ), 23.1 (s,  $\text{CH}_3^i\text{Pr}$ ), 17.1 (d,  $^1J_{\text{CP}} = 27$  Hz,  $\text{P-CH}_3$ ), 16.9 (d,  $^1J_{\text{CP}} = 26$  Hz,  $\text{P-CH}_3$ ).

$^{31}\text{P}\{^1\text{H}\}$  NMR (121 MHz,  $\text{C}_6\text{D}_6$ , 298 K):  $\delta$  -7.8 (s).

Elemental analysis (%), calculated (found) for  $\text{C}_{32}\text{H}_{48}\text{ClNiP}$ : C, 70.79 (70.50); H, 8.15 (8.30).

Yield: 0.60 g, 65%.

**II.4.7.3. [NiCl( $\eta^3$ -C<sub>3</sub>H<sub>4</sub>Me)(PMe<sub>2</sub>Ar<sup>Xyl2</sup>)] (14·L1).**


<sup>13</sup>C{<sup>1</sup>H} NMR (75 MHz, CD<sub>2</sub>Cl<sub>2</sub>, 298 K):  $\delta$  146.4 (d, <sup>2</sup>J<sub>CP</sub> = 9 Hz, *o*-C<sub>3</sub>H<sub>6</sub>), 142.5 (d, <sup>3</sup>J<sub>CP</sub> = 4 Hz, *ipso*-Xyl), 137.3 (s, *o*-Xyl), 137.3 (s, *o*-Xyl), 131.0 (d, <sup>3</sup>J<sub>CP</sub> = 6 Hz, *m*-C<sub>3</sub>H<sub>6</sub>), 130.8 (s, *p*-C<sub>3</sub>H<sub>6</sub>), 130.0 (d, <sup>1</sup>J<sub>CP</sub> = 29 Hz, *ipso*-C<sub>6</sub>H<sub>3</sub>), 128.2 (s, *p*-Xyl), 127.9 (s, *m*-Xyl), 111.1 (s, C<sub>meso</sub>), 87.1 (d, <sup>2</sup>J<sub>CP</sub> = 19 Hz, C<sub>trans-P</sub>), 41.2 (d, <sup>2</sup>J<sub>CP</sub> = 5 Hz, C<sub>cis-P</sub>), 22.2 (s, CH<sub>3</sub> Xyl), 17.3 (d, <sup>3</sup>J<sub>CP</sub> = 2 Hz, CH<sub>3</sub> crotyl), 16.5 (d, <sup>1</sup>J<sub>CP</sub> = 27 Hz, P-CH<sub>3</sub>), 16.4 (d, <sup>1</sup>J<sub>CP</sub> = 27 Hz, P-CH<sub>3</sub>).

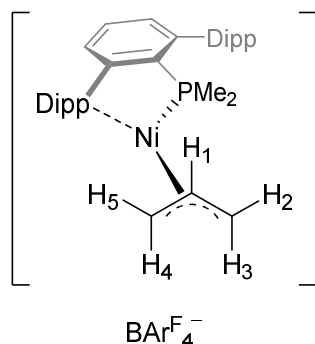
<sup>31</sup>P{<sup>1</sup>H} NMR (121 MHz, CD<sub>2</sub>Cl<sub>2</sub>, 298 K):  $\delta$  -7.1 (s).

Elemental analysis (%), calculated (found) for C<sub>28</sub>H<sub>34</sub>ClNiP: C, 67.85 (67.60); H, 6.91 (6.81).

Yield: 0.0795 g, 53%.

**II.4.8. General synthesis of complexes  $[\text{Ni}(\eta^3\text{-C}_3\text{H}_5)(\text{PR}_2\text{Ar}'')] \text{BAR}^{\text{F}}_4$  ( $15 \cdot \text{PR}_2\text{Ar}''$ ).**

To a suspension of  $\text{Ni}(\text{cod})_2$  (1-1.2 eq) in THF or  $\text{CH}_2\text{Cl}_2$  (*ca.* 3 mL per 0.1 mmol), cooled to  $-60$  °C, allyl chloride (1-2 eq) was added. The mixture was warmed up to  $0$  °C and stirred for 30 min at this temperature, after which  $\text{PR}_2\text{Ar}''$  (1 eq) was added. The mixture was stirred at room temperature for an additional hour and, if the solvent was THF, dried under vacuum and the residue dissolved in  $\text{CH}_2\text{Cl}_2$ .  $\text{NaBAR}^{\text{F}}_4$  (1 eq) was then added and the resulting mixture stirred for a further 3-18 h. Volatiles were removed under vacuum, the remaining residue was extracted in a pentane/ $\text{CH}_2\text{Cl}_2$  mixture and filtered. Evaporation of the solvents or, when specified, crystallisation at  $-20$  °C rendered the sought products as an orange powder or reddish orange crystals, respectively.

II.4.8.1.  $[\text{Ni}(\eta^3\text{-C}_3\text{H}_5)(\text{PMe}_2\text{Ar}^{\text{Dipp}})_2]\text{BAr}^{\text{F}}_4$  (15·L2).

$^1\text{H}$  NMR (300 MHz,  $\text{CD}_2\text{Cl}_2$ , 298 K):  $\delta$  *ca.* 7.75 (2 H, *m*-Dipp), 7.60 (td,  $^3J_{\text{HH}} = 7.7$  Hz,  $^5J_{\text{HP}} = 2.3$  Hz, 1 H, *p*- $\text{C}_6\text{H}_6$ ), 7.52-7.43 (m, 2 H, *p*-Dipp), 7.37 (ddd,  $^3J_{\text{HH}} = 7.6$ ,  $^4J_{\text{HP}} = 2.4$  Hz,  $^4J_{\text{HH}} = 1.2$  Hz, *m*- $\text{C}_6\text{H}_3$ ), 7.32 (d,  $^3J_{\text{HH}} = 7.8$  Hz, 2 H, *m*-Dipp), 6.79 (ddd,  $^3J_{\text{HH}} = 7.7$ ,  $^4J_{\text{HP}} = 2.8$  Hz,  $^4J_{\text{HH}} = 1.2$  Hz, 1 H, *m*- $\text{C}_6\text{H}_3$ ), *ca.* 5.33 (1 H,  $\text{H}_1$ ), 3.15 (dd,  $^3J_{\text{HH}} = 14.6$  Hz,  $^3J_{\text{HP}} = 5.6$  Hz, 1 H,  $\text{H}_4$ ), 2.47-2.28 (m, 4 H,  $\text{CH}^i\text{Pr}$ ), 1.83 (dd,  $^3J_{\text{HH}} = 8.0$  Hz,  $^3J_{\text{HP}} = 3.0$  Hz, 1 H,  $\text{H}_5$ ), 1.52 (d,  $^3J_{\text{HH}} = 7.0$  Hz, 6 H,  $\text{CH}_3^i\text{Pr}$ ), 1.36-1.26 (m, 12 H,  $\text{CH}_3^i\text{Pr}$ ,  $\text{P-CH}_3$ ), 1.08 (b d,  $^2J_{\text{HP}} = 6.8$  Hz, 6 H,  $\text{CH}_3^i\text{Pr}$ ), 1.02 (d,  $^3J_{\text{HP}} = 6.7$  Hz, 6 H,  $\text{CH}_3^i\text{Pr}$ ).

$^{13}\text{C}\{^1\text{H}\}$  NMR (75 MHz,  $\text{CD}_2\text{Cl}_2$ , 298 K):  $\delta$  147.4 (s, *o*-Dipp), 146.2 (d,  $^2J_{\text{CP}} = 32$  Hz, *o*- $\text{C}_6\text{H}_3$ ), 146.3 (s, *o*- $\text{C}_6\text{H}_3$ ), 144.1 (b s, *ipso*-Dipp), 134.0 (d,  $^3J_{\text{CP}} = 4$  Hz, *m*- $\text{C}_6\text{H}_3$ ), 132.6 (s, CH aromatic), 132.4 (d,  $^1J_{\text{CP}} = 46$  Hz, *ipso*- $\text{C}_6\text{H}_3$ ), 131.6 (s, CH aromatic), 131.0 (d,  $^3J_{\text{CP}} = 14$  Hz, *m*- $\text{C}_6\text{H}_3$ ), 130.6 (s, CH Dipp), 123.7 (s, CH Dipp), 120.5 (d,  $^2J_{\text{CP}} = 5$  Hz, *ipso*-Dipp), 115.7 (s,  $\text{C}_{\text{meso}}$ ), 96.1 (d,  $^2J_{\text{CP}} = 18$  Hz,  $\text{C}_{\text{trans-P}}$ ), 51.0 (d,  $^2J_{\text{CP}} = 4$  Hz,  $\text{C}_{\text{cis-P}}$ ), 33.3 (s, CH  $^i\text{Pr}$ ), 31.8 (s, CH  $^i\text{Pr}$ ), 26.4 (s,  $\text{CH}_3^i\text{Pr}$ ), 24.9 (s,  $\text{CH}_3^i\text{Pr}$ ), 24.7 (s,  $\text{CH}_3^i\text{Pr}$ ), 21.6 (s,  $\text{CH}_3^i\text{Pr}$ ), 14.5 (d,  $^1J_{\text{CP}} = 32$  Hz,  $\text{P-CH}_3$ ).

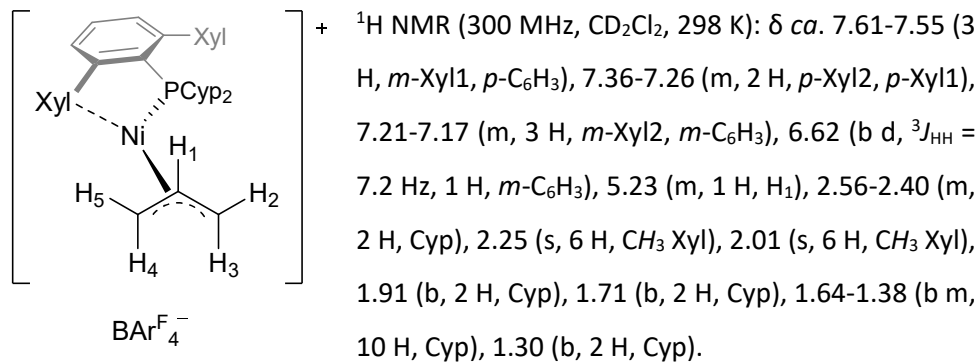
$^{31}\text{P}\{^1\text{H}\}$  NMR (121 MHz,  $\text{CD}_2\text{Cl}_2$ , 298 K):  $\delta$  15.9 (s).

Elemental analysis (%), calculated (found) for  $\text{C}_{67}\text{H}_{60}\text{BF}_4\text{NiP}$ : C, 56.61 (56.77); H, 4.25 (3.92).

Yield: 0.3157 g, 74% (after recrystallisation).

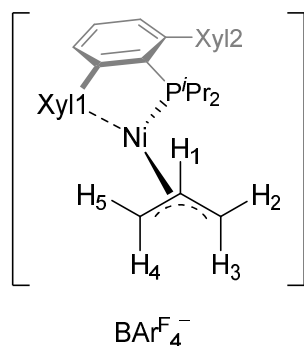


### II.4.8.2. $[\text{Ni}(\eta^3\text{-C}_3\text{H}_5)(\text{PCyp}_2\text{Ar}^{\text{Xyl}_2})]\text{BAr}^{\text{F}_4}$ (15·L3).



$^1\text{H}$  NMR (300 MHz,  $\text{CD}_2\text{Cl}_2$ , 223 K):  $\delta$  *ca.* 7.58-7.46 (3 H, *m*-Xyl1, *p*- $\text{C}_6\text{H}_3$ ) 7.30-7.21 (m, 2 H, *p*-Xyl2, *p*-Xyl1), 7.17-7.19 (m, 3 H, *m*-Xyl2, *m*- $\text{C}_6\text{H}_3$ ), 6.60 (b d,  $^3J_{\text{HH}} = 7.2$  Hz, 1 H, *m*- $\text{C}_6\text{H}_3$ ), 5.27 (m, 1 H,  $\text{H}_1$ ), 3.53 (b s, 1 H,  $\text{H}_5$ ), 3.15 (dd,  $^3J_{\text{HH}} = 14.6$  Hz,  $^3J_{\text{HP}} = 4.1$  Hz, 1 H,  $\text{H}_4$ ), 2.38 (s, 3 H,  $\text{CH}_3$  Xyl), 2.03 (s, 3 H,  $\text{CH}_3$  Xyl), 1.95 (s, 3 H,  $\text{CH}_3$  Xyl), 1.85 (s, 3 H,  $\text{CH}_3$  Xyl), *ca.* 1.81 (1 H,  $\text{H}_2$ ), *ca.* 1.69 (1 H,  $\text{H}_3$ ), 1.60-1.03 (b m, 15 H, Cyp), 0.87 (b, 1 H, Cyp).

$^{31}\text{P}\{^1\text{H}\}$  NMR (121 MHz,  $\text{CD}_2\text{Cl}_2$ , 298 K):  $\delta$  54.3 (s).

II.4.8.3.  $[\text{Ni}(\eta^3\text{-C}_3\text{H}_5)(\text{P}^i\text{Pr}_2\text{Ar}^{\text{Xyl}2})]\text{BAr}^{\text{F}_4}$  (15·L4).

$^1\text{H}$  NMR (400 MHz,  $\text{CD}_2\text{Cl}_2$ , 298 K):  $\delta$  7.60-7.55 (m, 3 H, *m*-Xyl1, *p*- $\text{C}_6\text{H}_3$ ), 7.36 (t,  $^3J_{\text{HH}} = 7.6$  Hz, 1 H, *p*-Xyl1), 7.28 (t,  $^3J_{\text{HH}} = 7.6$  Hz, 1 H, *p*-Xyl2), 7.21-7.17 (m, 3 H, *m*-Xyl2, *m*- $\text{C}_6\text{H}_3$ ), 6.61 (ddd,  $^3J_{\text{HH}} = 7.8$  Hz,  $^4J_{\text{HP}} = 2.6$  Hz,  $^3J_{\text{HH}} = 1.3$  Hz, 1 H, *m*- $\text{C}_6\text{H}_3$ ), 5.31 (m, 1 H, H<sub>1</sub>), 2.59-2.48 (m, 2 H, *CH*<sup>*i*</sup>Pr), 2.23 (b, 6 H,  $\text{CH}_3$  Xyl), 2.01 (s, 6 H,  $\text{CH}_3$  Xyl), 1.21 (dd,  $^3J_{\text{HP}} = 19.4$  Hz,  $^3J_{\text{HH}} = 7.2$  Hz, 6 H,  $\text{CH}_3$ <sup>*i*</sup>Pr), 0.80 (b, 6 H,  $\text{CH}_3$ <sup>*i*</sup>Pr).

$^1\text{H}$  NMR (400 MHz,  $\text{CD}_2\text{Cl}_2$ , 233 K):  $\delta$  7.58 (d,  $^3J_{\text{HH}} = 7.8$  Hz, 1 H, *m*-Xyl1), *ca.* 7.54 (1 H, *p*- $\text{C}_6\text{H}_3$ ), 7.48 (d,  $^3J_{\text{HH}} = 7.8$  Hz, 1 H, *m*-Xyl1), 7.31 (t,  $^3J_{\text{HH}} = 7.6$  Hz, 1 H, *p*-Xyl1), 7.26-7.18 (m, 2 H, *p*-Xyl2, *m*-Xyl2), 7.15 (d,  $^3J_{\text{HH}} = 7.6$  Hz, 1 H, *m*- $\text{C}_6\text{H}_3$ ), 7.11 (d,  $^3J_{\text{HH}} = 7.4$  Hz, 1 H, *m*-Xyl2), 6.59 (b d,  $^3J_{\text{HH}} = 7.7$  Hz, 1 H, *m*- $\text{C}_6\text{H}_3$ ), *ca.* 5.34 (H<sub>1</sub>), 3.67 (b s, 1 H, H<sub>5</sub>), 2.90 (dd,  $^3J_{\text{HH}} = 14.5$  Hz,  $^2J_{\text{HP}} = 5.0$  Hz, 1 H, H<sub>4</sub>), 2.65-2.51 (m, 1 H, *CH*<sup>*i*</sup>Pr), 2.44 (s, 3 H,  $\text{CH}_3$  Xyl), 2.38-2.24 (m, 1 H, *CH*<sup>*i*</sup>Pr), 2.08 (s, 3 H,  $\text{CH}_3$  Xyl), 1.87 (s, 3 H,  $\text{CH}_3$  Xyl), 1.82 (s, 3 H,  $\text{CH}_3$  Xyl), *ca.* 1.80 (1 H, H<sub>2</sub>), 1.71 (b s, 1 H, H<sub>3</sub>), 1.22-1.09 (m, 6 H,  $\text{CH}_3$ <sup>*i*</sup>Pr), 0.94 (dd,  $^3J_{\text{HP}} = 15.5$  Hz,  $^3J_{\text{HH}} = 6.8$  Hz, 3 H,  $\text{CH}_3$ <sup>*i*</sup>Pr), 0.40 (dd,  $^3J_{\text{HP}} = 13.0$  Hz,  $^3J_{\text{HH}} = 6.9$  Hz, 3 H,  $\text{CH}_3$ <sup>*i*</sup>Pr).

$^{13}\text{C}\{^1\text{H}\}$  NMR (100 MHz,  $\text{CD}_2\text{Cl}_2$ , 298 K):  $\delta$  148.7 (d,  $^2J_{\text{CP}} = 27$  Hz, *o*- $\text{C}_6\text{H}_3$ -Xyl2), 146.2 (s, *o*- $\text{C}_6\text{H}_3$ -Xyl1), 139.8 (s, *ipso*-Xyl1), 136.9 (s, *o*-Xyl2, *o*-Xyl1), 134.4 (s, *o*-Xyl2), 133.7-133.5 (m, *p*- $\text{C}_6\text{H}_3$ , *m*- $\text{C}_6\text{H}_3$ ), 131.6 (s, *p*-Xyl1), 130.6 (s,  $^3J_{\text{CP}} = 12$  Hz, *m*- $\text{C}_6\text{H}_3$ ), 128.7 (s, *m*-Xyl1, *m*-Xyl2), 121.2 (d,  $^3J_{\text{CP}} = 6$  Hz, *ipso*-Xyl2), 114.5 (s,  $\text{C}_{\text{meso}}$ ), 27.6 (d,  $^1J_{\text{CP}} = 23$  Hz, *CH*<sup>*i*</sup>Pr), 24.5 (b,  $\text{CH}_3$ <sup>*i*</sup>Pr), 23.0 (s,  $\text{CH}_3$  Xyl1), 21.3 (s,  $\text{CH}_3$  Xyl2), 19.4 (s,  $\text{CH}_3$ <sup>*i*</sup>Pr).

$^{31}\text{P}\{^1\text{H}\}$  NMR (121 MHz,  $\text{CD}_2\text{Cl}_2$ , 298 K):  $\delta$  65.1 (s).

Yield: 0.1113 g. This complex is obtained as a mixture, purportedly with the neutral chloride  $\text{NiCl}(\eta^3\text{-C}_3\text{H}_5)(\text{P}^i\text{Pr}_2\text{Ar}^{\text{Xyl}2})$  (<10%,  $\delta(^{31}\text{P}) = 32.0$  ppm). Attempts at crystallising this compound in an analytically pure form were unsuccessful.

#### II.4.8.4. Characterisation of $[(\text{CH}_2=\text{CHCH}_2)\text{PMe}_2\text{Ar}^{\text{Xyl}_2}]\text{BAr}^{\text{F}_4}$ (**14-L1**).

This compound was isolated when attempting to synthesise **15-L1** in THF.

$[(\text{CH}_2=\text{CHCH}_2)\text{PMe}_2\text{Ar}^{\text{Xyl}_2}]^+ \text{BAr}^{\text{F}_4-}$   $^1\text{H}$  NMR (400 MHz,  $\text{CD}_2\text{Cl}_2$ , 298 K):  $\delta$  7.94 (td,  $^3J_{\text{HH}} = 7.7$  Hz,  $^5J_{\text{HP}} = 2.1$  Hz, 1 H, *p*- $\text{C}_6\text{H}_3$ ), 7.41-7.35 (m, 4 H, *m*- $\text{C}_6\text{H}_3$ , *p*-Xyl), 7.25 (d,  $^3J_{\text{HH}} = 7.7$  Hz, 4 H, *m*-Xyl), 5.40-5.23 (m, 2 H,  $\text{CH}=\text{CH}_2$ ,  $\text{CH}=\text{CH}_2$ ), 5.12-5.02 (m, 1 H,  $\text{CH}=\text{CH}_2$ ), 2.64 (dd,  $^2J_{\text{HP}} = 15.6$  Hz,  $^3J_{\text{HH}} = 7.0$  Hz, 2 H,  $\text{P}-\text{CH}_2$ ), 2.07 (s, 12 H,  $\text{CH}_3$  Xyl), 1.22 (d,  $^2J_{\text{HP}} = 12.8$  Hz, 6 H,  $\text{P}-\text{CH}_3$ ).

$^{13}\text{C}\{^1\text{H}\}$  NMR (75 MHz,  $\text{CD}_2\text{Cl}_2$ , 298 K):  $\delta$  148.3 (d,  $^2J_{\text{CP}} = 11$  Hz, *o*- $\text{C}_6\text{H}_3$ ), 138.6 (d,  $^3J_{\text{CP}} = 4$  Hz, *ipso*-Xyl), 136.8 (s, *o*-Xyl), 136.4 (d,  $^4J_{\text{CP}} = 3$  Hz, *p*- $\text{C}_6\text{H}_3$ ), 133.3 (d,  $^3J_{\text{CP}} = 11$  Hz, *m*- $\text{C}_6\text{H}_3$ ), 130.6 (s, *p*-Xyl), 129.1 (s, *m*-Xyl), 126.9 (d,  $^3J_{\text{CP}} = 13$  Hz,  $\text{CH}=\text{CH}_2$ ), 122.9 (d,  $^2J_{\text{CP}} = 10$  Hz,  $\text{CH}=\text{CH}_2$ ), 31.5 (d,  $^1J_{\text{CP}} = 49$  Hz,  $\text{P}-\text{CH}_2$ ), 21.4 (s,  $\text{CH}_3$  Xyl), 10.6 (d,  $^1J_{\text{CP}} = 56$  Hz,  $\text{P}-\text{CH}_3$ ).

$^{31}\text{P}\{^1\text{H}\}$  NMR (121 MHz,  $\text{CD}_2\text{Cl}_2$ , 298 K):  $\delta$  19.8 (s).

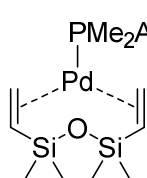
Elemental analysis (%), calculated (found) for  $\text{C}_{59}\text{H}_{44}\text{BF}_{24}\text{P}$ : C, 56.66 (56.54); H, 3.55 (3.41).

MS/ESI *m/z* (%): 387.2 ( $(\text{CH}_2=\text{CHCH}_2)\text{PMe}_2\text{Ar}^{\text{Xyl}_2}$ , 100).

### II.4.9. Nickel(0), palladium(0) and platinum(0) complexes.

#### II.4.9.1. Synthesis and characterisation of Pd(dvds)(PMe<sub>2</sub>Ar<sup>Xyl</sup>)<sub>2</sub> (16-L1).

To a suspension of [PdCl(μ-Cl)(PMe<sub>2</sub>Ar<sup>Xyl</sup>)<sub>2</sub>] (3-L1) (0.0523 g, 0.050 mmol) in THF (5 mL), 1,3-divinyltetramethyldisiloxane (46 μL, 0.200 mmol) were added, followed by Zn powder (0.0654 g, 1.00 mmol, 10 eq). After stirring for 1 day at room temperature, volatiles were removed under vacuum, and the resulting solid extracted in petroleum ether and filtered. The solution was cooled at -20 °C yielding the sought product as greyish crystals. Yield: 0.0289 g, 45%.

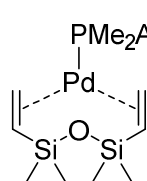


<sup>1</sup>H NMR (400 MHz, CDCl<sub>3</sub>, 298 K): δ 7.31 (td, <sup>3</sup>J<sub>HH</sub> = 7.7 Hz, <sup>5</sup>J<sub>HP</sub> = 1.1 Hz, 1 H, *p*-C<sub>6</sub>H<sub>3</sub>), 7.07 (dd, <sup>3</sup>J<sub>HH</sub> = 8.1 Hz, <sup>3</sup>J<sub>HH</sub> = 7.0 Hz, 2 H, *p*-Xyl), 6.93 (d, <sup>3</sup>J<sub>HH</sub> = 7.0 Hz, 4 H, *m*-Xyl), 6.84 (dt, <sup>3</sup>J<sub>HH</sub> = 7.6 Hz, <sup>4</sup>J<sub>HP</sub> = 2.4 Hz, 2 H, *m*-C<sub>6</sub>H<sub>3</sub>), 2.58-2.36 (m, 6 H, dvds), 1.95 (s, 12 H, CH<sub>3</sub> Xyl), 0.95 (d, <sup>2</sup>J<sub>HP</sub> = 5.1 Hz, 6 H, P-CH<sub>3</sub>), 0.10 (s, 6 H, Si-CH<sub>3</sub>), -0.53 (s, 6 H, Si-CH<sub>3</sub>).

<sup>31</sup>P{<sup>1</sup>H} NMR (121 MHz, CDCl<sub>3</sub>, 298 K): δ -11.2 (s).

**II.4.9.2. Synthesis and characterisation of Pd(dvds)(PMe<sub>2</sub>Ar<sup>Dipp2</sup>) (16·L2).**

To a suspension of [PdCl(μ-Cl)(PMe<sub>2</sub>Ar<sup>Dipp2</sup>)<sub>2</sub>] (3·L2) (0.0523 g, 0.050 mmol) in THF (5 mL), 1,3-divinyltetramethyldisiloxane (46 μL, 0.200 mmol, 100% excess) were added, followed by Zn powder (0.0654 g, 1.00 mmol, 10 eq). After stirring for 1 day at room temperature, volatiles were removed under vacuum, and the resulting solid extracted in petroleum ether and filtered. The solution was cooled at -20 °C yielding the sought product as greyish crystals. Yield: 0.0289 g, 45%.



<sup>1</sup>H NMR (300 MHz, C<sub>6</sub>D<sub>6</sub>, 298 K): δ 7.26 (dd, <sup>3</sup>J<sub>HH</sub> = 8.0 Hz, <sup>3</sup>J<sub>HH</sub> = 7.4 Hz, 2 H, *p*-Xyl), 7.10 (d, <sup>3</sup>J<sub>HH</sub> = 7.7 Hz, 4 H, *m*-Xyl), 7.04-6.94 (m, 3 H, *m*-C<sub>6</sub>H<sub>3</sub>, *p*-C<sub>6</sub>H<sub>3</sub>), 3.15 (ddd, <sup>3</sup>J<sub>HH</sub> = 15.3 Hz, <sup>3</sup>J<sub>HP</sub> = 12.4 Hz, <sup>3</sup>J<sub>HH</sub> = 5.1 Hz, CH dvds) 3.00-2.79 (m, 8 H, CH<sub>2</sub> dvds, CH <sup>*i*</sup>Pr), 1.30 (d, <sup>3</sup>J<sub>HH</sub> = 6.8 Hz, 6 H, CH<sub>3</sub> <sup>*i*</sup>Pr), 1.14 (d, <sup>2</sup>J<sub>HP</sub> = 5.1 Hz, 6 H, P-CH<sub>3</sub>), 0.97 (d, <sup>3</sup>J<sub>HH</sub> = 6.7 Hz, 6 H, CH<sub>3</sub> <sup>*i*</sup>Pr), 0.49 (s, 6 H, Si-CH<sub>3</sub>), -0.17 (s, 6 H, Si-CH<sub>3</sub>).

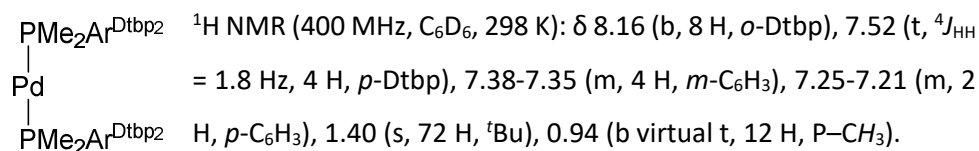
<sup>13</sup>C{<sup>1</sup>H} NMR (75 MHz, C<sub>6</sub>D<sub>6</sub>): δ 147.0 (s, *o*-Dipp), 143.6 (d, <sup>2</sup>J<sub>CP</sub> = 10 Hz, *o*-C<sub>6</sub>H<sub>3</sub>), 140.7 (d, <sup>3</sup>J<sub>CP</sub> = 3 Hz, *ipso*-Dipp), 136.2 (d, <sup>1</sup>J<sub>CP</sub> = 8 Hz, *ipso*-C<sub>6</sub>H<sub>3</sub>), 133.5 (d, <sup>3</sup>J<sub>CP</sub> = 5 Hz, *m*-C<sub>6</sub>H<sub>3</sub>), 129.0 (s, *p*-Dipp), 126.5 (s, *p*-C<sub>6</sub>H<sub>3</sub>), 123.1 (s, *m*-Dipp), 66.5 (d, <sup>2</sup>J<sub>CP</sub> = 9 Hz, CH dvds), 65.8 (d, <sup>2</sup>J<sub>CP</sub> = 2 Hz, CH<sub>2</sub> dvds), 31.4 (s, CH <sup>*i*</sup>Pr), 25.9 (s, CH<sub>3</sub> <sup>*i*</sup>Pr), 23.1 (s, CH<sub>3</sub> <sup>*i*</sup>Pr), 19.5 (d, <sup>1</sup>J<sub>CP</sub> = 18 Hz, P-CH<sub>3</sub>), 1.66 (Si-CH<sub>3</sub>), -0.78 (Si-CH<sub>3</sub>).

<sup>31</sup>P{<sup>1</sup>H} NMR (121 MHz, C<sub>6</sub>D<sub>6</sub>, 298 K): δ -13.5 (s).

Elemental analysis (%), calculated (found) for C<sub>40</sub>H<sub>61</sub>OPPdSi<sub>2</sub>: C, 63.93 (64.03); H, 8.18 (8.33).

**II.4.9.3. Synthesis and characterization of Pd(PMe<sub>2</sub>Ar<sup>Dtbp2</sup>)<sub>2</sub> (17·L5).**

To a vessel containing [Pd(η<sup>3</sup>-C<sub>3</sub>H<sub>5</sub>)<sub>2</sub>(μ-Cl)<sub>2</sub>] (0.0092 g, 0.025 mmol) and PMe<sub>2</sub>Ar<sup>Dtbp2</sup> (0.0516 g, 0.100 mmol), THF (1 mL) was added. After stirring at room temperature for 2 hours, the solvent was removed under reduced pressure and <sup>i</sup>PrOH (0.5 mL) was added, followed by a solution of KO<sup>t</sup>Bu (0.0062 g, 0.055 mmol, 10% excess) in <sup>i</sup>PrOH (1 mL). The mixture was stirred for a further 16 hours, followed by centrifugation. The supernatant solution was discarded and the remaining solid washed with <sup>i</sup>PrOH (1.5 mL), dissolved in Et<sub>2</sub>O and filtered. Removal of the solvent under vacuum rendered the sought product as a yellowish white solid. Yield: 0.027 g, 48%. Single crystals suitable for X-ray diffraction studies were grown by slow evaporation from a pentane solution at room temperature.



<sup>1</sup>H NMR (400 MHz, C<sub>6</sub>D<sub>6</sub>, 333 K): δ 8.08 (b d, <sup>4</sup>J<sub>HH</sub> ≈ 1 Hz, 8 H, *o*-Dtbp), 7.51 (t, <sup>4</sup>J<sub>HH</sub> = 1.8 Hz, 4 H, *p*-Dtbp), 7.35-7.33 (m, 4 H, *m*-C<sub>6</sub>H<sub>3</sub>), 7.27-7.24 (m, 2 H, *p*-C<sub>6</sub>H<sub>3</sub>), 1.39 (s, 72 H, <sup>t</sup>Bu), 0.93 (virtual t, *J*<sub>app</sub> = 1.4 Hz, 12 H, P-CH<sub>3</sub>).

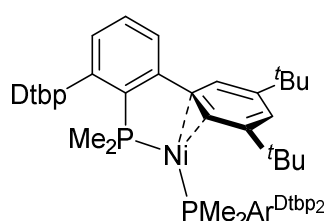
<sup>13</sup>C{<sup>1</sup>H} NMR (100 MHz, C<sub>6</sub>D<sub>6</sub>, 298 K): δ 150.9 (s, *m*-Dtbp), 146.6 (virtual t, *J*<sub>app</sub> = 4 Hz, *o*-C<sub>6</sub>H<sub>3</sub>), 144.3 (s, *ipso*-Dtbp), 138.6 (virtual t, *J*<sub>app</sub> = 7 Hz, *ipso*-C<sub>6</sub>H<sub>3</sub>), 131.8 (virtual t, *J*<sub>app</sub> = 2 Hz, *m*-C<sub>6</sub>H<sub>3</sub>), 127.5 (s, *p*-C<sub>6</sub>H<sub>3</sub>), 126.0 (s, *o*-Dtbp), 120.4 (s, *p*-Dtbp), 35.3 (s, C <sup>t</sup>Bu), 32.0 (s, CH<sub>3</sub> <sup>t</sup>Bu), 20.0 (virtual t, *J*<sub>app</sub> = 10 Hz, P-CH<sub>3</sub>).

<sup>31</sup>P{<sup>1</sup>H} NMR (202 MHz, C<sub>6</sub>D<sub>6</sub>, 298 K): δ -12.8 (s).

Elemental analysis (%), calculated (found) for C<sub>72</sub>H<sub>102</sub>P<sub>2</sub>Pd: C, 76.13 (76.08); H, 9.05 (9.17).

#### II.4.9.4. Synthesis and characterization of Ni(PMe<sub>2</sub>Ar<sup>Dtbp2</sup>)<sub>2</sub> (18·L5).

A Fischer-Porter vessel containing a mixture of Ni(cod)<sub>2</sub> (0.1375 g, 0.500 mmol, 100% excess) and PMe<sub>2</sub>Ar<sup>Dtbp2</sup> (0.5148 g, 0.500 mmol) in toluene (10 mL) was charged with H<sub>2</sub> (4 bar) and stirred at 50 °C for 3 hours. After that time, the H<sub>2</sub> atmosphere was discharged and volatiles removed under reduced pressure. Any remaining toluene and cod were removed by co-evaporating with pentane twice, and then the solid residue was extracted in pentane and filtered through silica. Concentration and crystallisation at -30 °C rendered the sought product as very dark reddish brown crystals. Yield: 0.1178 g, 43%.



<sup>1</sup>H NMR (500 MHz, C<sub>6</sub>D<sub>6</sub>, 298 K): δ 7.19 (b, 4 H, *p*-Dtbp), 7.11 (d, <sup>3</sup>J<sub>HH</sub> = 7.5 Hz, 4 H, *m*-C<sub>6</sub>H<sub>3</sub>), 6.98-6.93 (b m, 10 H, *p*-C<sub>6</sub>H<sub>3</sub>, *o*-Dtbp), 1.31 (s, 72 H, <sup>t</sup>Bu), 1.09 (b, 12 H, P-CH<sub>3</sub>).

<sup>13</sup>C{<sup>1</sup>H} NMR (100 MHz, C<sub>6</sub>D<sub>6</sub>, 298 K): δ 151.4-149.5 (b m, *o*-C<sub>6</sub>H<sub>3</sub>, *ipso*-Dtbp, *m*-Dtbp), 140.2 (virtual t, *J*<sub>app</sub> = 16 Hz, *ipso*-C<sub>6</sub>H<sub>3</sub>), 129.5 (s, *m*-C<sub>6</sub>H<sub>3</sub>), ca. 127.3 (*p*-C<sub>6</sub>H<sub>3</sub>), 118.1 (s, *p*-Dtbp), 35.0 (s, C <sup>t</sup>Bu), 31.7 (s, CH<sub>3</sub> <sup>t</sup>Bu), 17.1 (b s, P-CH<sub>3</sub>).

<sup>31</sup>P{<sup>1</sup>H} NMR (202 MHz, C<sub>6</sub>D<sub>6</sub>, 298 K): δ -4.3 (s).

Elemental analysis (%), calculated (found) for C<sub>72</sub>H<sub>102</sub>P<sub>2</sub>Ni: C, 79.47 (79.39); H, 9.45 (9.37).

**II.4.9.5. Synthesis and characterization of Pt(PMe<sub>2</sub>Ar<sup>Dtbp<sub>2</sub></sup>)<sub>2</sub> (19·L5).**

To an ampoule charged with PMe<sub>2</sub>Ar<sup>Dtbp<sub>2</sub></sup> (0.470 g, 0.913 mmol), K<sub>2</sub>PtCl<sub>4</sub> (0.205 g, 0.493 mmol) and KOH (0.071 g, 1.27 mmol), EtOH (8 mL) was added and the resulting suspension was stirred at 100 °C for 2 days. This was followed by centrifugation, removal of the supernatant liquid and washing the solid with EtOH until the solution was colourless (5 x 3 mL). After removal of remaining EtOH in vacuum, pentane was added until complete dissolution of the whitish solid (50 mL) and the remaining metallic platinum was separated by centrifugation. Thorough evaporation of volatiles followed by washing with pentane (3 x 2 mL) at 0 °C rendered **19·L5** as a pale yellow solid. Yield: 0.379 g, 68%. Single crystals suitable for X-ray diffraction studies were obtained by slow evaporation of pentane at room temperature.

$$\begin{array}{c} \text{PMe}_2\text{Ar}^{\text{Dtbp}_2} \\ | \\ \text{Pt} \\ | \\ \text{PMe}_2\text{Ar}^{\text{Dtbp}_2} \end{array}$$
<sup>1</sup>H NMR (400 MHz, C<sub>6</sub>D<sub>6</sub>, 298 K): δ 9.00 (b, 8 H, *o*-Dtbp), 7.53 (t, <sup>4</sup>J<sub>HH</sub> = 1.7 Hz, 4 H, *p*-Dtbp), 7.39 (b d, <sup>3</sup>J<sub>HH</sub> = 7.1 Hz, 4 H, *m*-C<sub>6</sub>H<sub>3</sub>), 7.23 (t, <sup>3</sup>J<sub>HH</sub> = 7.6 Hz, 2 H, *p*-C<sub>6</sub>H<sub>3</sub>), 1.41 (s, 72 H, <sup>t</sup>Bu), 1.43 (b, 12 H, P-CH<sub>3</sub>).

<sup>1</sup>H NMR (400 MHz, C<sub>6</sub>D<sub>6</sub>, 338 K): δ 8.18 (b, 8 H, *o*-Dtbp), 7.51 (t, <sup>4</sup>J<sub>HH</sub> = 1.8 Hz, 4 H, *p*-Dtbp), 7.37-7.35 (m, 4 H, *m*-C<sub>6</sub>H<sub>3</sub>), 7.28-7.25 (m, 2 H, *p*-C<sub>6</sub>H<sub>3</sub>), 1.40 (s, 72 H, <sup>t</sup>Bu), 1.01 (virtual t, J<sub>app</sub> = 2.3 Hz, 12 H, P-CH<sub>3</sub>).

<sup>13</sup>C{<sup>1</sup>H} NMR (100 MHz, C<sub>6</sub>D<sub>6</sub>, 298 K): δ 150.8 (s, *m*-Dtbp), 146.8 (virtual t, J<sub>app</sub> = 4 Hz, *o*-C<sub>6</sub>H<sub>3</sub>), 144.0 (s, *ipso*-Dtbp), 137.2 (virtual t, J<sub>app</sub> = 16 Hz, *ipso*-C<sub>6</sub>H<sub>3</sub>), 132.0 (s, *m*-C<sub>6</sub>H<sub>3</sub>), *ca.* 127.5 (s, *p*-C<sub>6</sub>H<sub>3</sub>), 126.3 (b, *o*-Dtbp), 120.5 (s, *p*-Dtbp), 35.3 (b s, C<sup>t</sup>Bu), 32.0 (b s, CH<sub>3</sub> <sup>t</sup>Bu), 20.7 (virtual t, J<sub>app</sub> = 17 Hz, P-CH<sub>3</sub>).

<sup>31</sup>P{<sup>1</sup>H} NMR (202 MHz, C<sub>6</sub>D<sub>6</sub>, 298 K): δ 14.2 (s, <sup>1</sup>J<sub>Pt</sub> = 3794).

Elemental analysis (%), calculated (found) for C<sub>72</sub>H<sub>102</sub>P<sub>2</sub>Pt: C, 70.62 (70.65); H, 8.42 (8.68).



## II.5. BIBLIOGRAPHY

1. a) Greenwood, N. N.; Earnshaw, A. *Chemistry of the Elements*, 2nd Ed.; Elsevier, 1997; b) *Chemistry of the Platinum Group Metals - Recent Developments*, 1st Ed.; Hartley, F. R., Ed.; Studies in Inorganic Chemistry; Elsevier, 1991; Vol. 11.
2. Zeise, W. C. *Ann. Phys. Chem.* **1831**, *97*, 497–541.
3. a) Dewar, M. J. S. *Bull. Soc. Chim. Fr.* **1951**, *18*, C71–C79.; b) Chatt, J.; Duncanson, L. A. *J. Chem. Soc.* **1953**, 2939–2947.
4. a) Pope, W. J.; Peachy, S. J. *Proc. Chem. Soc.* **1907**, *23*, 86–87; b) Donnay, G.; Coleman, L. B.; Krieghoff, N. G.; Cowan, D. O. *Acta Cryst.* **1968**, *B24*, 157–159.
5. Reppe, W.; Schlichting, O.; Klager, K.; Toepel, T. *Justus Liebigs Ann. Chem.* **1948**, *560*, 1–92.
6. a) *Handbook of Organopalladium Chemistry for Organic Synthesis*; Negishi, E., de Meijere, A., Eds.; Wiley Interscience: New York, 2002; b) *Palladium in Organic Synthesis*; Tsuji, J., Ed.; Topics in Organometallic Chemistry; Springer Berlin Heidelberg: Berlin, Heidelberg, 2005; Vol. 14.
7. Tsuji, J. *Synthesis* **1990**, 739–749.
8. King, A. O. Palladium-Catalyzed Homogeneous Hydrogenation: Palladium-Catalyzed Homogeneous Hydrogenation with Dihydrogen and Related Hydrogen Transfer Reactions. In *Handbook of Organopalladium Chemistry*

## Chapter II

*for Organic Synthesis*; Negishi, E., Ed.; John Wiley & Sons, Inc.: New York, USA, 2002; pp 2753–2758.

9. Zeni, G.; Larock, R. C. *Chem. Rev.* **2006**, *106*, 4644–4680.
10. Tietze, L. F.; Ila, H.; Bell, H. P. *Chem. Rev.* **2004**, *104*, 3453–3516.
11. a) *Metal-Catalyzed Cross-Coupling Reactions*; de Meijere, A., Diederich, F., Eds.; Wiley-VCH Verlag GmbH: Weinheim, Germany, 2004; b) *New Trends in Cross-Coupling*; Colacot, T., Ed.; Catalysis Series; Royal Society of Chemistry: Cambridge, 2014.
12. Beccalli, E. M.; Broggini, G.; Martinelli, M.; Sottocornola, S. *Chem. Rev.* **2007**, *107*, 5318–5365.
13. a) Smidt, J.; Hafner, W.; Jira, R.; Sedlmeier, J.; Sieber, R.; Rüttinger, R.; Kojer, H. *Angew. Chem.* **1959**, *71*, 176–182; b) Keith, J. A.; Henry, P. M. *Angew. Chem. Int. Ed.* **2009**, *48*, 9038–9049; c) Jira, R. *Angew. Chem. Int. Ed.* **2009**, *48*, 9034–9037.
14. Mizoroki, T.; Mori, K.; Ozaki, A. *Bull. Chem. Soc. Jpn.* **1971**, *44*, 581–581.
15. Heck, R. F.; Nolley, J. P. *J. Org. Chem.* **1972**, *37*, 2320–2322.
16. a) Nicolaou, K. C.; Bulger, P. G.; Sarlah, D. *Angew. Chem. Int. Ed.* **2005**, *44*, 4442–4489; b) Barnard, C. *Platinum Metals Rev.* **2008**, *52*, 38–45; c) Johansson Seechurn, C. C. C.; Kitching, M. O.; Colacot, T. J.; Snieckus, V. *Angew. Chem. Int. Ed.* **2012**, *51*, 5062–5085.
17. Nobel lectures 2010: a) Suzuki, A. *Angew. Chem. Int. Ed.* **2011**, *50*, 6722–6737; b) Negishi, E. *Angew. Chem. Int. Ed.* **2011**, *50*, 6738–6764.
18. Collman, J. P.; Hegedus, L. S.; Norton, J. R.; Finke, R. G. *Principles and Applications of Organotransition Metal Chemistry*, 2nd Ed.; University Science Books: Mill Valley, 1987.

19. a) Ozawa, F.; Ito, T.; Yamamoto, A. *J. Am. Chem. Soc.* **1980**, *102*, 6457–6463; b) Moravskiy, A.; Stille, J. K. *J. Am. Chem. Soc.* **1981**, *103*, 4182–4186; c) Tatsumi, K.; Hoffmann, R.; Yamamoto, A.; Stille, J. K. *Bull. Chem. Soc. Jpn.* **1981**, *54*, 1857–1867.
20. a) Driver, M. S.; Hartwig, J. F. *J. Am. Chem. Soc.* **1995**, *117*, 4708–4709; b) Mann, G.; Shelby, Q.; Roy, A. H.; Hartwig, J. F. *Organometallics* **2003**, *22*, 2775–2789.
21. a) Stambuli, J. P.; Bühl, M.; Hartwig, J. F. *J. Am. Chem. Soc.* **2002**, *124*, 9346–9347; b) Yamashita, M.; Hartwig, J. F. *J. Am. Chem. Soc.* **2004**, *126*, 5344–5345; c) Hanley, P. S.; Marquard, S. L.; Cundari, T. R.; Hartwig, J. F. *J. Am. Chem. Soc.* **2012**, *134*, 15281–15284.
22. a) Braunschweig, H.; Radacki, K.; Rais, D.; Scheschkewitz, D. *Angew. Chem. Int. Ed.* **2005**, *44*, 5651–5654; b) Braunschweig, H.; Radacki, K.; Uttinger, K. *Chem. Eur. J.* **2008**, *14*, 7858–7866; c) Berthon-Gelloz, G.; de Bruin, B.; Tinant, B.; Markó, I. E. *Angew. Chem. Int. Ed.* **2009**, *48*, 3161–3164; d) Rivada-Wheelaghan, O.; Ortuño, M. A.; Díez, J.; Lledós, A.; Conejero, S. *Angew. Chem. Int. Ed.* **2012**, *51*, 3936–3939; e) Kelly, C. M.; Kwon, D.-H.; Ferguson, M. J.; Bischof, S. M.; Sydora, O. L.; Ess, D. H.; Stradiotto, M.; Turculet, L. *Angew. Chem. Int. Ed.* **2015**, *54*, 14498–14502.
23. a) Stambuli, J. P.; Incarvito, C. D.; Bühl, M.; Hartwig, J. F. *J. Am. Chem. Soc.* **2004**, *126*, 1184–1194; b) Lavallo, V.; Canac, Y.; DeHope, A.; Donnadiou, B.; Bertrand, G. *Angew. Chem. Int. Ed.* **2005**, *44*, 7236–7239; c) Stambuli, J. P.; Weng, Z.; Incarvito, C. D.; Hartwig, J. F. *Angew. Chem. Int. Ed.* **2007**, *46*, 7674–7677; d) Walter, M. D.; White, P. S.; Brookhart, M. *New J. Chem.* **2013**, *37*, 1128–1133; e) Baratta, W.; Stoccoro, S.; Doppiu, A.; Herdtweck, E.; Zucca, A.; Rigo, P. *Angew. Chem. Int. Ed.* **2003**, *42*, 105–109; f) Ingleson, M. J.; Mahon, M. F.; Weller, A. S. *Chem. Commun.* **2004**, 2398–2399; g) Rivada-Wheelaghan, O.; Donnadiou, B.; Maya, C.; Conejero, S. *Chem. Eur.*

## Chapter II

- J.* **2010**, *16*, 10323–10326; h) Campos, J.; Ortega-Moreno, L.; Conejero, S.; Peloso, R.; López-Serrano, J.; Maya, C.; Carmona, E. *Chem. Eur. J.* **2015**, *21*, 8883–8896.
24. See for example: a) Barder, T. E.; Walker, S. D.; Martinelli, J. R.; Buchwald, S. L. *J. Am. Chem. Soc.* **2005**, *127*, 4685–4696; b) DeAngelis, A. J.; Gildner, P. G.; Chow, R.; Colacot, T. J. *J. Org. Chem.* **2015**, *80*, 6794–6813.
25. a) Moreno, J. J.; Espada, M. F.; Krüger, E.; López-Serrano, J.; Campos, J.; Carmona, E. *Eur. J. Inorg. Chem.* **2018**, 2309–2321; b) Marín, M.; Moreno, J. J.; Navarro-Gilabert, C.; Álvarez, E.; Maya, C.; Peloso, R.; Nicasio, M. C.; Carmona, E. *Chem. Eur. J.* **2019**, *25*, 260–272; c) Moreno, J. J.; Espada, M. F.; Campos, J.; López-Serrano, J.; Macgregor, S. A.; Carmona, E. *J. Am. Chem. Soc.* **2019**, *141*, 2205–2210.
26. a) Ortega-Moreno, L.; Fernández-Espada, M.; Moreno, J. J.; Navarro-Gilabert, C.; Campos, J.; Conejero, S.; López-Serrano, J.; Maya, C.; Peloso, R.; Carmona, E. *Polyhedron* **2016**, *116*, 170–181; b) Ortega-Moreno, L.; Peloso, R.; López-Serrano, J.; Iglesias-Sigüenza, J.; Maya, C.; Carmona, E. *Angew. Chem. Int. Ed.* **2017**, *56*, 2772–2775.
27. a) Green, M. L. H.; Nagy, P. L. I. In *Advances in Organometallic Chemistry*, Vol. 2; Stone, F. G. A., West, R., Eds.; Academic Press, 1965; pp 325–363; b) *Synthetic Methods of Organometallic and Inorganic Chemistry*, Vol. 9; Herrmann, W. A., Ed.; Georg Thieme Verlag: New York, 2000.
28. a) Wilke, G.; Bogdanović, B.; Hardt, P.; Heimbach, P.; Keim, W.; Kröner, M.; Oberkirch, W.; Tanaka, K.; Steinrücke, E.; Walter, D.; Zimmermann, H. *Angew. Chem. Int. Ed. Engl.* **1966**, *5*, 151–164; b) Clarke, H. L. *J. Organomet. Chem.* **1974**, *80*, 155–173.
29. See for example ref. 24b, and also: Werner, H.; Kühn, A. *Angew. Chem. Int. Ed. Engl.* **1977**, *16*, 412–413.

30. See for example: a) Raper, G.; McDonald, W. S. *J. Chem. Soc., Dalton Trans.* **1972**, 265–269; b) Bandoli, G.; Dolmella, A.; Fanizzi, F. P.; Di Masi, N. G.; Maresca, L.; Natile, G. *Organometallics* **2001**, *20*, 805–807.
31. a) Smith, A. E. *Acta Cryst.* **1965**, *18*, 331–340; b) Mason, R.; Wheeler, A. G. *J. Chem. Soc. A* **1968**, 2543–2549.
32. a) Smidt, J.; Hafner, W. *Angew. Chem.* **1959**, *71*, 284–284; b) Wilke, G.; Bogdanovič, B. *Angew. Chem.* **1961**, *73*, 756–756.
33. a) *Comprehensive Organometallic Chemistry, Vol. 8*; Wilkinson, G., Stone, F. G. A., Abel, E. W., Eds.; Pergamon Press: New York, 1982; b) Jolly, P. W.; Wilke, G. *The Organic Chemistry of Nickel, Vol. 2*; Wiley: New York, 1975.
34. Hartwig, J. F. *Organotransition Metal Chemistry: From Bonding to Catalysis.*; University Science Books: Sausalito, 2010.
35. Takacs, J. M. Transition Metal Allyl Complexes: Telomerization of Dienes. In *Comprehensive Organometallic Chemistry II, Vol. 12*; Elsevier, 1995; pp 785–796.
36. Oppolzer, W. Transition Metal Allyl Complexes: Intramolecular Alkene and Alkyne Insertions. In *Comprehensive Organometallic Chemistry II, Vol. 12*; Elsevier, 1995; pp 905–921.
37. Harrington, P. J. Transition Metal Allyl Complexes: Pd, W, Mo-assisted Nucleophilic Attack. In *Comprehensive Organometallic Chemistry II, Vol. 12*; Elsevier, 1995; pp 797–904.
38. Trost, B. M.; Crawley, M. L. *Chem. Rev.* **2003**, *103*, 2921–2944.
39. Some recent examples include: a) Chartoire, A.; Frogneux, X.; Nolan, S. P. *Adv. Synth. Catal.* **2012**, *354*, 1897–1901; b) Bastug, G.; Nolan, S. P. *J. Org. Chem.* **2013**, *78*, 9303–9308; c) Marelli, E.; Chartoire, A.; Le Duc, G.; Nolan, S. P. *ChemCatChem* **2015**, *7*, 4021–4024.

## Chapter II

40. a) Hill, L. L.; Crowell, J. L.; Tutwiler, S. L.; Massie, N. L.; Hines, C. C.; Griffin, S. T.; Rogers, R. D.; Shaughnessy, K. H.; Grasa, G. a.; Johansson Seechurn, C. C. C.; Li, H.; Colacot, T. J. *J. Org. Chem.* **2010**, *75*, 6477–6488; b) Seechurn, C. C. C. J.; Parisel, S. L.; Colacot, T. J. *J. Org. Chem.* **2011**, *76*, 7918–7932.
41. a) Li, H.; Johansson Seechurn, C. C. C.; Colacot, T. J. *ACS Catal.* **2012**, *2*, 1147–1164; b) Hazari, N.; Melvin, P. R.; Beromi, M. M. *Nat. Rev. Chem.* **2017**, *1*, 0025.
42. a) Melvin, P. R.; Nova, A.; Balcells, D.; Dai, W.; Hazari, N.; Hruszkewycz, D. P.; Shah, H. P.; Tudge, M. T. *ACS Catal.* **2015**, *5*, 3680–3688; b) Melvin, P. R.; Balcells, D.; Hazari, N.; Nova, A. *ACS Catal.* **2015**, *5*, 5596–5606.
43. For some recent reviews on catalysis by first-row transition metals, see: a) *Chem. Rev.* **2019**, *119*, 2089–3032 (whole issue); b) Miao, J.; Ge, H. *Eur. J. Org. Chem.* **2015**, 7859–7868; c) Zweig, J. E.; Kim, D. E.; Newhouse, T. R. *Chem. Rev.* **2017**, *117*, 11680–11752
43. For some recent reviews centred on nickel catalysis, see: a) Han, F.-S. *Chem. Soc. Rev.* **2013**, *42*, 5270–5298; b) Ananikov, V. P. *ACS Catal.* **2015**, *5*, 1964–1971; c) Ritleng, V.; Henrion, M.; Chetcuti, M. J. *ACS Catal.* **2016**, *6*, 890–906; d) Tasker, S. Z.; Standley, E. A.; Jamison, T. F. *Nature* **2014**, *509*, 299–309.
44. a) Iglesias, M. J.; Prieto, A.; Nicasio, M. C. *Adv. Synth. Catal.* **2010**, *352*, 1949–1954; b) Iglesias, M. J.; Prieto, A.; Nicasio, M. C. *Org. Lett.* **2012**, *14*, 4318–4321; c) Martin, A. R.; Nelson, D. J.; Meiries, S.; Slawin, A. M. Z.; Nolan, S. P. *Eur. J. Org. Chem.* **2014**, 3127–3131; d) Makida, Y.; Marelli, E.; Slawin, A. M. Z.; Nolan, S. P. *Chem. Commun.* **2014**, *50*, 8010–8013; e) Fernández-Salas, J. a.; Marelli, E.; Cordes, D. B.; Slawin, A. M. Z.; Nolan, S. P. *Chem. Eur. J.* **2015**, *21*, 3906–3909; f) Marelli, E.; Fernández Salas, J.; Nolan, S. P. *Synthesis* **2015**, *47*, 2032–2037.

46. Ge, S.; Hartwig, J. F. *Angew. Chem. Int. Ed.* **2012**, *51*, 12837–12841.
47. Pauling, L. *The Nature of the Chemical Bond*; Cornell University Press: Ithaca, New York (United States), 1960.
48. a) Eastes, J. W.; Burgess, W. M. *J. Am. Chem. Soc.* **1942**, *64*, 1187–1189; b) Burbage, J. J.; Fernelius, W. C. *J. Am. Chem. Soc.* **1943**, *65*, 1484–1486.
49. Malatesta, L.; Ugo, R.; Cenini, S. Chemistry of Zerovalent Nickel, Palladium, and Platinum Derivatives. In *Werner Centennial*; Kauffman, G. B., Ed.; 1967; pp 318–356.
50. a) Chatt, J. *Nature* **1950**, *165*, 637–638; b) Wilkins, R. G. *Nature* **1951**, *167*, 434–435.
51. a) Malatesia, L.; Angoletta, M. *J. Chem. Soc.* **1957**, 1186–1188; b) Malatesta, L.; Cariello, C. *J. Chem. Soc.* **1958**, 2323–2328.
52. a) Wilke, G.; Müller, E. W.; Kröner, M. *Angew. Chem.* **1961**, *73*, 33–34; b) Schunn, R. A. *Inorg. Synth.* **2007**, *13*, 124–126.
53. Ugo, R. *Coord. Chem. Rev.* **1968**, *3*, 319–344.
54. a) Matsumoto, M.; Yoshioka, H.; Nakatsu, K.; Yoshida, T.; Otsuka, S. *J. Am. Chem. Soc.* **1974**, *96*, 3322–3324; b) Immirzi, A.; Musco, A. *J. Chem. Soc., Chem. Commun.* **1974**, 400–401; c) Otsuka, S.; Yoshida, T.; Matsumoto, M.; Nakatsu, K. *J. Am. Chem. Soc.* **1976**, *98*, 5850–5858; d) Tanaka, M. *Acta Cryst.* **1992**, *C48*, 739–740.
55. a) Ugo, R.; La Monica, G.; Cariati, F.; Cenini, S.; Conti, F. *Inorganica Chim. Acta* **1970**, *4*, 390–394; b) Goel, R. G.; Ogini, W. O.; Srivastava, R. C. *J. Organomet. Chem.* **1981**, *214*, 405–417.
56. a) Englert, M.; Jolly, P. W.; Wilke, G. *Angew. Chem. Int. Ed. Engl.* **1971**, *10*, 77–77; b) Otsuka, S.; Tani, K.; Kato, I.; Teranaka, O. *J. Chem. Soc. Dalton Trans.* **1974**, 2216–2219.

## Chapter II

57. a) Paul, F.; Patt, J.; Hartwig, J. F. *J. Am. Chem. Soc.* **1994**, *116*, 5969–5970; b) Hartwig, J. F.; Paul, F. *J. Am. Chem. Soc.* **1995**, *117*, 5373–5374; c) Littke, A. F.; Dai, C.; Fu, G. C. *J. Am. Chem. Soc.* **2000**, *122*, 4020–4028; d) Christmann, U.; Vilar, R. *Angew. Chem. Int. Ed.* **2005**, *44*, 366–374; e) Xue, L.; Lin, Z. *Chem. Soc. Rev.* **2010**, *39*, 1692–1705; f) Schoenebeck, F.; Houk, K. N. *J. Am. Chem. Soc.* **2010**, *132*, 2496–2497; g) Proutiere, F.; Schoenebeck, F. *Angew. Chem. Int. Ed.* **2011**, *50*, 8192–8195.
58. a) Krause, J.; Cestarcic, G.; Haack, K.-J.; Seevogel, K.; Storm, W.; Pörschke, K.-R. *J. Am. Chem. Soc.* **1999**, *121*, 9807–9823; b) Selvakumar, K.; Zapf, A.; Beller, M. *Org. Lett.* **2002**, *4*, 3031–3033; c) Clement, N. D.; Cavell, K. J.; Ooi, L. *Organometallics* **2006**, *25*, 4155–4165; d) Clement, N. D.; Routaboul, L.; Grotevendt, A.; Jackstell, R.; Beller, M. *Chem. Eur. J.* **2008**, *14*, 7408–7420; e) Komine, N.; Abe, M.; Suda, R.; Hirano, M. *Organometallics* **2015**, *34*, 432–437; f) Komine, N.; Ito, R.; Suda, H.; Hirano, M.; Komiya, S. *Organometallics* **2017**, *36*, 4160–4168.
59. a) Reid, S. M.; Boyle, R. C.; Mague, J. T.; Fink, M. J. *J. Am. Chem. Soc.* **2003**, *125*, 7816–7817.; b) Li, H.; Grasa, G. A.; Colacot, T. J. *Org. Lett.* **2010**, *12*, 3332–3335.
60. a) Böhm, V. P. W.; Gstöttmayr, C. W. K.; Weskamp, T.; Herrmann, W. A. *J. Organomet. Chem.* **2000**, *595*, 186–190; b) Caddick, S.; Cloke, F. G. N.; Clentsmith, G. K. B.; Hitchcock, P. B.; McKerrecher, D.; Titcomb, L. R.; Williams, M. R. V. *J. Organomet. Chem.* **2001**, *617–618*, 635–639; c) Titcomb, L. R.; Caddick, S.; Cloke, F. G. N.; Wilson, D. J.; McKerrecher, D. *Chem. Commun.* **2001**, 1388–1389; d) Gstöttmayr, C. W. K.; Böhm, V. P. W.; Herdtweck, E.; Grosche, M.; Herrmann, W. A. *Angew. Chem. Int. Ed.* **2002**, *41*, 1363–1365; e) Altenhoff, G.; Goddard, R.; Lehmann, C. W.; Glorius, F. *Angew. Chem. Int. Ed.* **2003**, *42*, 3690–3693; f) Arentsen, K.; Caddick, S.; Cloke, F. G. N.; Herring, A. P.; Hitchcock, P. B. *Tetrahedron Lett.* **2004**, *45*,



- 3511–3515; g) Yamashita, M.; Goto, K.; Kawashima, T. *J. Am. Chem. Soc.* **2005**, *127*, 7294–7295; h) Fantasia, S.; Nolan, S. P. *Chem. Eur. J.* **2008**, *14*, 6987–6993; i) Lee, E.; Yandulov, D. V. *J. Organomet. Chem.* **2011**, *696*, 4095–4103.
61. Schmid, T. E.; Jones, D. C.; Songis, O.; Diebolt, O.; Furst, M. R. L.; Slawin, A. M. Z.; Cazin, C. S. J. *Dalton Trans.* **2013**, *42*, 7345–7353.
62. Velian, A.; Lin, S.; Miller, A. J. M.; Day, M. W.; Agapie, T. *J. Am. Chem. Soc.* **2010**, *132*, 6296–6297.
63. Ortega-Moreno, L.; Peloso, R.; Maya, C.; Suárez, A.; Carmona, E. *Chem. Commun.* **2015**, *51*, 17008–17011.
64. Ortega Moreno, L. Synthesis, Structure and Some Catalytic Applications of Platinum Complexes with Terphenyl Phosphine Ligands. PhD thesis, Universidad de Sevilla, 2016.
65. a) Harris, R. K. *Can. J. Chem.* **1964**, *42*, 2275–2281; b) Ault, A. J. *Chem. Educ.* **1970**, *47*, 812–818; c) Redfield, D. A.; Cary, L. W.; Nelson, J. H. *Inorg. Chem.* **1975**, *14*, 50–59.
66. Cordero, B.; Gómez, V.; Platero-Prats, A. E.; Revés, M.; Echeverría, J.; Cremades, E.; Barragán, F.; Alvarez, S. *Dalton Trans.* **2008**, 2832–2838.
67. Vicente, J.; Lagunas, M. C.; Bleuel, E.; Ramirez de Arellano, M. C. CCDC 100877: Experimental Crystal Structure Determination, 1998, DOI: 10.5517/cc3cz3j
68. Demchuk, O. M.; Kaplon, K.; Mazur, L.; Strzelecka, D.; Pietrusiewicz, K. M. *Tetrahedron* **2016**, *72*, 6668–6677.
69. a) Kinzhalov, M. A.; Buldakov, A. V.; Petrov, A. V.; Mahmudov, K. T.; Ivanov, A. Y.; Suslonov, V. V. *Russ. J. Gen. Chem.* **2017**, *87*, 2605–2611; b) Martínez-Martínez, A. J.; Chicote, M. T.; Bautista, D. *Inorganica Chim. Acta* **2012**, *382*,

Chapter II

203–206.

70. Pregosin, P. S. *NMR in Organometallic Chemistry*; WILEY-VCH: Weinheim, Germany, 2012.
71. gNMR, Version 5.0.6.0, Budzelaar, P. H. M. Ivorysoft 2006.
72. a) *Dynamic Nuclear Magnetic Resonance Spectroscopy*; Jackman, L. M., Cotton, F. A., Eds.; Academic Press: New York, 1975; b) Solin, N.; Szabó, K. *J. Organometallics* **2001**, *20*, 5464–5471.
73. Marion, N.; Navarro, O.; Mei, J.; Stevens, E. D.; Scott, N. M.; Nolan, S. P. *J. Am. Chem. Soc.* **2006**, *128*, 4101–4111.
74. Silva, L. C.; Gomes, P. T.; Veiros, L. F.; Pascu, S. I.; Duarte, M. T.; Namorado, S.; Ascenso, J. R.; Dias, A. R. *Organometallics* **2006**, *25*, 4391–4403.
75. a) Henning, H.; Hofbauer, K.; Handke, K.; Stich, R. *Angew. Chem. Int. Ed. Engl.* **1997**, *36*, 408–410; b) Milne, J. E.; Jarowicki, K.; Kocienski, P. J. *Synlett* **2002**, 0607–0609; c) Sheina, E. E.; Liu, J.; Iovu, M. C.; Laird, D. W.; McCullough, R. D. *Macromolecules* **2004**, *37*, 3526–3528; d) Ananikov, V. P.; Gayduk, K. A.; Orlov, N. V.; Beletskaya, I. P.; Khrustalev, V. N.; Antipin, M. Y. *Chem. Eur. J.* **2010**, *16*, 2063–2071; e) Cornella, J.; Gómez-Bengoa, E.; Martin, R. *J. Am. Chem. Soc.* **2013**, *135*, 1997–2009; f) Standley, E. A.; Jamison, T. F. *J. Am. Chem. Soc.* **2013**, *135*, 1585–1592.
76. Mastrorilli, P.; Moro, G.; Nobile, C. F.; Latronico, M. *Inorganica Chim. Acta* **1992**, *192*, 183–187.
77. Tschan, M. J. L.; García-Suárez, E. J.; Freixa, Z.; Launay, H.; Hagen, H.; Benet-Buchholz, J.; van Leeuwen, P. W. N. M. *J. Am. Chem. Soc.* **2010**, *132*, 6463–6473.
78. Neff, R. K.; Frantz, D. E. *J. Am. Chem. Soc.* **2018**, *140*, 17428–17432.
79. Hoshimoto, Y.; Hayashi, Y.; Suzuki, H.; Ohashi, M.; Ogoshi, S.

## Bibliography

- Organometallics* **2014**, *33*, 1276–1282.
80. Cook, C. D.; Koo, C. H.; Nyburg, S. C.; Shiomi, M. T. *Chem. Commun. (London)*, **1967**, 426b–427.
81. Smith, R. C.; Woloszynek, R. A.; Chen, W.; Ren, T.; Protasiewicz, J. D. *Tetrahedron Lett.* **2004**, *45*, 8327–8330.
82. Wielandt, J. W.; Ruckerbauer, D., *Inorg. Synth.* **2010**, *35*, 120–125.
83. Jensen, K. A.; Nielsen, E. J.; Reiter, R.; Schønfeldt, E.; Steensgaard, I.; Rosenberg, T. *Acta Chem. Scand.* **1953**, *7*, 866–868.



## CONCLUSIONES

Una serie de dialquil terfenil fosfinas,  $PR_2Ar''$ , han sido sintetizadas, caracterizadas y sus estabilidades con respecto a la oxidación al aire examinadas. En el estado sólido, tanto las nuevas fosfinas como las previamente reportadas adoptan una de tres posibles conformaciones, dependiendo de la disposición de los grupos alquilo.

Complejos  $Ni(CO)_3(PR_2Ar'')$  de las fosfinas menos voluminosas (con  $R = Me$  o  $Et$ ) han sido sintetizados y caracterizados. El estudio de sus espectros de IR desvela que las fosfinas  $PR_2Ar''$  dan lugar a valores de TEP más bajos que sus análogas  $PR_2Ph$ , indicando una mayor capacidad donadora de las primeras.

Para los miembros más voluminosos de la familia ( $R = iPr$ ,  $Cyp$  o  $Cy$ ), el calentamiento de las mezclas de reacción en vacío resultó en complejos de fórmula  $Ni(CO)_2(PR_2Ar'')$ , donde un segundo ligando carbonilo es reemplazado por una interacción  $\eta^2$  con uno de los anillos laterales de la fosfina.

Cálculos DFT sugieren que la presencia de grupos alquilo voluminosos en el átomo de fósforo causan una desestabilización de las moléculas de  $Ni(CO)_3(PR_2Ar'')$ , facilitando de esta manera la pérdida de un ligando carbonilo.

No se obtuvo una buena correlación entre los valores de TEP obtenidos de los espectros de IR de complejos  $IrCl(CO)_2(PR_2Ar'')$  y aquellos encontrados para el sistema  $Ni(CO)_3(PR_2Ar'')$ .

Las dialquil terfenil fosfinas estudiadas son, en la mayor parte de los casos, capaces de estabilizar complejos de níquel, paladio y platino en estado de oxidación 0 y +II, exhibiendo un mayor grado de éxito en compuestos coordinativamente insaturados.

## Conclusiones

Los compuestos de fórmula empírica  $\text{PdCl}_2(\text{PR}_2\text{Ar}'')$  existen en disolución como monómeros o como dímeros con puentes cloruro, según los estudios de RMN. La preferencia por una forma o la otra depende de varios factores, tal como el disolvente, la concentración y la naturaleza del ligando fosfina. Estos complejos reaccionan con bases de Lewis para generar los correspondientes aductos  $\text{PdCl}_2(\text{L})(\text{PR}_2\text{Ar}'')$ .

El comportamiento dinámico de los complejos de  $\eta^3$ -alilo de níquel y paladio con ligandos dialquil terfenil fosfina ha sido investigado. El fragmento alilo en los derivados de paladio sufre un intercambio *sin-anti*, presumiblemente a través de un mecanismo de isomerización  $\eta^3$ - $\eta^1$ - $\eta^3$ . Tanto la naturaleza de la fosfina como la sustitución del ligando alilo afectan a la velocidad de dicho intercambio. Por otro lado, un intercambio *sin-sin anti-anti* parece ser la causa del comportamiento fluxional de los análogos de níquel.

Los complejos donde el metal se encuentra en estado de oxidación 0 y que contienen dialquil terfenil fosfinas pueden ser sintetizados siguiendo diferentes estrategias. Los compuestos coordinativamente insaturados se estabilizan por impedimento estérico o bien por interacción con los anillos laterales de la fosfina.